AD/A-004 416

STRUCTURAL MODE EFFECTS ON FLYING
QUALITIES IN TURBULENCE

Carl A. Crother, et al

Rockwell International Corporation

Prepared for:

Air Force Flight Dynamics Laboratory

August 1973

AD/A-004416

DOCUMENT CONTROL DATA - R & D

(Security classification of title, body of abstract and indexing annotation must be entered when the overall report is classified)

1 ORIGINATING ACTIVITY *(Corporate author)*	2a. REPORT SECURITY CLASSIFICATION
Los Angeles Aircraft Division of Rockwell International Corporation, Los Angeles International Airport, Los Angeles, California 90009	UNCLASSIFIED
	2b. GROUP N/A

3 REPORT TITLE

STRUCTURAL MODE EFFECTS ON FLYING QUALITIES IN TURBULENCE

4 DESCRIPTIVE NOTES *(Type of report and inclusive dates)*

Final Report — 6 December 1971 to 19 August 1973

5 AUTHOR(S) *(First name, middle initial, last name)*

Carl A. Crother, Brian Gabelman, Del Langton

6 REPORT DATE	7a. TOTAL NO. OF PAGES	7b. NO. OF REFS
August 1973	4-12	11

8a. CONTRACT OR GRANT NO.	9a. ORIGINATOR'S REPORT NUMBER(S)
F33615-71-C-1418	
b. PROJECT NO 8219	
c. Task No. 821904	9b. OTHER REPORT NO(S) *(Any other numbers that may be assigned this report)*
d.	AFFDL-TR-73-88

10 DISTRIBUTION STATEMENT

Approved for public release; distribution unlimited

11 SUPPLEMENTARY NOTES	12. SPONSORING MILITARY ACTIVITY
None	AFFDL Control Criteria Branch Wright-Patterson AFB, Ohio 45435

13 ABSTRACT

Pilot performance parameters, such as pilot ratings, tracking errors, and pilot response characteristics, are determined for two longitudinal tracking tasks, using a large, flexible bomber in a turbulent environment. The two tasks, terrain following and air refueling, were accomplished on a limited, six-degrees-of-freedom motion simulator. The effect of structural motion on pilot performance and opinion and the correlation with pilot ratings are of concern for potential application in pilot rating prediction methods. The study results indicate the motion effects of turbulence and structural flexibility do not affect pilot performance or pilot opinion in the two tasks evaluated.

DD FORM 1 NOV 65 1473

i

14 KEY WORDS	LINK A		LINK B		LINK C	
	ROLE	WT	ROLE	WT	ROLE	WT
Pilot Opinion Turbulence Structural Flexibility Pilot Model						

STRUCTURAL MODE EFFECTS ON

FLYING QUALITIES IN TURBULENCE

C. A. Crother
B. Gabelman
D. Langton

August 1973

NOTICE

When Government drawings, specifications, or other data are used for any purpose other than in connection with a definitely related Government procurement operation, the United States Government thereby incurs no responsibility nor any obligation whatsoever; and the fact that the government may have formulated, furnished, or in any way supplied the said drawings, specifications, or other data, is not to be regarded by implication or otherwise as in any manner licensing the holder or any other person or corporation, or conveying any rights or permission to manufacture, use, or sell any patented invention that may in any way be related thereto.

Copies of this report should not be returned unless return is required by security considerations, contractual obligations, or notice on a specific document.

X
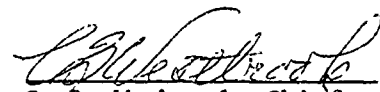
FOREWORD

This document is the final technical report on a study of structural motion effects on pilot opinion and performance during tracking in a large flexible vehicle in turbulence. The study was conducted at the Los Angeles Aircraft Division, Rockwell International Corporation, International Airport, Los Angeles, Calif. 90009, under USAF Contract F33615-71-C-1418. The contract work was sponsored by the Air Force Flight Dynamics Laboratory under Project 8219, Task No. 821904, and was under the direction of Mr. Frank L. George (AFFDL/FGC) of the Air Force Flight Dynamics Laboratory, Wright-Patterson AFB, Ohio. The inclusive dates of research were 6 December 1971 to 19 August 1973.

The research was performed under the supervision of L. U. Nardi at the Los Angeles Aircraft Division. Project personnel included C. A. Crother, Principal Investigator; B. Gabelman; and D. Langton.

This report was submitted on 19 August 1973.

This technical report has been reviewed and is approved.

C. B. Wesbrook, Chief
Control Criteria Branch
Flight Control Division

ABSTRACT

Pilot performance parameters, such as pilot ratings, tracking errors, and pilot response characteristics, are determined for two longitudinal tracking tasks, using a large, flexible bomber in a turbulent environment. The two tasks, terrain following and air refueling, were accomplished on a limited, six-degrees-of-freedom motion simulator. The effect of structural motion on pilot performance and opinion and the correlation with pilot ratings are of concern for potential application in pilot rating prediction methods. The study results indicate that the motion effects of turbulence and structural flexibility do not affect pilot performance or pilot opinion in the two tasks evaluated.

TABLE OF CONTENTS

LIST OF ILLUSTRATIONS

LIST OF TABLES

SECTION I

INTRODUCTION

The analytical prediction of pilot ratings was successfully demonstrated for the hover task through the work of R. O. Anderson of the Air Force Flight Dynamics Laboratory. In his study (reference 1), Anderson utilized the large mass of experimental hover data to develop a relationship between pilot rating and measurable pilot task parameters. The potential significance of this methodology is in its application to pilot/vehicle/task analyses and evaluation in terms of handling qualities specifications. The extension of this concept to conventional vehicle tasks in the longitudinal axis was undertaken recently by Anderson (reference 2) and extended to the lateral/directional axis by E. D. Onstott of Northrop (reference 3). A degree of success was achieved, but specific criteria have not been developed to date, and part of the difficulty seems to lie in the poor correlation between pilot ratings and pilot task parameters when the vehicle is subject to higher levels of turbulence or exhibits poor damping characteristics. Additionally, there is some concern that structural mode motions adversely affect flying qualities opinions. In order to develop this methodology for application to the large flexible vehicle where structural mode motions are significant, a study was made to determine the effects on pilot opinion and performance of structural mode excitation and to incorporate these effects into the methodology of predicting flying qualities in a turbulent environment. The successful development of pilot rating predictions based on this data base would enhance the potential for ultimately specifying or evaluating flying qualities criteria through these methods.

This report details the results of that study in structural mode effects on pilot opinion and performance during two tracking tasks. Section III describes briefly the background effort in the prediction of pilot ratings based on Anderson's method. Section IV covers the program objectives, a description of the study vehicle, and the tracking tasks and data analysis methods employed. The simulation results of the terrain-following and air-refueling tasks are presented in sections V and VI, respectively. Application of the simulation results to the paper pilot method is covered in section VII, while the study conclusions are given in section VIII.

1

SECTION II

SUMMARY

Considerable effort has been and is being expended to improve and extend current flying qualities specifications. One of the areas of technical activity has been in the use of prediction methods of pilot ratings based on closed-loop analyses and pilot modeling. Limitations in the method have appeared in recent work for conditions involving high turbulence with or without poor aircraft short period damping. This study examines the application of predictive pilot ratings to a large, flexible bomber in a turbulent environment where structural motion is significant.

Two longitudinal mission tasks were evaluated using a six-degrees-of-freedom simulation of the aircraft equations of motion. The piloting tasks were conducted on a limited six-degrees-of-freedom motion simulator to generate a data base for deriving a suitable pilot rating algorithm. Pilot comments and performance in the terrain-following and air-refueling tasks, however, revealed little correlation between rating and turbulence or structural flexibility effects. Pilot model characteristics were well defined for the terrain-following task and, in the resulting lead-lag transfer function, the lag time constant correlated well with turbulence level. In the air-refueling task, considerable variation occurred in the pilot frequency response characteristics. A frequency dependent, large time delay was found necessary for good phase matching between pilot model and bode plot. Although some evidence exists of a correlation between pilot rating and pilot pitch stick spectral density function, the general conclusion of the simulation effort is that the pilots rated the vehicle-task problem and were not influenced by turbulence or structural mode excitation. This is attributable to the fact that the primary tracking tasks were in terrain following and air refueling and that turbulence and structural effects were additive to these tasks and were not of sufficient magnitude to dominate the pilot's display tracking capabilities.

The current concept of predicting pilot ratings which isolates flying qualities from ride qualities appears to be valid based on these results. The parametric variations conducted in the study proved to be of little influence in pilot rating determination and, consequently, the data base generated could not be used to develop flying qualities specifications. Unfortunately, the simulation and simulator availability did not permit a timely and beneficial reorientation of the study program.

SECTION III

BACKGROUND OF ANALYTICAL METHOD

The VTOL vehicle exhibits basic instability in the hover mode, necessitating the use of stability augmentation systems. Since the degree of artificial stabilization drastically affects the vehicle's response characteristics, a simple statement of flying qualities requirements in the conventional terms was not possible. In an effort to circumvent this problem, R. O. Anderson developed analytical methods of evaluation and prediction of pilot ratings based upon closed loop analyses of the hover task. Using experimental hover data available, he showed a correlation between pilot ratings and pilot task parameters and then developed an analytical method for predicting such ratings (reference 1). The developed relationship between pilot rating and pilot task parameters for a hover situation was found to be:
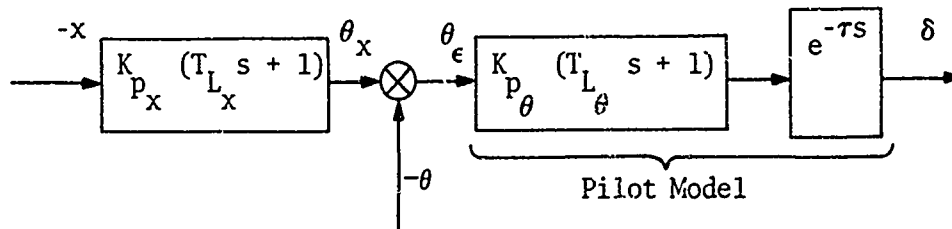
$$R = R_1 + R_2 + R_3 + 1.0$$

where

$$R_1 = \frac{\sigma - \sigma_m}{\sigma_m}, \quad \sigma_m = 0.80 = \text{required performance}$$

$$\sigma = \sigma_x + 10\sigma_q$$

$$0 \leq R_1 \leq 2.50$$

and

σ_x = standard deviation of x displacement in feet

σ_q = standard deviation of pitch rate in rad per second

$$R_2 = 2.5\, T_{L_\theta}, \quad R_2 \leq 3.25$$

$$R_3 = 1.0\ T_{L_x}\ ,\ R_3 \leq 1.20$$

T_{L_θ} = Pilot lead time constant in pitch in seconds

T_{L_x} = Pilot lead time constant in displacement in seconds

In an attempt to expand the concept to provide predictions, Anderson said that, if the pilot naturally works to minimize his rating, the aforementioned pilot rating function could be used as an algorithm for minimizing pilot ratings based on the trade-off between workload and performance. He applied this prediction method to additional hover data and obtained good results. In an effort to automate the application of the prediction method and thus elimi- nate the laborious computational chore, J. D. Dillow developed the "paper pilot" which is a digital computer program for predicting pilot ratings for the hover task (reference 4).

G. L. Teper of STI undertook to further assess the Anderson prediction method for the hover task (reference 5). Although the pilot rating criteria in the hover task used in Teper's work was considerably different from Anderson's, Teper showed that the Anderson pilot model can be used successfully if the time delay is assumed to be variable. Additionally, in order to improve the performance prediction, remnant injection was found necessary.

Extension of the paper pilot to conventional vehicles and a pitch track- ing task was examined by Anderson in reference 2. In general, the results proved promising, but the data base was admittedly limited. The form of the pilot model and the rating algorithm used are as follows:

Pilot Model
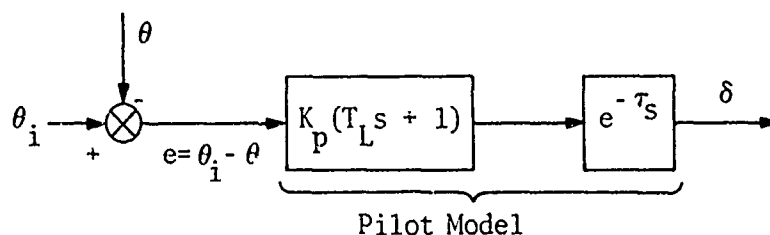
where

$$PR = \begin{cases} R1 + R2 + 1.0, & PERF + R2 + 1.0 \leq 10 \\ 10 & , & PERF + R2 + 1.0 > 10 \end{cases}$$

$$R1 = \frac{0.1}{0.974 - \sigma} \qquad\qquad R_2 = \begin{cases} -2.5\, T_L, & T_L < 0 \\[2mm] 2.5\, T_L, & 0 \leq T_L \leq 1.3 \\[2mm] 3.25, & T_L > 1.3 \end{cases}$$

$$PERF = \begin{cases} \dfrac{0.1}{0.974 - \sigma}, & \sigma < 0.9739 \\[4mm] 10^{11}\,(0.974-\sigma)^2 - 3\times10^7\,(0.974-\sigma) + 3\times10^3, & \sigma \geq 0.9739 \end{cases}$$

One interesting aspect of the study results is that, for a high dynamic pressure (high aircraft longitudinal frequency) flight condition, an open-loop prediction algorithm based on damping provided better correlation with the experimental data, while for a low dynamic pressure (low frequency) case (power approach), the closed-loop paper pilot did better. Additionally, the open-loop prediction was better even for the low dynamic pressure condition whenever poor damping existed.

In reference 3, E. D. Onstott and E. P. Salmon of Northrop Corp, attempted to further extend analytical prediction methods to the lateral-directional control of the conventional air vehicle in a turbulent environment. Although their work showed relatively good prediction of performance measures in roll and heading control, no real success was achieved in predicting pilot ratings. However, the data base generated and the performance prediction methods used provide necessary ingredients for further work in this area. In an extension of this effort, Onstott et al further applied their performance prediction methods to two other fighter-type vehicles with the objective of generating flying qualities specifications (AFFDL Contract F33615-71-C-1067). A pitch tracking task was also added to the study. Results similar to those presented in reference 3 were obtained, and flying qualities specifications were proposed in terms of performance measures. One interesting conclusion of the study was that pilot ratings alone are insufficient for flying qualities in turbulence evaluations, a position comparable to that expressed in reference 5 which indicated correlation with pilot rating but not with performance is insufficient for satisfactory specifications.

Drawing on this background in the use of the Anderson method, an investigation was made to determine the paper pilot's applicability to flying qualities specification development based on a large, flexible bomber in turbulence. The results of that study are presented hereafter.

SECTION IV

PROGRAM OBJECTIVES AND SCOPE

PROGRAM PLAN

The study objectives, as indicated earlier, are to define flying qualities in turbulence criteria through the application of Anderson's paper pilot concept. The vehicle being evaluated is a large, swingwing bomber. Two flight conditions representative of mission tasks requiring precise vehicle attitude control were selected for the application of the analytical methods.

The sequence of steps which were to be followed in the study are as follows:

1. Incorporate the bomber characteristics and flight controls into the pitch paper pilot.

2. Modify the pilot model and rating algorithm as necessary to reflect the piloting tasks involved.

3. Identify flying qualities criteria based on these paper pilot applications to the vehicle in turbulence.

4. Develop flight controls for the vehicle based on the flying qualities criteria previously identified.

5. Test the method by conducting a simulation program to verify the flight controls design and the pilot model and performance.

Unfortunately, the uniqueness of the terrain-following task and display necessitated the running of the simulation first in order to identify the pilot model to be used in the paper pilot program. In addition, the other task (air refueling) was sufficiently different as to require still another pilot model. Thus, the program was essentially reversed, with the simulation being used to generate data for the analytical program and the flying qualities specifications being based on the paper pilot and simulation results.

DESCRIPTION OF VEHICLE, TASKS, AND PILOT MODEL IDENTIFICATION

VEHICLE DESCRIPTION

The vehicle selected for the study is a large, swingwing bomber. Its primary mission is a low-altitude, high-speed condition, and it uses a structural model control system to minimize its structural flexibility effects.

Preceding page blank

The command stability augmentation systems (SAS) are conventional, and the longitudinal control system is shown in block diagram form in figure 1. The vehicle characteristics are listed in table I for the two flight conditions of interest, and the vehicle longitudinal equations of motion used in the analytical evaluations are given in figure 2. These equations, including the structural mode effects, are described in reference 6.

TASK DESCRIPTIONS

The two vehicle mission tasks selected, which require precise attitude control, are terrain following (TF) and air refueling (AR). Since turbulence effects are of significance at these conditions, they are ideally suited for the study. A brief description of each follows.

The TF task occurs at the low-altitude, high-speed flight condition. The TF algorithm developed for the vehicle is the ADLAT system. For manual control, the display of g error to the pilot is augmented by a lagged pitch stick displacement signal. The g error is generated by multiplying the flight path-error by 12.7 g per rad. Extensive simulation studies conducted in support of a bomber development program have shown that such display lead information is necessary for satisfactory manual terrain following. For this study, the TF task was restricted to the pitch axis (vertical plane) with the longitudinal SAS operative.

The simulation tests used the B-1 motion simulator (figure 3), and the vehicle six-degrees-of-freedom rigid body equations of motion (described in reference 6) were simulated in the hybrid computer facility. The simulator pilots flew TF tests using a conventional ADI where the horizontal flight director needle indicated the g error (scaled for 1 inch per g). Although six degrees of freedom were simulated, the vehicle was well behaved lateral-directionally such that the pilot task was restricted to the vertical plane only (the complete lateral-directional stability augmentation was always operative and pilot comments indicated no coupling occurred). The turbulence inputs were also restricted to W_g effects only. The TF task was flown over a specific terrain profile, and the runs were from 3 to 7 minutes in duration. The runs always began at the same point along the ground track (the statistical characteristics of the task are described later). The turbulence was generated through filtered white noise to approximate the Dryden form of the power spectra of the turbulence and then recorded on FM tape, thus providing a constant turbulence time history, desirable because of the relatively short simulation runs. The turbulence characteristics used are shown in figure 4.

In order to assess the effects of turbulence or pilot-induced structural mode excitation on the pilot, the vehicle simulation, which was for a rigid vehicle, had to be slightly modified. In keeping the simulation changes as

10
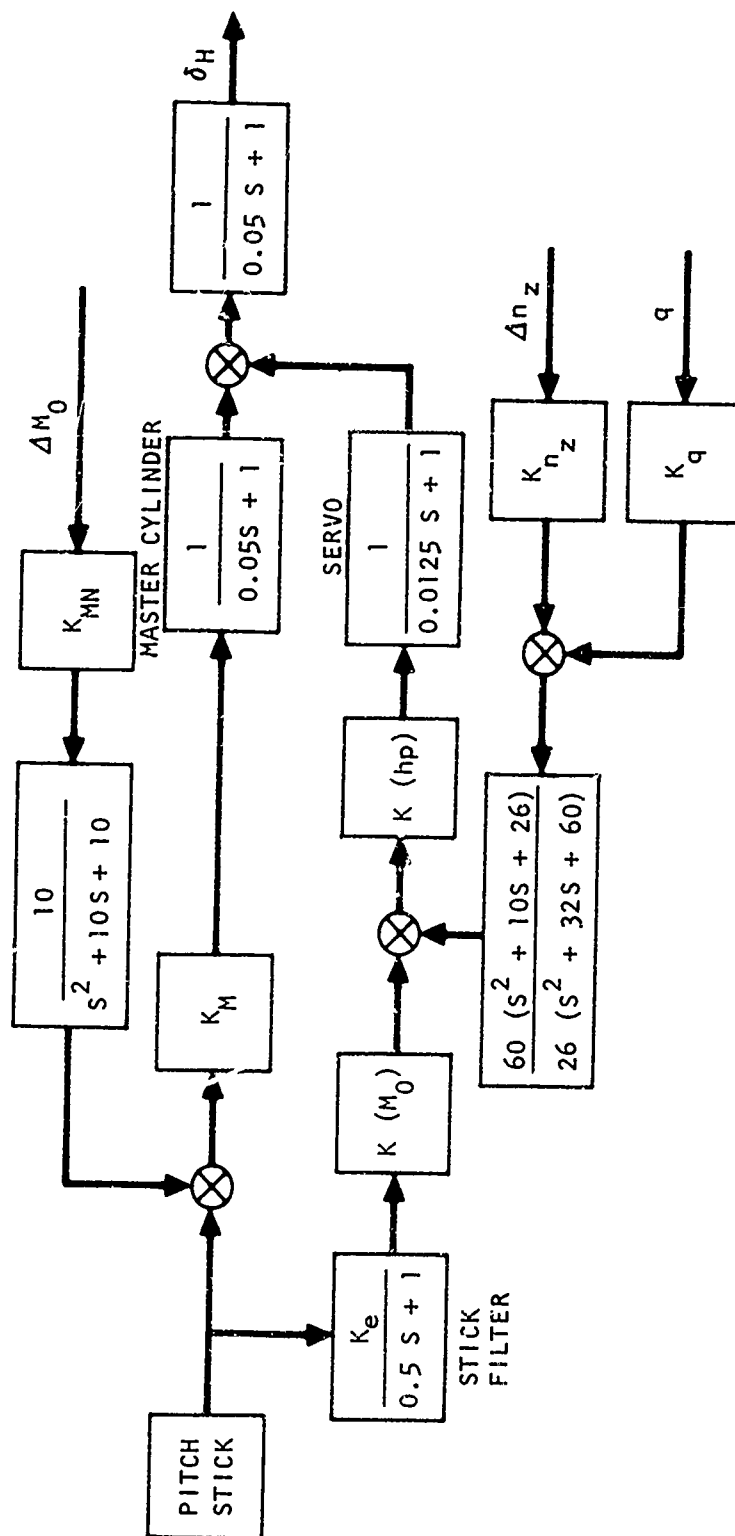
Figure 1. Command Stability Augmentation System Block Diagram

TABLE I. VEHICLE CHARACTERISTICS

TERRAIN-FOLLOWING (TF) DATA			
Stability Derivatives			

$X_u = -0.02505$ $Z_w = -0.9498$ $M_\delta = -9.006$ $X_{w_g} = -0.05644$

$X_w = -0.05644$ $Z_\delta = -165.79$ $M_q = -0.6517$ $M_{w_g} = -0.00158$

$X_\delta = 0$ $M_u = -0.0003$ $M_w = -0.00023$

$Z_u = -0.1055$ $M_w = -0.00158$

Modal Data	Mode 1	Mode 2	Mode 3
ω (rad/sec)	13.59	14.12	21.30
Z_{η_i} (ft/sec^2)	8.749	-91.135	-4.7821
M_{η_i} (rad/sec^2)	-0.2028	-0.09777	0.21949
$E_{\eta_{1_{w_g}}}$ (1/ft sec)	2.529	-0.9948	-0.5867
$E_{\eta_{i_\delta}}$ (1/rad-sec^2)	-2227.06	-217.05	614.67
$E_{\eta_{i_q}}$ (1/rad-sec)	-136.87	23.152	50.266
$E_{\eta_{1\eta_i}}$ (1/sec^2)	7.826	-16.673	66.807
$E_{\eta_{2\eta_i}}$ (1/sec^2)	13.877	-305.86	6.9015
$E_{\eta_{3\eta_i}}$ (1/sec^2)	7.755	34.891	-8.239
$\phi_{\eta_i}^A$	-0.0887	0.0531	-0.1097
$\phi_{\eta_i}^{'G}$ (1/ft)	-0.0036	-0.0079	-0.0030
$\phi_{\eta_i}^{'P}$ (1/ft)	0.0289	0.0287	0.03585
ζ_{η_i}	0.02	0.02	0.02

TABLE I. VEHICLE CHARACTERISTICS (CONT)

Pitch Control System Gains

$K_q \cdot K(h_p) = -0.4176$ sec $K_e \cdot K(M_0) \cdot K(h_p) = 0.0649$ rad/in.

$K_{n_Z} \cdot K(h_p) = -0.04716$ rad/g $K_m = 0.01099$ 1/in., $K_{MN} = -0.00627$ in./fps

AIR-REFUELING (AR) DATA

Stability Derivatives

$X_u = -0.0049$	$Z_w = -0.6121$	$M_\delta = -37.188$	$X_{w_g} = 0.02237$
$X_w = 0.02237$	$Z_\delta = -50.44$	$M_q = -0.4259$	$M_{w_g} = -0.003768$
$X_\delta = 0$	$M_u = 0.000042$	$M_{\dot{w}} = -0.000253$	
$Z_u = -0.0998$	$M_w = -0.003768$		

Modal Data	Mode 1	Mode 2	Mode 3
ω (rad/sec)	9.0138	12.2792	18.7314
Z_{η_i} (ft/sec^2)	-15.805	1.2688	4.724
M_{η_i} (rad/sec^2)	-0.002227	-0.001889	-0.01544
$E_{\eta_{1_{w_g}}}$ (1/ft-sec)	0	0	0
$E_{\eta_{i_\delta}}$ (1/rad-sec^2)	-16.381	-548.69	-0.7316
$E_{\eta_{i_q}}$ (1/rad-sec)	3.750	-25.376	-0.05473
$E_{\eta_{1_{\eta_i}}}$ (1/sec^2)	-29.732	1.2584	1.1284
$E_{\eta_{2_{\eta_i}}}$ (1/sec^2)	-10.279	3.3782	-27.690

TABLE I. VEHICLE CHARACTERISTICS (CONCL)

Modal Data (Continued)			
$E_{\eta_{3}\eta_i}$ (1/sec^2)	-0.03545	-0.00160	-0.04398
$\phi_{\eta_i}^{A}$	0.3626	-0.0620	-0.1500
$\phi_{\eta_i}^{'G}$ (1/ft)	-0.01239	-0.003238	-0.01105
$\phi_{\eta_i}^{'P}$ (1/ft)	0.0198	0.0288	0.0363
ζ_{η_i}	0.02	0.02	0.02
Pitch Control System Gains			
$K_q \cdot K(h_p) = -0.6118$ sec $K_e \cdot K(M_0) \cdot K(h_p) = 0.1005$ rad/in.			
$K_{n_Z} \cdot K(h_p) = -0.06118$ rad/g $K_m = 0.01536$ 1/in., $K_{MN} = -0.00087$ in./fps			

$$\dot{\theta} = q$$

$$\dot{u} = -32.2\theta + X_u u + X_w w + X_\delta \delta + X_{w_g} w_g$$

$$\dot{w} = U_o + Z_u u + Z_w w + Z_\delta \delta + \sum_{i=1}^{3} Z_{\eta_i}\eta_i$$

$$\dot{q} = \left(M_q + U_o M_{\dot{w}}\right)q + \left(M_u + M_{\dot{w}}Z_u\right)u + \left(M_w + M_{\dot{w}}Z_w\right)w$$
$$+ \left(M_\delta + M_{\dot{w}}Z_\delta\right)\delta + \sum_{i=1}^{3}\left(M_{\eta_i} + Z_{\eta_i}M_w\right)\eta_i + M_{w_g}w_g$$

$$\ddot{\eta}_i = -\zeta_{\eta_i}\omega_i \dot{\eta}_i - \omega_i^2 \eta_i + E_{\eta_{i\delta}}\delta + E_{\eta_{iq}}q + \sum_{j=1}^{3}E_{\eta_{j\eta_i}}\eta_i + E_{\eta_{iw_g}}w_g$$

$$n_Z^{ACC} = U_o q - \dot{w} - \sum_{i=1}^{3}\phi_i^{A}\ddot{\eta}_i$$

$$q^{GYRO} = q - \sum_{i=1}^{3}\phi_i^{'G}\dot{\eta}_i$$

Figure 2. Vehicle Longitudinal Equations
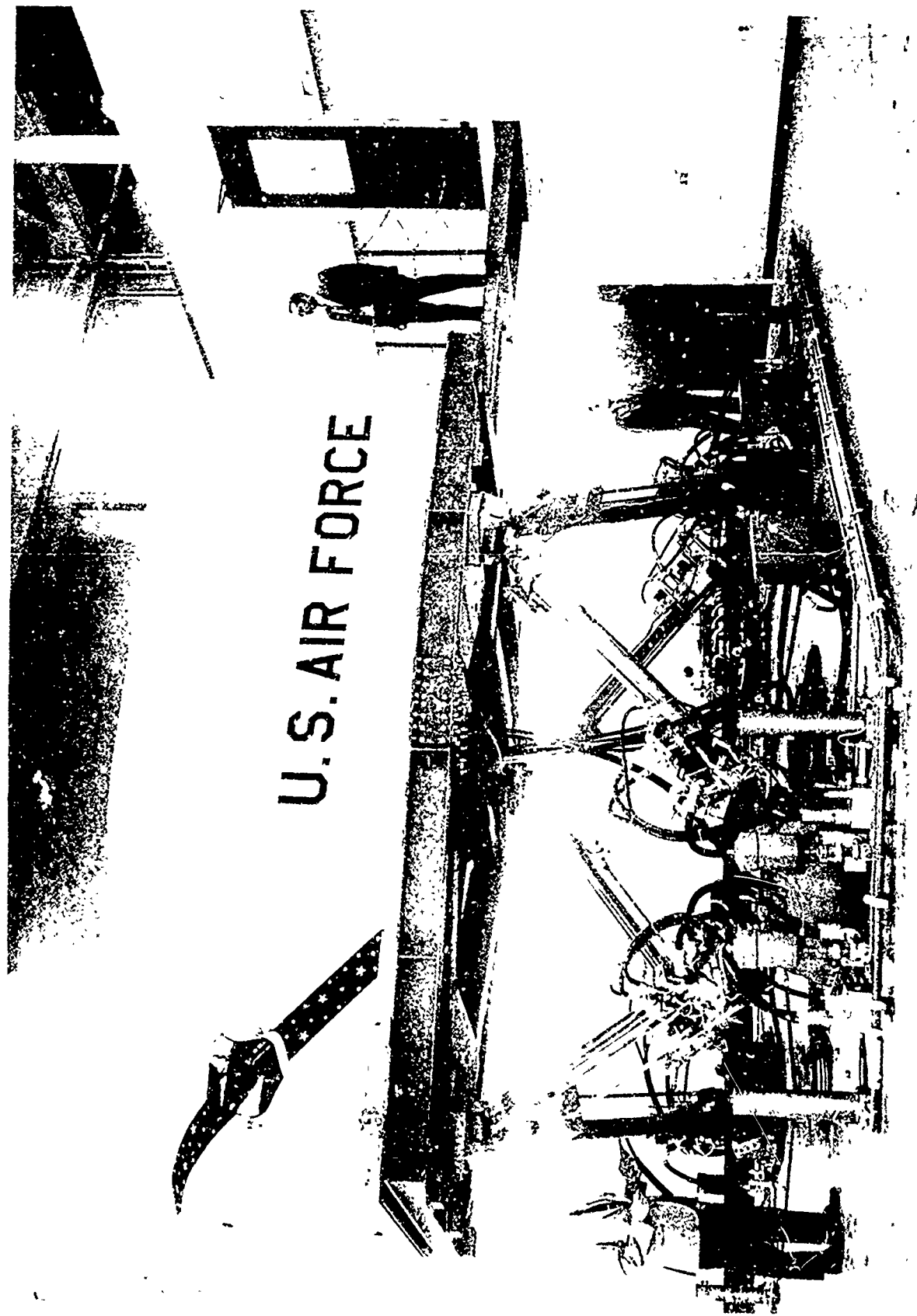
Figure 3. Study Program Motion Simulator
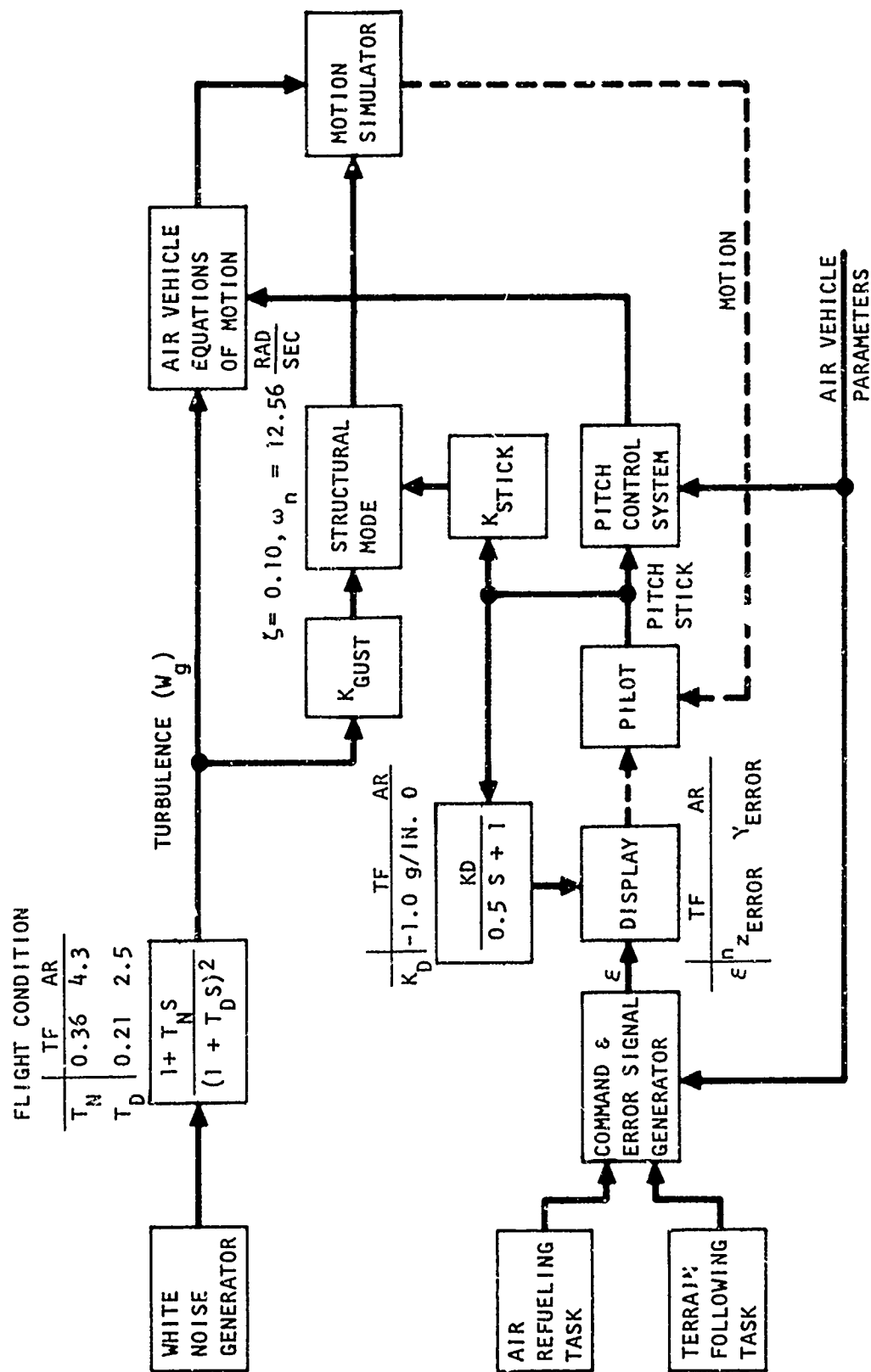
Figure 4. Simulation Setup Block Diagram

16

simple as possible, the following was adopted. A single, 2 Hz structural mode was simulated, capable of being excited by either gust or pitch stick displacements or both. The effect of the mode on pilot acceleration was fed into the motion system. The sensitivity of the mode to the gust and pitch stick was varied in order to assess their effects on the pilot rating of and performance in the task. Since the objective was to assess pilot motion effects as a function of magnitude of structural oscillations, it was assumed that one mode, with excitation sensitivity as a variable, would suffice. A block diagram of this portion of the simulation setup is shown in figure 4.

Two subjects were used in the TF simulation:

• Subject A has 16 years in military and civil aviation as a pilot and engineering/experimental test pilot on a variety of military and civil aircraft and helicopters. He is presently assigned as project pilot for the B-1 program. His past flight experience includes the F-8, SR-71, F-101, F-100, F-84F, T-38, B-57, and the

Rockwell Sabreliner. He is a graduate of the USAF Experimental Test Pilot School at Edwards AFB, Calif.

• Subject B is a member of the technical staff at the B-1 Division of North American Aerospace Group and, as an engineer in the Flight Control Analysis Group, has had over 10 years of experience in evaluation of flying qualities of fighters, bombers, and transports simulated in the Flight Simulation Laboratory. He has a commercial pilot's rating, both single and multiengine, with over 1,000 flight hours experience.

The subjects were asked to evaluate the TF task as presented to them and not the motion environment in which they found themselves. Hence, their Cooper-Harper ratings should vary due to motion effects only if their performance is impaired.

Those simulation parameters important to the paper pilot program and to the task performance measurements were recorded on FM tape for later data analysis. Unfortunately, one sensor (the accelerometer measuring actual pilot g on the motion simulator) operated intermittently at best, and no confident record of that parameter was obtained.

The AR task was conducted at 0.7 mach at a medium altitude. Unlike the low-altitude, high-speed condition, the wings are swept forward and, hence, the vehicle is more sensitive to turbulence. To provide a repeatable tracking task for the evaluating pilots, a simulation run was recorded during which altitude changes were made approximating the workload involved during air refueling. The resulting flight path angle (γ) time history was then used as a tracking command for the simulator data runs (the γ command characteristics are given later). Initial attempts at running the simulation using the ADI horizontal flight director needle as the flight path error indicator proved unsuccessful because of the conflict in cues displayed by the pitch attitude ball directly behind the needle. To separate the task display from the ADI, a cathode-ray tube (CRT) display was used with only the flight path error and cross bar reference mark being shown (scaled for 1 inch per 10 degrees of flight path error). Since the simulation included six degrees of freedom, the pilot had to hold speed and wings level, but pilot comments indicated this was not a factor in their performance. A picture of the CRT display is given in figure 5 (the runway is a TV picture being provided as a background for demonstration purposes). Both the tracking task and the turbulence time histories were recorded and repeated for the different runs to hold these parameters constant. The turbulence inputs and structural mode representations were similar to those used in the TF task. The one difference is that the AR data include turbulence effects alone on the rigid aircraft, in addition to the structural mode excitation effects.

Two subjects were used in the AR simulation:

● Subject B is the same one who participated in the TF simulation.

● Subject C is a former engineering test pilot with 27 years of flight experience. With a total of 10,000 flight hours (5,000 test hours), he has flown a wide spectrum of large aircraft including the B-29, B 50, B-47, B-52, KC-135, and Boeing 707. He has considerable B-52 AR flight experience. As was done in the TF simulation, both subjects were asked to rate the vehicle during the AR task.

In both tasks, the basic problem presented the pilot is one of γ tracking. The pitch stick to γ transfer functions (SAS on) for the two flight conditions are given in table II for the rigid body aerodynamics. The inclusion of the three structural modes would add three poorly damped second orders to the transfer functions with the associated frequencies close to those shown in table I. As will be seen later in the discussion on the paper pilot results, the addition of the structural modes does not significantly affect pilot motion relative to the task.

18
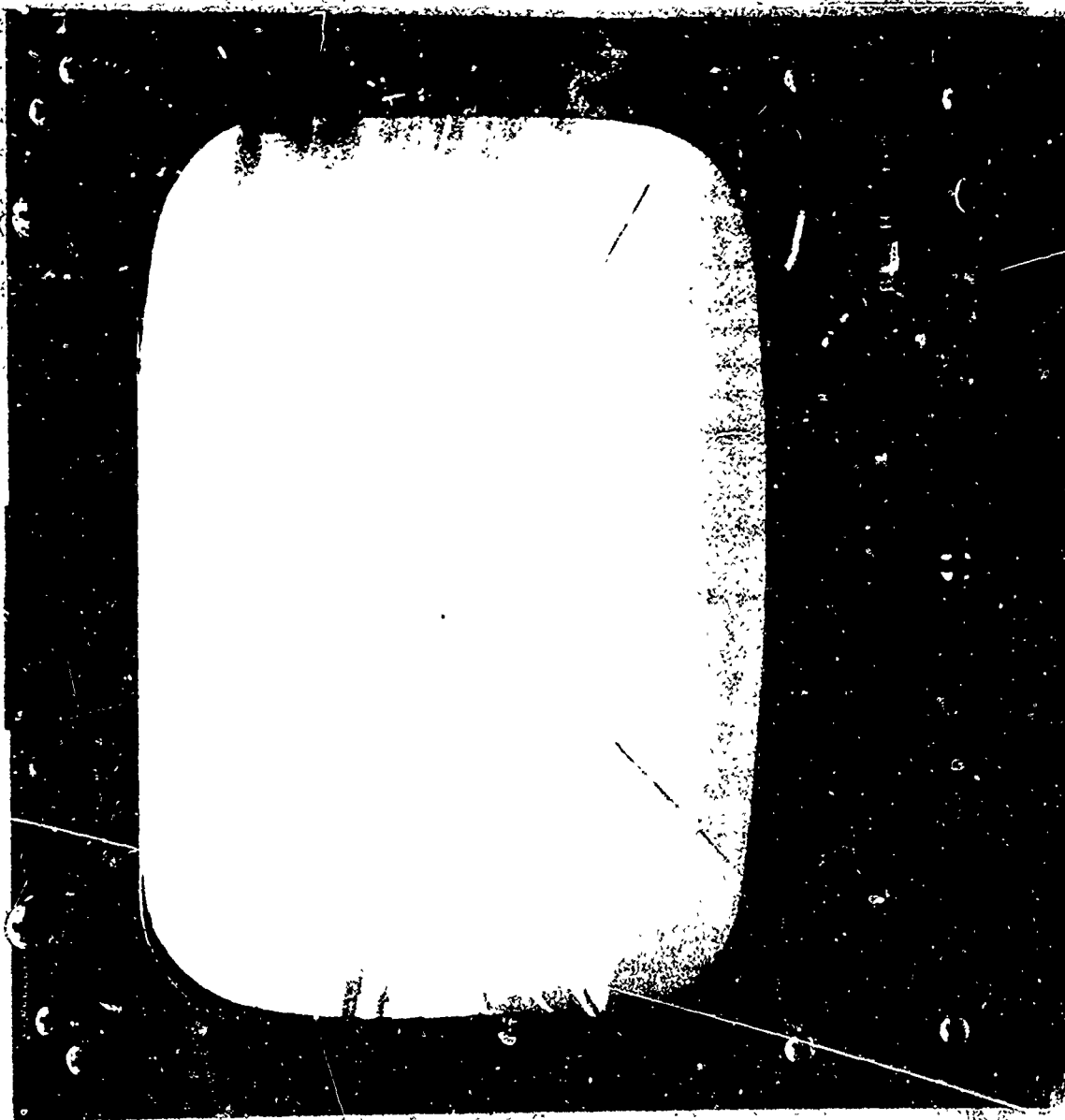
Figure 5. Study Program CRT Display

19

TABLE II. γ/Xp TRANSFER FUNCTIONS FOR THE TWO TASK FLIGHT CONDITIONS

Terrain-Following (TF) Task

$$\frac{\gamma^*}{Xp} = \frac{0.0384 (S + 0.0152)(S + 7.343)(S - 6.463)(S + 30.0)(S + 13.8)(S + 80.0)}{(S + 2.58)(S + 98.0)(S + 0.0087 \pm 0.0275j)(S + 1.97 \pm 3.165j)(S + 14.64 \pm 16.37j)} \quad \text{rad/in.}$$

$$\frac{\gamma^{**}}{Xp} = \frac{0.0384 (S + 0.0152)(S + 1.127)(S - 6.463)(S + 7.343)}{(S + 1.093)(S + 20.0)(S + 0.011 \pm 0.083j)(S + 0.928 \pm 1.129j)} \quad \text{rad/in.}$$

Air-Refueling (AR) Task

$$\frac{\gamma^*}{Xp} = \frac{0.0218 (S + 0.00114)(S + 15.09)(S + 18.14)(S - 17.53)(S + 30.0)(S + 80.0)}{(S + 1.95)(S + 99.7)(S + 0.0017 \pm 0.0218j)(S + 3.95 \pm 2.54j)(S + 11.83 \pm 30.28j)} \quad \text{rad/in.}$$

$$\frac{\gamma^{**}}{Xp} = \frac{0.0218 (S + 0.00141)(S - 17.53)(S + 18.14)}{(S + 20.0)(S + 0.0912 \pm 0.0876j)(S + 0.610 \pm 1.60j)} \quad \text{rad/in.}$$

* SAS ON
** SAS OFF
RIGID BODY

20

PILOT MODEL IDENTIFICATION METHOD

The simulation data generated had to be analyzed to provide task performance measures and pilot models suitable for the respective tasks. The primary tool used to accomplish this is a data processing and frequency analysis program already developed and in use at the North American Aerospace Group. This program calculates the autocorrelation and crosscorrelation functions for one pair of time measurement records and estimates spectral density functions from these calculations. Coherence estimates (similar to the linear correlation function described in reference 7) are also calculated and can be used to identify pilot remnant effects. The program also provides the gain and phase relationships between the two input records based on the appropriate spectral density, cospectral density, and quadrature spectral density functions. Finally, the program may be used to obtain a complex curve fit based on an iterative least squares approximation to the spectral data. The mathematical expression for this curve represents the system (pilot model) linear transfer function. The two time histories may also be shifted in time relative to each other to remove the nonlinear phase effects of a constant time delay. A more detailed description of this analysis program is given in appendix I.

For use in the aforementioned computer program, the simulation time histories recorded on FM tape were digitized at 50 samples/second with a resolution of about 0.05 percent. To prevent frequency folding effects, the FM data were filtered through a 0.0072-second filter because of noise presence (primarily 400 Hz).

21

SECTION V

TERRAIN-FOLLOWING DATA EVALUATION

SIMULATION DATA ANALYSIS

The terrain-following (TF) simulation data were analyzed through the data processing and frequency analysis program to identify those test characteristics important to the paper pilot program. A typical set of data produced by the analysis program is given here as an example.

A strip chart trace of a typical terrain and vehicle flight path time history is shown in figure 6. The difference between the command flight path and the actual flight path, augmented by a signal which is a function of stick displacement, was converted to an acceleration error and presented to the pilot on the ADI as described earlier. Typical time histories of the display signal and the pilot's pitch stick for that TF segment are shown in figure 7. In addition, the commanded flight path angle time history is also shown in figure 8. The results of the data analysis for this run are shown in figures 9, 10, 11, and 12. Figure 9 shows the autocorrelation functions for the input-output signals (the horizontal bar and pitch stick, respectively). Of particular interest in these plots are the autocorrelation values at zero lag number since they are the variances (σ^2) for the two signals (0.103 inch^2 and 0.017 g^2). Figure 10 depicts the spectral density functions for the two signals, while figure 11 shows the cospectra, quadrature spectra, and coherence functions. (Refer to appendix I for a description of these functions.) Finally, figure 12 presents the bode plots for the input-output signals. This frequency response, computed from the spectral data for this run, represents the linear pilot model. The two data points on the phase plot, seemingly separate from the others, actually should be plotted at -189.4 and -187.1 degrees but, because the plotting routine restricts the data points to between ±180 degrees, such points are folded over. The smooth lines on the amplitude and phase plots represent the results of an automatic routine for a curve fit to those data points which exhibit a coherence value greater than 0.5. The match is good except for the dc level of the gain. Th ·omputer-provided transfer function is

$$3.87 \ \frac{(-0.297S + 1)}{1.18S + 1}$$

while a better dc gain fit would be 3.4 rather than 3.87.

FLIGHT PATH PROFILE

TERRAIN PROFILE

10
SEC

500 FT

400

200

0

+.1 RAD

0

-.1

TERRAIN &
FLIGHT PATH
PROFILES

TERRAIN
CLEARANCE

VEHICLE
FLIGHT PATH
ANGLE
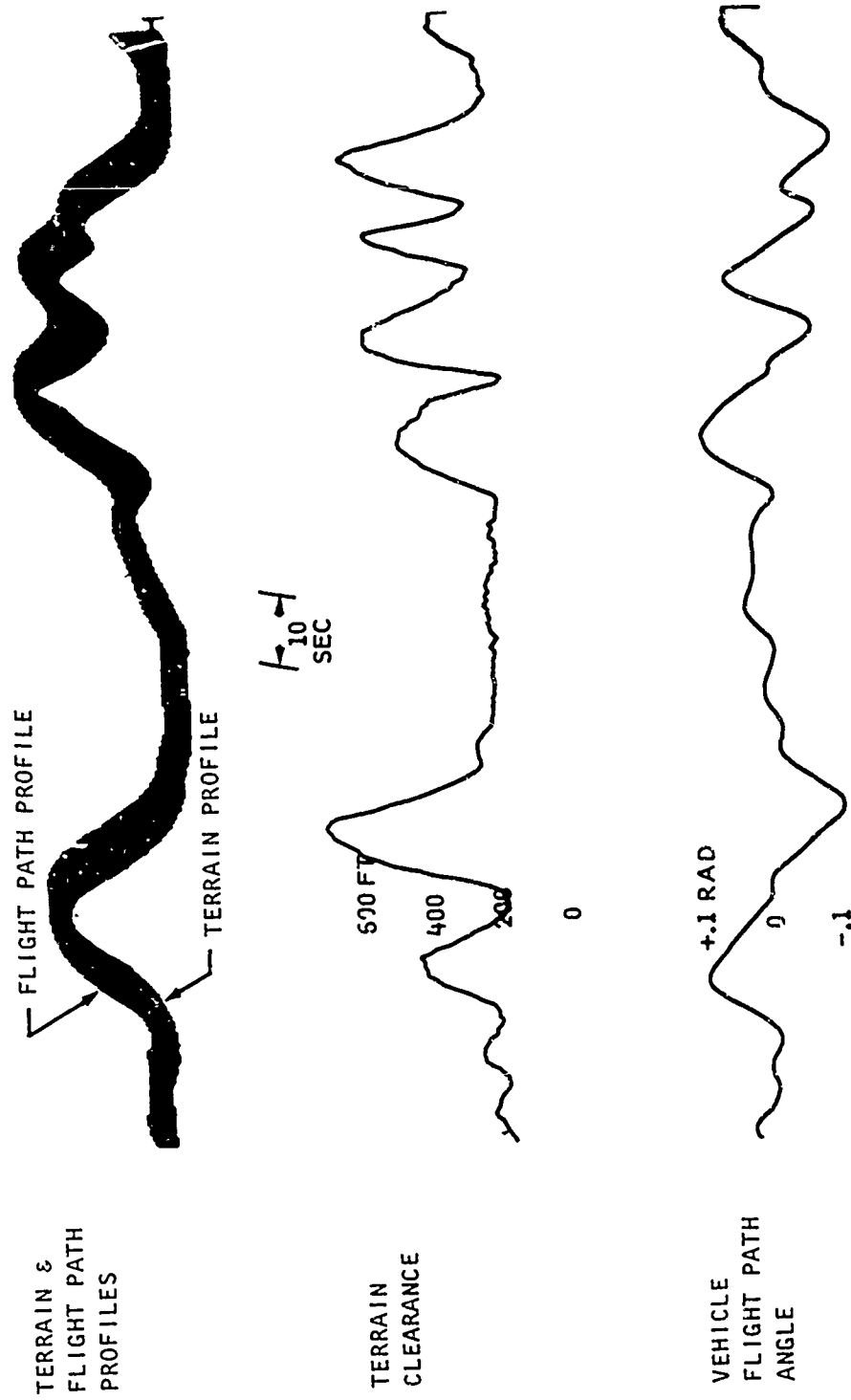
Figure 6. Typical Terrain and Flight Time Histories (No. 0418)

24
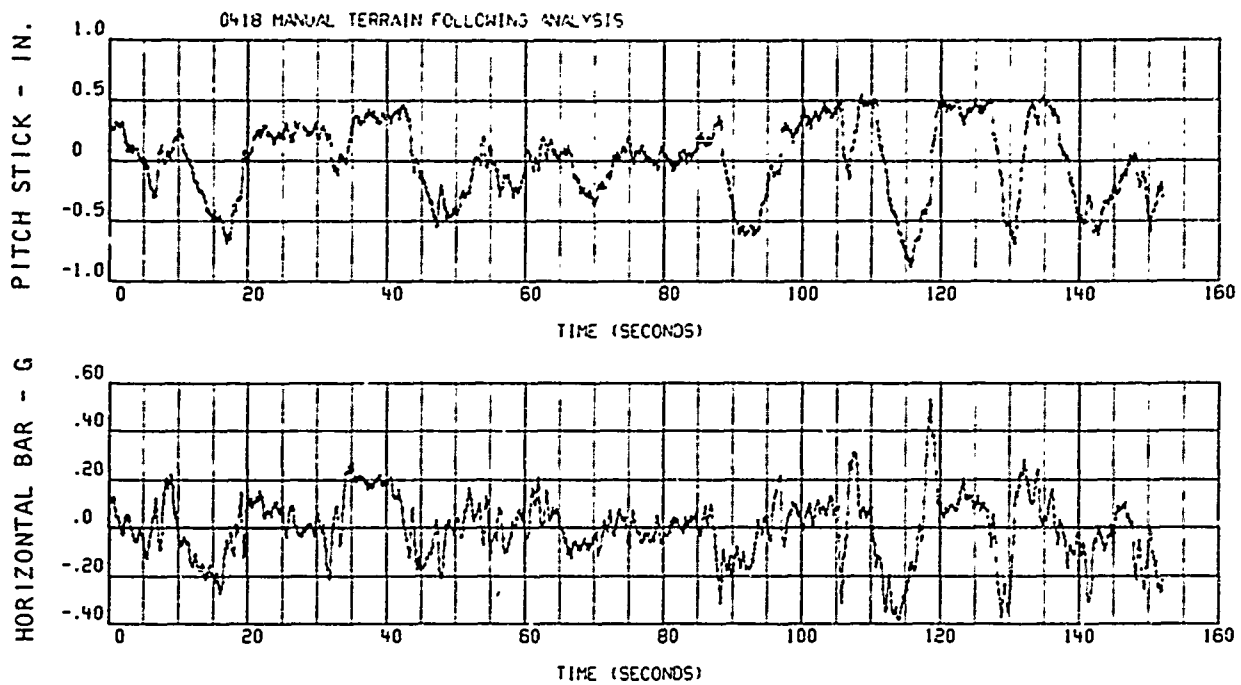
Figure 7. Time Histories of Pitch Stick and Horizontal Bar (No. 0418)
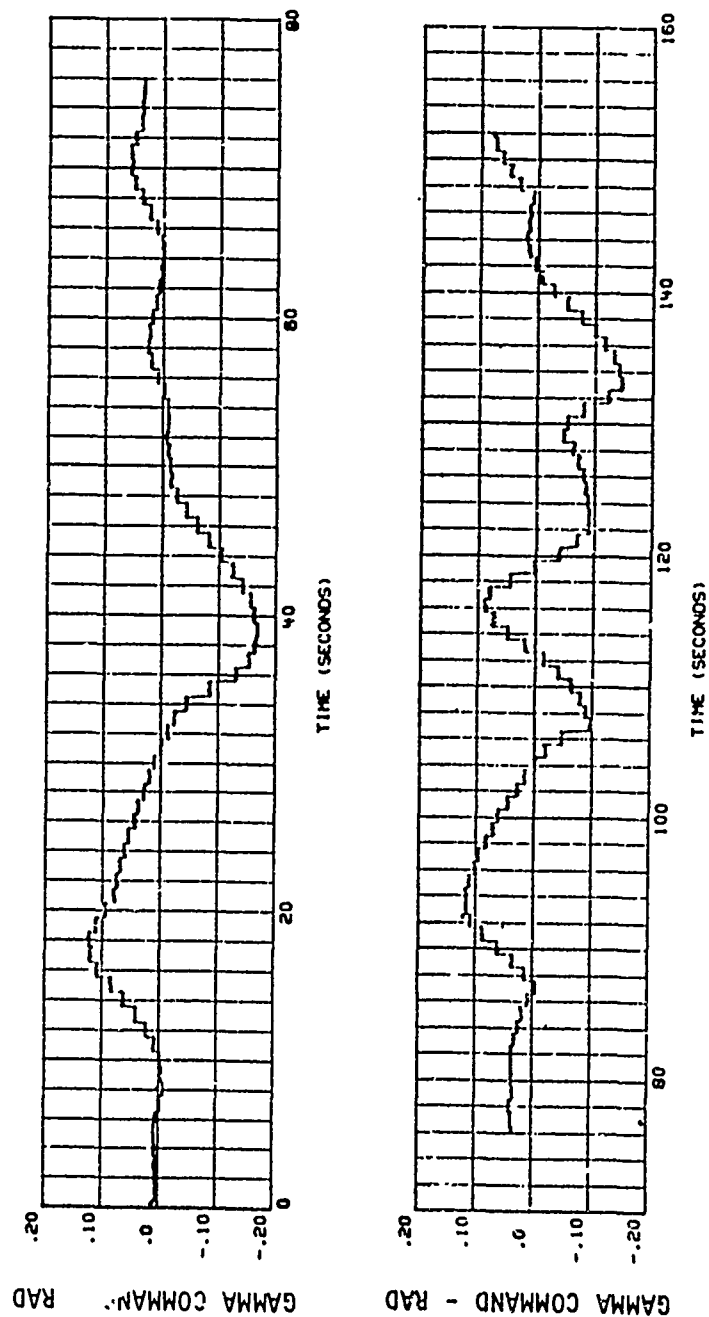
Figure 8. Gamma Command (γ_c) Time History (No. 0418)

SPECTRAL DENSITY FUNCTIONS
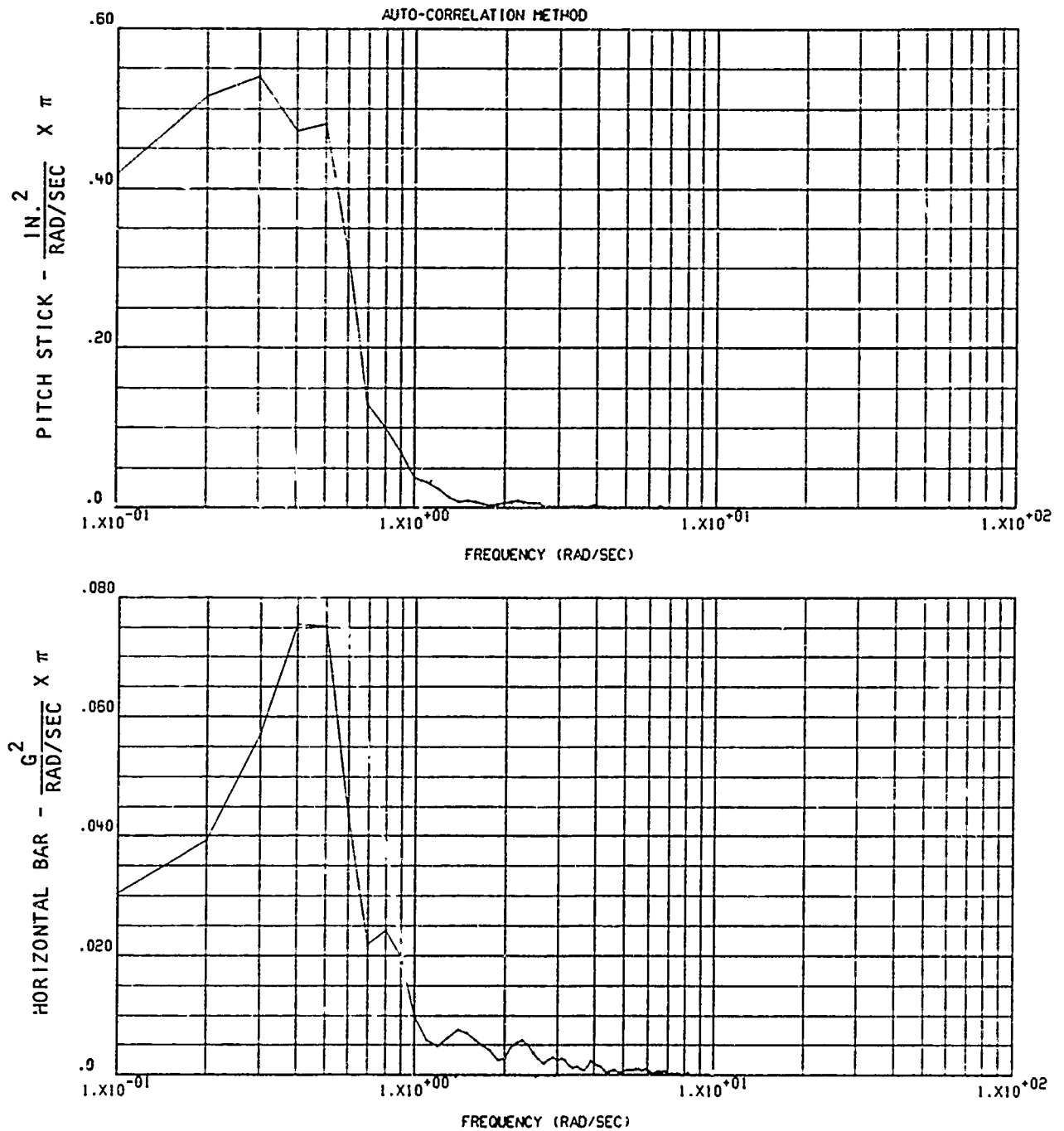
Figure 10. Spectral Density Functions of Pitch Stick and Horizontal Bar (No. 0418)
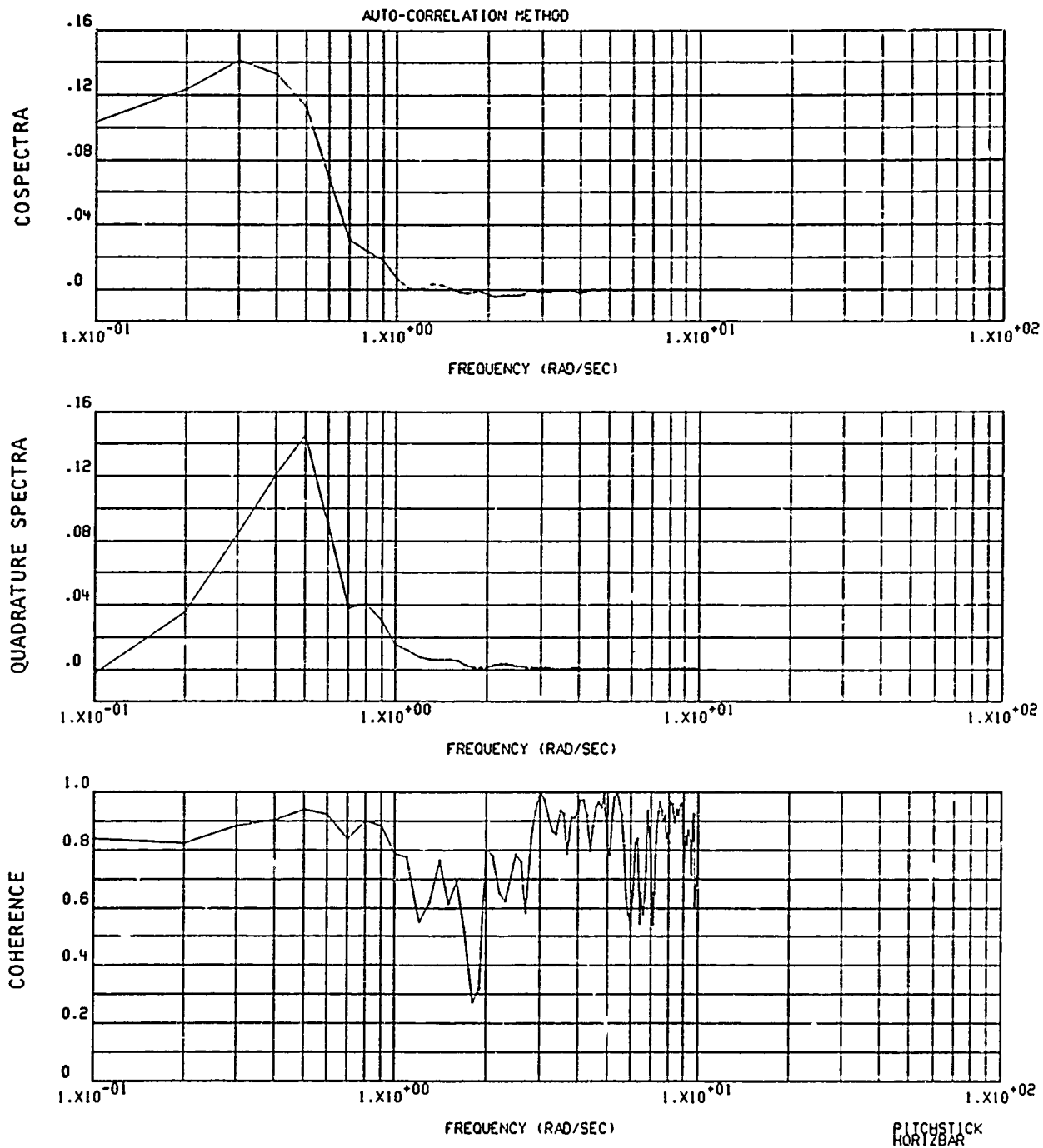
Figure 11. Cospectra, Quadrature Spectra, and Coherence Functions
of Pitch Stick and Horizontal Bar (No. 0418)
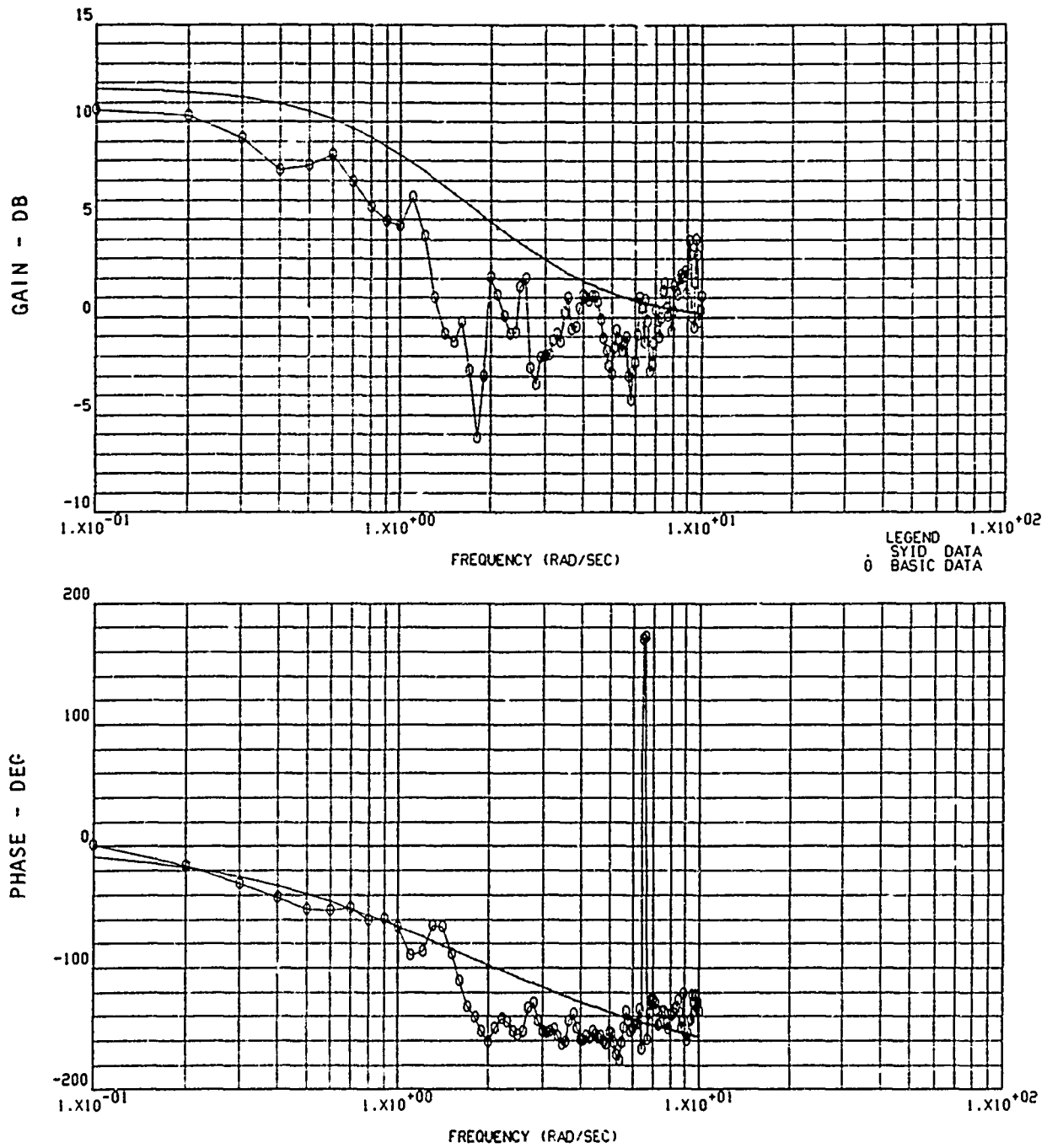
Figure 17   Pilot Bode Plot (No. 0418)

The negative lead indicated in the computed pilot model is a common characteristic of all the TF runs analyzed. Although at first glance it seems to be at odds with most literature on pilot models, this model is not unreasonable when it is realized that this is a linear model being fitted to data which probably exhibit a time delay; i.e., a linear model including a first-order Pade' approximation for the time delay would also have a negative lead term. As will be seen in section VII, the computed paper pilot model (first-order lag with first-order Pade' approximation for a time delay) compared well with the measured pilot model of the form previously shown. Since the time series analysis program could time-shift the output relative to the input, some early attempts were made to account for pilot time delays before the spectral analyses occurred. However, since the process is an iterative one (to find the proper time delay) and, since the program did well in model computation without time shifting, further attempts were ceased.

Although the spectral analysis program does not specifically compute the remnant effects of the pilot, it does compute the coherence function (R) which is an indication of the linear relationship between input and output. As mentioned earlier, this is the same as the linear correlation function described in reference 7. Since, as shown in appendix I, the coherence function (R) is given as

$$R^2(\omega) = 1 - \frac{S_{nn}(j\omega)}{S_{xx}(j\omega)}$$

where $S_{xx}(j\omega)$ is the spectral density function of the pilot's total output, then $S_{nn}(j\omega)$, the spectral density function of the remnant (noise), can be computed. If the remnant is small, then it can be ignored and the linear model justified. If the remnant is large, then quite possibly nonlinear or uncorrelated effects are occurring and the linear model is restricted in applicability. In general, all of the TF runs showed good correlation as evidenced by the coherence function plots shown in figure 11 and in appendix II. Figure 13 shows the PSD of the computed remnant for the pilot transfer function previously shown. The ratio of the remnant standard deviation to that of the pilot's total output $(\sigma_{S_{nn}}/\sigma_{S_{xx}})$ is 0.48. It should be further noted that the time series analysis program curve fit only uses frequency data points which exhibit a specified level of coherence. For the TF runs, a value of 0.5 was used.

The spectral density and autocorrelation functions for the corresponding γ_c for this particular run are shown in figure 14.

31
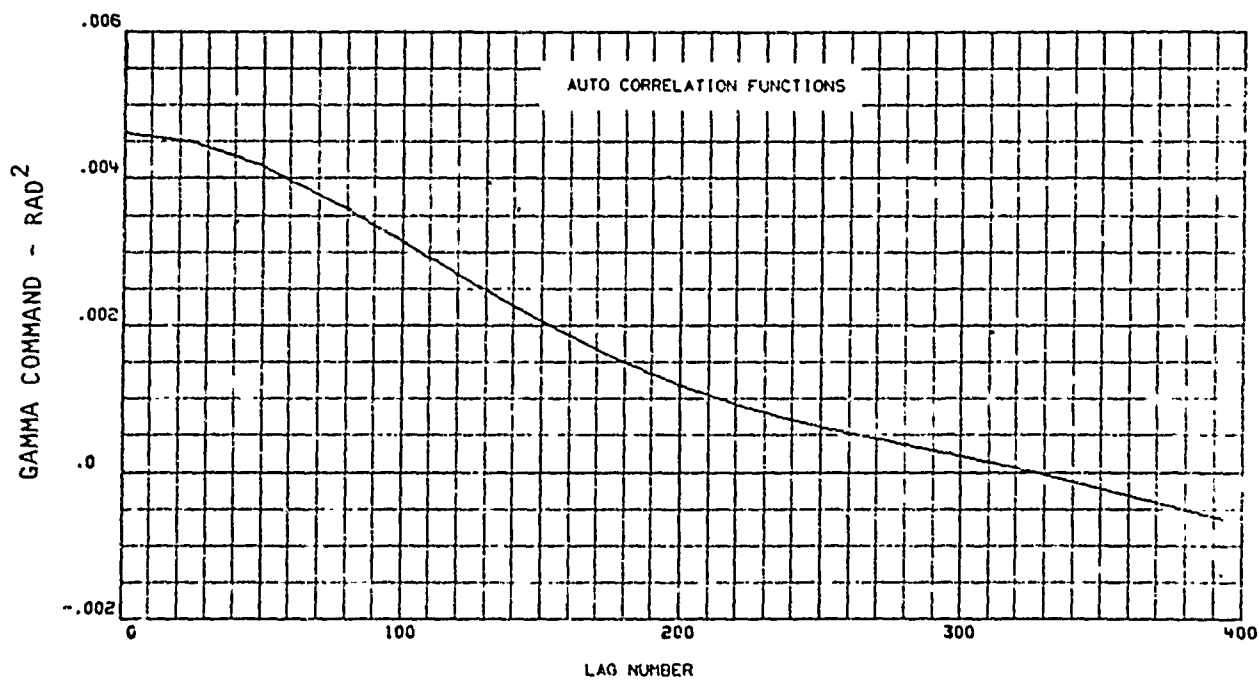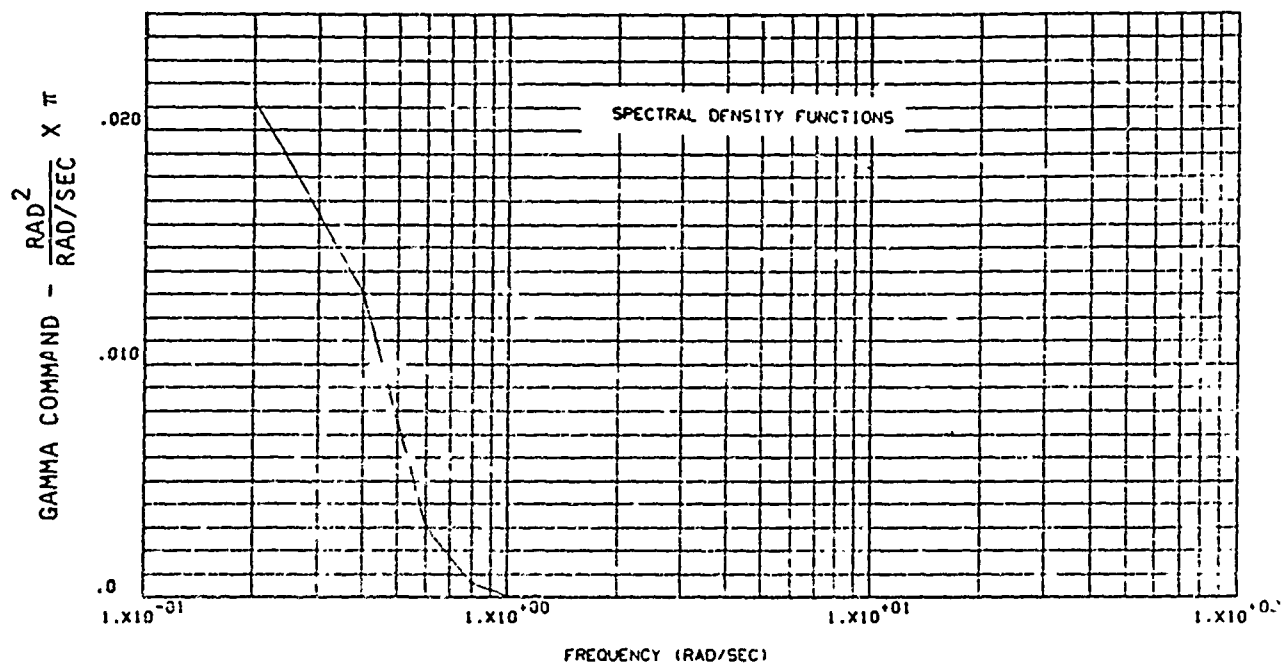
Figure 14. Spectral Density Function for γ_c (No. 0418)
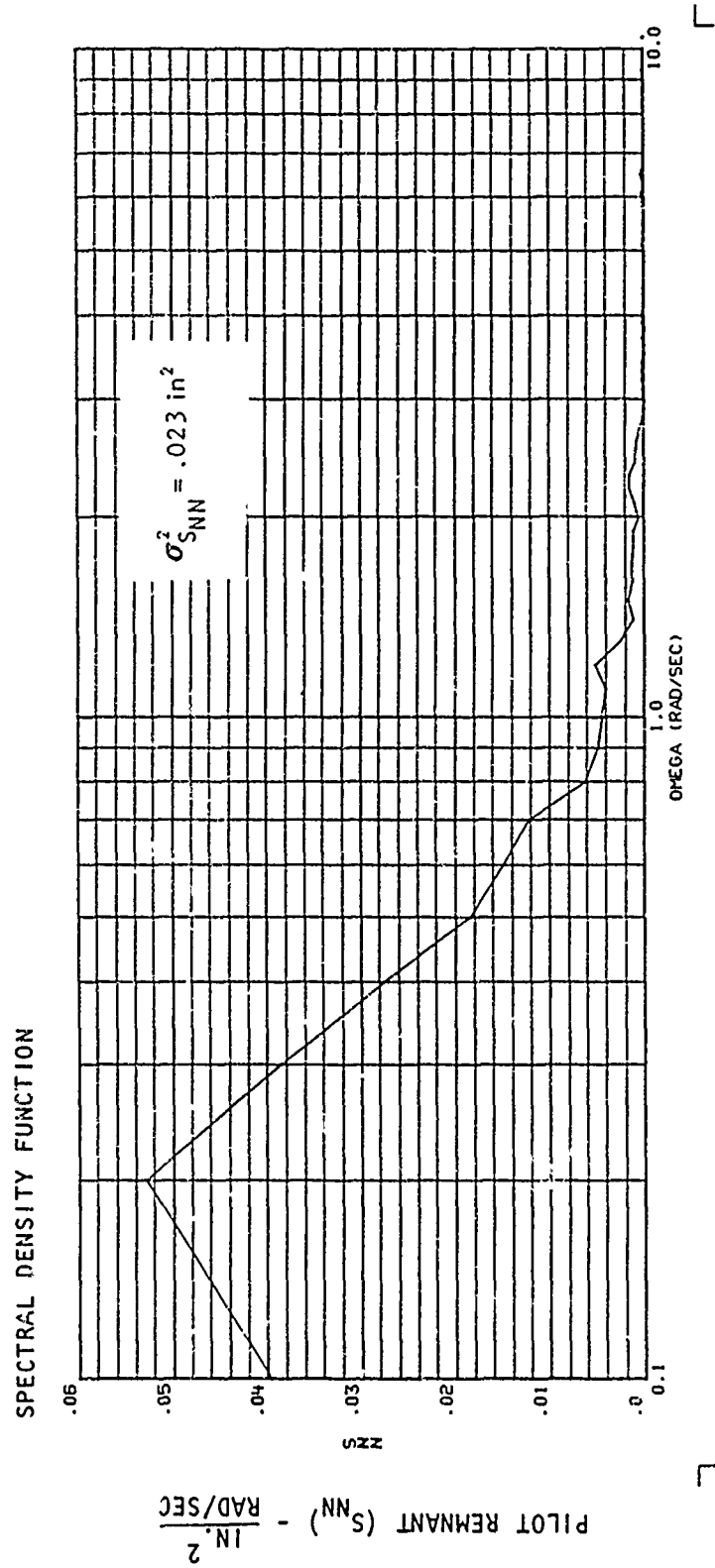
Figure 13. Spectral Density Function of Pilot Remnant (No. 0418)

33

The flight path command time history naturally depends upon how well the pilot follows the terrain. However, it can be expected that the actual variation in the statistical description of this signal will be small if the pilot's capabilities are not widely disparate and if the pilot's performance is not significantly different between runs. Figure 15 shows the change in spectral density function for one pilot as the stick effect on structural mode excitation progresses from nill to very heavy (curves 1 to 3). The corresponding autocorrelation functions are also shown in figure 15 with the resulting standard deviations (σ) of 0.065 rad, 0.077 rad, and 0.078 rad, respectively. Figure 16 shows the γ_c time histories for these runs. These variations are typical of the extremes encountered and, for application in the paper pilot program, the σ of the γ_c used was obtained by averaging over a number of runs with the average being 0.069 rad.

An interesting application of the pilot mod. 1 generated in this program provided tentative validation of the model characteristics. Computer runs were made with a TF system using the pilot model to close the g control loop. The run was made for an encounter with an isolated peak. Comparative computer runs were made using an automatic TF system. Figure 59 in appendix II shows the two runs and illustrates how well the pilot model performed.

SIMULATION RESULTS

The TF simulation data were examined to determine the effects of turbulence and structural mode excitation on pilot ratings and performance parameters. Additionally, data evaluation was made to identify any correlation existing between pilot ratings and performance parameters. These results are presented herein.

Pilot rating influence due to the variables of gust and stick excitation of pilot motion differed between pilots A and B, as shown in figure 17. Pilot A maintained constant rating of 2 across the board of parameter variations. Even for the case of maximum effects of gust and stick simultaneously, his comment was "motion doesn't seem to affect any stick motion or control." Pilot A's rating of 2 for the task continued even when a subjective rating of E for vibration intensity was given (on a scale of A to F for increasing intensity.) Pilot B showed a rating degradation for high stick effects on pilot motion, but not for gust excitations even though his subjective rating for vibration intensity was higher (D versus B) for the worst gust case compared to the worst stick case. The effect of large stick excitation on performance parameters is not pronounced as will be seen later. The explanation seems to tie in with the fact that the stick input into the structural mode was not rate limited in the simulation; hence, stick-effect gains large enough to provide noticeable pilot motion for small, tracking-type stick displacements could cause a relatively severe jolt if the stick were pulsed or moved
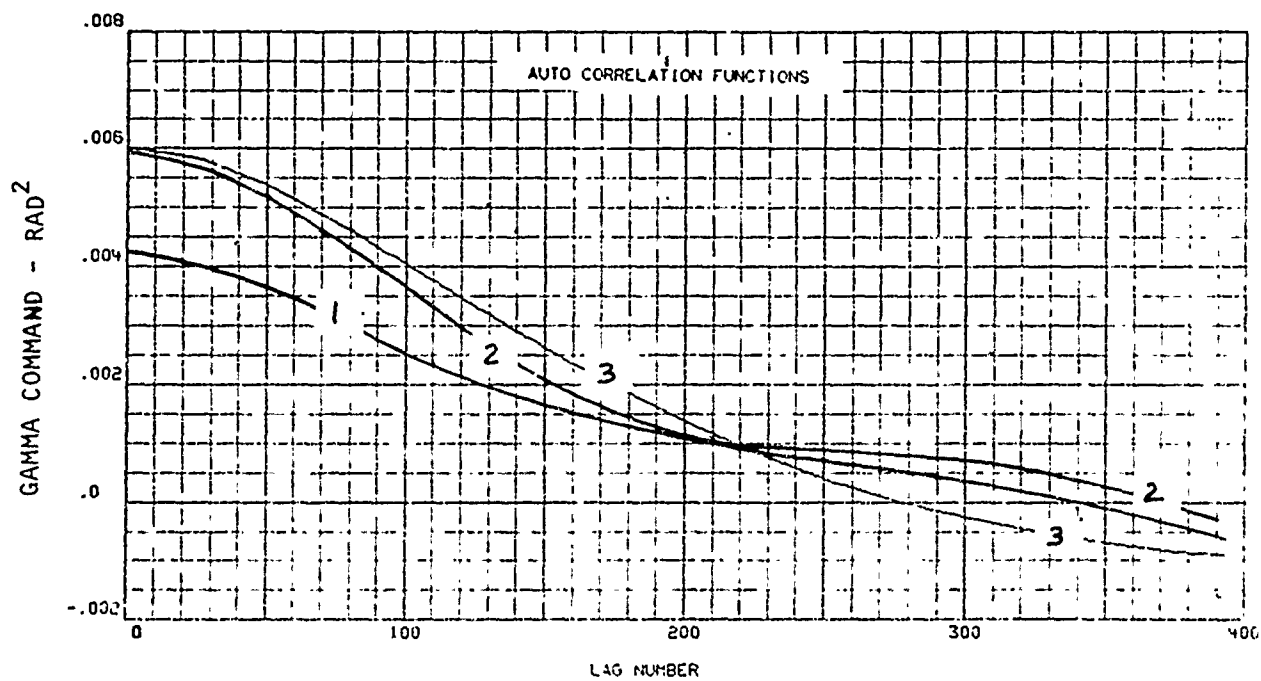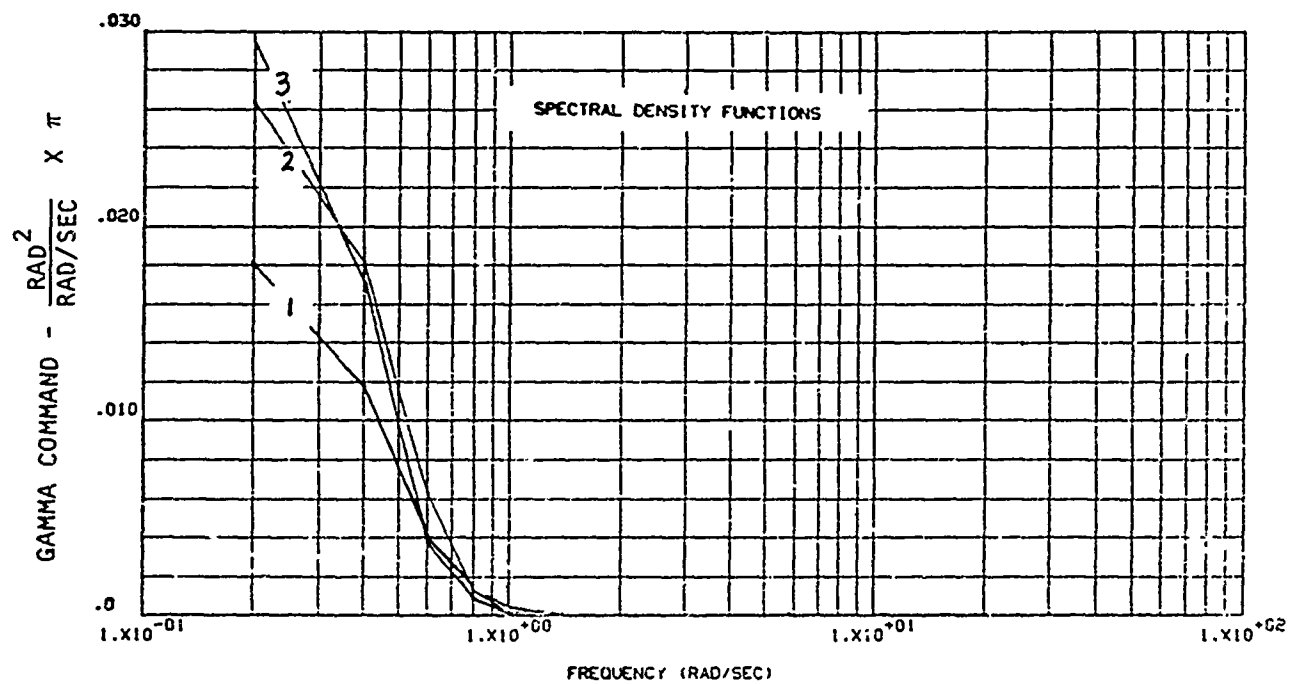
Figure 15. Effects of Turbulence on γ_c Spectral Density and Autocorrelation

Figure 16. γ_c Time Histories

36
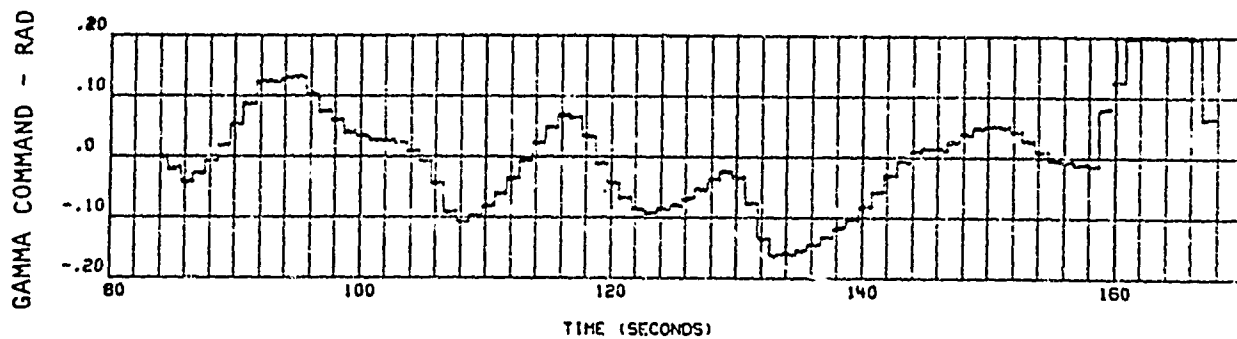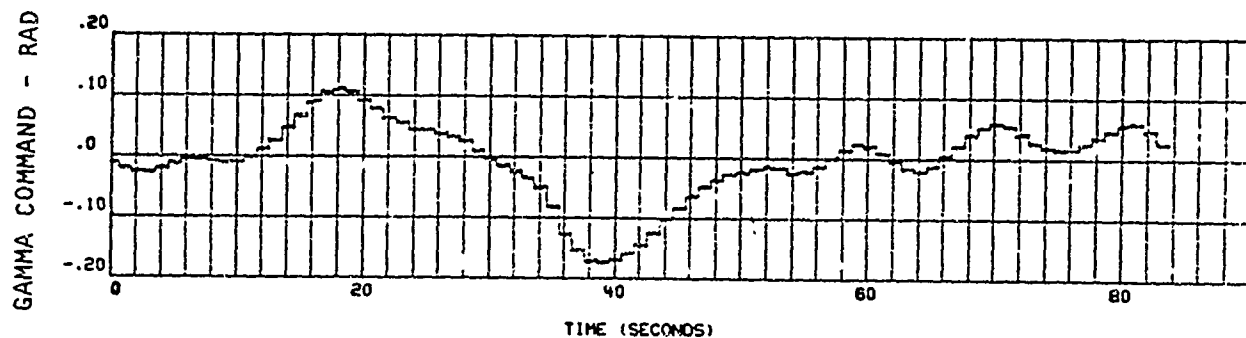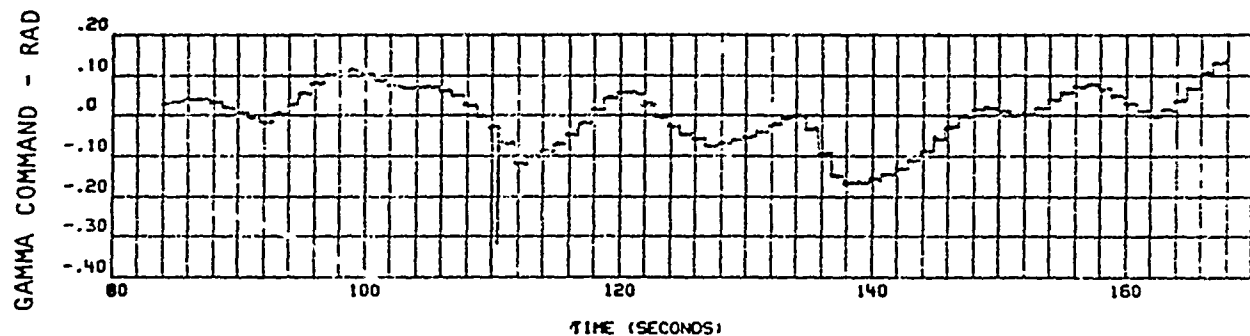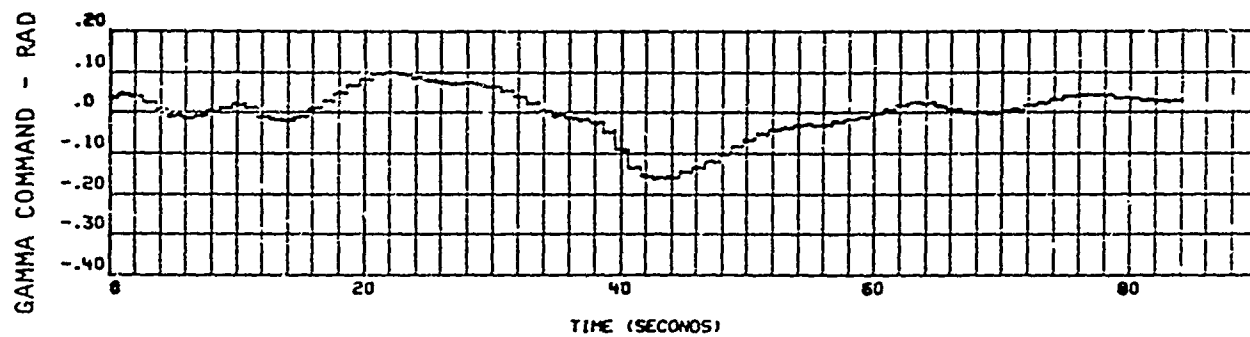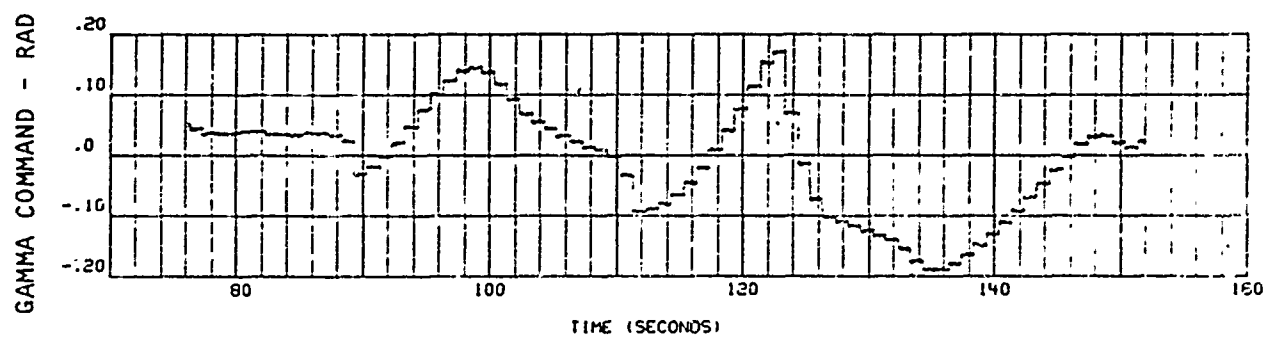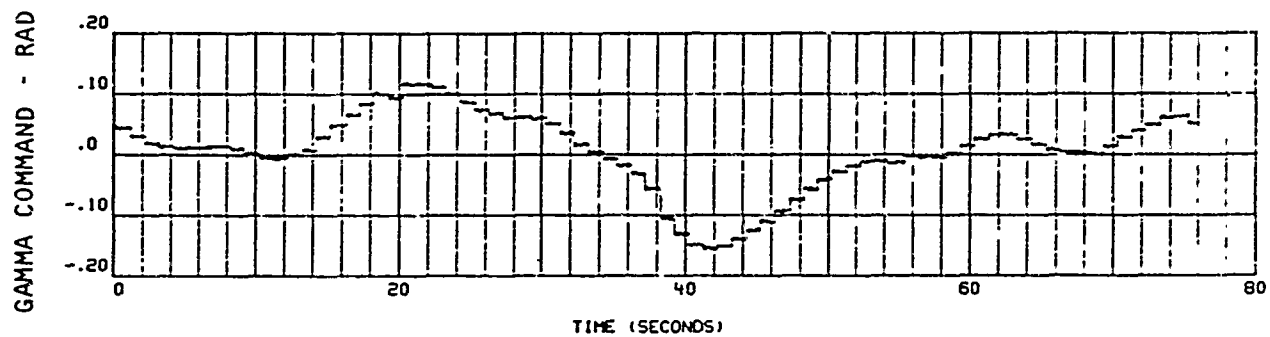
Figure 16. γ_c Time Histories (Concl)

37
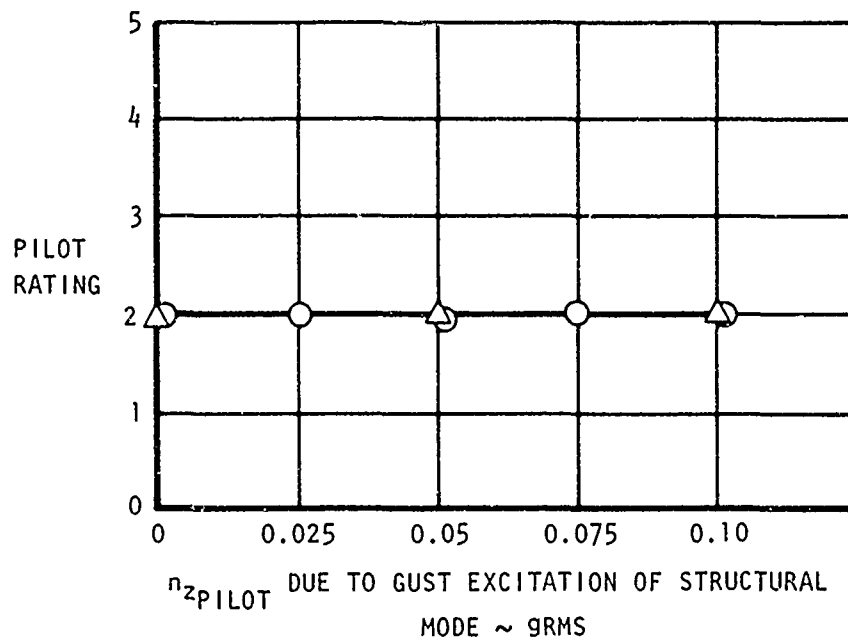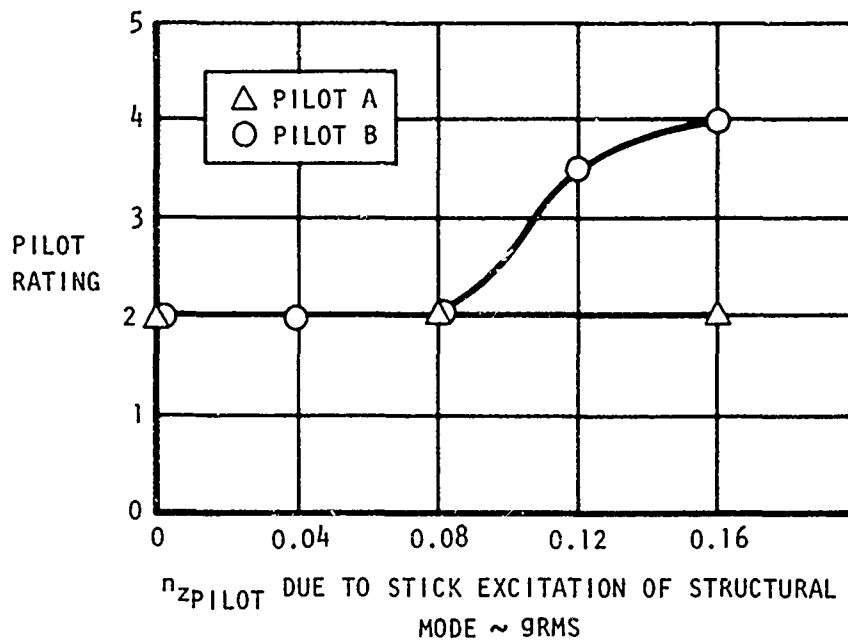
Figure 17. Terrain-Following Pilot Rating Versus N_{zPILOT}

stepwise. This presumed mental inhibition seems to have caused the pilot rating to deteriorate even though his performance did not. (See figure 19.)

Pilot rating is also plotted versus four pilot performance parameters as shown in figures 18 and 19. In the latter plot, the ratings as a function of the standard deviation (σ) of horizontal bar (needle) and pitch stick are depicted. No obvious relationships exist (note pilot B shows ratings of 2, 3.5, and 4 for essentially the same value of error signal, σ_{HB}). In figure 18, the ratings are plotted versus measured pilot model lag and lead time constants. (It should be noted that pilot model computations were not made for all pilot B test cases, but only those to show the range of gust and stick effects.) It would be expected that the pilot rating would increase with decreasing τ_{LAG} and increasing τ_{LEAD}, but only in the case for pilot B is this seen, even to a slight extent, with decreasing τ_{LAG}; i.e., rating increases above 2 only when τ_{LAG} goes below 0.90 second.

Performance parameters descriptive of the pilot model and task activity are shown in figures 20 through 24. The first figure shows how the standard deviation of pitch stick activity varies with gust and stick effects on structural motion. Pilot A shows a slight decrease in stick σ_{PS} with an increase in stick effect on motion. Since, in this simulation, the increase in stick effect does not result in an increase in vehicle moment control but only in pilot motion through the structural mode excitation, it might be expected that the stick activity should remain relatively constant since the tracking task doesn't really change. (The pilot motion was never large enough to cause consistent involuntary stick motion.) Pilot B shows a more constant activity with only a slight increase for both the stick and gust effects. However, pilot A does show a definite trend in σ_{PS} with gust effects. This tendency to decrease stick activity as high-frequency motion effects increase is not unexpected. The pilot will tend to decrease the frequency of his inputs and follow the lower frequency tracking errors. This is seen in figure 25 which shows the spectral density functions for the three conditions being discussed. The curves labeled 1 to 3 (for increasing gust excitation) shows the frequency corresponding to peak power drops off from 0.5 to 0.3 and finally below 0.1 rad per second.

In figure 21, the standard deviation in the horizontal bar (needle) movements is presented versus the pilot acceleration resulting from gust and stick excitation of the structural modes. Between the two pilots, the most obvious difference is in level of the signal, particularly at the zero level for structural motion. Since stick displacement feeds into the display, it could be expected higher stick activity would result in higher display activity. However, figure 20 does not support that contention since both pilots show about the same σ_{PS}. Examination of the stick and horizontal bar PSDs for both pilots reveals a significant difference, however. Pilot A shows the same peak frequency in both stick and horizontal bar (figure 49) PSD's, while pilot B
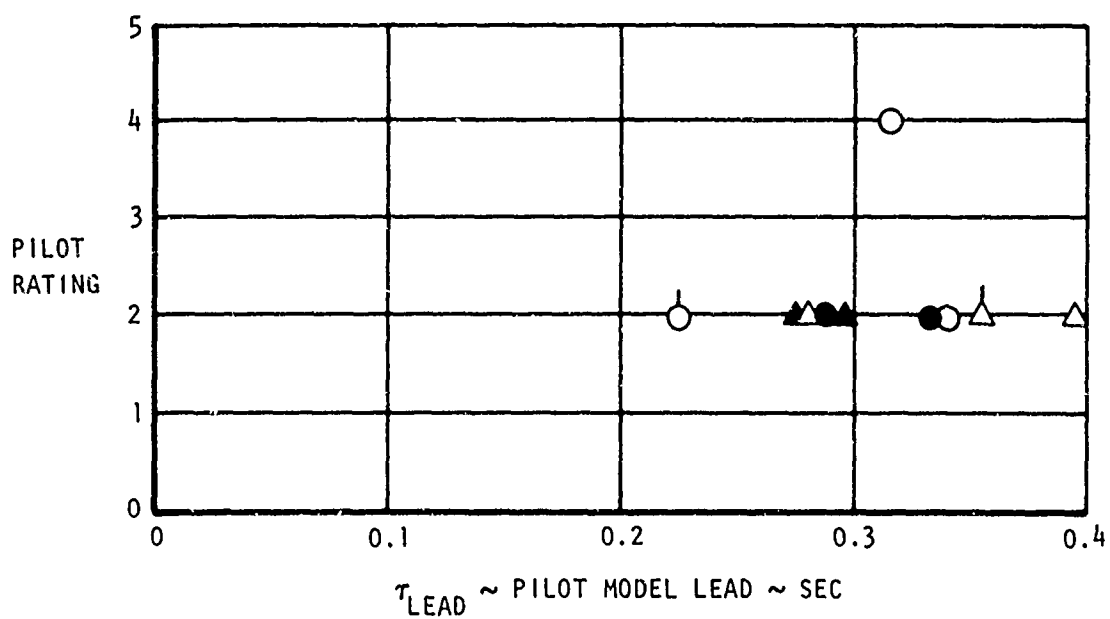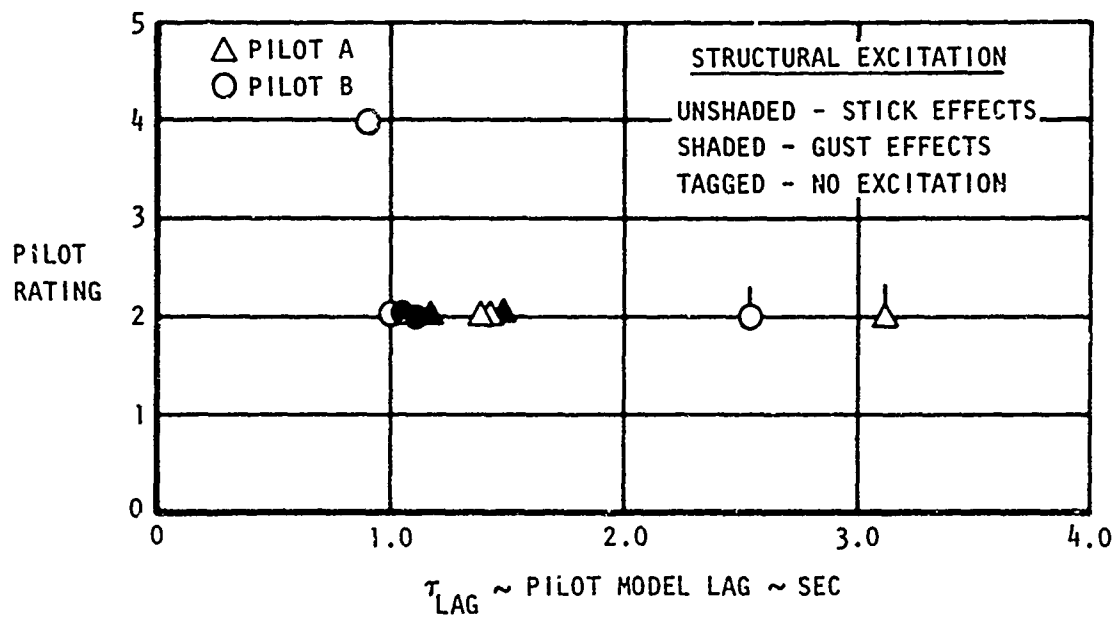
Figure 18. Terrain-Following Pilot Rating Versus τ_{LAG} and τ_{LEAD}
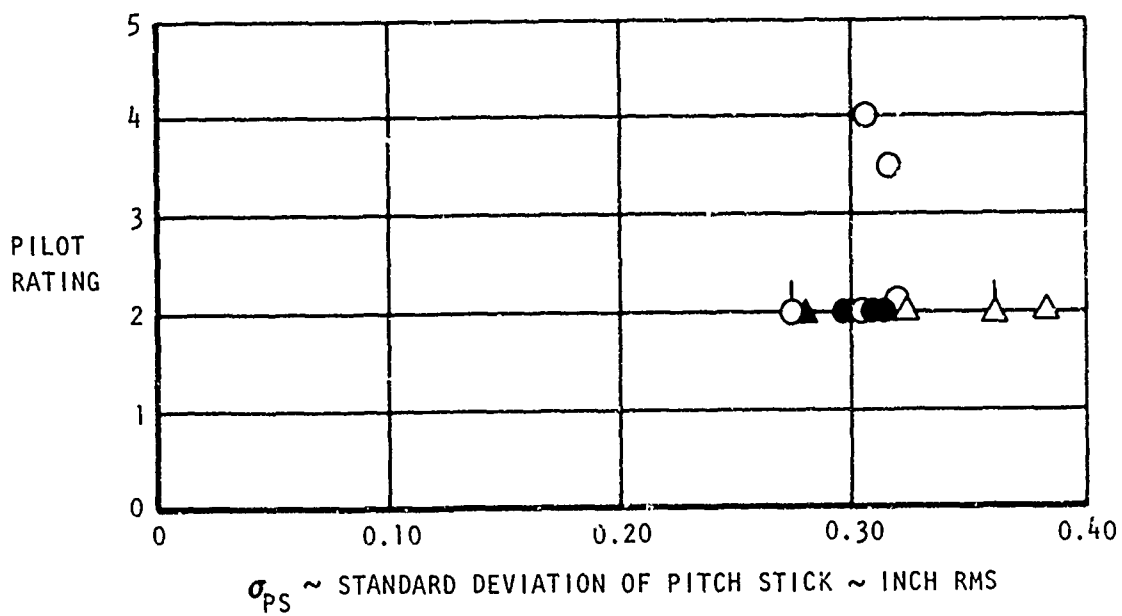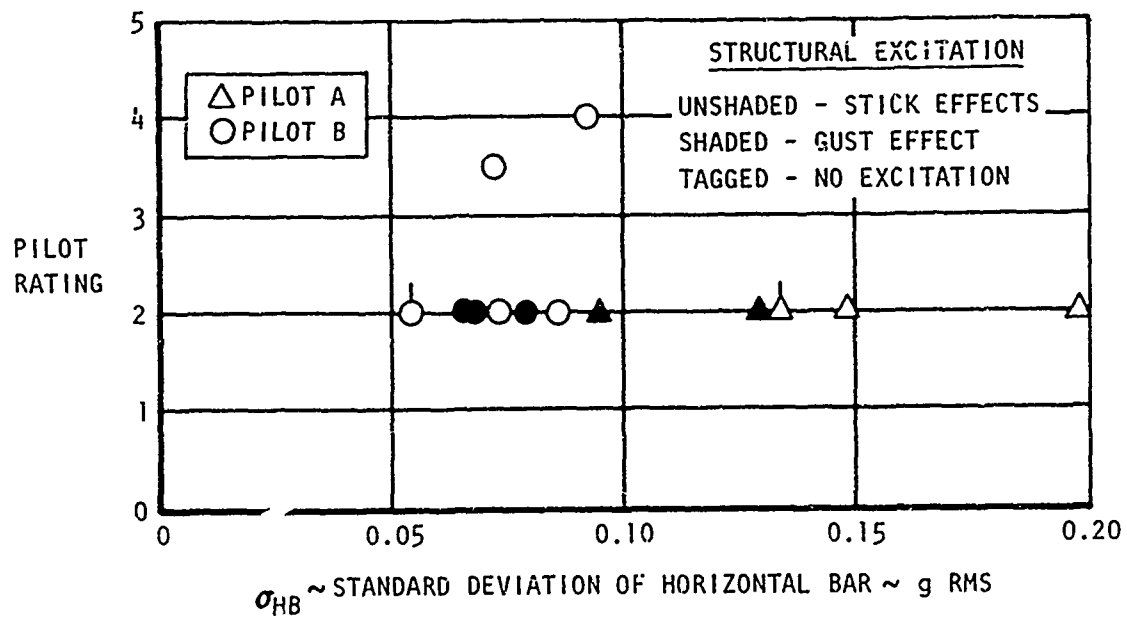
Figure 19. Terrain-Following Pilot Rating Versus σ_{HB} and σ_{PS}

Figure 20. σ_{PS} Versus N_{zPILOT} (Gust) and N_{zPILOT} (Stick)
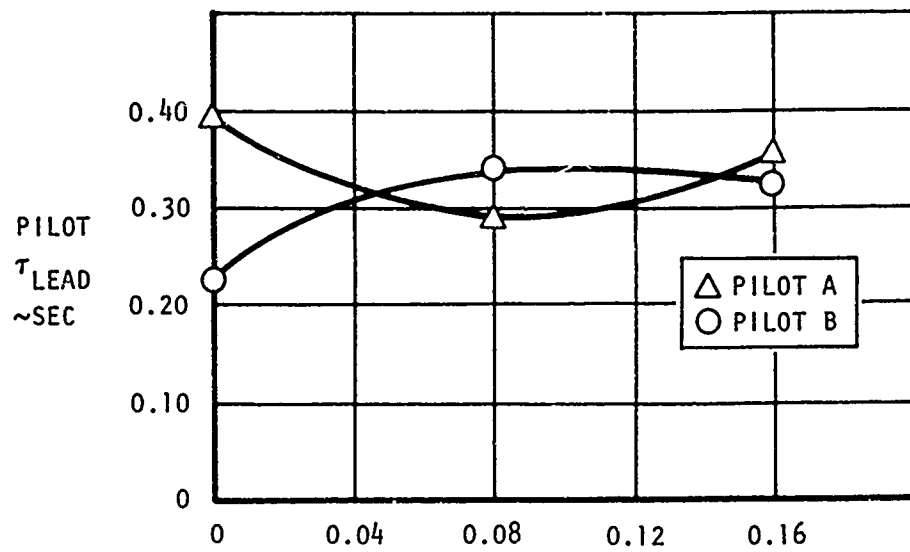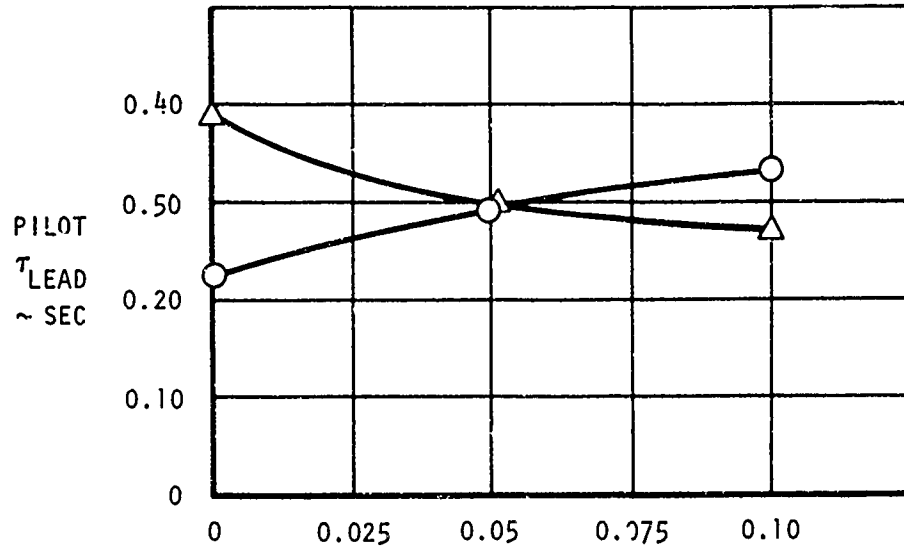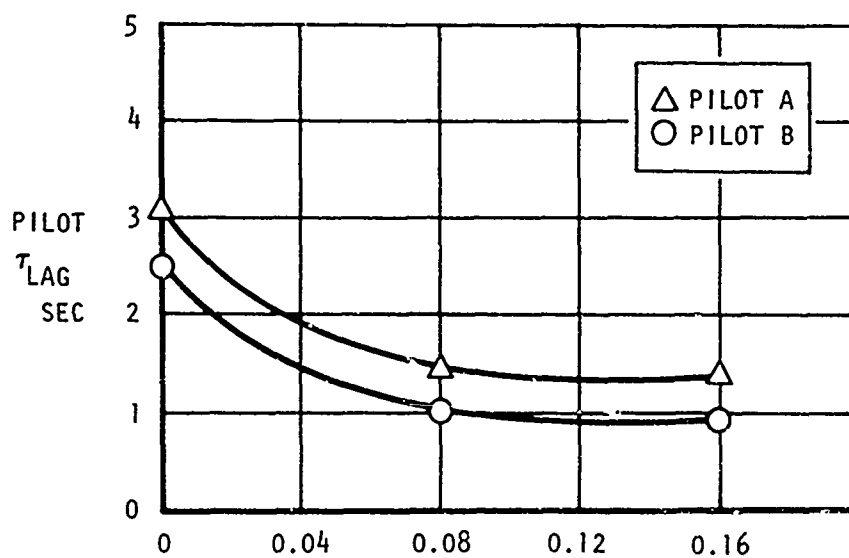
Figure 21. σ_{HB} Versus N_{zPILOT} (Gust) and N_{zPILOT} (Stick)
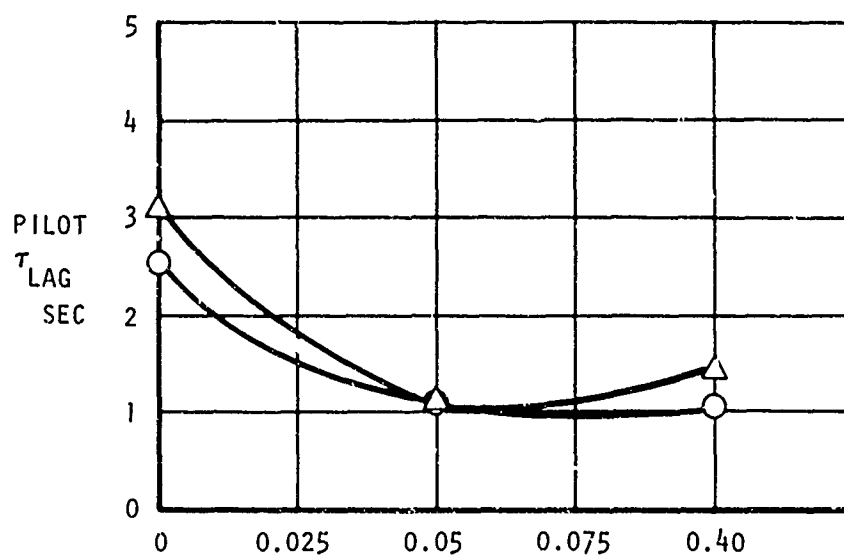
Figure 22. τ_{LEAD} Versus N_{zPILOT} (Gust) and N_{zPILOT} (Stick)

Figure 23. τ_{LAG} Versus N_{zPILOT} (Gust) and N_{zPILOT} (Stick)

Figure 24. Normalized Pilot Gain Versus $N_{z_{PILOT}}$ (Gust) and $N_{z_{PILOT}}$ (Stick)
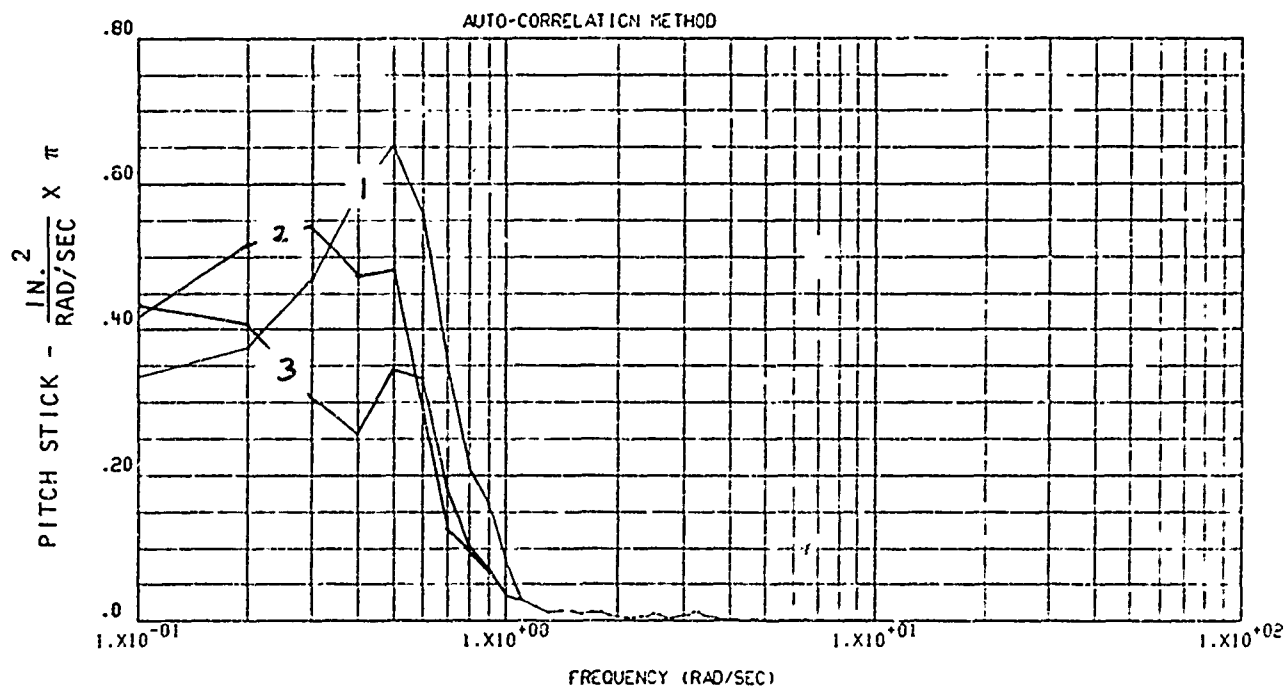
Figure 25. Effect of Increased Gust on Stick Spectral Density

47

(figure 54) indicates the influence of stick on horizontal bar is not nearly as significant. Hence, pilot A's large σ_{HB} can be attributed to the large power content in pitch stick at about 0.5 rad per second frequency. This effect of frequency is further borne out by noting that the convergence in σ_{HB} values for large stick effects is duplicated by convergence in PSD similarities as seen in figures 51 and 56.

The variation in pilot model parameters are shown in the next three figures. The lead time constant remains relatively steady for both pilots as seen in figure 22. Both pilots converge on a value of 0.30 second with increasing pilot motion resulting from increased structural effects. Pilot lag time constant shows a definite trend with increased turbulent motion. (See figure 23.) Both pilots decrease their lag time constants from about 2.5 to 3.0 seconds to about 1 to 1.5 seconds. Finally, the pilot model low-frequency gain (dc) is shown in figure 24. The gains, normalized to the no structural motion case, decrease with increasing pilot motion due to increasing structural effects. Percentagewise, pilot B shows a larger decrease than does pilot A. This is due primarily to the fact that pilot B's initial gain is higher than pilot A's (refer to table IV in appendix II) because of pilot B's greater activity in the low-frequency range as mentioned earlier.

The TF simulation revealed the ability of the pilots to maintain fairly constant performance over the range of structural motion effects studied without any significant trend in pilot workload. This is reflected in the pilots' unchanging rating of the TF task even when subjected to a high level of turbulent type of motion. This is undoubtedly due to a large extent to the fact that the tracking task was a low-frequency one and that the high-frequency disturbance did not appear in the display, but only affected his "ride." Hence, in this respect, the TF task was unlike other tracking tasks described in earlier referenced works where the turbulence provided the tracking problem.

The form of the measured pilot model was consistent throughout the runs, and the data exhibited good coherence throughout the frequency range sampled. The negative lead characteristic identified in the pilot model is not unexpected if the assumption is true that it represents part of the first-order linear approximation of the time delay existing in the pilot's response.

48

SECTION VI

AIR REFUELING DATA EVALUATION

SIMULATION DATA ANALYSIS

The air refueling (AR) simulation data were analyzed in a manner similar to that done for the terrain-following (TF) data. Aside from the change in flight condition, the significant differences in task were:

1. The display did not have lagged pitch stick displacement summing with γ_{ERROR}.

2. The γ tracking task was generated in an open-loop fashion.

A typical set of AR traces and data are presented herein with a discussion of the AR simulation data in later paragraphs.

Figure 26 shows the tracking task, γ_c, as a function of time ($\sigma = 0.88$ degree RMS and the mean = -0.49 degree) and its spectral density function. For a typical AR run, time histories of the display signal (γ_{ERROR}) and pitch stick are shown in figure 27. Figures 28 and 29 show the autocorrelation and crosscorrelation functions, respectively. The spectral density functions are presented in figure 30, while figure 31 shows the cospectra, quadrature spectra, and coherence functions. And finally, figure 32 presents the bode plots for these input-output signals. It is at this point that the data processing and frequency analysis results differ from those obtained in the TF task. Automatic curve fitting to these data was not achieved. The bode plot indicates the transfer functions consists primarily of lead terms. The analysis program failed to find acceptable curve fits for these lead-only situations. Hence, limited curve fitting was done by hand and, as will be seen later, even linear lead-only transfer functions (as suggested in this bode plot) were often inadequate. Complexities arose primarily because of the nonlinear phase behavior (evident in the referenced figure) of many of the plots.

SIMULATION RESULTS

As was evident in the TF task, the pilot ratings obtained were not a function of turbulence or structural mode excitation but, for the AR task, reflected whether the stability augmentation system (SAS) was off or on. Figure 33 shows that pilot B rated the AR task with SAS on as a 3 regardless of turbulence while, for SAS off, his rating was a 5 for no turbulence and a 9 for 3 fps RMS of turbulence. This latter rating must

49
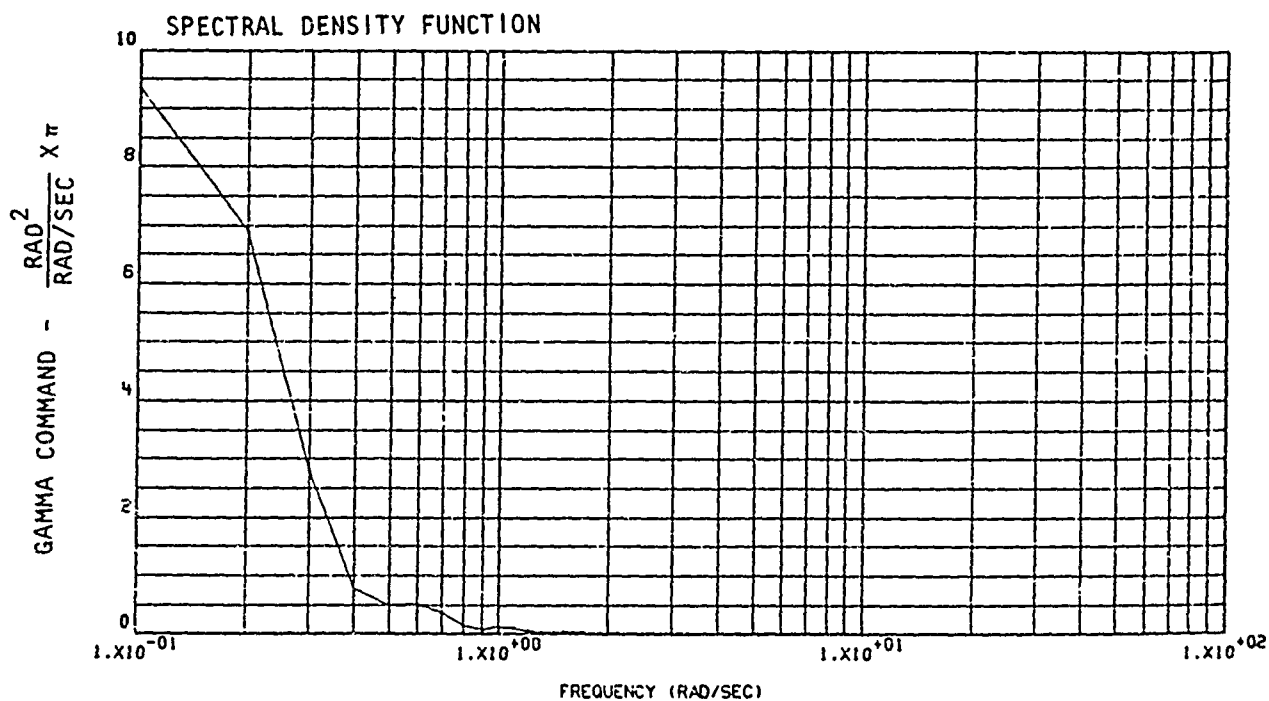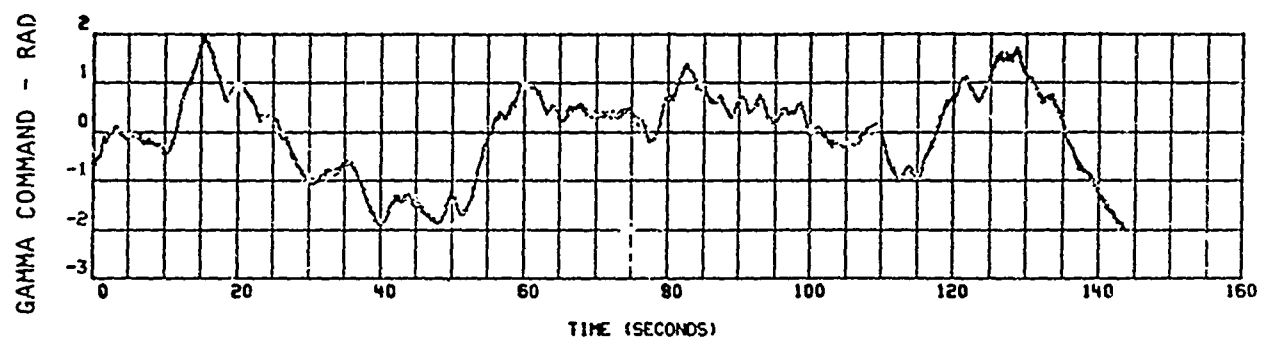
Figure 26. AR Gamma Command (γ_c) Time History and
Spectral Density Function

50
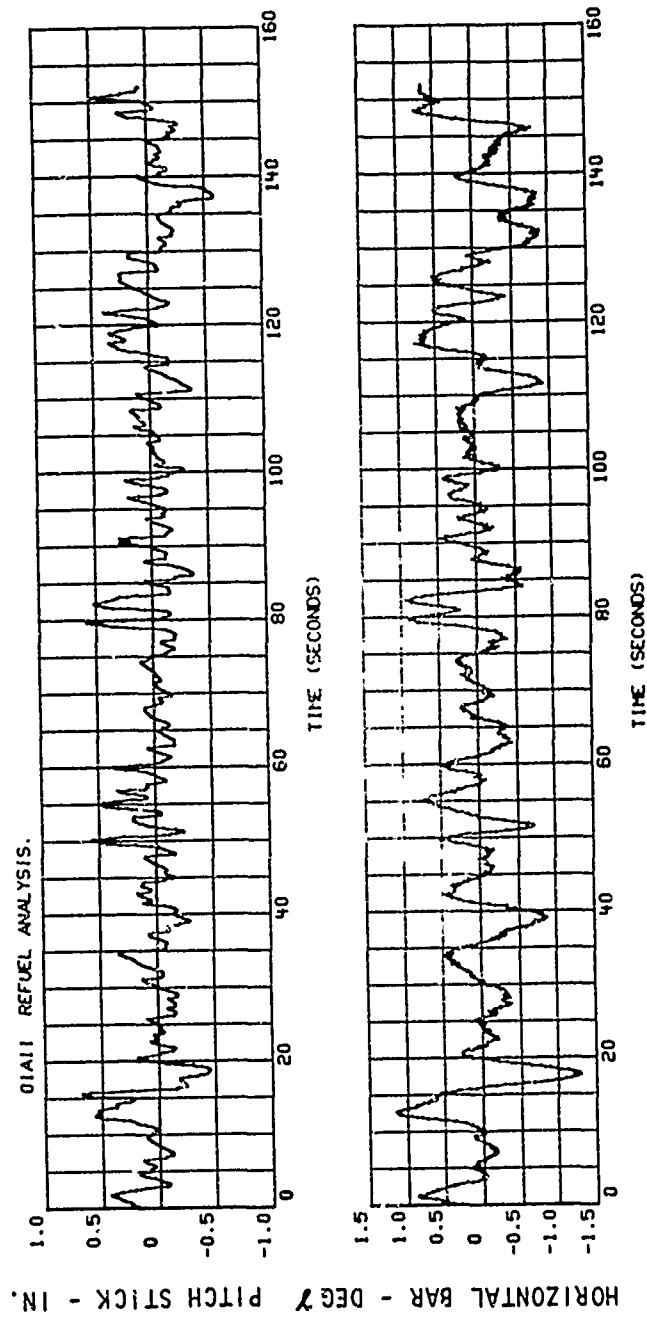
Figure 27. Typical AR Pitch Stick and Display (γ_{ERROR}) Time Histories (No. 01A11)
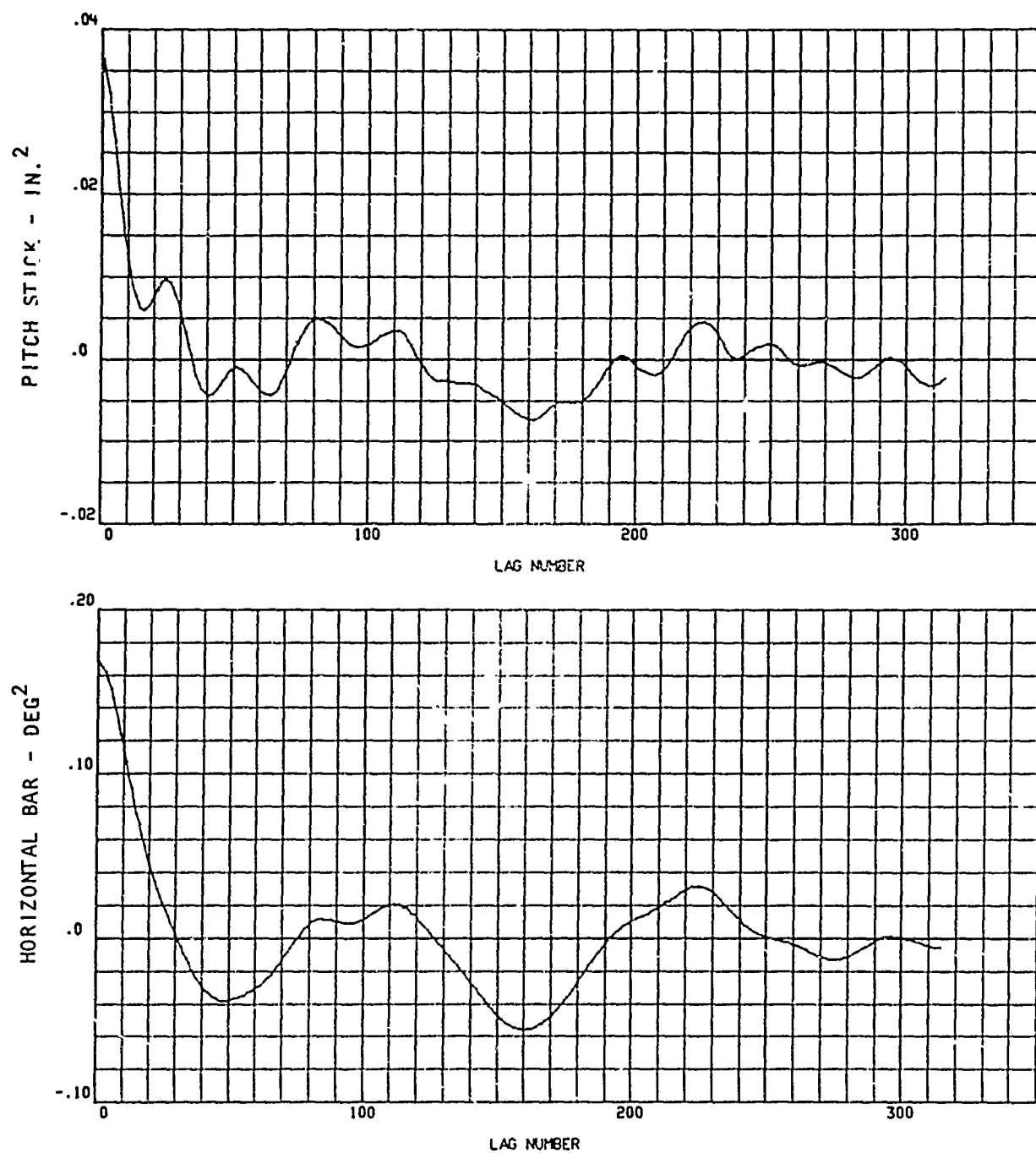
Figure 28. Autocorrelation Functions of Pitch Stick and Display (No. 01A11)
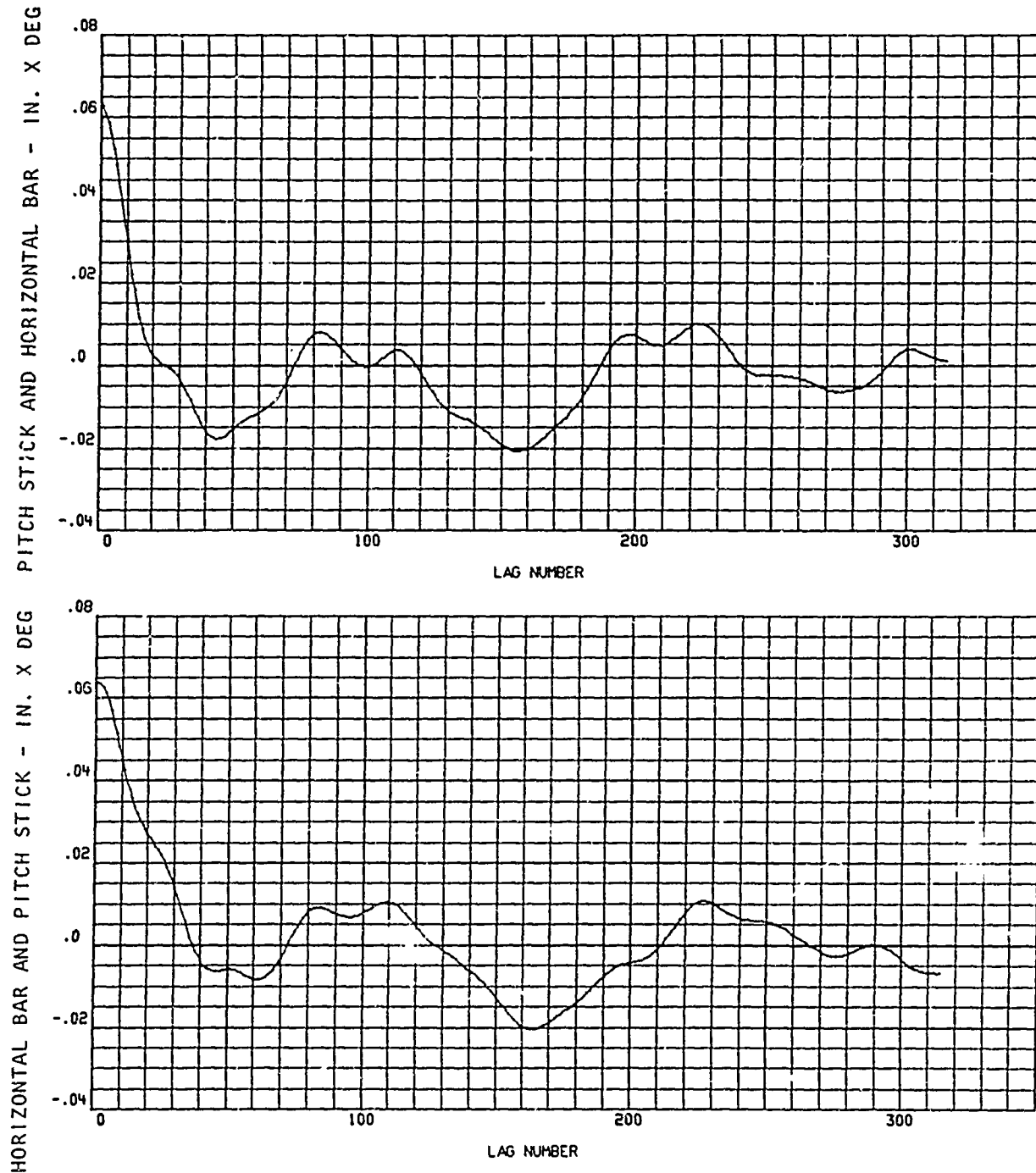
Figure 29.   Crosscorrelation Functions of Pitch Stick and
Display (No. 01A11)

SPECTRAL DENSITY FUNCTIONS
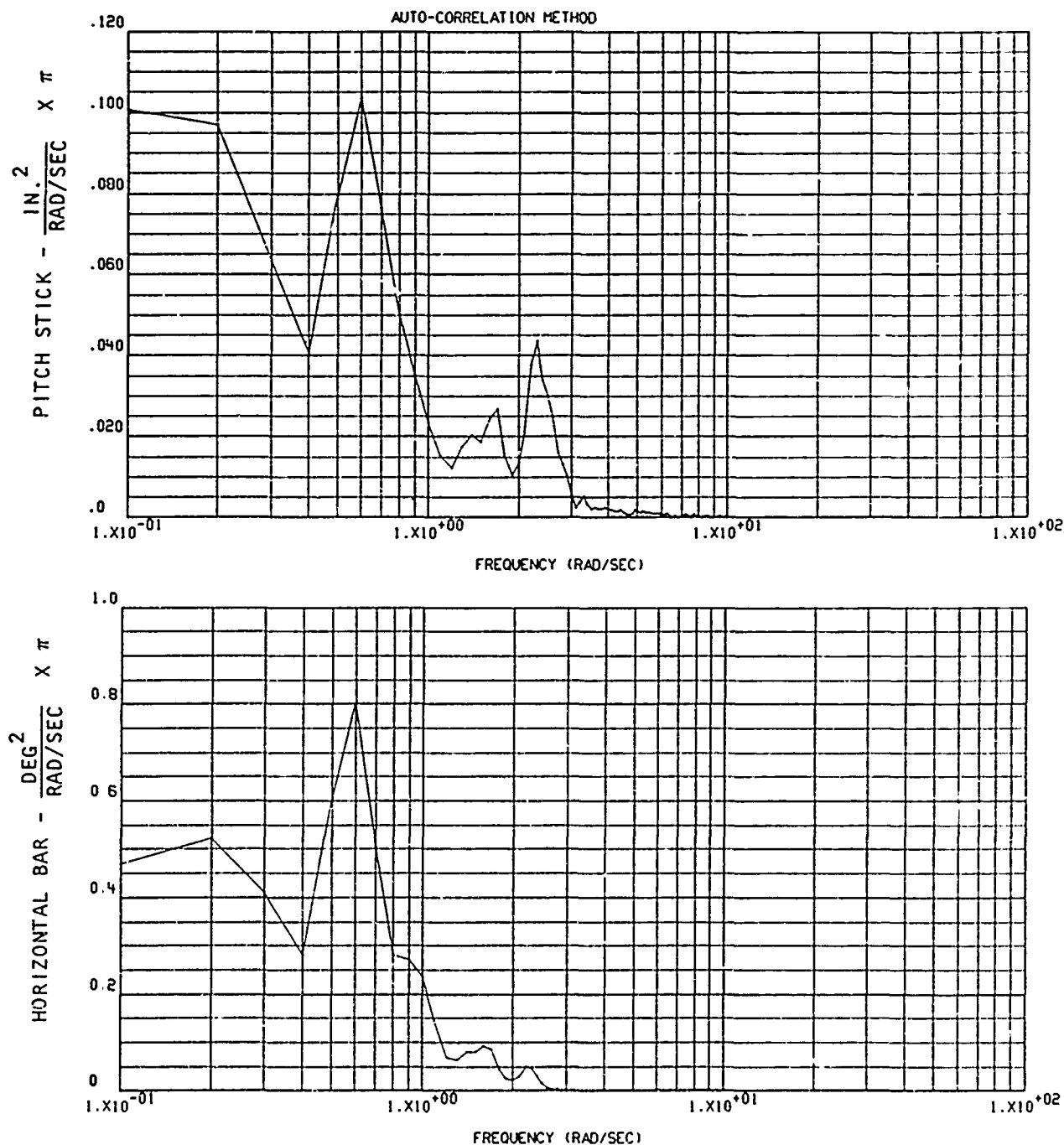
Figure 30. Spectral Density Functions of Pitch Stick and
Display (No. 01A11)

AUTO-CORRELATION METHOD

Figure 31.   Cospectra, Quadrature Spectra, and Coherence Functions
of Pitch Stick and Display (No. 01A11)

55

01A11 REFUEL ANALYSIS.
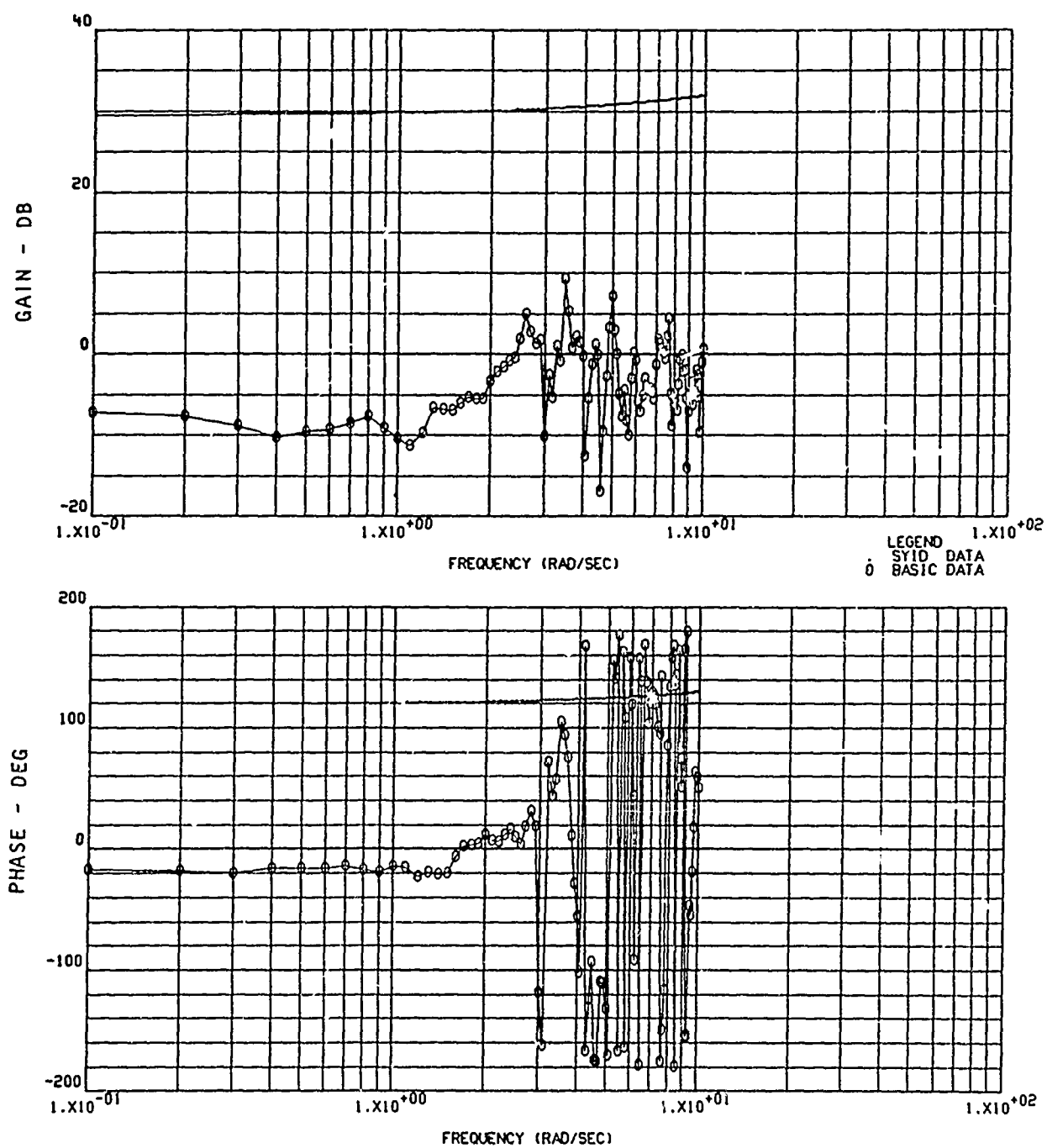
Figure 32. Pilot Bode Plot (No. 01A11)
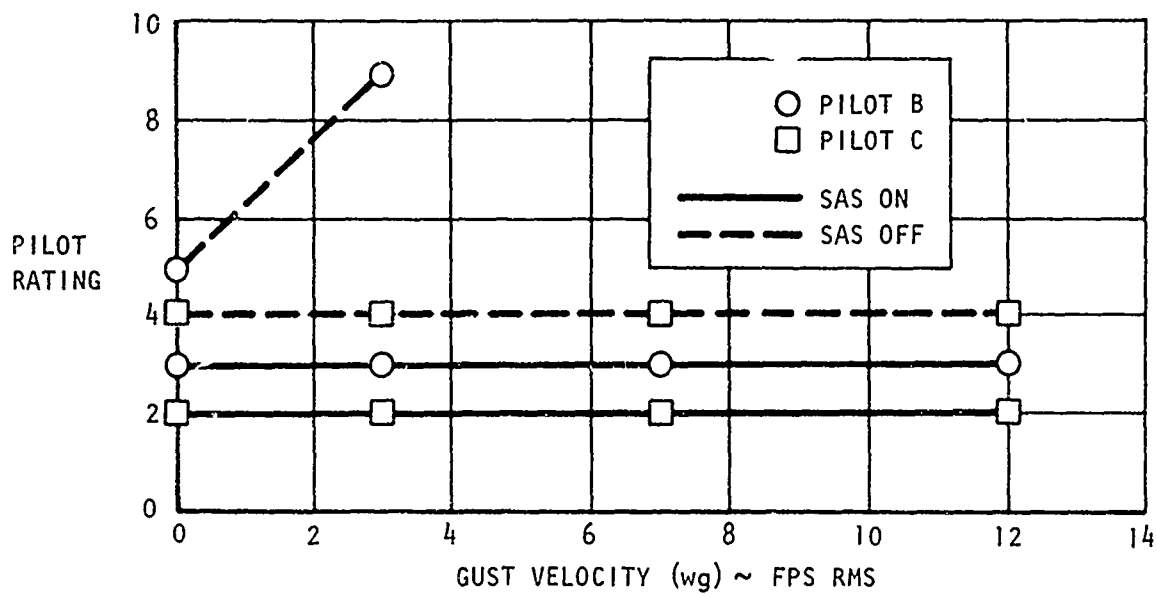
Figure 33. Pilot Ratings Versus Gust Velocity for Air-Refueling Task

be considered something of an anomaly because, in subsequent runs with SAS off and with more extreme turbulence, the task was rated a 5. Pilot comment and the data indicate a PIO condition existed (see figure 78 in appendix III) of sufficient severity to cause him to give a 9 rating. Such a PIO condition, however, did not reoccur. The time histories in the figure show the oscillations at about 0.3 Hz, and the pitch stick spectral density function in the same figure shows the significant power contained in the 0.3 Hz or 2 rad-per-second frequency region (compare this plot with that shown in figure 79 for SAS off, the same turbulence level and with structural mode effects but with no power peak unrelated to the task). Although the rating seems extreme for a PIO condition, the pilot felt he could not accomplish the AR task safely. Based on his performance and ratings for similar conditions, it is felt this case is an isolated one where, probably, pilot motivation was temporarily insufficient.

Pilot C was likewise consistent in his ratings, a 2 for SAS on and a 4 for SAS off regardless of the level of turbulence or mode of excitation.

These data indicate that the primary parameters of variation used in the study are not those which influence pilot ratings of the task. Turbulence level, structural mode·excitation, pilot acceleration, and other parameters which may correlate with these are insufficient to develop a pilot rating prediction algorithm. In the AR task, only SAS affected pilot ratings. The gain of the command SAS had to be reduced by a factor of 4 at the beginning of the simulation to provide an acceptable pilot rating, and this gain effect is shown in figure 34. Increasing the gain caused an increase in stick activity, γ_{ERROR} and pilot acceleration, all for zero turbulence. Unfortunately, this correlation is not easily verified in the paper pilot scheme since that algorithm was developed on the assumption that the optimum pilot input sensitivity had been selected and, as a consequence, pilot gain is not a variable in the rating algorithm or cost function. Examination of the pitch stick spectral density plots for the three SAS pilot input gains indicates that, as the frequency content of the activity decreased, the ratings improved (figures 39, 76, and 75 correspond to the normalized electrical gains of 1, 2, and 4 shown in figure 34). The pilot obviously prefers to work at a lower frequency. This certainly is in an indication of why the TF and AR tasks are well rated by the pilots, in spite of their motion environment, as long as the frequency content of the task remains low. The effect of SAS on the frequency content of pilot activity is illustrated in figure 35 for runs No. 01A11 and 04A1 which show SAS on and off, respectively. Even though the pitch stick σ is higher for the SAS-on case (0.192 versus 0.173 in RMS), there is a well-pronounced frequency peak at 2 rad per second for the SAS-off situation.

Another SAS control system parameter was evaluated, the stick pre-filter which, however, proved to have little effect on pilot ratings in the
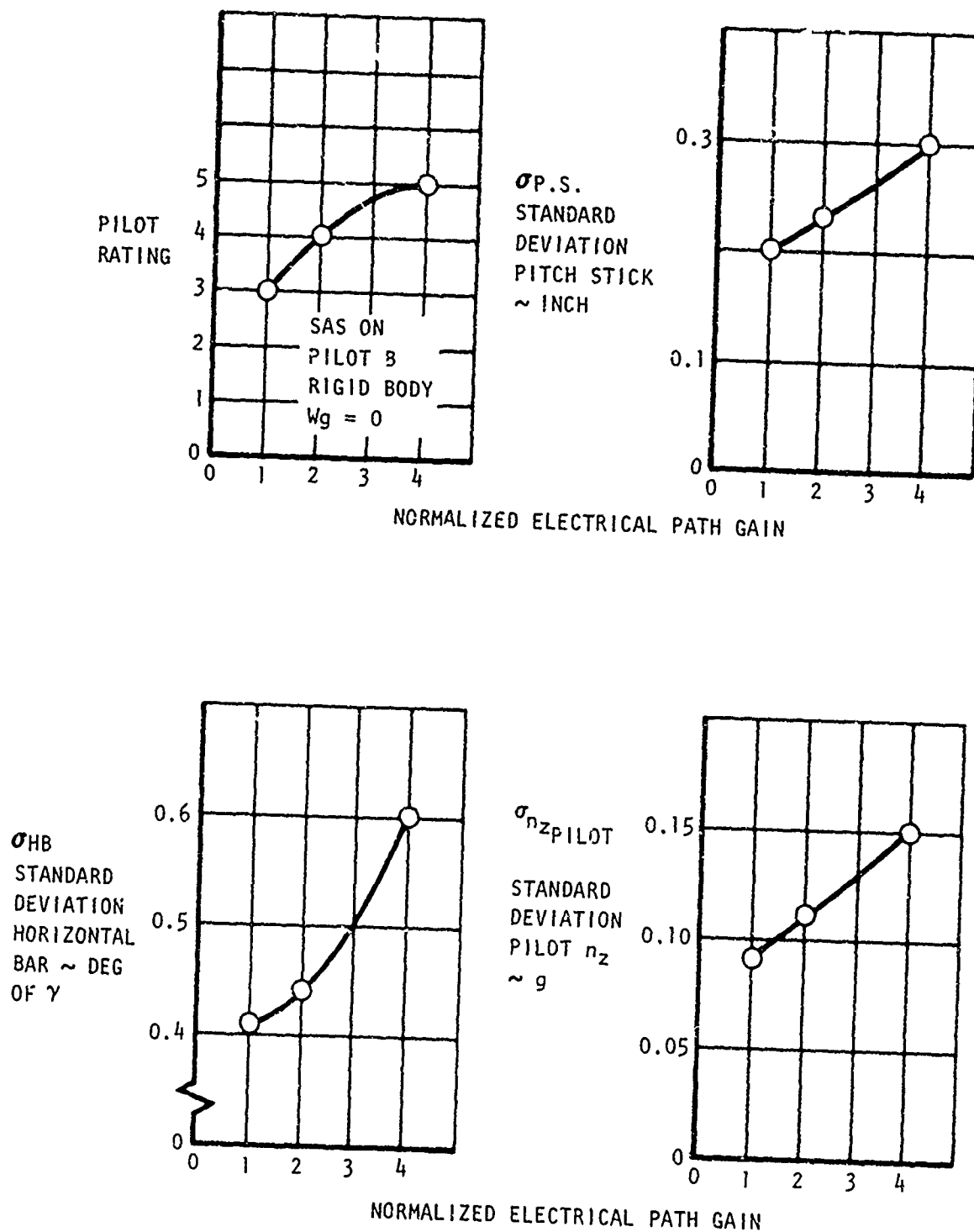
Figure 34. Effects of SAS Command Gains of Air-Refueling Task and Performance
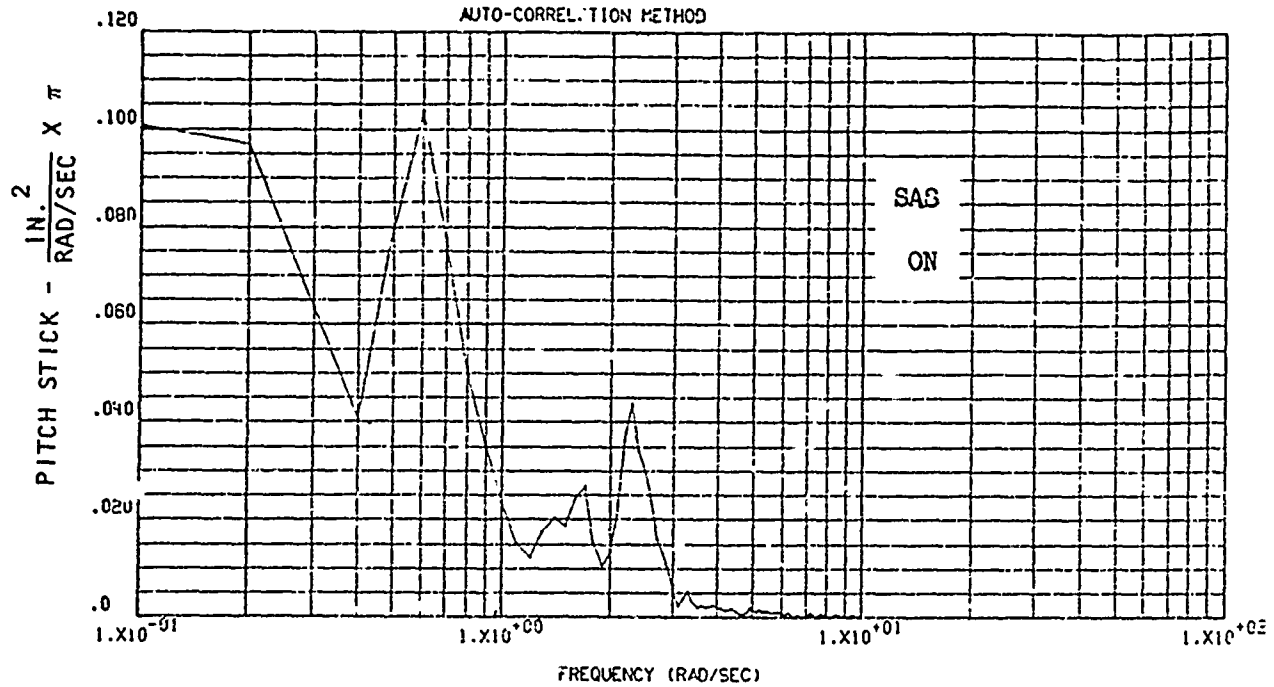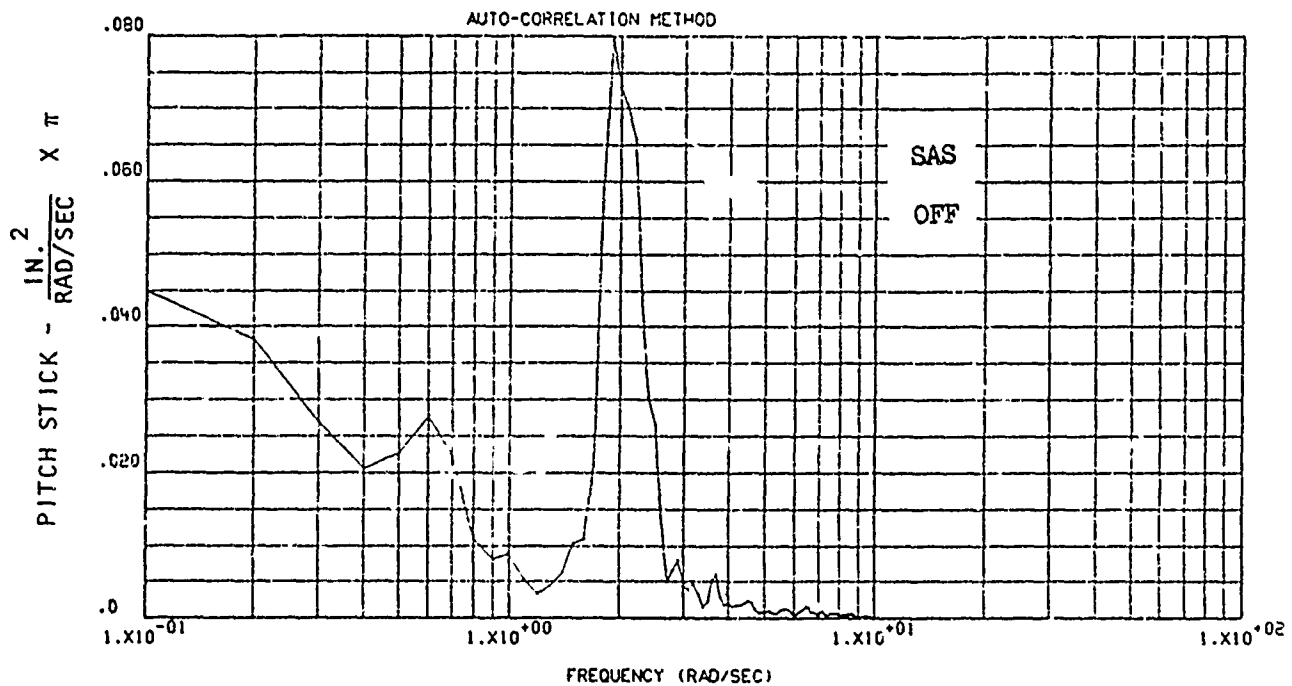
Figure 35. Pitch Stick Spectral Density Functions

lag range evaluated. Performance parameters resulting from the lag
variations of from 0.10 to 1.0 second are shown in figure 36. Pilot B shows
relatively little difference in stick activity with turbulence or stick lag
variation, while the tracking error σ_{HB} does show the effects of increased
stick lag. This, however, did not significantly influence pilot rating.

Additional effects of SAS on task performance parameters are given in
figure 37 which presents the standard deviations in pitch stick and
horizontal bar (γ_{ERROR}) as a function of turbulence level, turbulence
excitation of structural mode, and SAS status. No obvious correlations
exist except for the higher σ's for the high turbulence and SAS-off cases.
Figure 38 shows similar SAS effects for the rigid body vehicle for various
turbulence levels. Pilot B does show more tracking error for the SAS-off
case, while pilot C shows a reduced tracking error for SAS off. Stick
activity data shown are also not instructive except for the one SAS-off
case for 3 fps RMS of gust velocity which was described earlier.

Pilot acceleration, in the AR study, was generated through the pilot
tracking effort, the rigid body motion due to turbulence and the acceleration
due to structural mode excitation by the turbulence and stick. Figure 39
shows how pilot acceleration is affected by these variations. Structural
mode excitations by turbulence are the dominant contributors for both
pilots. The pilots really have no control over these effects. The rigid
body accelerations are considerably different for the two pilots for the
low levels of turbulence, but are identical for the high levels. Although
the stick activity for the two pilots is almost the same (0.235 and
0.225 σ_{ps}) for 3 fps RMS of gust, the difference in rigid body accelerations
can be explained by examining the stick spectral density functions. (See
figures 84 and 60.) In the former plot (pilot C) the power is concentrated
at about 2 rad per second, while, for the latter plot (pilot B), the
dominance is in the lower frequencies. The higher frequency inputs by
pilot C result in attenuated rigid body acceleration effects, while
pilot B's lower frequencies result in more acceleration effects. This can
be seen in figure 40 which presents the pilot acceleration spectral density
functions for the two cases. Pilot B, the lower plot, shows the higher
acceleration levels existing at the lower frequencies, thus giving a
larger standard deviation as shown in figure 39. For the higher turbulence
level (w_g = 12 fps RMS), the standard deviations in pilot acceleration
is about the same as seen in figure 40, and this is evident in the similarity
of the spectral density plots for the two pilots, shown in figure 41.

Pilot acceleration data show little correlation with pitch stick
activity and horizontal bar (γ_{ERROR}), as shown in figure 42. The arrows
shown on the curves indicate the direction of increasing turbulence level.
No obvious trend exists for the set of data, although some of the indicated
subsets show a degree of correlation with turbulence.
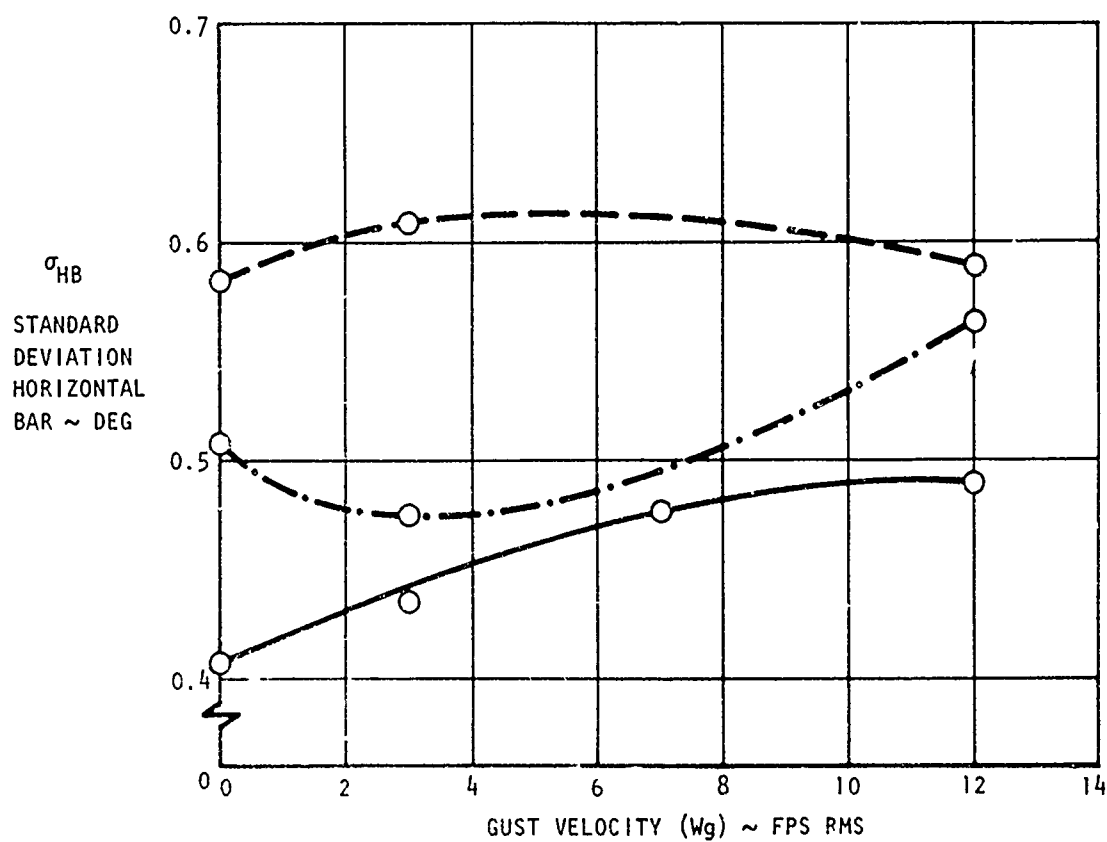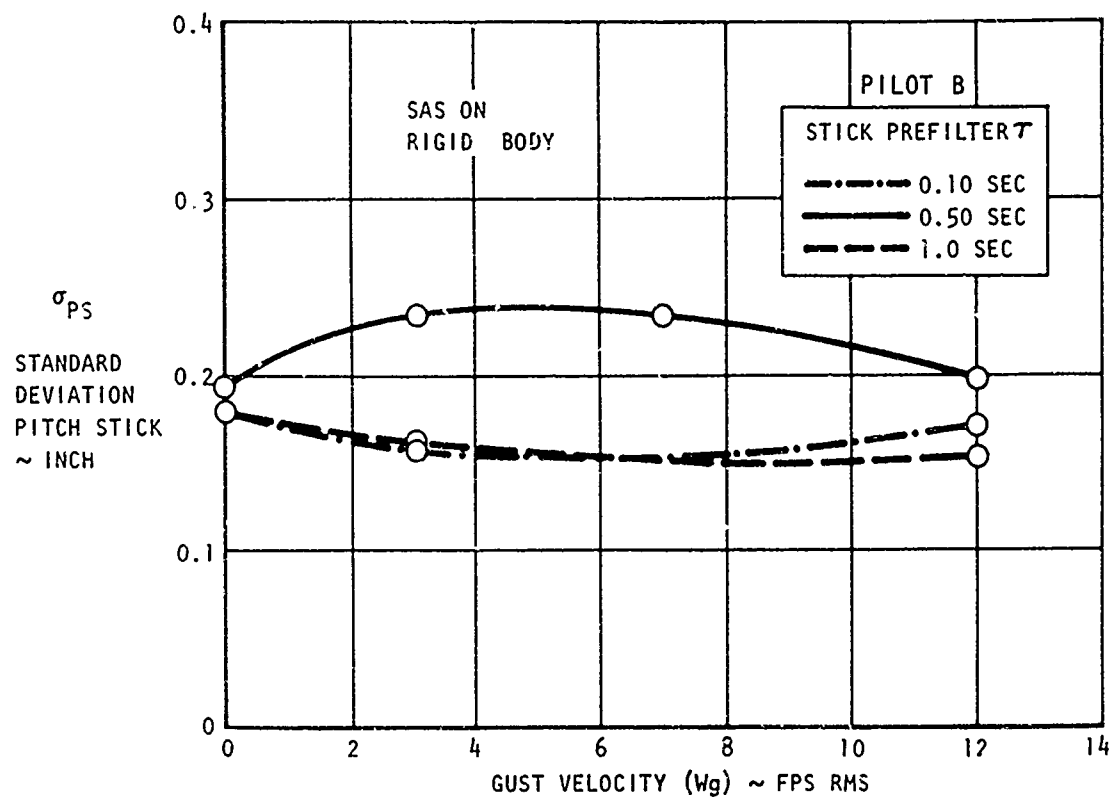
Figure 30. Air-Retueling Task Performance Parameter Variation Due to Stick Prefilter Time Constant
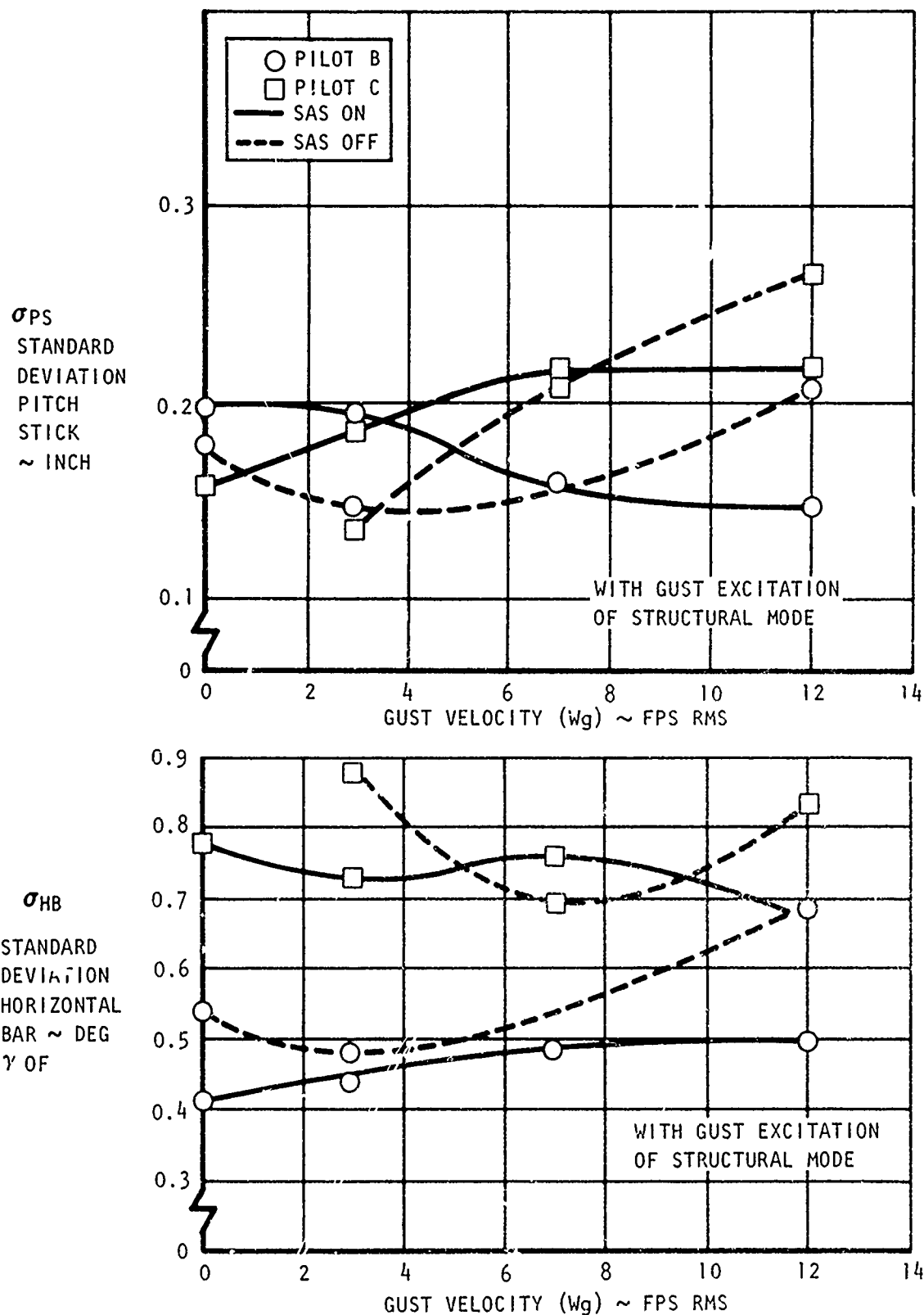
Figure 37. SAS Effects on Air-Refueling Performance Parameters with Gust
Excitation of Structural Mode

63
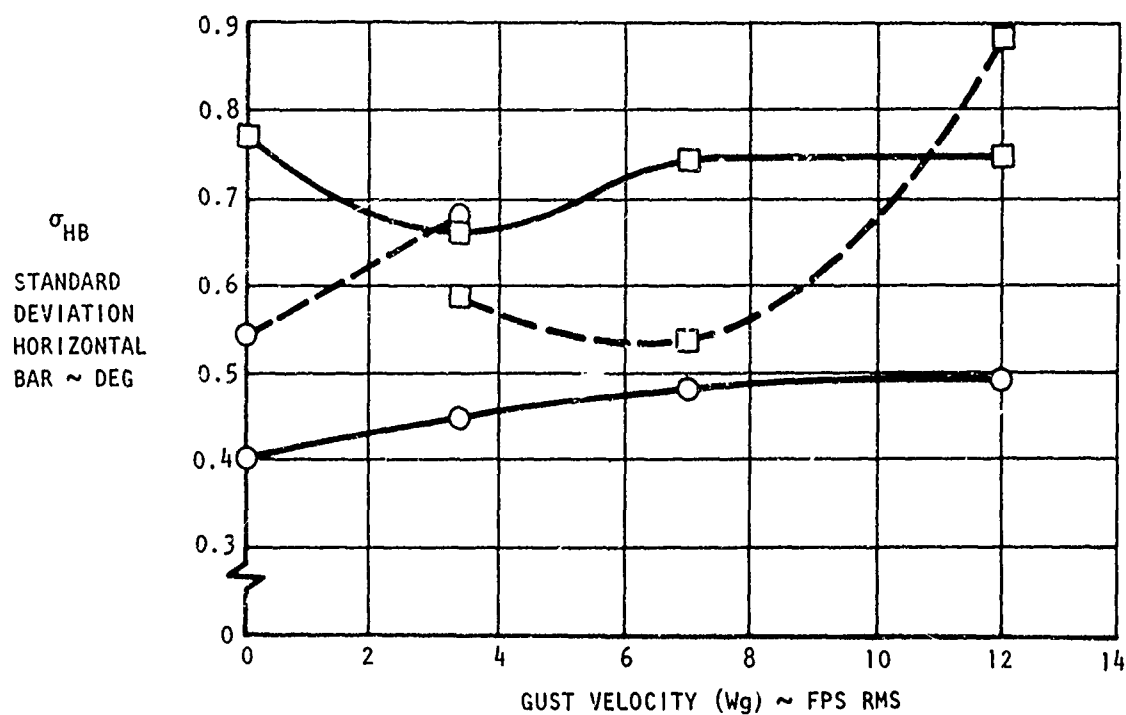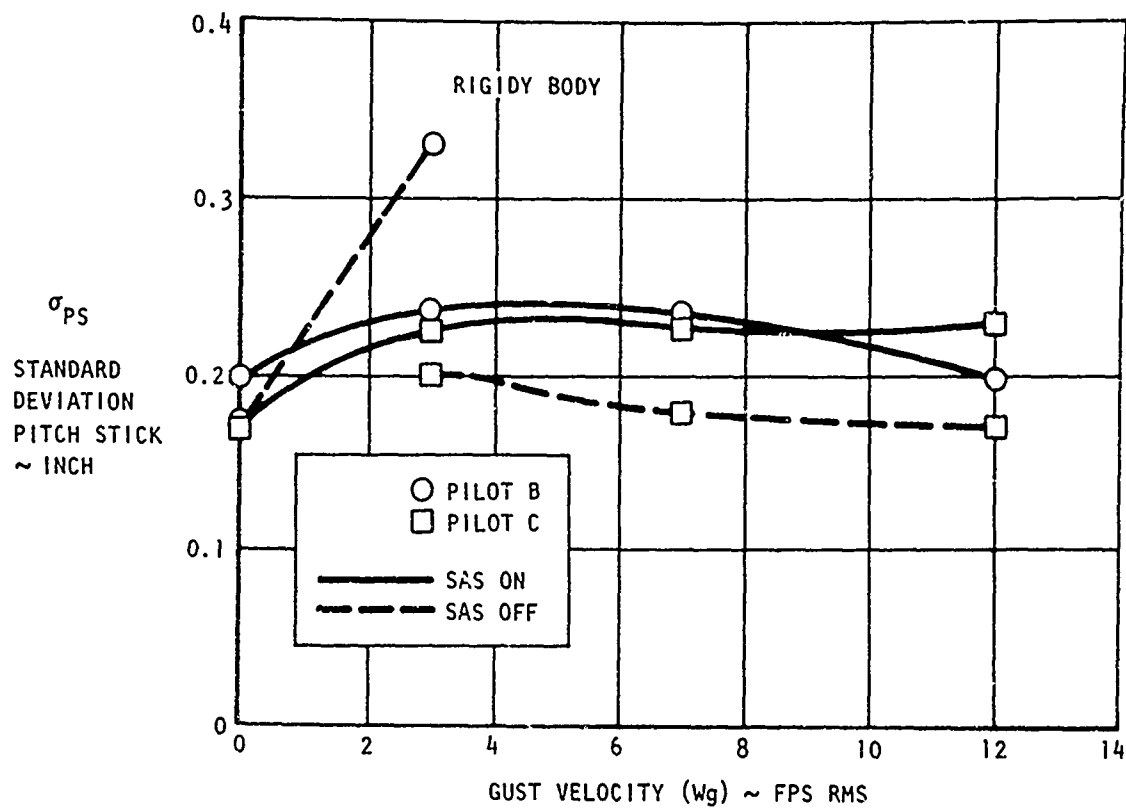
Figure 38. SAS Effects on Rigid Body Air-Refueling Performance Parameters
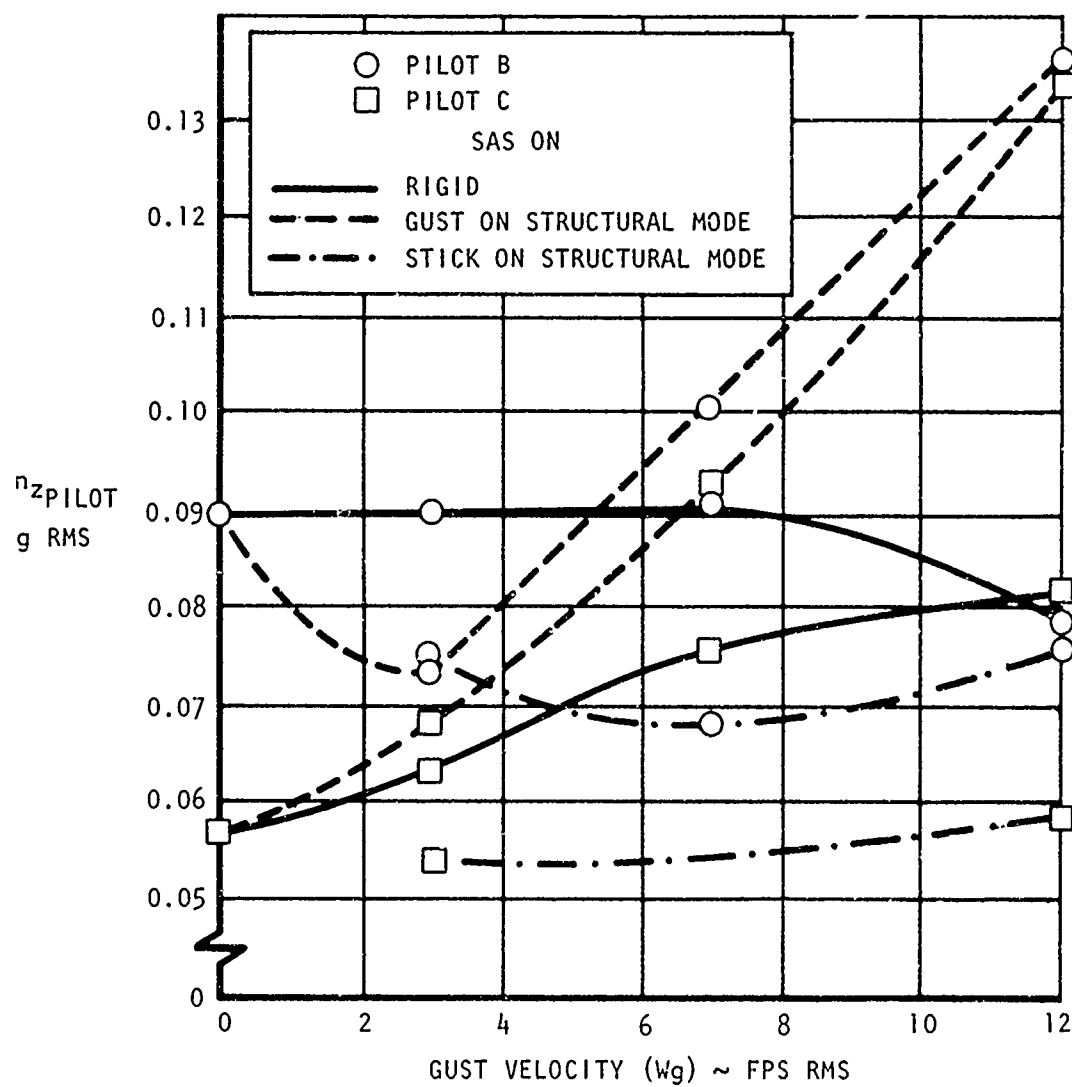
Figure 39. Pilot Acceleration Versus Gust Velocity
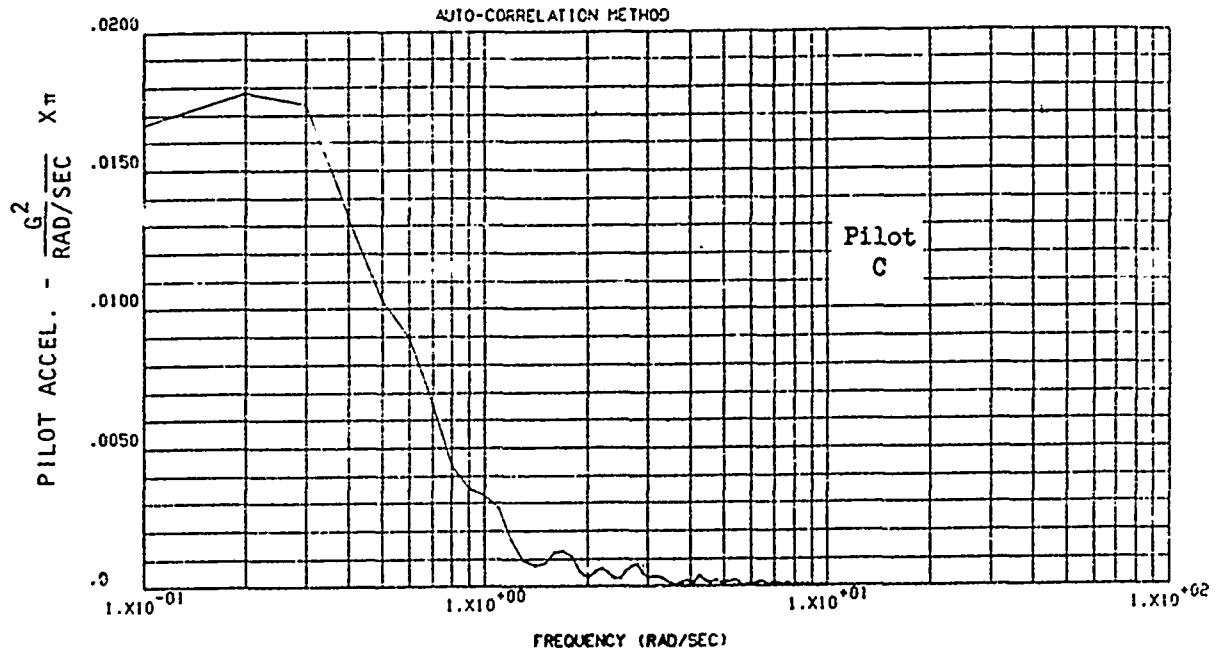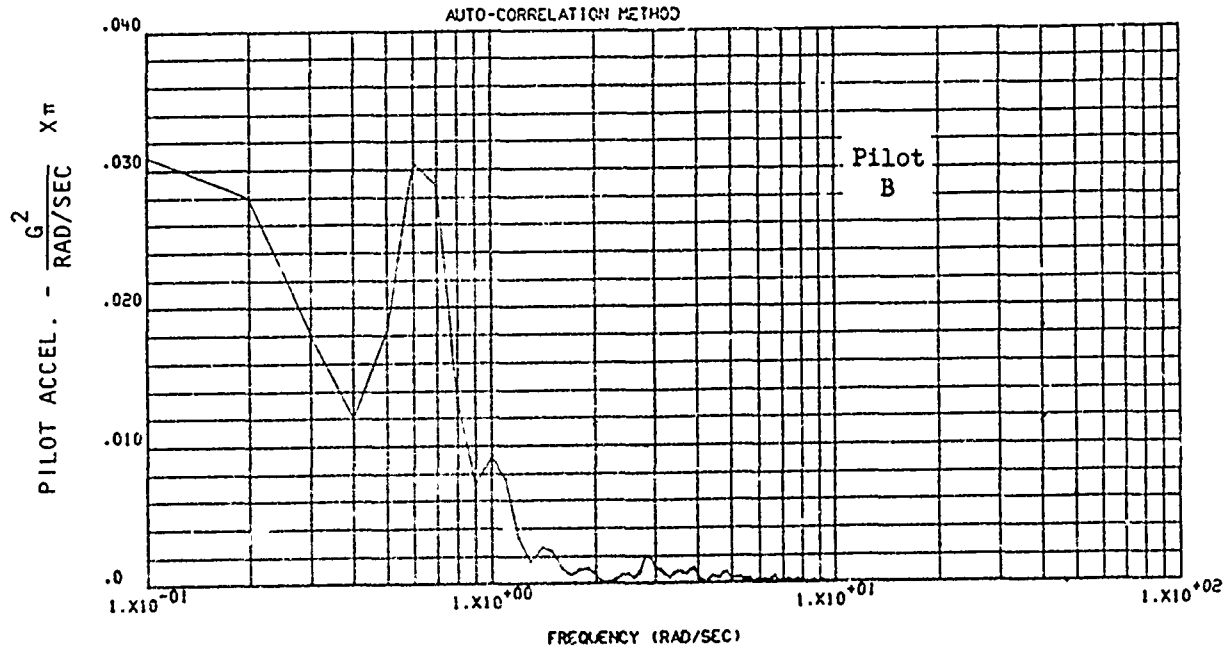
Figure 40.   Variation of Pilot Acceleration Spectral Density Functions

66
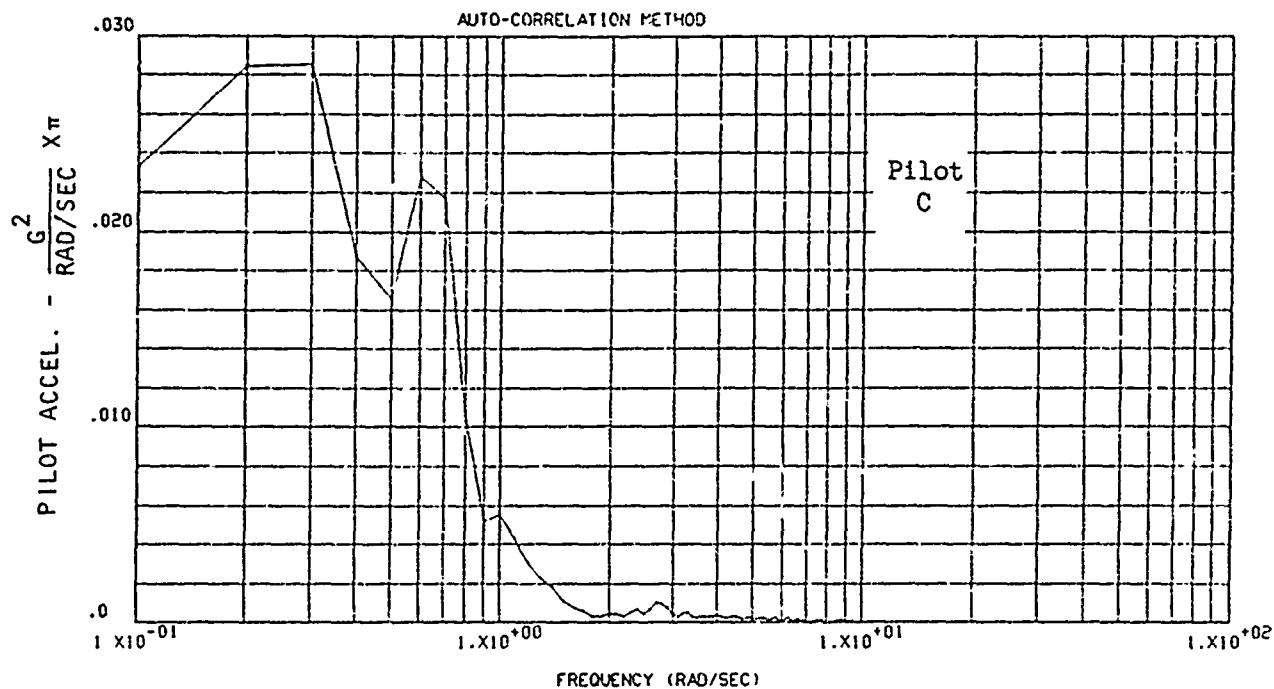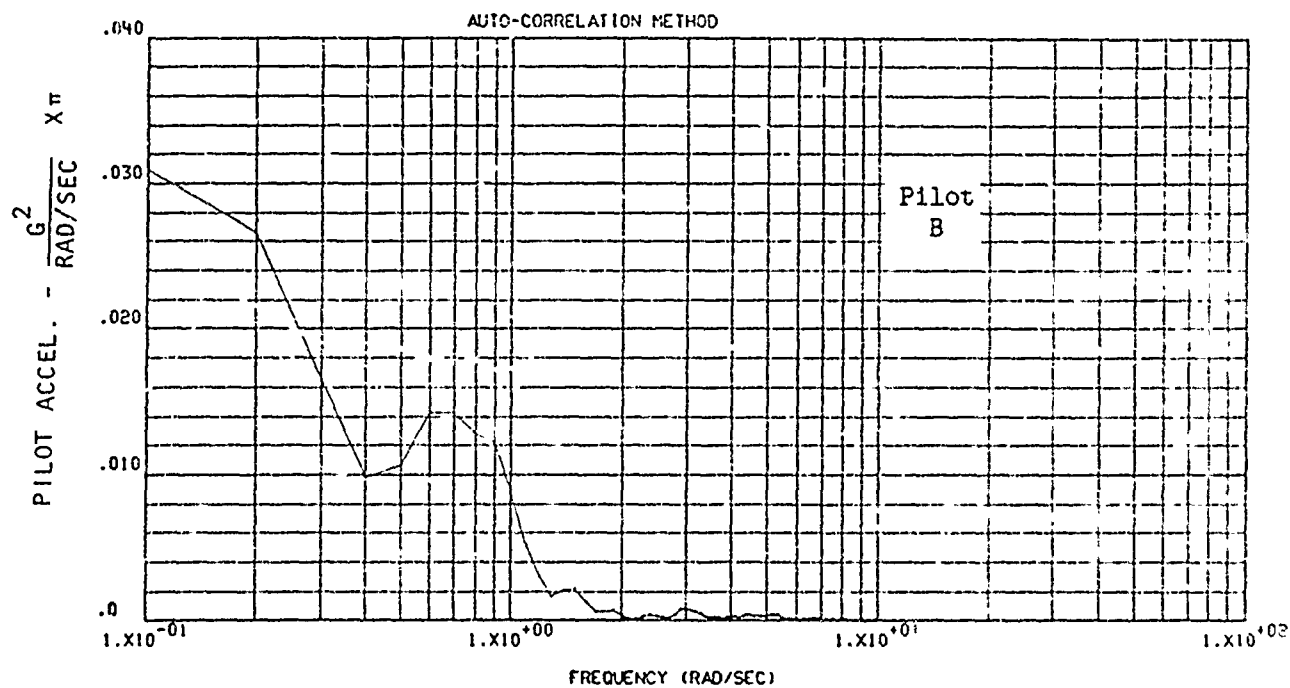
Figure 41. Variation of Pilot Acceleration Spectral Density
Functions for High Gust Levels

67
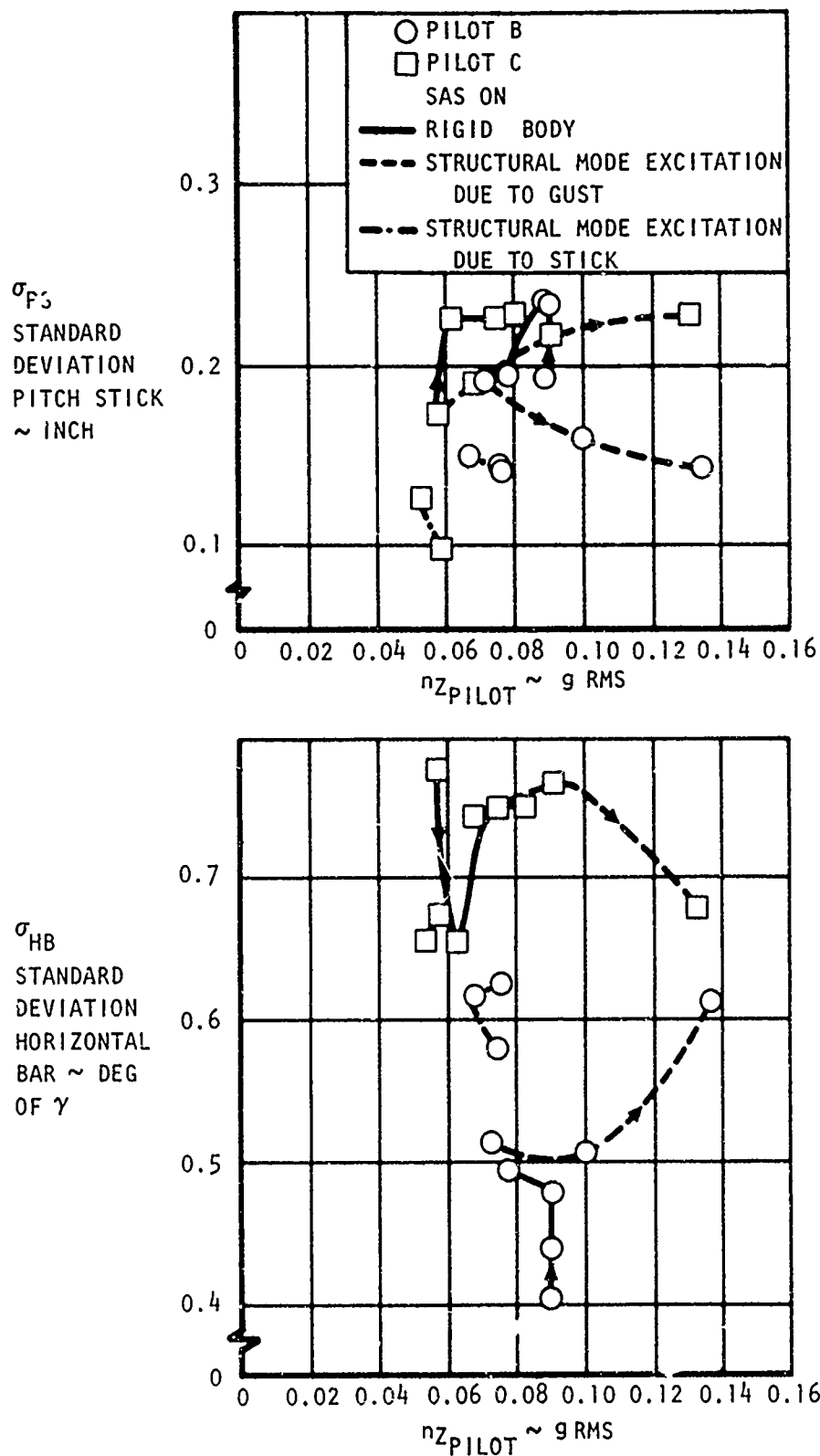
Figure 42. Air-Refueling Performance Parameters Versus Pilot Acceleration

Pitch stick activity trends do show up as a function of structural mode excitation. Figure 43 shows σ_{ps} decreases with gust level when the stick excites the structural mode. The effect of gust on the structural mode differs between the pilots with pilot B displaying a reduction with increased gust level while pilot C does the opposite. Both pilots show a slight increase in σ_{ps} with rigid body gusts. In the lower plot, the tracking error (σ_{HB}) effects are more pronounced between pilots than between gust levels. Pilot B does indicate an increase in σ_{HB} with gust increase and with gust and stick excitation of the structural mode. On the other hand, pilot C decreases his tracking error standard deviation slightly with increasing gust level. The large difference in tracking error RMS (σ_{HB}) between the pilots can be seen in the horizontal bar time histories in figures 27 and 83. In figure 83, it is evident pilot C allows larger tracking errors to exist for longer times than does pilot B (figure 27).

Analysis of the pilot bode plots proved difficult because of the variation in the form of the data and the apparent need for complex models. Compared to the TF data, the coherence estimates of the AR data were poor. As described in appendix I, the coherence estimate is an indication of the adequacy of a linear, time-invariant transfer function in fitting the input-output time histories.

Figure 11 gives the coherence function for a TF run (No. 0418) which can be compared with that shown in figure 31 for an AR run (No. 01A11). The spectral density function of the remnant for AR run (No. 01A11) is given in figure 44 which can be compared to figure 13. The obvious difference is the consistently poor coherence estimate for frequencies above 2.5 rad per second for the AR case. This is typical of most of the AR data, and examination of the bode plots indicates a significant leveling off or dropping in amplitude ratio for frequencies above 2.5 to 3.0 rad per second. For those AR cases where a double lead pilot model was assumed and shown on the data plots, the amplitude ratio linear model must be restricted to frequencies below 2.5 to 3.0 rad per second, as is apparent from the plots.

Even in the lower frequency ranges, a considerable variation in amplitude ratio form is indicated by the bode plots. They range from simple lead (figure 66) to double lead (figure 75) to lead-lag (figure 82) to a notch filter (figure 94) and, finally, to a simple lag (figure 68). In each case, the phase plot does not match the amplitude ratio form. The respective coherence functions vary as can be seen in appendix III. The simple lead coherence function is high to 2 rad per second, the double lead coherence is high to 3.5 rad per second, the lead-lag is relatively poor throughout, the notch filter is poor at the notch frequency and above 2 rad per second, while the simple lag is high to 1.3 rad per second. In general, however, if the data points exhibiting low coherence values are ignored, the common tendency is to a lead only transfer function.
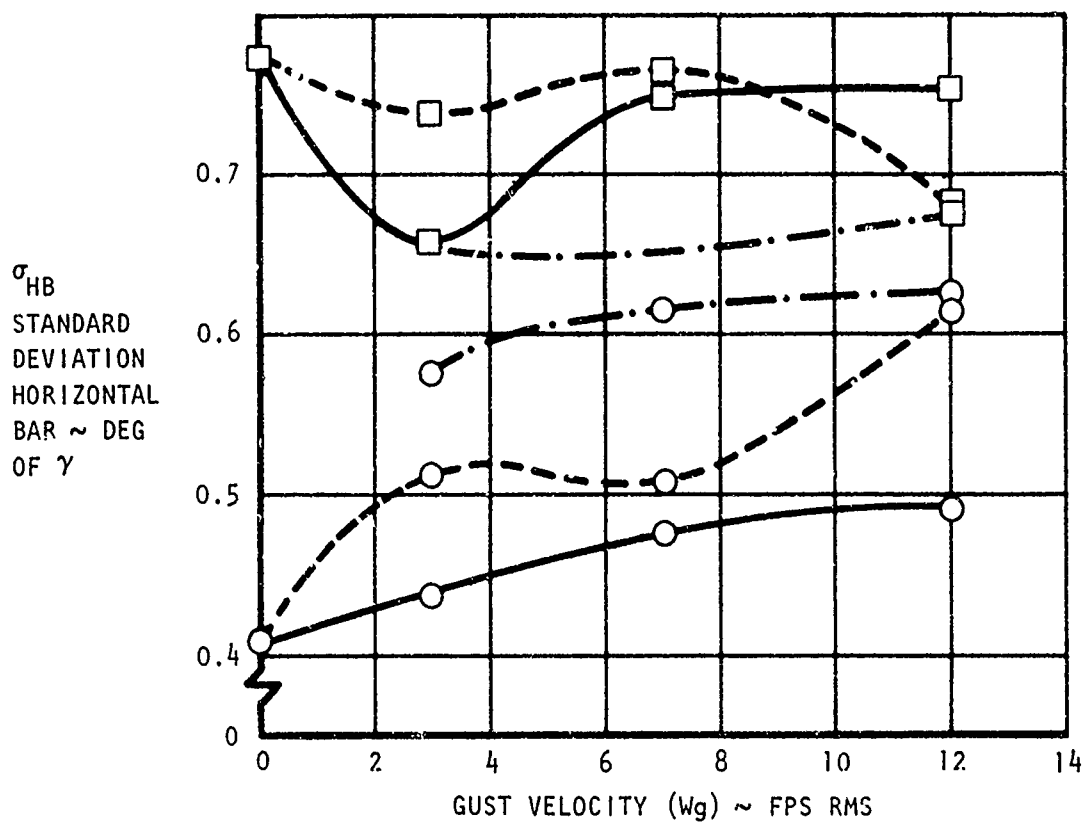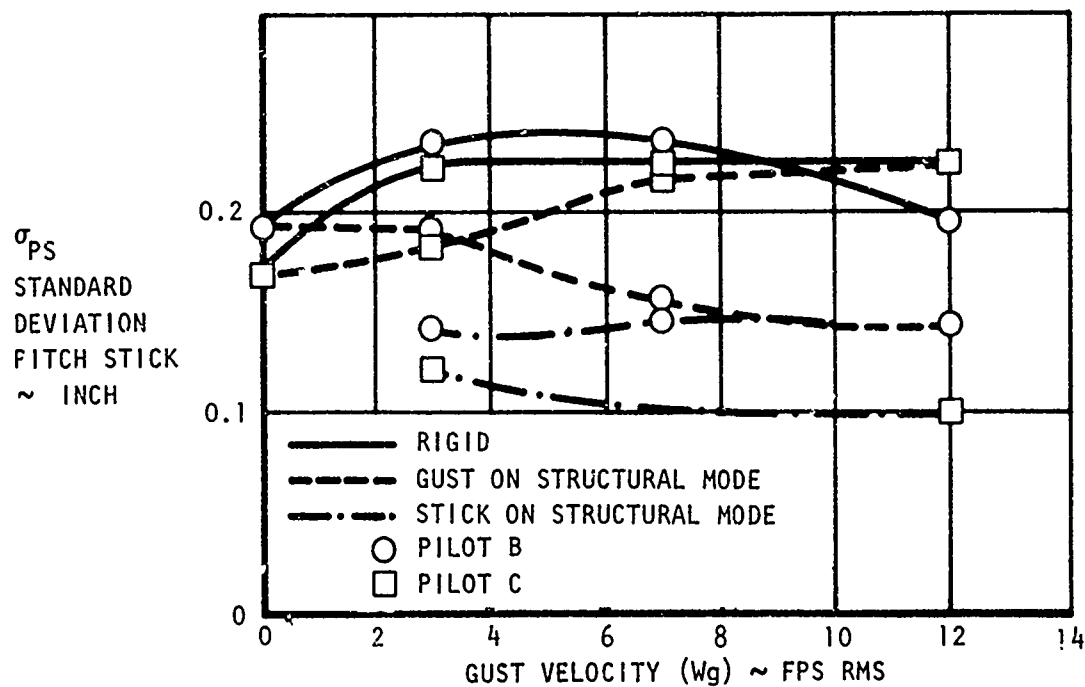
Figure 43. Air-Refueling Performance Parameters for Gust and Stick Effects on Structural Mode
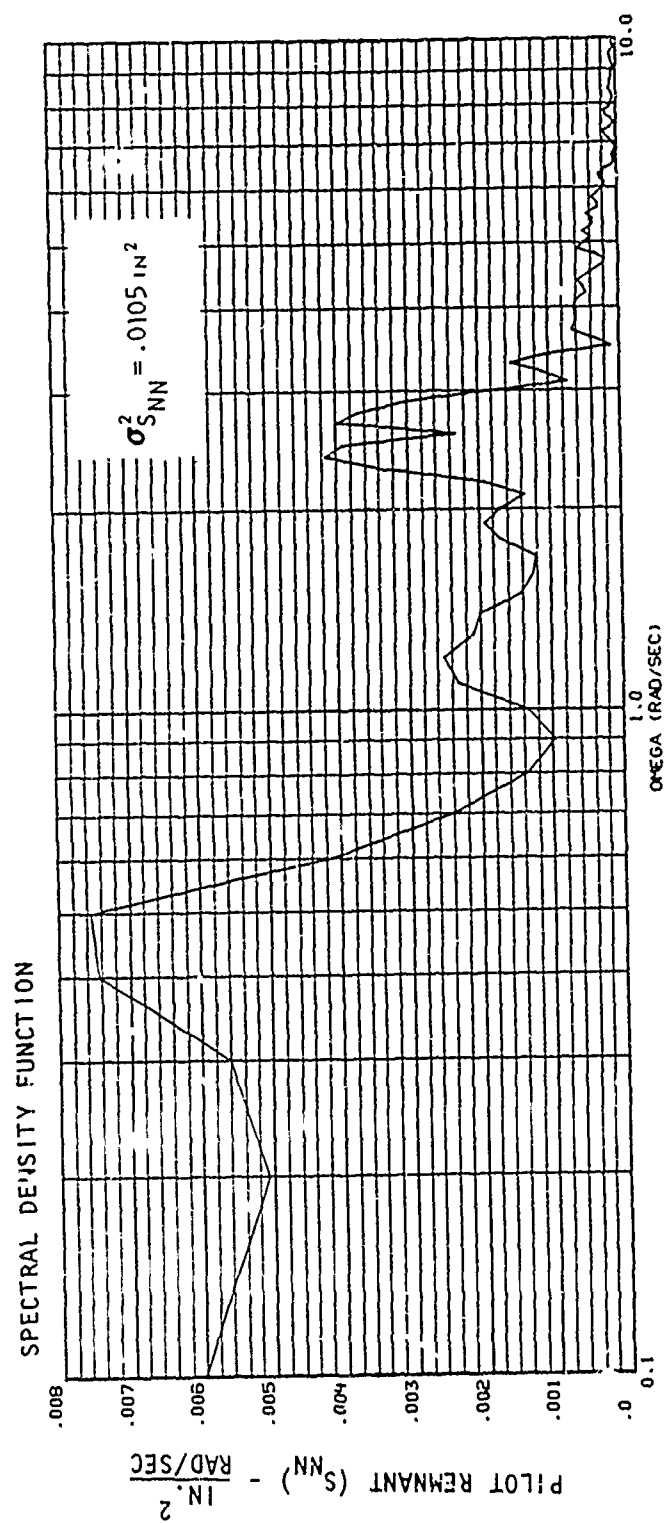
Figure 44. Power Spectral Density of Pilot Remnant (No. 01A11)

71

The phase plots, in general, are poor matches to the amplitude ratio plots. Even where a rather positive indication of lead behavior is evident, as in figure 75, the phase noticeably exhibits less lead than expected. A simple time delay, unfortunately, will not solve the phase mismatch. A rather complex time delay with the delay time constant, τ_D, being a function of frequency is required. Run No. 01A11, mentioned earlier, is shown again in figure 45 with a postulated pilot model curve fit shown. The frequency response data can be matched by assuming the pilot adopted a lead term and a variable time delay. In the low-frequency range, he would exhibit a time delay of 1.0 second which is removed as the frequency increases until, at 3 rad per second, the time delay is zero. Figure 45 shows the resulting curve fit. It can be expected that the majority of the AR cases can be handled by using a variable time delay to account for the phase mismatch. Without the benefit of an automatic curve fit program (as was achievable for the TF data), such pilot model construction would require lengthy and tedious effort. However, since the AR task did reflect a variation in pilot rating with SAS status, another pilot model construction was made for run No. 02A2 which was a SAS-off condition with a pilot rating of 9. Figure 46 shows the bode plot obtained from the pilot traces and a pilot model curve fit based on a double lead and a variable time delay. For the curve fit, a larger time delay (1.5 seconds) was necessary than for the SAS-on condition in figure 45. In addition, a double lead of 1.0 second was also necessary for a better amplitude match. The physical significance or even the possibility of such frequency-dependent time delay relative to pilot behavior is not considered. The pilot remnant PSD for this run is shown in figure 47. No further attempts were made to develop pilot models for the various AR data involving turbulence and structural mode variations.

Examination of the spectral density functions for the AR cases reveals a characteristic which might be of use in correlating pilot ratings with pilot activity. In many of the SAS-off cases, the pitch stick spectral density function exhibits a high frequency peak which is as large or larger than any existing in the frequency range associated with the tracking task. Figure 36 illustrates the case for run No. 01A11 which is SAS-on with a rating of 3 and run No. 04A1 which is SAS-off with a rating of 5. Assuming this is a distinguishing characteristic between good and bad pilot ratings, the rest of the AR data were examined for such traits. For pilot B, of the seven cases with a 5 rating, four checked out in the manner previously described, while for 17 cases with a 3 rating, all checked out. For pilot C, all eight of the cases rated 4 checked out, while six of the 10 cases rated 2 checked out. Since, in general, the tracking error spectral density function does not show a similar behavior, this additional pilot activity is similar in function to pilot remnant effects. As indicated earlier, however, the pitch stick standard deviation does not correlate with pilot rating. Further work in this area of spectral density function analysis may be fruitful.

72
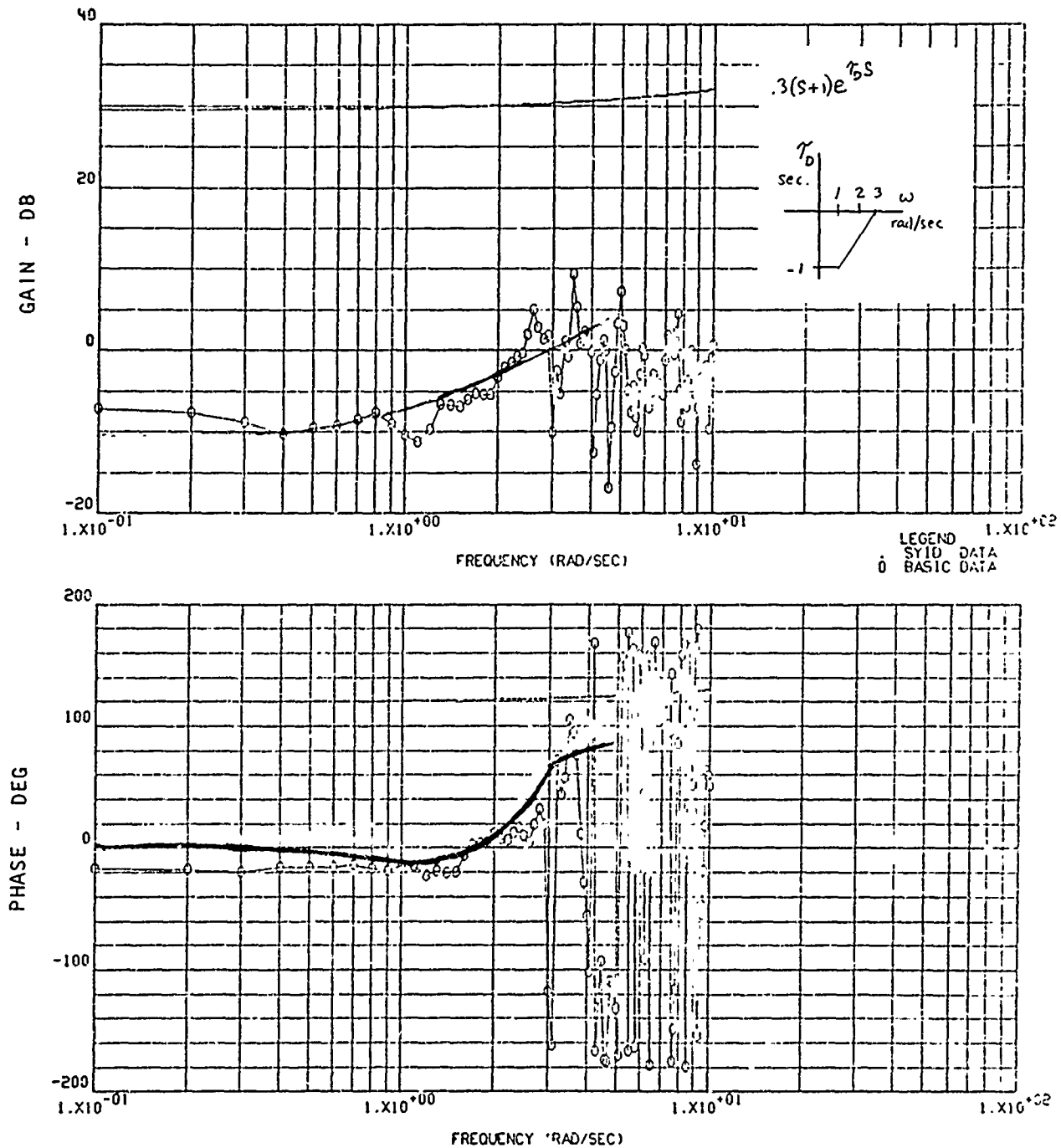
Figure 45. Pilot Model Curve Fit for AR SAS-ON Case (No. 01A11)

73
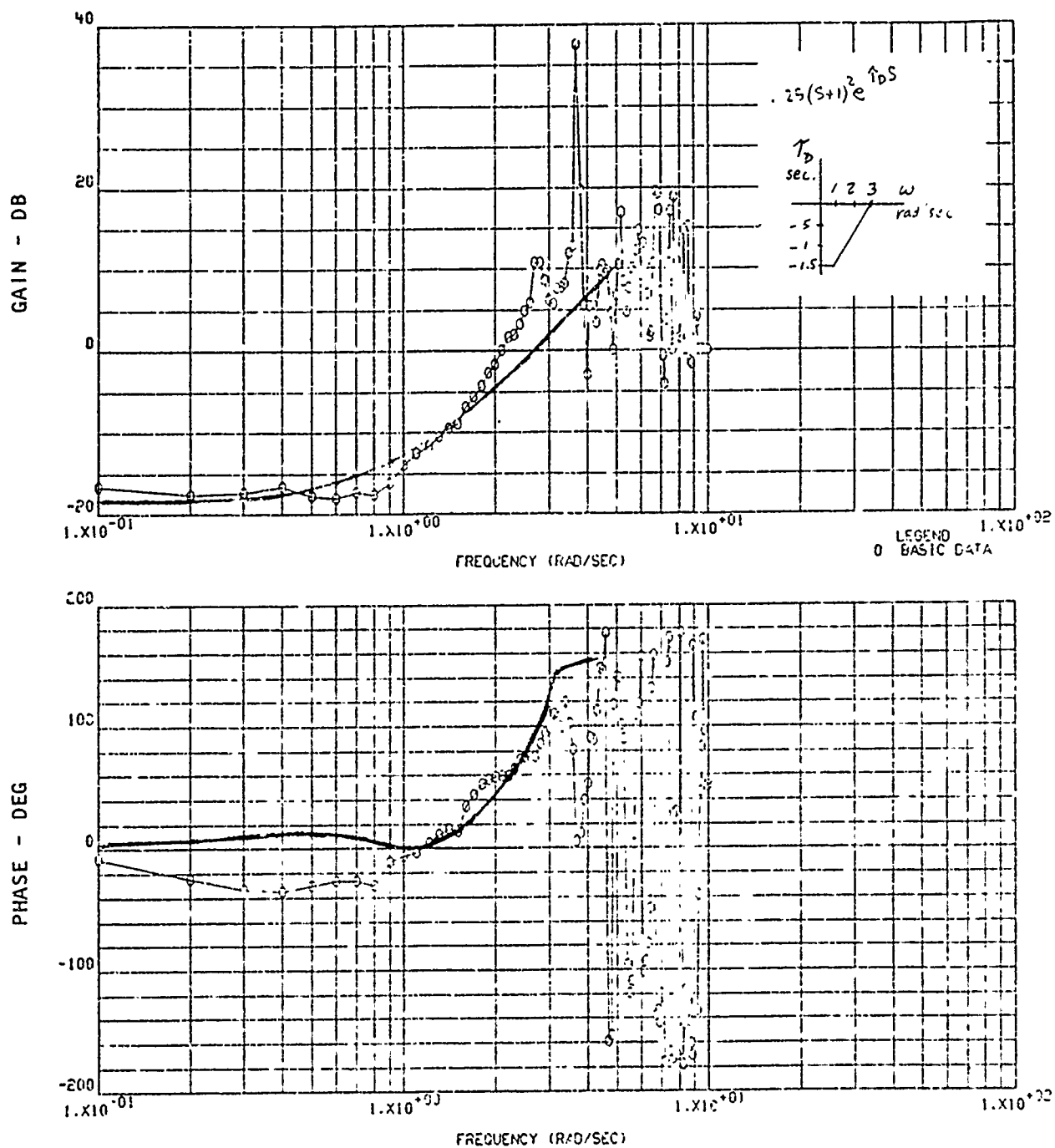
Figure 46. Pilot Model Curve Fit for AR SAS-OFF Case (No. 02A2)

74
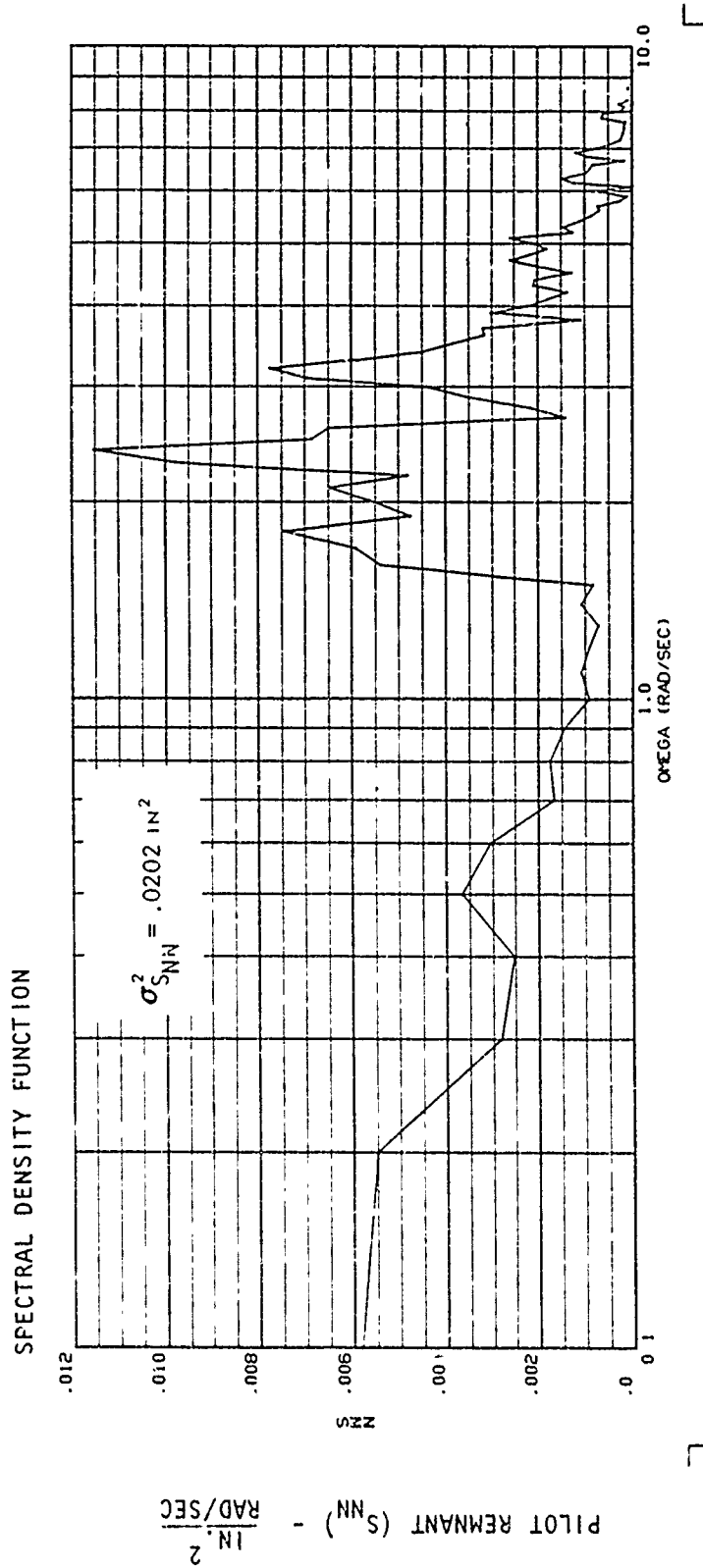
Figure 47. Power Spectral Density of Pilot Remnant (No. 02A2)

75

SECTION VII

DISCUSSION OF PILOT RATING PREDICTION

PAPER PILOT MODIFICATIONS

Since the terrain-following (TF) simulation did not corroborate past investigations relative to adverse effects of turbulence on pilot ratings, the rating algorithm used in reference 2 was not modified. However, the pilot model was changed to reflect the characteristic lead-lag form found in the simulation data. Further modifications were made to incorporate the selected vehicle's aerodynamic characteristics, its three primary longitudinal structural modes, and its control system and display signal format. The shaping of the tracking command signal was also changed from a first-order lag to a second order so as to more closely approximate the characteristics of the simulated γ_c. This modified paper pilot computer program is available at the Air Force Flight Dynamics Laboratory, Wright-Patterson AFB, Ohio.

TERRAIN-FOLLOWING RESULTS

For the TF runs, the pilot lag term was set as a constant with the pilot gain and lead time constant being the variable parameters. For the rigid aircraft and zero turbulence level, the paper pilot computed a pilot rating of 1.15 with a pilot gain of 4.0 inch per g and a zero lead time constant. A pilot time delay of 0.42 second was included in the paper pilot. These results can be compared directly with TF run No. 1015 which, as shown in table IV, has the same task conditions. The computed pilot model from this simulation run is also shown in table IV and plotted in figure 49. For convenience, the pilot model plot is reshown as figure 48 but with the addition of the paper pilot computed pilot model. The match including the steady-state gain is surprisingly good.

Additional paper pilot runs with different turbulence levels and with structural modes included showed very little variation in pilot rating and pilot model parameters. Table III lists the values obtained for the various combinations evaluated. Although the analytically derived pilot ratings are low compared to those in the TF simulation, the same insensitivity to turbulence and structural mode effects is evident.

AIR REFUELING RESULTS

The inconsistency in the pilot model data obtained in the air-refueling (AR) simulation made it difficult to generate paper pilot data for

Preceding page blank
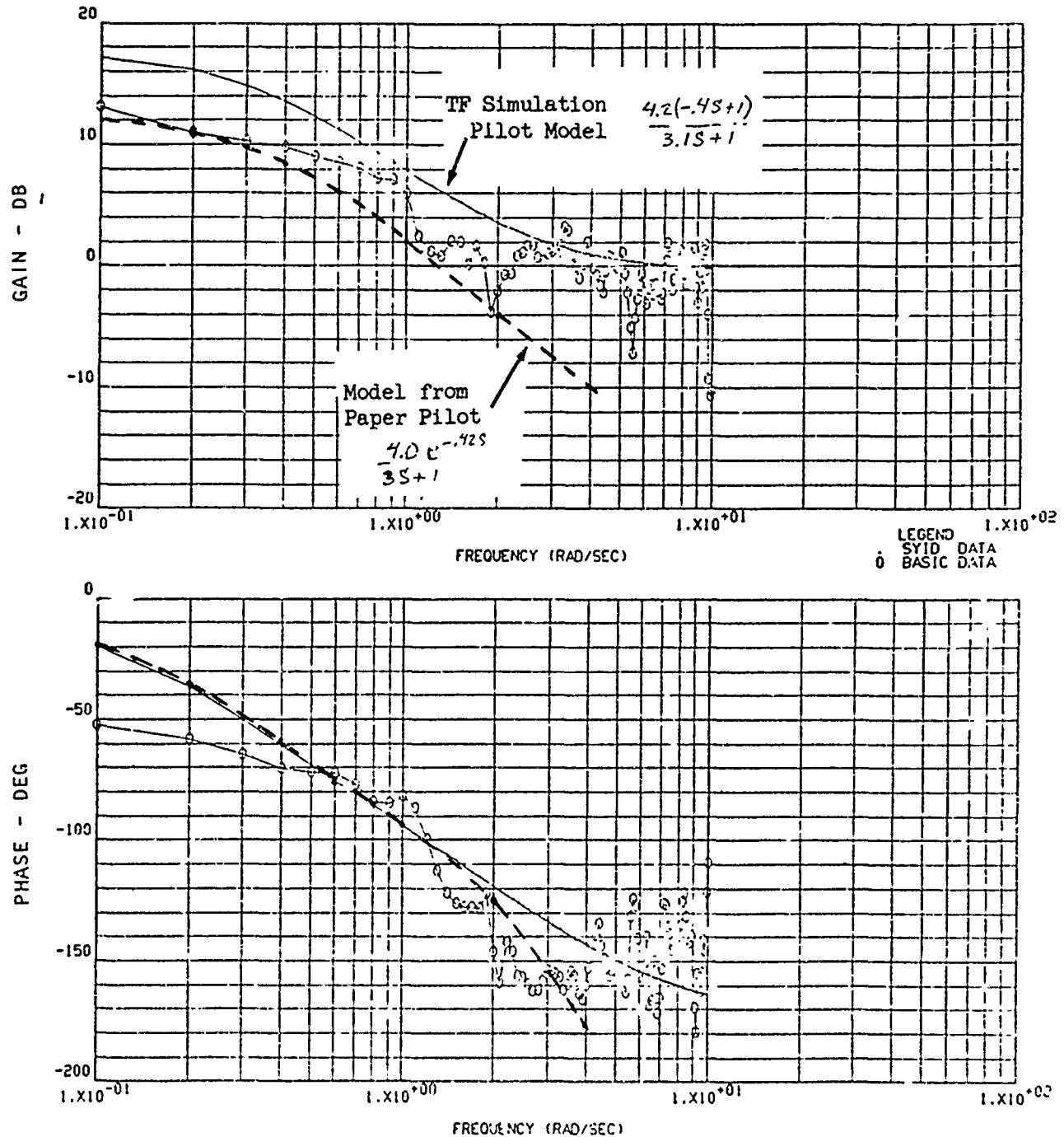
Figure 48. Comparison of TF Simulation Pilot Model and Paper
Pilot Generated Pilot Model

78

comparison. Since the TF and AR results showed little effect due to turbulence and structural modes, only three runs are shown in table III for the AR results. These represent conditions similar to those evaluated in the AR simulation which resulted in pilot rating changes. The first two AR conditions represented the change in SAS command augmentation gains, as depicted in figure 34. The primary effect is in pilot gain and, not unexpectedly, little difference in paper pilot results is shown. The third condition is for the SAS-off case and again little change is noted, unlike the simulation. The ratings are also consistently lower than those obtained in the simulation, again as was observed for the terrain following. However, the AR paper pilot did reflect a lead required task compared to TF by reducing the pilot lag to zero. This direction of pilot model change agrees with the simulation data.

TABLE III. PAPER PILOT RESULTS FOR SIMULATION TASKS

Task	Structural Modes	SAS Status	Gust Level (fps)	Pilot Rating	σ_γ (rad)	σ_q (rad/sec)	$\sigma_{n_{z_p}}$ (g)	σ_w (fps)	σ_{δ_s} (rad)	K_p	T_1	T_p	T_d
Terrain Following	No	On	0	1.149	0.0729	0.0197	0.4614	16.04	0.0296	4	0	3	0.42
			6	1.150	0.0729	0.0208	0.4766	17.08	0.0300	4	0	3	0.42
			12	1.1511	0.0730	0.0239	0.5197	19.89	0.0311	4	0	3	0.42
	Yes	On	0	1.150	0.0728	0.0194	0.4580	16.10	0.0293	4	0	3	0.42
			6	1.150	0.0729	0.0205	0.4802	16.66	0.0308	4	0	3	0.42
			12	1.151	0.0730	0.0245	0.5413	18.26	0.0350	4	0	3	0.42
Air Refueling	No	On KeX4	0	1.22	0.0171	0.005	0.0836	6.67	0.0077	8	0	0	0.42
		On KeX1	0	1.17	0.0176	0.007	0.0989	7.59	0.0093	35	0	0	0.42
		Off	0	1.20	0.0175	0.0127	0.1445	7.73	0.00	6	0	0	0.42

$$-K_p \frac{(T_1 S + 1)}{(T_p S + 1)} e^{-T_d S}$$

SECTION VIII

CONCLUSIONS

The examination in this study of a large, flexible bomber in a turbulent environment was engendered because of past difficulties, reported by other investigators, of correlating increasing pilot rating with pilot characteristics and performance parameters when turbulence levels were increasing. Piloted simulation, conducted in this study, of two longitudinal tracking tasks under high levels of turbulence revealed little consistent correlation between pilot rating and turbulence levels. Pilot acceleration, aggravated by both turbulence and structural mode excitation, did not influence pilot rating. The pilots participating in the simulation seemed able to divorce their task rating from their motion environment. Only when the vehicle short period characteristics were varied (e.g., SAS off) did pilot rating change, an indication that the higher frequency effects of turbulence and structural mode excitation did not influence their primary tracking task.

Pilot performance and response parameters used in past pilot rating prediction methods did not correlate with pilot ratings. Pilot acceleration, likewise, did not provide any consistent clue to the pilot ratings. Examination of the spectral density functions for the pitch stick (pilot output) and horizontal bar (pilot input) revealed a degree of correlation between pilot rating and the pitch stick power distribution in terms of frequency. A dominant peak in the spectral density function unrelated to the tracking task frequency content seemed to indicate a poorer control of the vehicle by the pilot and, as a result, a poorer pilot rating.

The pilot models constructed from the terrain-following (TF) simulation are considerably different from those required for the air-refueling (AR) simulation. A lead-lag model with a negative lead consistently fitted the TF task data which showed generally good coherence characteristics. The AR data varied in form considerably from simple leads to complex lead lags, to notch filters, and to simple lags. In general, however, if only data showing high coherence are used, the characteristic linear pilot model is of a lead-only transfer function. A frequency dependent time delay is required to provide reasonably good phase matching.

The results of the study indicate that current flying qualities specifications should continue to maintain a separation from ride qualities considerations. Longitudinal tracking tasks of the nature evaluated were rated on the basis of the vehicle short-period dynamics and not on the high-frequency pilot motion caused by turbulence and/or structural modes.

DATA PROCESSING AND FREQUENCY ANALYSIS PROGRAM

PRINCIPAL THEORIES

Statistical spectral analysis is a widely recognized tool for analyzing time-varying data from a variety of experimental situations. In this program, the emphasis is placed on cross-spectral analysis of paired time records representing an input time sequence and an output time sequence from some experimental time-invariant system. Cross-spectral analysis provides a measurement of the frequency response function of that system. This is possible even when the output is contaminated by noise disturbances arising, for example, from measurement errors or instrumentation variation. A transfer function can often be determined from the frequency response function by an iterative least squares technique. The principal theories (computing formulas) for the program are discussed herein.

NUMERICAL FOURIER TRANSFORMS

This program uses a rectangular integration with end-point corrections to obtain the numerical (also called finite discrete) Fourier transform. Because Fourier transforms are, in general, complex quantities (i.e., of the form $Z(j\omega) = U(j\omega) + jV(j\omega)$), the numerical or finite discrete Fourier transform may be represented in two parts as

$$U(j\omega_r) = T\sum_{k=n}^{N-n} x(kT) \cdot \cos k\omega_r T$$

and

$$V(j\omega_r) = T\sum_{k=n}^{N-n} x(kT) \cdot \sin k\omega_r T$$

where

T = sampling period in seconds

N = number of data points in the data set

n = number of end points to be weighted with end-point corrections

x(kT) = the time sequence (or correlation sequence) to be transformed

AUTOCORRELATION AND CROSS-CORRELATION FUNCTIONS

The following formulas apply to jointly stationary time series with zero mean values.

Autocorrelation of Input

The input time series is denoted by $y(t)$. The corresponding auto-correlation function is denoted by $R_{yy}(mT)$ and is given by

$$R_{yy}(mT) = \frac{1}{N-m} \sum_{k=1}^{N-m} y_k \cdot y_{k+m} \qquad m = 0,1,2,\ldots M$$

where

m = "lag number"

M = maximum number of lags

T = sampling period in seconds

Note that this calculation is for positive lag numbers only because R_{yy} is an even function, i.e.,

$$R_{yy}(mT) = R_{yy}(-mT)$$

Autocorrelation of Output

The output time series is denoted by $x(t)$ and its corresponding autocorrelation function by $R_{xx}(mT)$, which is given by

84

$$R_{xx}(mT) = \frac{1}{N-m} \sum_{k=1}^{N-m} x_k \cdot x_{k+m} \qquad m = 0,1,2,\ldots M$$

where "M," and "T" are as previously defined, and R_{xx} is, likewise, an even function.

Cross-Correlation Functions

Both time series $x(t)$ and $y(t)$ play a role in the calculations of the cross-correlation functions. The cross-correlation function $R_{xy}(mT)$ between output $x(t)$ and input $y(t)$ is given by

$$R_{xy}(mT) = \frac{1}{N-m} \sum_{k=1}^{N-m} x_k \cdot y_{k+m} \qquad m = 0,1,2,\ldots M$$

and the cross-correlation function $R_{yx}(mT)$ between input $y(t)$ and output $x(t)$ by

$$R_{yx}(mT) = \frac{1}{N-m} \sum_{k=1}^{N-m} y_k \cdot x_{k+m} \qquad m = 0,1,2,\ldots M$$

These functions are neither odd nor even, but satisfy the relation (reference 8).

$$R_{xy}(mT) = R_{yx}(-mT)$$

AUTOCORRELATION AND CROSS-SPECTRAL DENSITY FUNCTIONS

Two procedures are described, each leading to one-sided estimates of the same spectral density functions, which are defined for positive frequencies only. The first procedure is called the "direct" method. The second procedure is called the "autocorrelation" method, but it applies to cross-correlation as well. Either or both methods may be requested.

Direct Method

The direct method starts with output time sequence $x(t)$ and input time sequence $y(t)$ and obtains the numerical or finite discrete Fourier transforms of both sequences; i.e., it calculates $X(j\omega)$ and $Y(j\omega)$ for a specified arbitrary set of frequencies ω. These transforms are complex values and may be represented as real $RX(j\omega)$, $RY(j\omega)$, and imaginary $IX(j\omega)$, $IY(j\omega)$ parts according to

$$X(j\omega) = RX(j\omega) + jIX(j\omega)$$

and

$$Y(j\omega) = RY(j\omega) + jIY(j\omega)$$

Estimates of the spectral density functions are then obtained as indicated:

$$S_{xx}(j\omega) = [RX(j\omega)-jIX(j\omega)] \; [RX(j\omega)+jIX(j\omega)]$$

$$S_{xy}(j\omega) = [RX(j\omega)-jIX(j\omega)] \; [RY(j\omega)+jIY(j\omega)]$$

$$S_{yx}(j\omega) = [RY(j\omega)-jIY(j\omega)] \; [RX(j\omega)+jIX(j\omega)]$$

$$S_{yy}(j\omega) = [RY(j\omega)-jIY(j\omega)] \; [RY(j\omega)+jIY(j\omega)]$$

By introducing the notion of cospectral density $C_{xy}(j\omega)$ and quadrature-spectral density $Q_{xy}(j\omega)$, the cross-spectral density terms $S_{xy}(j\omega)$ and $S_{yx}(j\omega)$ may be expressed as follows:

$$S_{xy}(j\omega) = C_{xy}(j\omega) + jQ_{xy}(j\omega)$$

and

$$S_{yx}(j\omega) = C_{yx}(j\omega) + jQ_{yx}(j\omega)$$

it may be seen that

$$C_{xy}(j\omega) = RX(j\omega)*RY(j\omega)+IX(j\omega)*IY(j\omega)$$

$$C_{yx}(j\omega) = RX(j\omega)*RY(j\omega)+IX(j\omega)*IY(j\omega)$$

and

$$Q_{xy}(j\omega) = RX(j\omega)*IY(j\omega)-RY(j\omega)*IX(j\omega)$$

$$Q_{yx}(j\omega) = RX(j\omega)*IY(j\omega)+RY(j\omega)*IX(j\omega)$$

Therefore

$$C_{xy}(j\omega) = C_{yx}(j\omega)$$

and

$$Q_{xy}(j\omega) = -Q_{yx}(j\omega)$$

The time sequences $x(t)$ and $y(t)$ are neither even nor odd. Because the sequences are of finite duration, the end-points introduce integration errors which may be partially compensated by an end-point correction scheme. A three-point correction formula known as Simpsons half rule (reference 9) with weights 5/12, 8/12, and -1/12 is used in the direct method.

Autocorrelation Method

This method starts with correlation sequences R_{xx}, R_{xy}, R_{yy} and obtains the numerical or finite discrete Fourier transforms for an arbitrary set of frequencies, on individual or combined correlation sequences, as follows:

$$S_{xx}(j\omega_h) = \text{Re} \left[\mathcal{F}\{R_{xx}(mt)\} \right]$$

$$S_{yy}(j\omega_h) = \text{RE} \left[\mathcal{F}\{R_{yy}(mt)\} \right]$$

$$C_{xy}(j\omega_h) = \text{RE} \left[\mathcal{F}\{\rho_c(mt)\} \right]$$

$$Q_{xy}(j\omega_h) + \text{Im} \left[\mathcal{F}\{\rho_q(mt)\} \right] \quad h = 0,1,\ldots M$$

where

$$\rho_c(mt) = 1/2 \left[R_{xy}(mt) + R_{yx}(mt) \right]$$

$$\rho_q(mt) = 1/2 \left[R_{yx}(mt) - R_{xy}(mt) \right]$$

As previously noted

$$S_{xy}(j\omega) = C_{xy}(j\omega) + jQ_{xy}(j\omega)$$

$$S_{yx}(j\omega) = C_{xy}(j\omega) - jQ_{xy}(j\omega)$$

The autocorrelation sequences $R_{xx}(mT)$ and $R_{yy}(mT)$ are both even functions extending to negative values of the argument mT.

The Fourier transform for either function, say $R_{xx}(mT)$, may be expressed as

$$S_{xx}(j\omega_h) = T \sum_{mT=1}^{M} R_{xx}(mT)\cos m\omega_h T$$

$$= TR_{xx}(0) + 2T \sum_{mT=1}^{M} R_{xx}(mT)\cos m\omega_h T$$

Using a two-point correction for the end-points with equal weights of 1/2 results in the algorithm as given by equations 11 through 14 of reference 10. The same corrections are used in this program. The resulting expressions are

$$S_{xx}(j\omega_h) = T\left[R_{xx}(0) + 2 \sum_{mT=1}^{M-1} R_{xx}(mT)\cos m\omega_h T \right.$$
$$\left. + R_{xx}(MT)\cos M\omega_h T \right]$$

Likewise,

$$S_{yy}(j\omega_h) = T\left[R_{yy}(0) + 2 \sum_{mT=1}^{M-1} R_{yy}(mT)\cos m\omega_h T \right.$$
$$\left. + R_{yy}(MT)\cos M\omega_h T \right]$$

Since $\rho_c(mT)$ is an even function, its Fourier transform may be obtained in the same manner as for R_{xx} and R_{yy} previously noted, i.e.,

$$C_{xy}(j\omega_h) = \frac{T}{2}\left[\rho_c(0) + 2 \sum_{mT=1}^{M-1} \rho_c(mT)\cos m\omega_h T \right.$$
$$\left. + \rho_c(MT)\cos M\omega_h T \right]$$

89

Since $\rho_q(mT)$ is an odd function, its Fourier transform may be expressed as

$$Q_{xy}(j\omega_h) = \frac{T}{2}\left[0 + 2\sum_{mT=1}^{M-1}\rho_q(mT)\sin m\omega_h T + \rho_q(MT)\sin M\omega_h T\right]$$

Variability of Spectral Density Estimates

This discussion applies to the autocorrelation method only.

Variability of the spectral density calculations is said to be chi-squared distributed with degrees of freedom $2N/M$ when S_{xx} and S_{yy} are suitably normalized. This drops to N/M at frequencies $\omega = 0$ and $\omega = \pi/T$. The parameters N, M, and T are, respectively, the number of time data points, the number of lags used to calculate the autocorrelation sequence, and the sampling period in seconds. The required conditions for a chi-squared variate are that $x(t)$ and $y(t)$ be Gaussian and their ideal spectral density functions S_{xx} and S_{yy} be reasonably constant in the interval

$$\omega_h - \frac{2\pi}{mT} \le \omega \le \omega_h + \frac{2\pi}{mT}$$

These considerations rest with the user to interpret for his own use. Refer to Part 1, section 14, of reference 11 for more detail.

This program was designed so that the ratio of N/M would not be less than 2 whenever the autocorrelation method is specified. This is the recommended minimum for that ratio and is equivalent to two degrees of freedom in the chi-square sense. The program calculates the value of M from the punched card entry for DF, the frequency increment, according to

$$M = \frac{\pi}{T*DF} \qquad M < 500$$

Since the program requires

$$\frac{N}{M} \geq 2$$

then, substituting from $M = \dfrac{\pi}{T*DF}$ and rearranging gives the required range for DF, i.e.,

$$DF \geq \frac{2\pi}{N*T} \qquad\qquad N \leq 10,000$$

If DF<2π/N*T the program will increase its punched card value 25 percent, i.e.,

$$DF' = \frac{5}{4} DF$$

Then, if

$$DF' < \frac{2\pi}{N*T}$$

the program will substitute the direct method for the autocorrelation method and continue.

Very often, a choice in sampling rate f_s for the time sequences x(t) and y(t) may be exercised before the data are digitized. For data sampled several factors above the bandwidth of the system producing the data, the program offers a simple reduction feature. However, one must be careful not to alias the data by sample reduction. Aliasing is said to occur whenever the sampling frequency is less than twice the highest frequency of interest. For example, consider a low bandwidth system bandlimited at 10 radians per second. The slowest sampling rate that avoids aliasing is

$$f_s = \frac{10}{\pi} \approx 3 \text{ samples per second}$$

91

SMOOTHING TO IMPROVE SPECTRAL ESTIMATES

In estimating spectral densities, an ideal representation for the time function x(t) is a record of infinite length. In practical situations, only short intervals of time are available for analysis. Also, e may require shorter intervals of time for other considerations than are actually available. A mathematical means which literally accounts for "turning the time function on and off" is to use a spectral filter or window. A so-called hanning window is used in this program (reference 11). This filter smooths the spectral density estimates across three spectral points.

COHERENCE ESTIMATES

Coherence is a measure of the degree to which two time series x(t) and y(t) are related by a linear model of the type shown here.
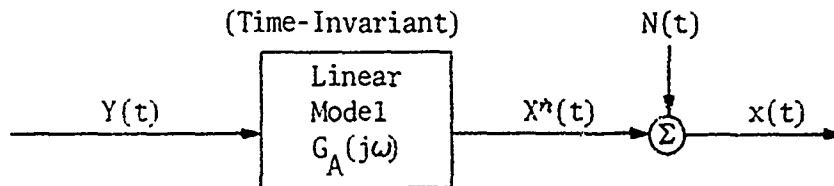
where N(t) is extraneous noise. The two time series x(t) and y(t) are supposed to be jointly "weakly" stationary (i.e., the values of their first and second moments are independent of the choice of the time origin). The noise disturbance, N(t), must be uncorrelated with the input. For classical correlation analysis, the linear model, $G_A(j\omega)$ may be viewed on a conceptual basis only. In any event, cross-spectral analysis seeks to determine the degree to which a linear relationship prevails between two time series and to characterize the linear model (or filter) which may be thought of as providing this relationship. Then, in terms of the spectral density functions, the coherence functions, denoted by $R^2(\omega)$, is given by

$$R^2(\omega) = \frac{C^2_{xy}(j\omega) + Q^2_{xy}(j\omega)}{S_{xx}(j\omega)S_{yy}(j\omega)}$$

92

As long as the linear model holds, the coherence function can also be expressed as

$$R^2(\omega) = 1 - \frac{S_{nn}(j\omega)}{S_{xx}(j\omega)}$$

where $S_{nn}(j\omega)$ is the spectral density function of the output disturbance, $N(t)$. The "total" spectral density of the output can be written in terms of $S_{nn}(j\omega)$ and $S_{x^*x^*}(j\omega)$ as

$$S_{xx}(j\omega) = S_{x^*x^*}(j\omega) + S_{nn}(j\omega)$$

where

$$S_{x^*x^*}(j\omega) = \text{the spectral density of } x^*(t)$$

Thus, it is apparent that coherence always assumes values between zero and one. In the absence of an output disturbance (i.e., if $S_{nn}(j\omega) = 0$ at some frequency ω_k) then $R^2(\omega_k) = 1$, and $x(t)$ and $y(t)$ are "perfectly coherent" (at that frequency. The opposite condition is where $R^2(\omega_k) = 0$, then $x(t)$ and $y(t)$ are "perfectly incoherent.")

It should be noted there is no theoretical significance to the preceding calculations of coherence when the <u>direct method</u> is specified, since the equation results in values of unity for all frequencies.

GAIN AND PHASE ESTIMATEES

Gain and phase estimates are obtained from the linear model as the ratio of $X(j\omega)/Y(j\omega)$, i.e.,

$$G_A(j\omega) = X(j\omega)/Y(j\omega)$$

where $G_A(j\omega)$ may be regarded as the frequency response function relating the input $y(t)$ to the output $x(t)$. It may also be regarded as the transfer function. If we multiply both numerator and denominator by the conjugate of $Y(j\omega)$, denoted by $\overline{Y}(j\omega)$, then

$$G_A(j\omega) = \frac{\overline{Y}(j\omega) * X(j\omega)}{\overline{Y}(j\omega) * Y(j\omega)}$$

but

$$\overline{Y}(j\omega) * X(j\omega) = C_{yx}(j\omega) + jQ_{yx}(j\omega)$$

and

$$\overline{Y}(j\omega) * Y(j\omega) = S_{yy}(j\omega)$$

so

$$G_A(j\omega) = \frac{C_{yx}(j\omega) + jQ_{yx}(j\omega)}{S_{yy}(j\omega)}$$

Therefore, the gain of this transfer function is computed as

$$\left| G_A(j\omega) \right| = \frac{\sqrt{C_{yx}^2(j\omega) + Q_{yx}^2(j\omega)}}{S_{yy}(j\omega)}$$

or since

$$C_{yx} = C_{xy} \quad \text{and} \quad Q_{yx} = -Q_{xy}$$

94

Then

$$G_A(j\omega) = \frac{\sqrt{C_{xy}^2(j\omega) + Q_{xy}^2(j\omega)}}{S_{yy}(j\omega)}$$

The phase of the transfer function is computed as

$$\phi_A(j\omega) = \tan^{-1}\left(-\frac{Q_{xy}(j\omega)}{C_{xy}(j\omega)}\right)$$

APPENDIX II

DATA ANALYSIS RESULTS FOR TERRAIN-FOLLOWING SIMULATION RUNS

The extensiveness of the data presented in this appendix is to provide a complete data base for the simulation tests.

A listing of the terrain-following (TF) runs and the significant data analysis results are given in table IV. Figures 49 through 58 present the data output plots obtained from the computer data processing of the listed runs. Each figure shows the pitch stick and horizontal bar (ADI flight director horizontal needle) time histories; the autocorrelation functions; the spectral density functions; the cospectra, quadrature spectra, and coherence functions; and finally the bode plots with the computed curve fit transfer functions. In many instances, it can be seen that a better amplitude ratio fit can be obtained if the curve fit is lowered in the amplitude plots without any phasing changes. This corresponds to just lowering the dc level of the transfer function. The values listed in table IV reflect these changes.

Figure 59 presents data generated using the pilot model as a means of closing the g control loop for the TF task. The specific model used is that listed under run No. 0418 in table IV. Computer runs were with this pilot model and also with an automatic TF system. The graphs indicate the pilot model performed quite satisfactorily.

Preceding page blank

TABLE IV. TERRAIN-FOLLOWING SIMULATION DATA ANALYSIS

| | | | | | Std Deviation | | | |
Figure	Run No.	Pilot	N_{z_p} Stick Effects	N_{z_p} Gust Effects	σ_{PS} Pitch Stick (in.)	σ_{HB} Horiz Bar (g)	Pilot Model	Pilot Rating
49	1015	A	None	None	0.361	0.134	$\dfrac{-4.2(0.40s - 1)}{3.1s + 1}$	2
50	0416	A	0.08 g RMS	None	0.386	0.198	$\dfrac{-2.5(0.28s - 1)}{1.5s + 1}$	2
51	0417	A	0.16 g RMS	None	0.321	0.149	$\dfrac{-2.8(0.36s - 1)}{1.4s + 1}$	2
52	0418	A	None	0.05 g RMS	0.321	0.130	$\dfrac{-3.4(0.30s - 1)}{1.2s + 1}$	2
53	0234	A	None	0.10 g RMS	0.280	0.096	$\dfrac{-4.7(0.28s - 1)}{1.4s + 1}$	2
54	0248	B	None	None	0.274	0.055	$\dfrac{-10\ (0.22s - 1)}{2.6s + 1}$	2
55	0252	B	0.08 g RMS	None	0.318	0.087	$\dfrac{-4.2(0.34s - 1}{1.0s + 1}$	2
56	0254	B	0.16 g RMS	None	0.307	0.092	$\dfrac{-3.7(0.31s - 1)}{0.90s + 1}$	4
57	0256	B	None	0.05 g RMS	0.297	0.066	$\dfrac{-6.0(0.29s - 1)}{1.1s + 1}$	2
58	0258	B	None	0.10 g RMS	0.314	0.079	$\dfrac{-5.0(0.33s - 1)}{1.1s + 1}$	2

Figure 49. TF Simulation Run No. 1015 Data

AUTO CORRELATION FUNCTIONS

Figure 49. TF Simulation Run No. 1015 Data (Cont)

100

CROSS CORRELATION FUNCTIONS

Figure 49.   TF Simulation Run No. 1015 Data (Cont)

101

SPECTRAL DENSITY FUNCTIONS

AUTO-CORRELATION METHOD
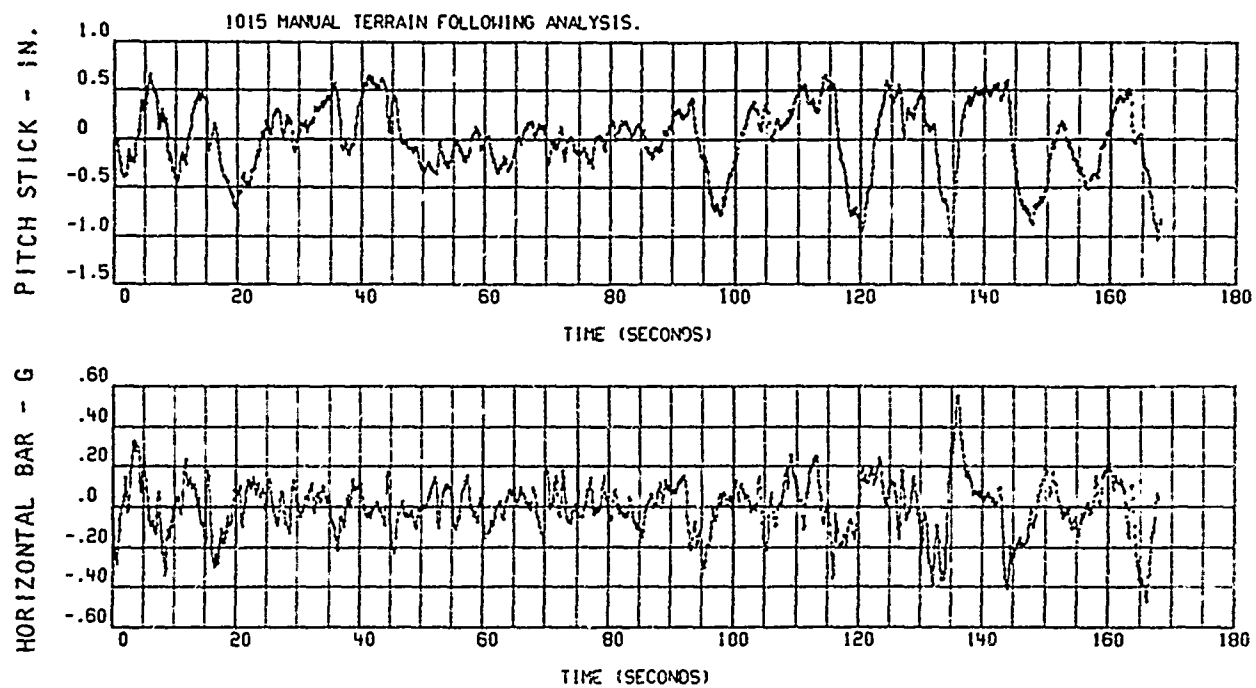
Figure 49. TF Simulation Run No. 1015 Data (Cont)
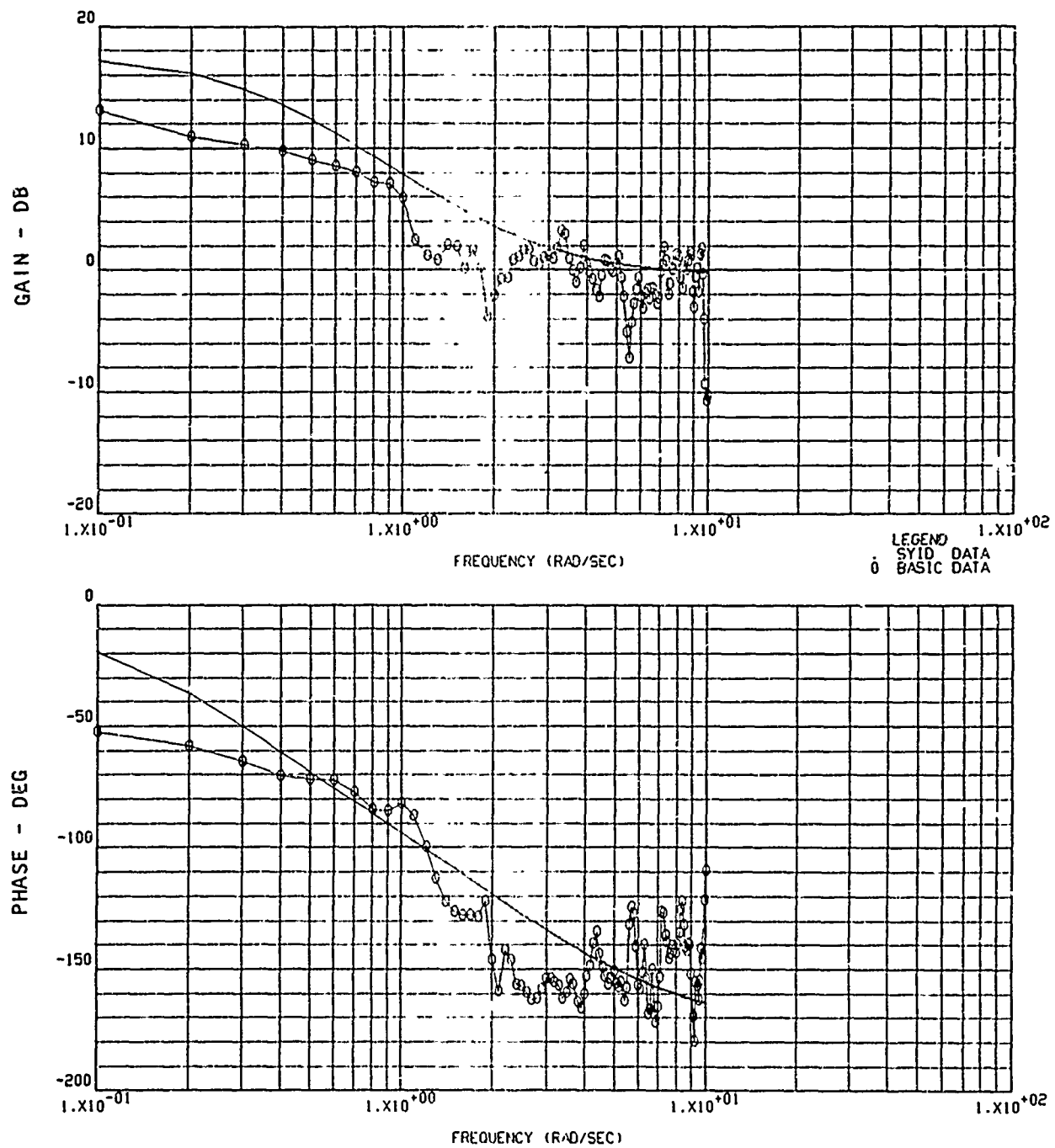
1015 MANUAL TERRAIN FOLLOWING ANALYSIS.

AUTO-CORRELATION METHOD
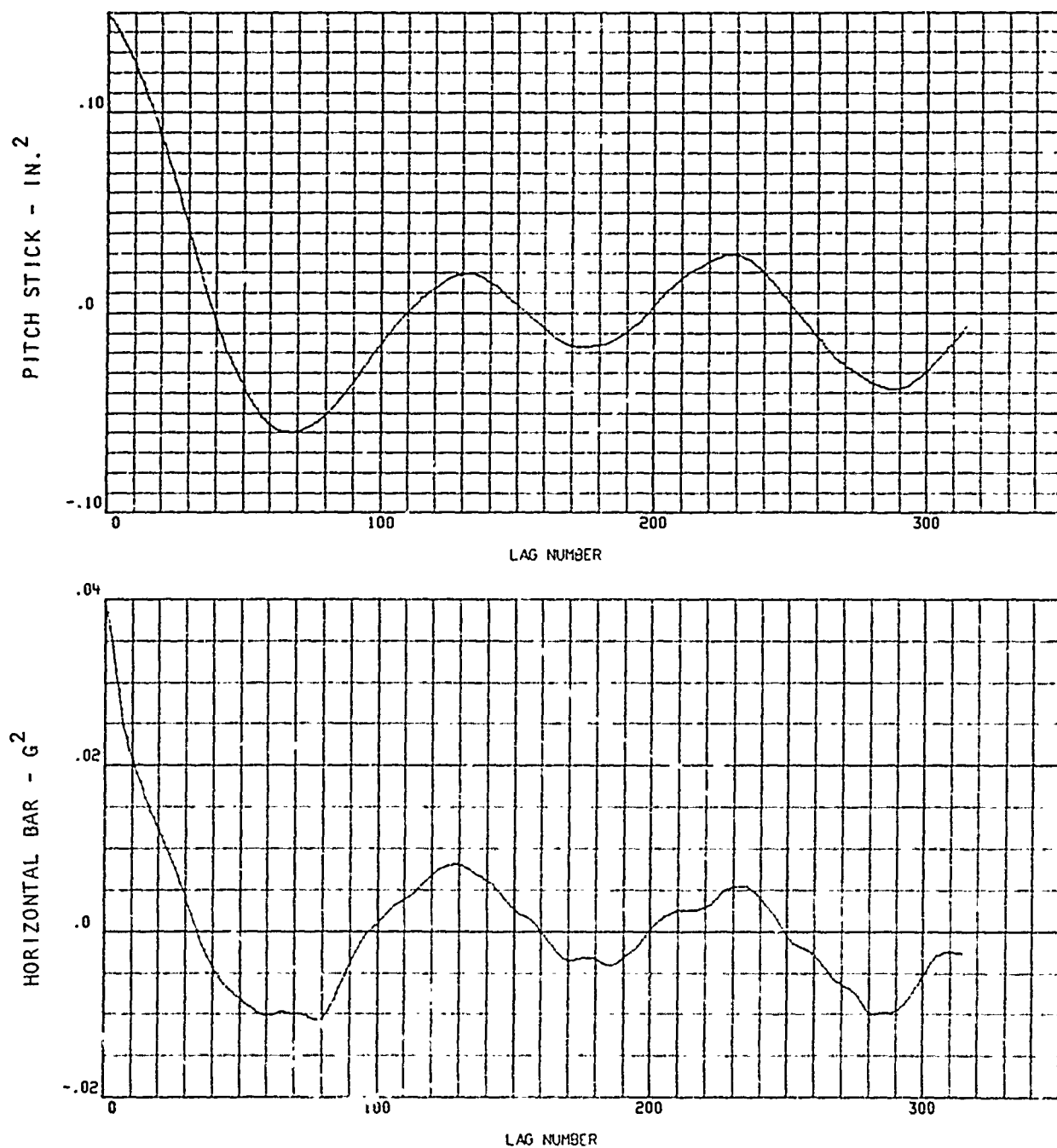
Figure 49. TF Simulation Run No. 1015 Data (Cont)

103
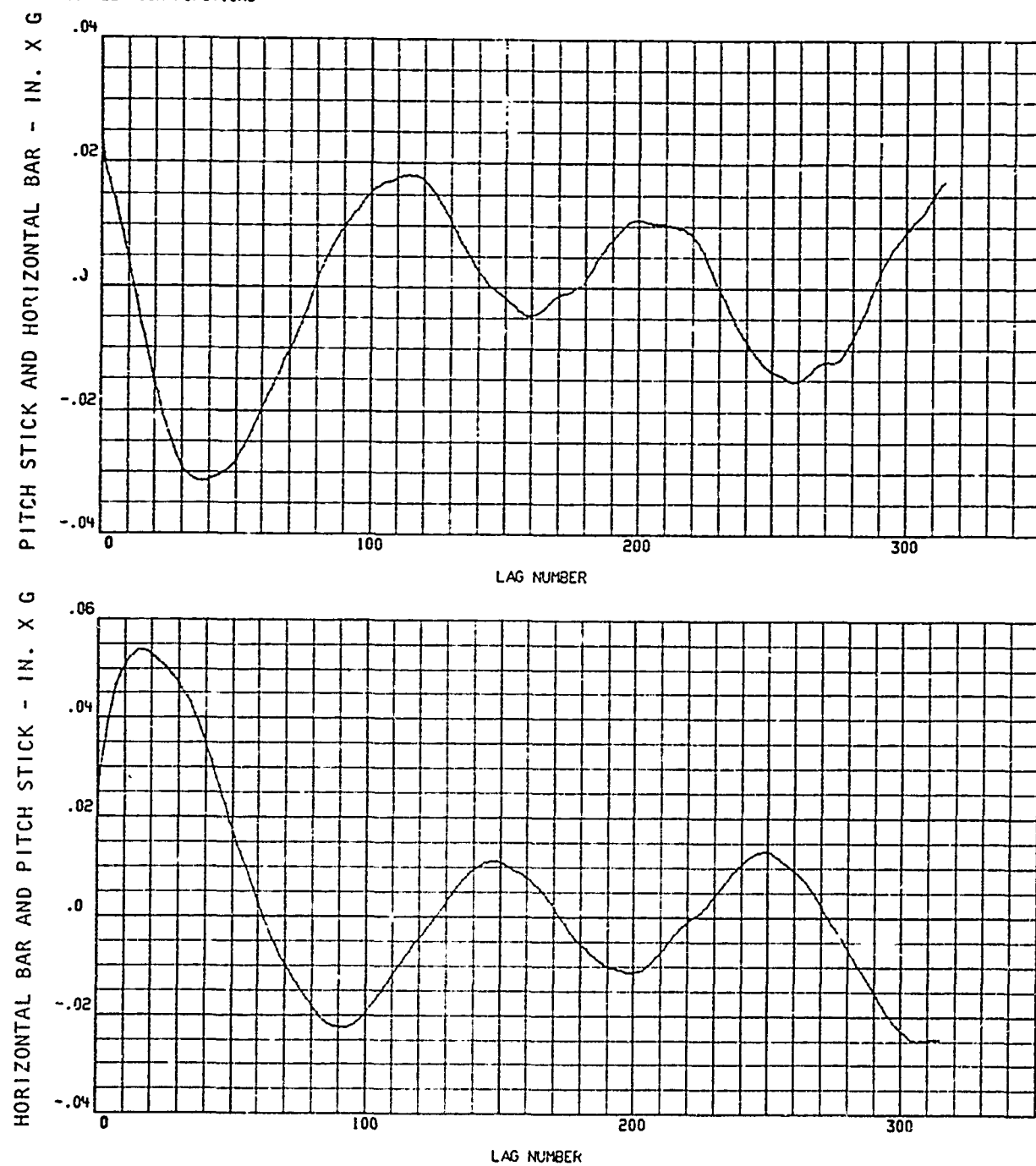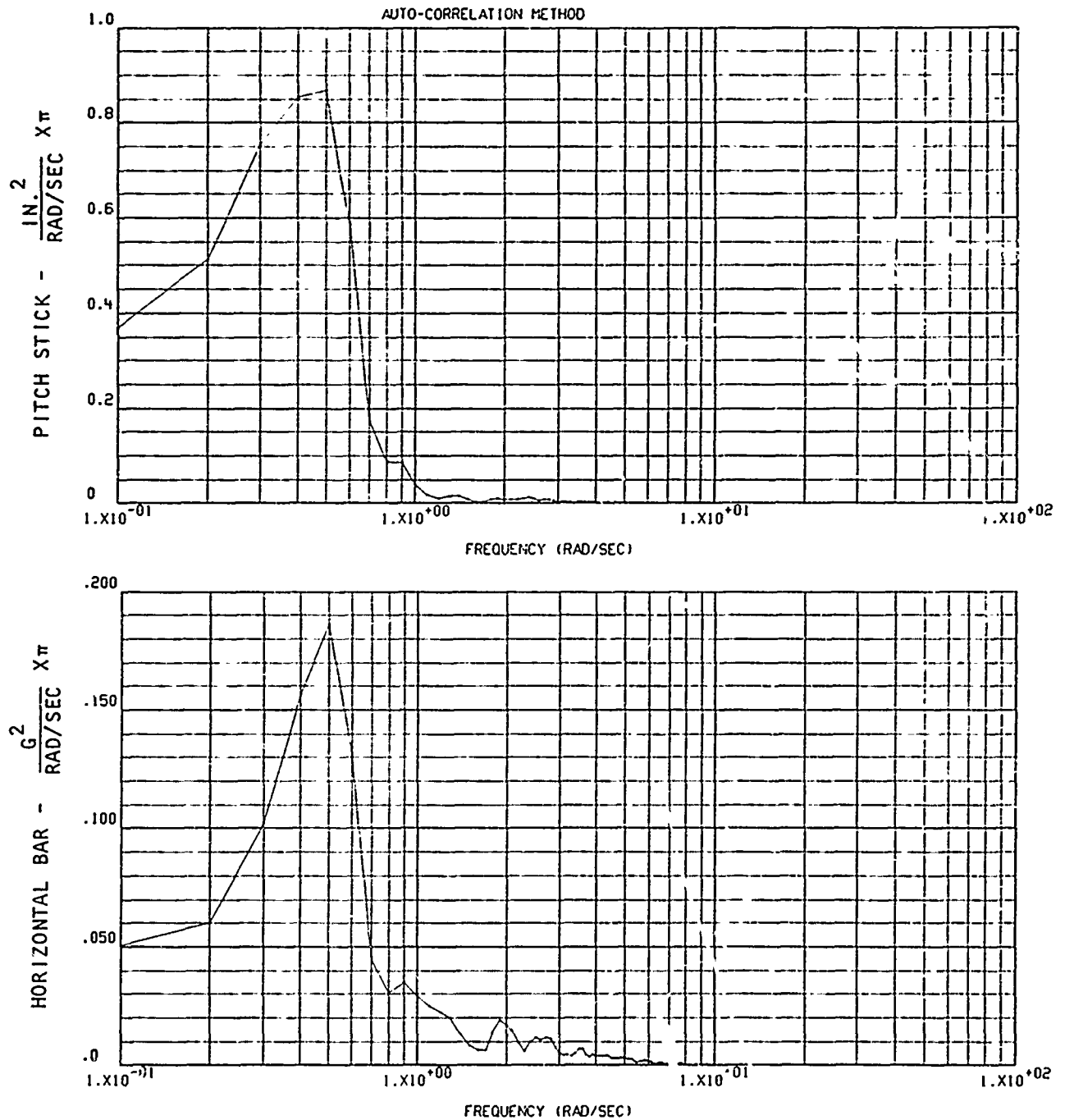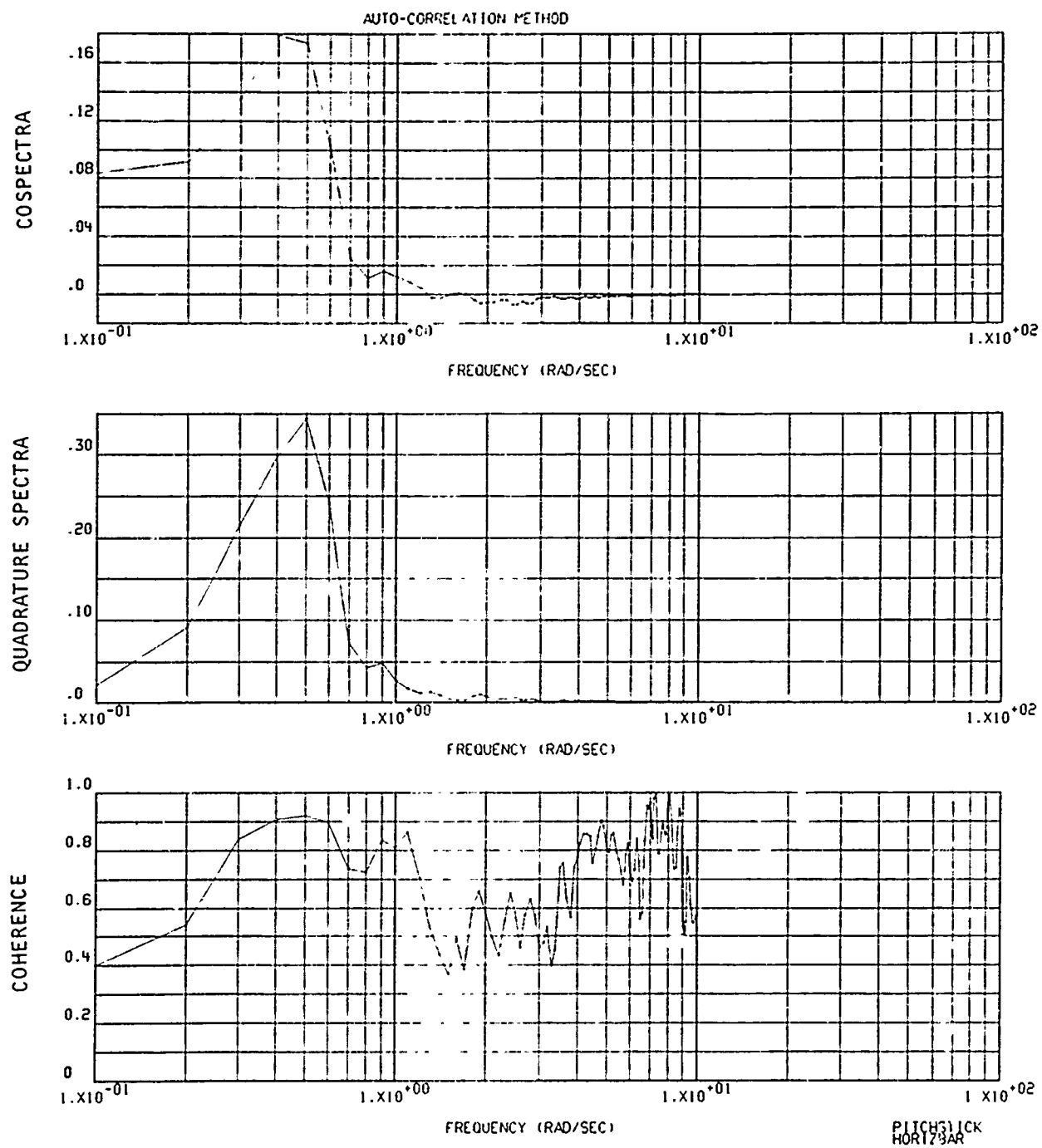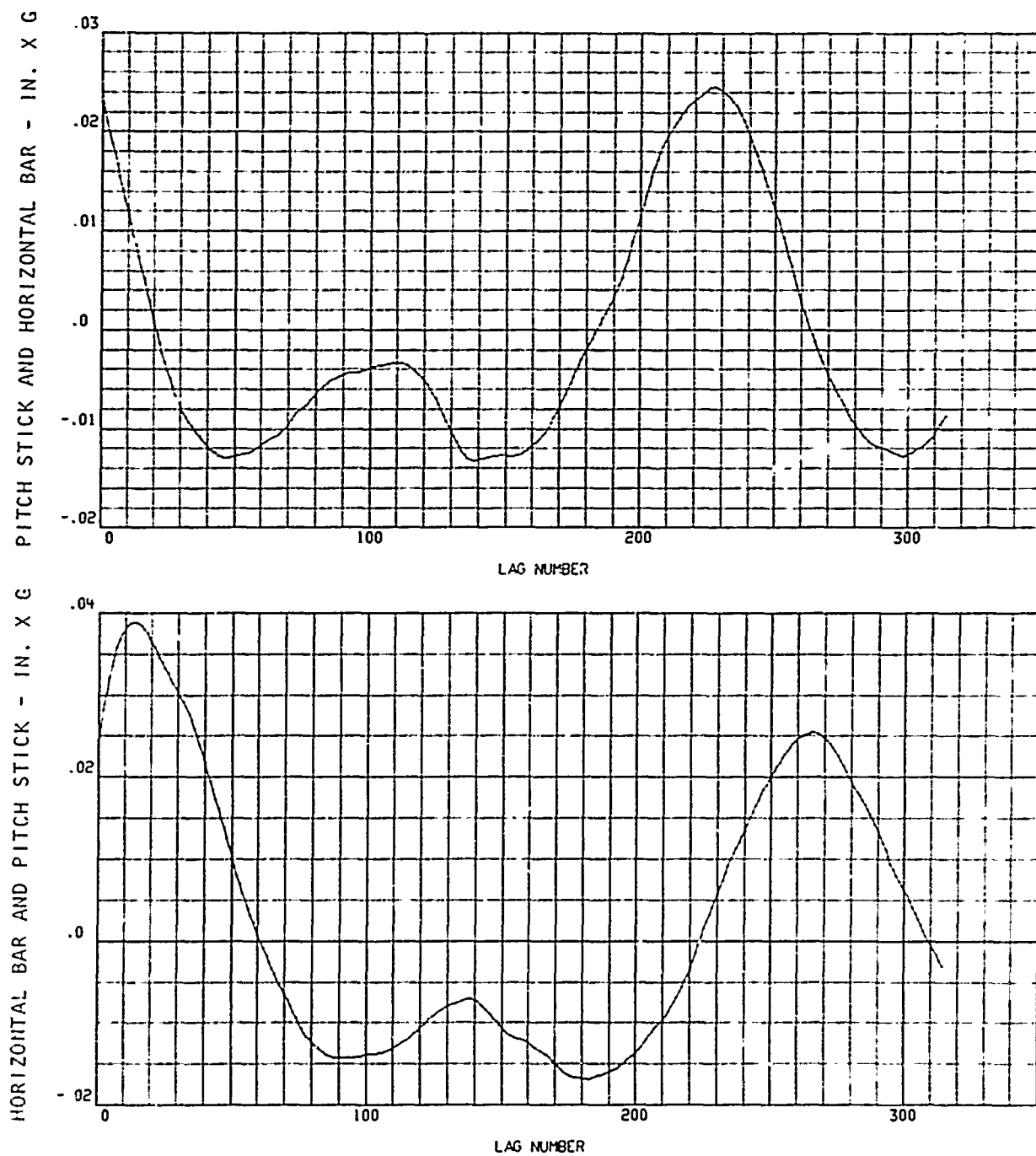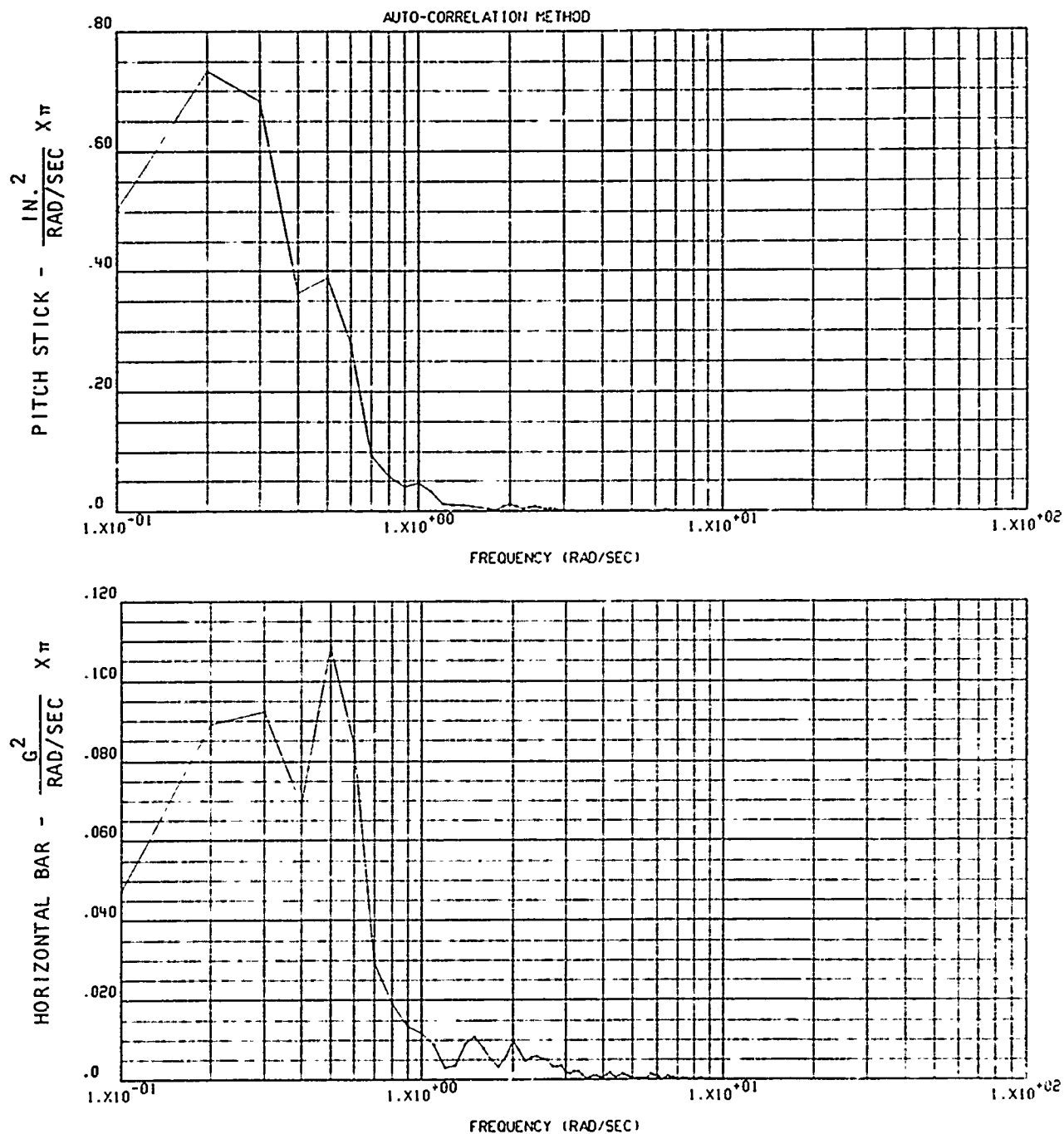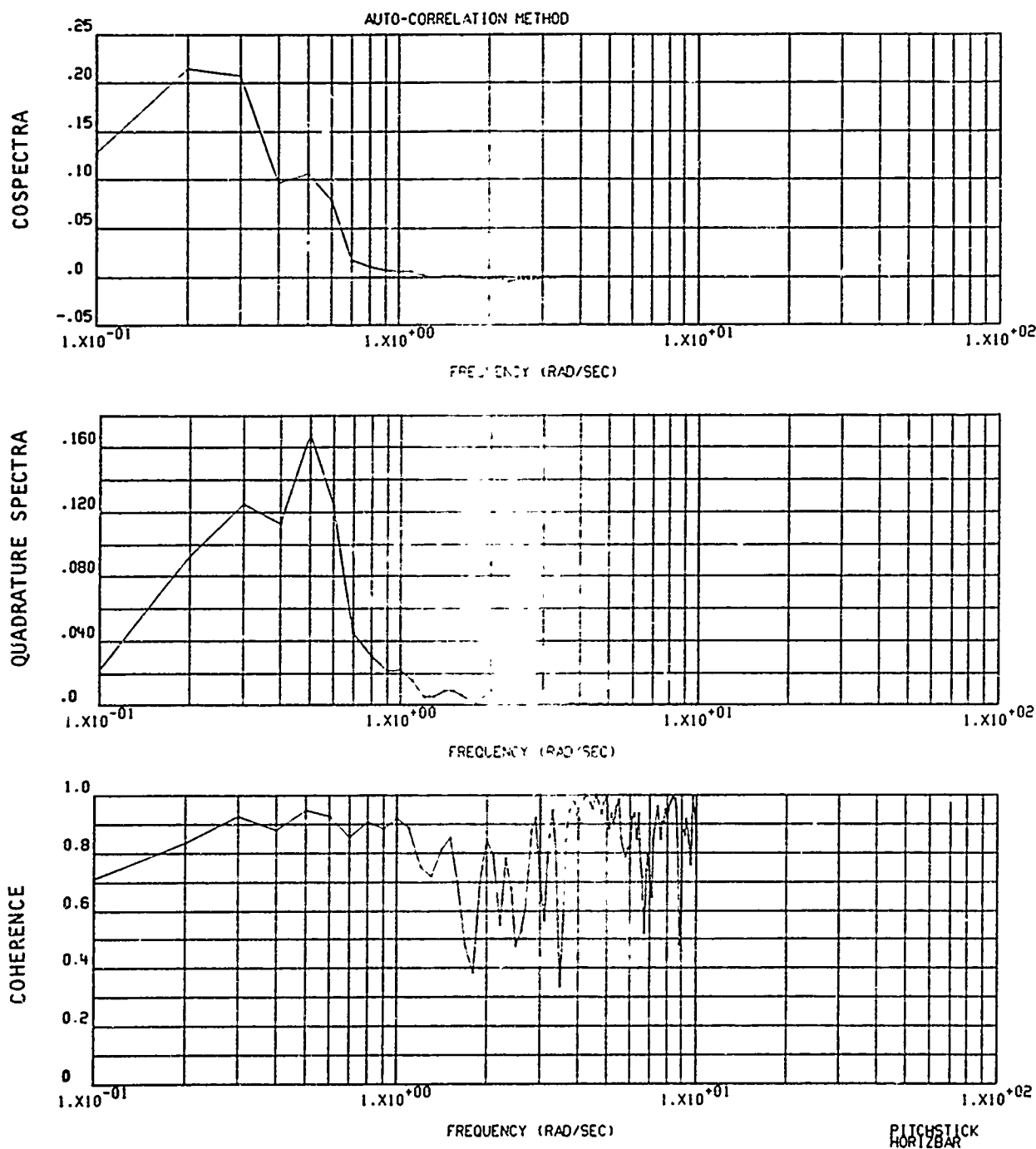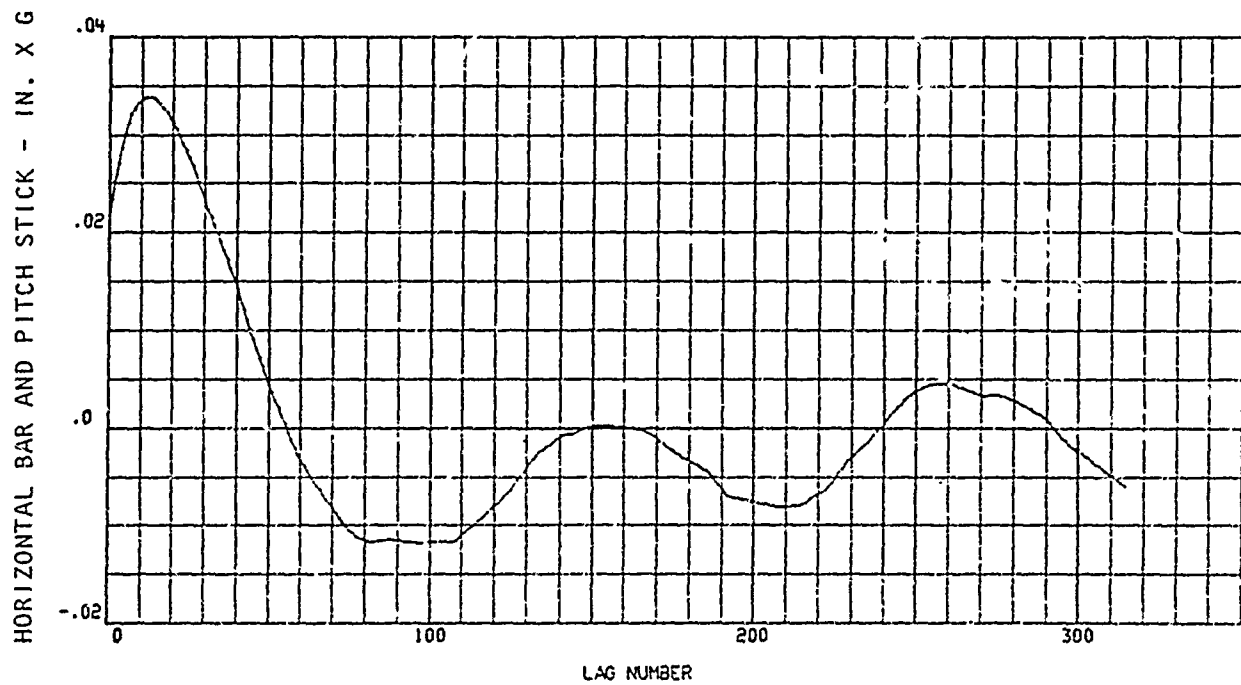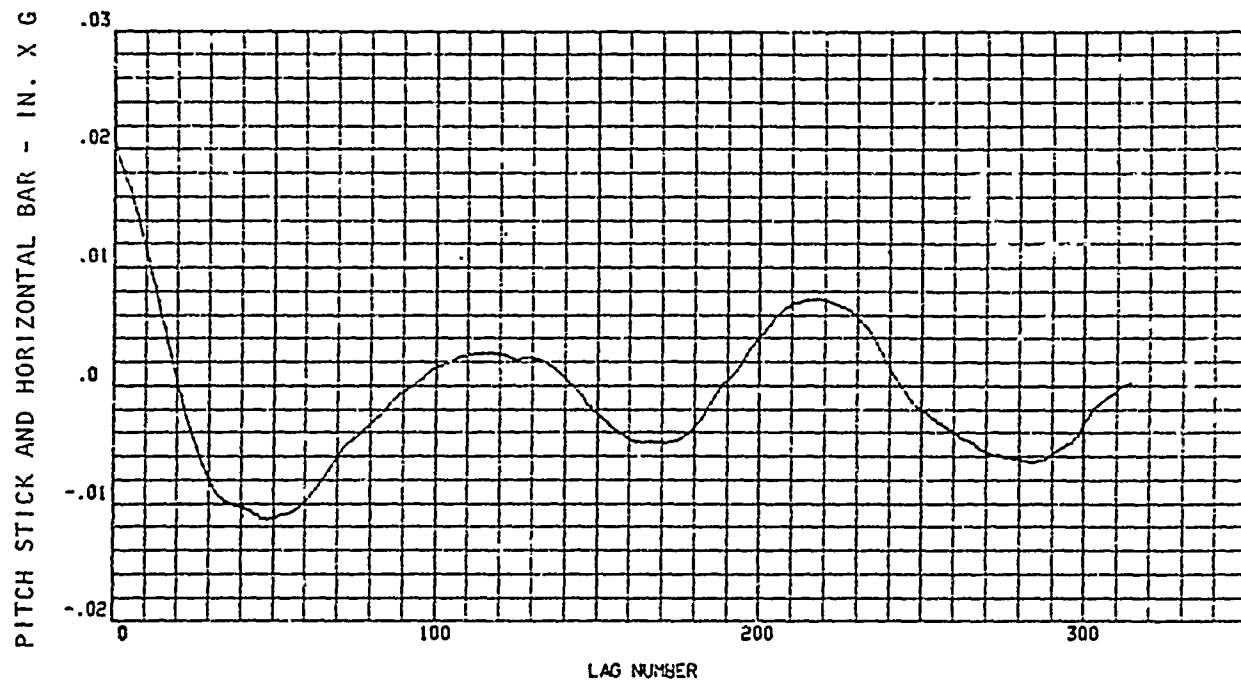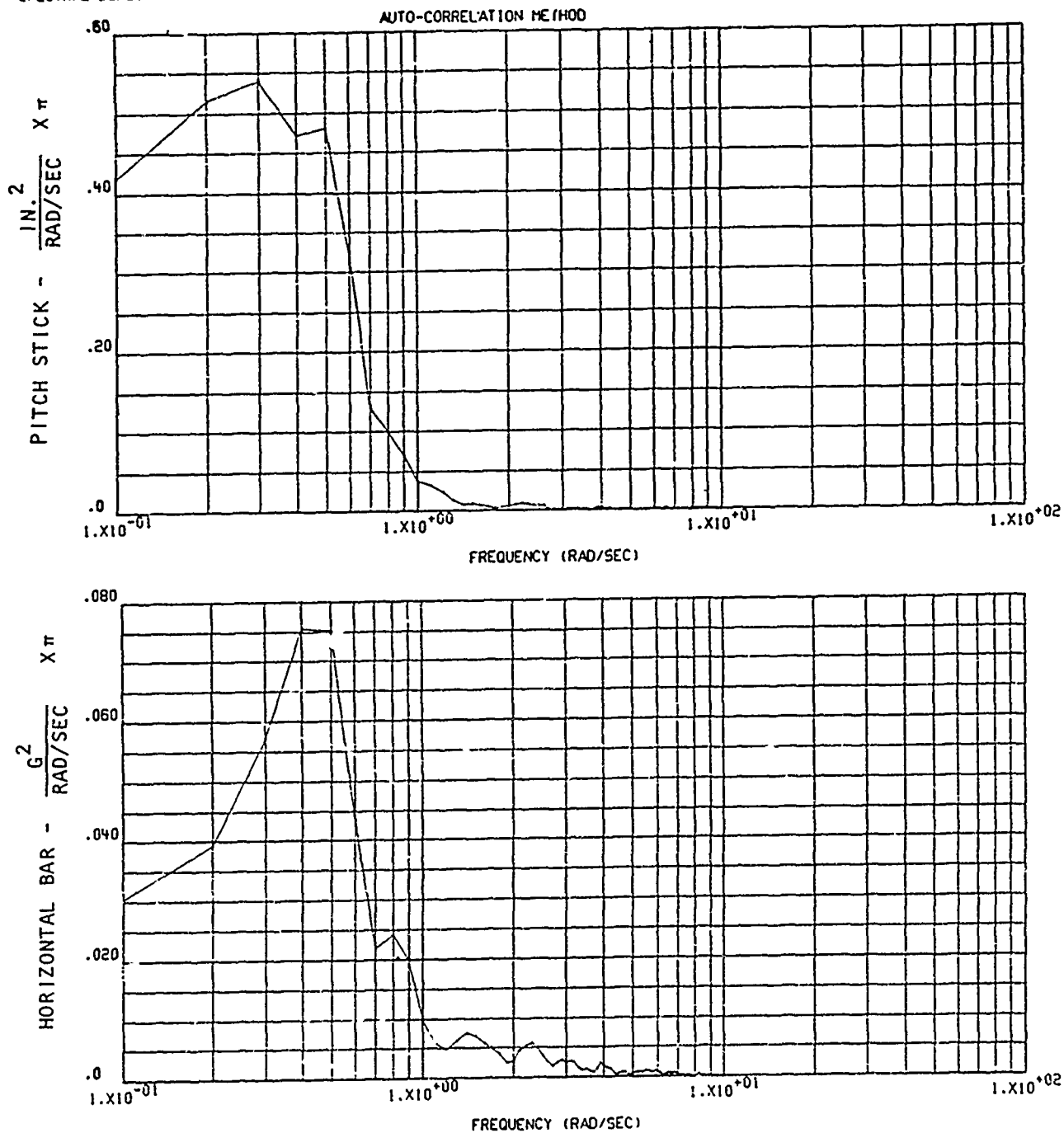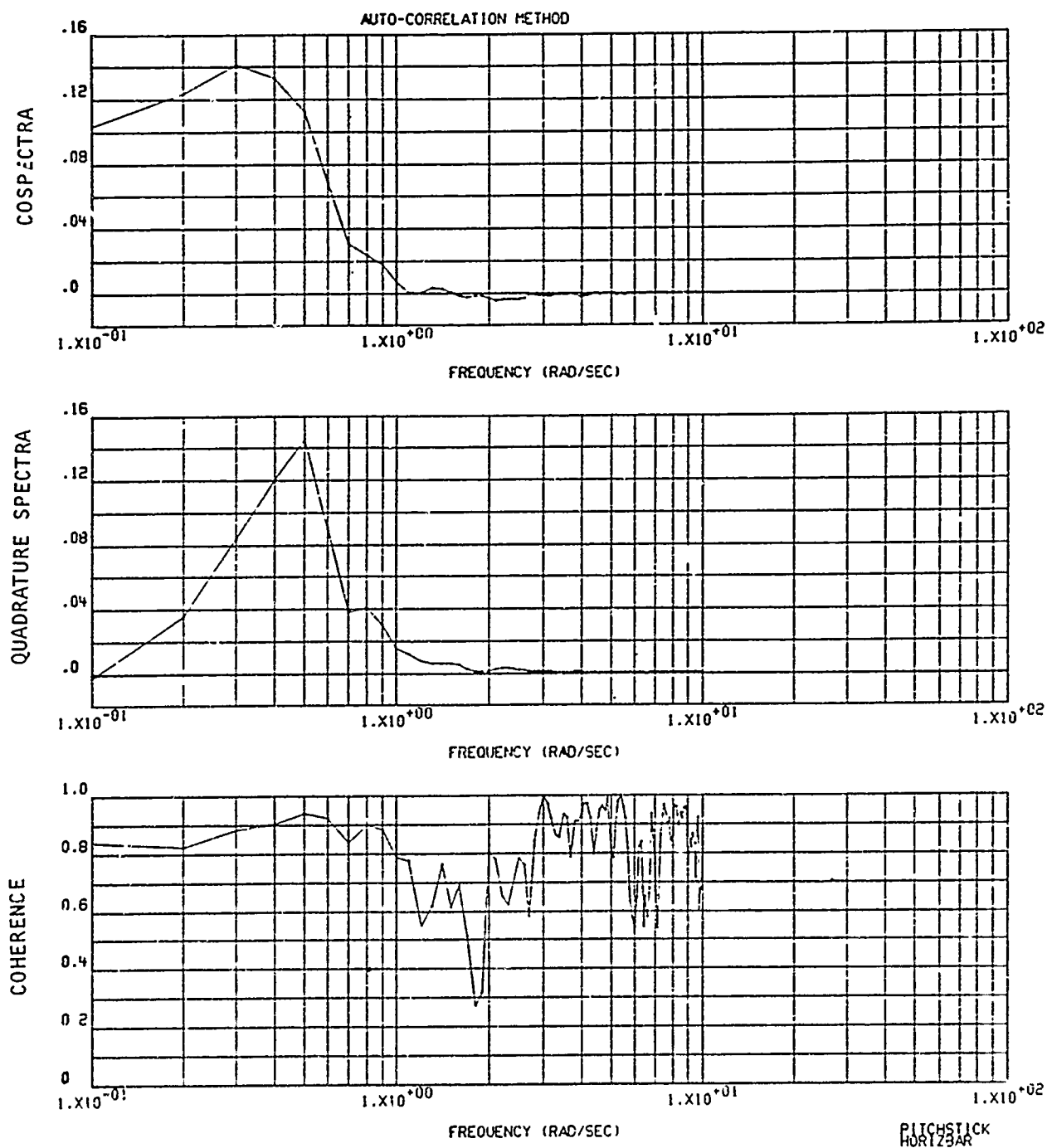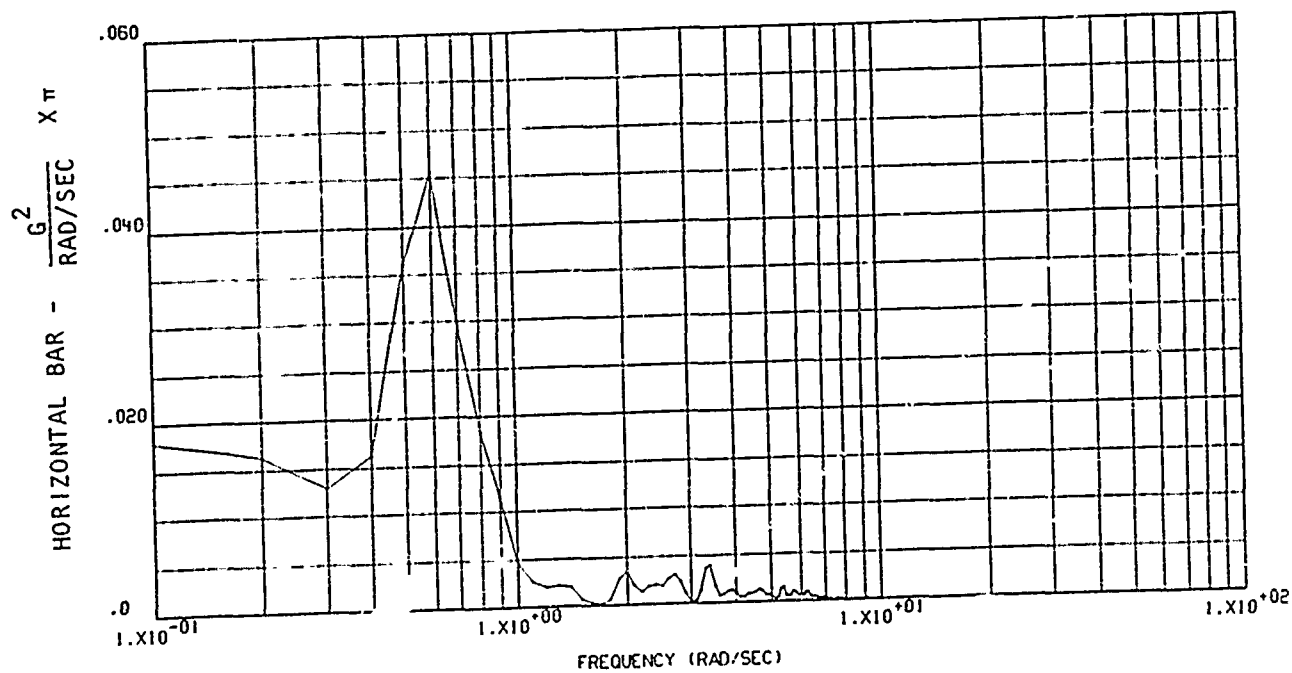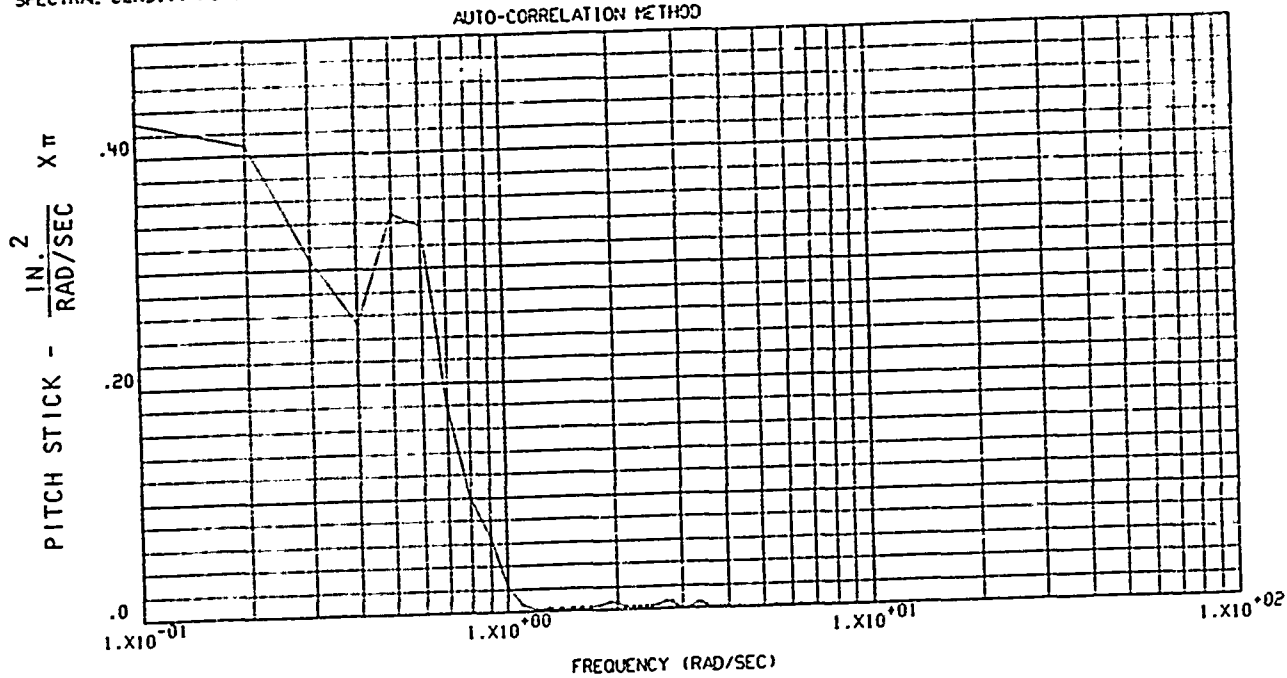
1015 MANUAL TERRAIN FOLLOWING ANALYSIS.

Figure 49. TF Simulation Run No. 1015 Data (Concl)

104

Figure 50. TF Simulation Run No. 0416 Data

AUTO CORRELATION FUNCTIONS

Figure 50. TF Simulation Run No. 0416 Data (Cont)

106

CROSS CORRELATION FUNCTIONS

Figure 50. TF Simulation Run No. 0416 Data (Cont)

Figure 50. TF Simulation Run No. 0416 Data (Cont)

Figure 50. TF Simulation Run No. 0416 Data (Cont)

109

Figure 50. TF Simulation Run No. 0416 Data (Concl)

Figure 51. TF Simulation Run No. 0417 Data

111

AUTO CORRELATION FUNCTIONS

Figure 51. TF Simulation Run No. 0417 Data (Cont)

CROSS CORRELATION FUNCTIONS

Figure 51. TF Simulation Run No. 0417 Data (Cont)

113

SPECTRAL DENSITY FUNCTIONS

AUTO-CORRELATION METHOD

Figure 51. TF Simulation Run No. 0417 Data (Cont)

114

Figure 51. TF Simulation Run No. 0417 Data (Cont)

Figure 51. TF Simulation Run No.0417 Data (Concl)

Figure 52. TF Simulation Run No. 0418 Data

AUTO CORRELATION FUNCTIONS

Figure 52.   TF Simulation Run No. 0418 Data (Cont)

118

CROSS CORRELATION FUNCTIONS

Figure 52. TF Simulation Run No. 0418 Data (Cont)

119

SPECTRAL DENSITY FUNCTIONS

Figure 52.   TF Simulation Run No. 0418 Data (Cont)

Figure 52.   TF Simulation Run No. 0418 Data (Cont)

121

Figure 52. TF Simulation Run No. 0418 Data (Concl)

122

Figure 53. TF Simulation Run No. 0234 Data

123

AUTO CORRELATION FUNCTIONS

Figure 53.   TF Simulation Run No. 0234 Data (Cont)

CROSS CORRELATION FUNCTIONS

Figure 53. TF Simulation Run No. 0234 Data (Cont)

SPECTRAL DENSITY FUNCTIONS

AUTO-CORRELATION METHOD

Figure 53. TF Simulation Run No. 0234 Data (Cont)

126

Figure 53. TF Simulation Run No. 0234 Data (Cont)

127

Figure 53. TF Simulation Run No. 0234 Data (Concl)

Figure 54.   TF Simulation Run No. 0248 Data

129

AUTO CORRELATION FUNCTIONS

Figure 54. TF Simulation Run No. 0248 Data (Cont)

0248 MANUAL TERRAIN FOLLOWING ANALYSIS

CROSS CORRELATION FUNCTIONS

Figure 54. TF Simulation Run No. 0248 Data (Cont)

131

SPECTRAL DENSITY FUNCTIONS

Figure 54. TF Simulation Run No. 0248 Data (Cont)

AUTO-CORRELATION METHOD

Figure 54. TF Simulation Run No. 0248 Data (Cont)
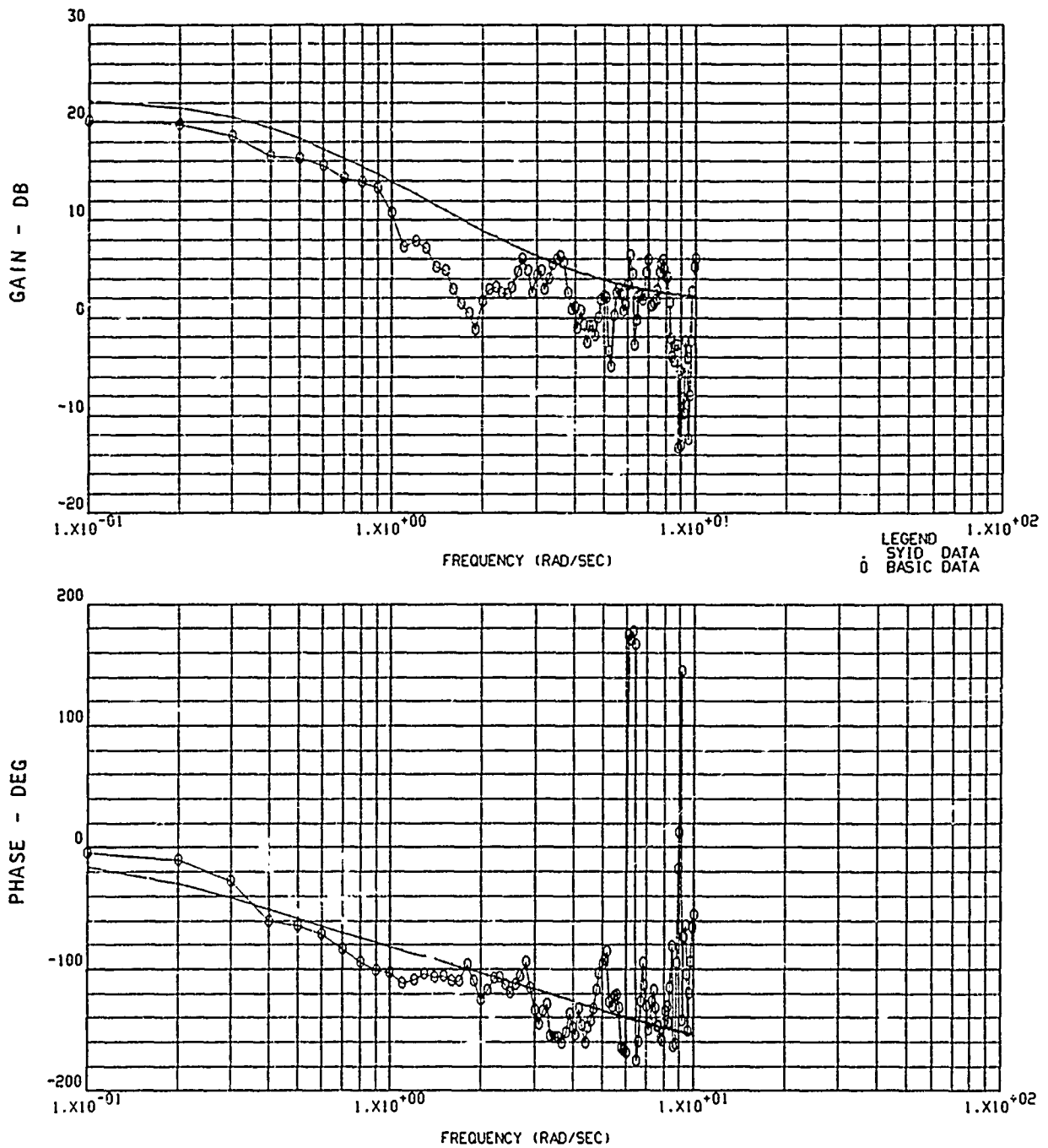
Figure 54. TF Simulation Run No. 0248 Data (Concl)

Figure 55. TF Simulation Run No. 0252 Data

AUTO CORRELATION FUNCTIONS

Figure 55. TF Simulation Run No. 0252 Data (Cont)

CROSS CORRELATION FUNCTIONS

Figure 55. TF Simulation Run No. 0252 Data (Cont)

Figure 55. TF Simulation Run No. 0252 Data (Cont)

Figure 55. TF Simulation Run No. 0252 Data (Cont)

139

Figure 55. TF Simulation Run No. 0252 Data (Concl)

140

Figure 56. TF Simulation Run No. 0254 Data

AUTO CORRELATION FUNCTIONS

Figure 56.   TF Simulation Run No. 0254 Data (Cont)

0254 MANUAL TERRAIN FOLLOWING ANALYSIS.
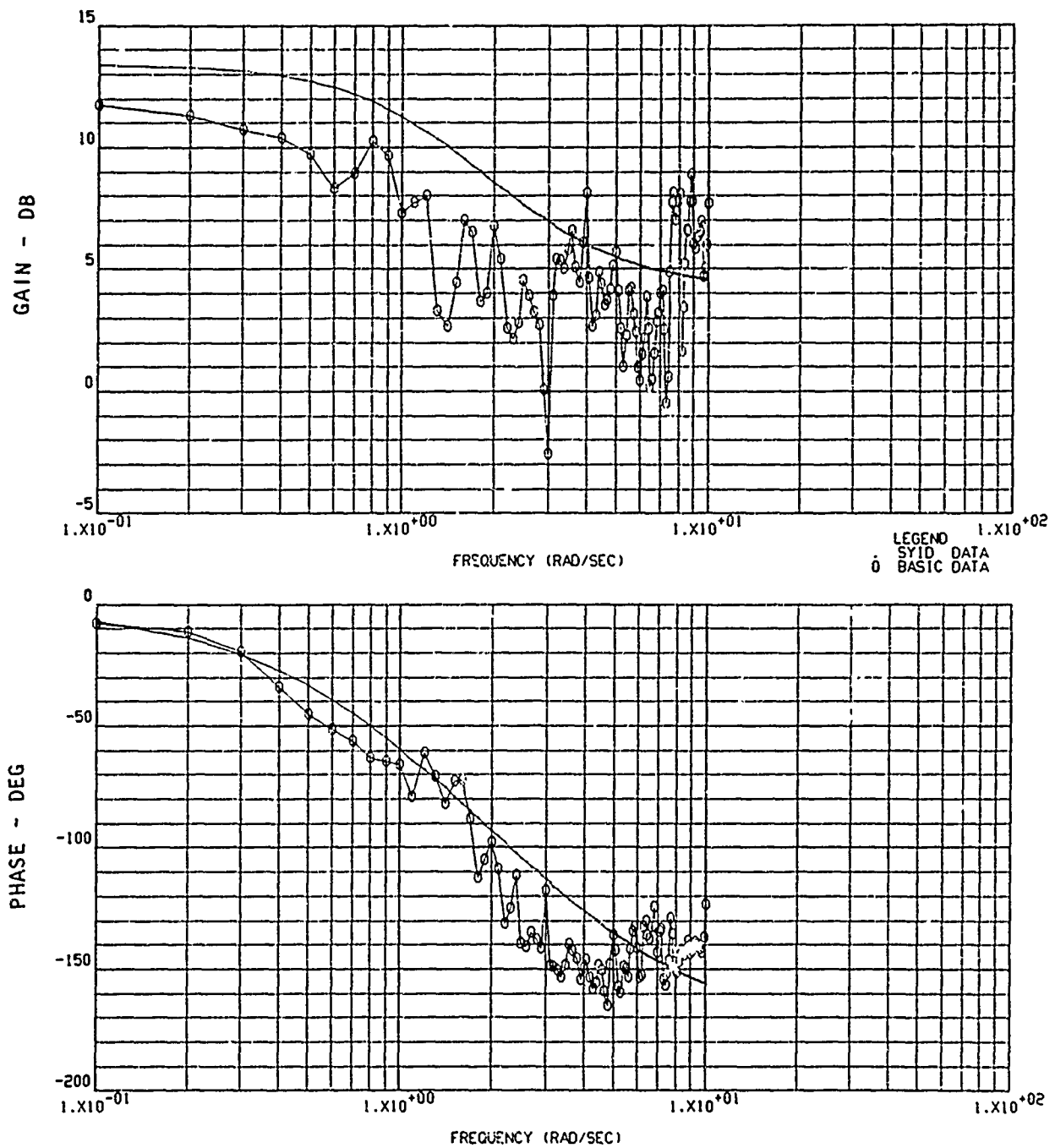
CROSS CORRELATION FUNCTIONS

Figure 56. TF Simulation Run No. 0254 Data (Cont)

143

SPECTRAL DENSITY FUNCTIONS

Figure 56. TF Simulation Run No. 0254 Data (Cont)

144

Figure 56.   TF Simulation Run No. 0254 Data (Cont)

Figure 56. TF Simulation Run No. 0254 Data (Concl)
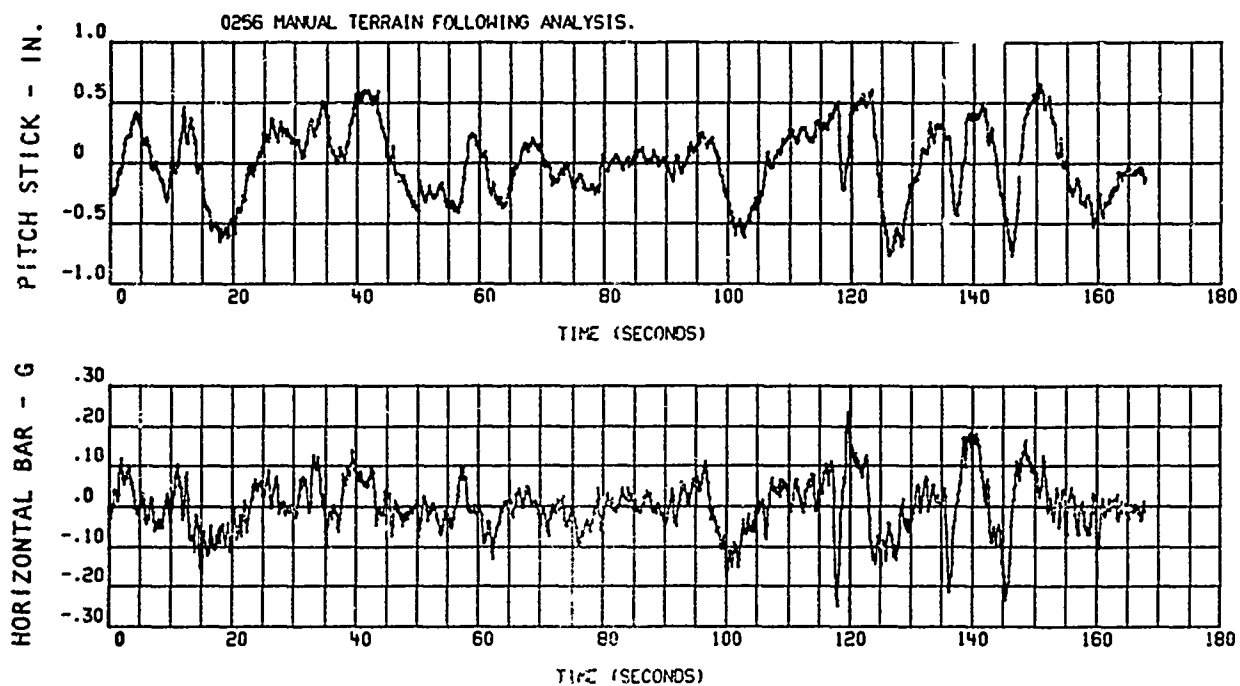
146

Figure 57. TF Simulation Run No. 0256 Data

147

AUTO CORRELATION FUNCTIONS

Figure 57. TF Simulation Run No. 0256 Data (Cont)

CROSS CORRELATION FUNCTIONS

Figure 57. TF Simulation Run No. 0256 Data (Cont)

149

SPECTRAL DENSITY FUNCTIONS

Figure 57. TF Simulation Run No. 0256 Data (Cont)

Figure 57.   TF Simulation Run No. 0256 Data (Cont)

151
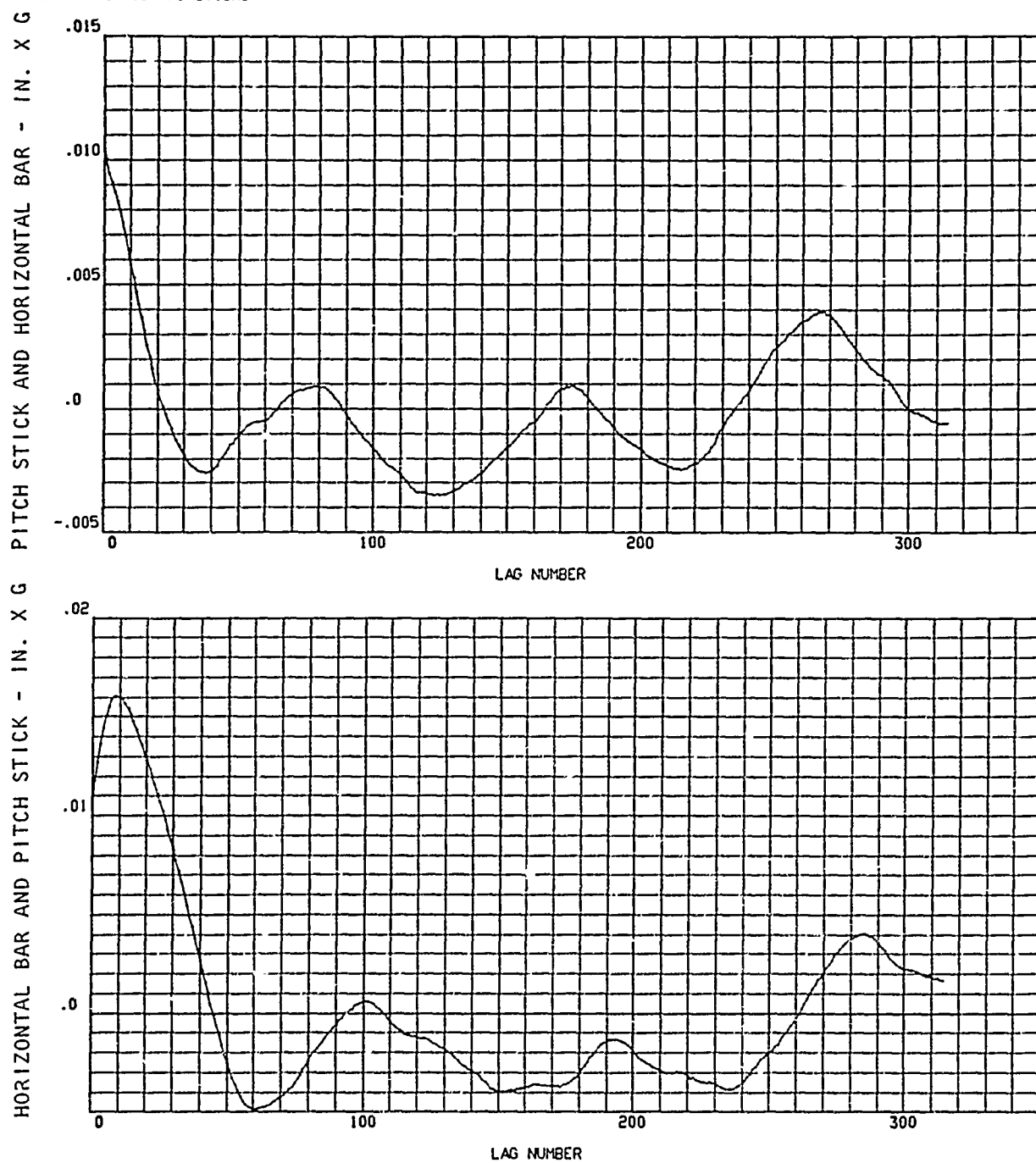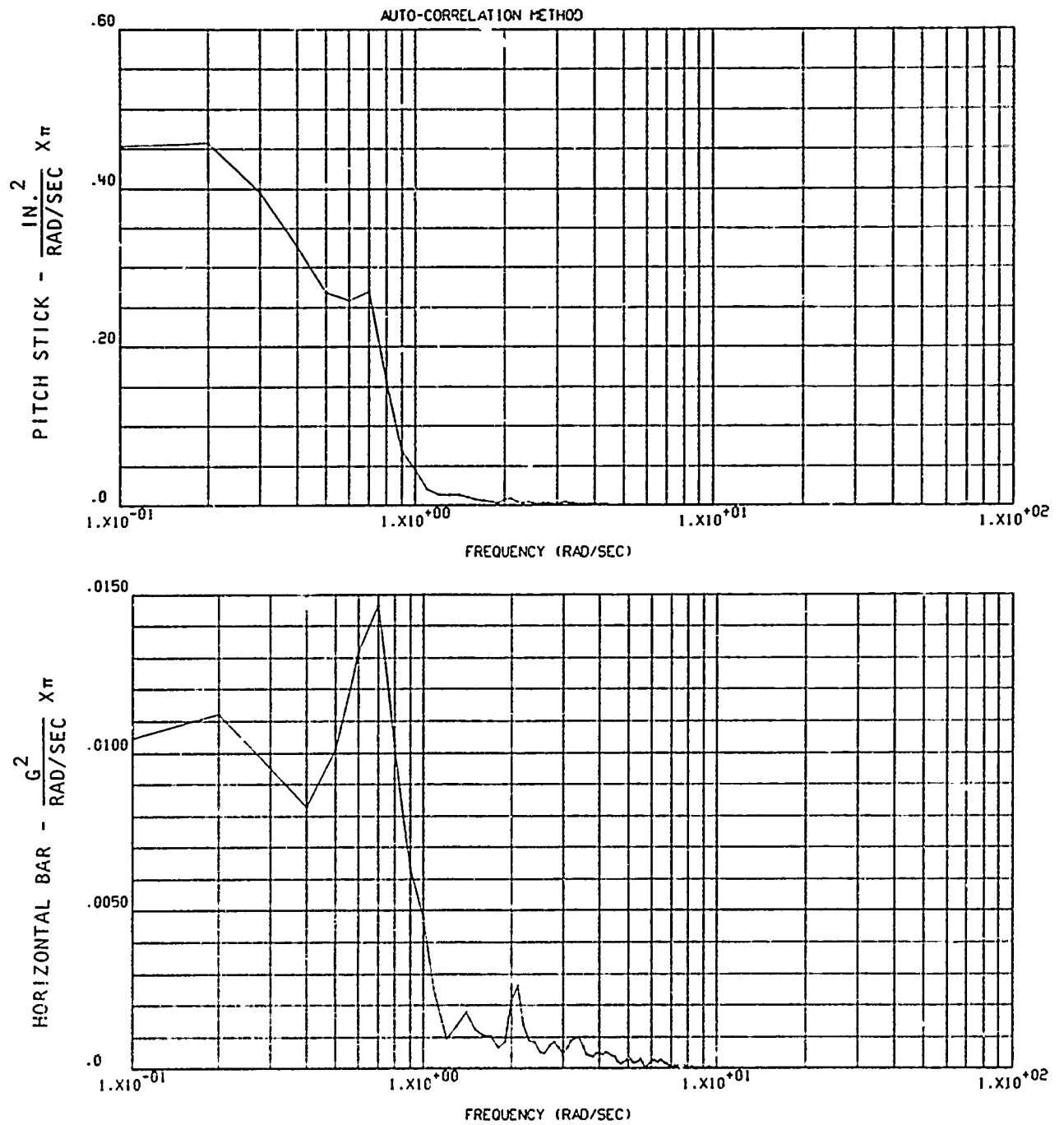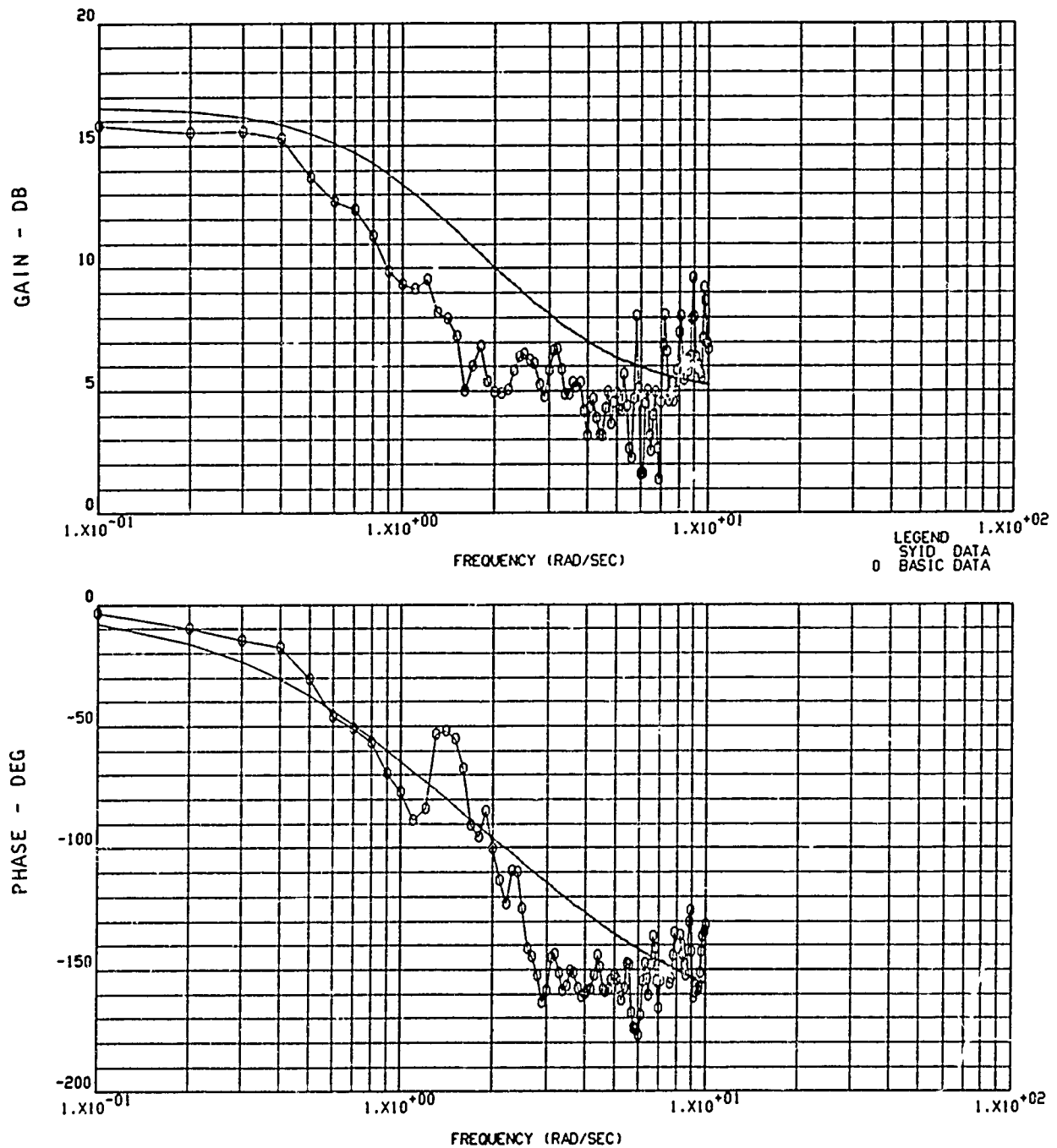
Figure 57. TF Simulation Run No. 0256 Data (Concl)

Figure 58. TF Simulation Run No. 0258 Data

153

AUTO CORRELATION FUNCTIONS

Figure 58. TF Simulation Run No. 0258 Data (Cont)

CROSS CORRELATION FUNCTIONS

Figure 58. TF Simulation Run No. 0258 Data (Cont)

SPECTRAL DENSITY FUNCTIONS

Figure 58. TF Simulation Run No. 0258 Data (Cont)

Figure 58.   TF Simulation Run No. 0258 Data (Cont)

Figure 58.   TF Simulation Run No. 0258 Data (Concl)

158

ACCELERATION VS GROUND RANGE

ACCEL G'S

TERRAIN AND AIRCRAFT ALTITUDE VS GROUND RANGE

ALTITUDE - FEET

GROUND RANGE - XNM
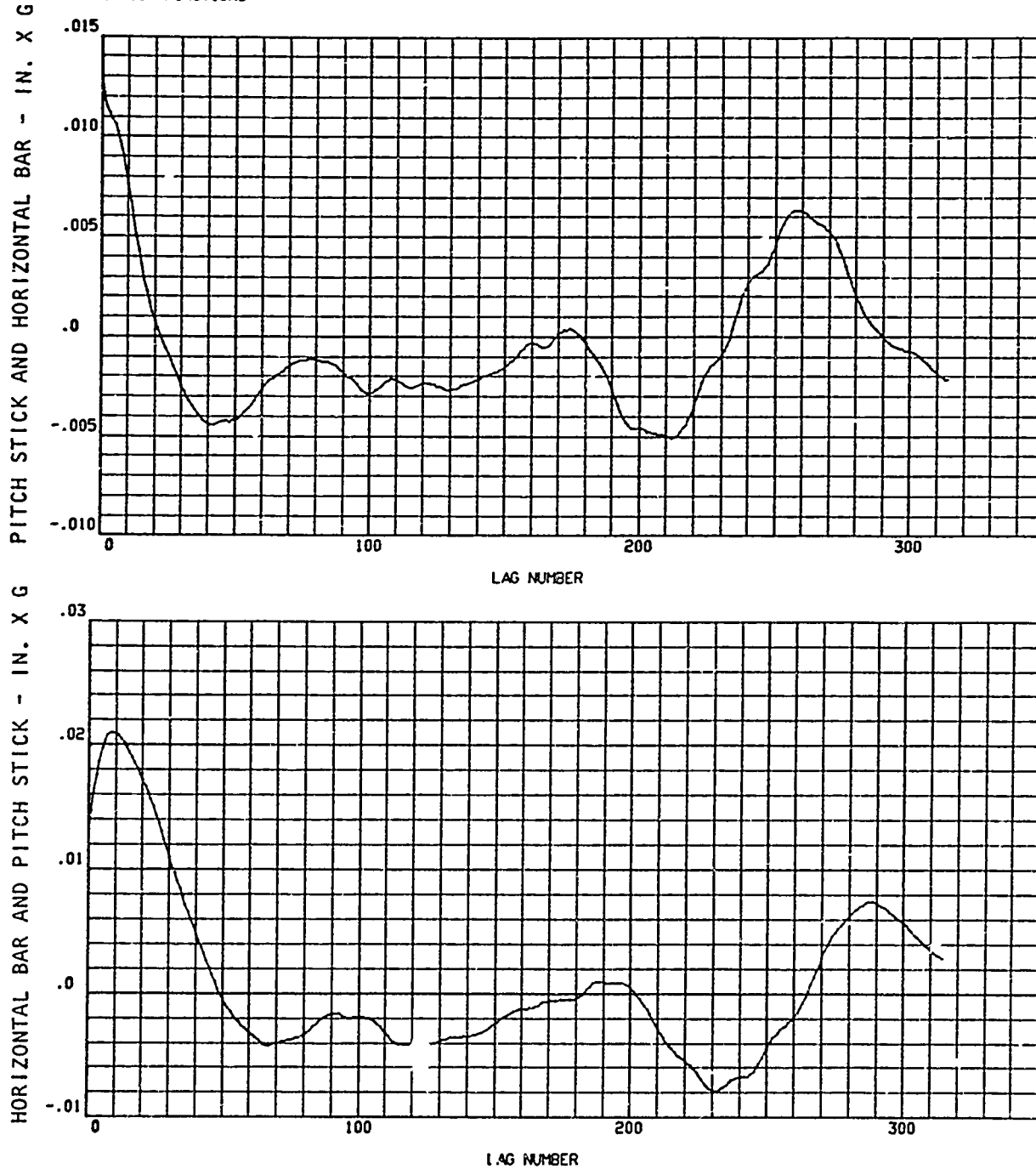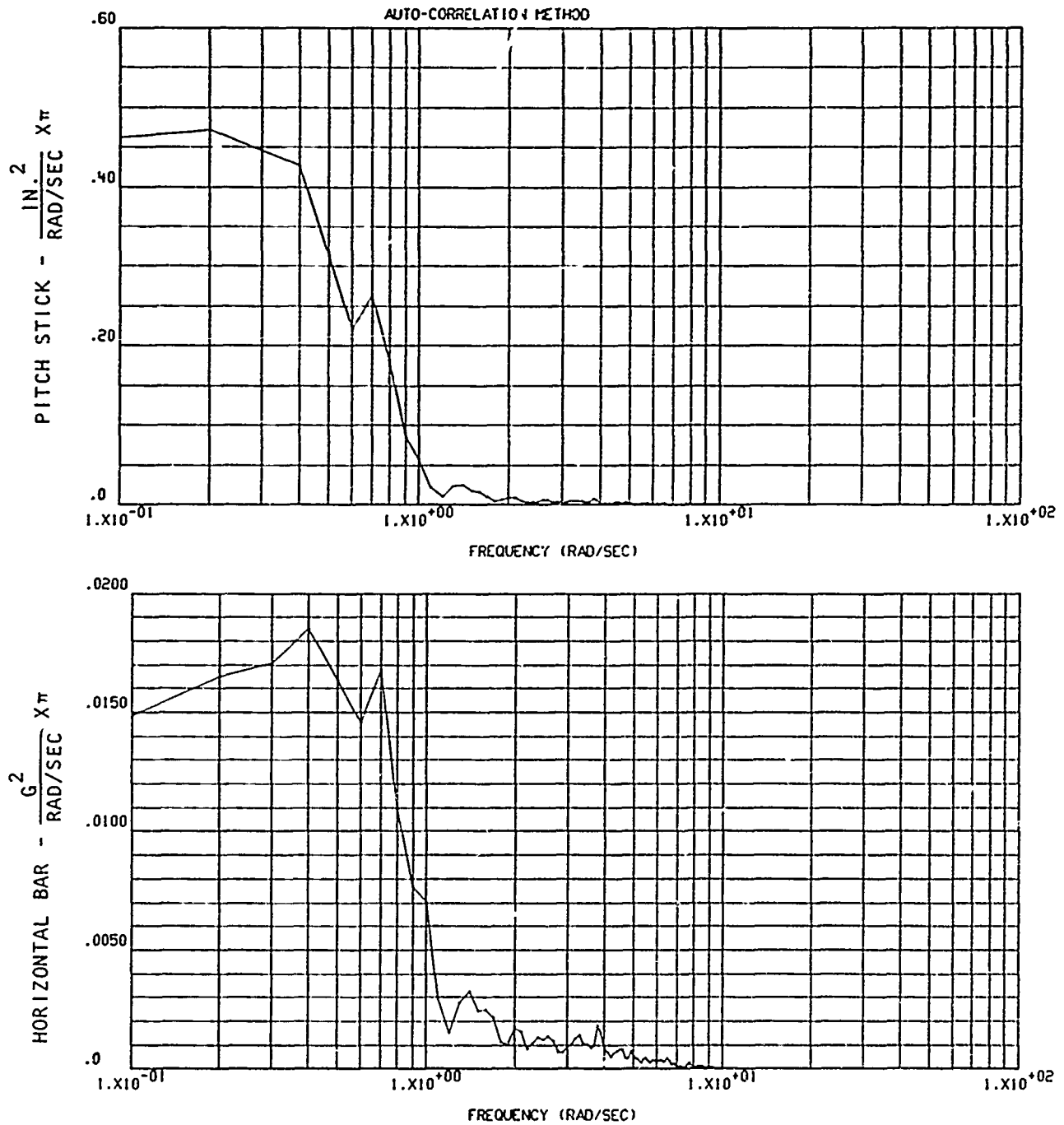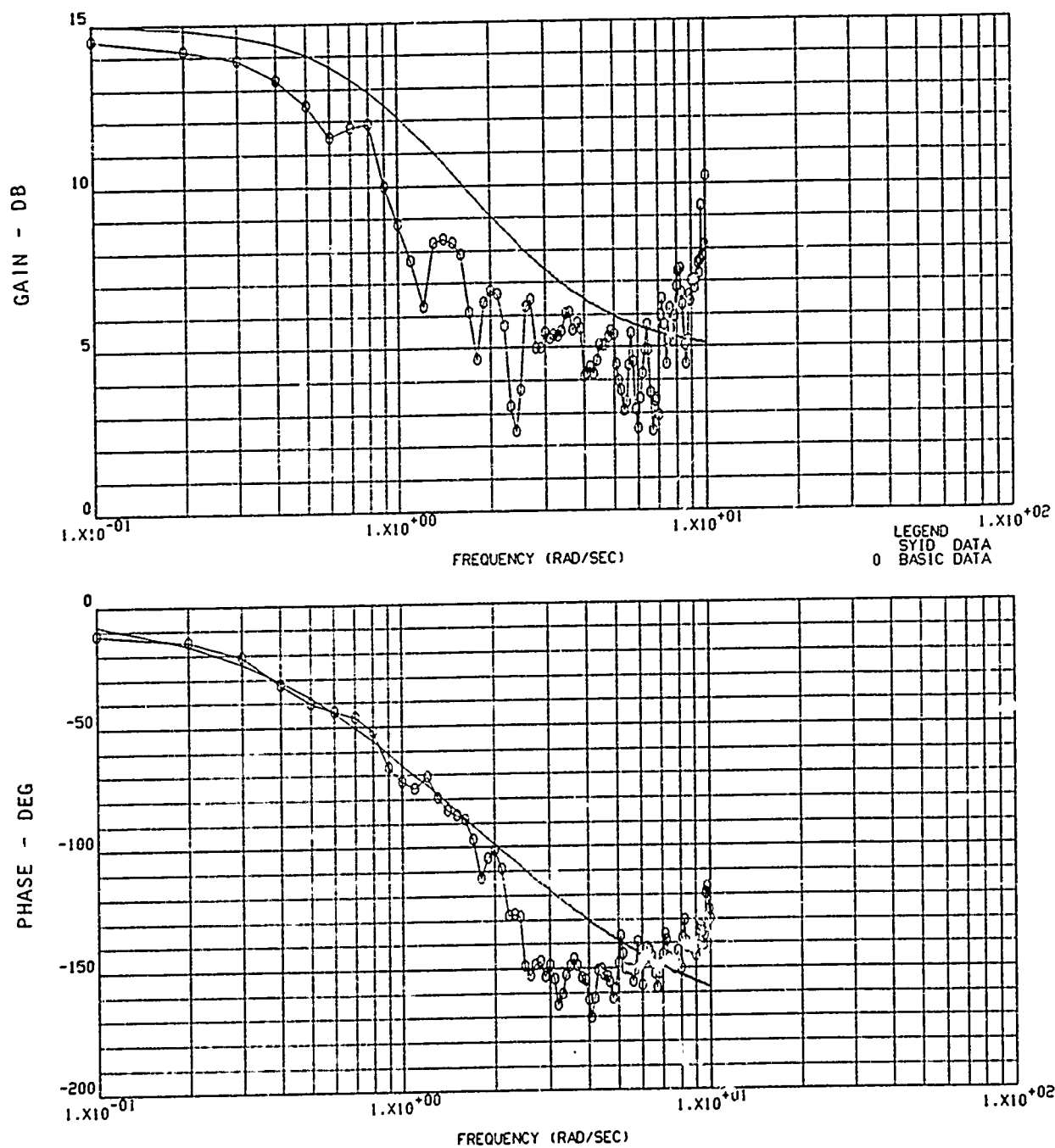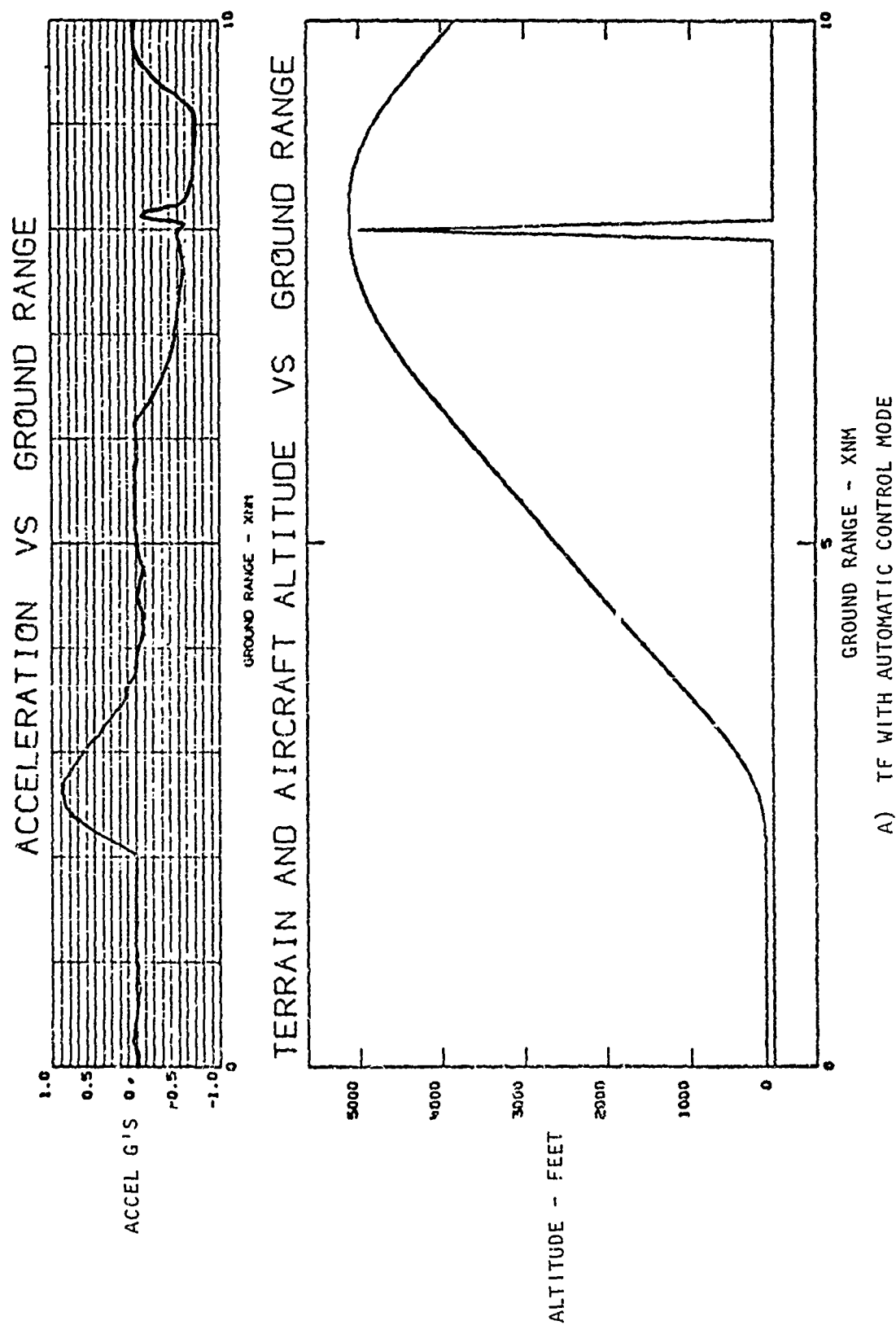
A) TF WITH AUTOMATIC CONTROL MODE

Figure 59.   Comparative TF Runs With Pilot Model and Automatic TF System

159

ACCELERATION VS GROUND RANGE

TERRAIN AND AIRCRAFT ALTITUDE VS GROUND RANGE
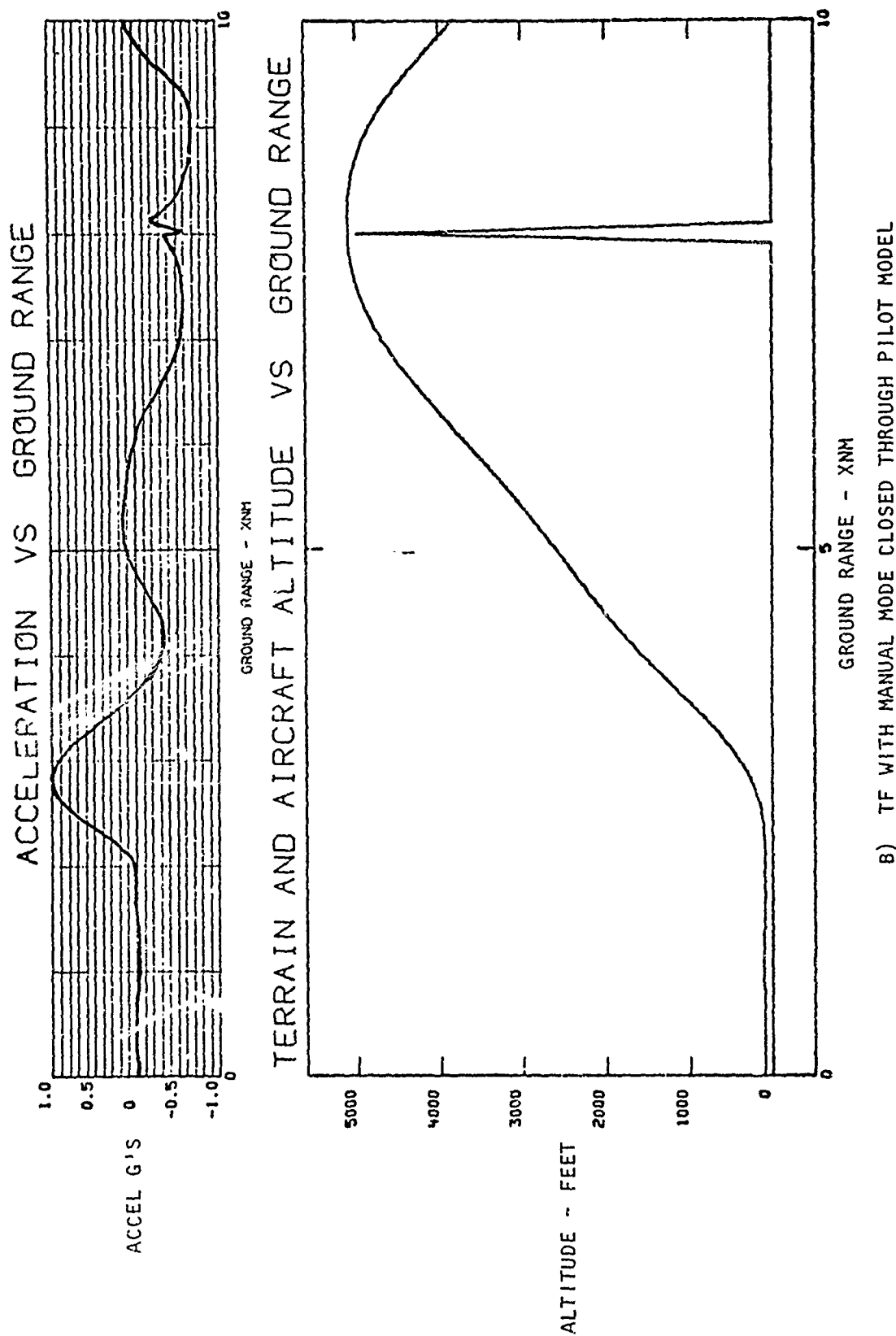
B) TF WITH MANUAL MODE CLOSED THROUGH PILOT MODEL

Figure 59. Comparative TF Runs With Pilot Model and Automatic TF System (Concluded)

APPENDIX III

DATA ANALYSIS RESULTS FOR AIR REFUELING SIMULATION RUNS

As for the terrain-following (TF) data, the extensiveness of the data in this appendix is to provide a complete data base for the simulation tests.

Identification and data results for the air refueling (AR) simulation runs are listed in table V. Figures 60 through 99 show the data plots obtained from the computer processing of the simulation data. Each figure shows the pitch stick and horizontal bar time histories; the autocorrelation and cross-correlation functions; the spectral density functions; the cospectra, quadrature spectra, and coherence functions; and, finally, the bode plots for the pilot transfer functions. As indicated earlier, no automatic curve fitting was achieved and, therefore, none are shown on the bode plots.

TABLE V. AIR REFUELING SIMULATION DATA ANALYSIS RESULTS

Figure	Run No.	Pilot	SAS Status	Gust Level σ_{W_G} (fps)	Gust/ Struct Mode	Stick/ Struct Mode	$\sigma_{N_{Z_P}}$ Pilot Accel (g)	σ_{PS} Pitch Stick (in.)	σ_{HB} Horiz Bar (deg)	Pilot Rating
59-52	01A11	B	On	0	No	No	0.089	0.192	0.410	3
60	01A12	B	On	3	No	No	0.089	0.235	0.436	3
61	01A13	B	On	7	No	No	0.091	0.234	0.479	3
62	01A14	B	On	12	No	No	0.078	0.194	0.489	3
63	01A15	B	On	3	Yes	No	0.073	0.190	0.511	3
64	01A16	B	On	7	Yes	No	0.100	0.158	0.507	3
65	01A17	B	On	12	Yes	No	0.136	0.144	0.611	3
66	01A22	B	On	3	No	Yes	0.075	0.142	0.579	3
67	01A23	B	On	7	No	Yes	0.068	0.147	0.617	3
68	01A24	B	On	12	No	Yes	0.076	0.140	0.624	3
69	01A33	B	On	0	No	No	0.078	0.181	0.581	3.5
70	01A34	B	On_1	3	No	No	0.071	0.162	0.607	3.5
71	01A35	B	On_1	12	No	No	0.066	0.160	0.588	3.5

TABLE V. AIR REFUELING SIMULATION DATA ANALYSIS RESULTS (CONT)

Figure	Run No.	Pilot	SAS Status	Gust Level σ_{W_G} (fps)	Gust/ Struct Mode	Stick/ Struct Mode	σ_N Z_p Pilot Accel (g)	σ_{PS} Pitch Stick (in.)	IIB Horiz Bar (deg)	Pilot Rating
72	01A38	B	On$_2$	0	No	No	0.076	0.178	0.506	3
73	01A39	B	On$_2$	3	No	No	.077	.161	.476	3
74	01A40	B	On$_2$	12	No	No	.080	.173	.563	3
75	01A3	B	On$_3$	0	No	No	.149	.305	.593	5
76	01A10	B	On$_4$	0	No	No	.108	.228	.434	4
77	04A1	B	Off	0	No	No	.092	.173	.528	5
78	02A2	B	Off	3	No	No	.124	.330	.675	9
79	01A19	B	Off	0	Yes	No	.072	.138	.481	5
80	01A20	B	Off	12	Yes	No	.154	.209	.681	5
81	01A31	B	Off	0	No	Yes	.078	.111	.633	5
82	01A32	B	Off	12	No	Yes	.067	.092	.455	5
83	02A49	C	On	0	No	No	.057	.170	.775	2
84	01A50	C	On	3	No	No	.063	.225	.657	2

163

TABLE V. AIR REFUELING SIMULATION DATA ANALYSIS RESULTS (CONT)

Figure	Run No.	Pilot	SAS Status	Gust Level σ_{W_G} (fps)	Gust/ Struct Mode	Stick/ Struct Mode	$\sigma_{N_{Z_P}}$ Pilot Accel (g)	σ_{PS} Pitch Stick (in.)	IIB Horiz Bar (deg)	Pilot Rating
85	01A51	C	On	7	No	No	0.075	0.223	0.744	2
86	01A52	C	On	12	No	No	.081	.226	.749	2
87	01A56	C	On	3	Yes	No	.068	.186	.737	2
88	01A57	C	On	7	Yes	No	.092	.217	.762	2
89	01A58	C	On	12	Yes	No	.134	.224	.680	2
90	01A63	C	On	3	No	Yes	.054	.125	.657	2
91	01A64	C	On	12	No	Yes	.058	.098	.674	2
92	01A46	C	Off	3	No	No	.093	.199	.584	4
93	01A47	C	Off	7	No	No	.079	.179	.537	4
94	01A48	C	Off	12	No	No	.094	.168	.877	4
95	01A53	C	Off	3	Yes	No	.076	.125	.882	4
96	01A54	C	Off	7	Yes	No	.158	.275	.839	4
97	01A55	C	Off	12	Yes	No	.075	.177	.694	4

TABLE V. AIR REFUELING SIMULATION DATA ANALYSIS RESULTS (CONCL)

Figure	Run No.	Pilot	SAS Status	Gust Level σ_{W_G} (fps)	Gust/ Struct Mode	Stick/ Struct Mode	$\sigma_{N_{Z_P}}$ Pilot Accel (g)	σ_{PS} Pitch Stick (in.)	HB Horiz Bar (deg)	Pilot Rating
98	01A61	C	Off	5	No	Yes	0.107	0.166	0.880	4
99	01A62	C	Off	12	No	Yes	.070	.122	.871	4

SAS   Status Subscripts

On   SAS operative and normal

Off   Longitudinal SAS inoperative

On_1 SAS on and stick prefilter = 1.0 sec

On_2 SAS on and stick prefilter = 0.10 sec

On_3 SAS on and pitch stick normalized electrical gain = 4.0

On_4 SAS on and pitch stick normalized electrical gain = 2.0

165
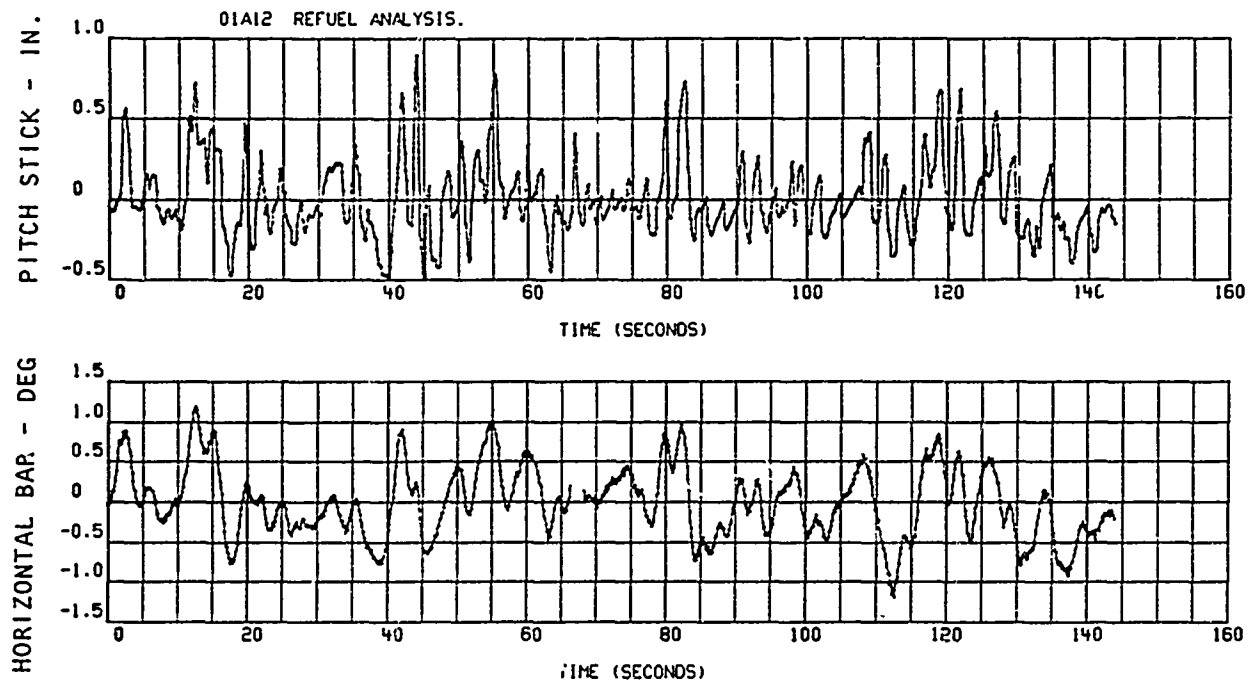
Figure 60. AR Simulation Run No. 01A12 Data

01A12 REFUEL ANALYSIS.
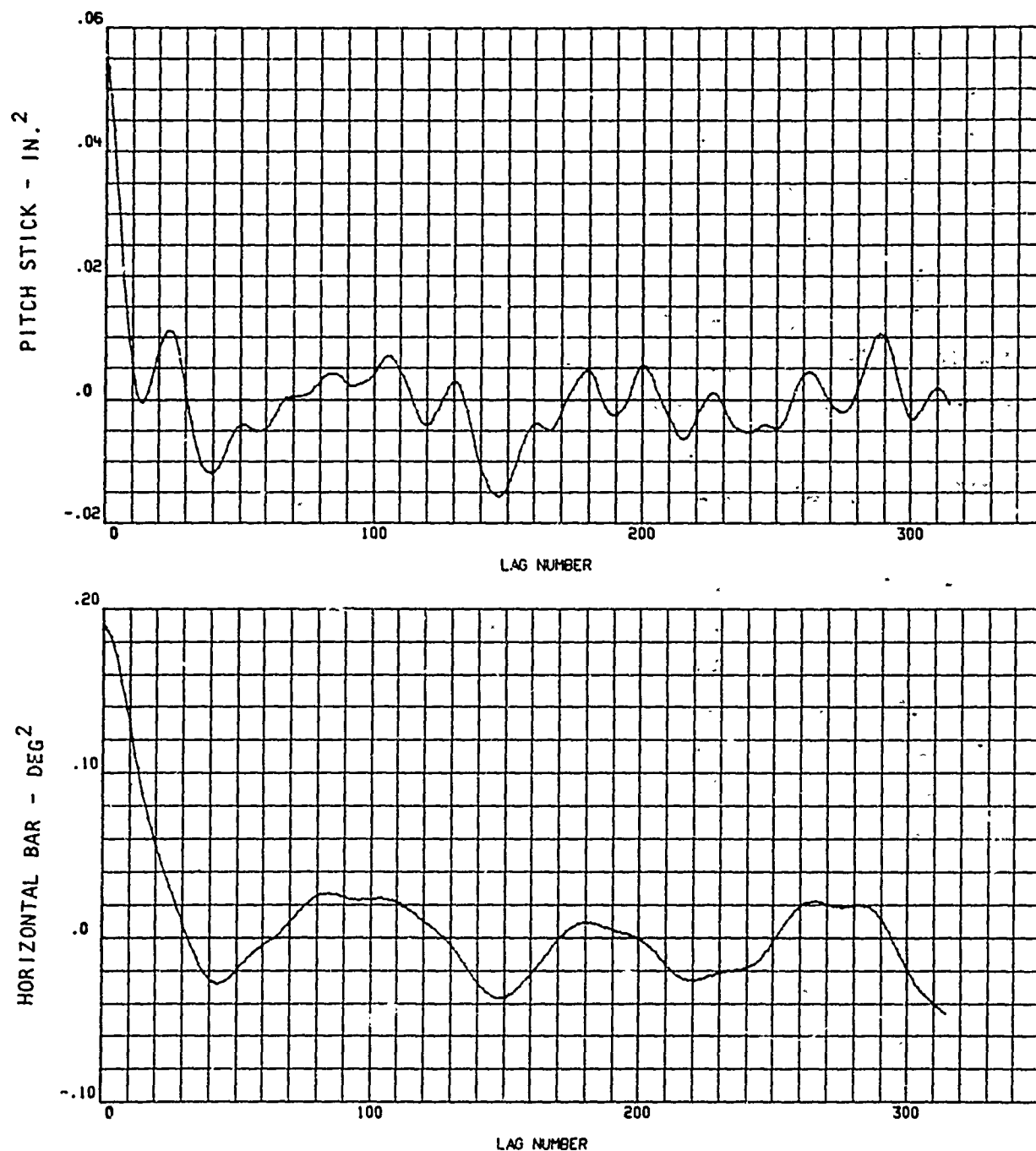
AUTO CORRELATION FUNCTIONS

Figure 60.   AR Simulation Run No. 01A12 Data (Cont)

167

Figure 60. AR Simulation Run No. 01A12 Data (Cont)

OIAI2 REFUEL ANALYSIS.

SPECTRAL DENSITY FUNCTIONS

Figure 60.   AR Simulation Run No. 01A12 Data (Cont)

169
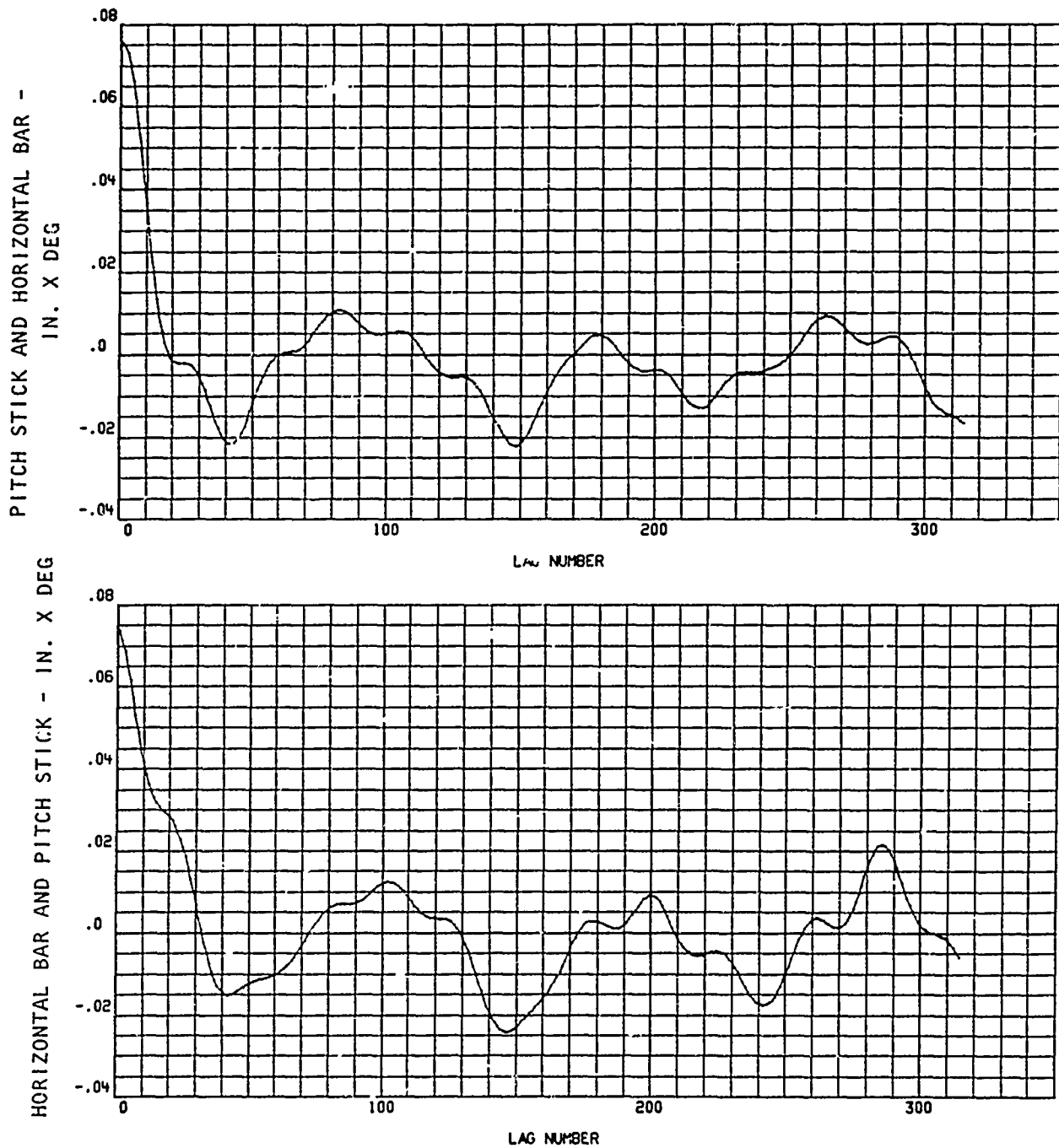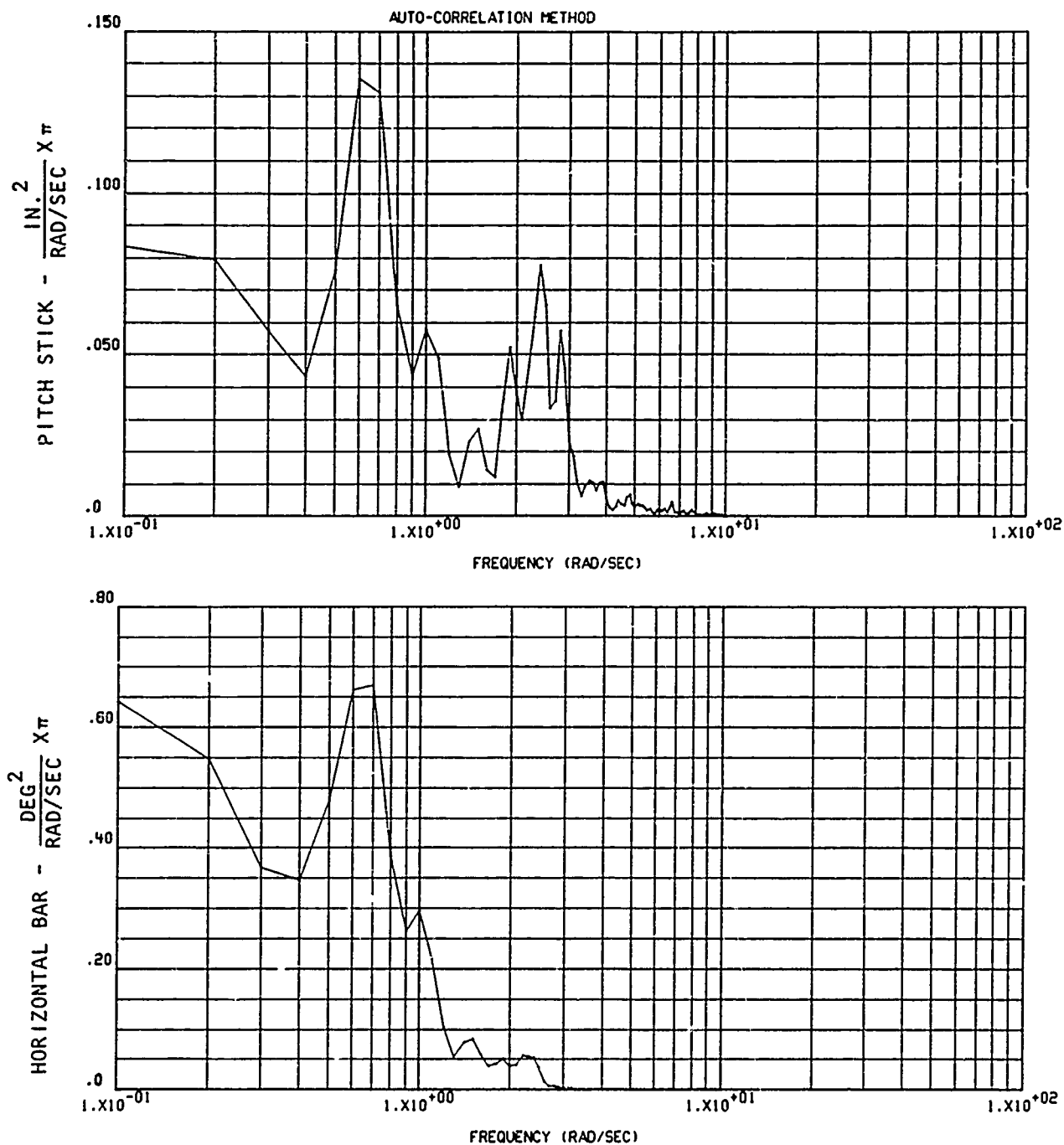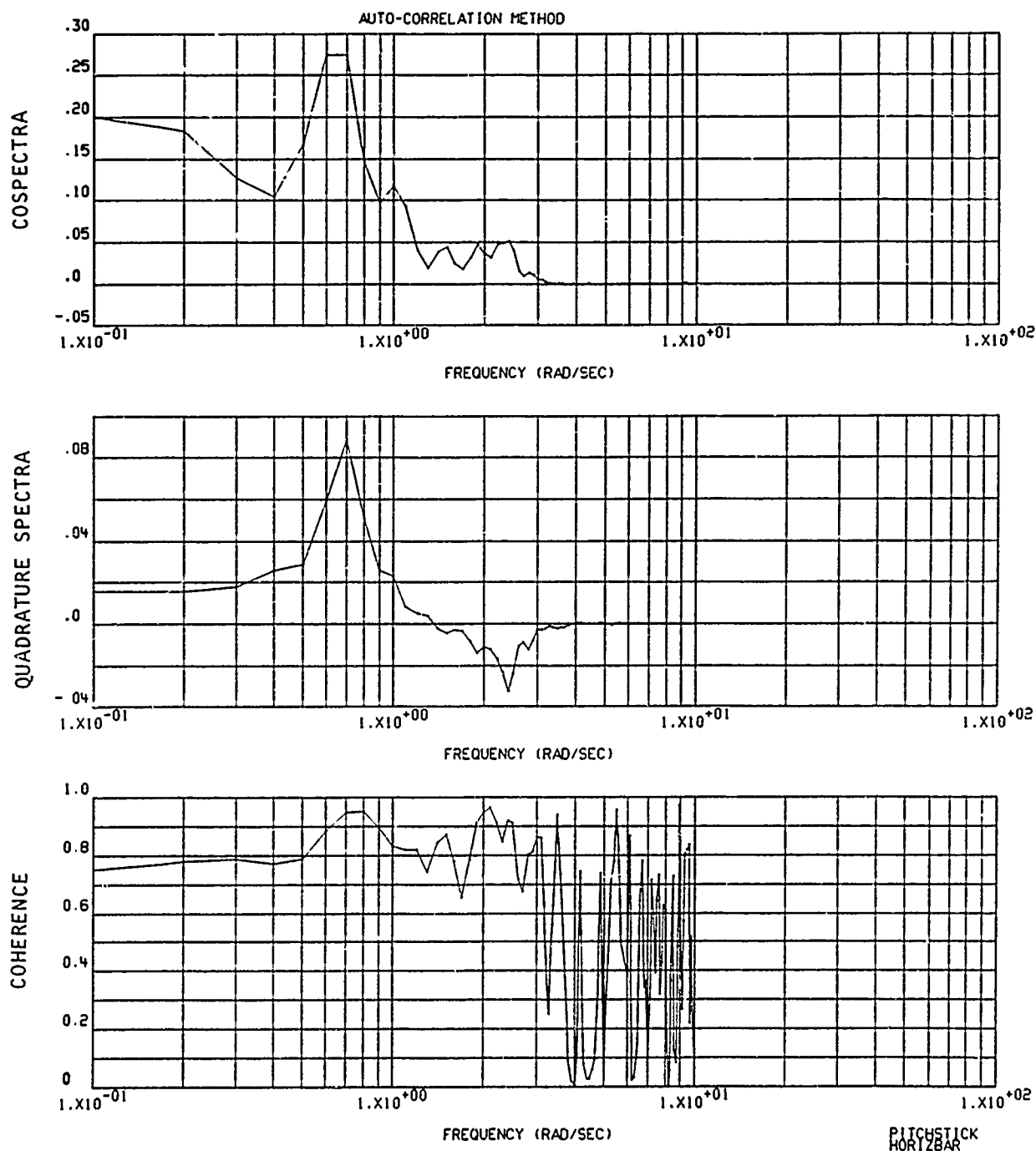
01A12 REFUEL ANALYSIS.

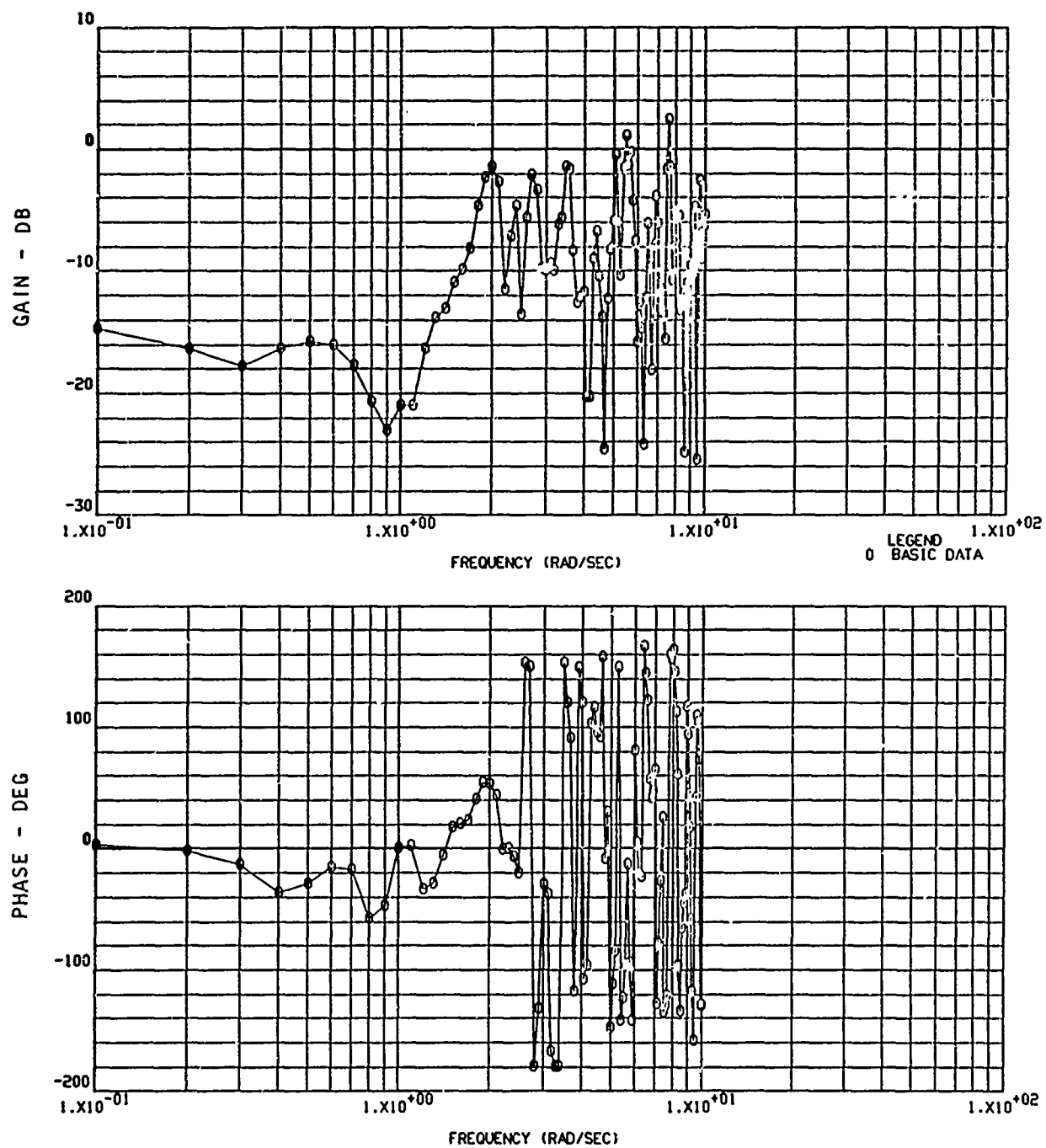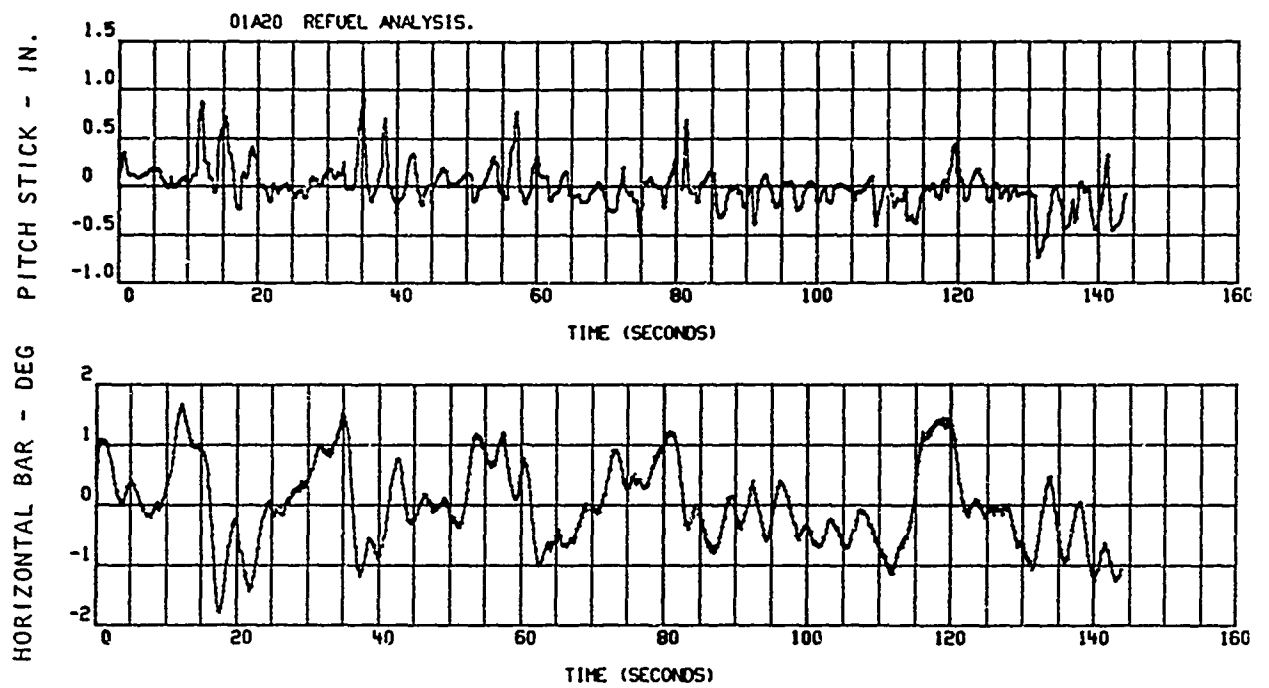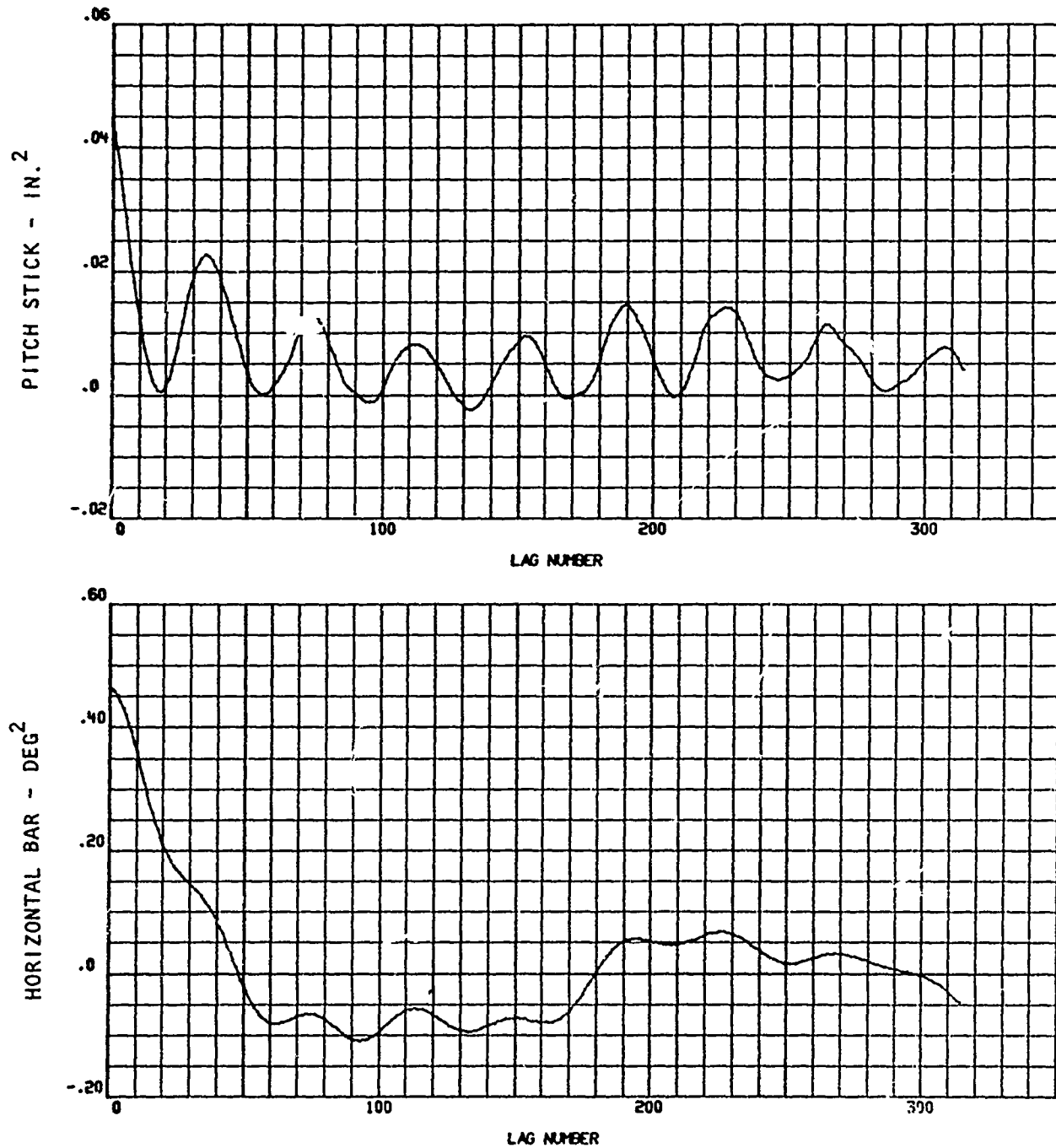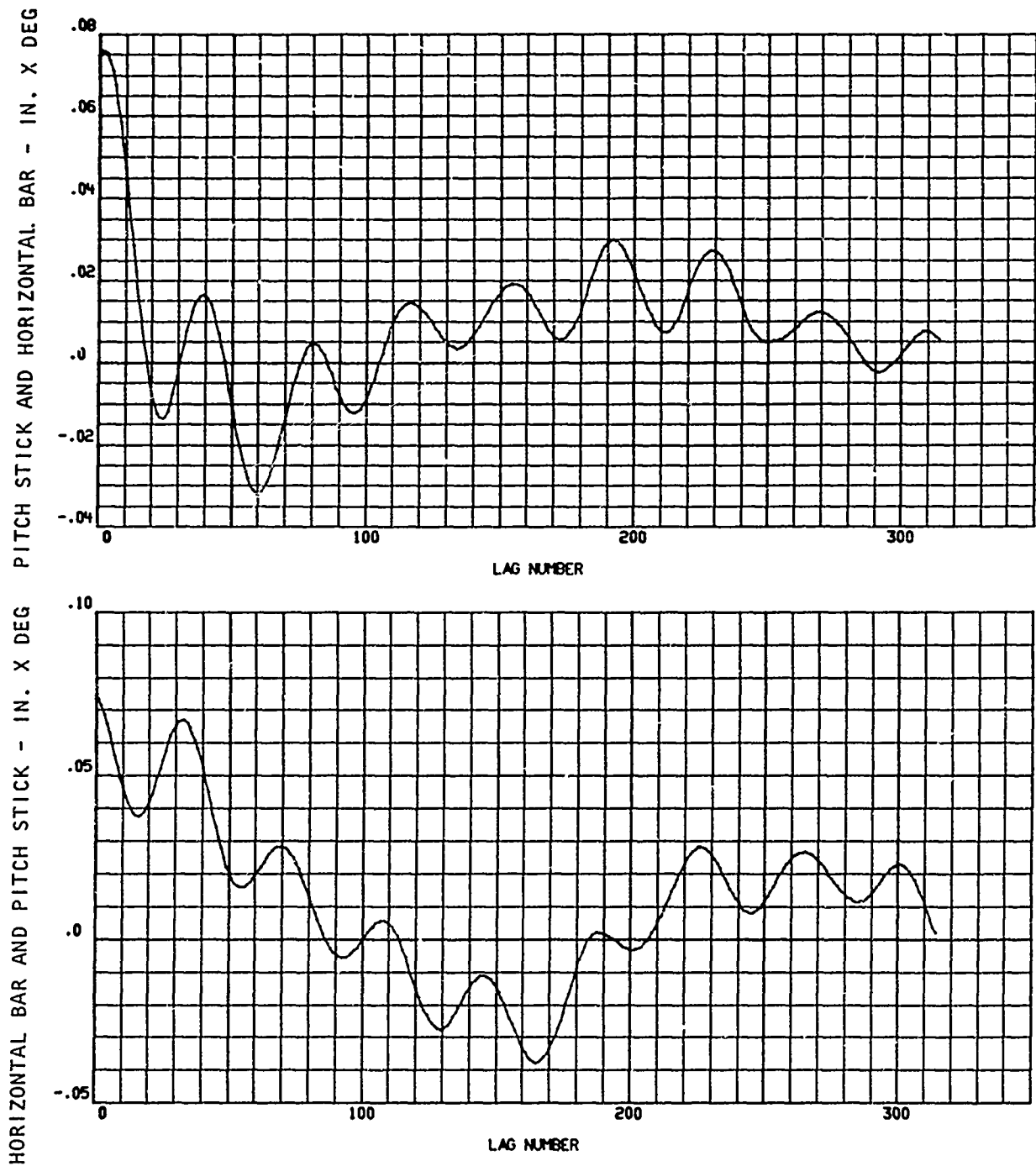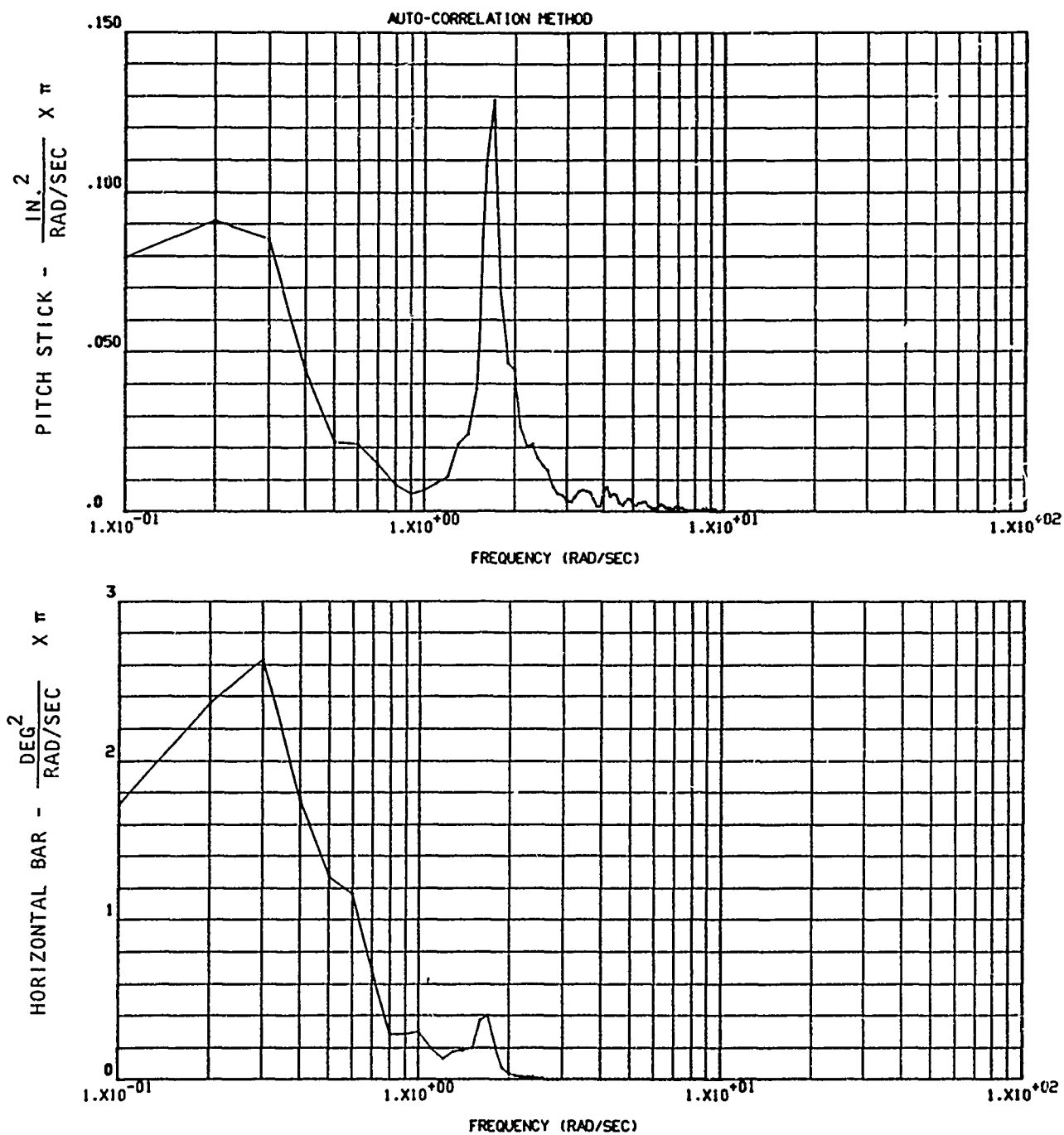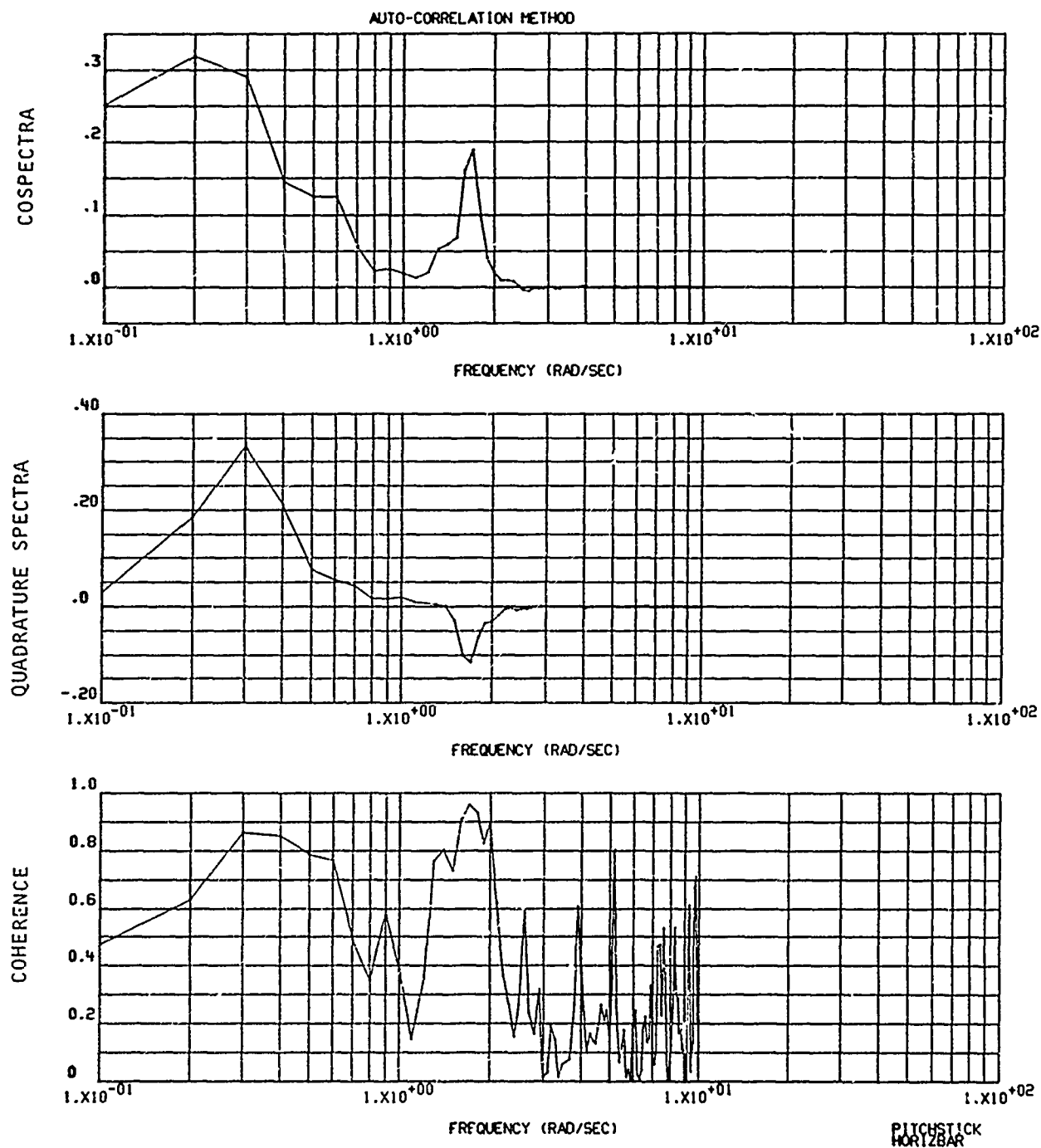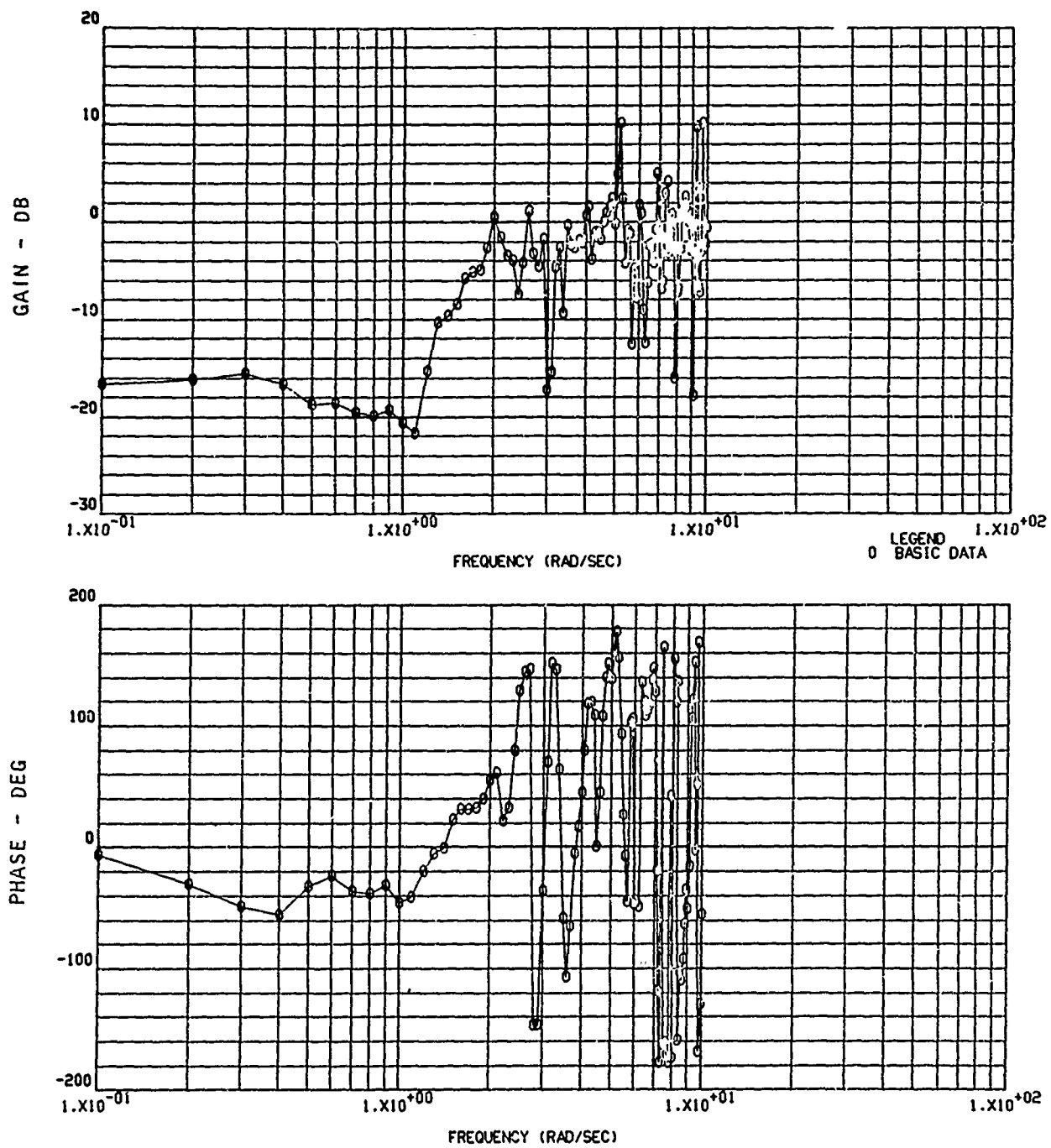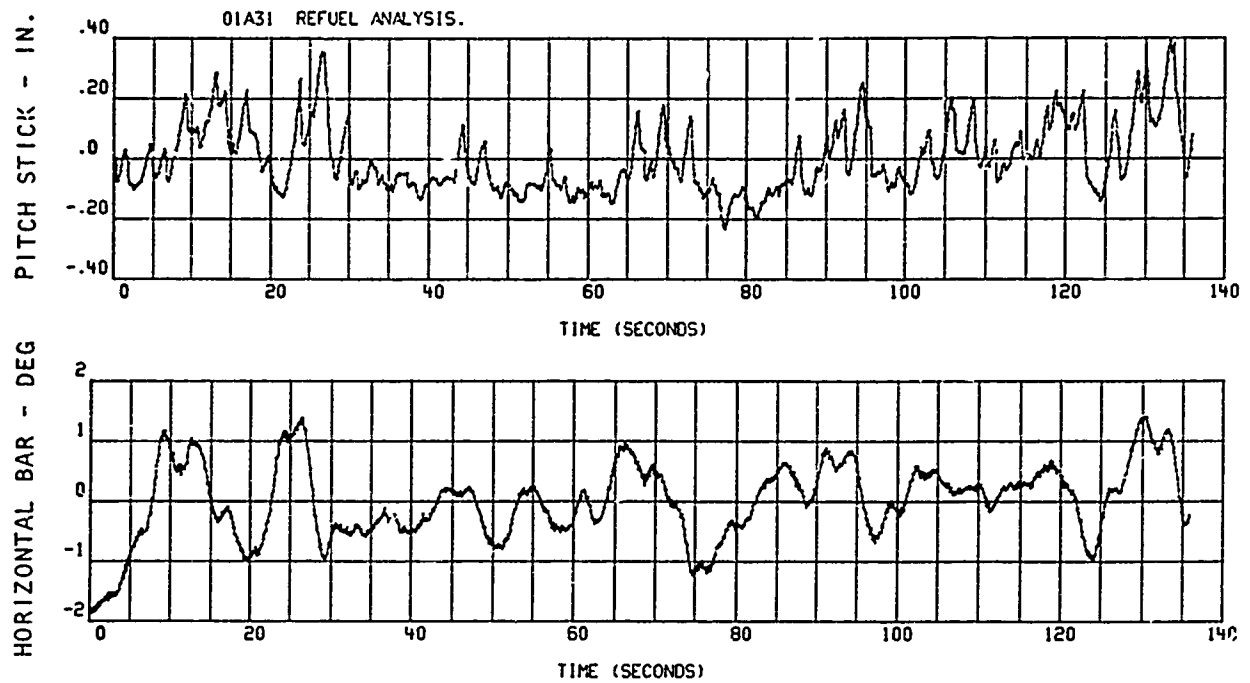Figure 60. AR Simulation Run No. 01A12 Data (Cont)

170
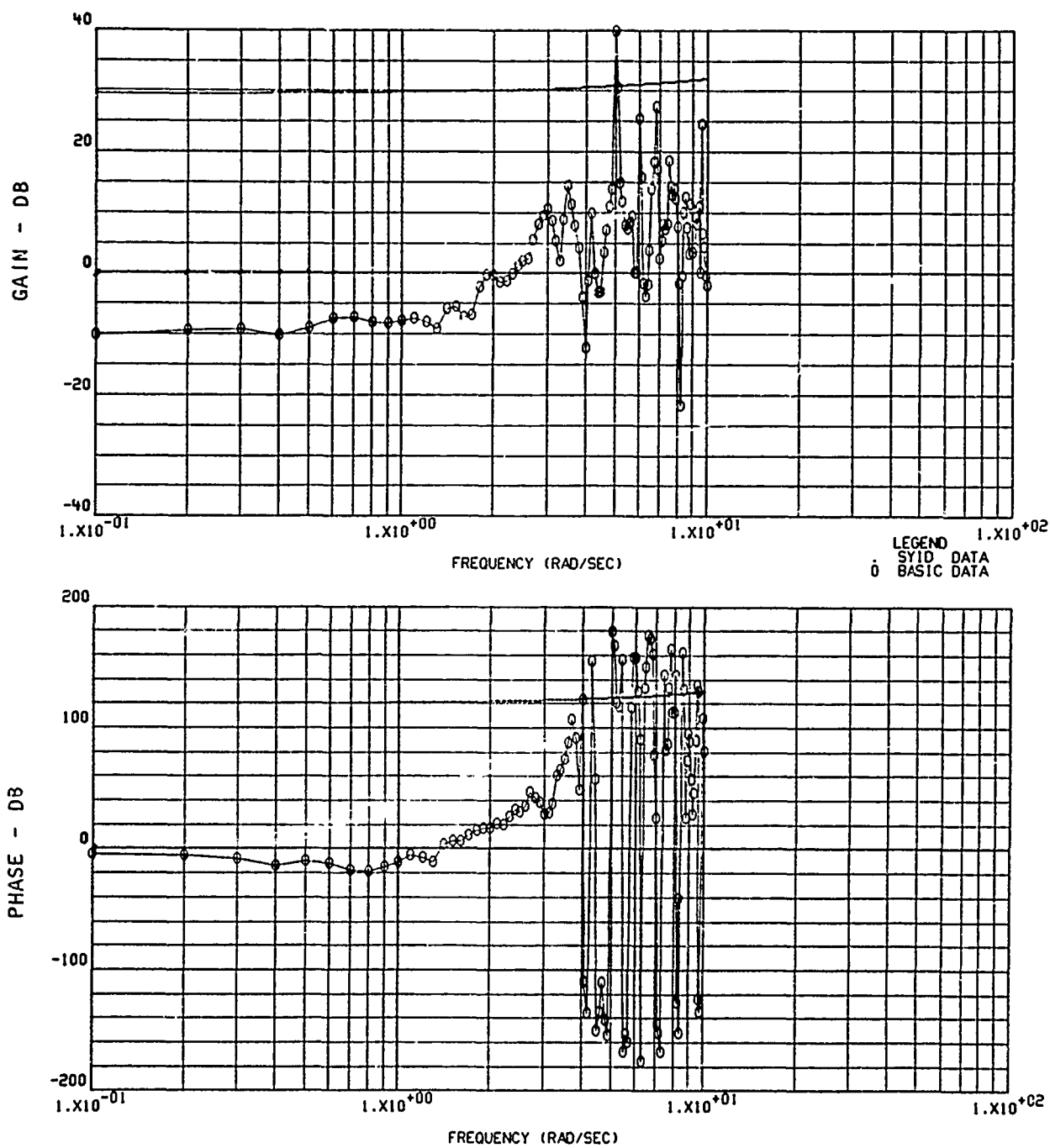
Figure 60. AR Simulation Run No. 01A12 Data (Concl)

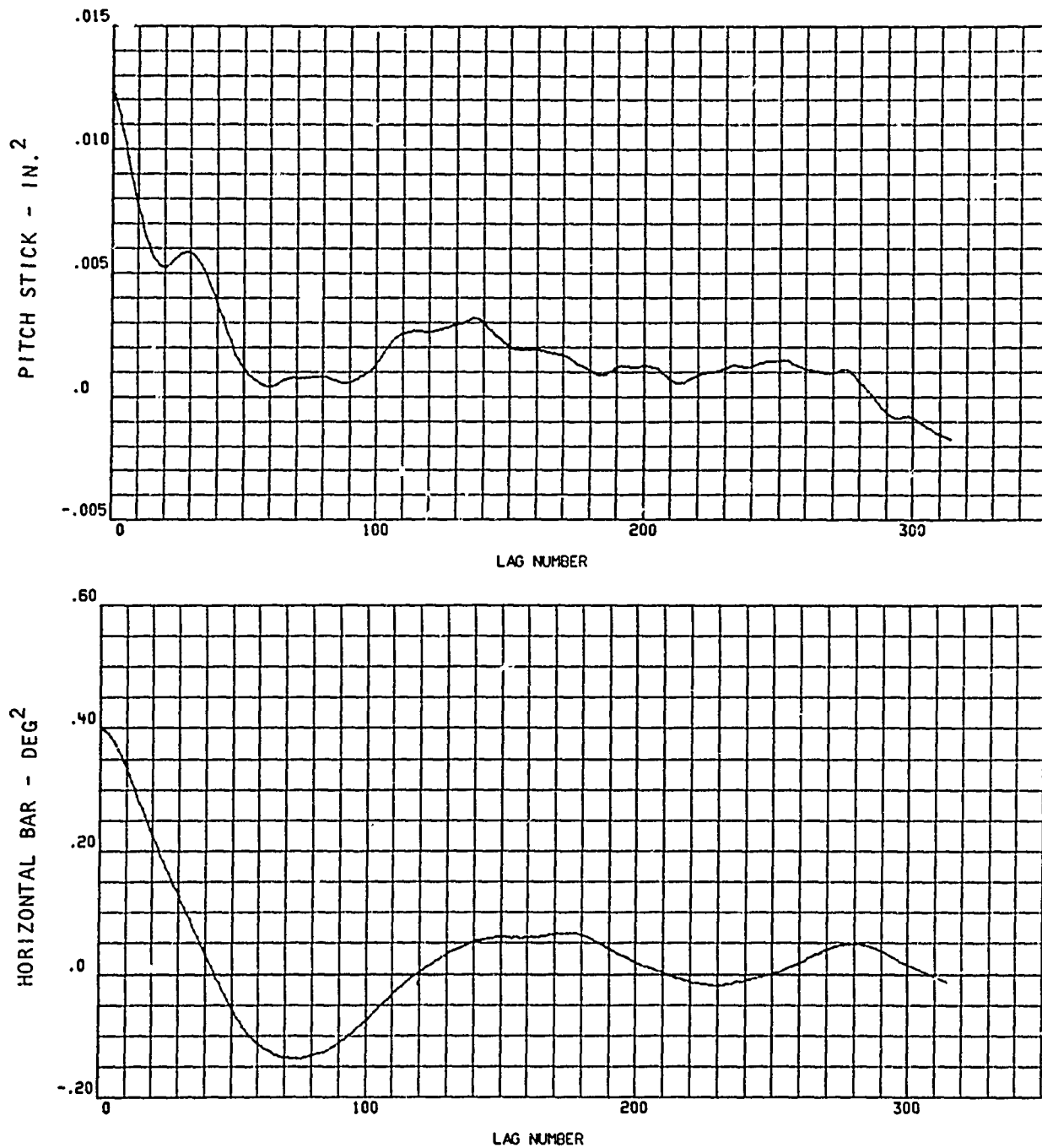171
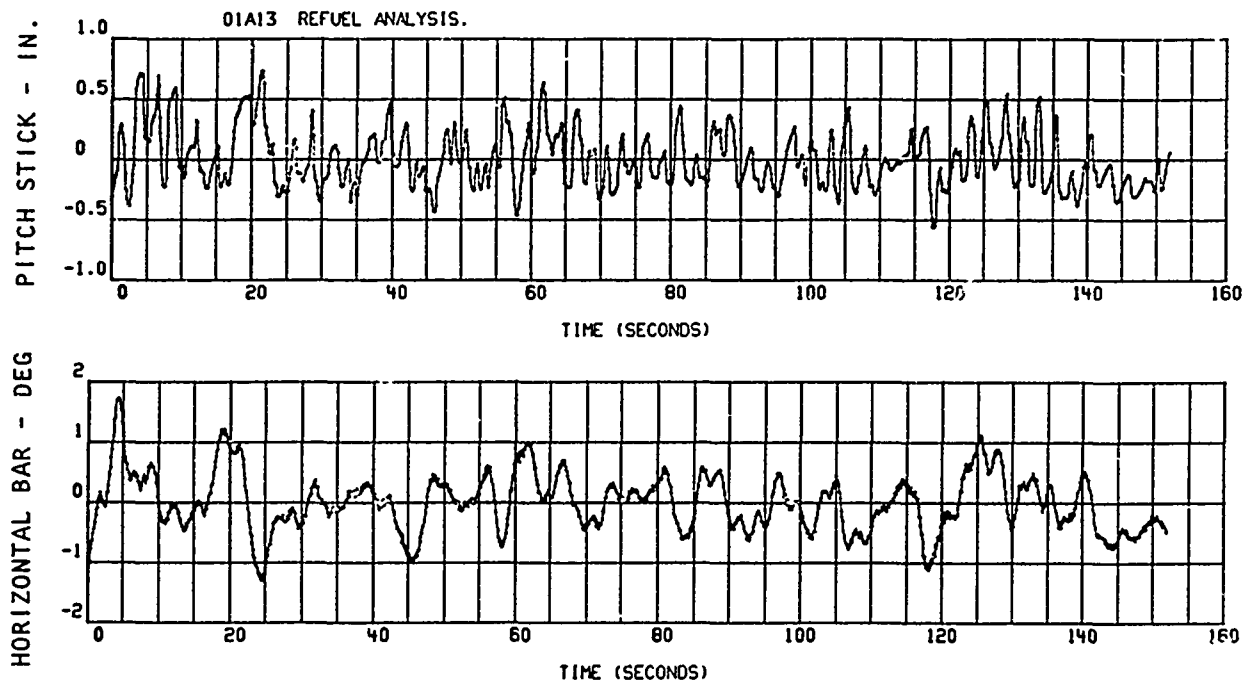
Figure 61. AR Simulation Run No. 01A13 Data

01A13 REFUEL ANALYSIS.
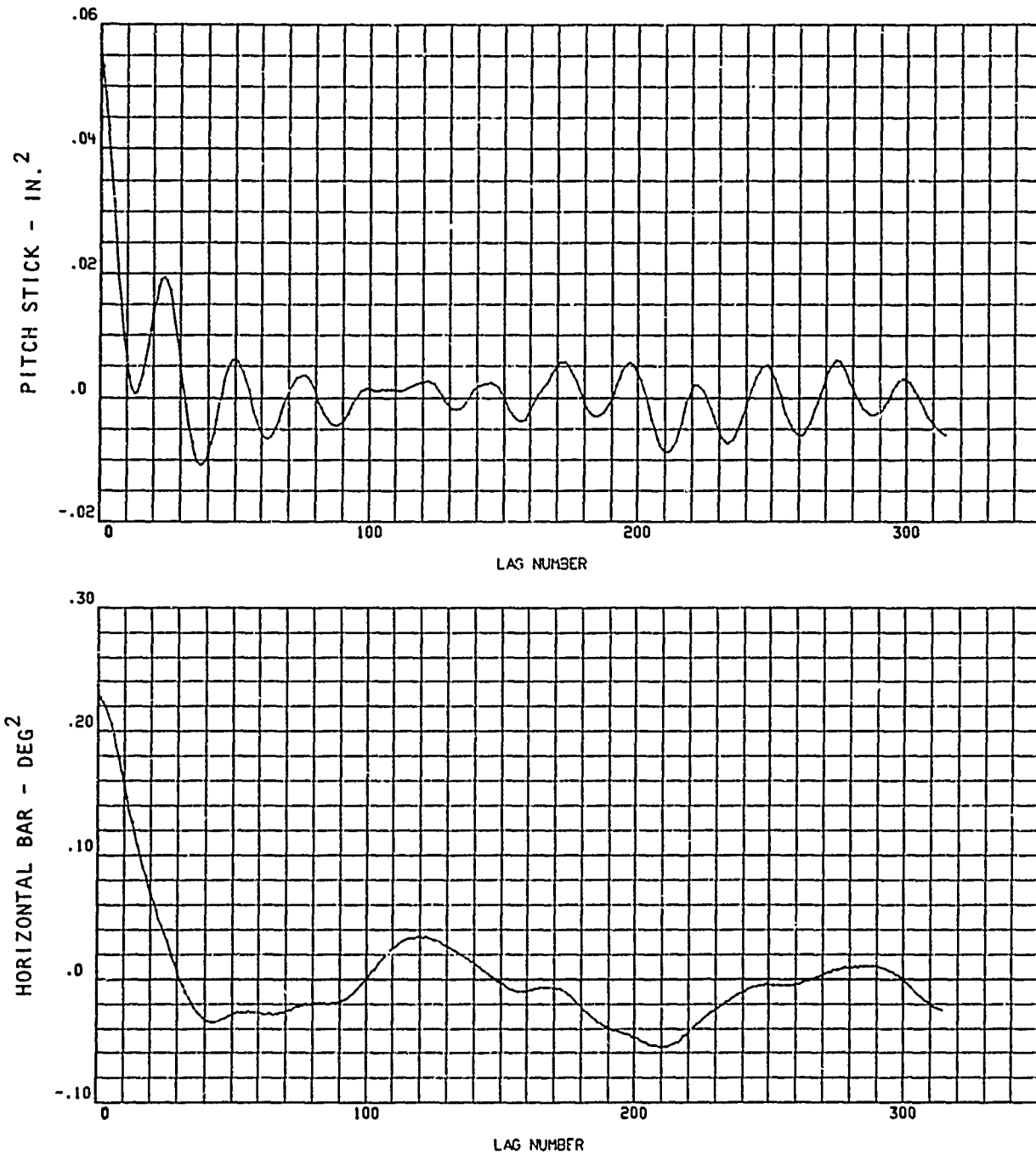
Figure 61.   AR Simulation Run No. 01A13 Data (Cont)

CROSS CORRELATION FUNCTIONS

Figure 61.   AR Simulation Run No. 01A13 Data (Cont)

174

SPECTRAL DENSITY FUNCTIONS

Figure 61.   AR Simulation Run No. 01A13 Data (Cont)

175

Figure 61.   AR Simulation Run No. 01A13 Data (Cont)

176
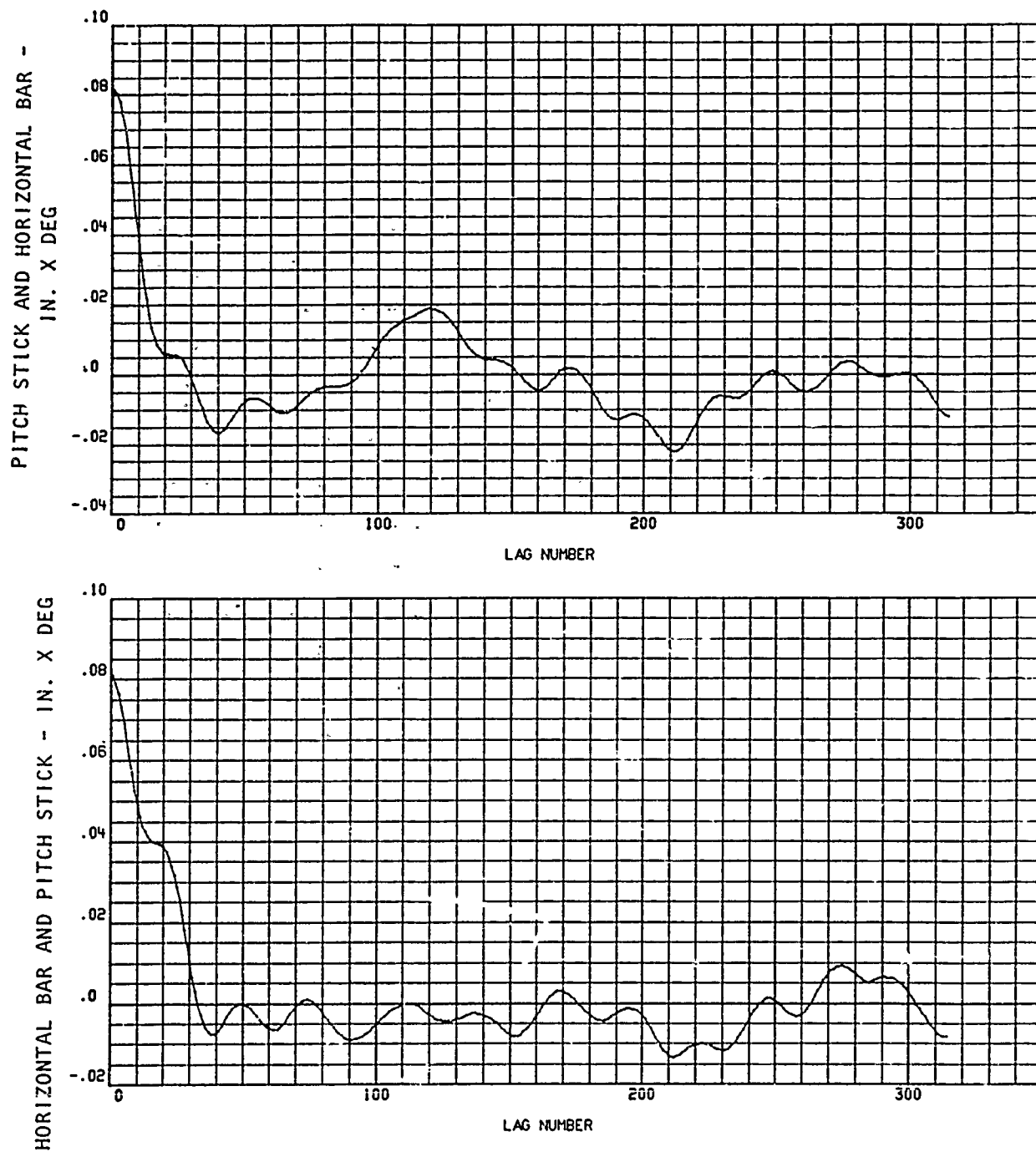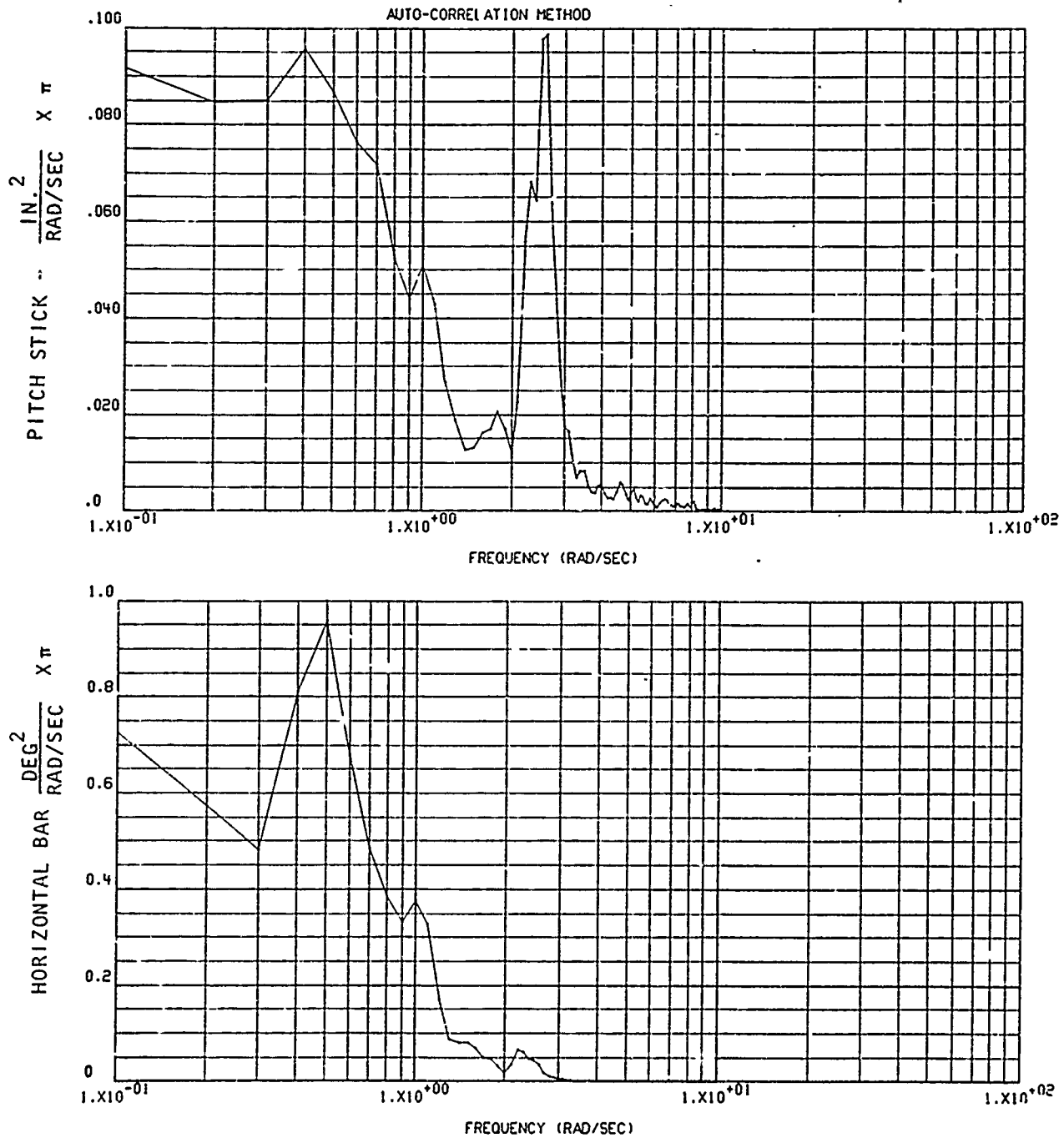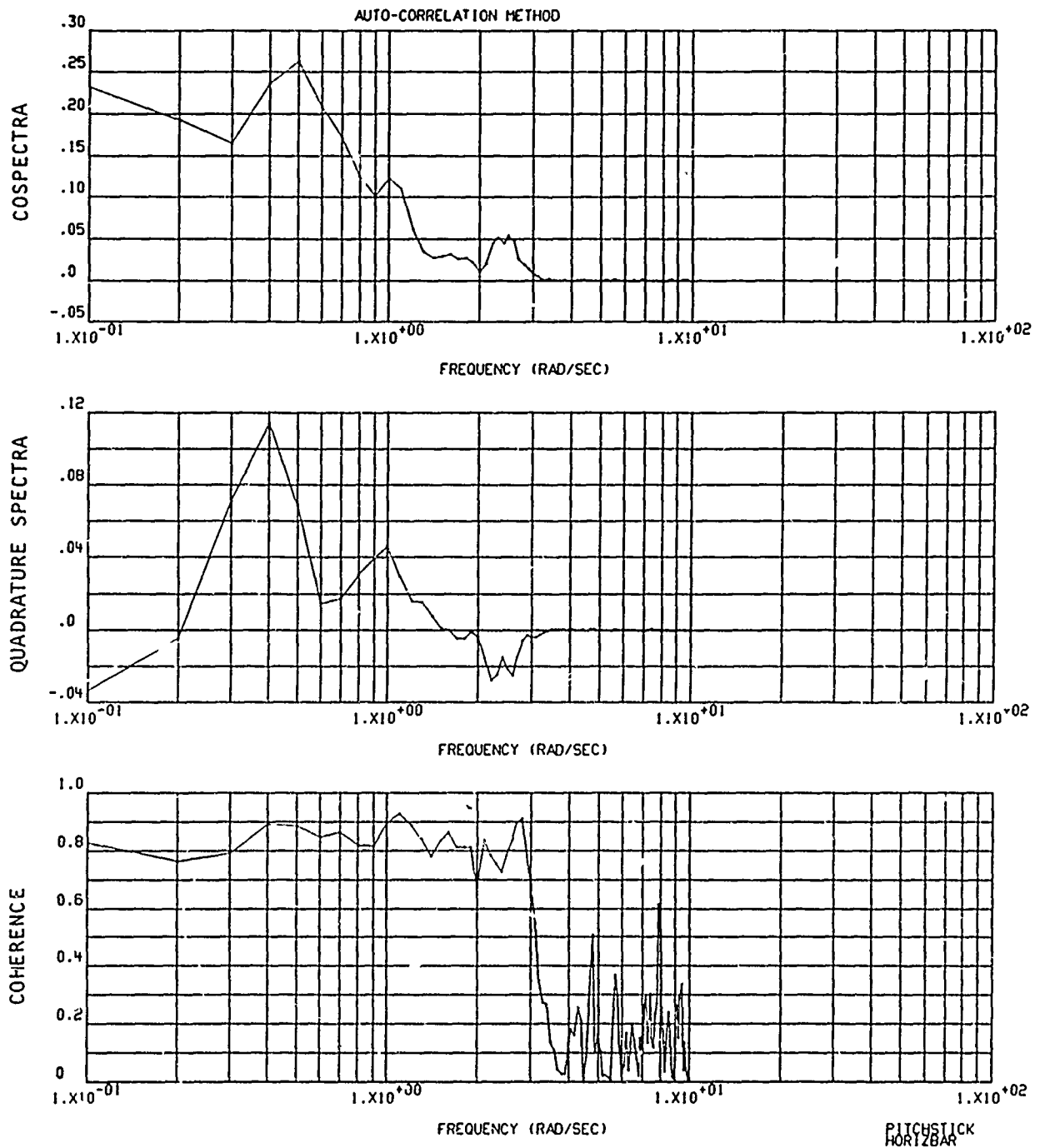
01A13 REFUEL ANALYSIS.
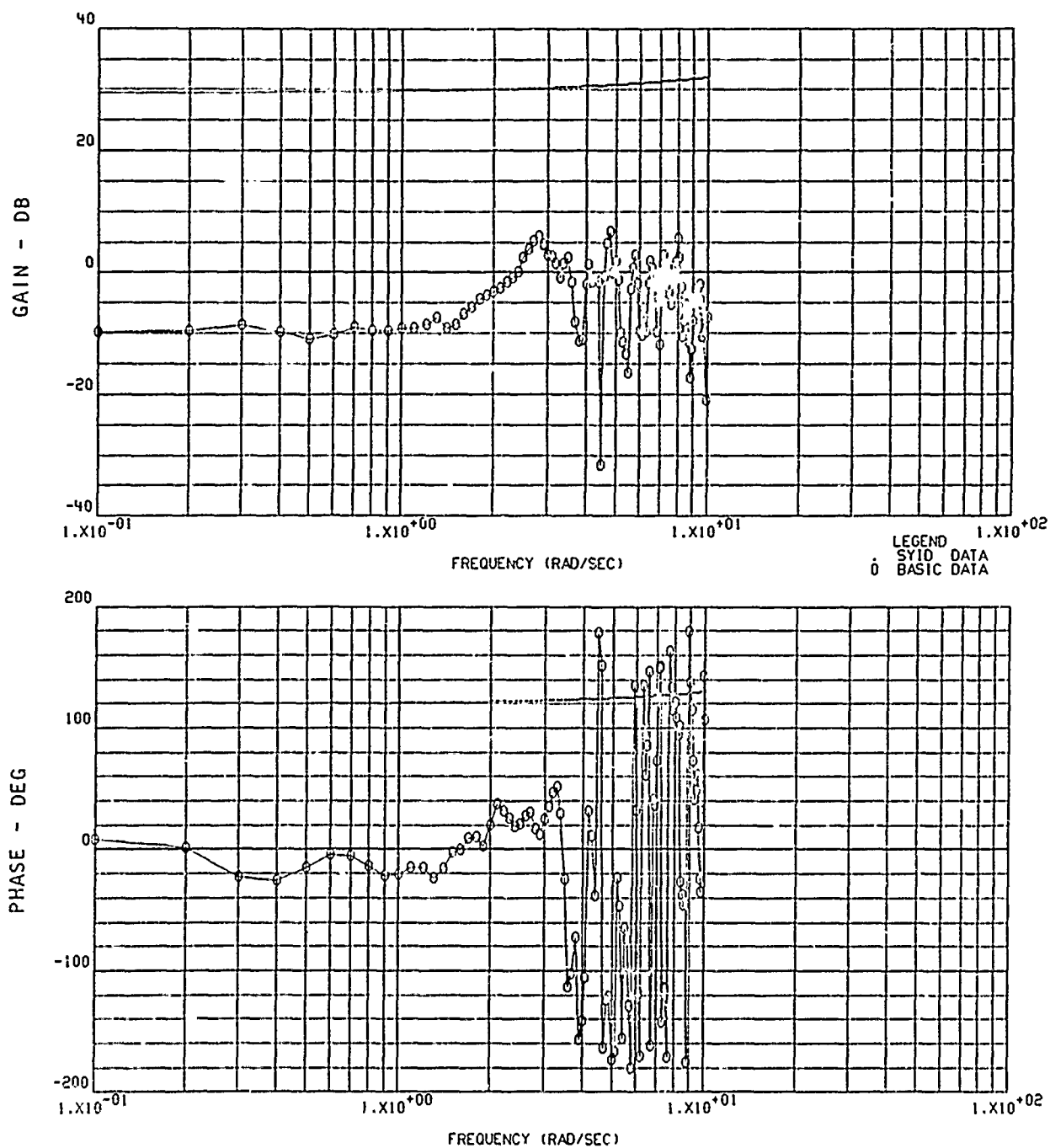
Figure 61. AR Simulation Run No. 01A13 Data (Concl)
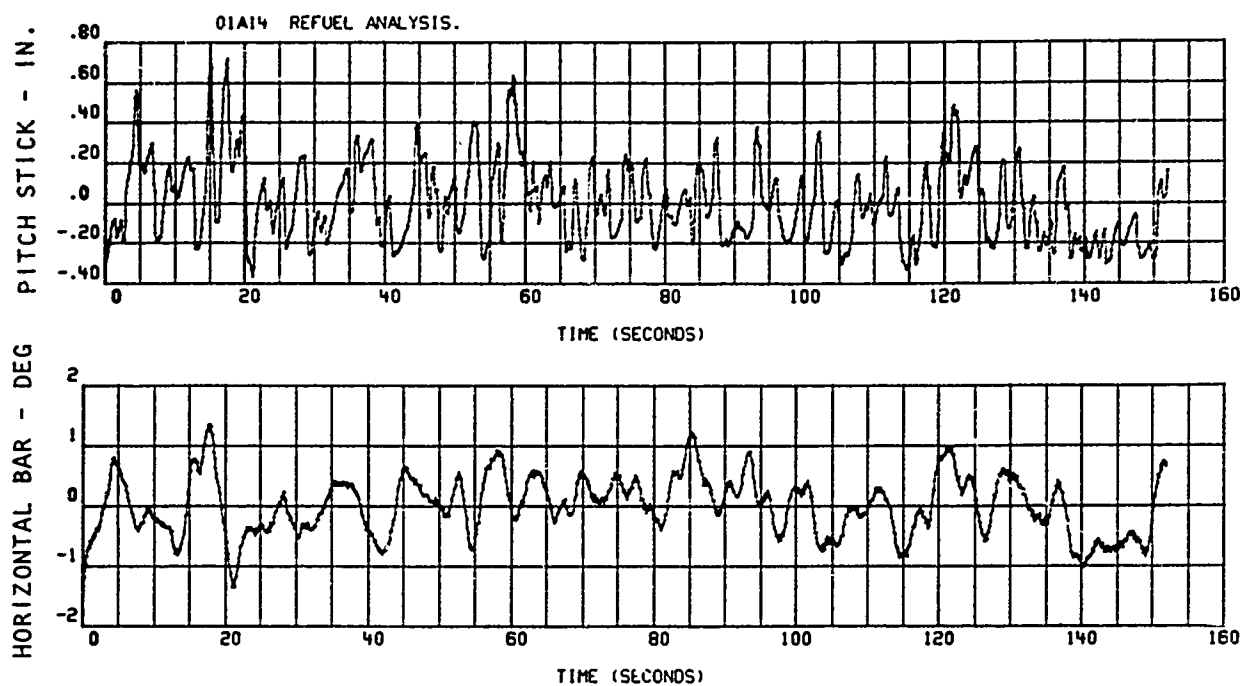
Figure 62.   AR Simulation Run No. 01A14 Data

01A14 REFUEL ANALYSIS.

AUTO CORRELATION FUNCTIONS

Figure 62. AR Simulation Run No. 01A14 Data (Cont)

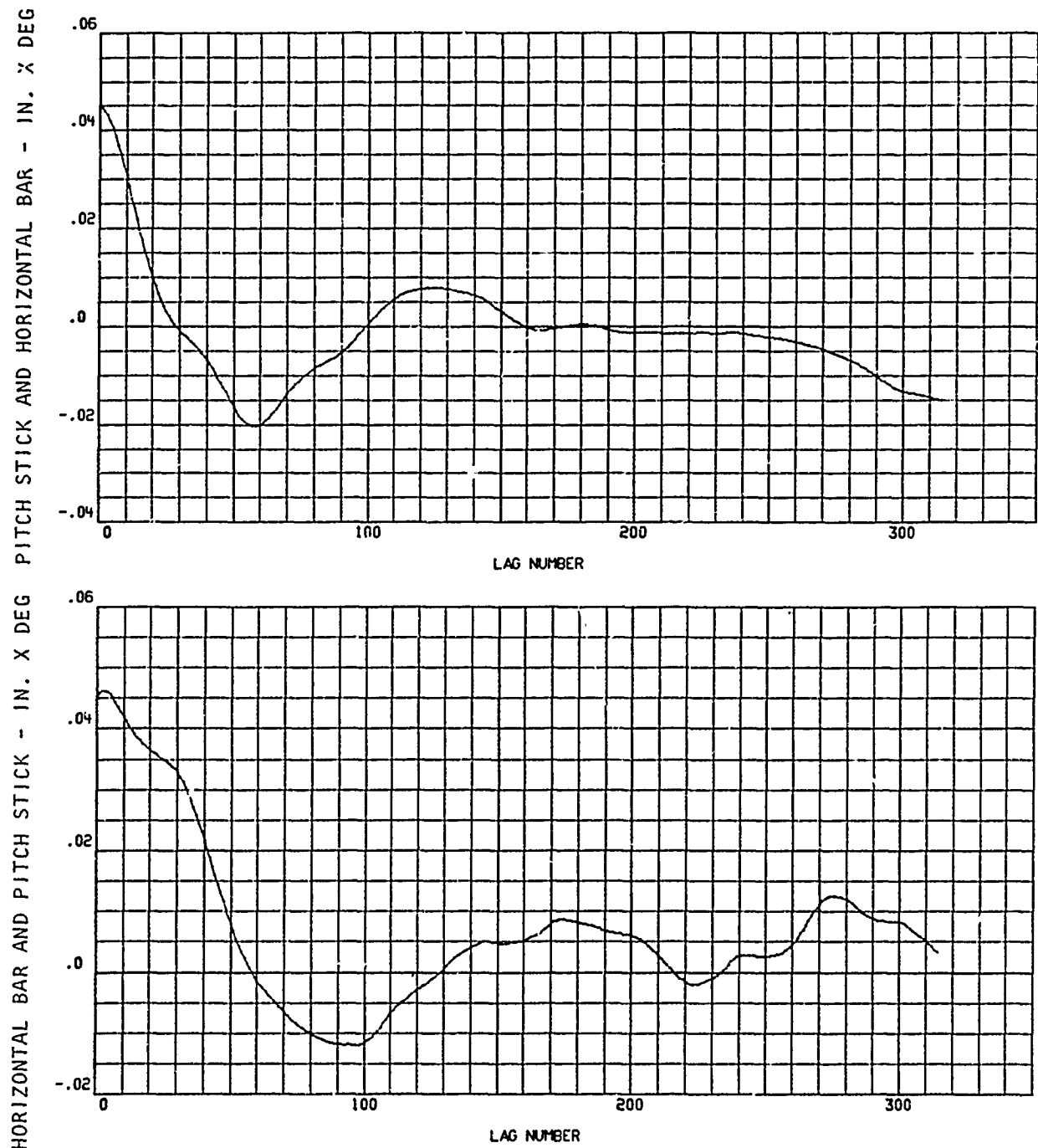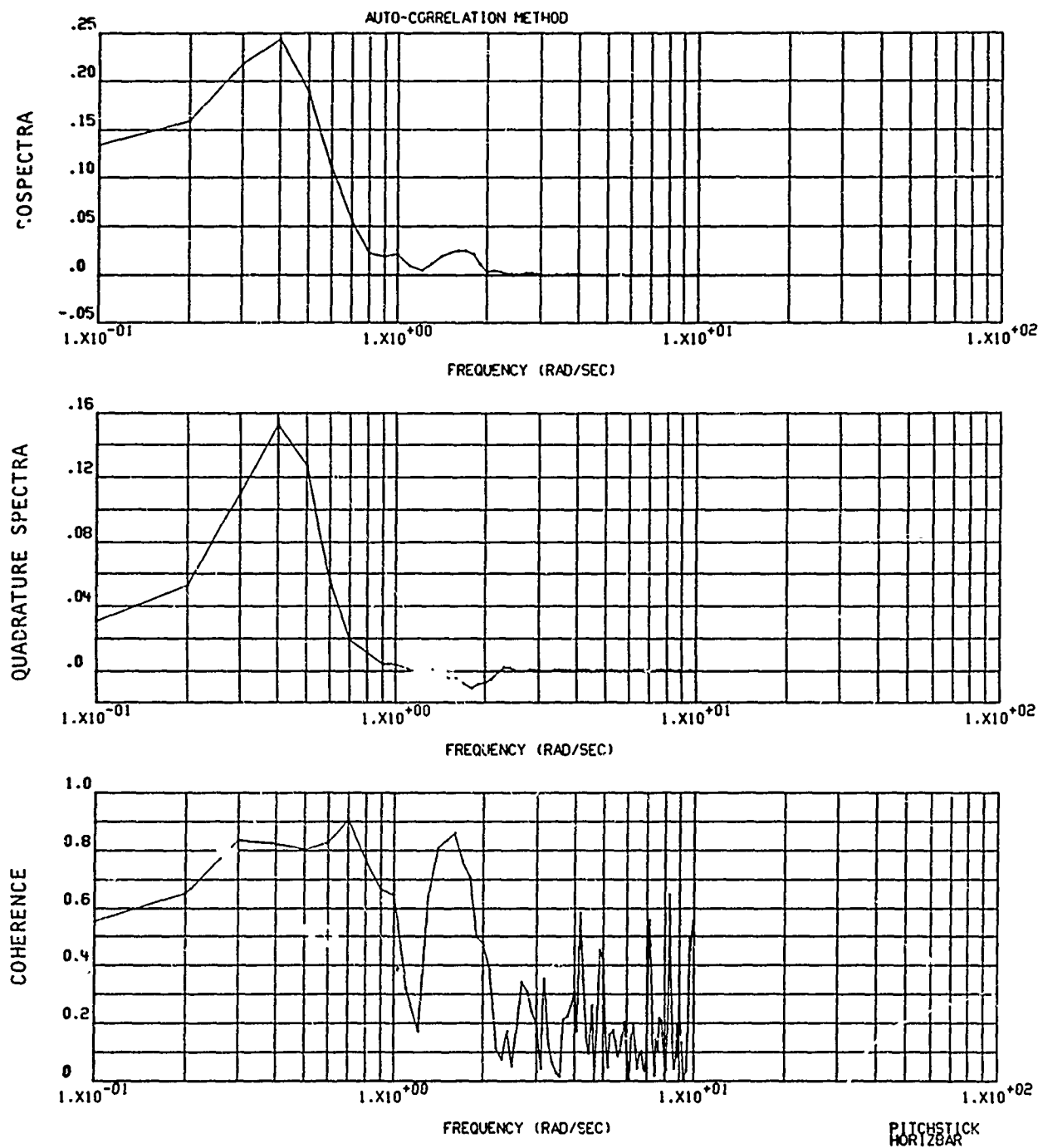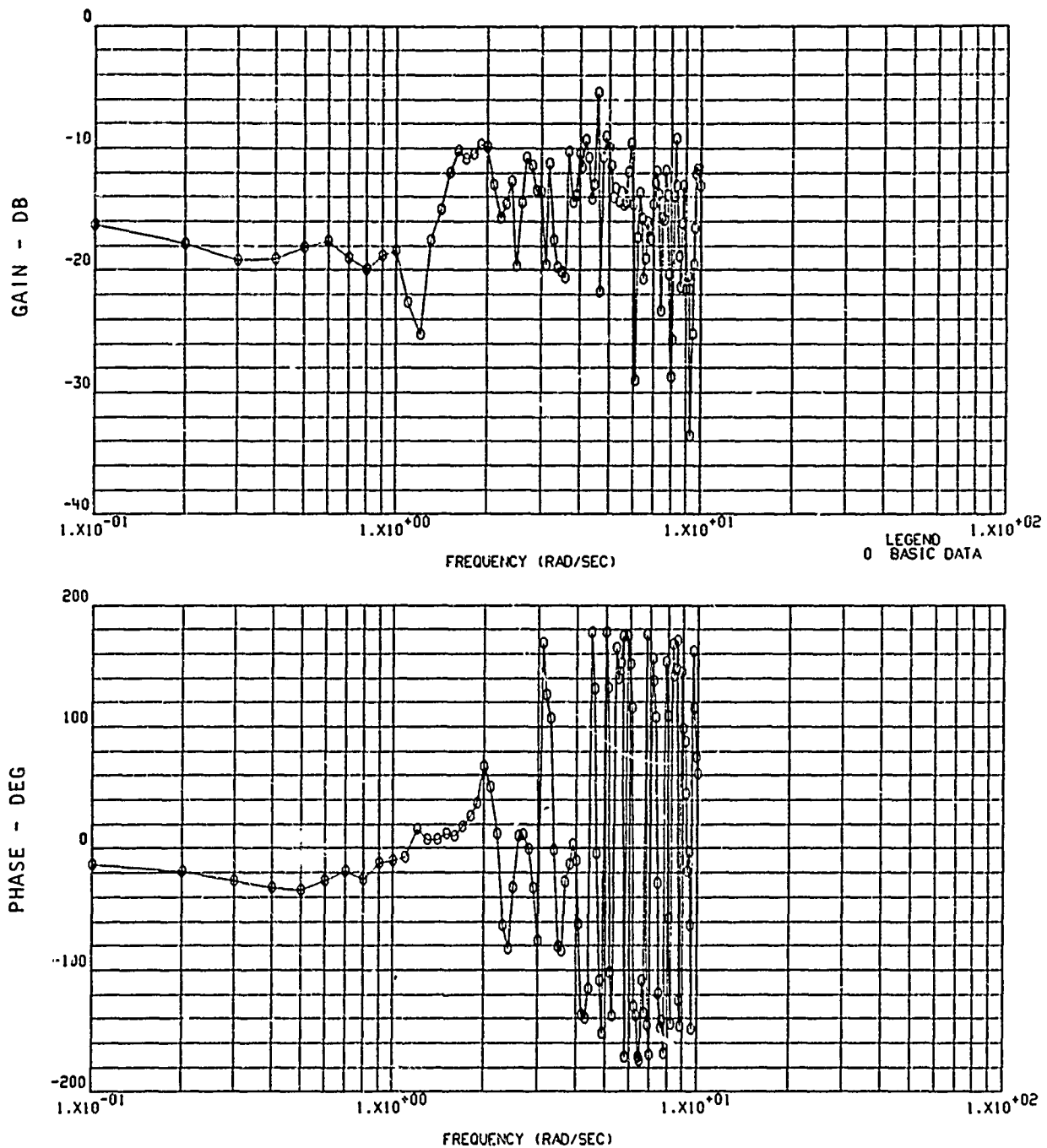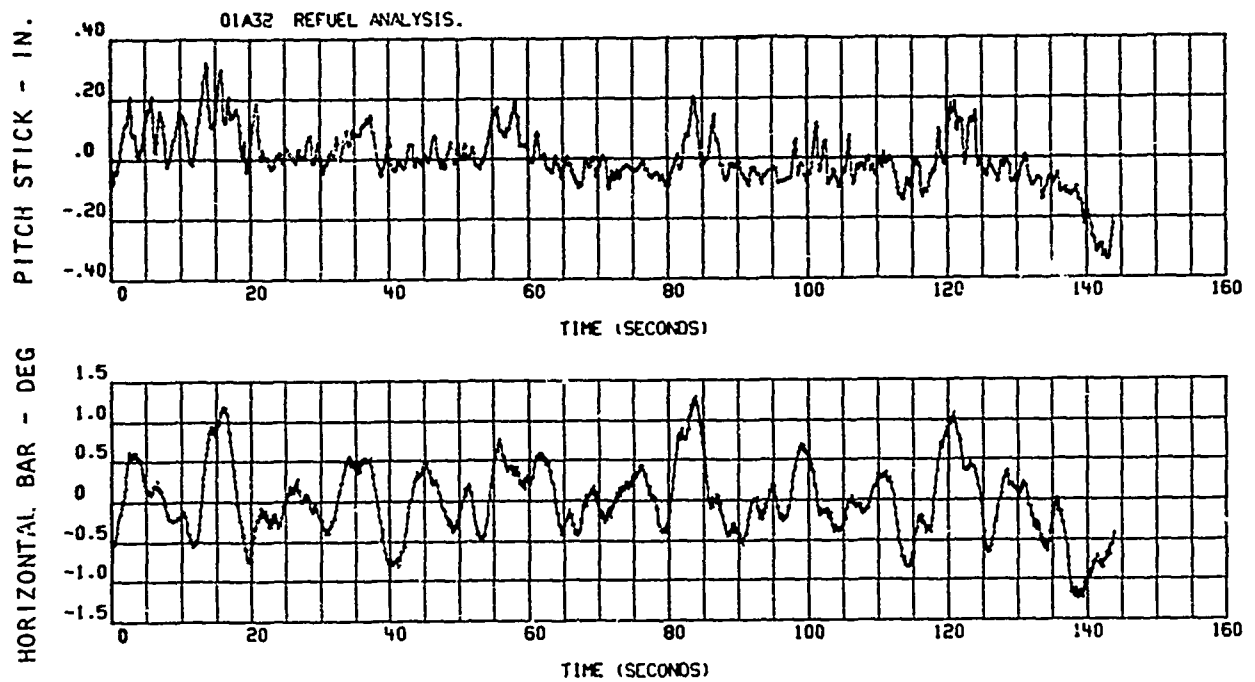179

01A14 REFUEL ANALYSIS.

CROSS CORRELATION FUNCTIONS

Figure 62.   AR Simulation Run No. 01A14 Data (Cont)

180

Figure 62. AR Simulation Run No. 01A14 Data (Cont)

Figure 62. AR Simulation Run No. 01A14 Data (Cont)

Figure 62. AR Simulation Run No. 01A14 Data (Concl)

183

Figure 63.   AR Simulation Run No. 01A15 Data

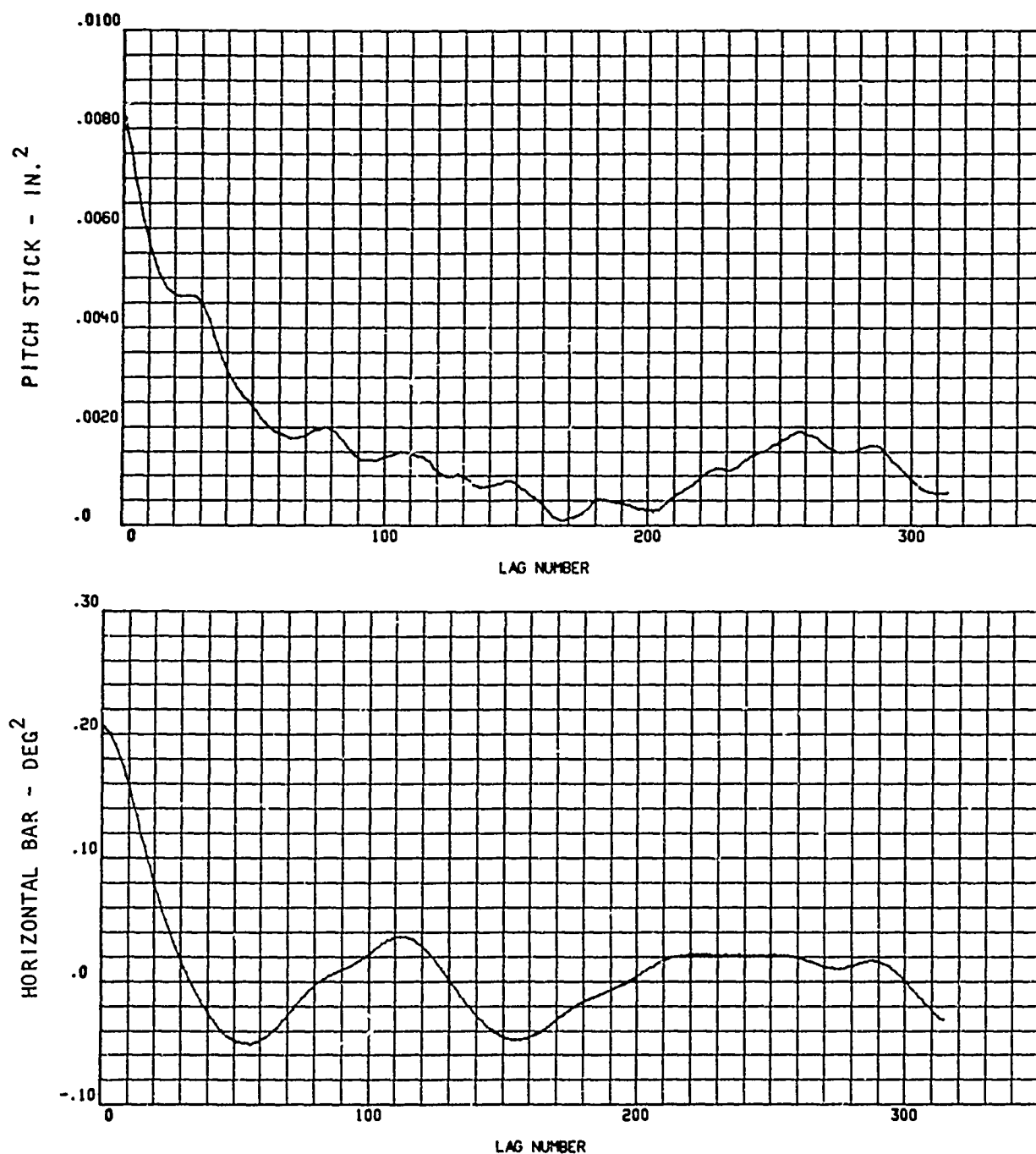AUTO CORRELATION FUNCTIONS

Figure 63. AR Simulation Run No. 01A15 Data (Cont)

185
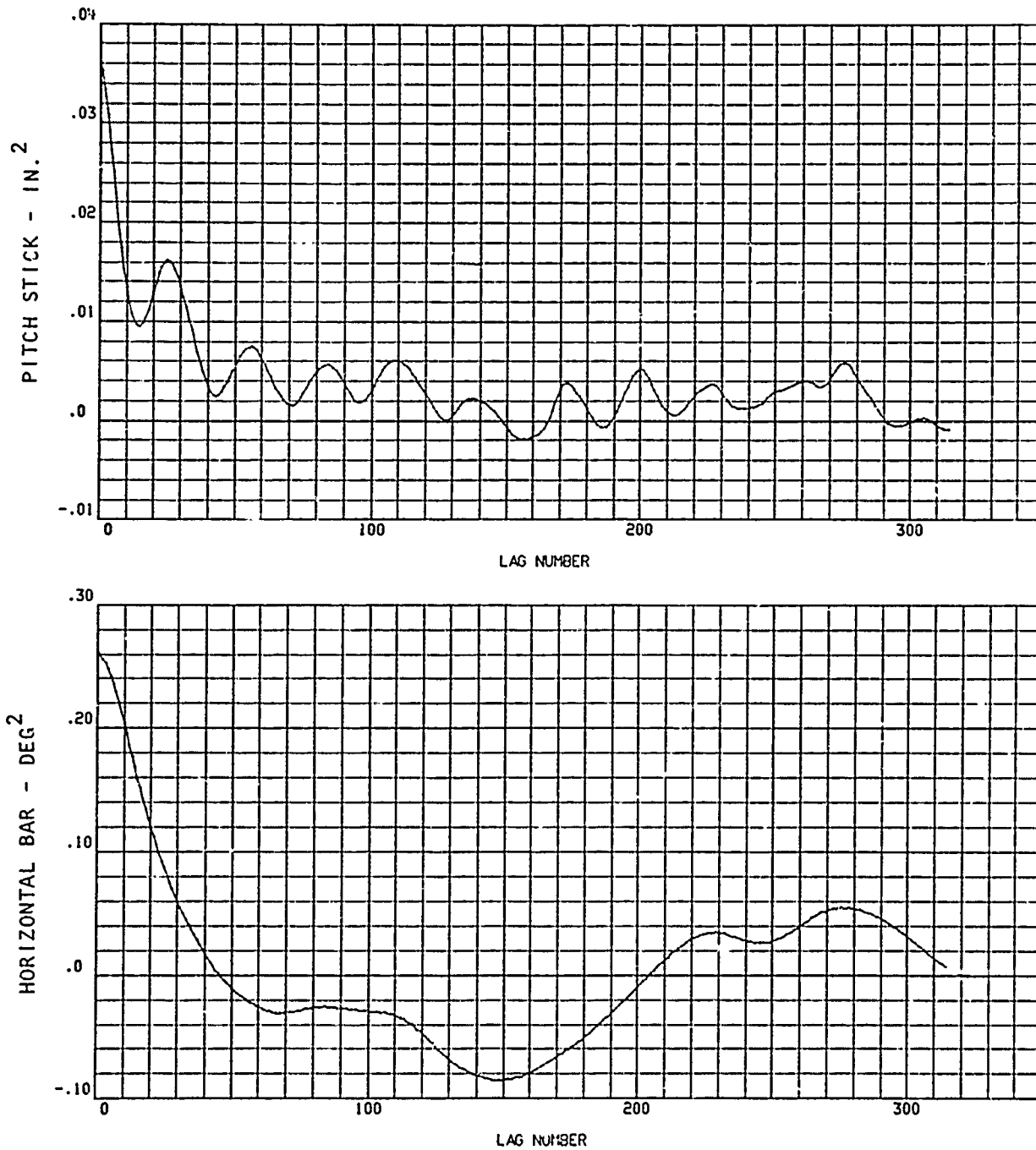
01A15 REFUEL ANALYSIS.

CROSS CORRELATION FUNCTIONS

Figure 63. AR Simulation Run No. 01A15 Data (Cont)
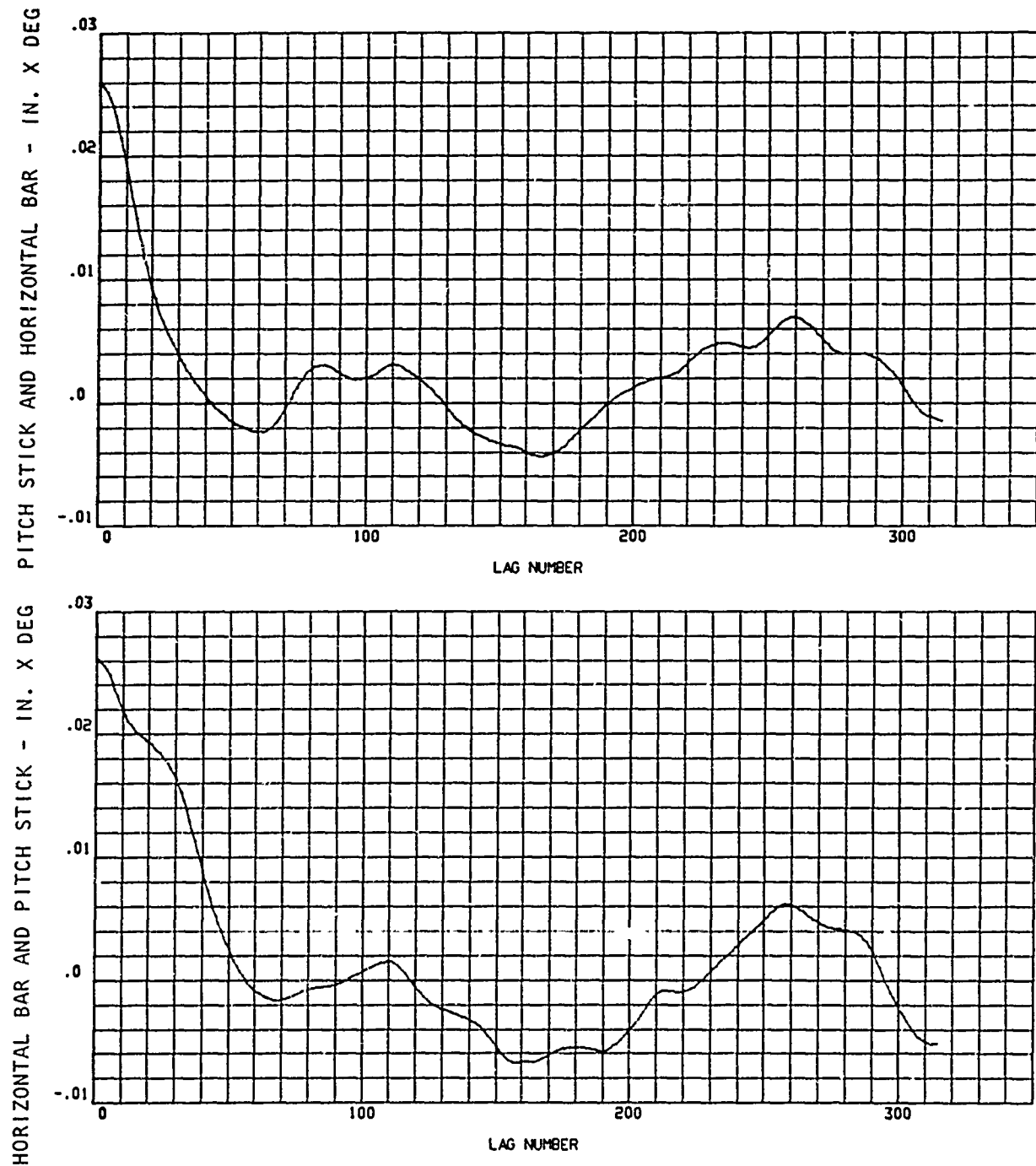
Figure 63.   AR Simulation Run No. 01A15 Data (Cont)

187

01A15 REFUEL ANALYSIS.

SPECTRAL DENSITY FUNCTIONS

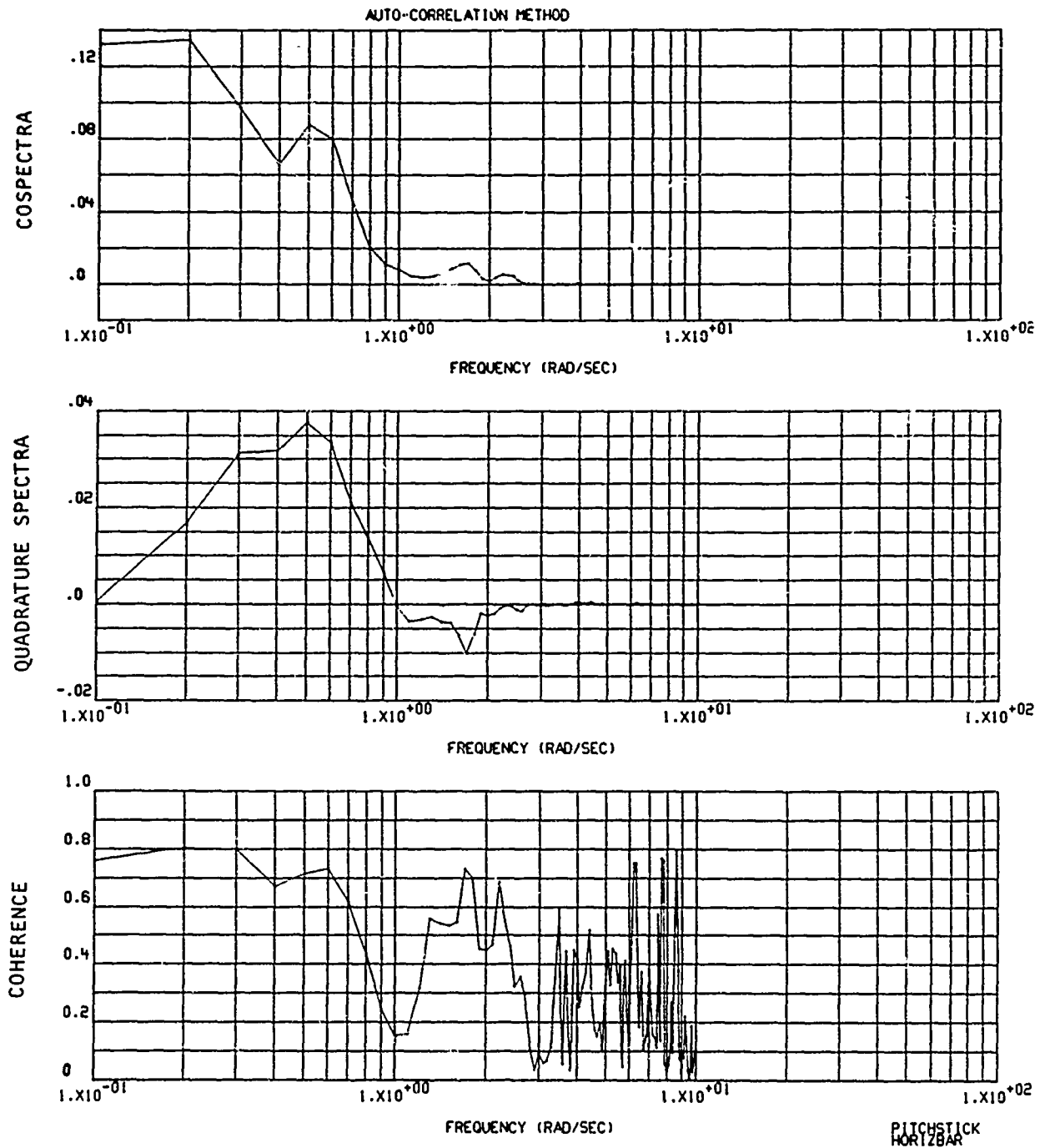Figure 63.   AR Simulation Run No. 01A15 Data (Cont)

187

Figure 63. AR Simulation Run No. 01A15 Data (Cont)

188

01A15 REFUEL ANALYSIS.

GAIN - DB vs FREQUENCY (RAD/SEC)

LEGEND
O BASIC DATA

PHASE - DEG vs FREQUENCY (RAD/SEC)

Figure 63.   AR Simulation Run No. 01A15 Data (Concl)

189

Figure 64. AR Simulation Run No. 01A16 Data

190

AUTO CORRELATION FUNCTIONS

Figure 64.   AR Simulation Run No. 01A16 Data (Cont)

01A16 REFUEL ANALYSIS.

CROSS CORRELATION FUNCTIONS

Figure 64. AR Simulation Run No. 01A16 Data (Cont)

Figure 64. AR Simulation Run No. 01A16 Data (Cont)

193

01A16 REFUEL ANALYSIS.

AUTO-CORRELATION METHOD

Figure 64. AR Simulation Run No. 01A16 Data (Cont)

194
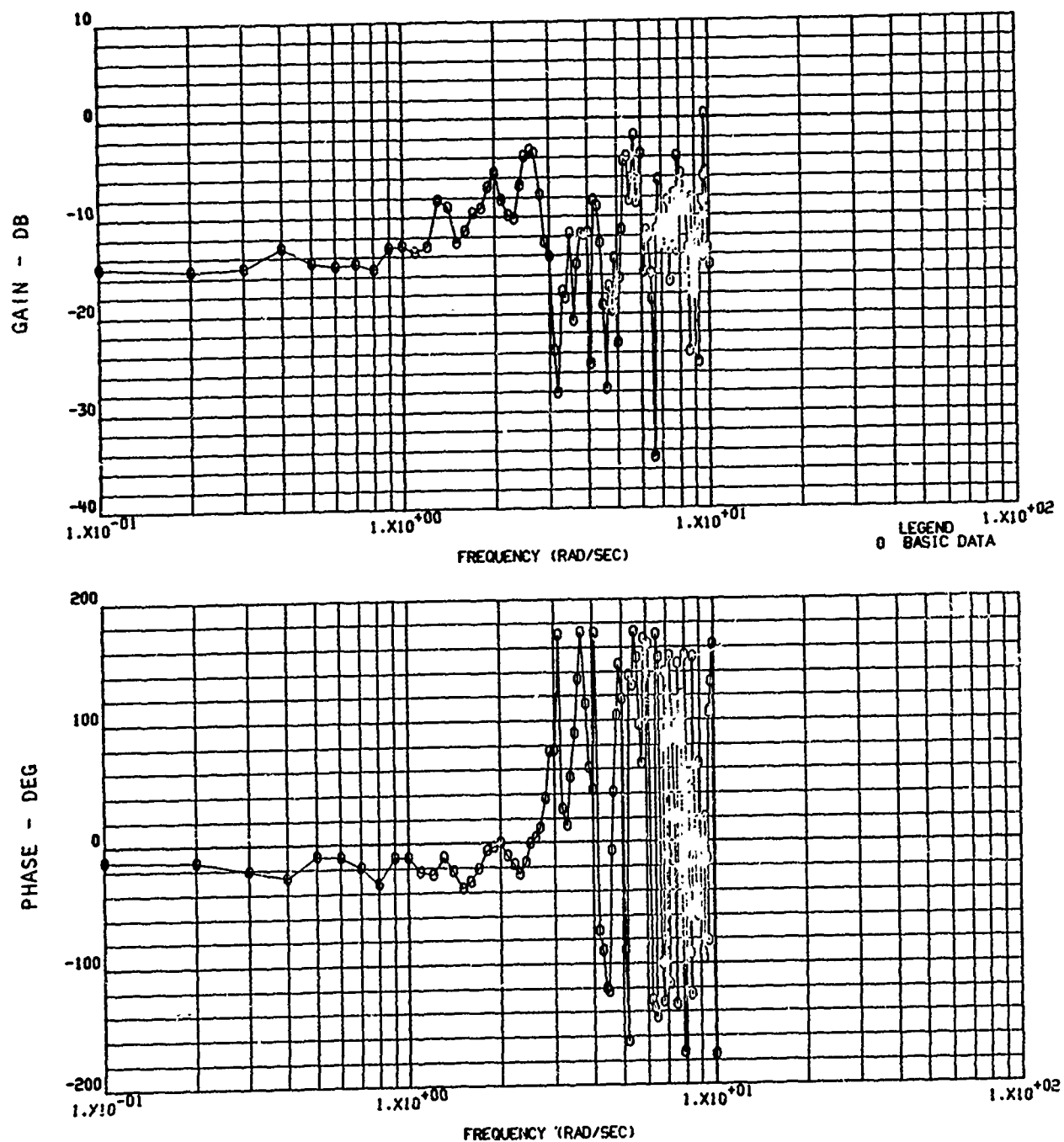
Figure 64. AR Simulation Run No. 01A16 Data (Concl)
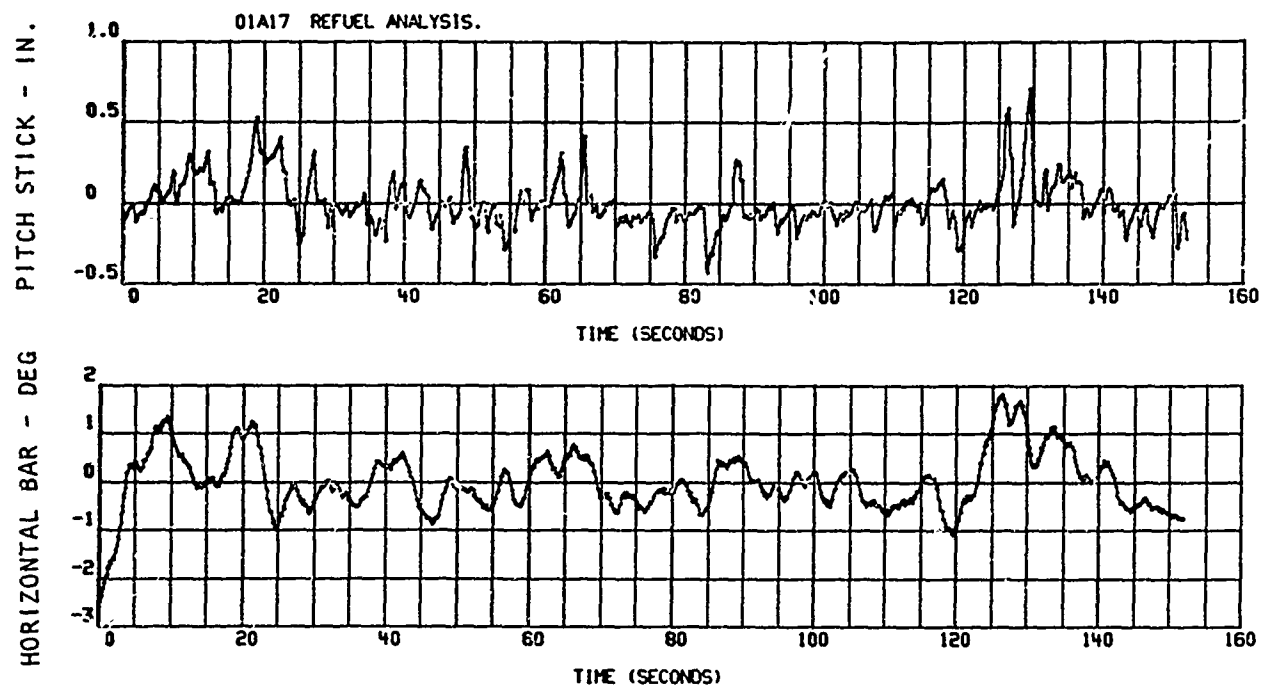
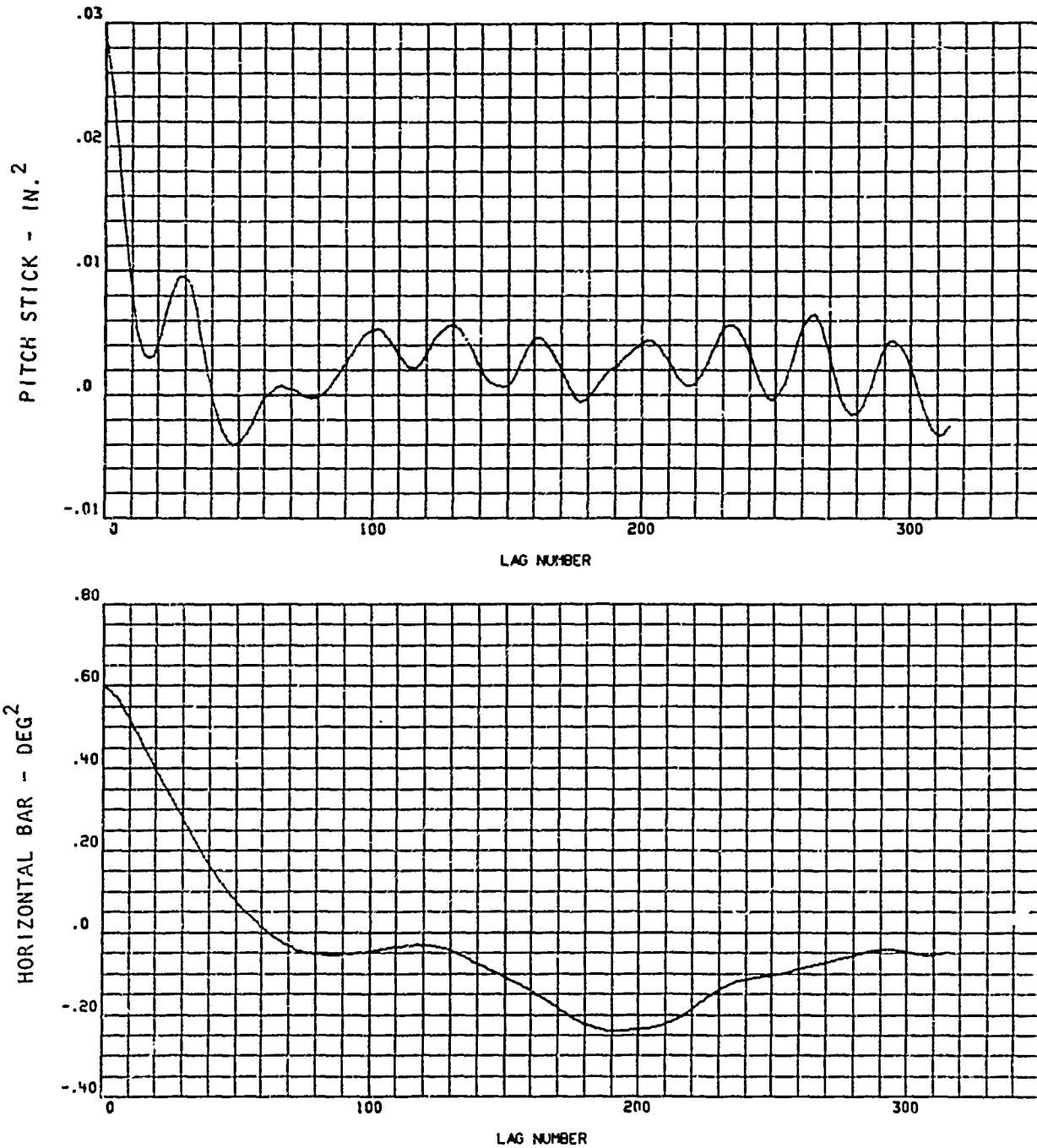Figure 65. AR Stimulation Run No. 01A17 Data
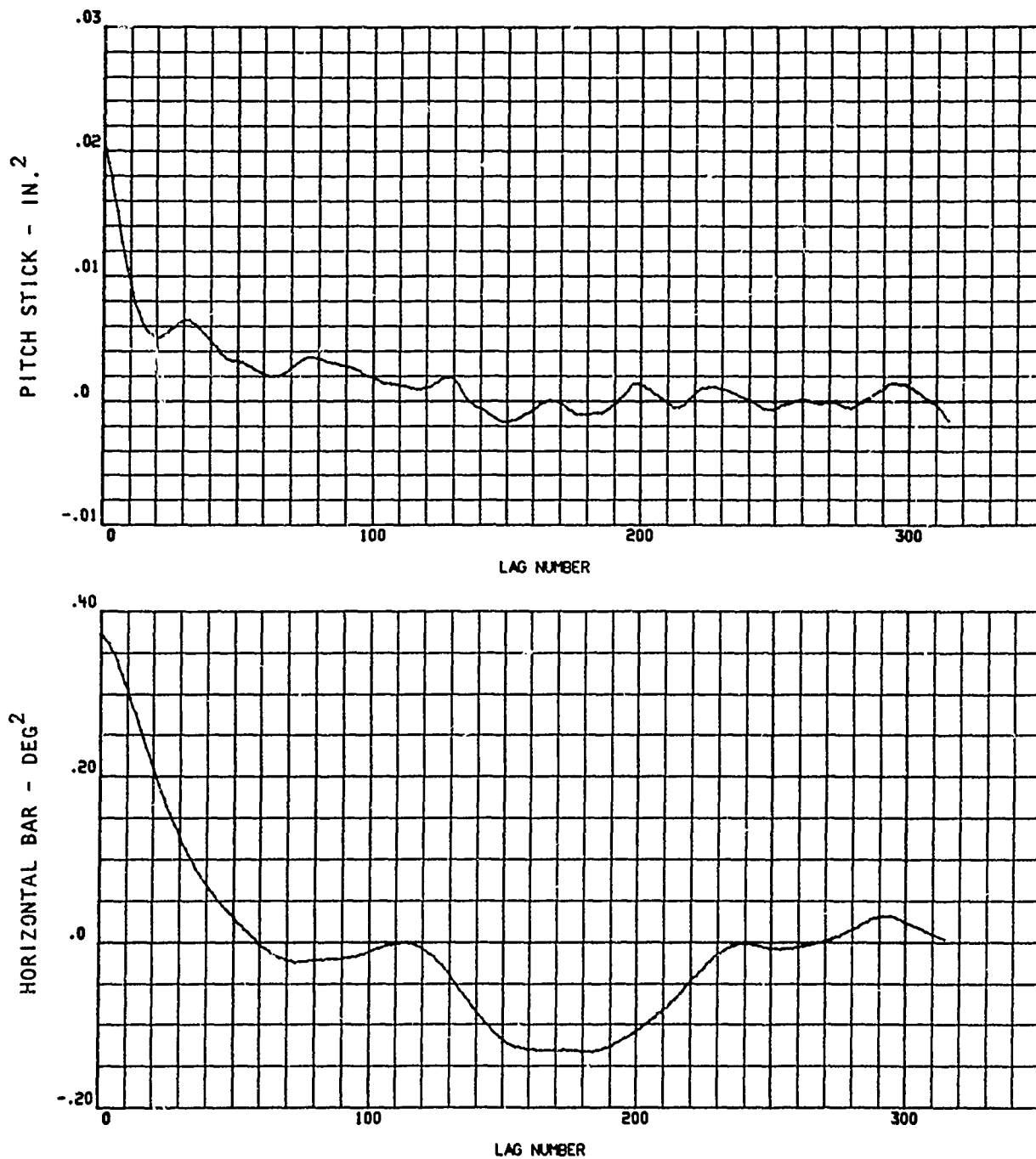
196

Figure 65. AR Simulation Run No. 01A17 Data (Cont)

01A17 REFUEL ANALYSIS.

CROSS CORRELATION FUNCTIONS

Figure 65. AR Simulation Run No. 01A17 Data (Cont)
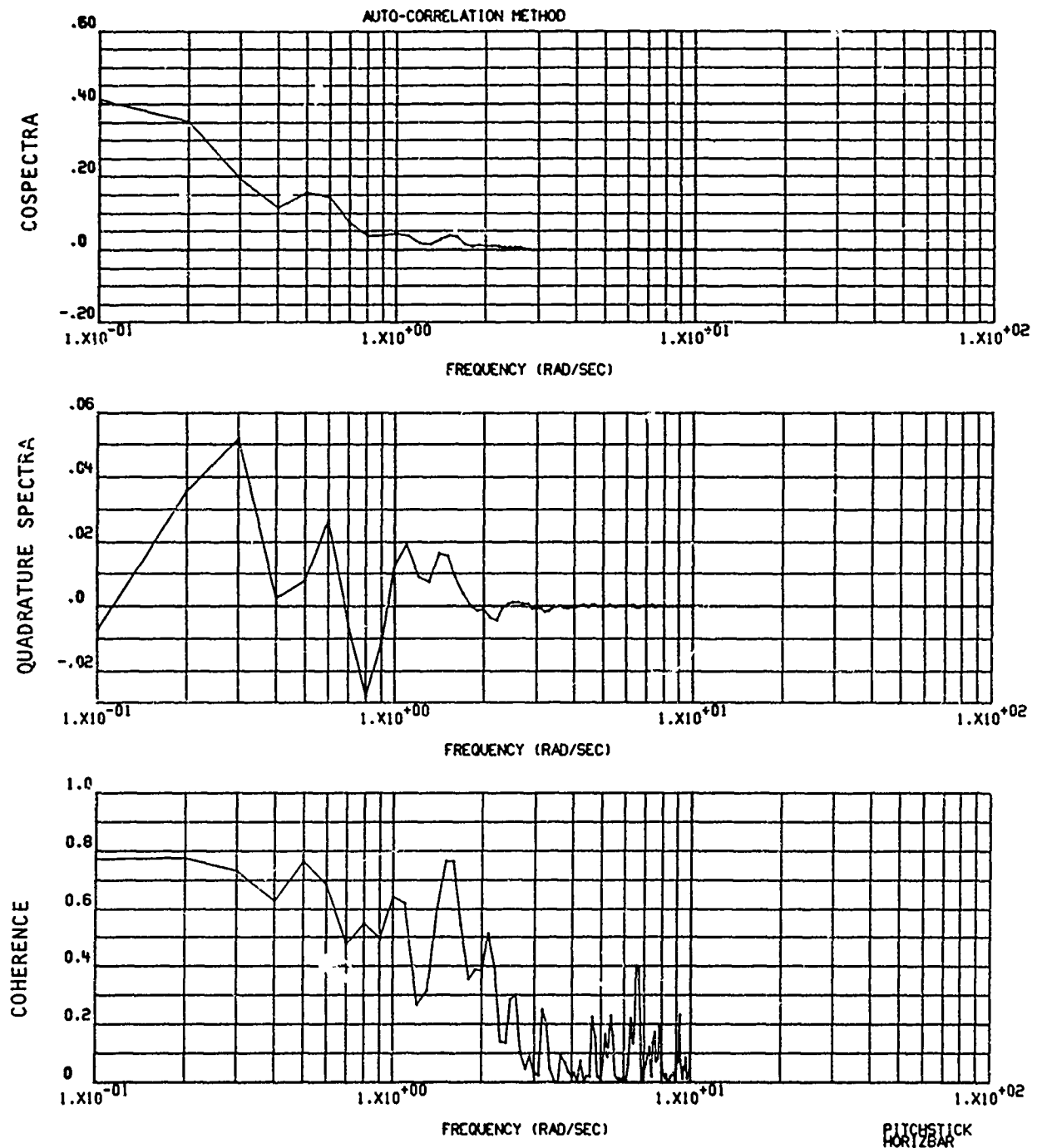
198

Figure 65. AR Simulation Run No. 01A17 Data (Cont)
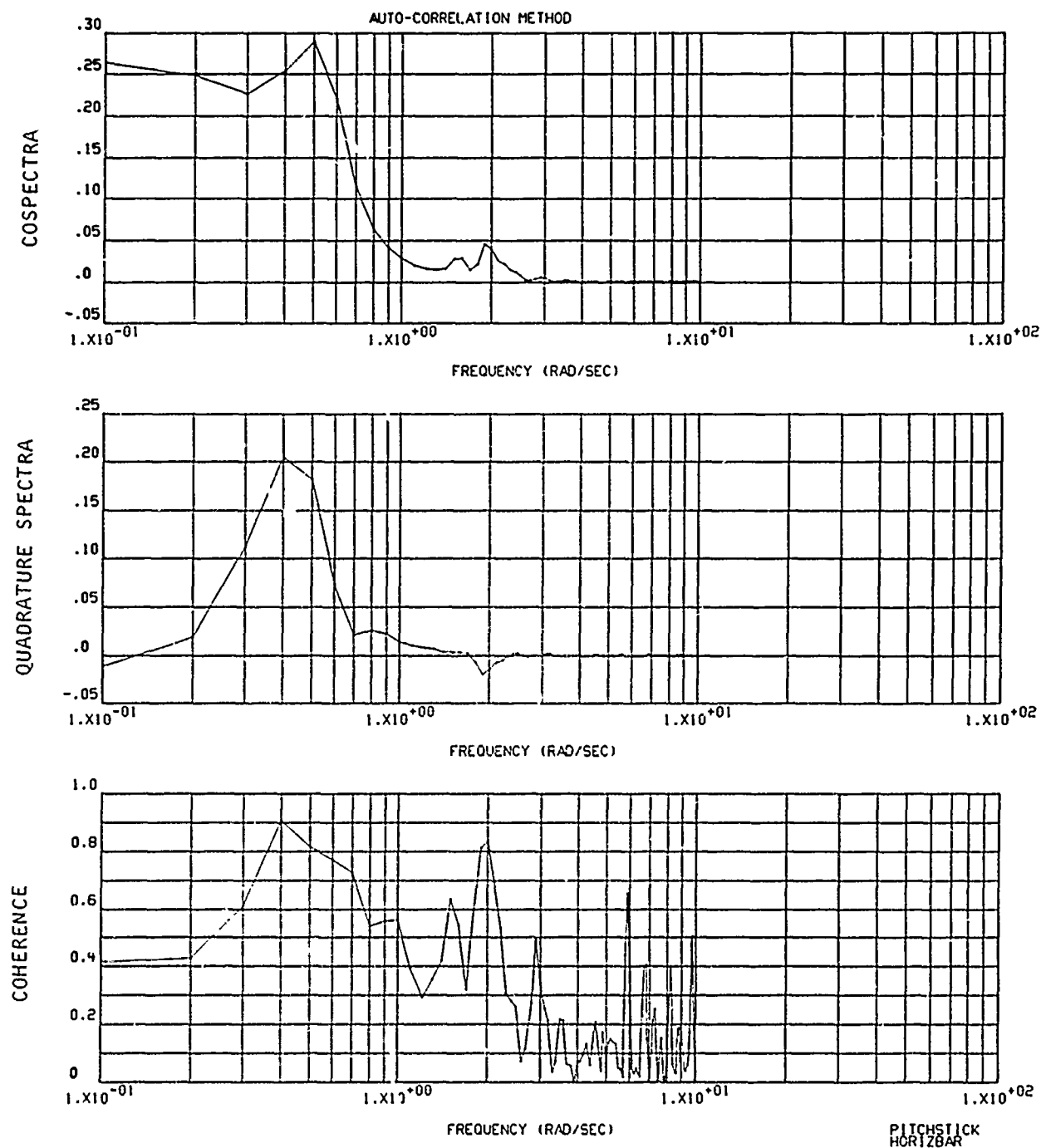
01A17 REFUEL ANALYSIS.

Figure 65.   AR Simulation Run No. 01A17 Data (Cont)

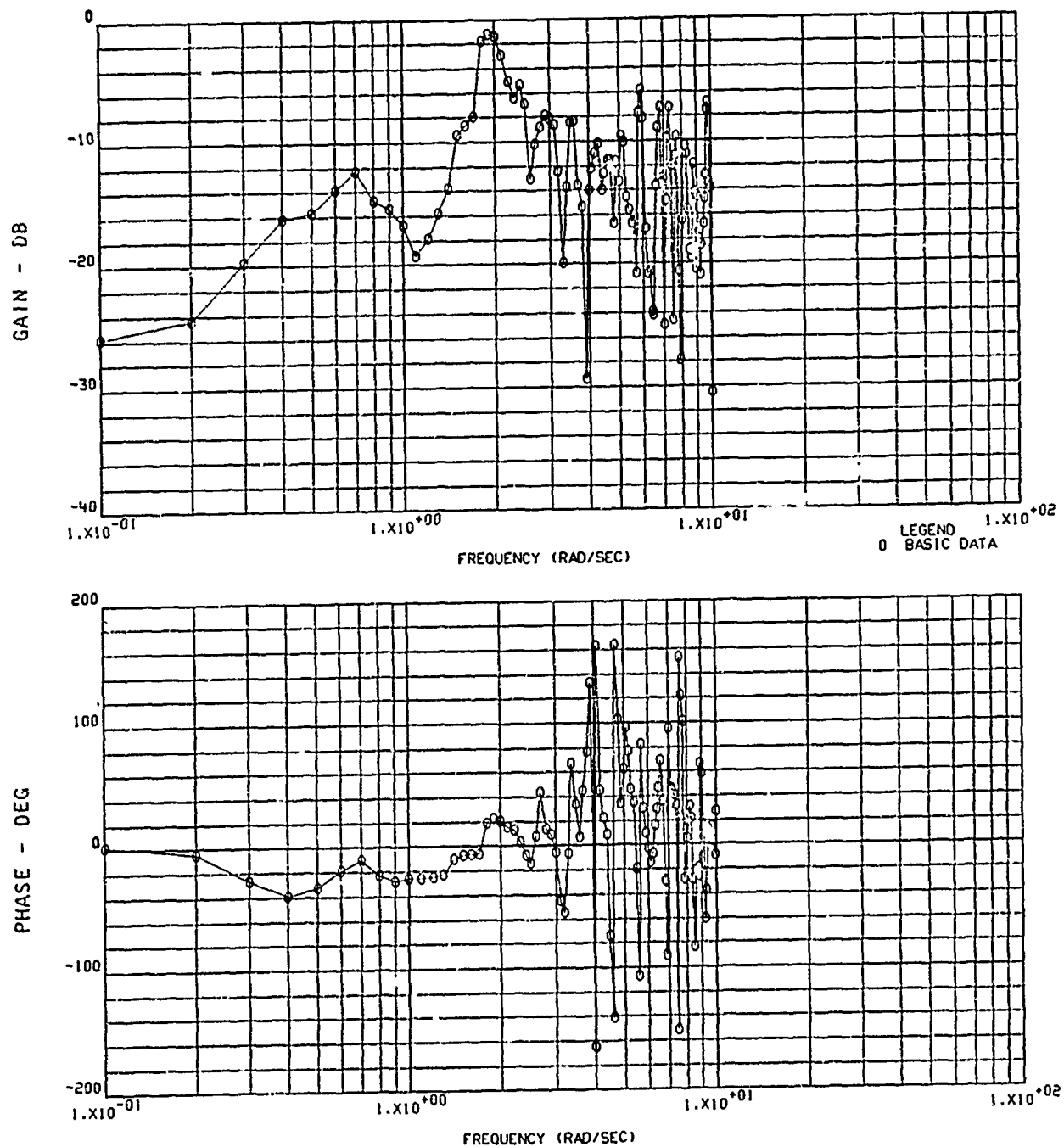200

01A17 REFUEL ANALYSIS.
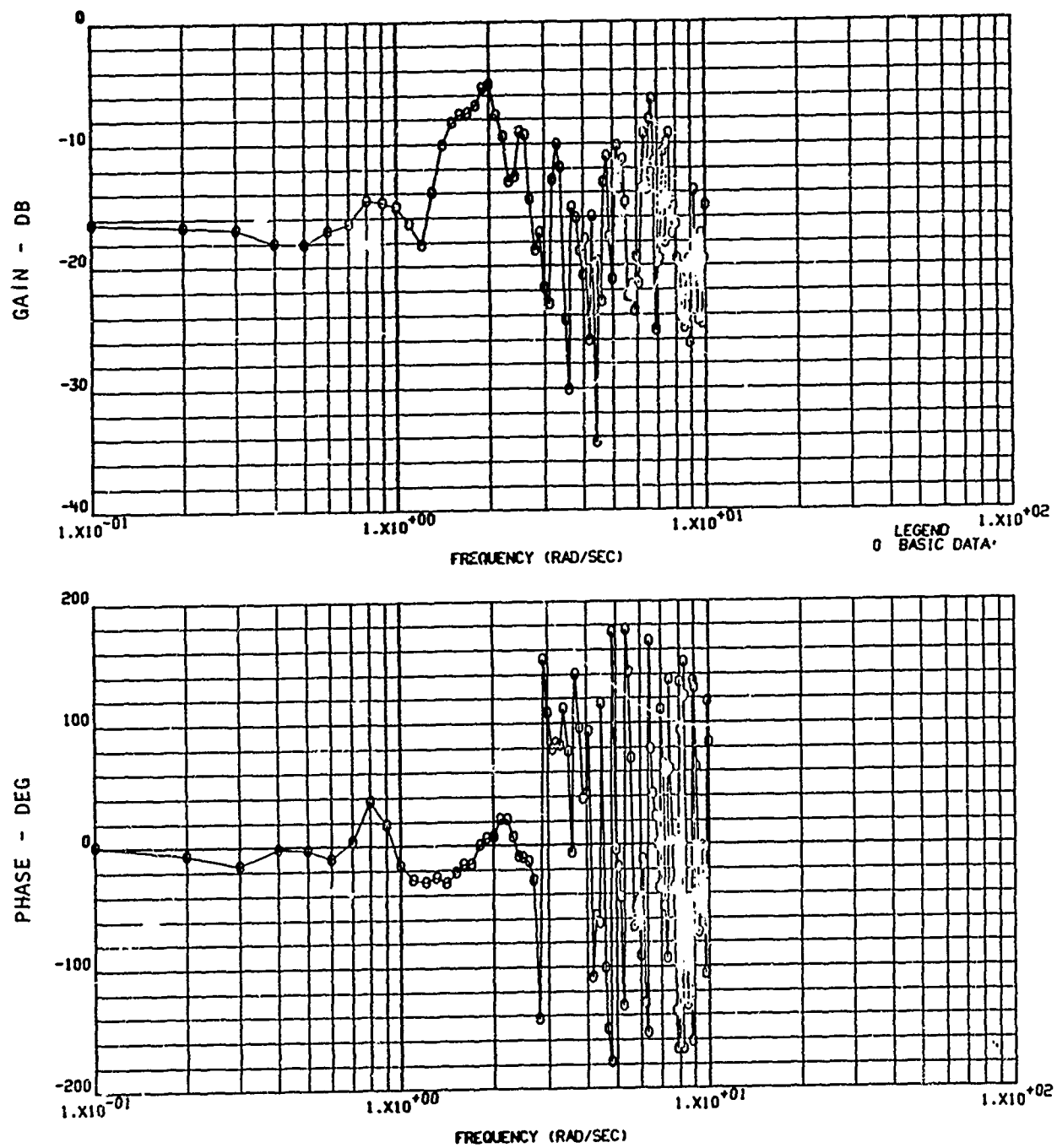
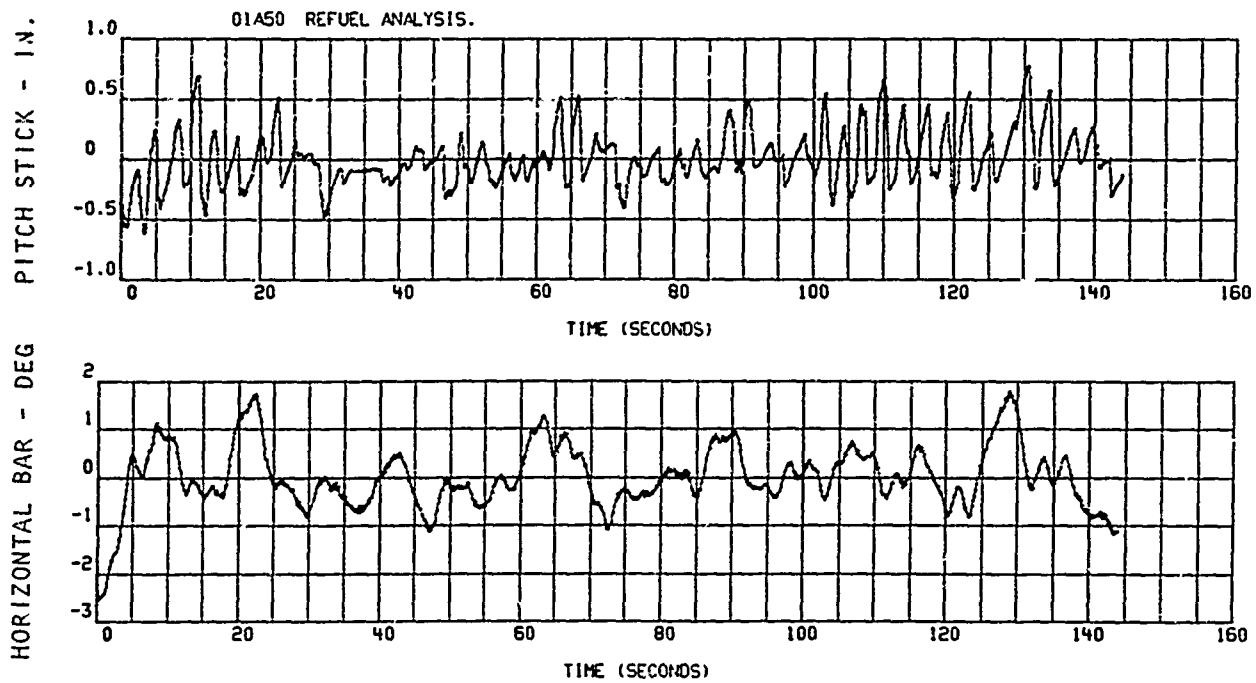Figure 65. AR Simulation Run No. 01A17 Data (Concl)
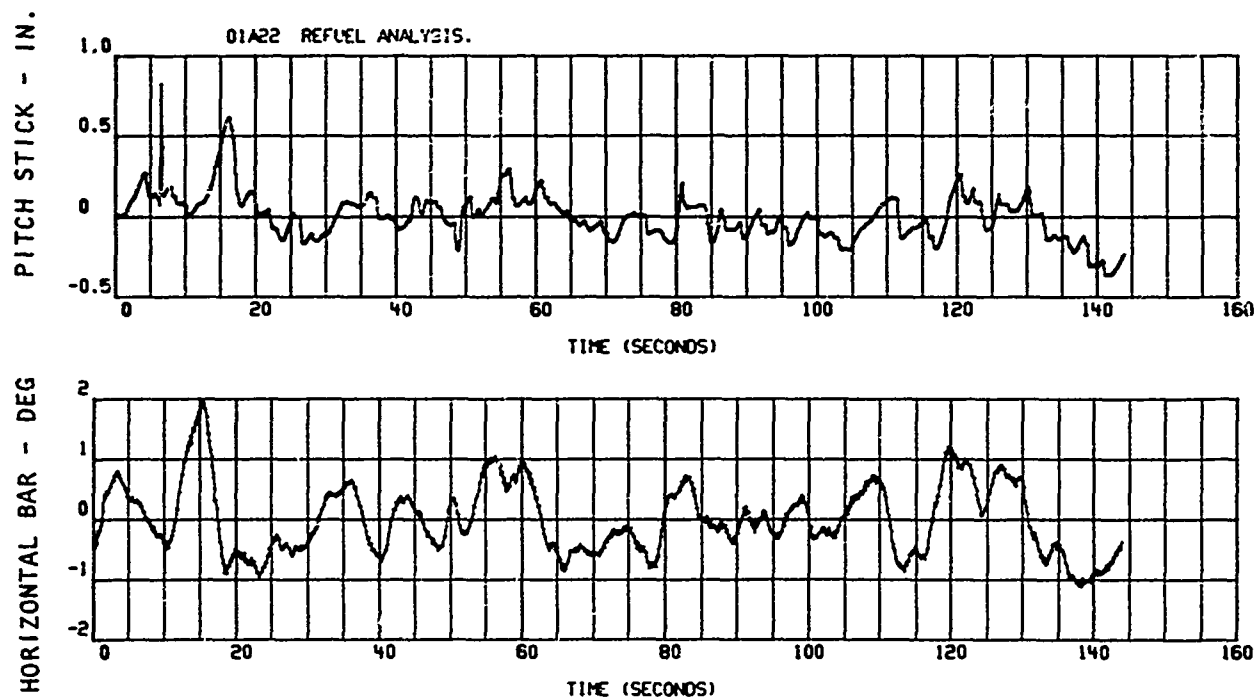
Figure 66.   AR Simulation Run No. 01A22 Data

01A22 REFUEL ANALYSIS.
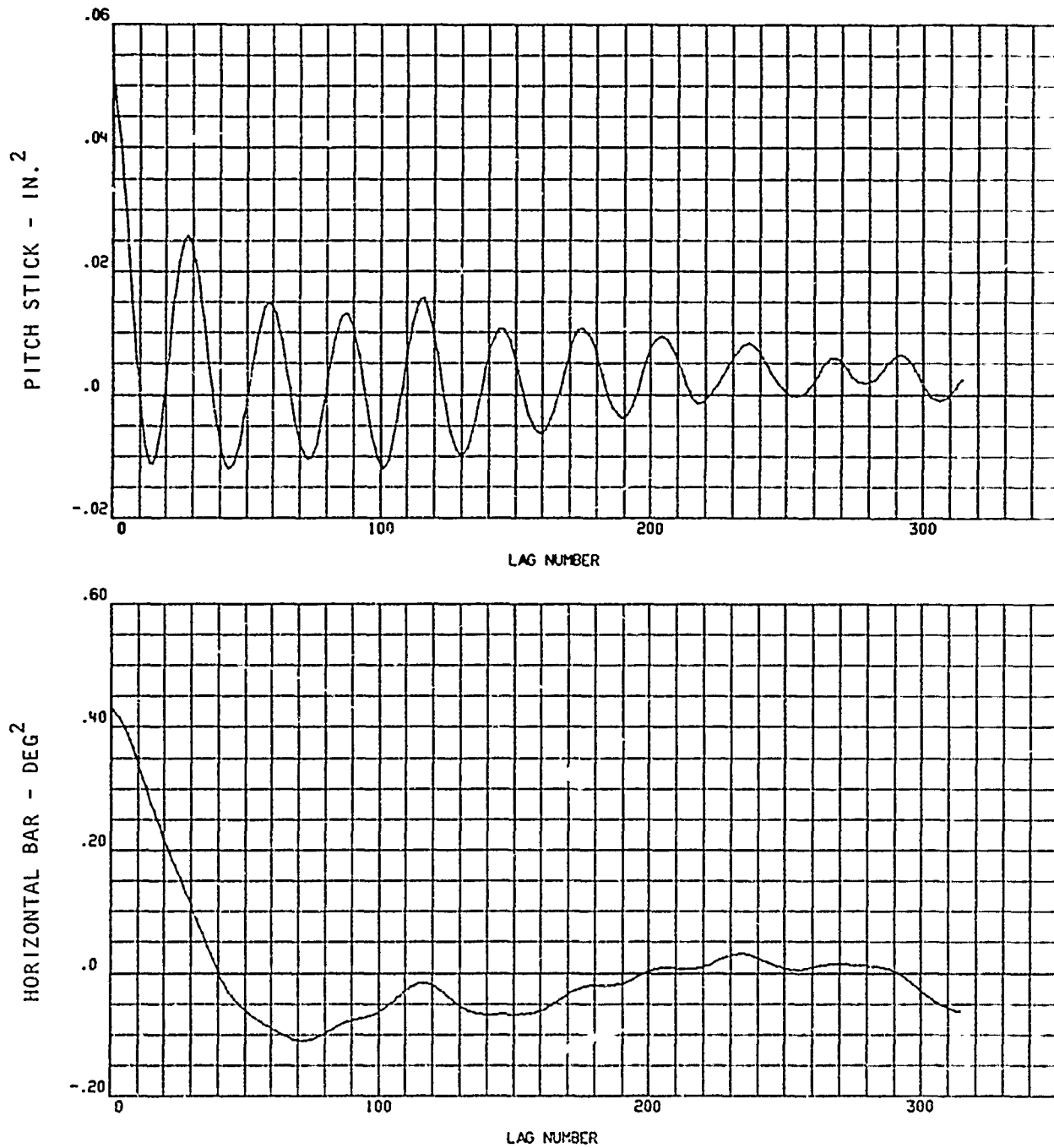
AUTO CORRELATION FUNCTIONS
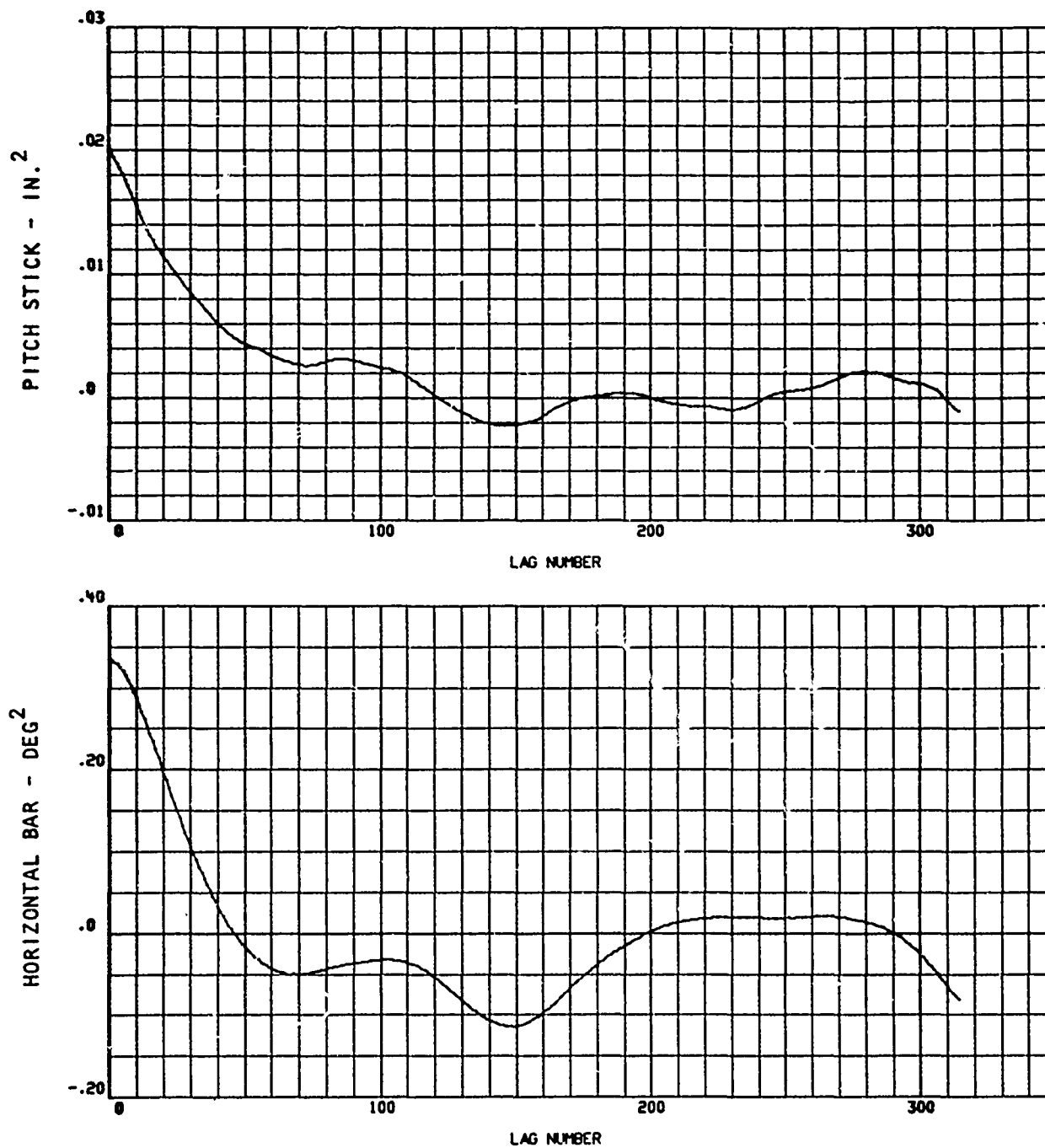
Figure 66.   AR Simulation Run No. 01A22 Data (Cont)

01A22 REFUEL ANALYSIS.

CROSS CORRELATION FUNCTIONS

Figure 66. AR Simulation Run No. 01A22 Data (Cont)

Figure 66. AR Simulation Run No. 01A22 Data (Cont)

Figure 66.   AR Simulation Run No. 01A22 Data (Cont)
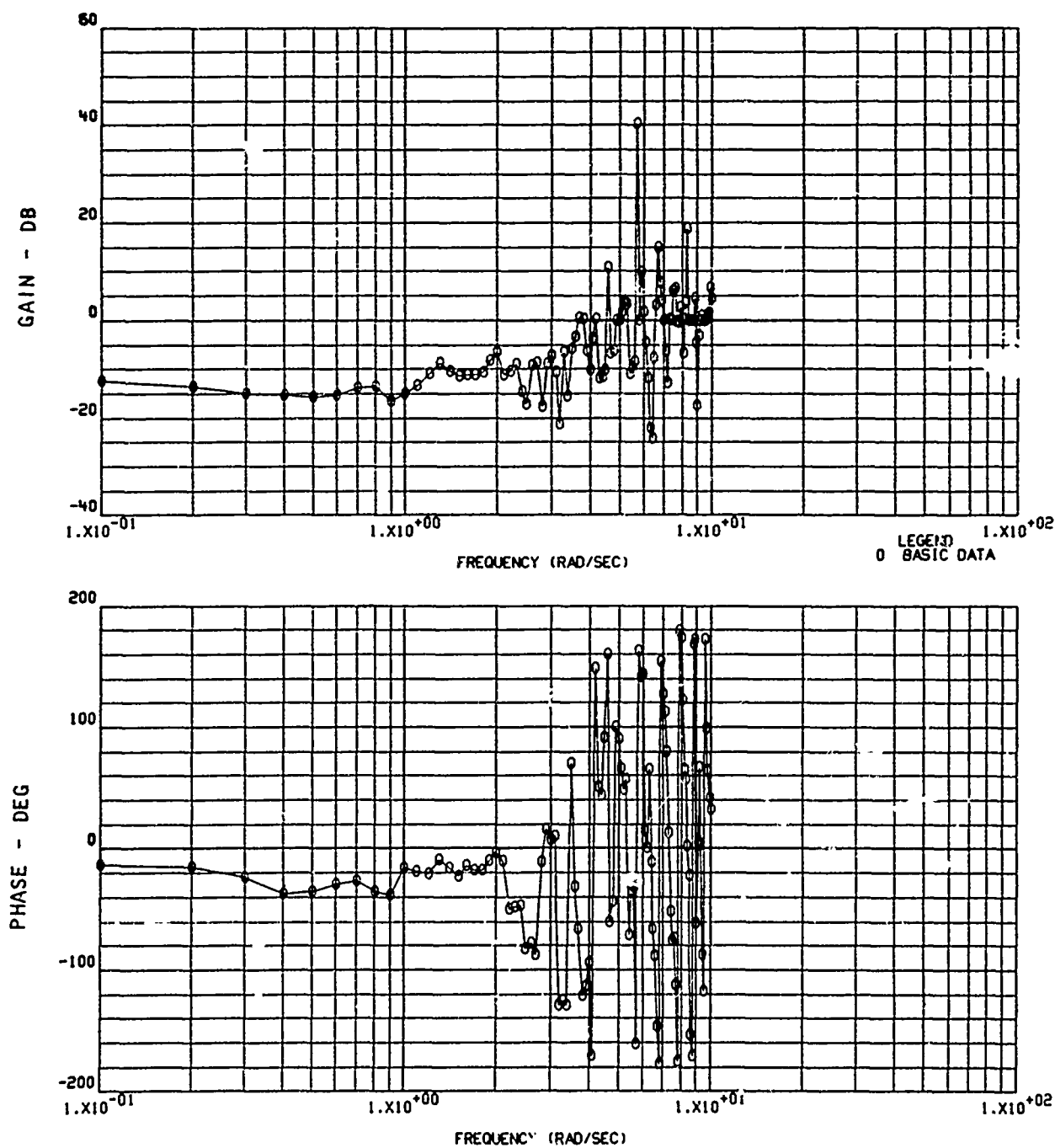
Figure 66. AR Simulation Run No. 01A22 Data (Concl)
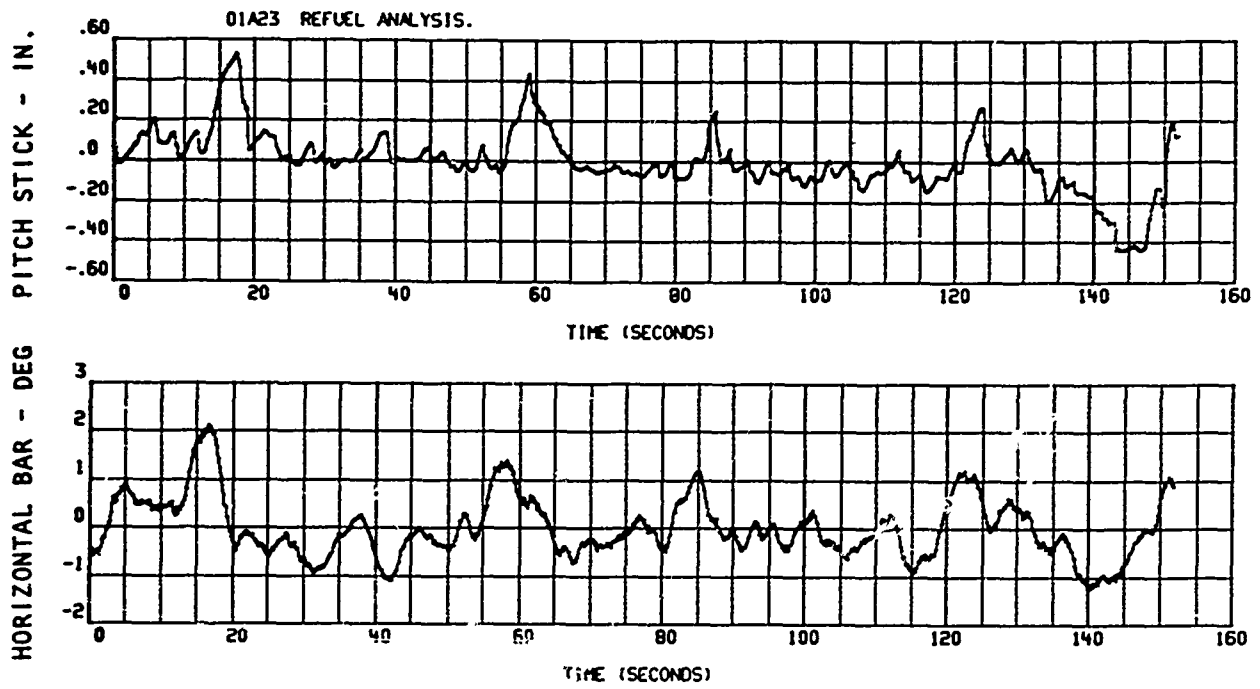
Figure 67. AR Simulation Run No. 01A23 Data

Figure 67.   AR Simulation Run No. 01A23 Data (Cont)
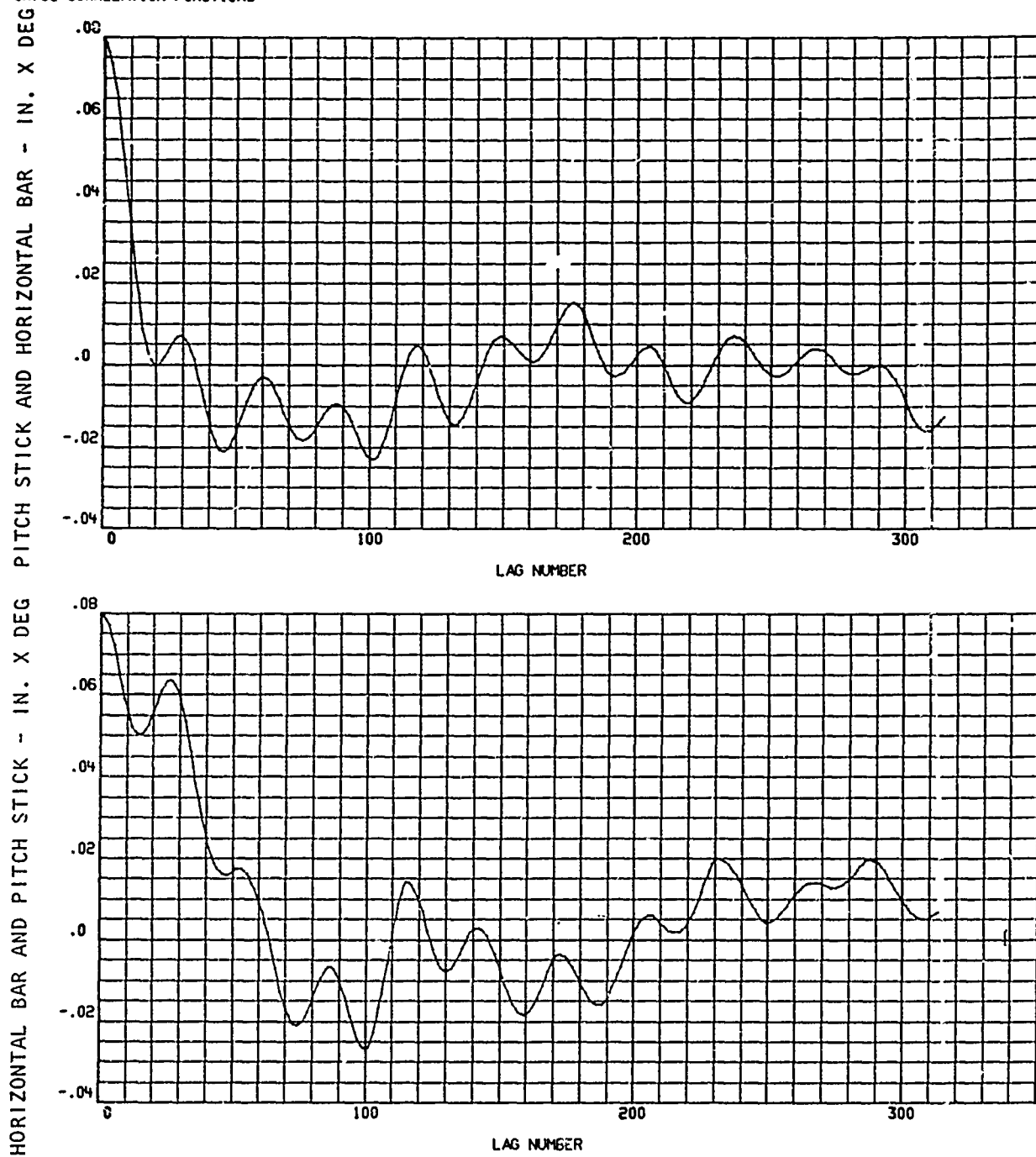
209

CROSS CORRELATION FUNCTIONS
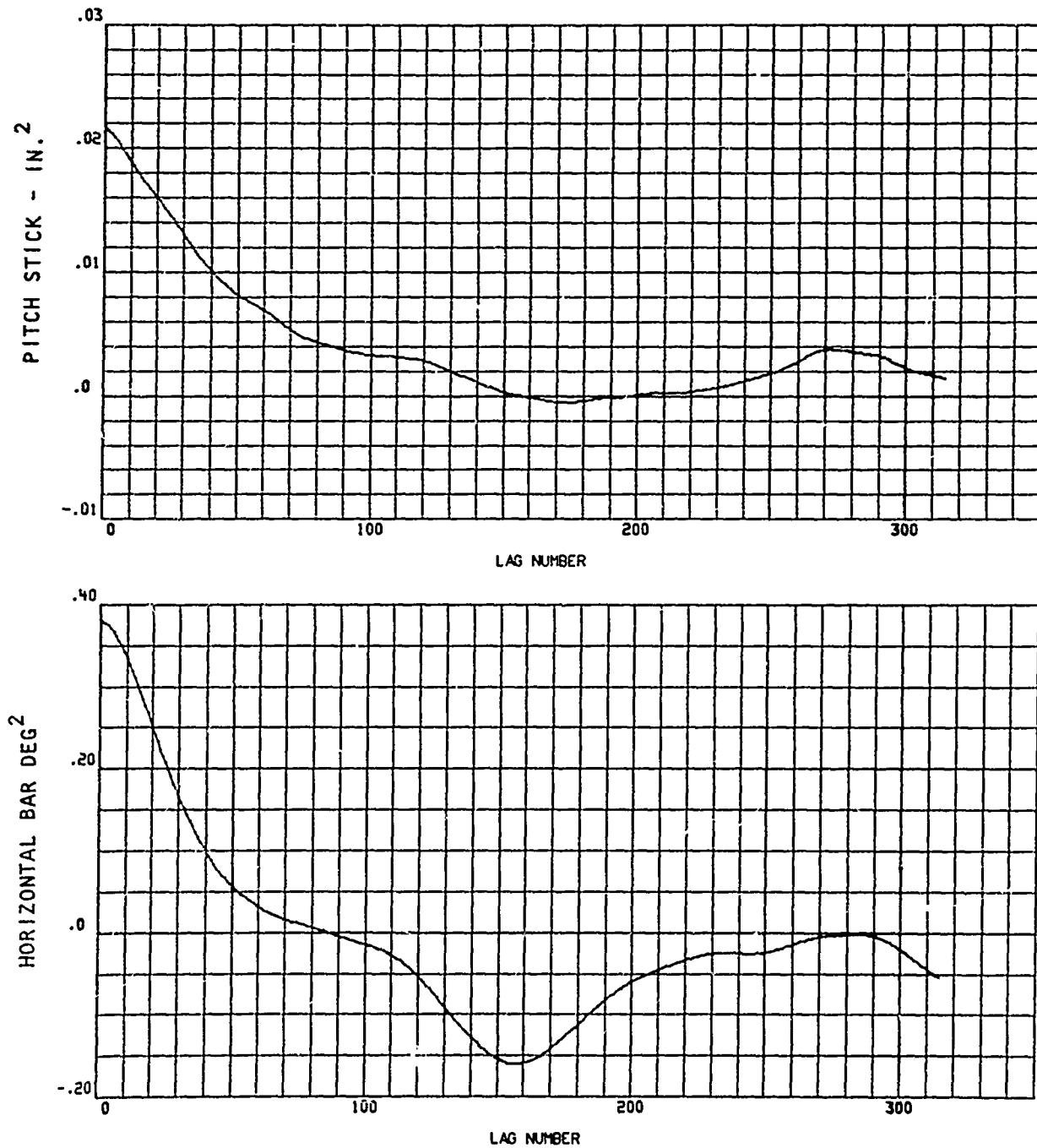
Figure 67.   AR Simulation Run No. 01A23 Data (Cont)
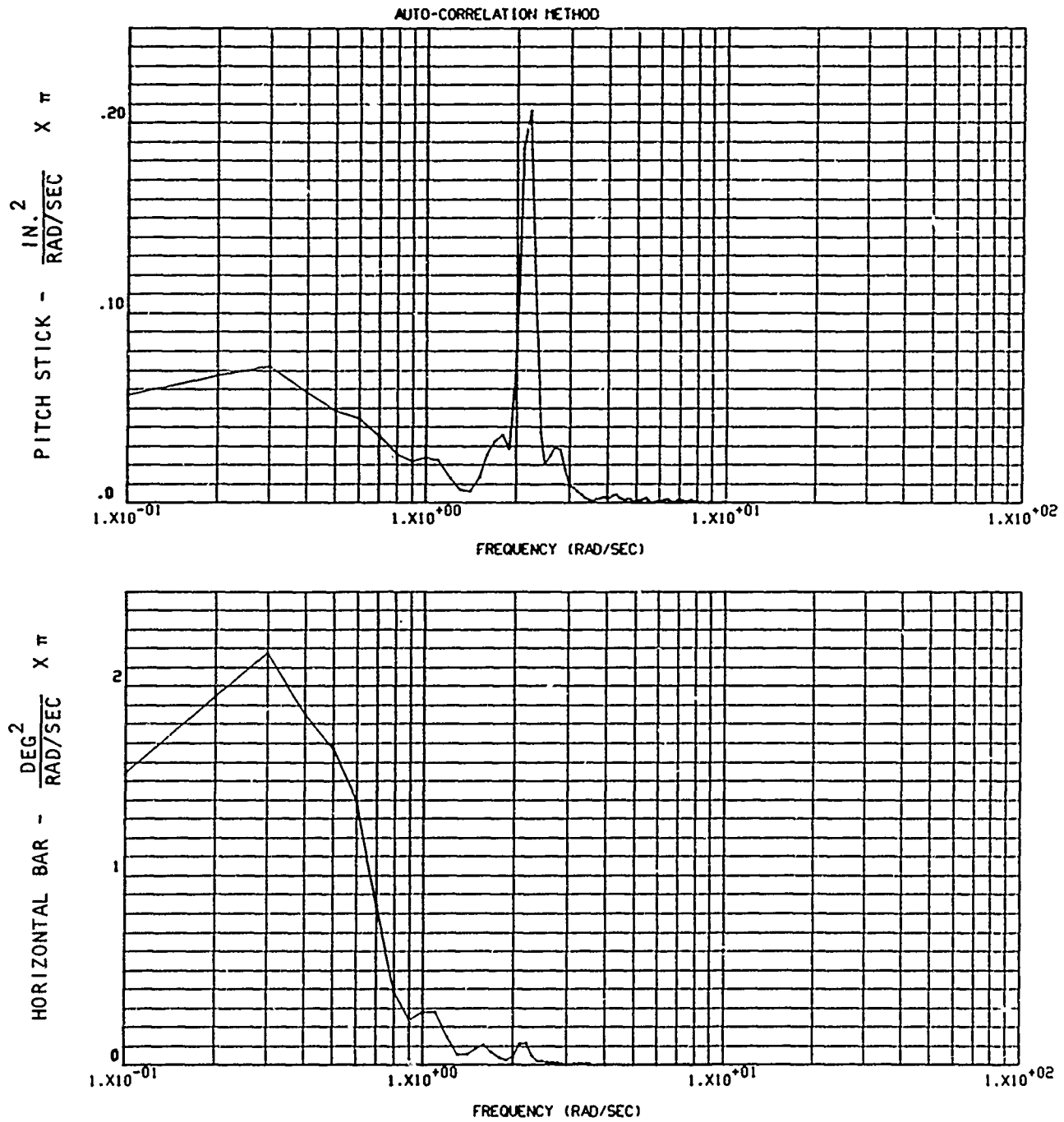
'01A23 REFUEL ANALYSIS.
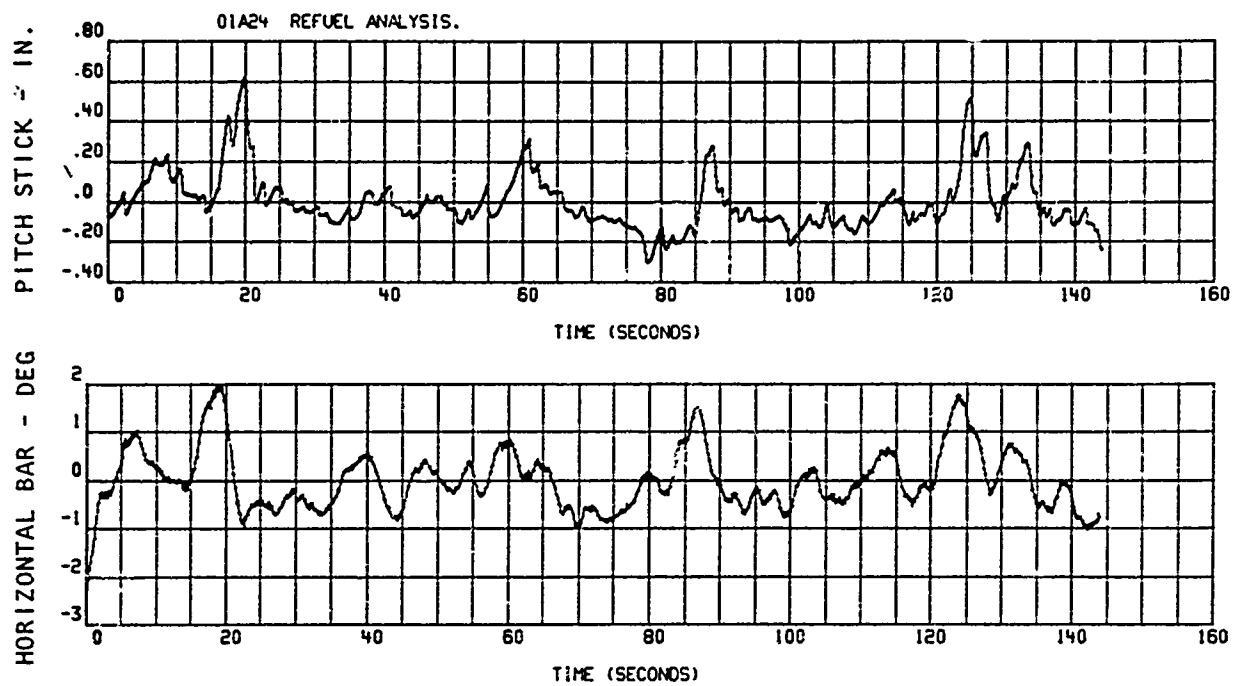
SPECTRAL DENSITY FUNCTIONS

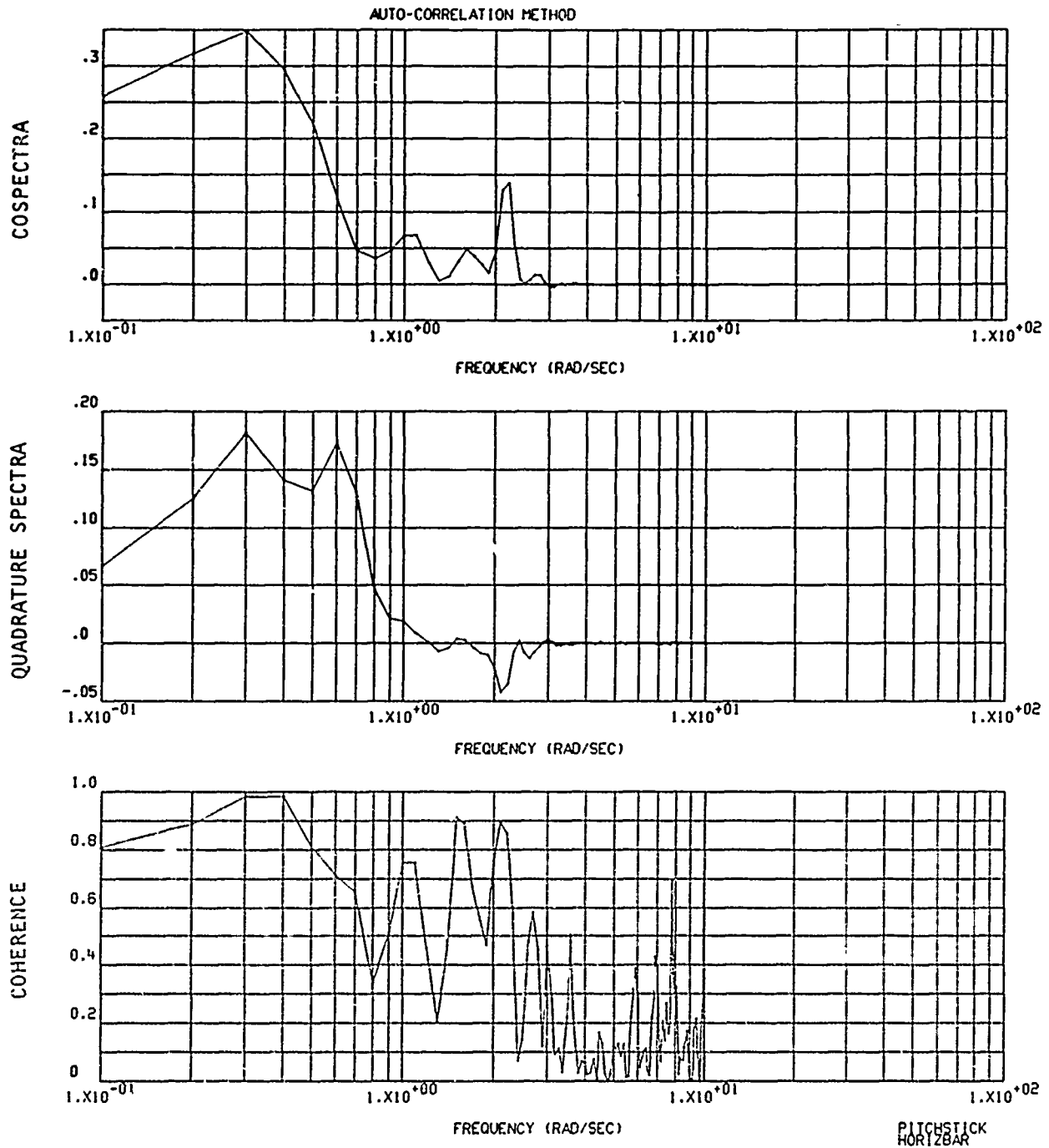Figure 67. AR Simulation Run No. 01A23 Data (Cont)

211

01A23 REFUEL ANALYSIS.

AUTO-CORRELATION METHOD

COSPECTRA

FREQUENCY (RAD/SEC)

QUADRATURE SPECTRA

FREQUENCY (RAD/SEC)

COHERENCE

FREQUENCY (RAD/SEC)

PITCHSTICK
HORIZBAR

Figure 67.   AR Simulation Run No. 01A23 Data (Cont)

212

Figure 67. AR Simulation Run No. 01A23 Data (Concl)

Figure 68. AR Simulation Run No. 01A24 Data
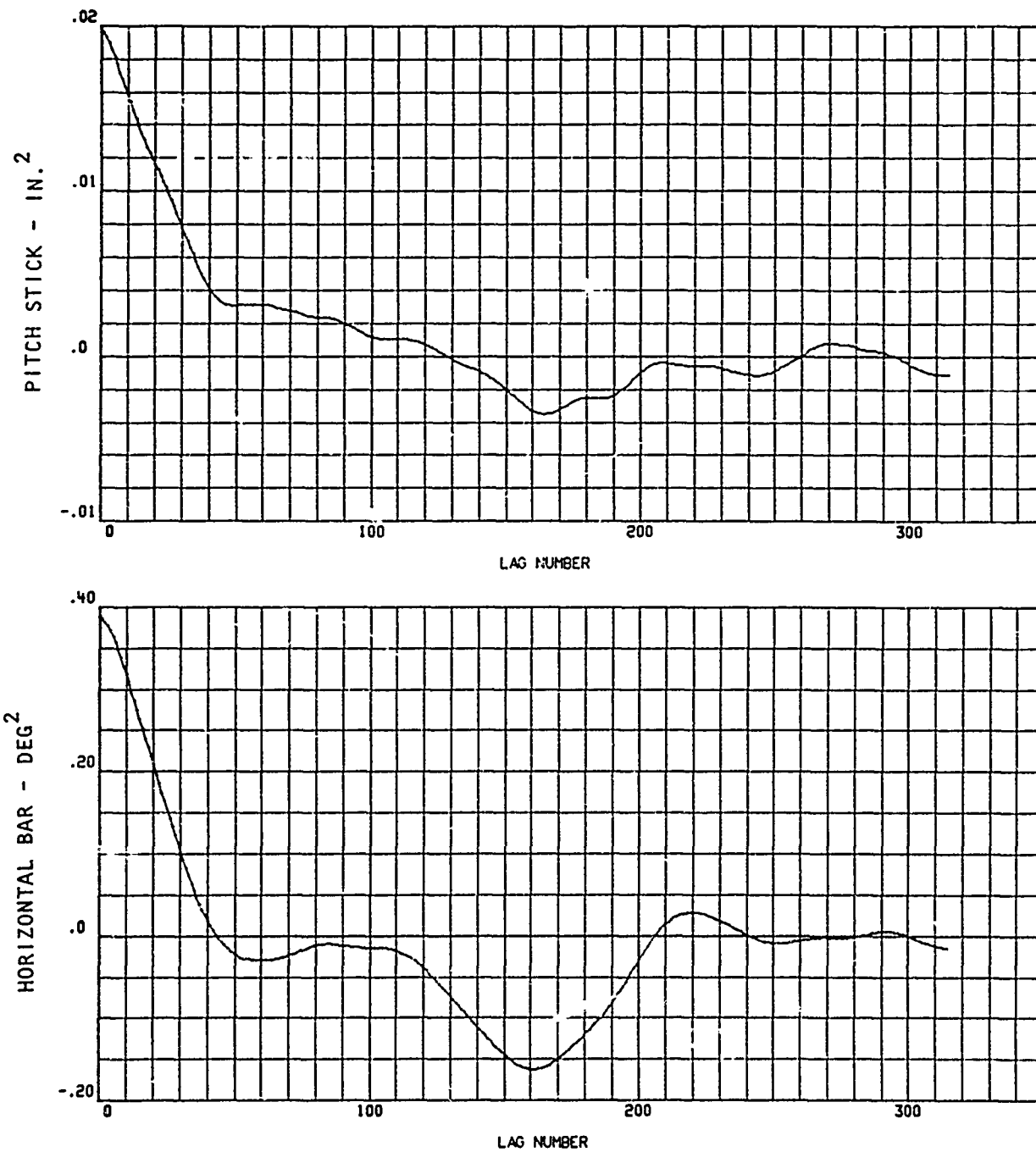
AUTO CORRELATION FUNCTIONS

Figure 68.   AR Simulation Run No. 01A24 Data (Cont)

215

Figure 68. AR Simulation Run No. 01A24 Data (Cont)

216

Figure 68. AR Simulation Run No. 01A24 Data (Cont)

217

Figure 68. AR Simulation Run No. 01A24 Data (Cont)

218
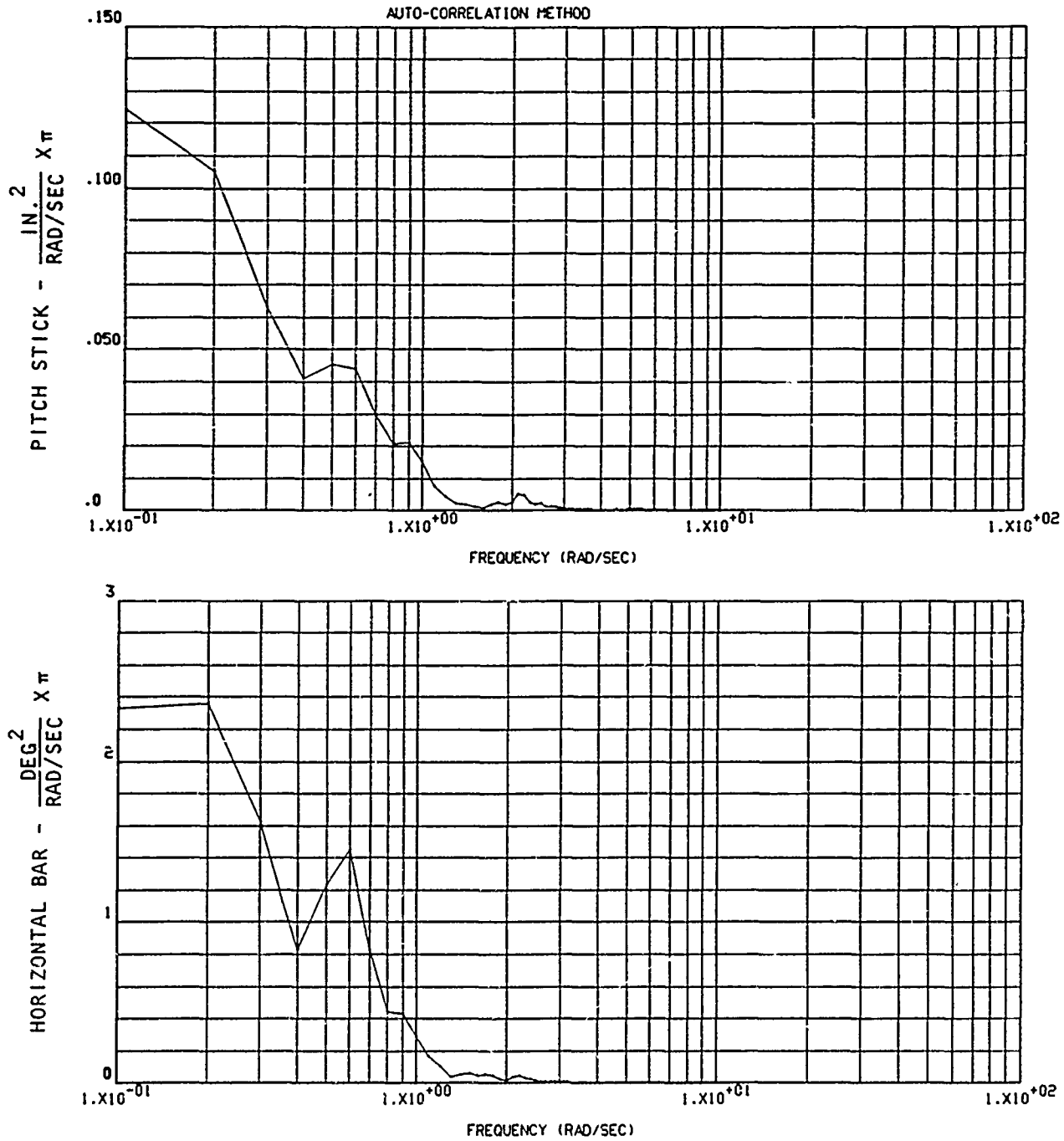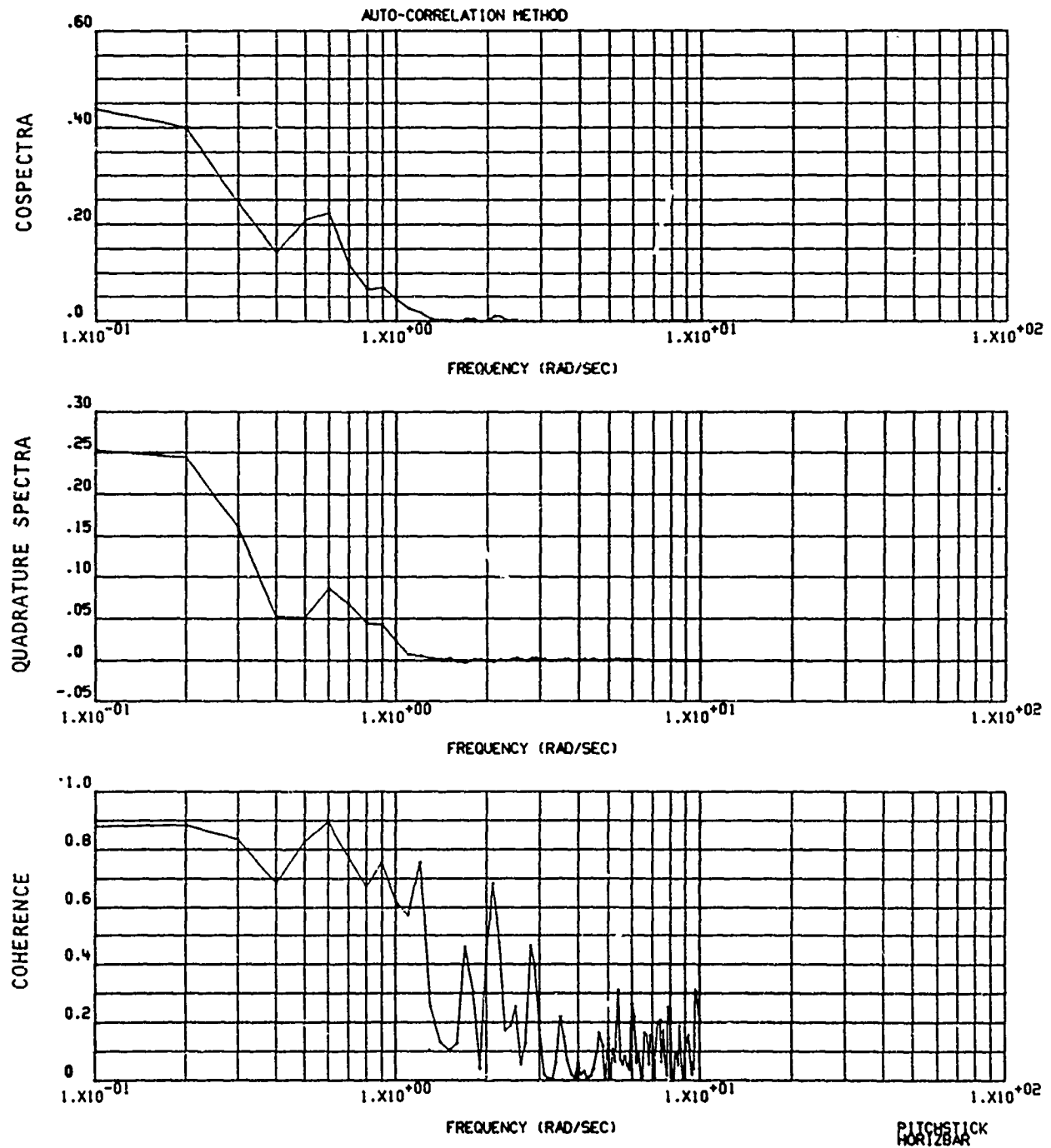
01A24 REFUEL ANALYSIS.
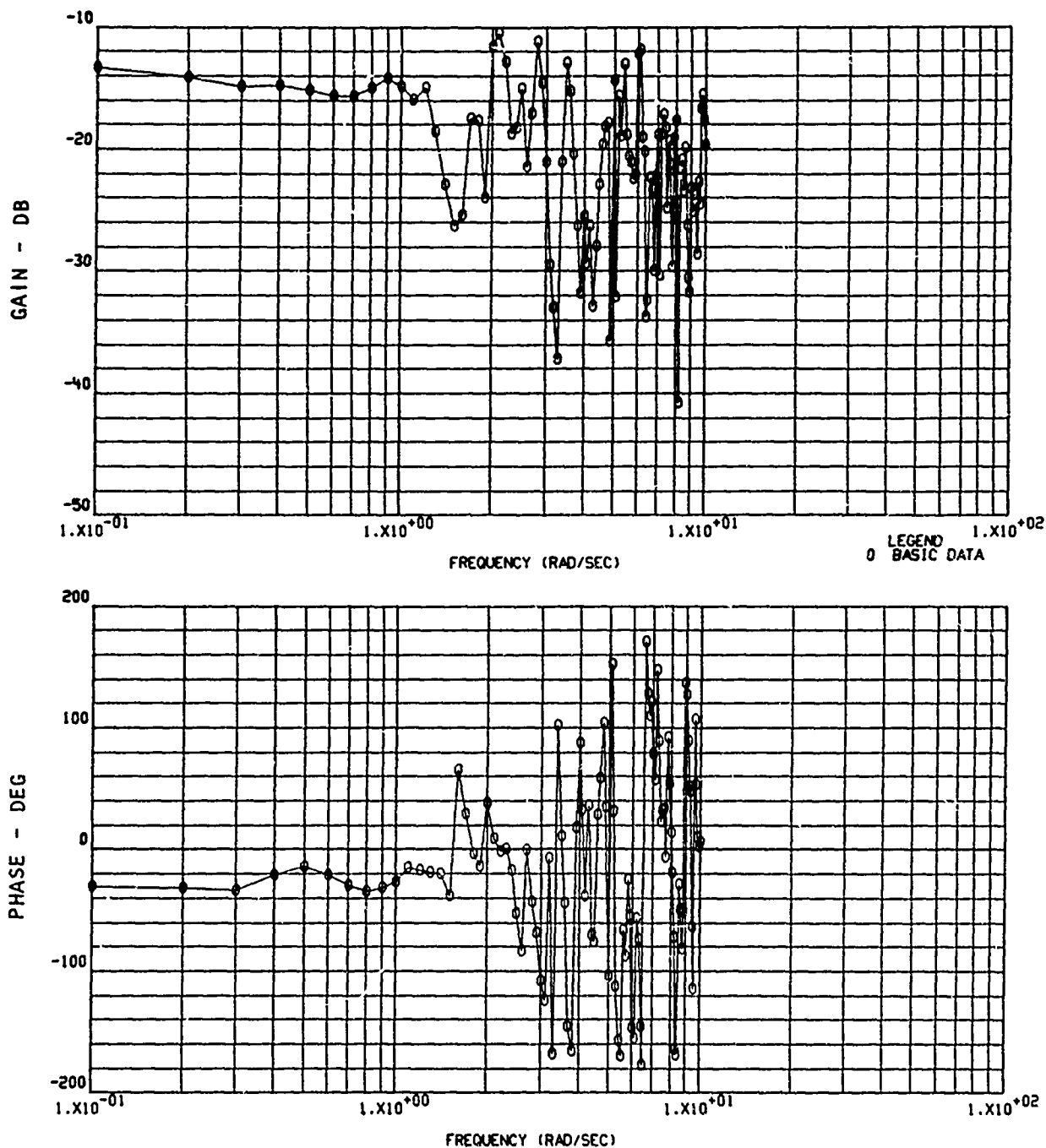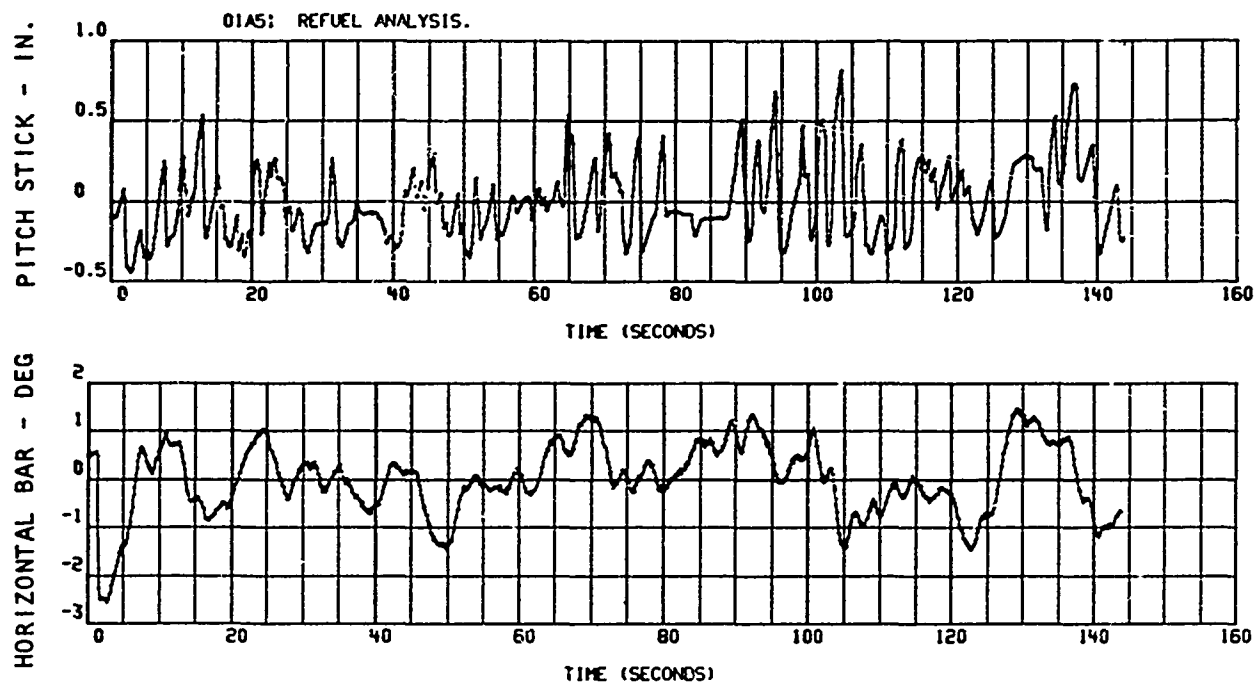

Figure 68.   AR Simulation Run No. 01A24 Data (Concl)
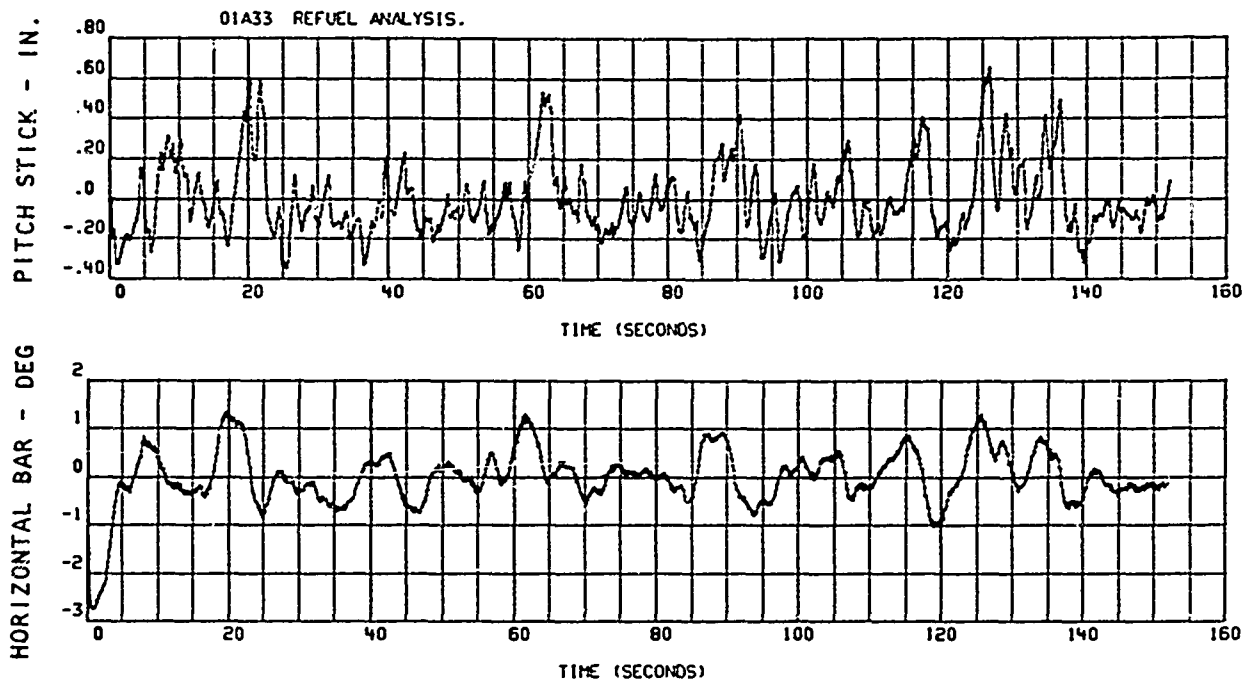
219

Figure 69. AR Simulation Run No. 01A33 Data
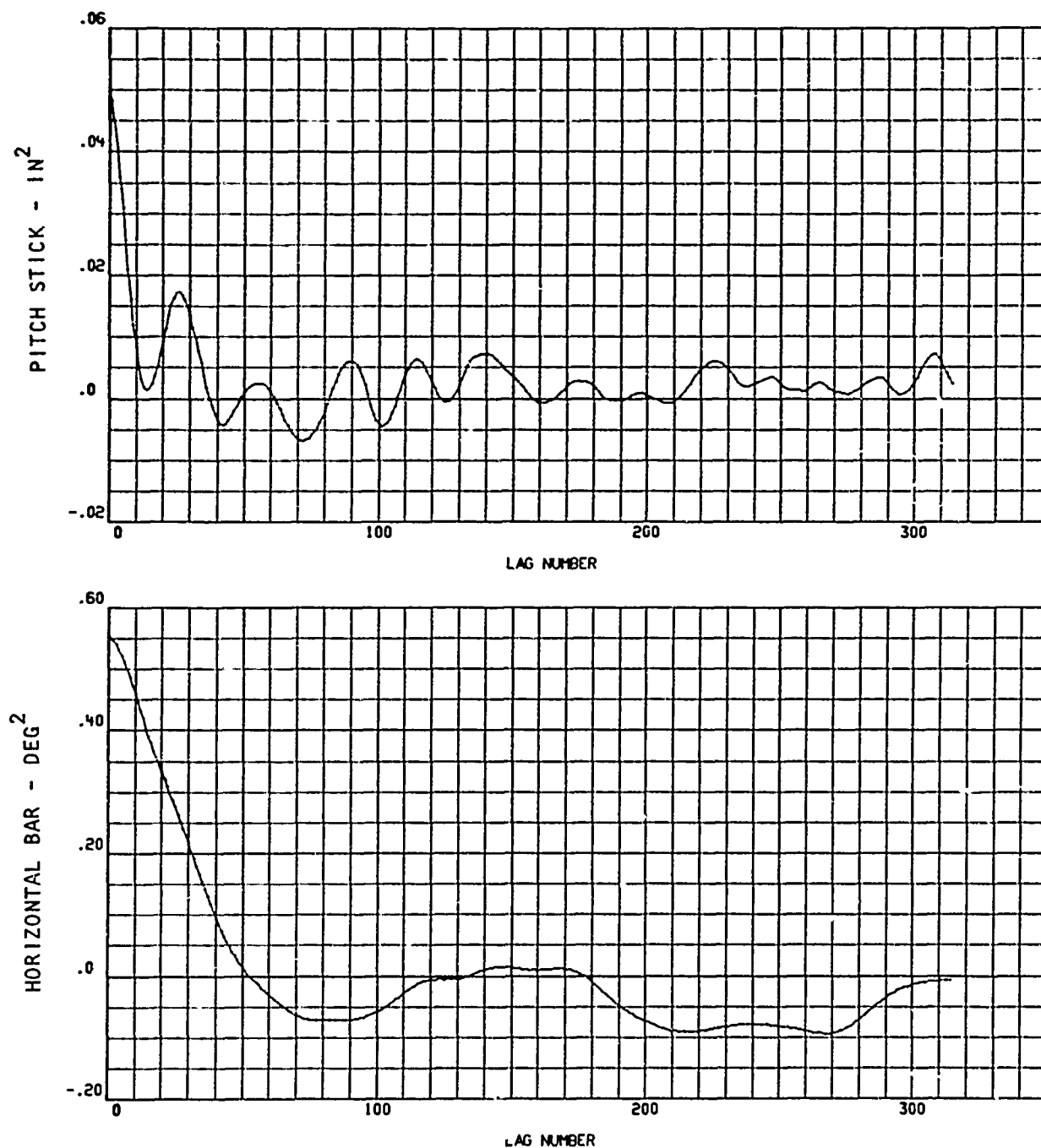
220

AUTO CORRELATION FUNCTIONS
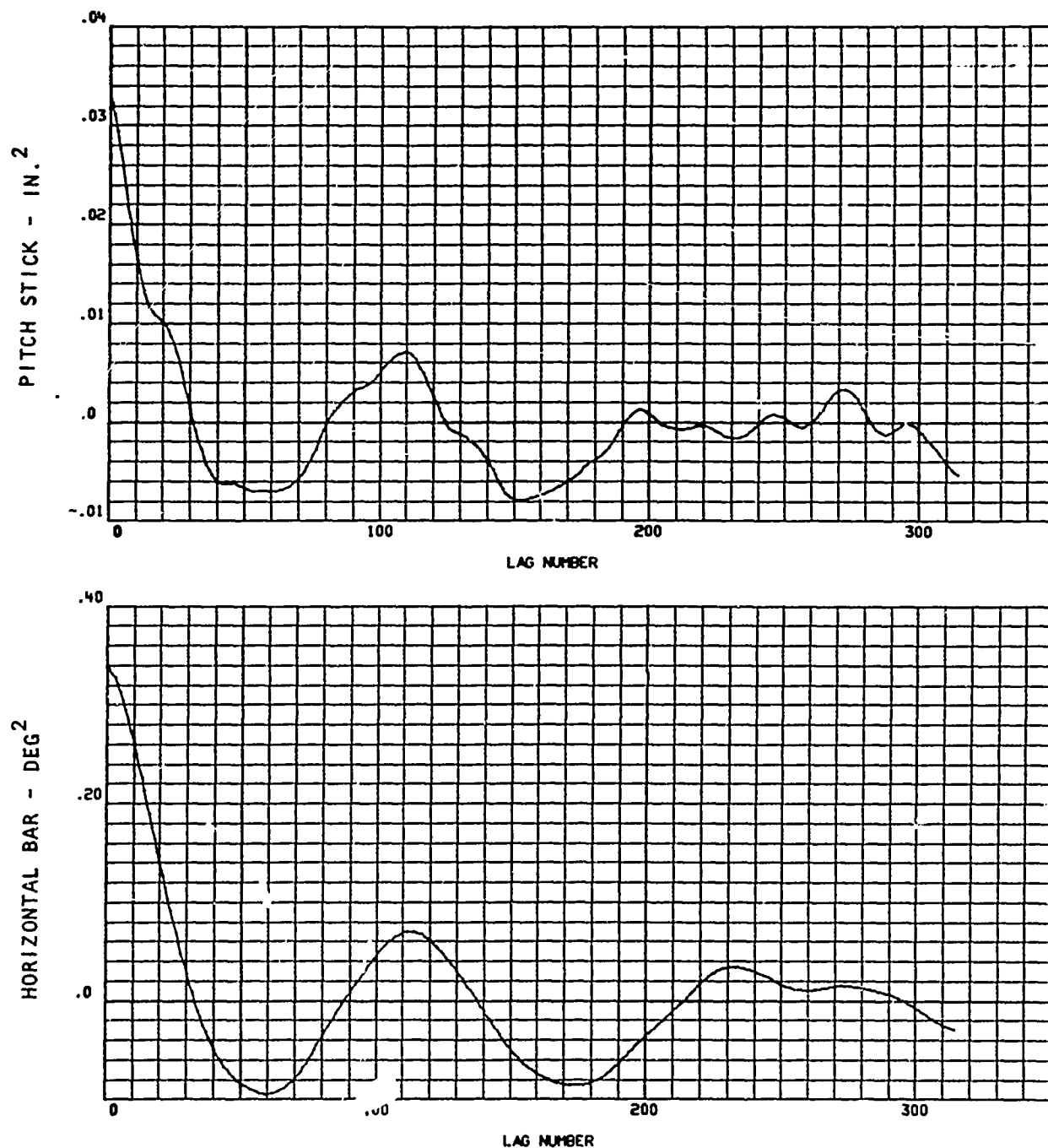
Figure 69.   AR Simulation Run No. 01A33 Data (Cont)

01A33 REFUEL ANALYSIS.
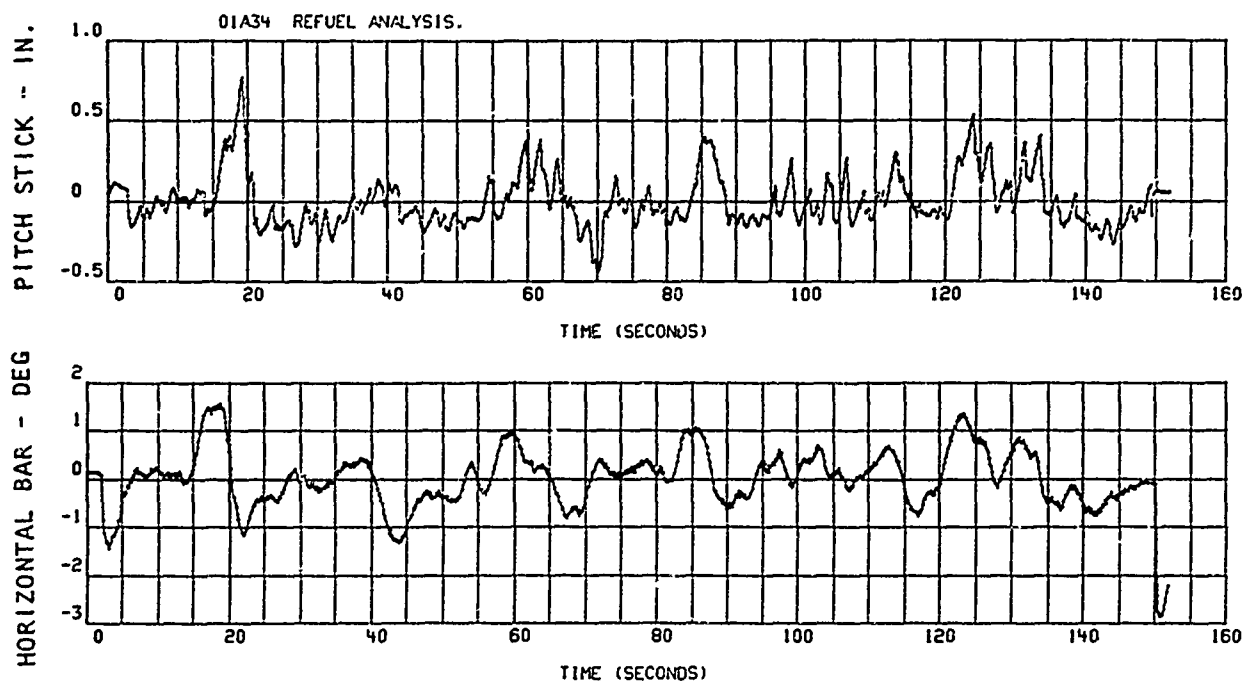
CROSS CORRELATION FUNCTIONS

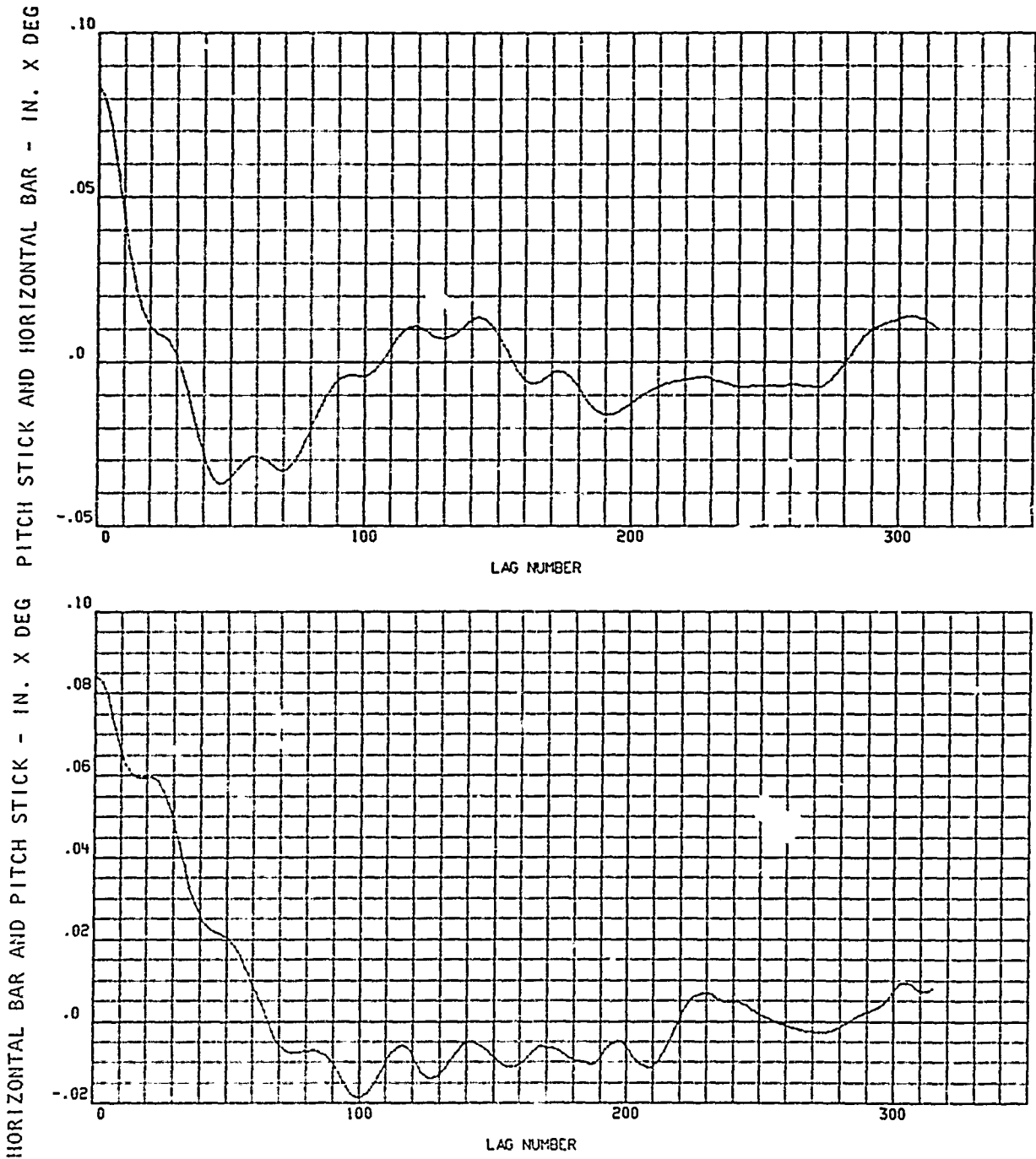Figure 69. AR Simulation Run No. 01A33 Data (Cont)
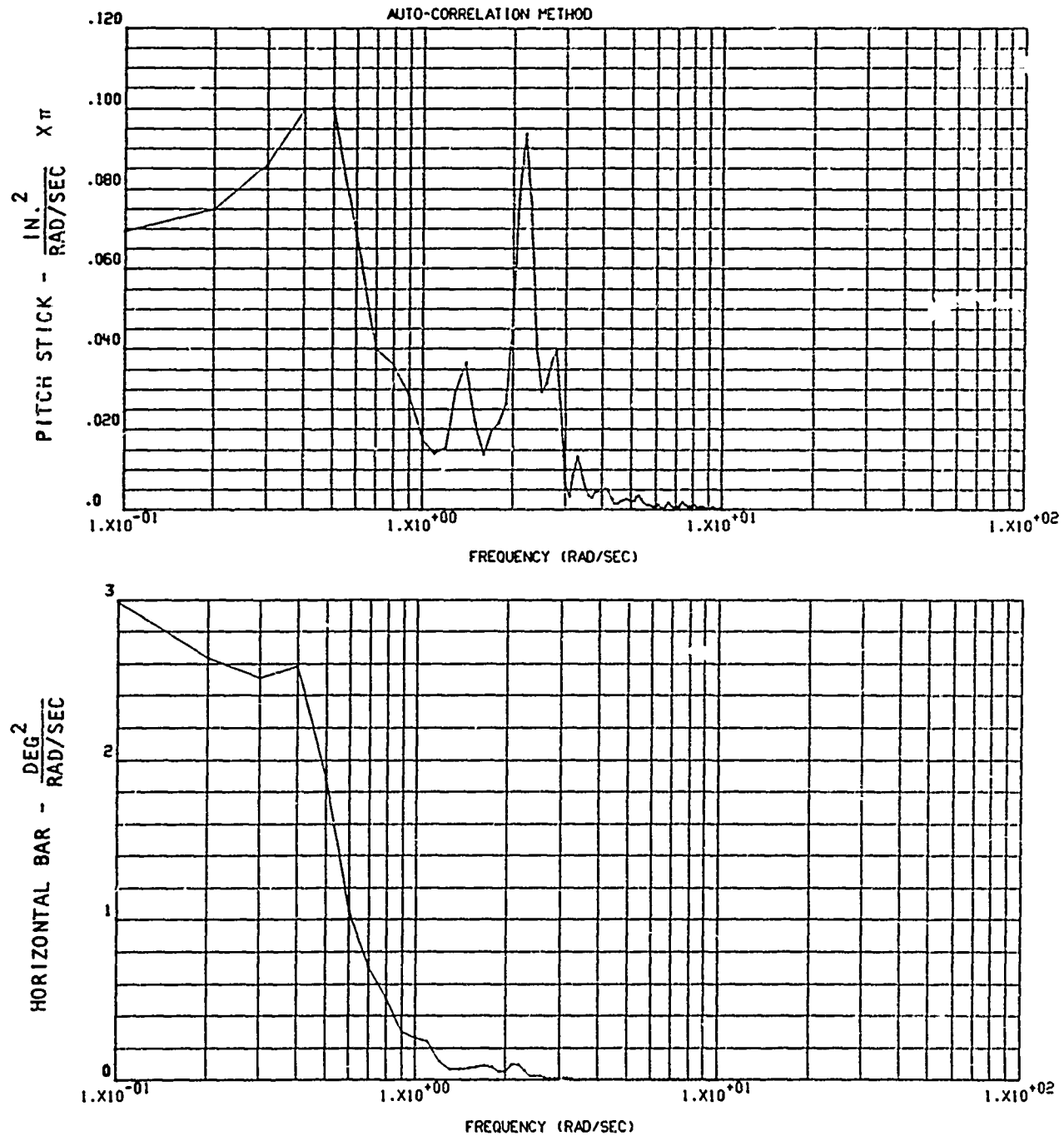
Figure 69. AR Simulation Run No. 01A33 Data (Cont)

223

01A33 REFUEL ANALYSIS.

Figure 69. AR Simulation Run No. 01A33 Data (Cont)

224

01A33 REFUEL ANALYSIS.

Figure 69. AR Simulation Run No. 01A33 Data (Concl)

225

Figure 70. AR Simulation Run No. 01A34 Data

Figure 70. AR Simulation Run No. 01A34 Data (Cont)

227

01A34 REFUEL ANALYSIS.

CROSS CORRELATION FUNCTIONS

Figure 70. AR Simulation Run No. 01A34 Data (Cont)

228

Figure 70. AR Simulation Run No. 01A34 Data (Cont)

229

01A34 REFUEL ANALYSIS.

AUTO-CORRELATION METHOD
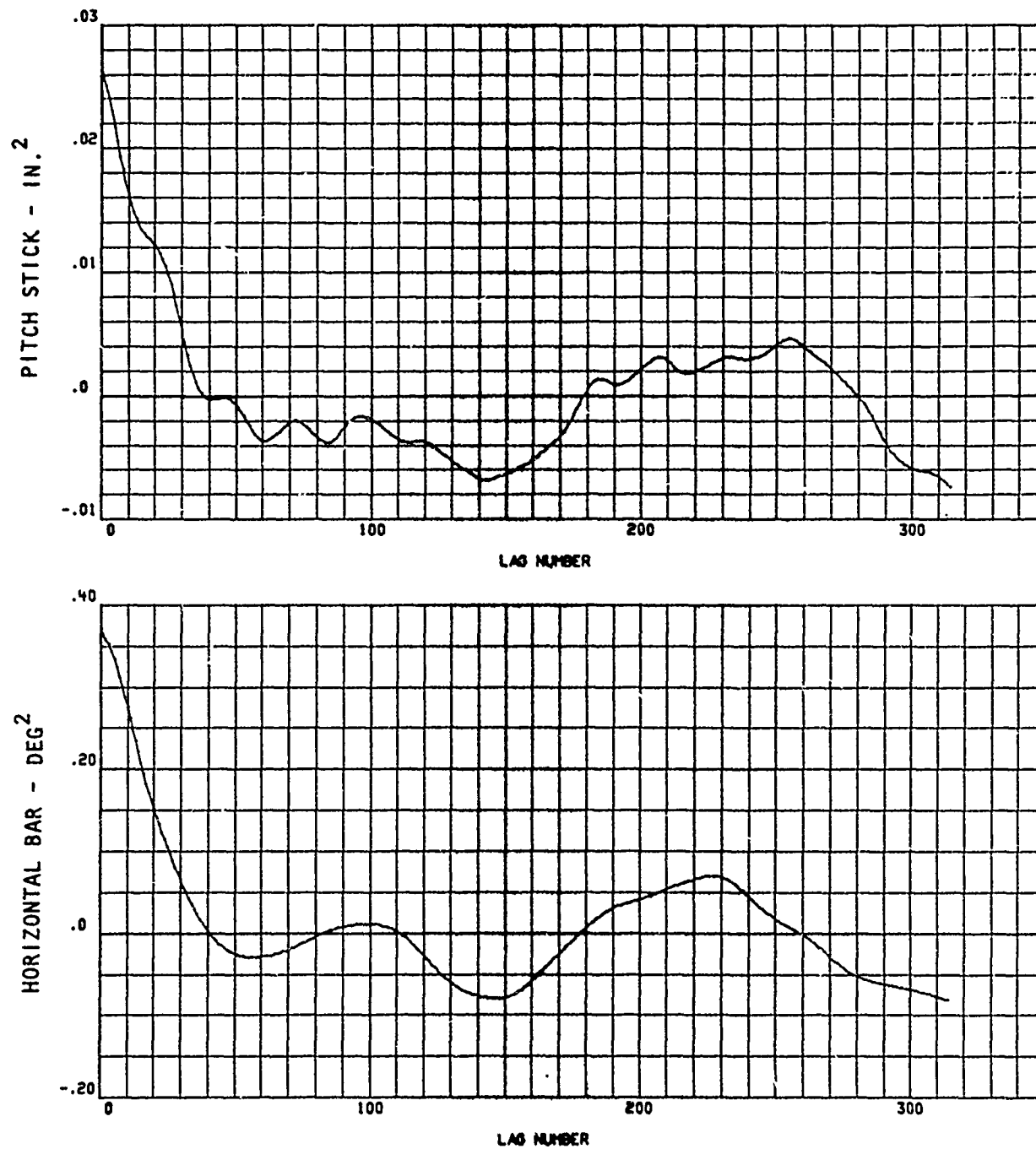
Figure 70. AR Simulation Run No. 01A34 Data (Cont)

01A34 REFUEL ANALYSIS.
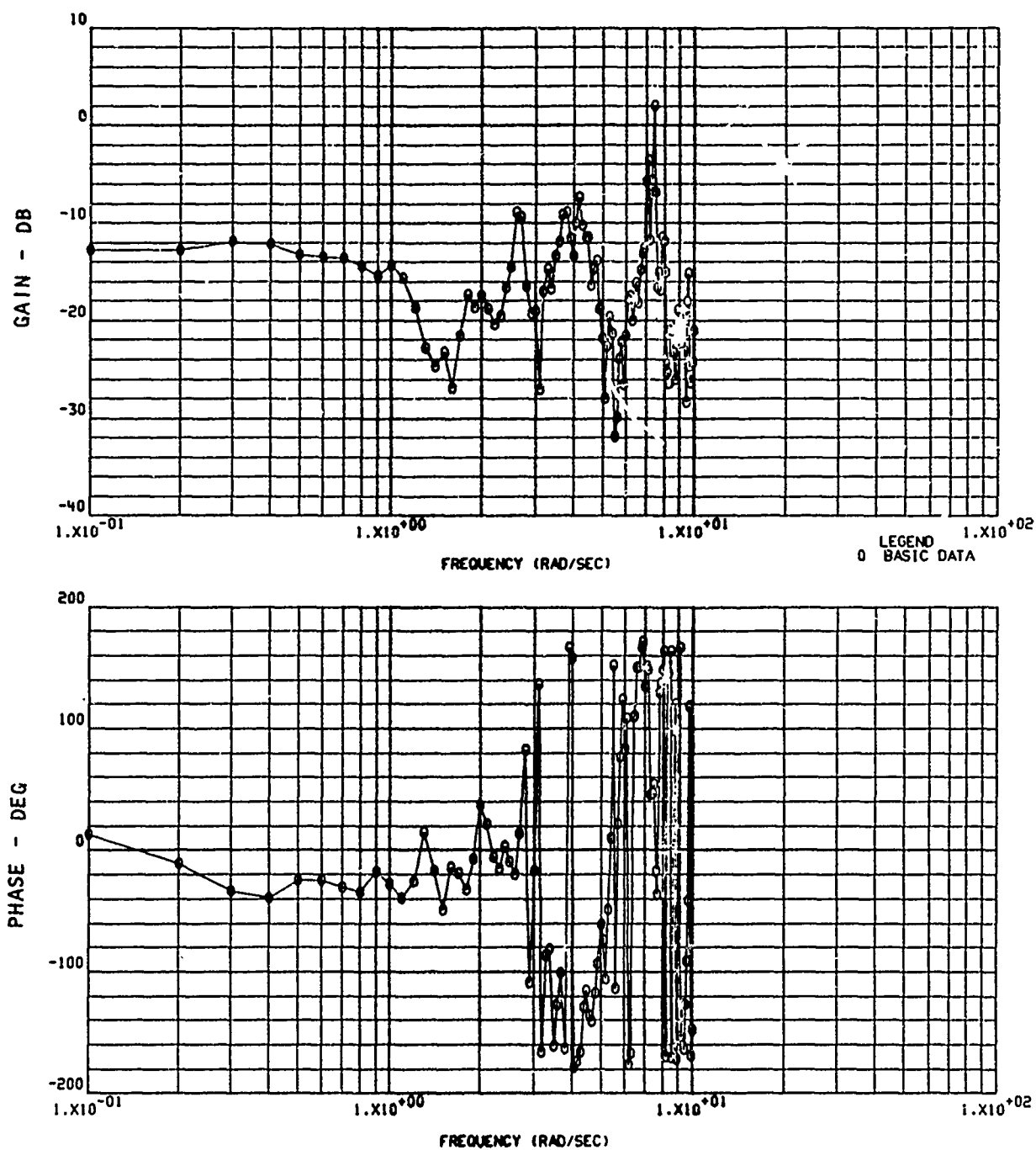
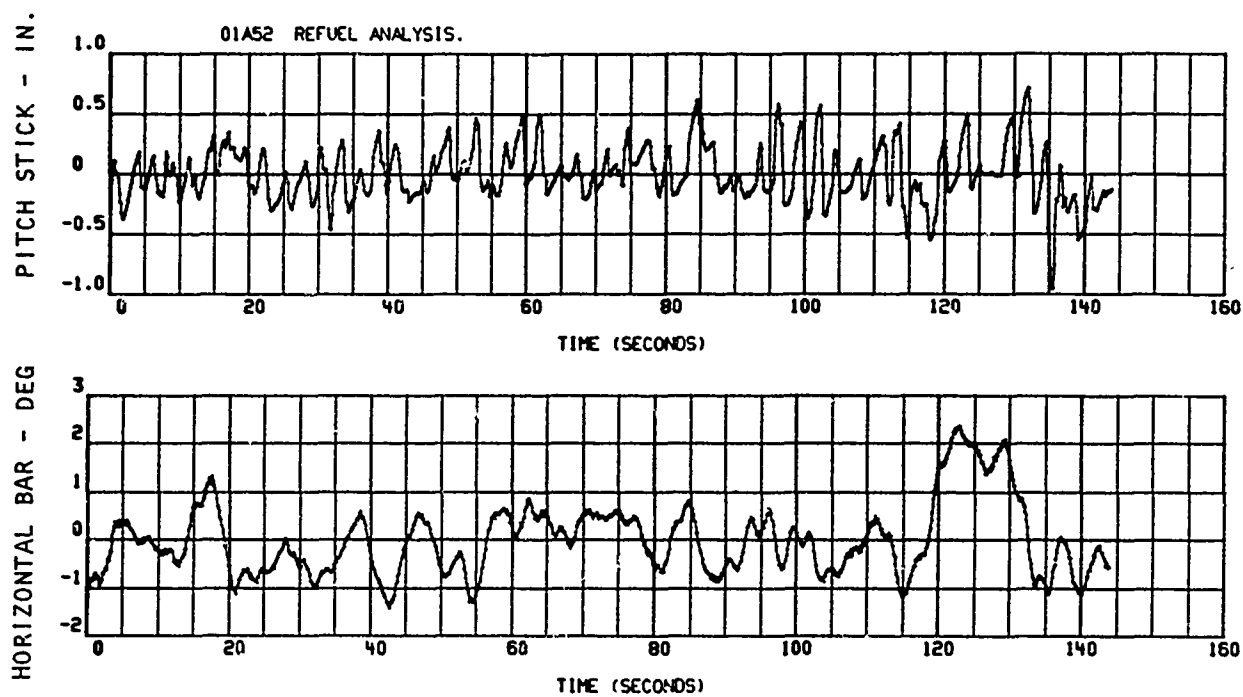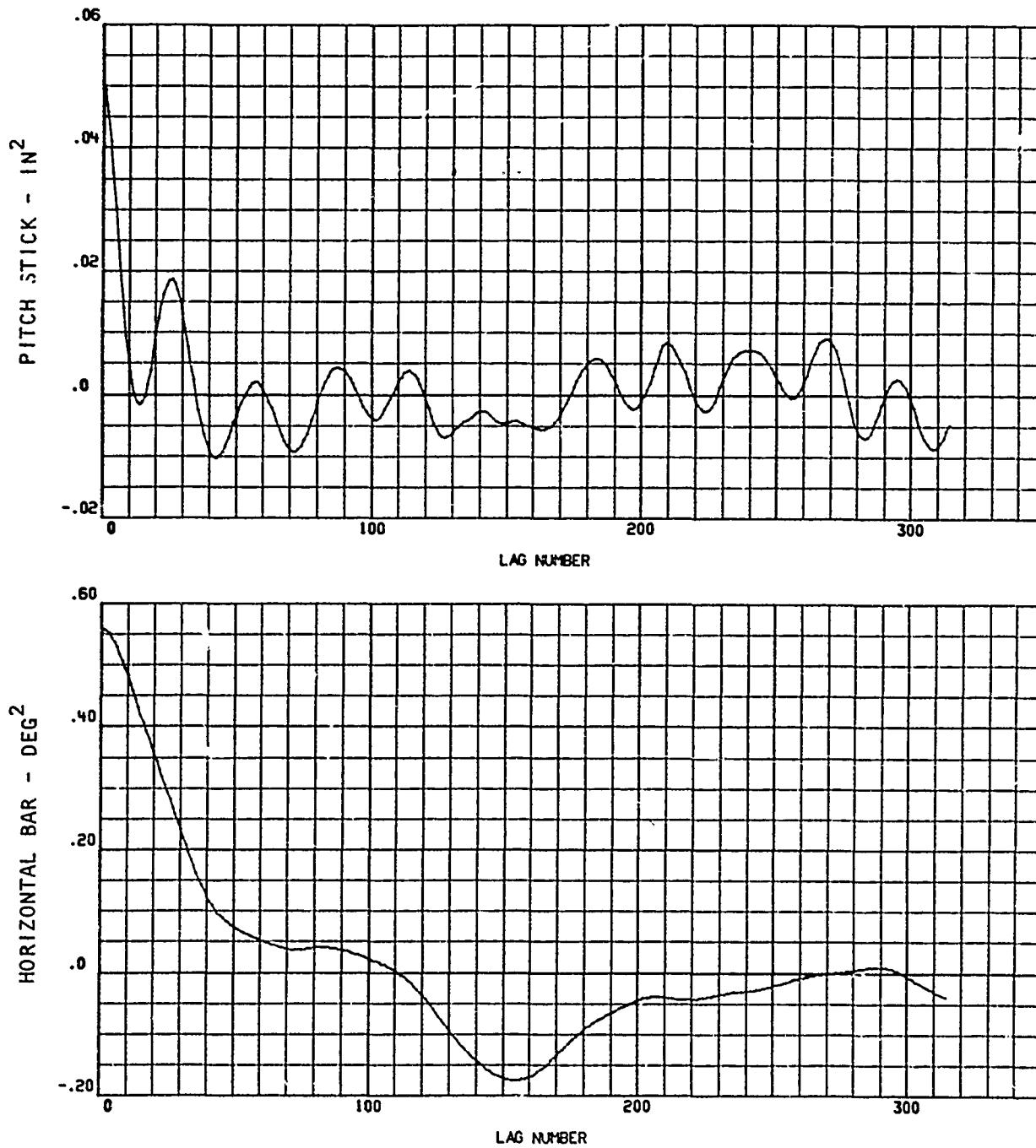Figure 70. AR Simulation Run No. 01A34 Data (Concl)

231
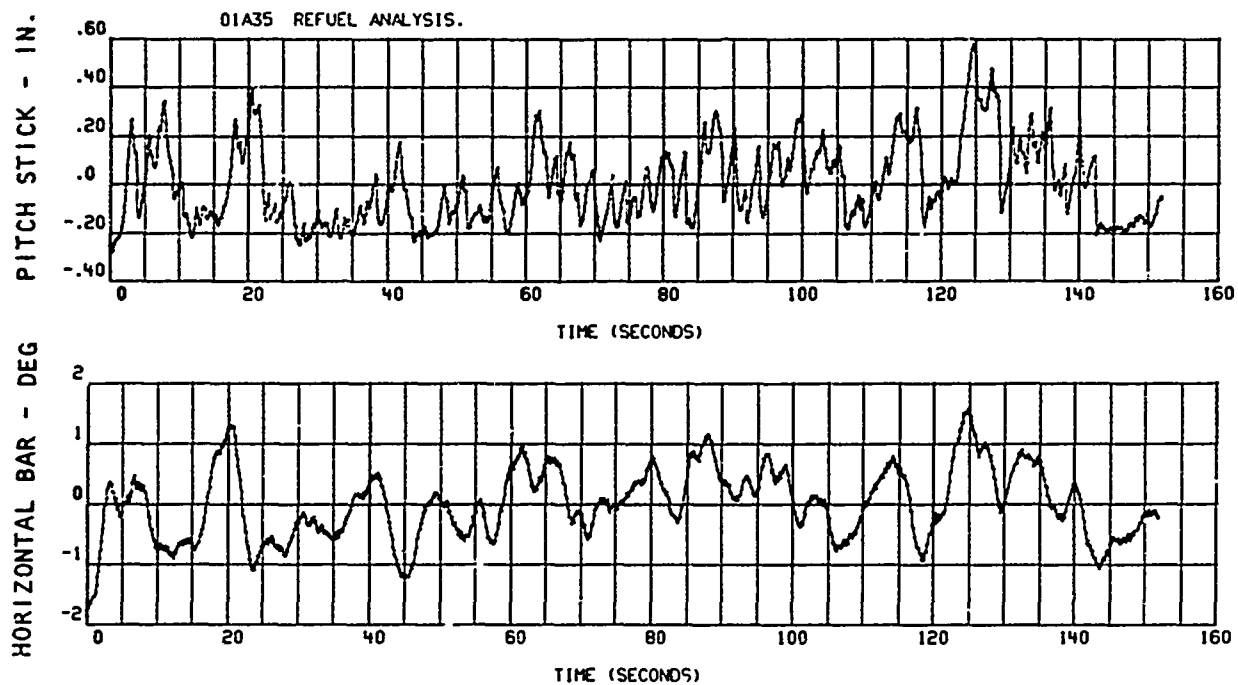
Figure 71. AR Simulation Run No. 01A35 Data

01A35 REFUEL ANALYSIS.
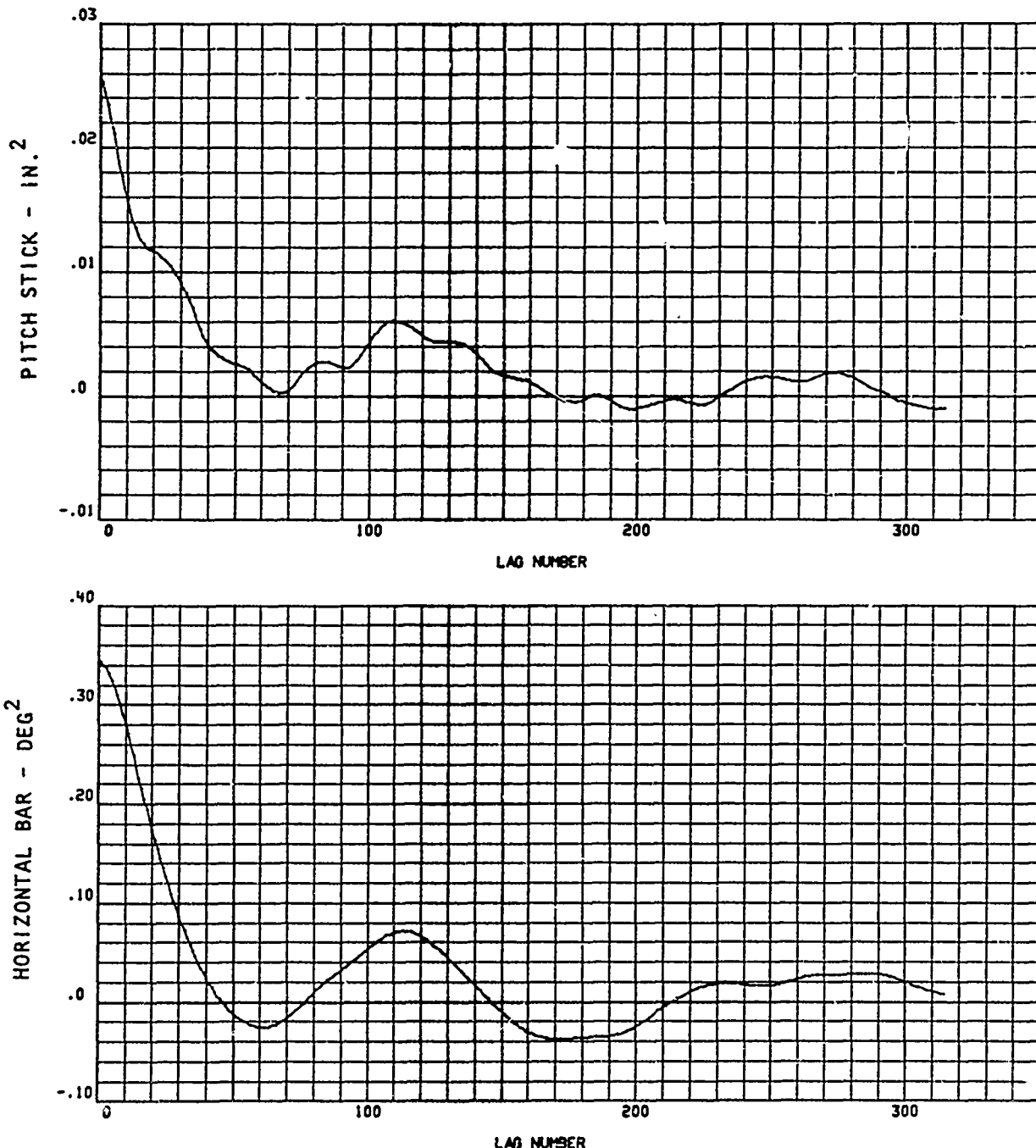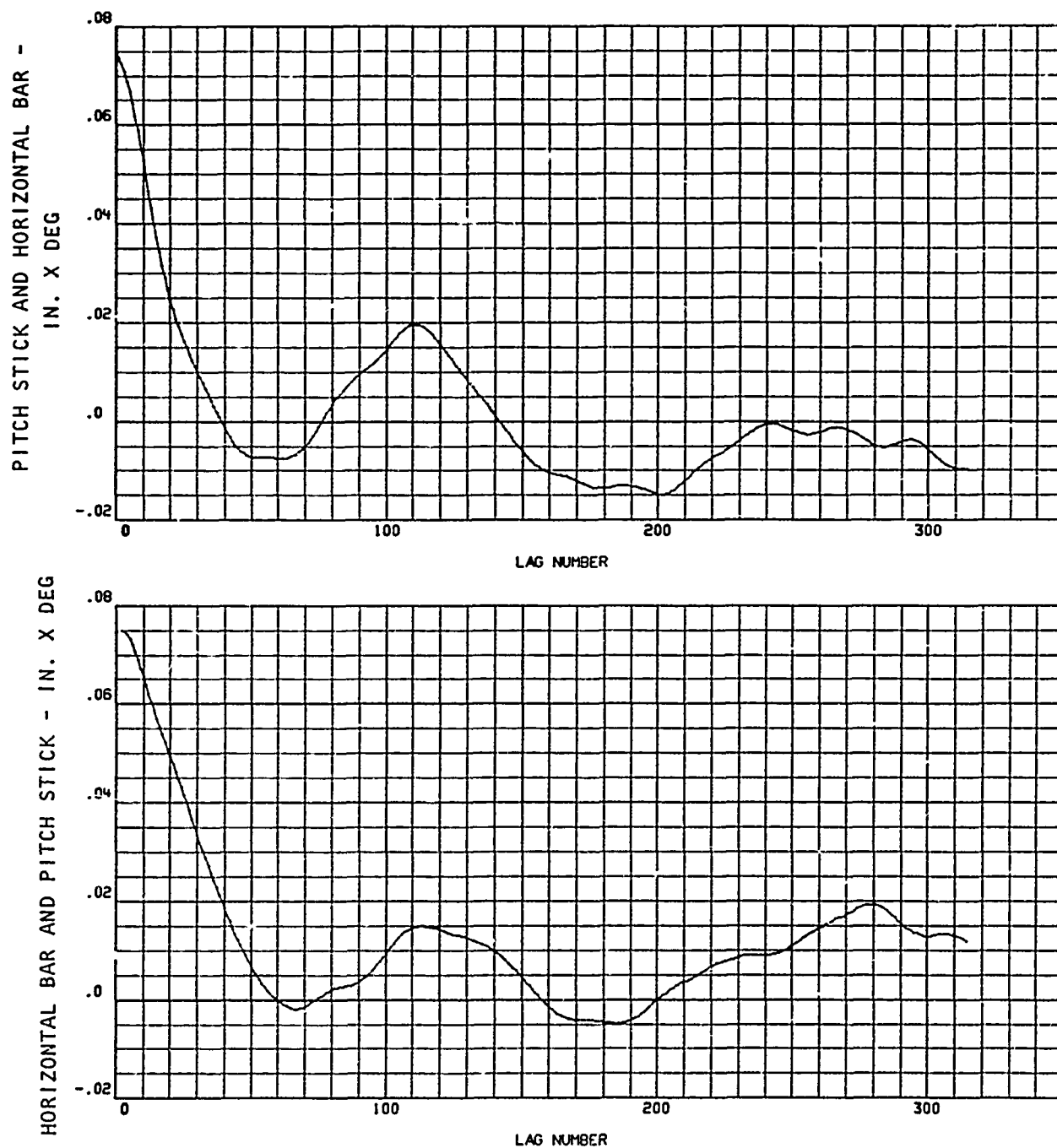
Figure 71. AR Simulation Run No. 01A35 Data (Cont)

233

CROSS CORRELATION FUNCTIONS

Figure 71.   AR Simulation Run No. 01A35 Data (Cont)

Figure 71. AR Simulation Run No. 01A35 Data

Figure 71. AR Simulation Run No. 01A35 Data (Cont)
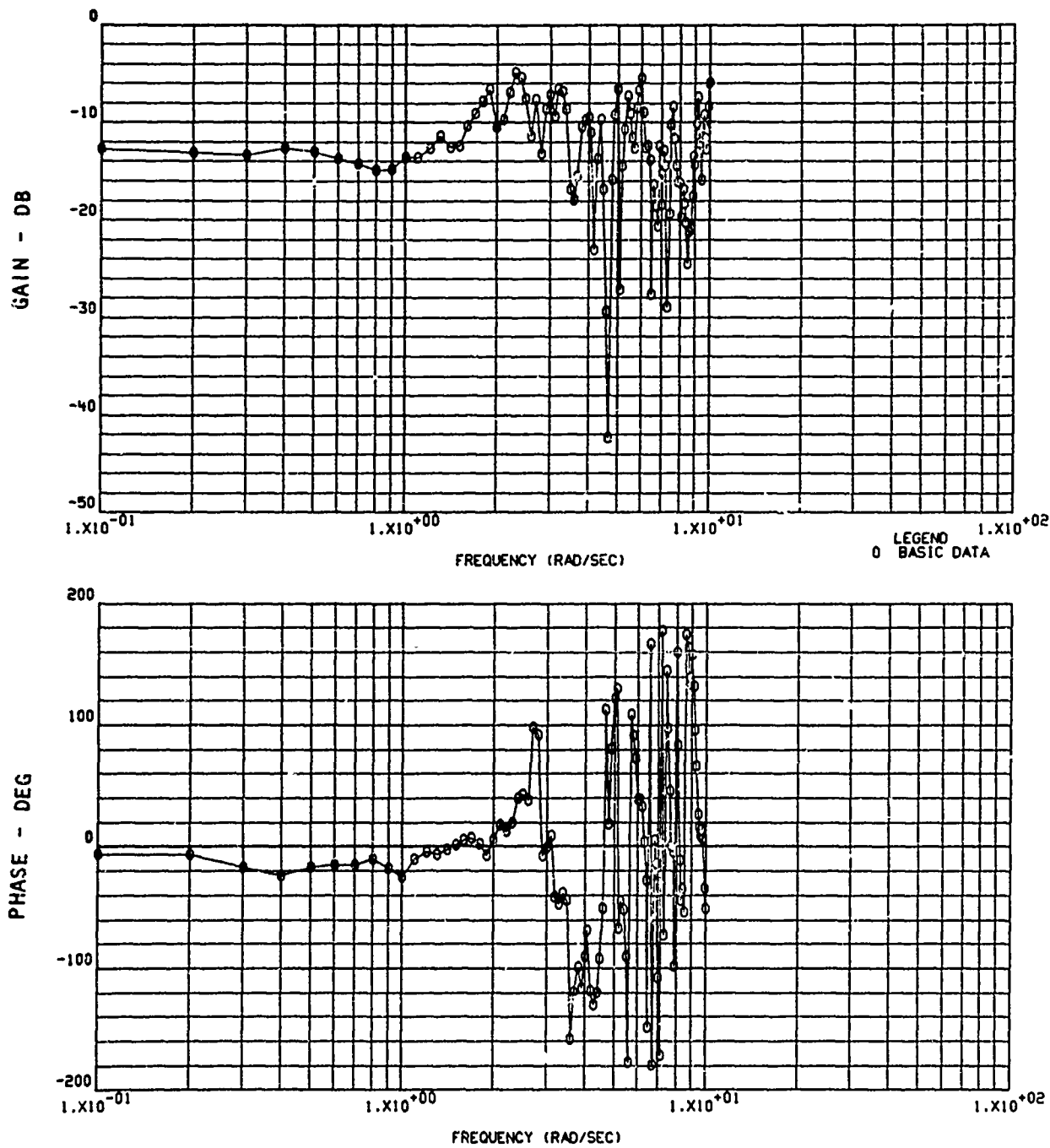
Figure 71. AR Simulation Run No. 01A35 Data (Concl)
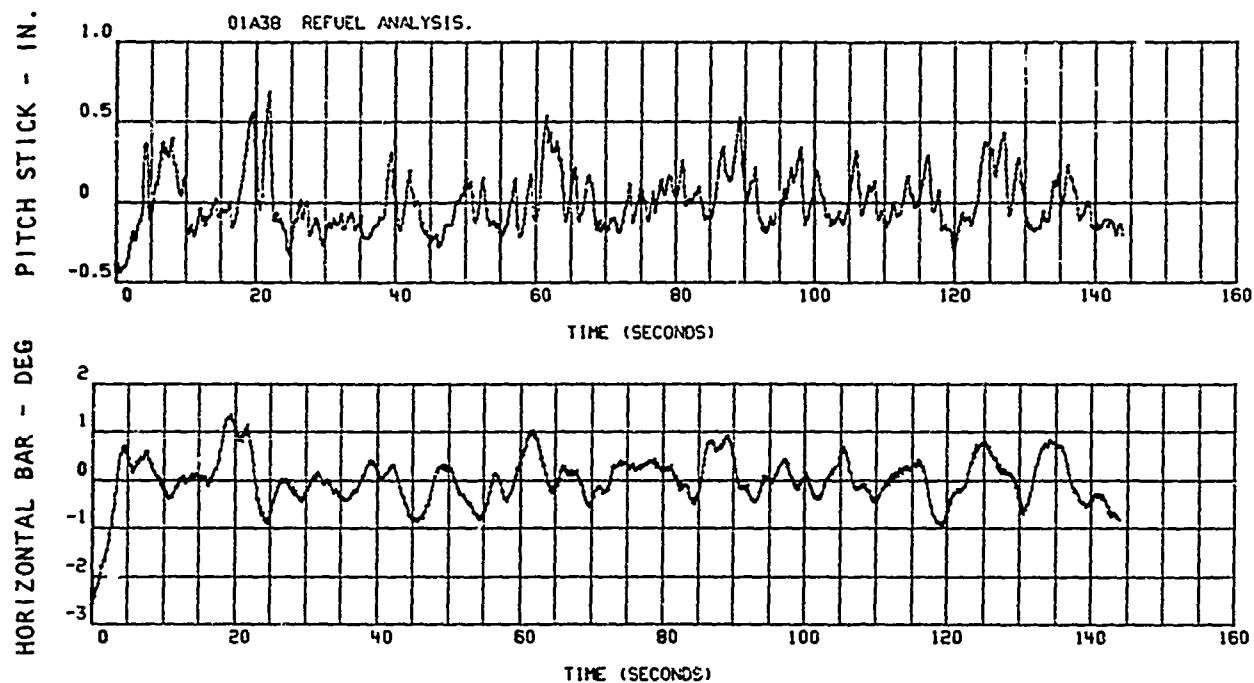
237

Figure 72. AR Simulation Run No. 01A38 Data

AUTO CORRELATION FUNCTIONS

Figure 72.   AR Simulation Run No. 01A38 Data (Cont)
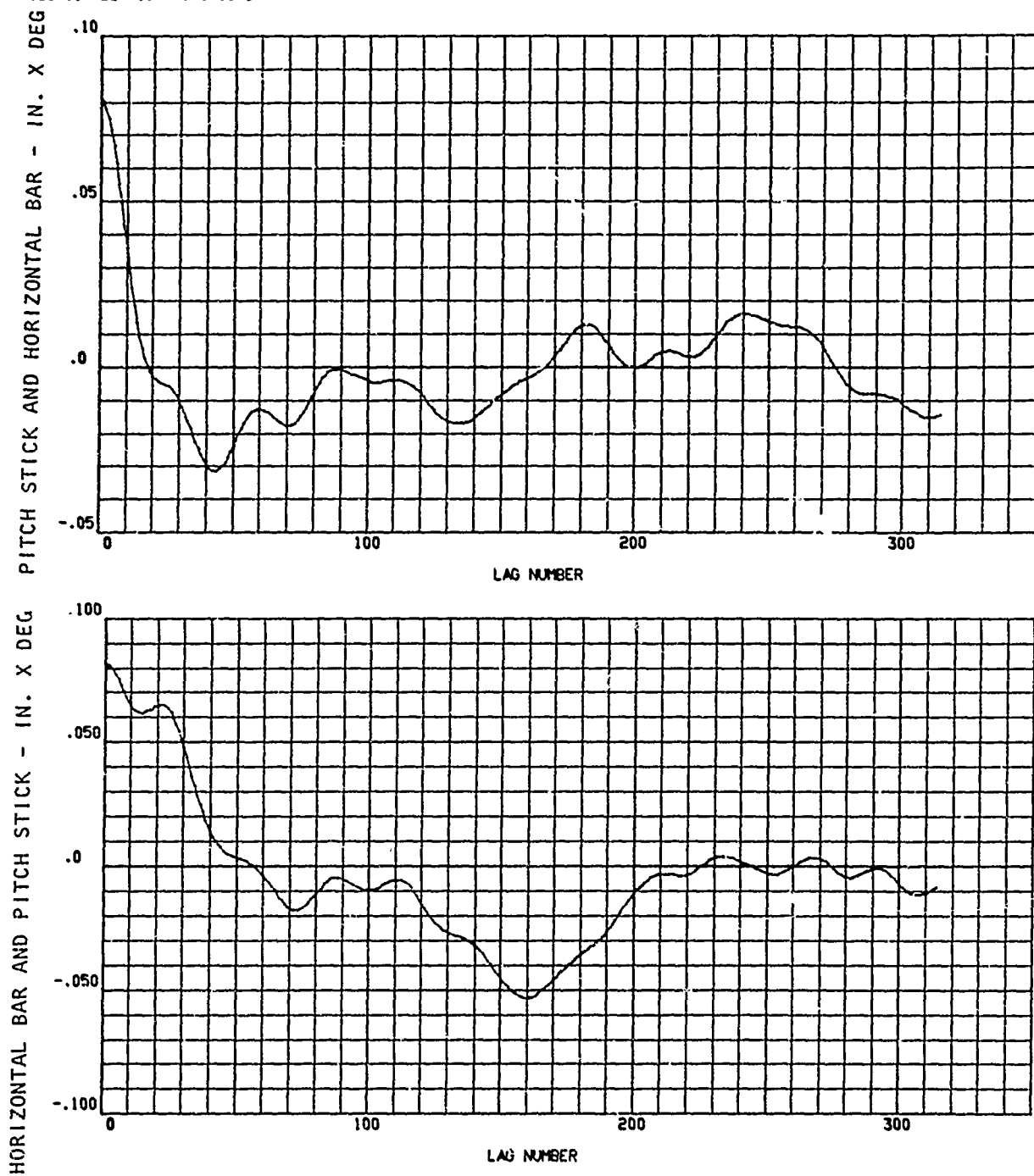
239

01A38 REFUEL ANALYSIS.

CROSS CORRELATION FUNCTIONS

Figure 72.   AR Simulation Run No. 01A38 Data (Cont)

240

SPECTRAL DENSITY FUNCTIONS

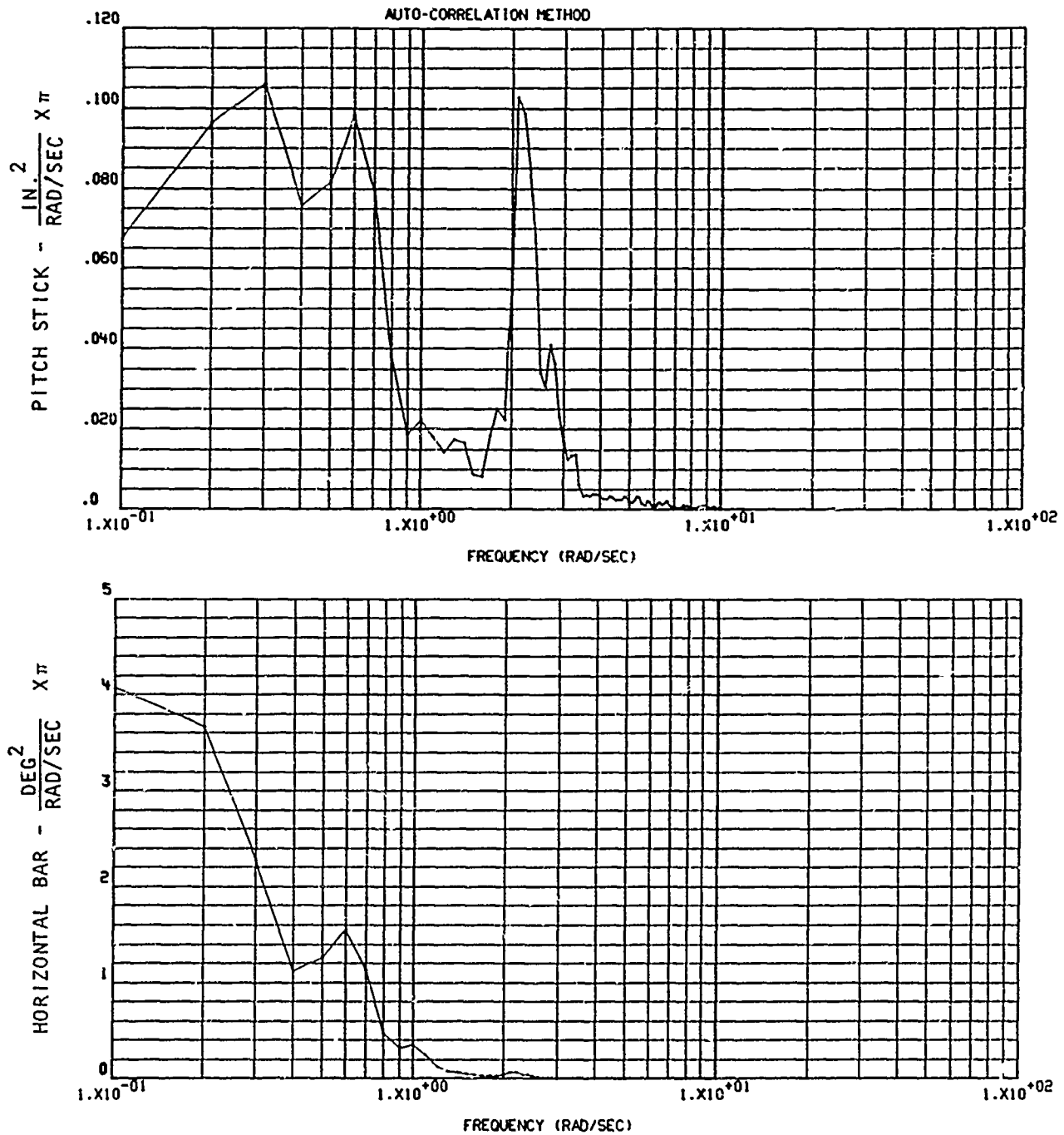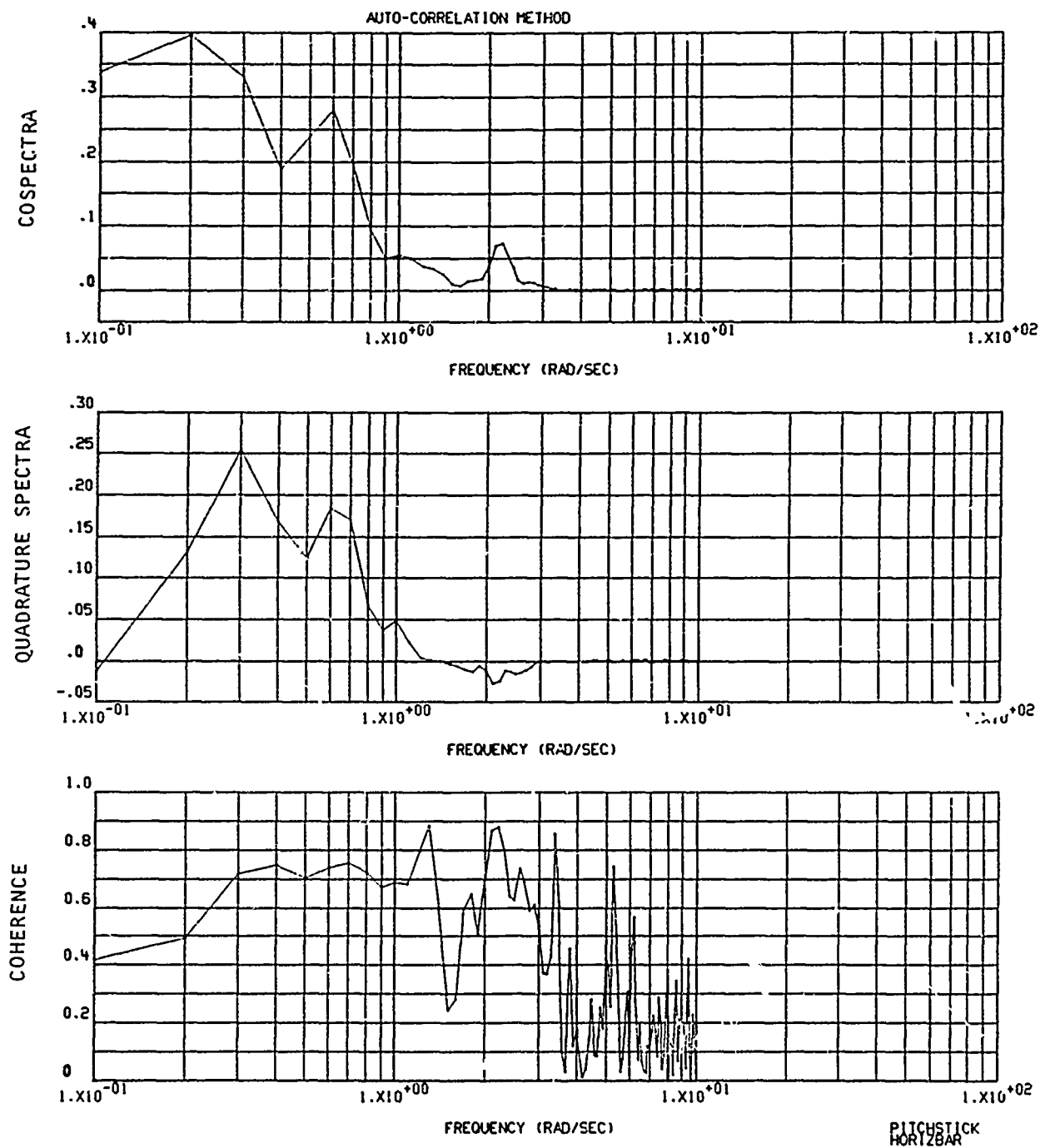Figure 72. AR Simulation Run No. 01A38 Data (Cont)

Figure 72. AR Simulation Run No. 01A38 Data (Cont)

242
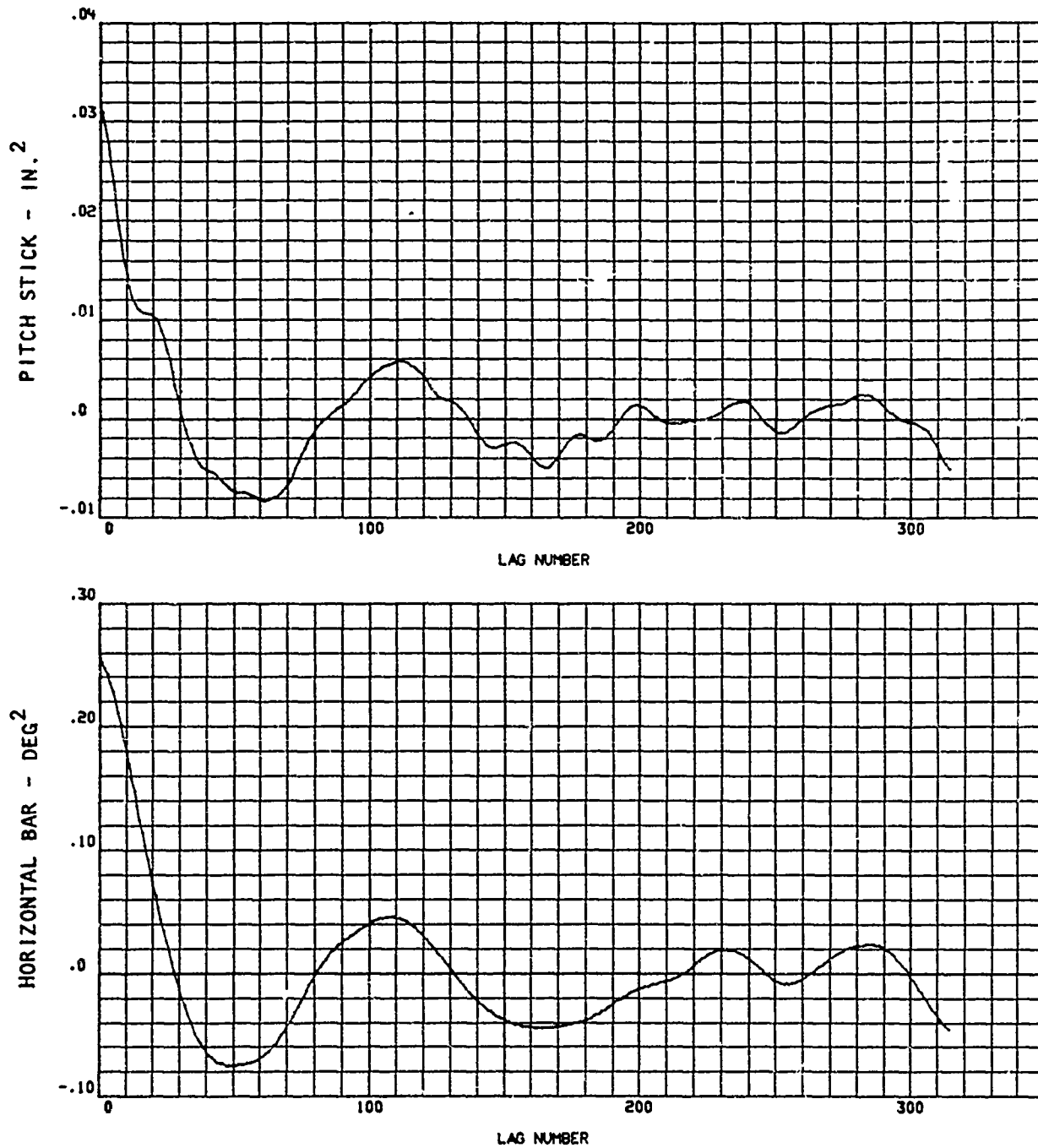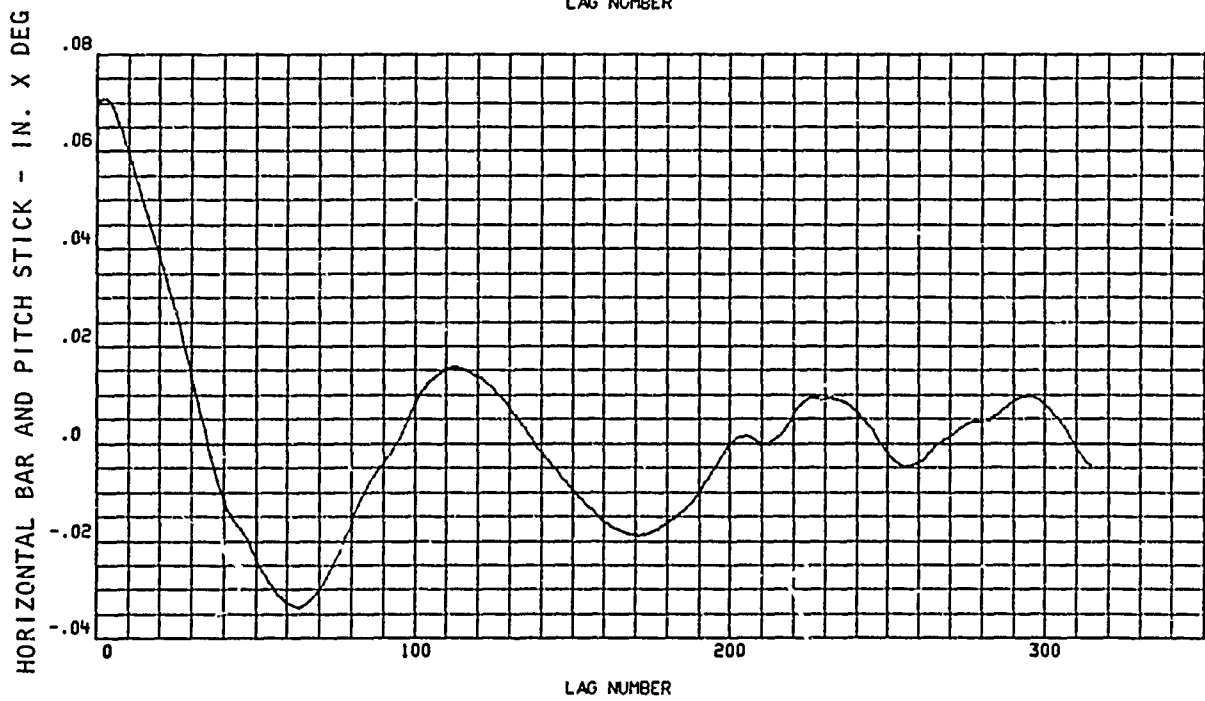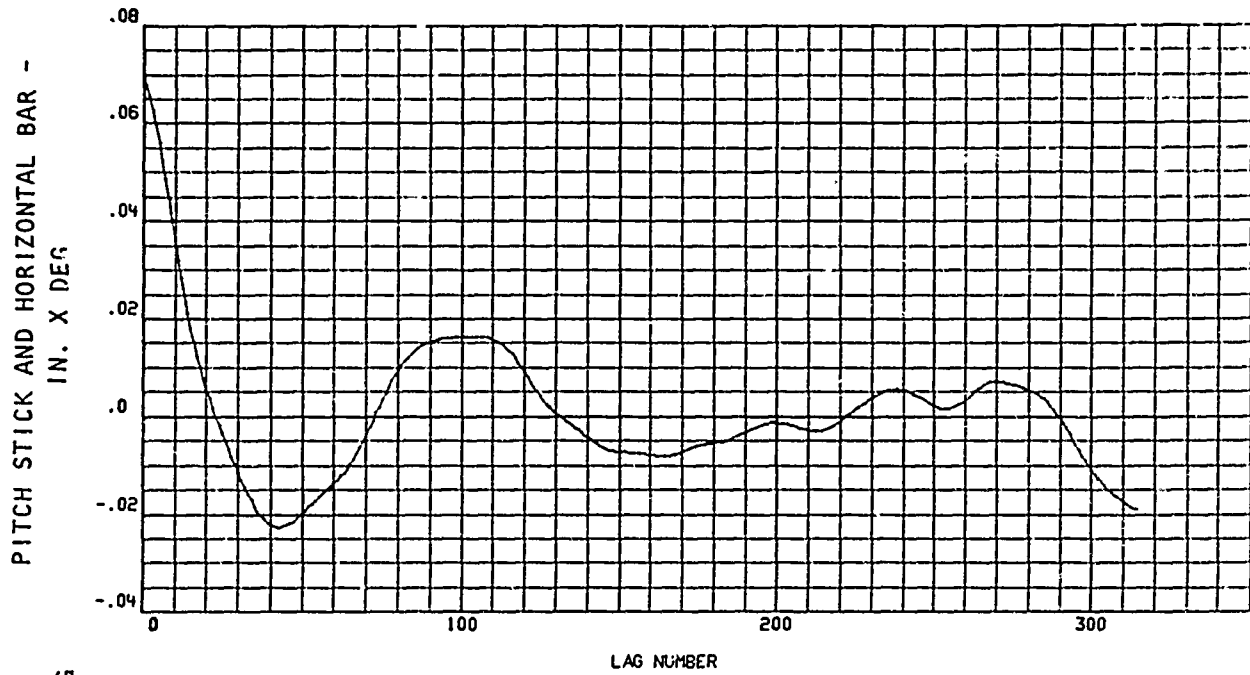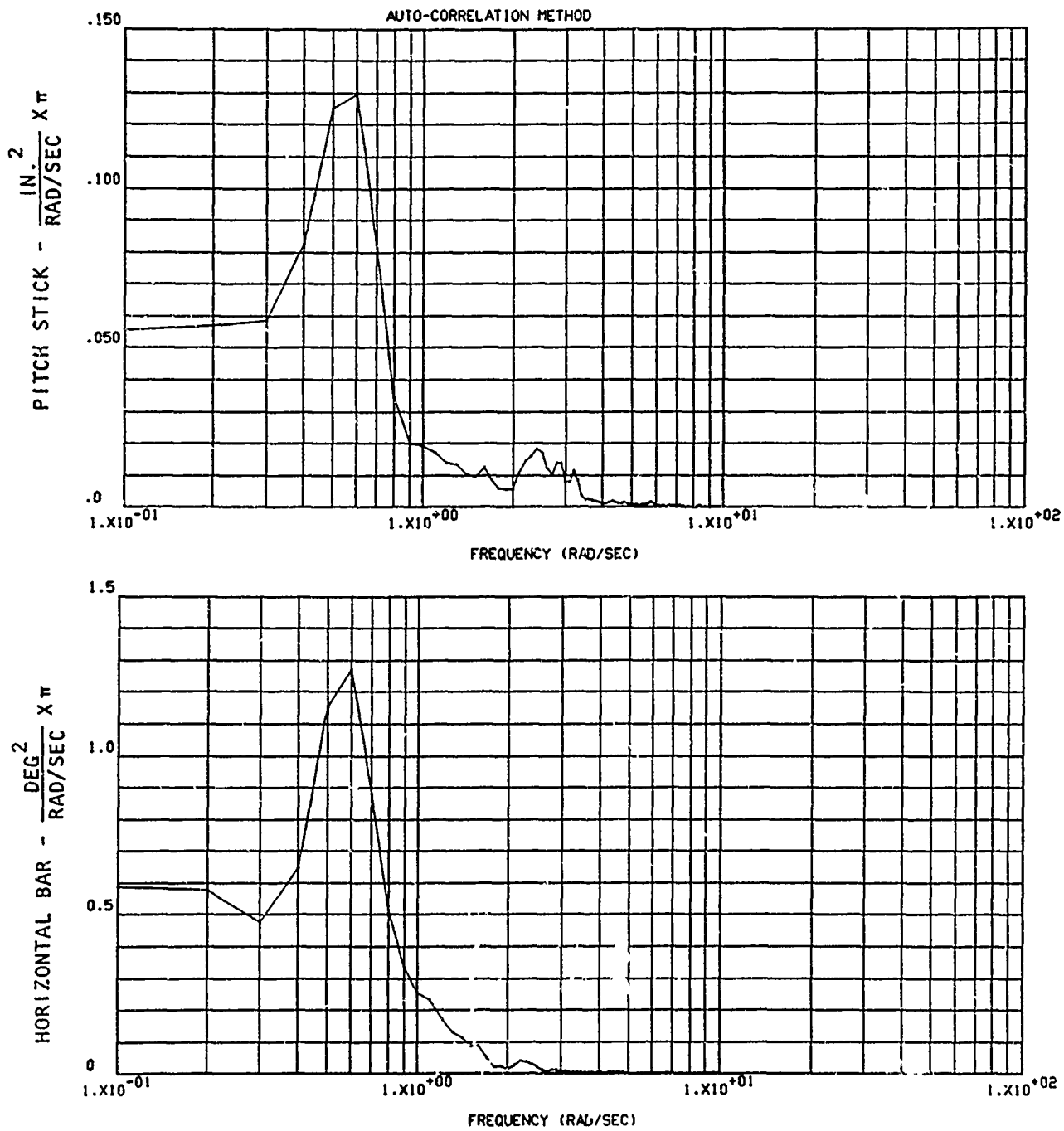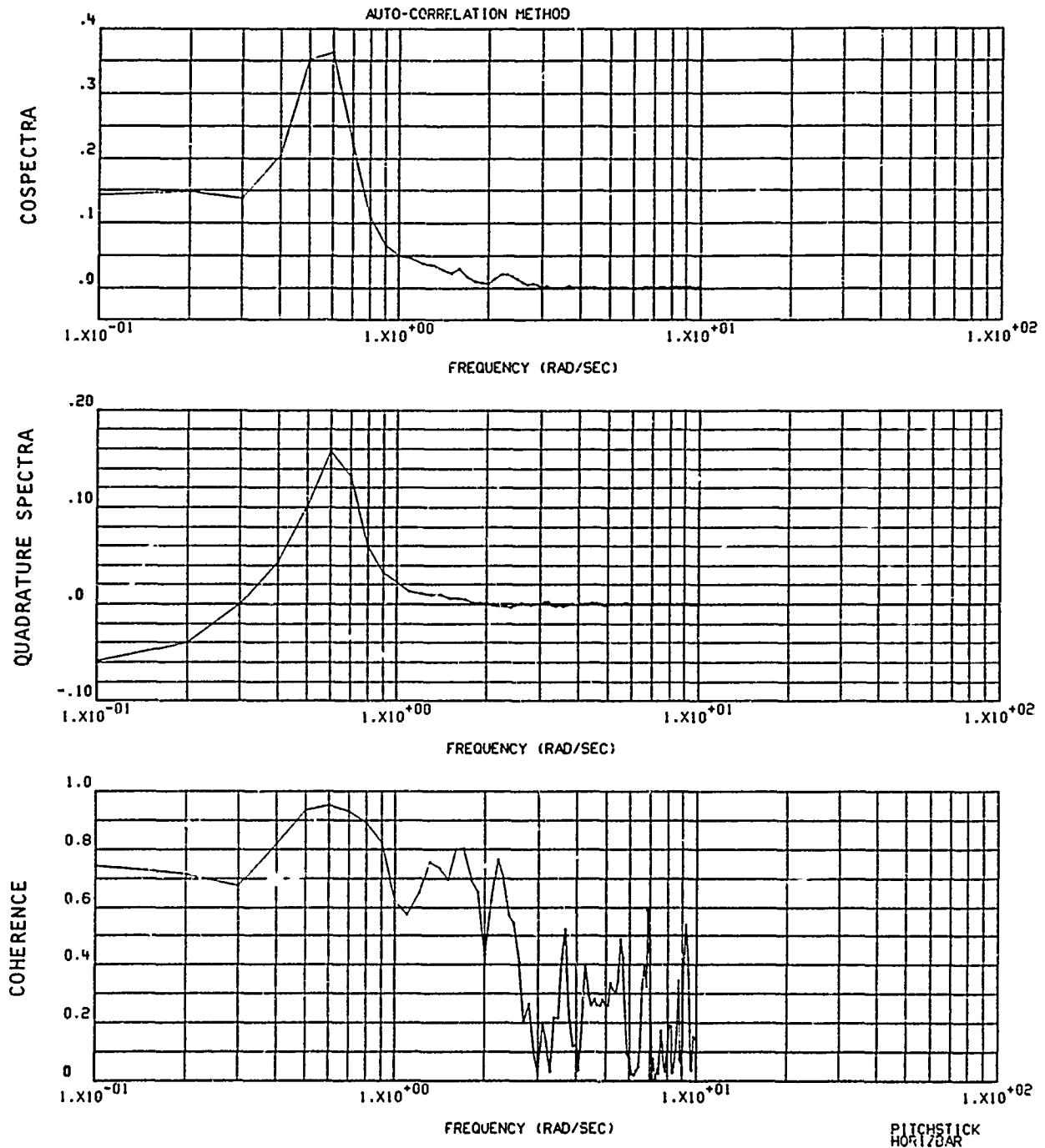
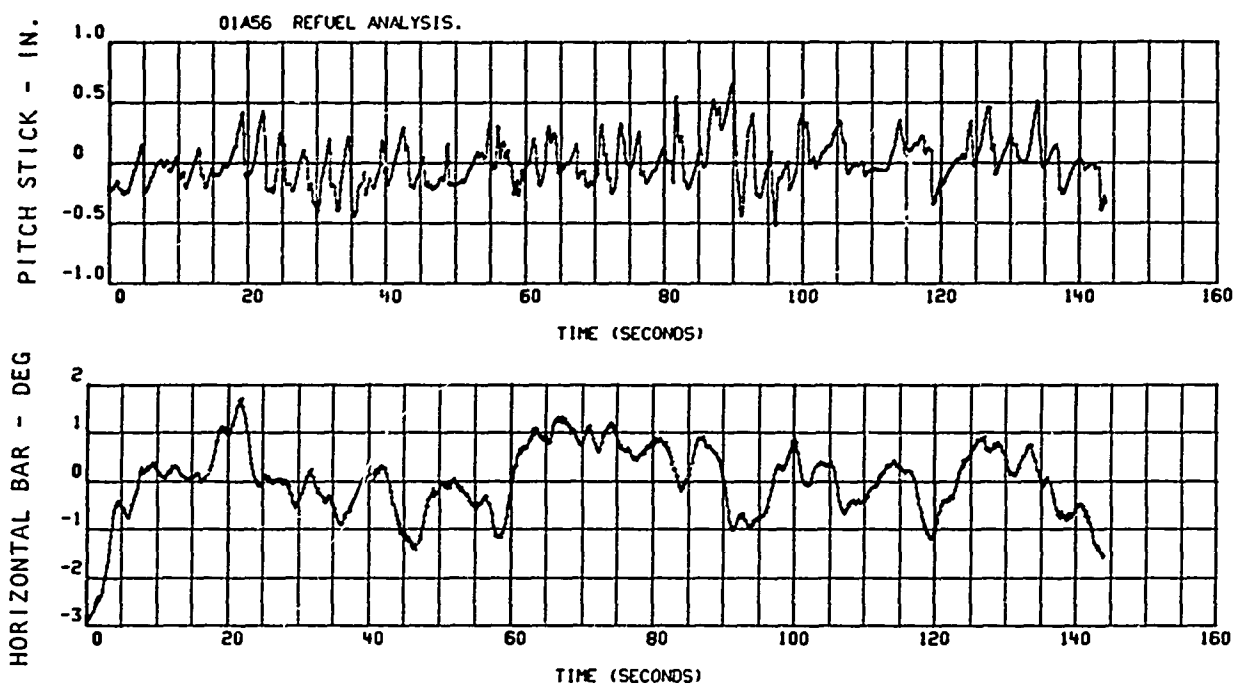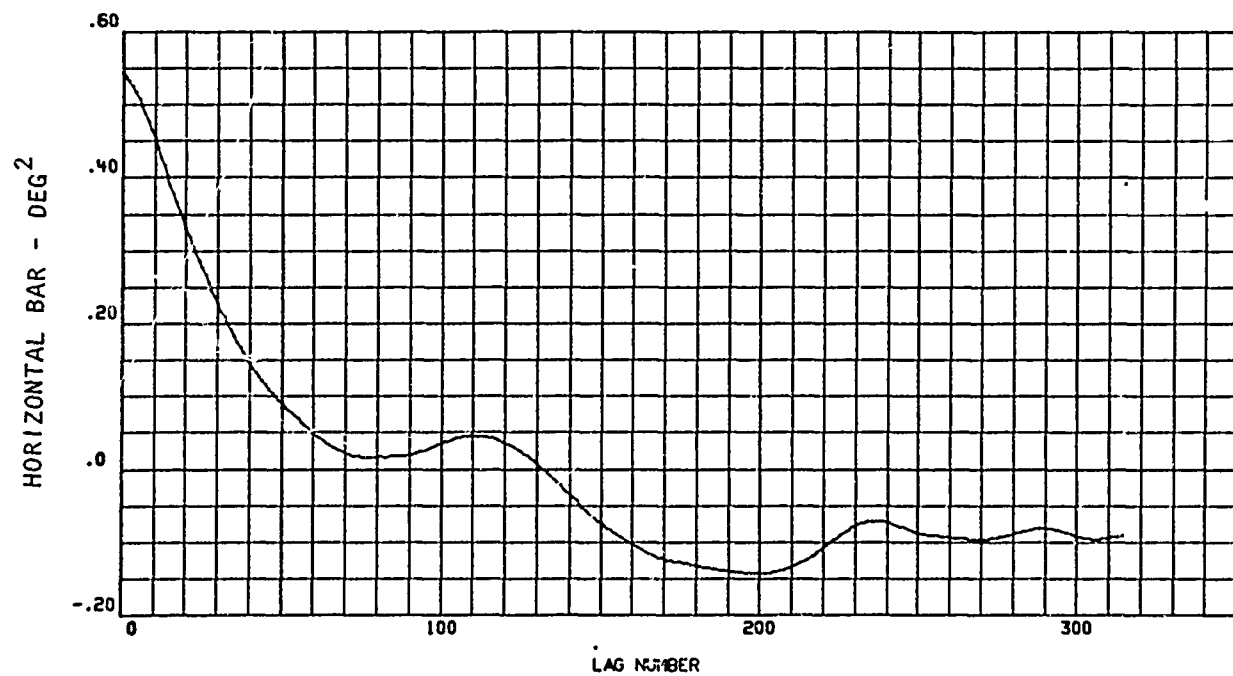01A38 REFUEL ANALYSIS.

Figure 72. AR Simulation Run No. 01A38 Data (Concl)
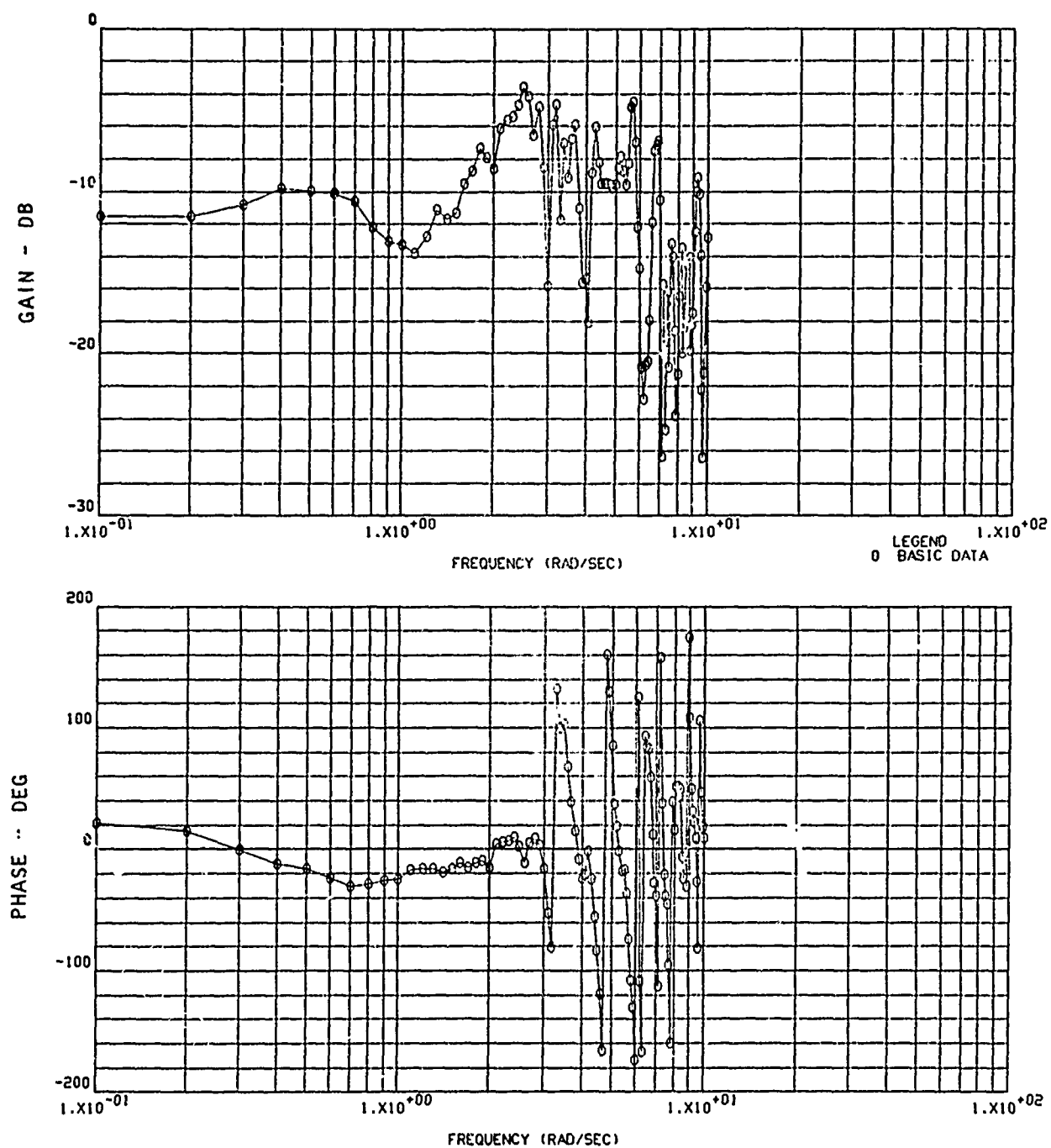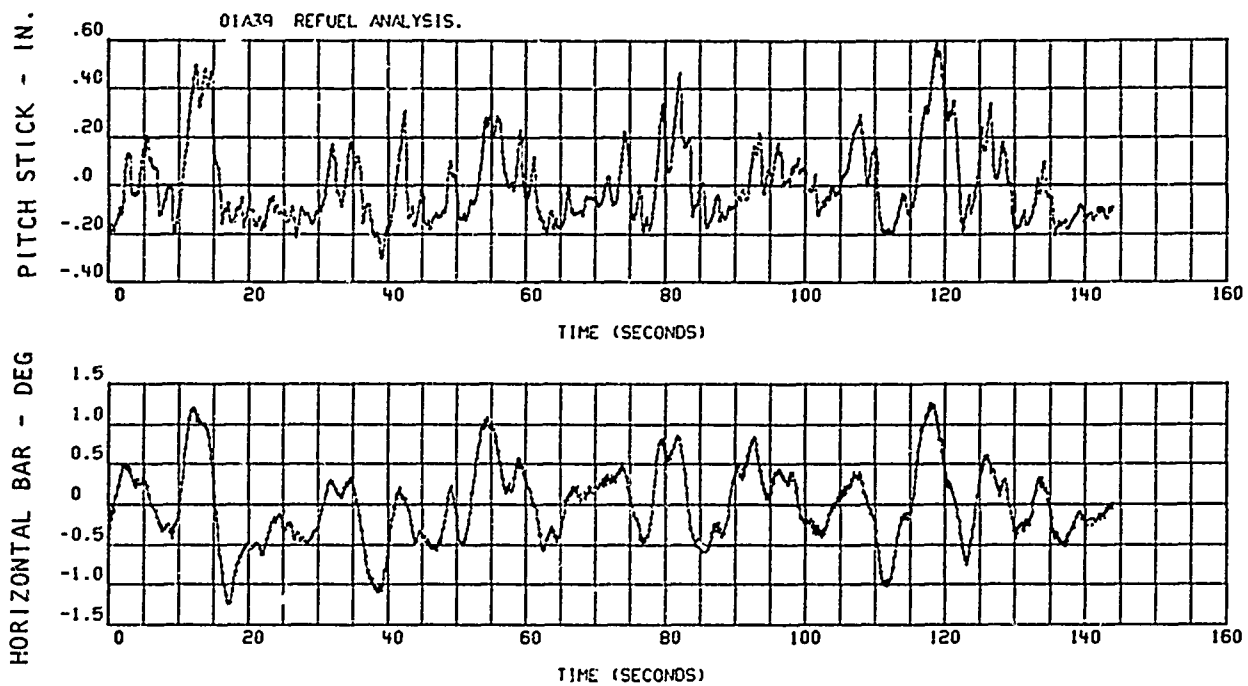
243

Figure 73. AR Simulation Run No. 01A39 Data

AUTO CORRELATION FUNCTIONS

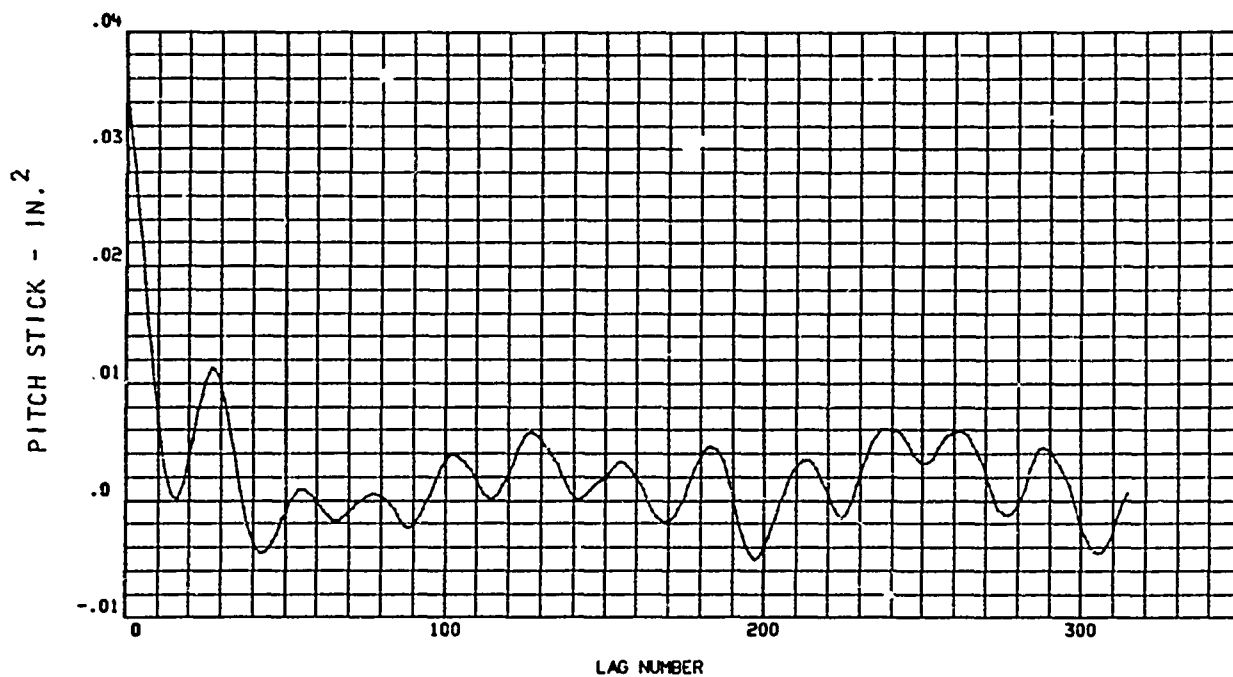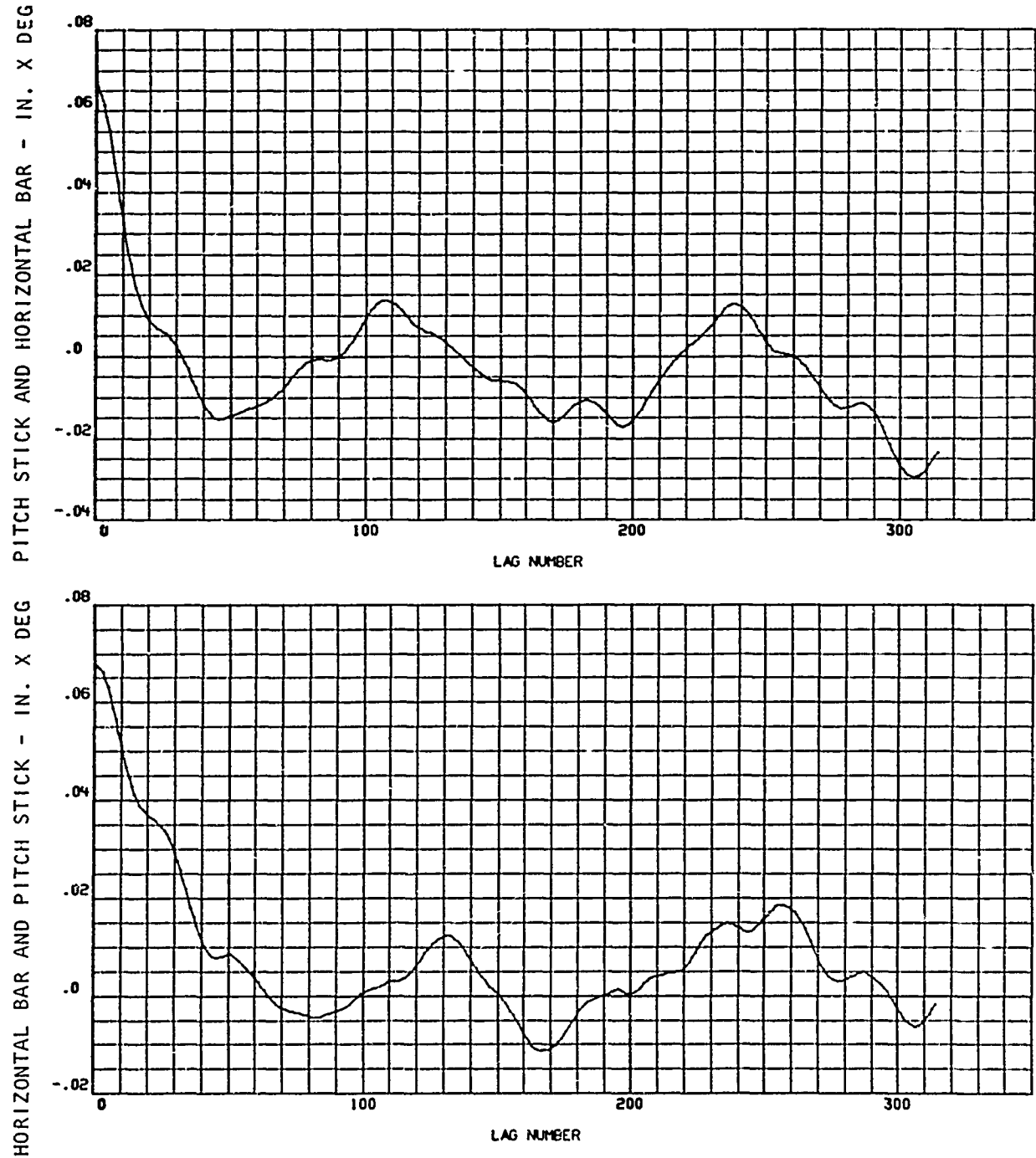Figure 73.   AR Simulation Run No. 01A39 Data (Cont)

245
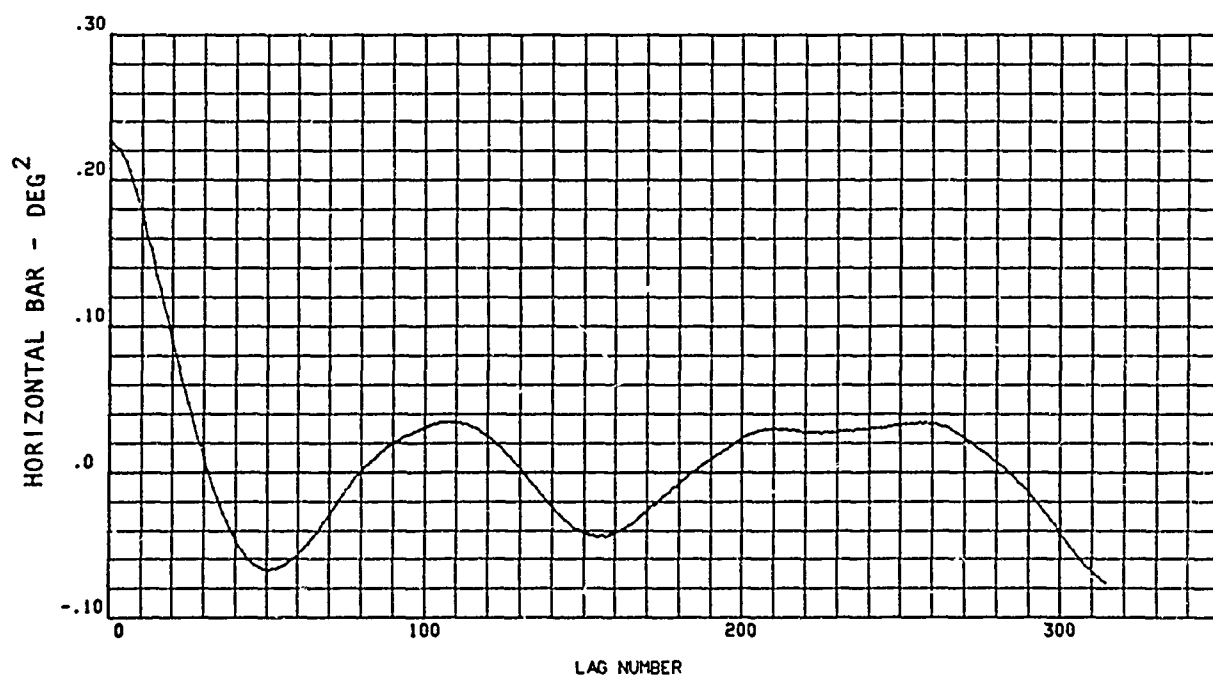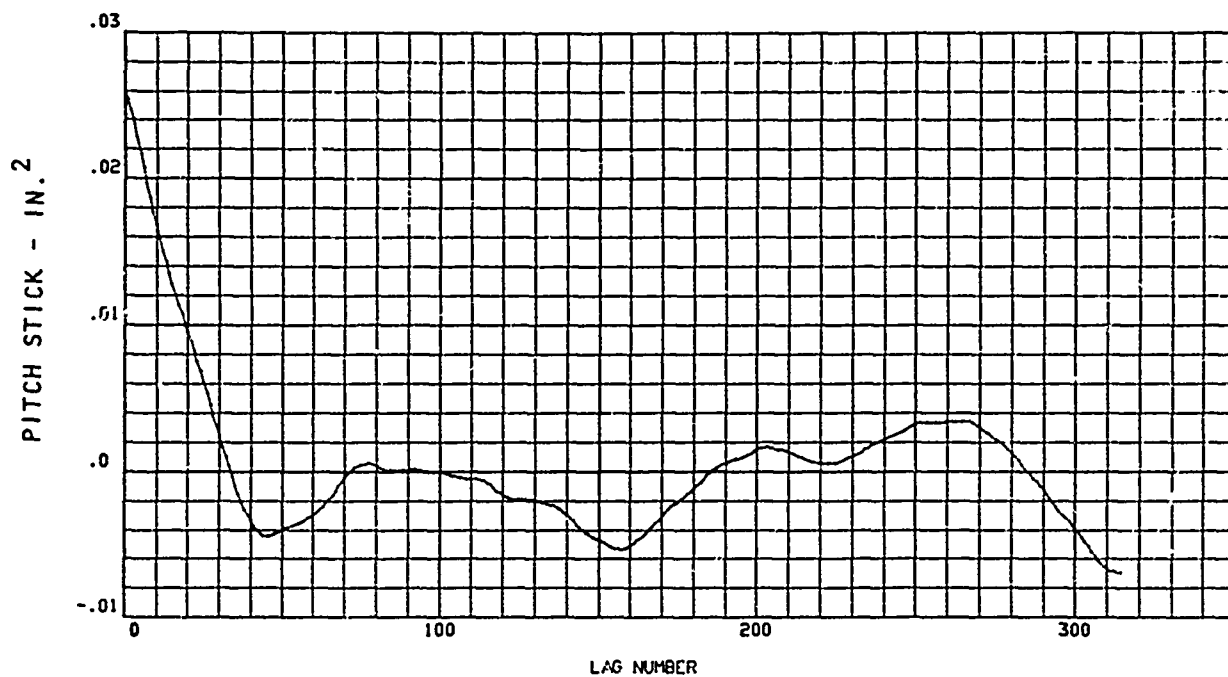
Figure 73. AR Simulation Run No. 01A39 Data (Cont)

01A39 REFUEL ANALYSIS.

SPECTRAL DENSITY FUNCTIONS

Figure 73.   AR Simulation Run No. 01A39 Data (Cont)

247

01A39 REFUEL ANALYSIS.

AUTO-CORRELATION METHOD

Figure 73. AR Simulation Run No. 01A39 Data (Cont)

248

01A39 REFUEL ANALYSIS.
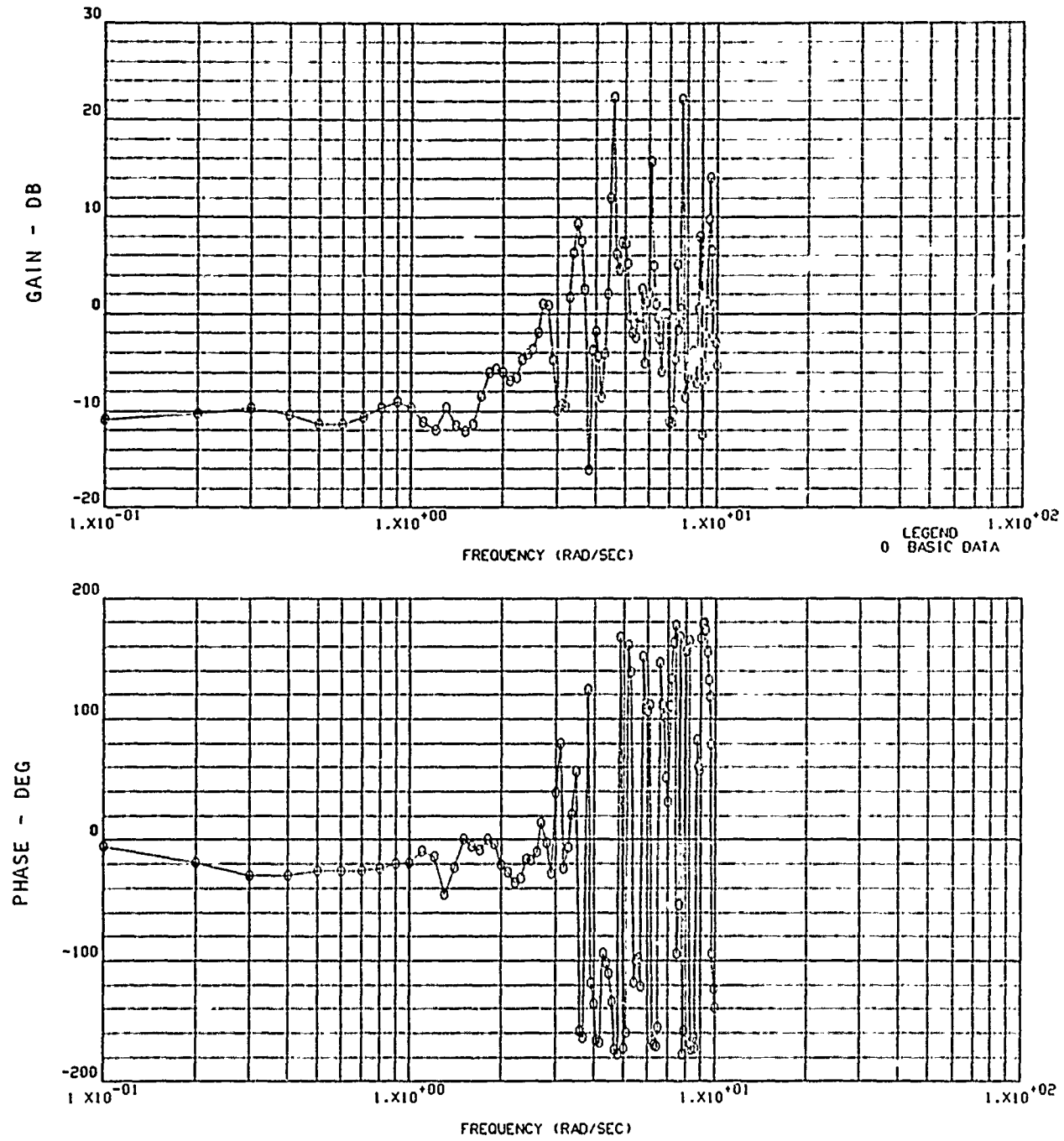
Figure 73. Simulation Run No. 01A39 Data (Concl)
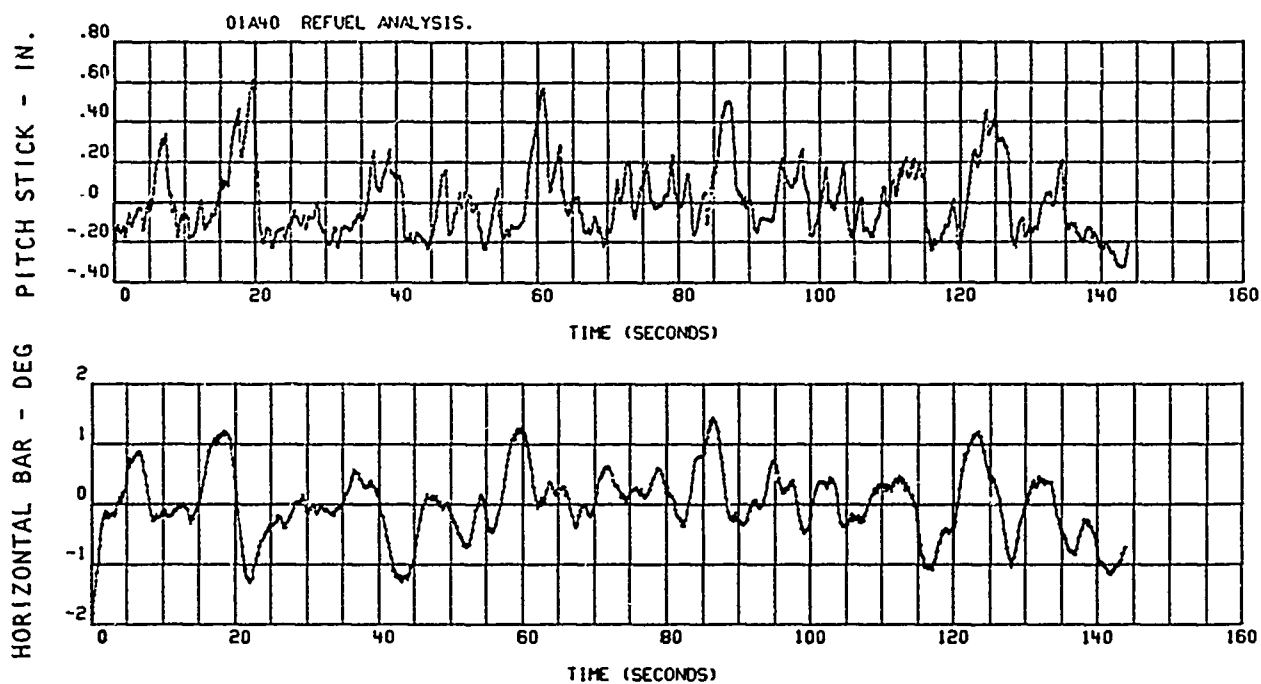
249.

Figure 74. AR Simulation Run No. 01A40 Data

Figure 74.   AR Simulation Run No. 01A40 Data (Cont)

251

01A40 REFUEL ANALYSIS.

CROSS CORRELATION FUNCTIONS
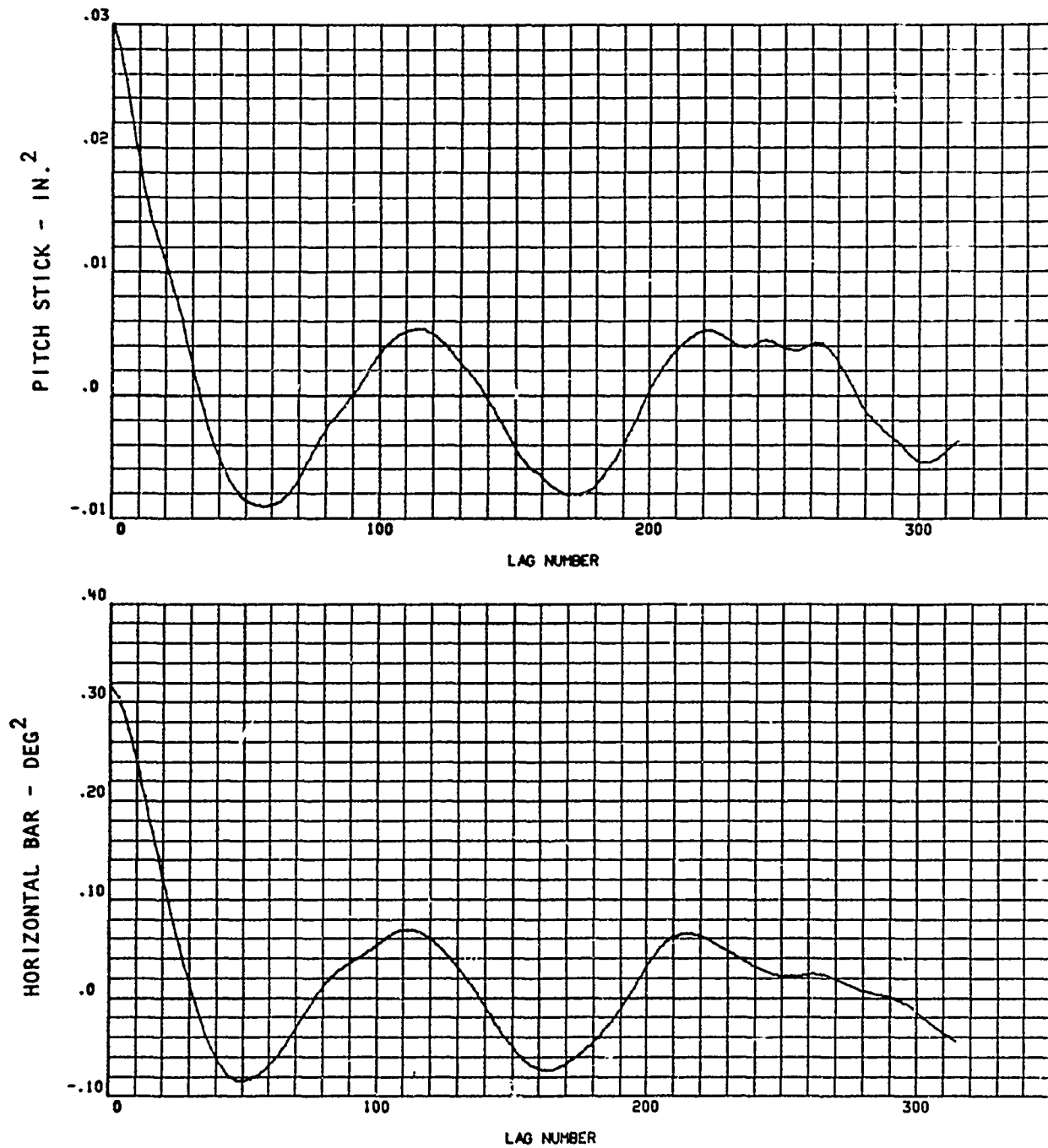
Figure 74. AR Simulation Run No. 01A40 Data (Cont)
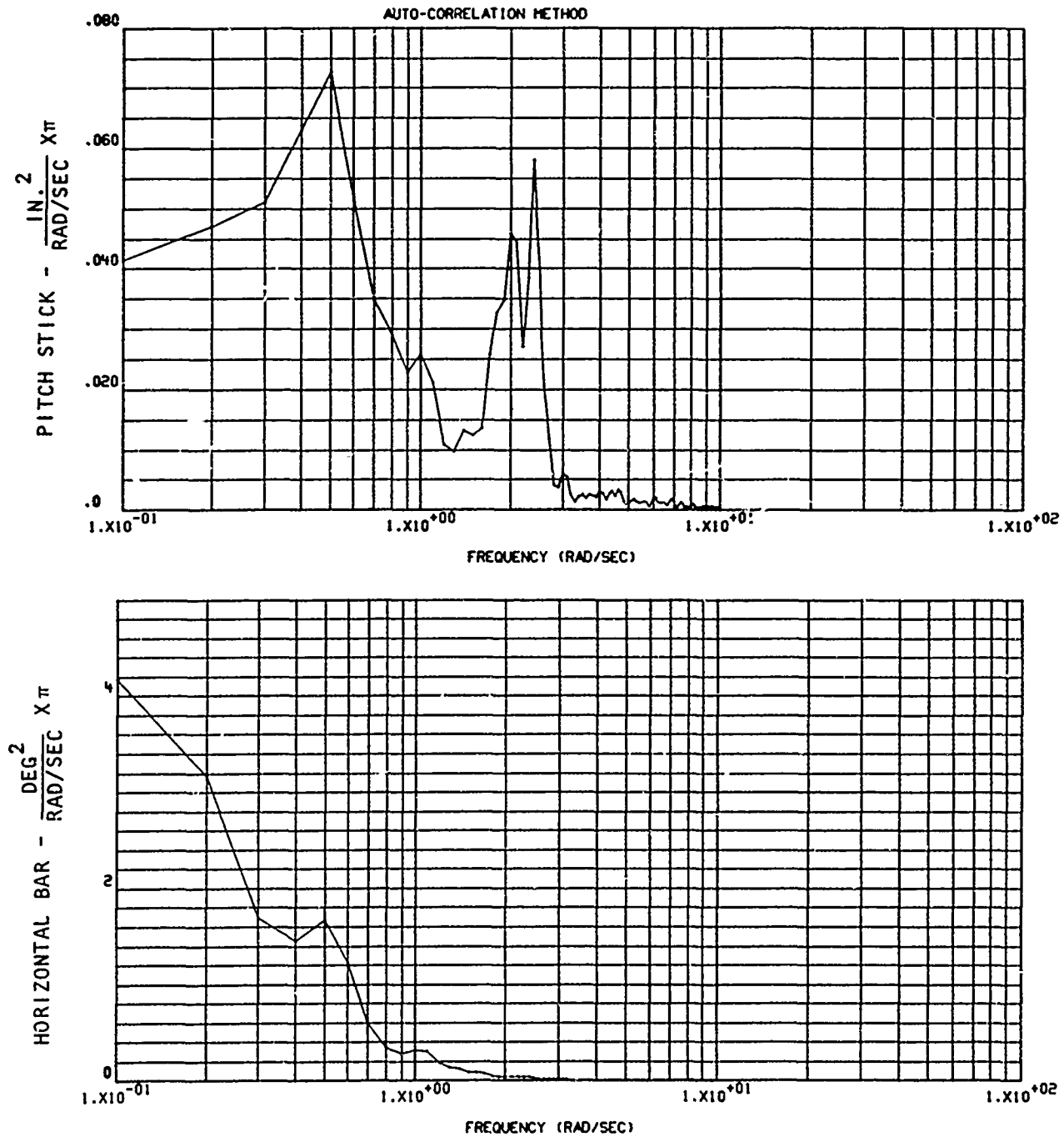
01A40 REFUEL ANALYSIS.

SPECTRAL DENSITY FUNCTIONS

Figure 74.   AR Simulation Run No. 01A40 Data (Cont)
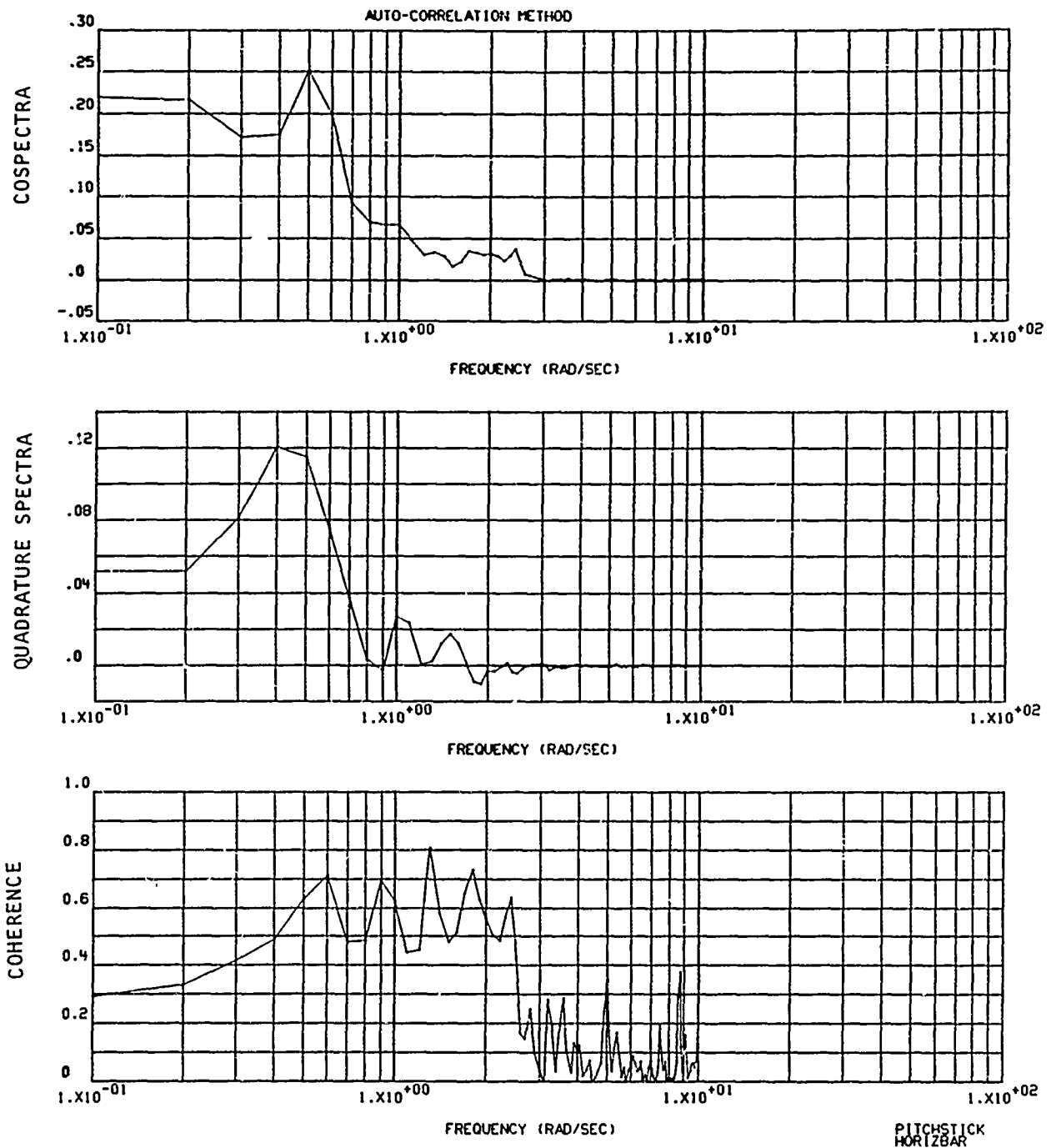
253

01A40 REFUEL ANALYSIS.

Figure 74. AR Simulation Run No. 01A40 Data (Cont)
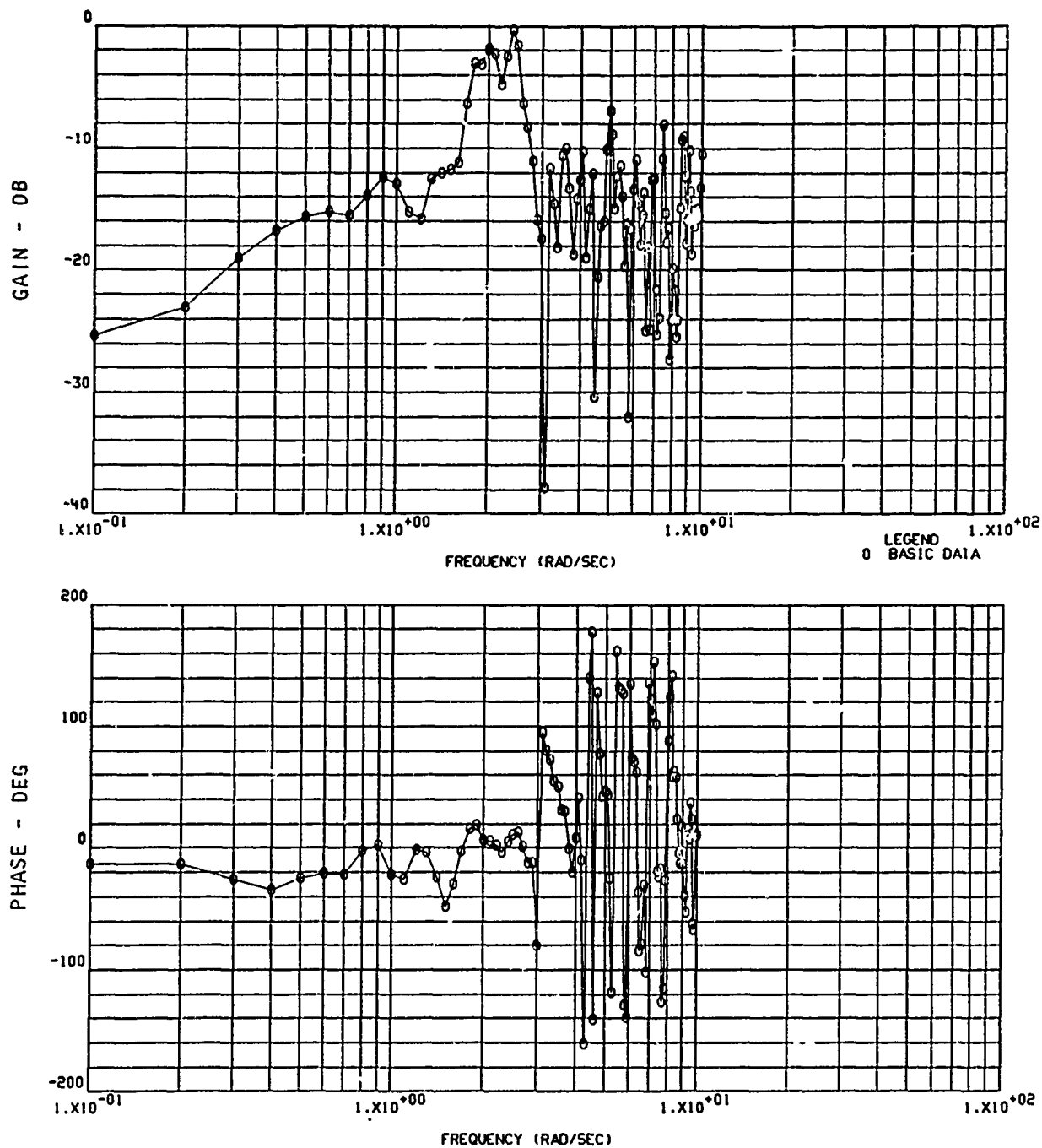
254

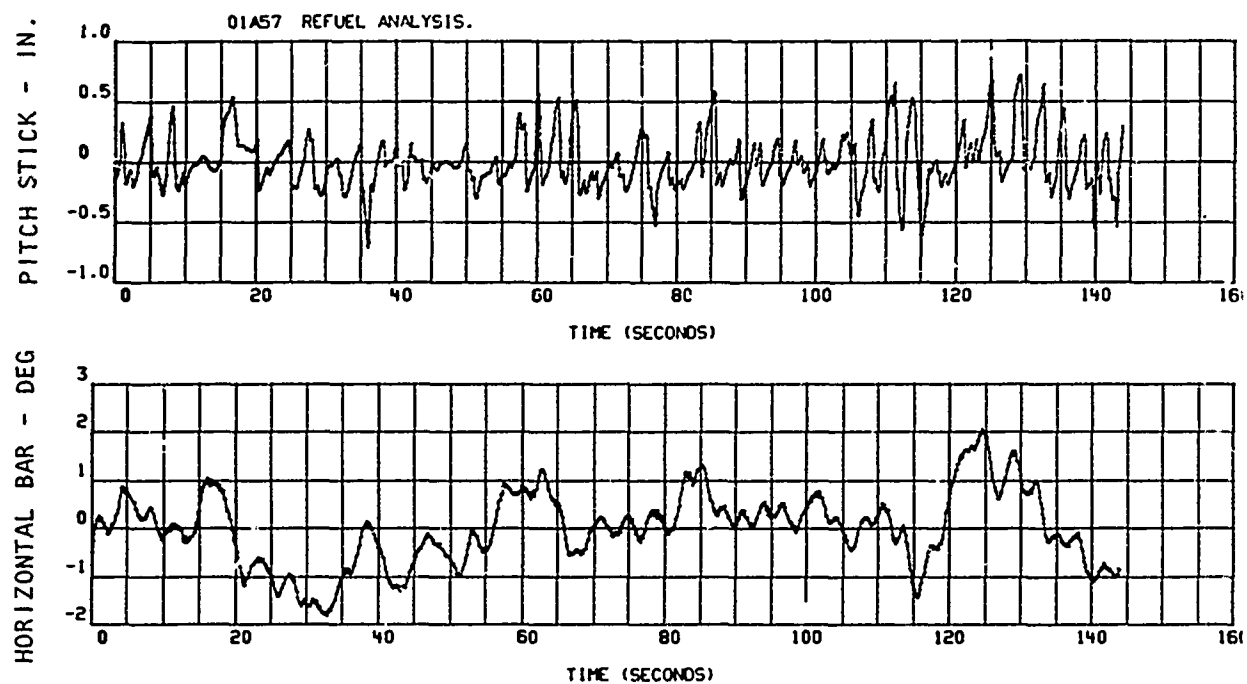01A40 REFUEL ANALYSIS.

Figure 74. AR Simulation Run No. 01A40 (Concl)

255

Figure 75. AR Simulation Run No. 01A3 Data

Figure 75. AR Simulation Run No. 01A3 Data (Cont)

Figure 75.   AR Simulation Run No. 01A3 Data (Cont)

258

Figure 75. AR Simulation Run No. 01A3 Data (Cont)

AUTO-CORRELATION METHOD

Figure 75. AR Simulation Run No. 01A3 Data (Cont)

Figure 75.   AR Simulation Run No. 01A3 Data (Concl)

261

Figure 76. AR Simulation Run No. 01A10 Data

Figure 76. AR Simulation Run No. 01A10 Data (Cont)

263

O1A10 REFUEL ANALYSIS.
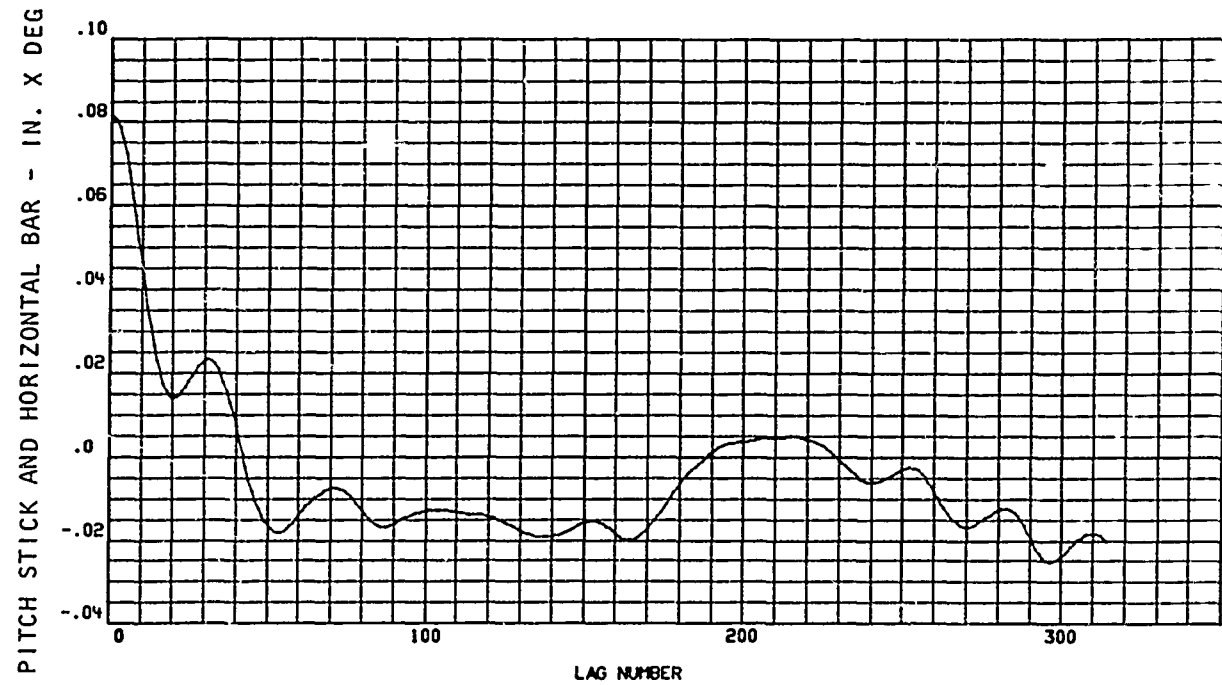
CROSS CORRELATION FUNCTIONS

Figure 76. AR Simulation Run No. 01A10 Data (Cont)

264
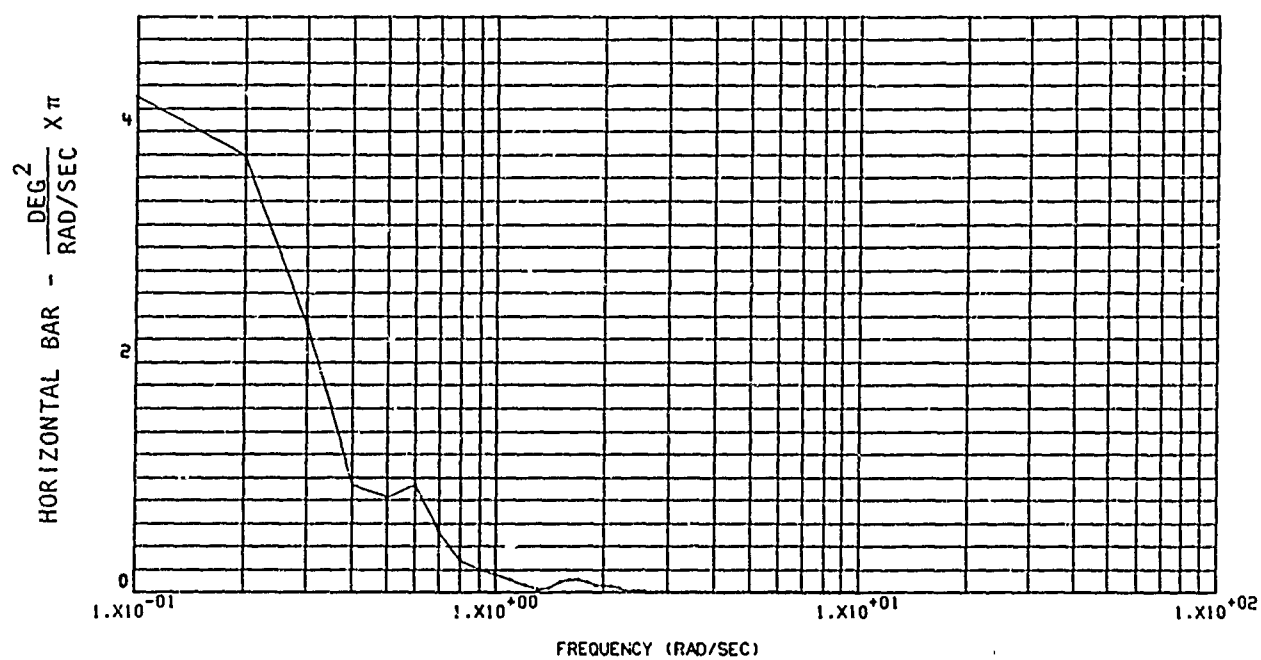
01A10 REFUEL ANALYSIS.

SPECTRAL DENSITY FUNCTIONS

Figure 76.   AR Simulation Run No. 01A10 Data (Cont)

265

01A10 REFUEL ANALYSIS.

AUTO-CORRELATION METHOD

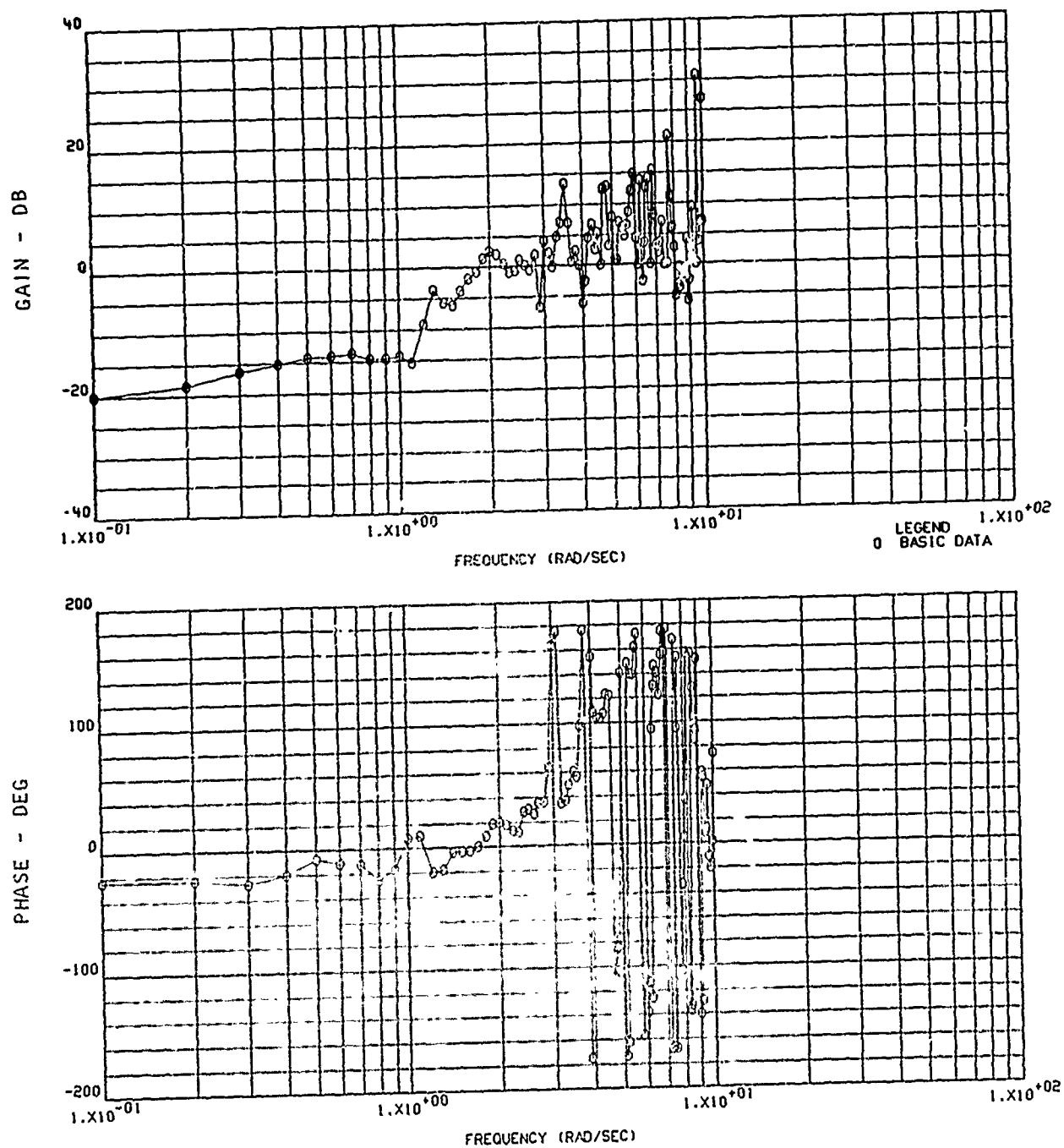Figure 76. AR Simulation Run No. 01A10 Data (Cont)

266
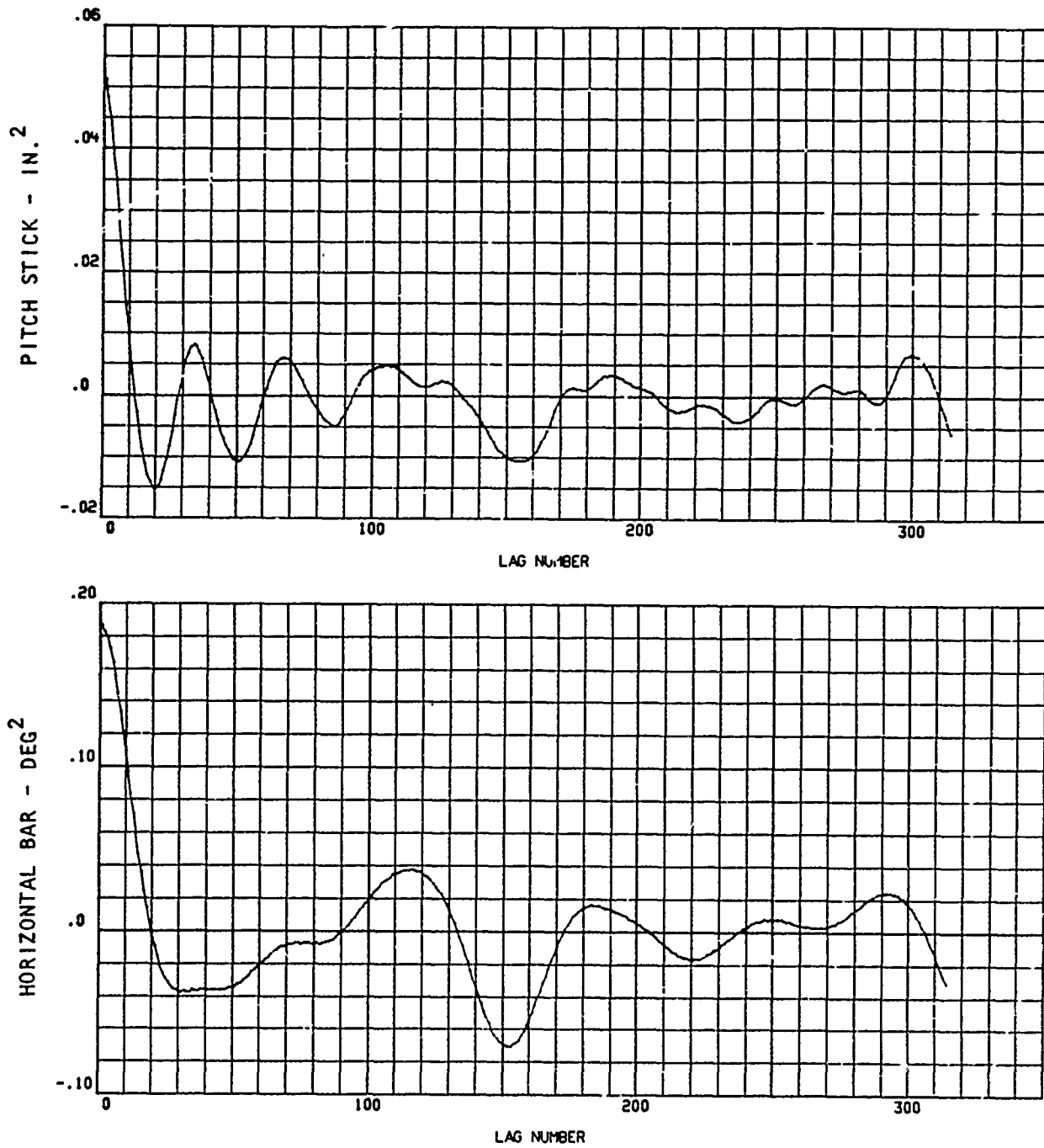
Figure 76. AR Simulation Run No. 01A10 Data (Concl)
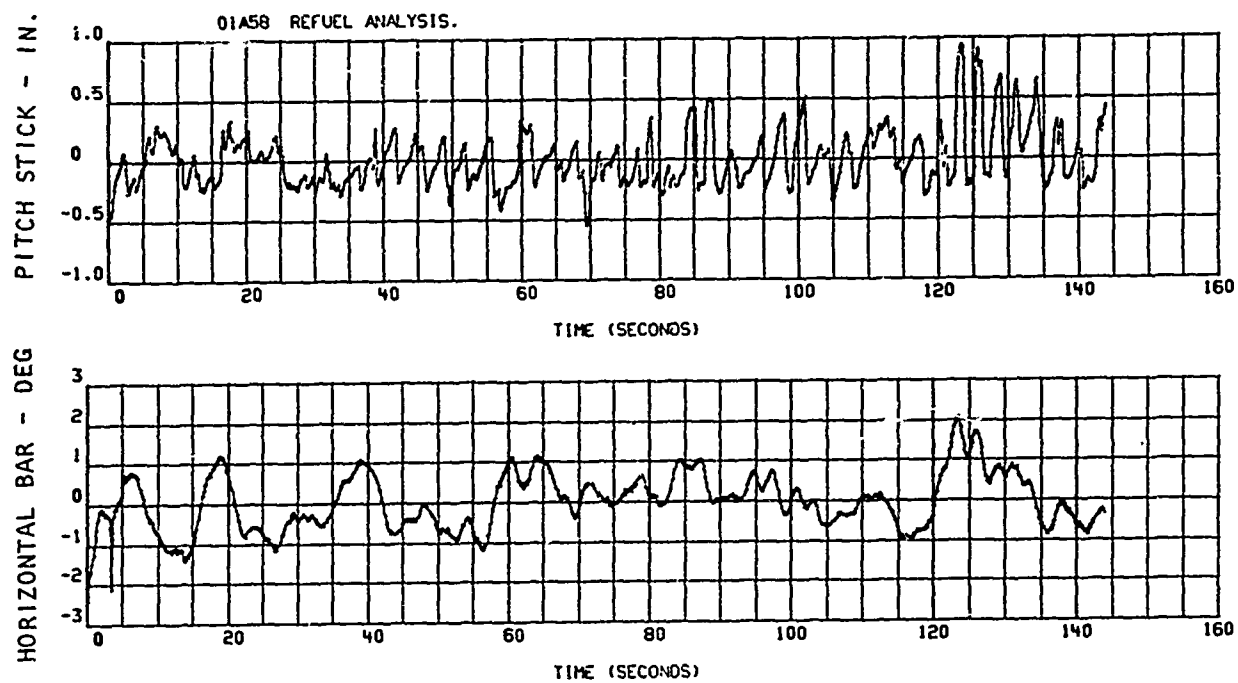
Figure 77. AR Simulation Run No. 04A1 Data

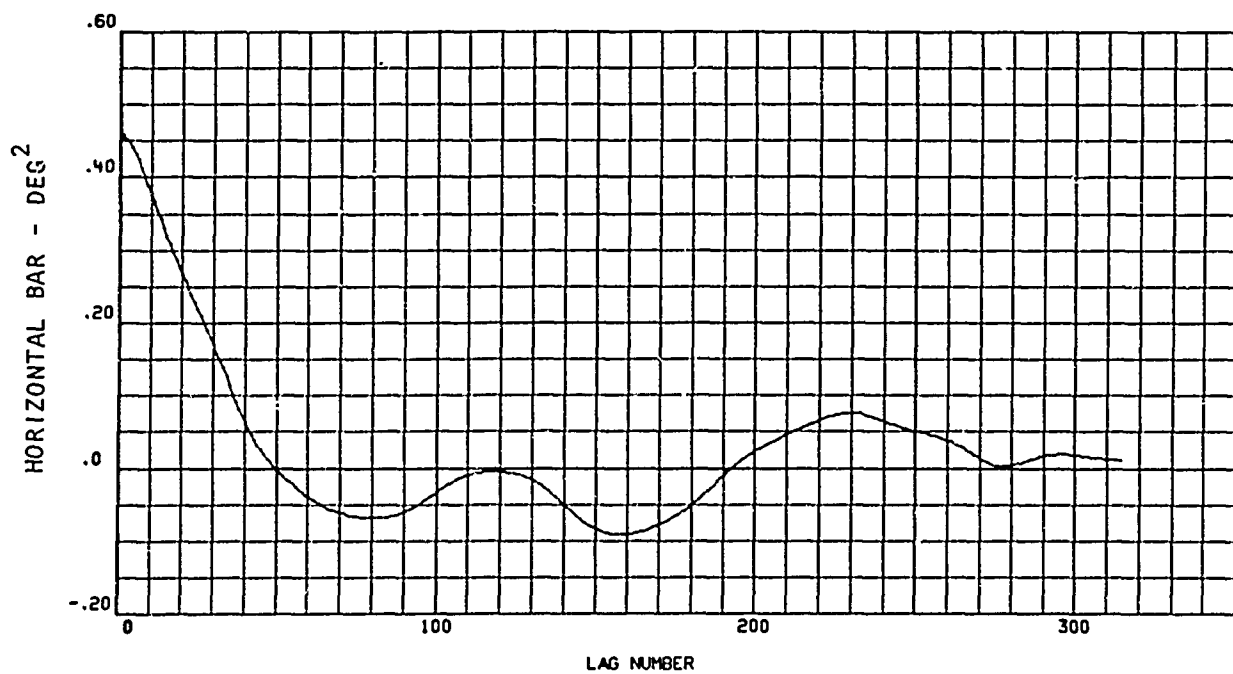04A1   REFUEL ANALYSIS.
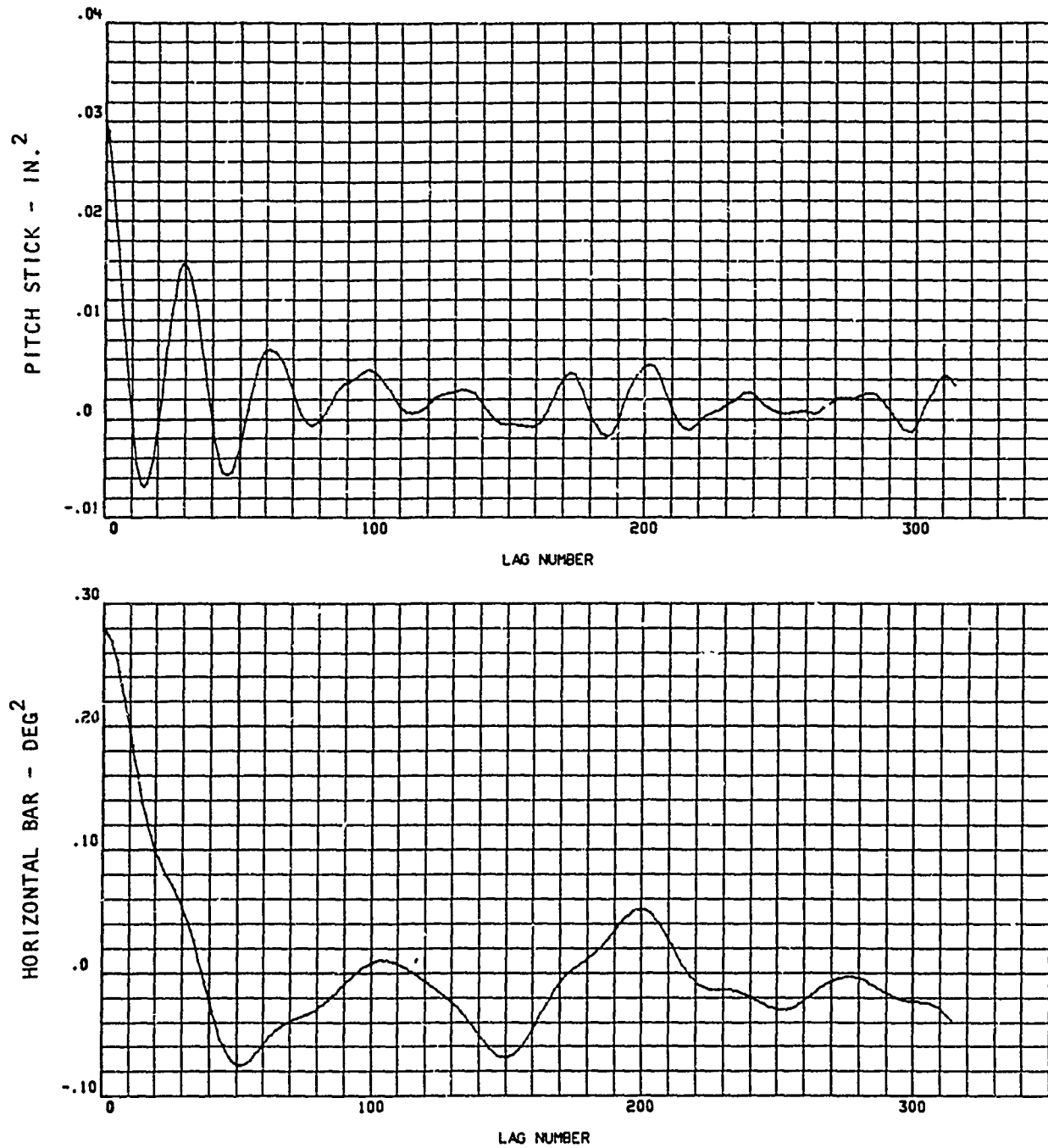
AUTO CORRELATION FUNCTIONS
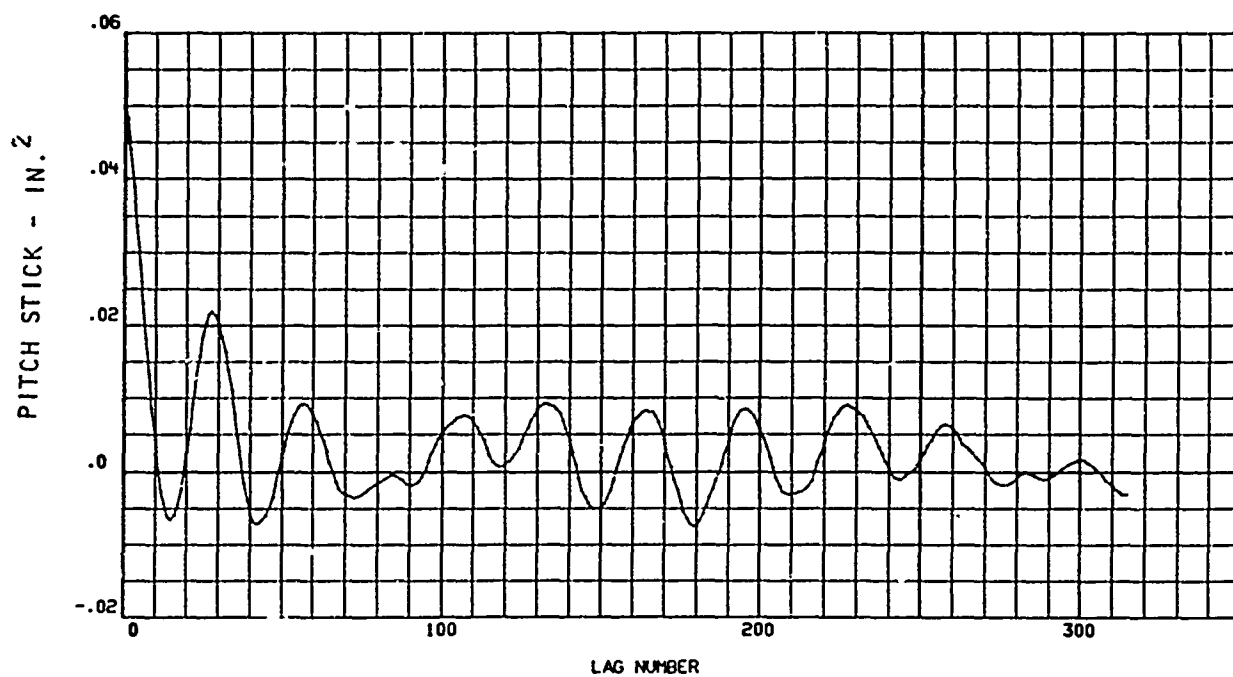

Figure 77.   AR Simulation Run No. 04A1 Data (Cont)

CROSS CORRELATION FUNCTIONS

Figure 77.   AR Simulation Run No. 04A1 Data (Cont)

270

Figure 77.   AR Simulation Run No. 04A1 Data (Cont)

271
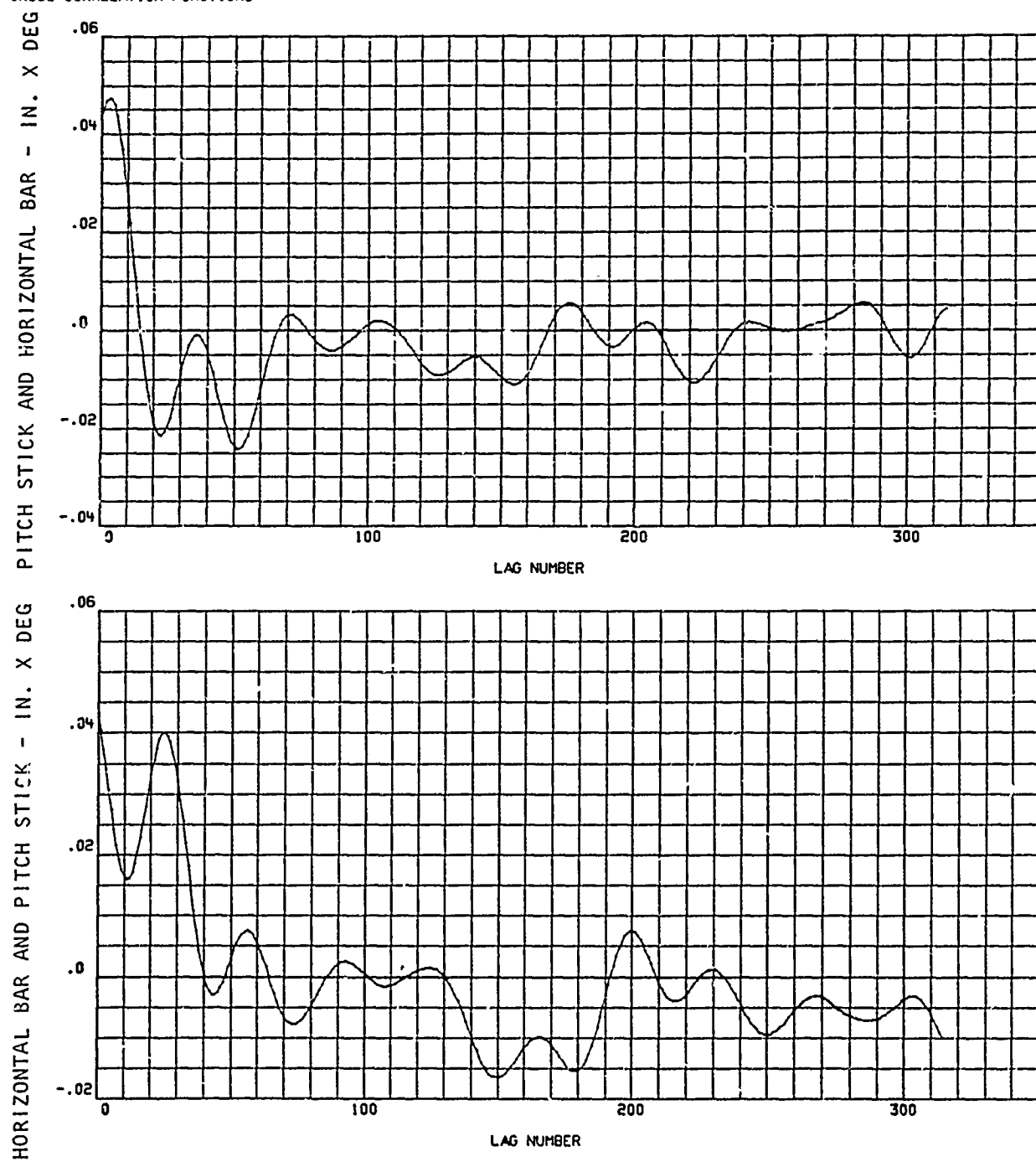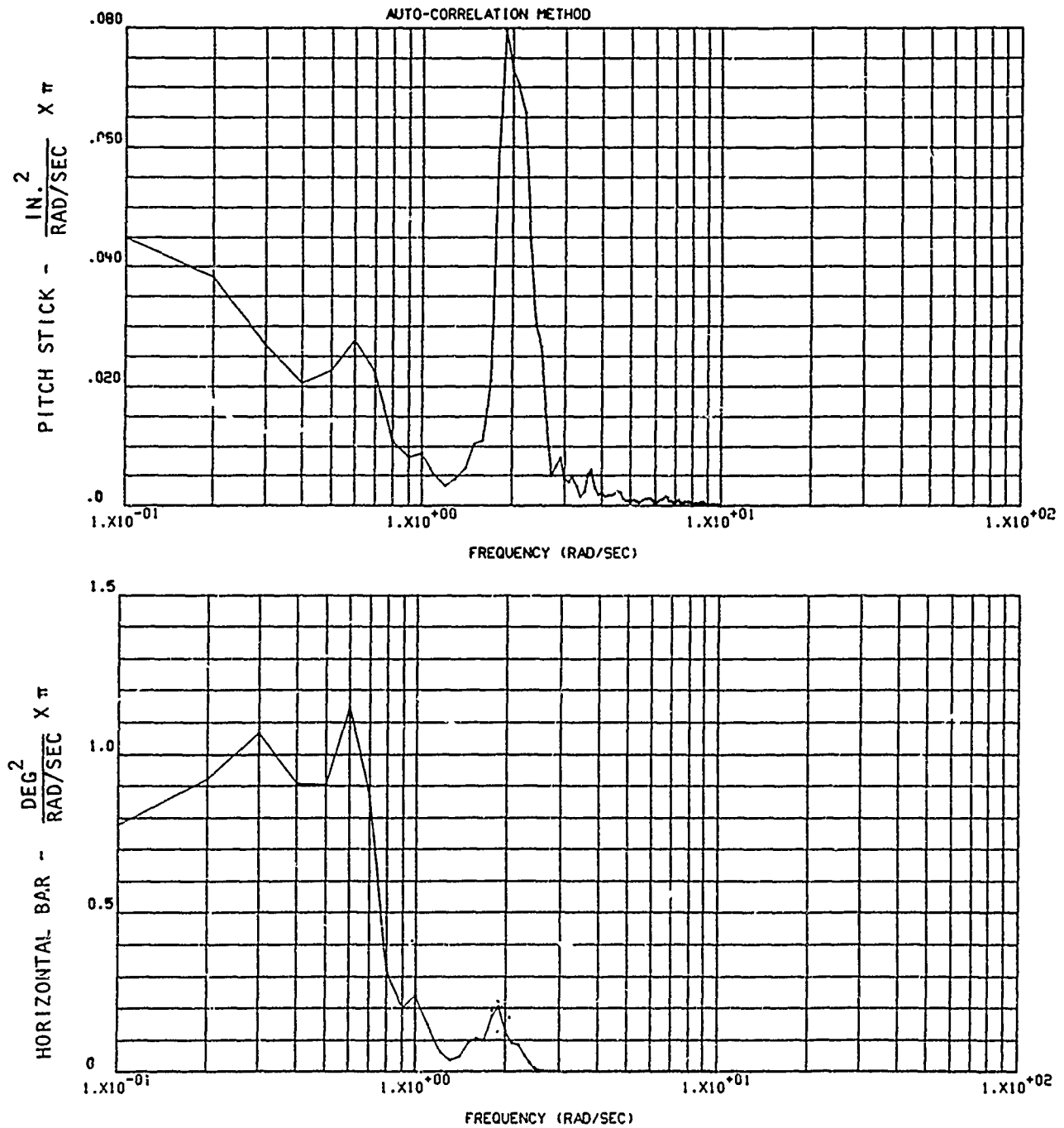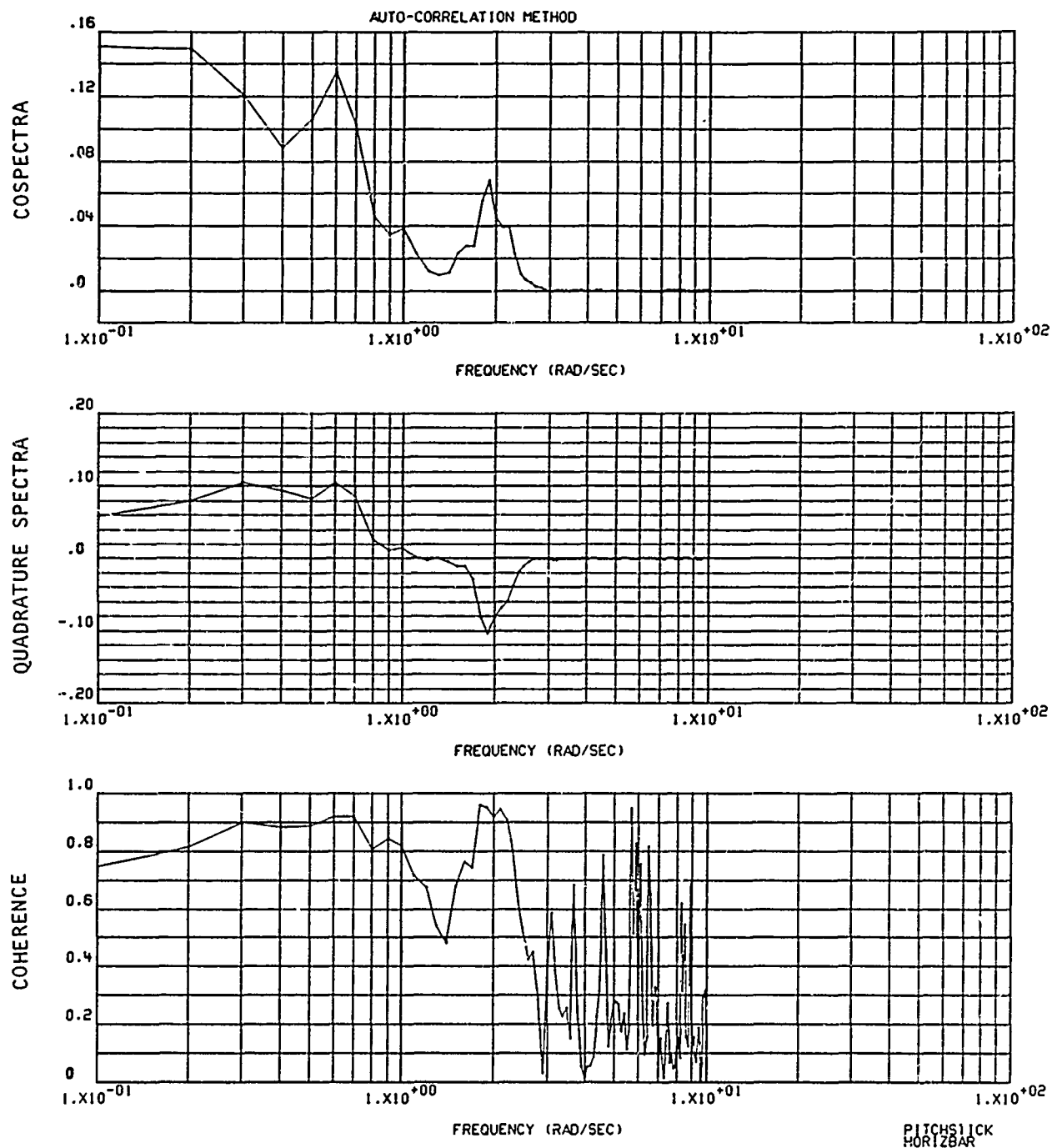
Figure 77. AR Simulation Run No. 04A1 Data (Cont)
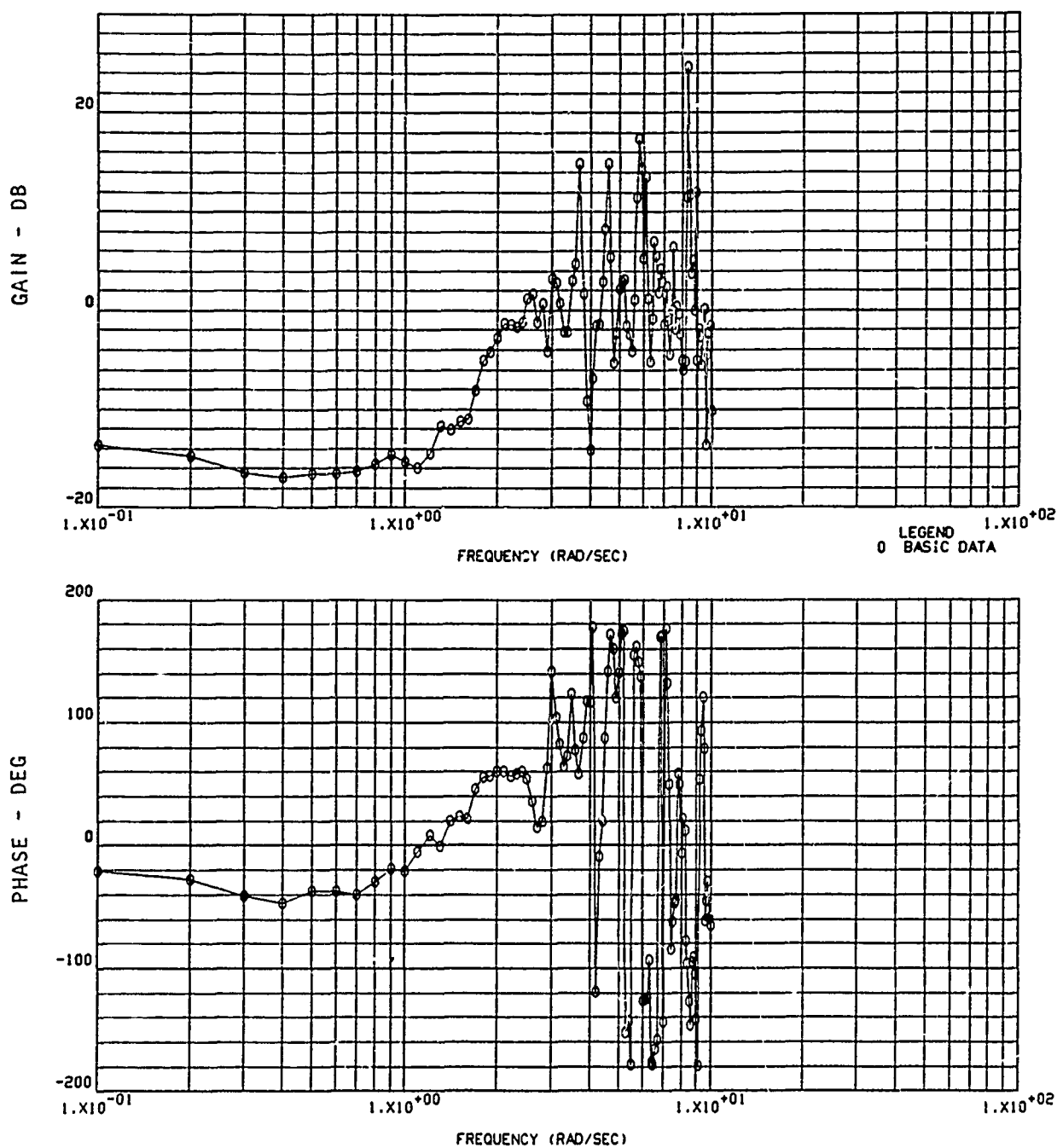
Figure 77.   AR Simulation Run No. 04A1 Data (Concl)

273

Figure 78. AR Simulation Run No. 02A2 Data

AUTO CORRELATION FUNCTIONS

Figure 78.   AR Simulation Run No. 02A2 Data (Cont)

CROSS CORRELATION FUNCTIONS

LAG NUMBER

LAG NUMBER

Figure 78.   AR Simulation Run No. 02A2 Data (Cont)

Figure 78. AR Simulation Run No. 02A2 Data (Cont)
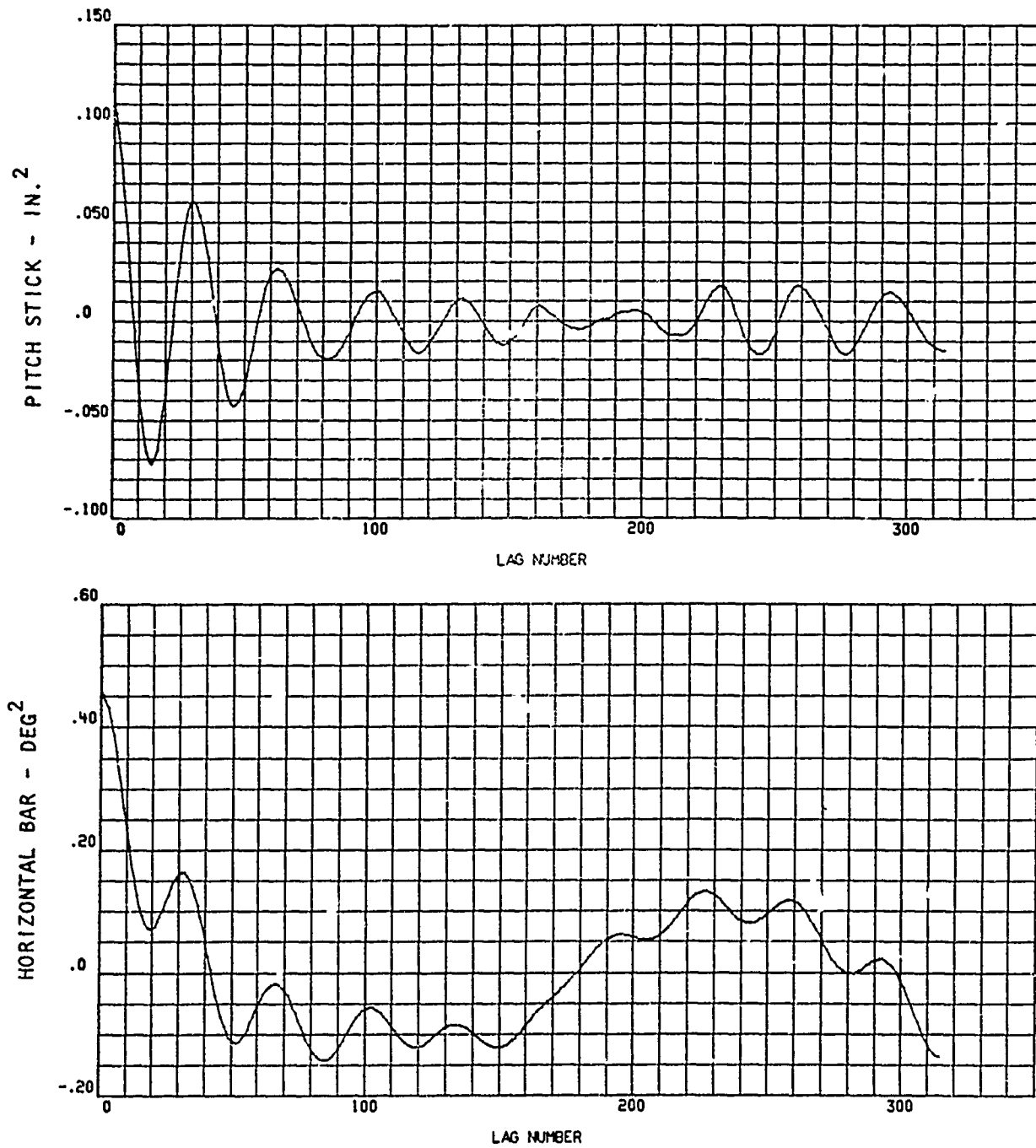
Figure 78. AR Simulation Run No. 02A2 Data (Cont)

02A2   REFUEL ANALYSIS.

LEGEND
0 BASIC DATA
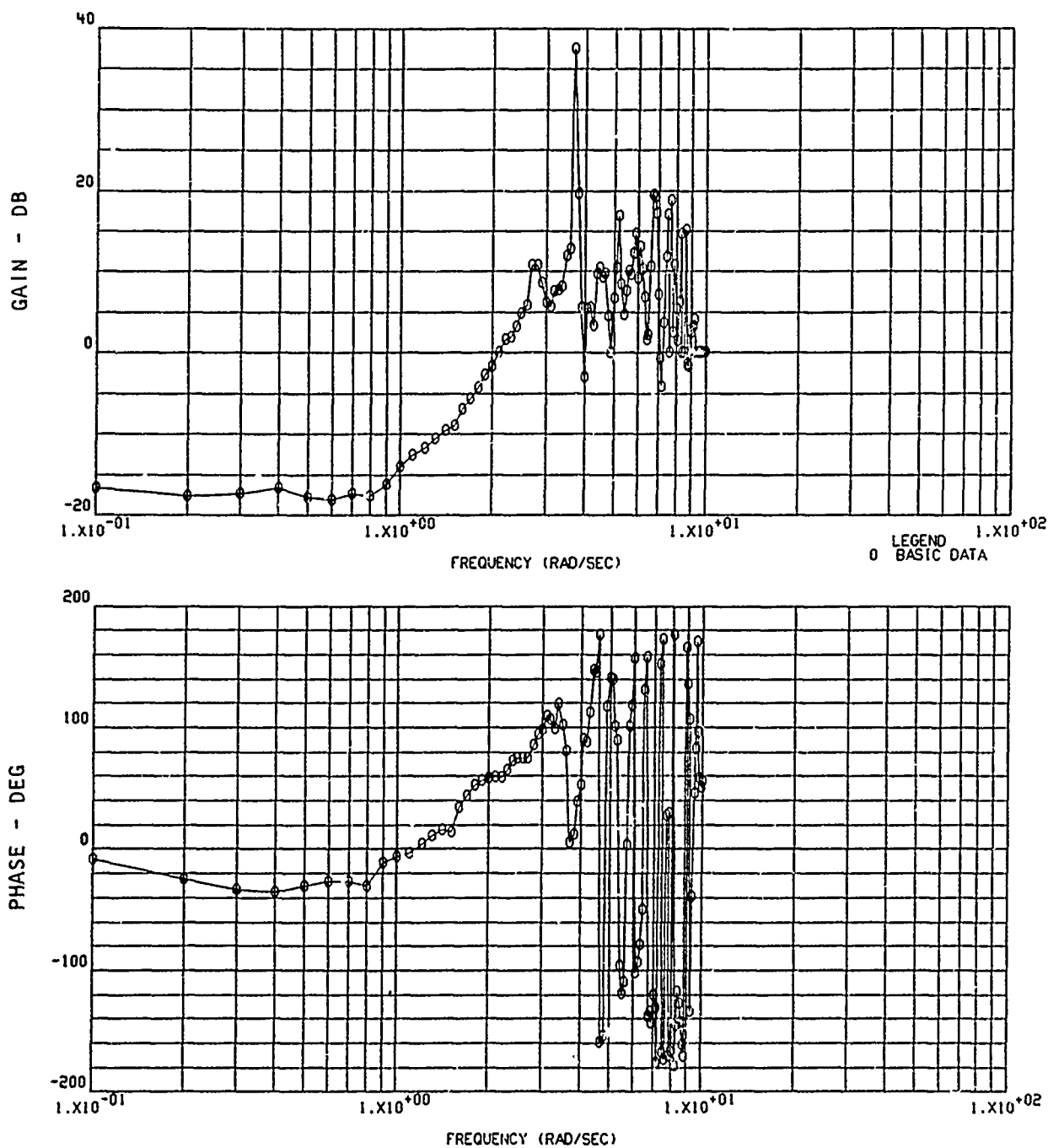
Figure 78. AR Simulation Run No. 02A2 Data (Concl)
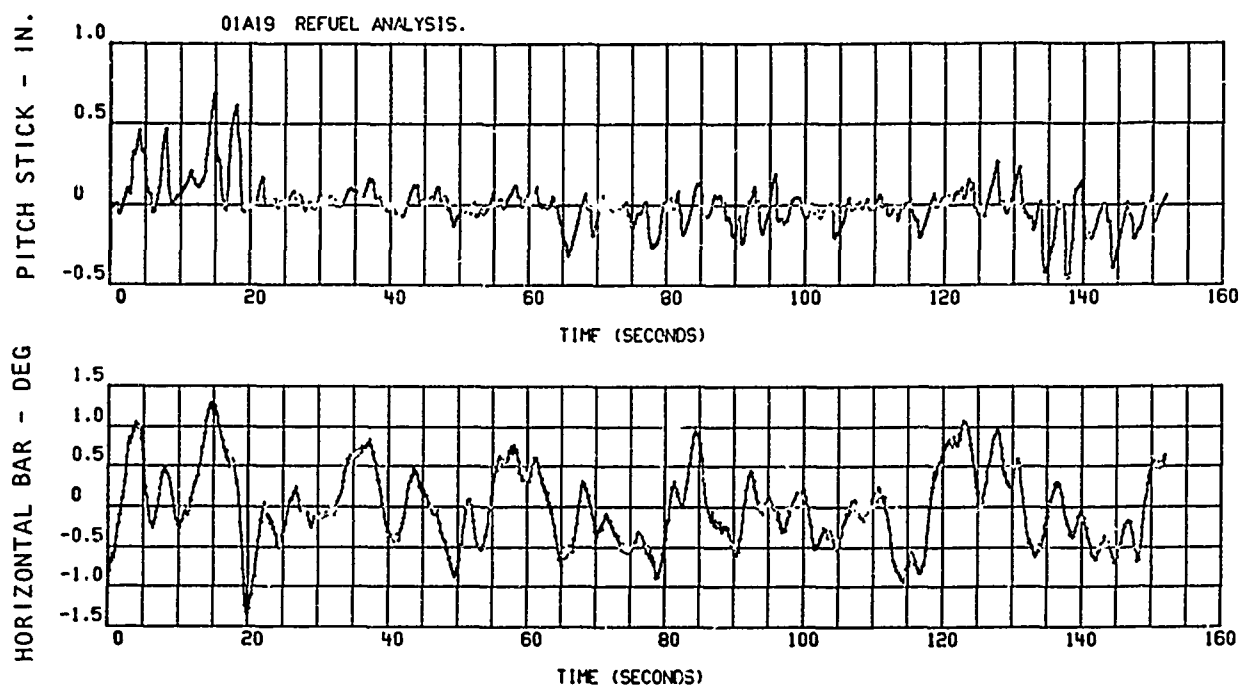
279
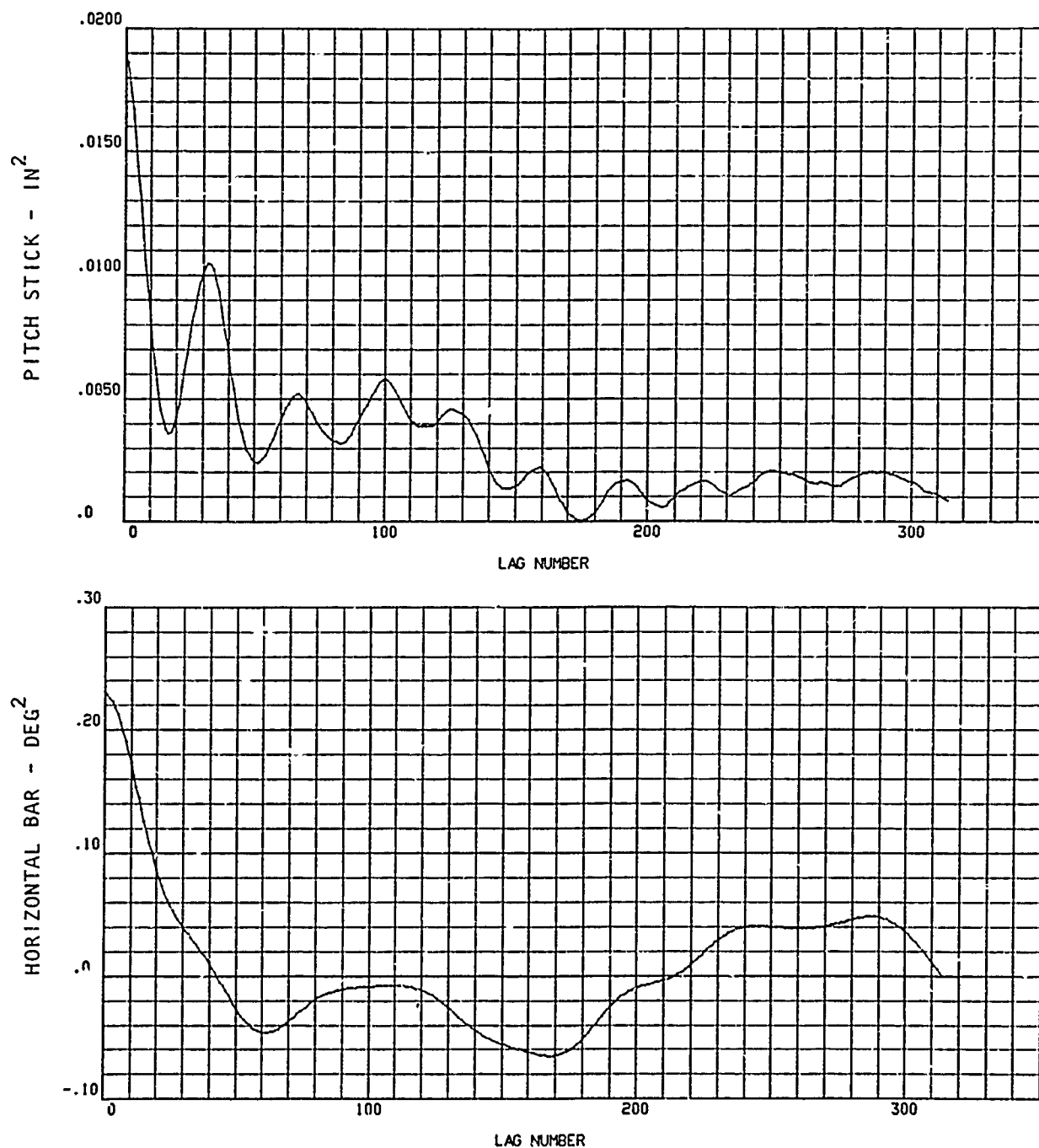
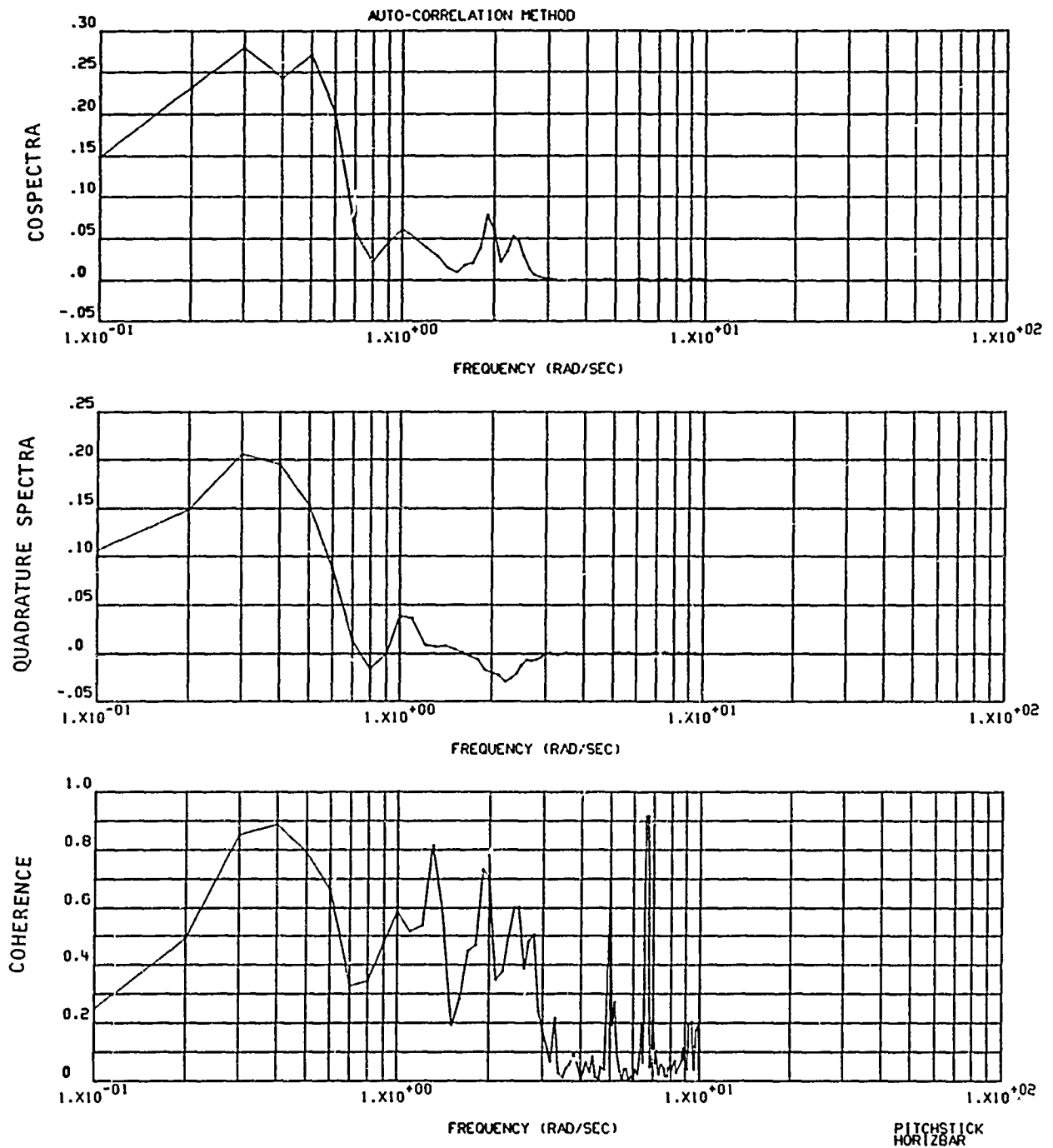Figure 79. AR Simulation Run No. 01A19 Data

AUTO CORRELATION FUNCTIONS
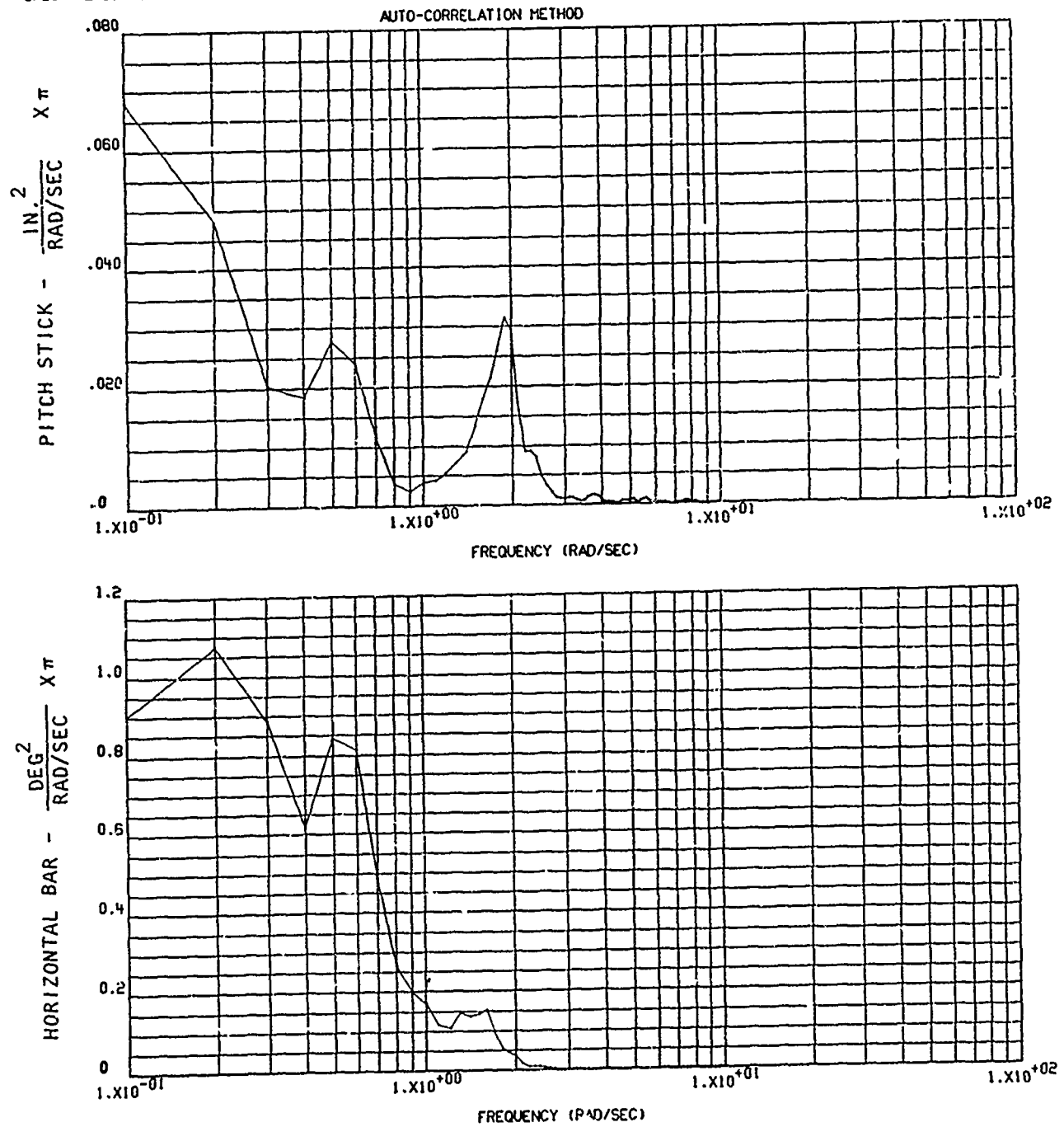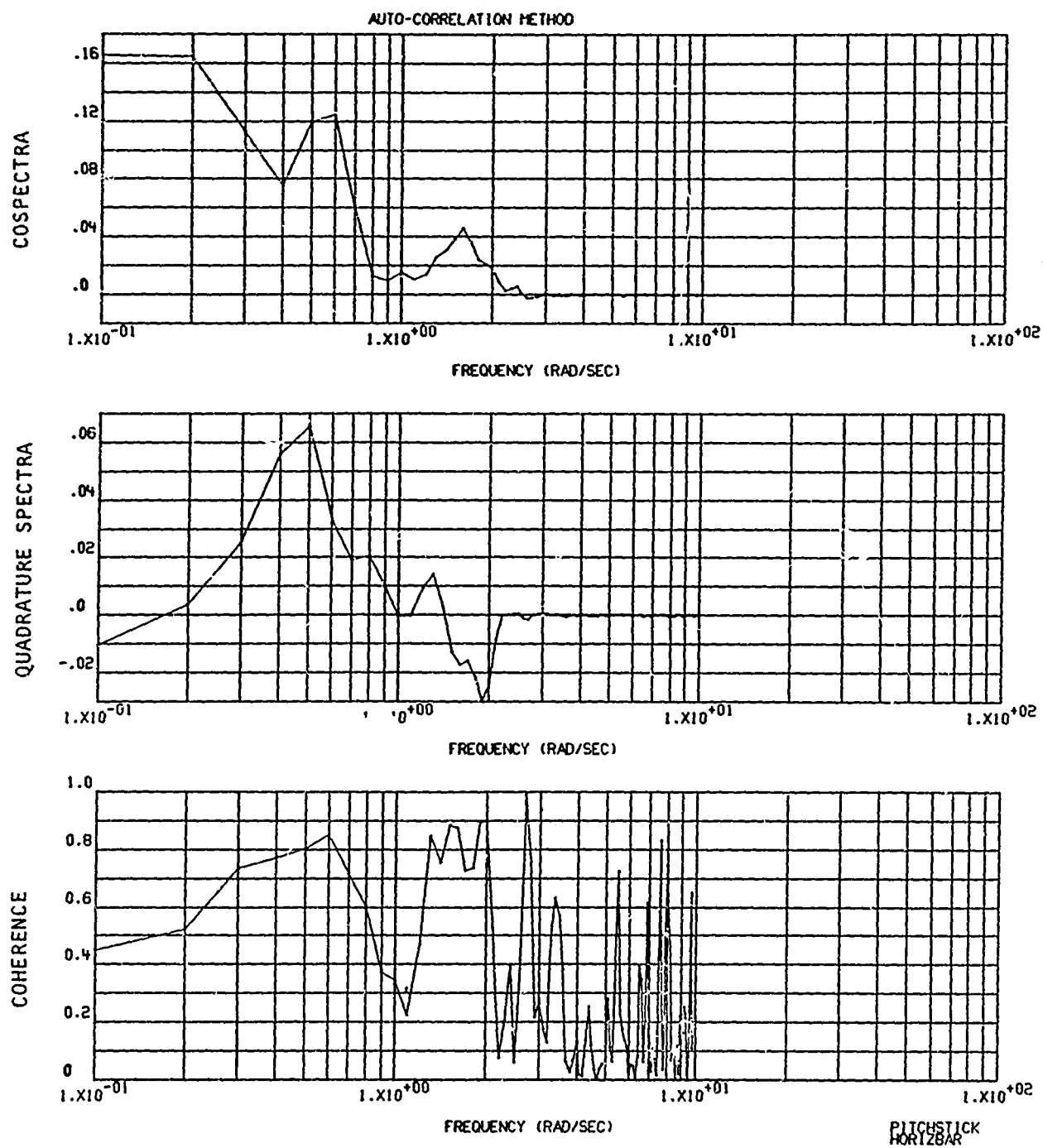
Figure 79.   AR Simulation Run No. 01A19 Data (Cont)

281

Figure 79. AR Simulation Run No. 01A19 Data (Cont)

Figure 79. AR Simulation Run No. 01A19 Data (Cont)

283

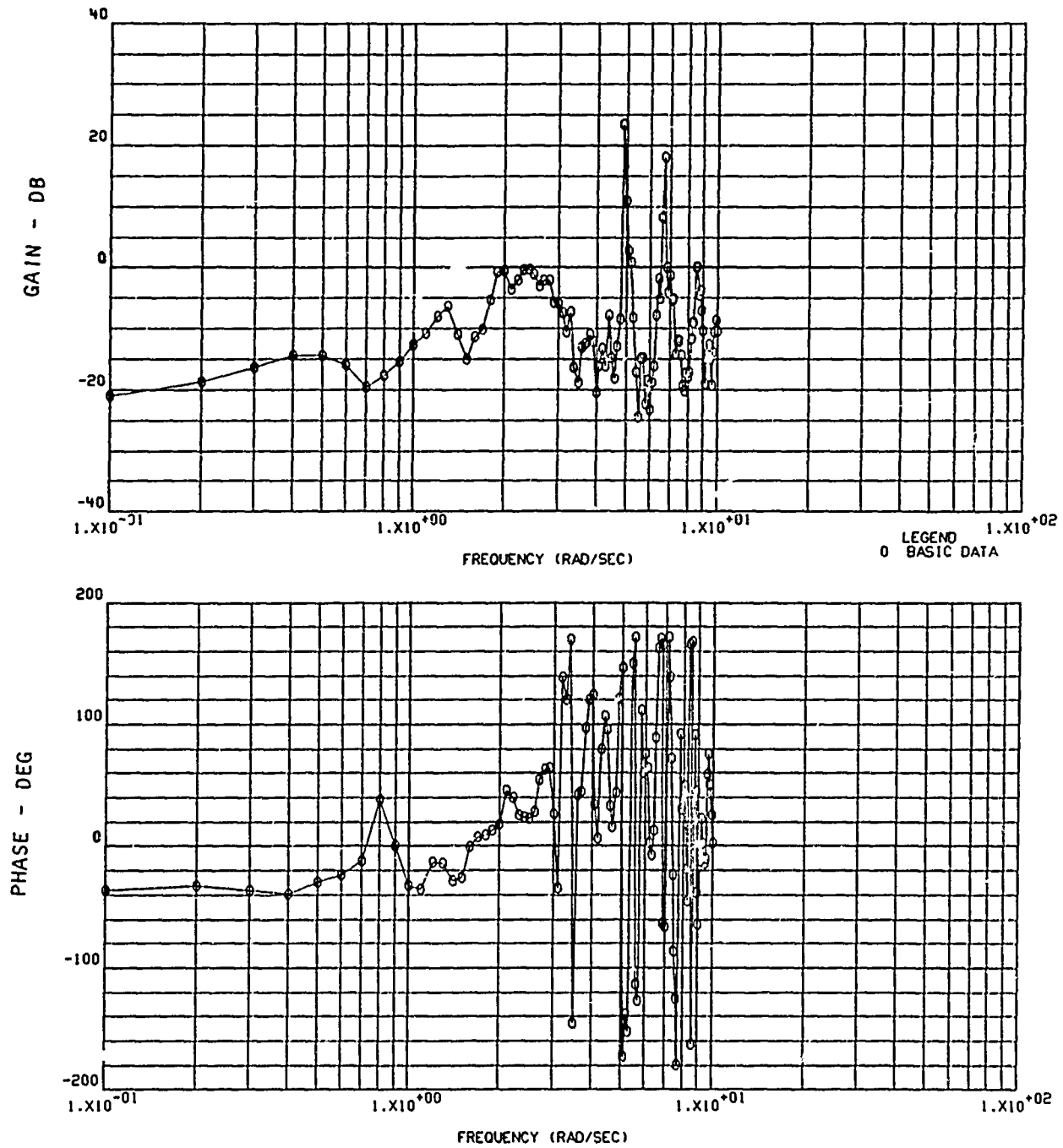Figure 79. AR Simulation Run No. 01A19 Data (Cont)

284

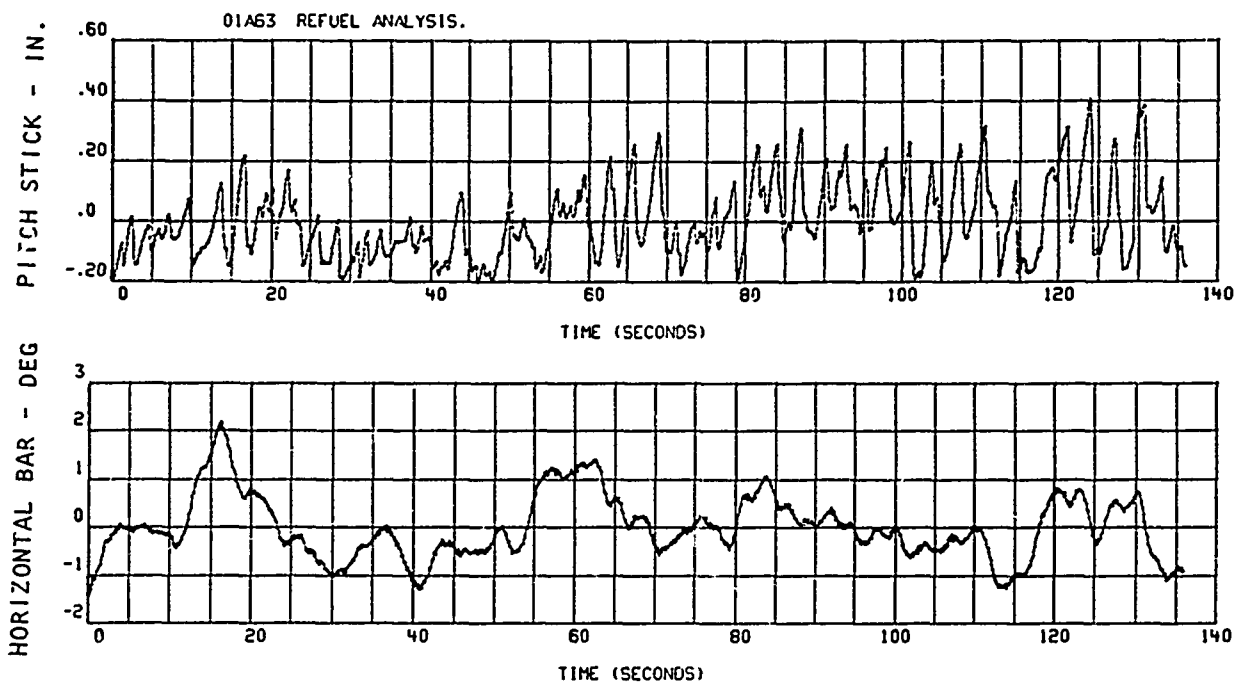Figure 79. AR Simulation Run No. 01A19 Data (Concl)

285

Figure 80.   AR Simulation Run No. 01A20 Data

01A20 REFUEL ANALYSIS.

AUTO CORRELATION FUNCTIONS

Figure 80.   AR Simulation Run No. 01A20 Data (Cont)

287

Figure 80. AR Simulation Run No. 01A20 Data (Cont)

288

Figure 80. AR Simulation Run No. 01A20 Data (Cont)

01A20 REFUEL ANALYSIS.

Figure 80. AR Simulation Run No. 01A20 Data (Cont)

290

01A20 REFUEL ANALYSIS.

Figure 80.   AR Simulation Run No. 01A20 Data (Concl)

291

Figure 81. AR Simulation Run No. 01A31 Data

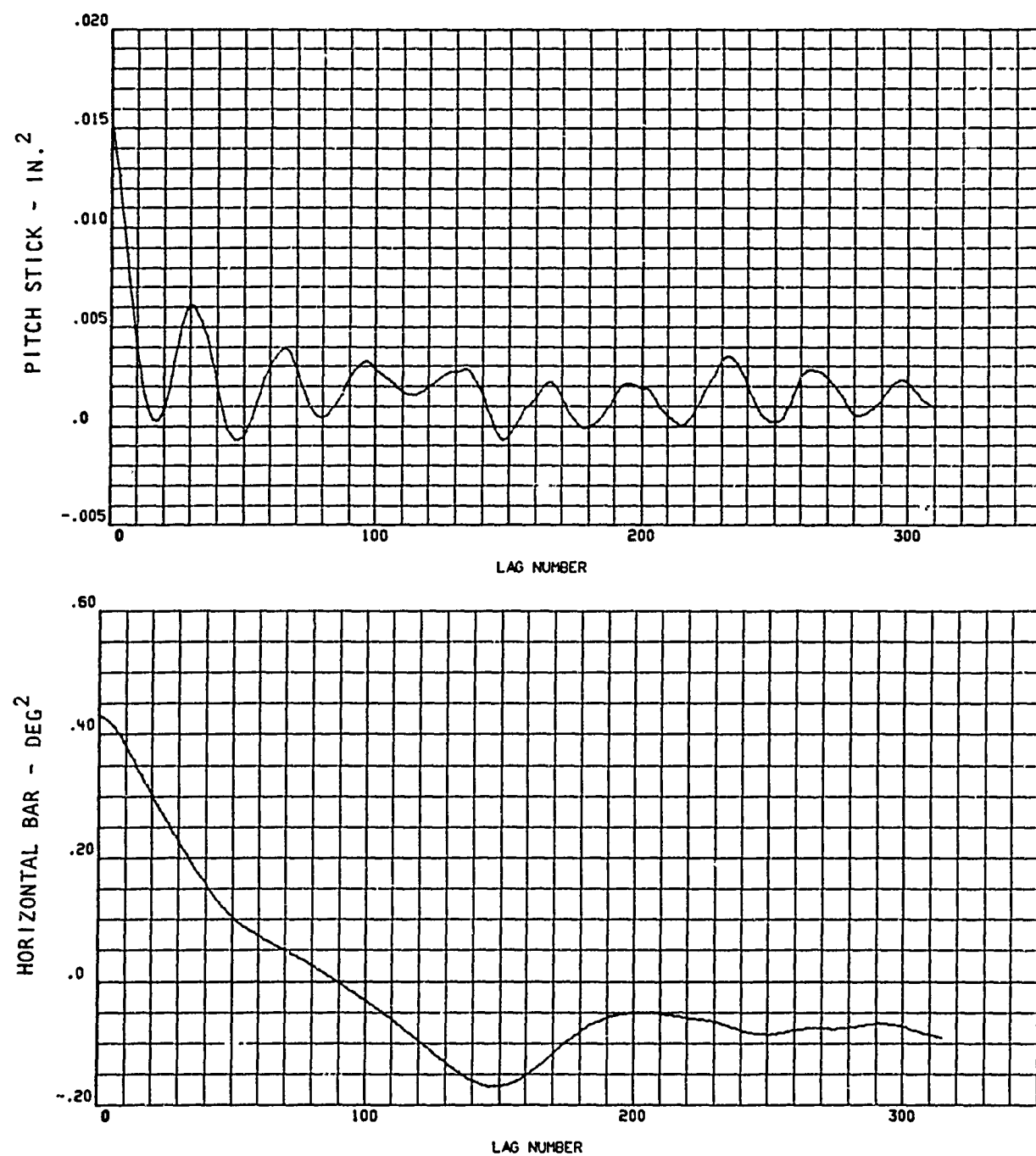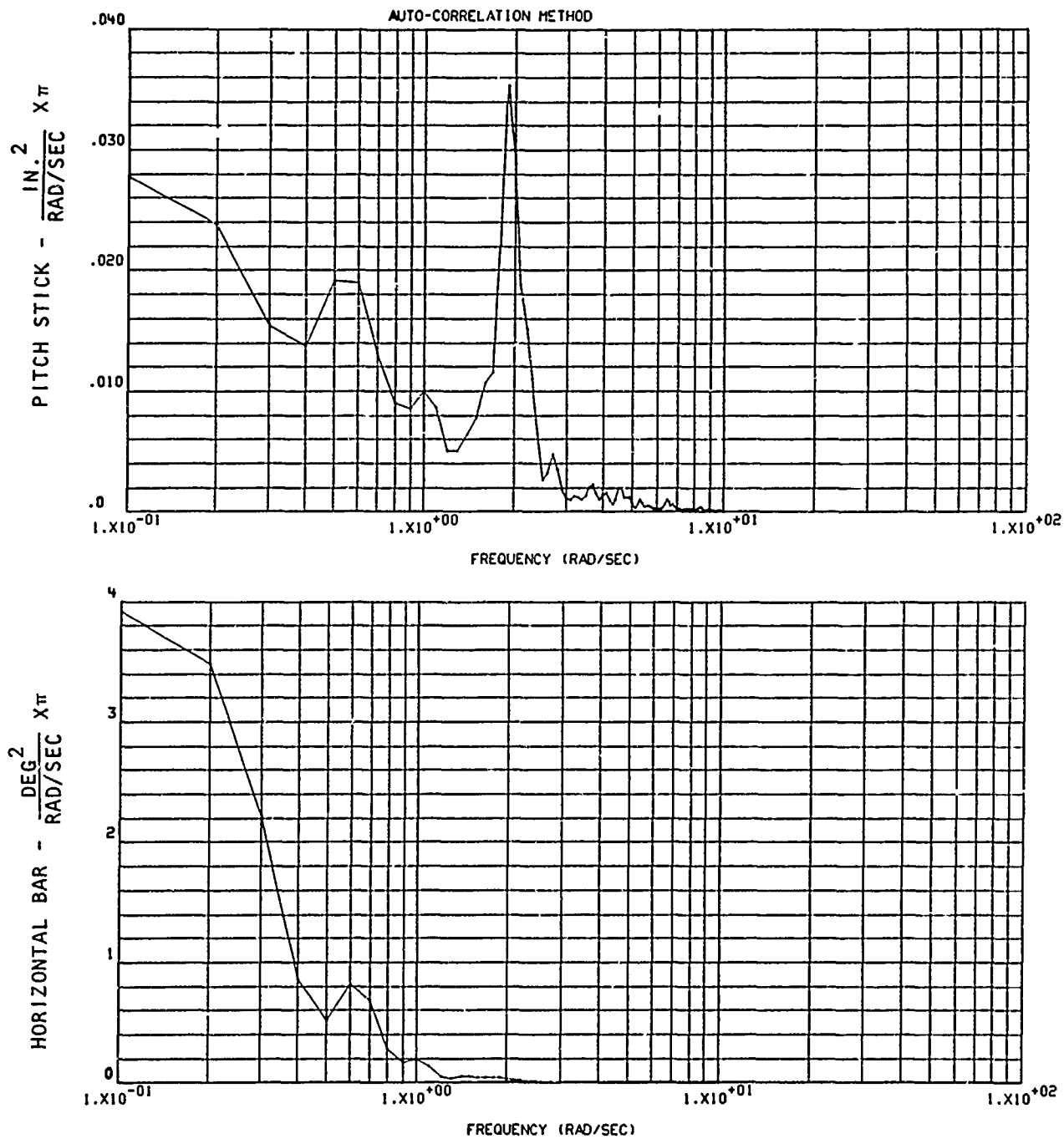01A31 REFUEL ANALYSIS.

AUTO CORRELATION FUNCTIONS

Figure 81. AR Simulation Run No. 01A31 Data (Cont)

293

Figure 81. AR Simulation Run No. 01A31 Data (Cont)

294

01A31 REFUEL ANALYSIS.

SPECTRAL DENSITY FUNCTIONS

AUTO-CORRELATION METHOD

Figure 81.   AR Simulation Run No. 01A31 Data (Cont)

295

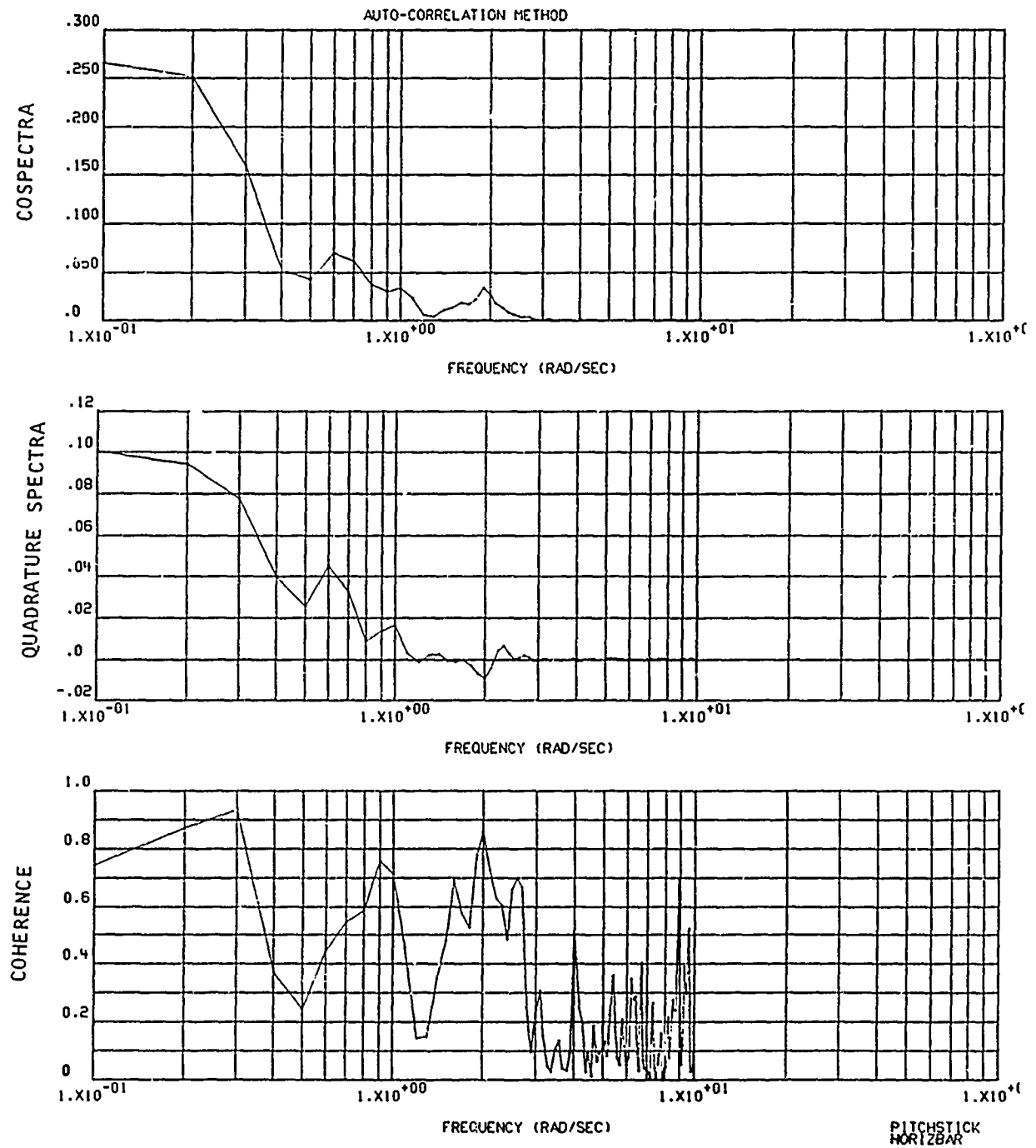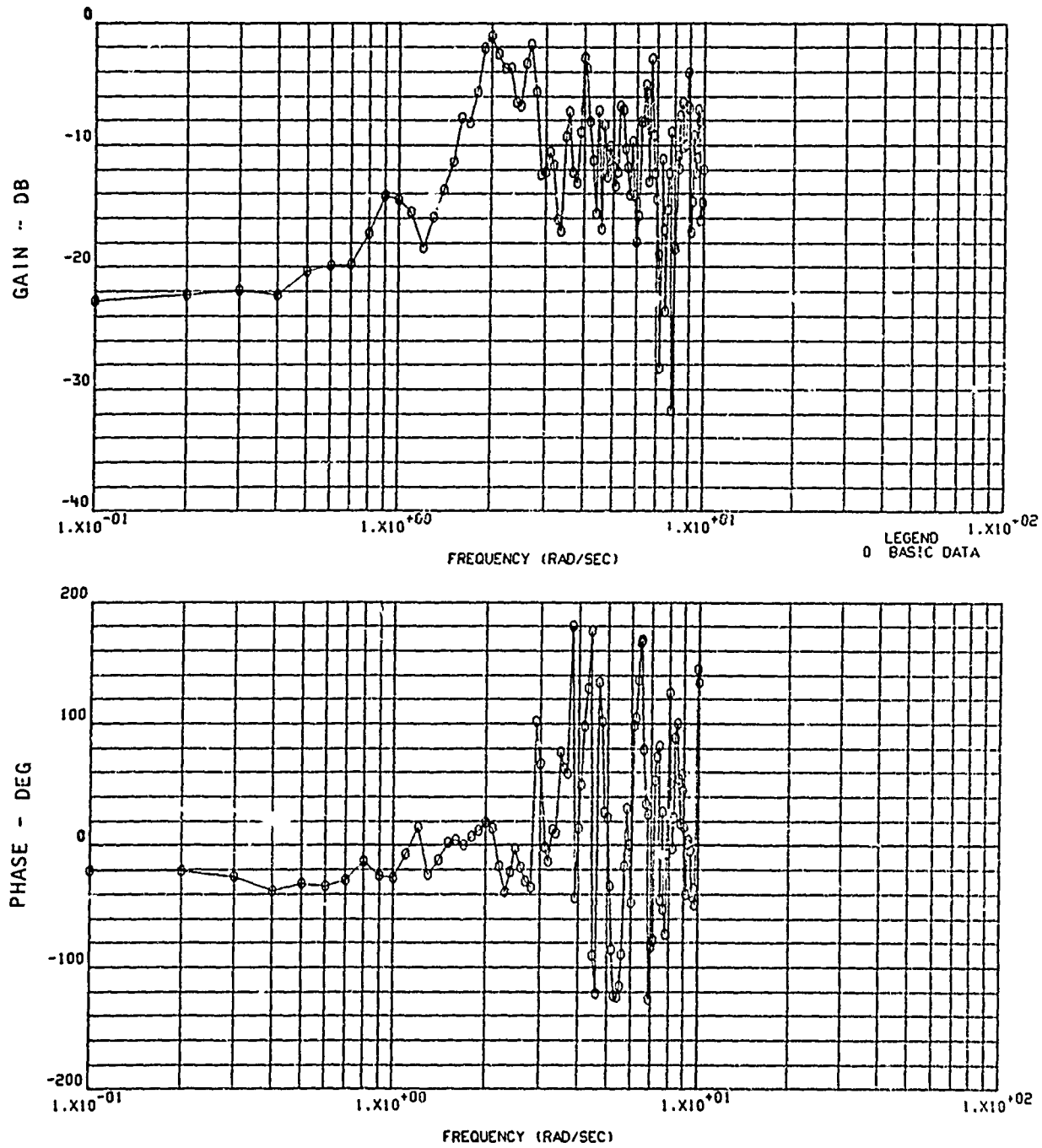01A31 REFUEL ANALYSIS.

AUTO-CORRELATION METHOD

Figure 81.   AR Simulation Run No. 01A31 Data (Cont)

296
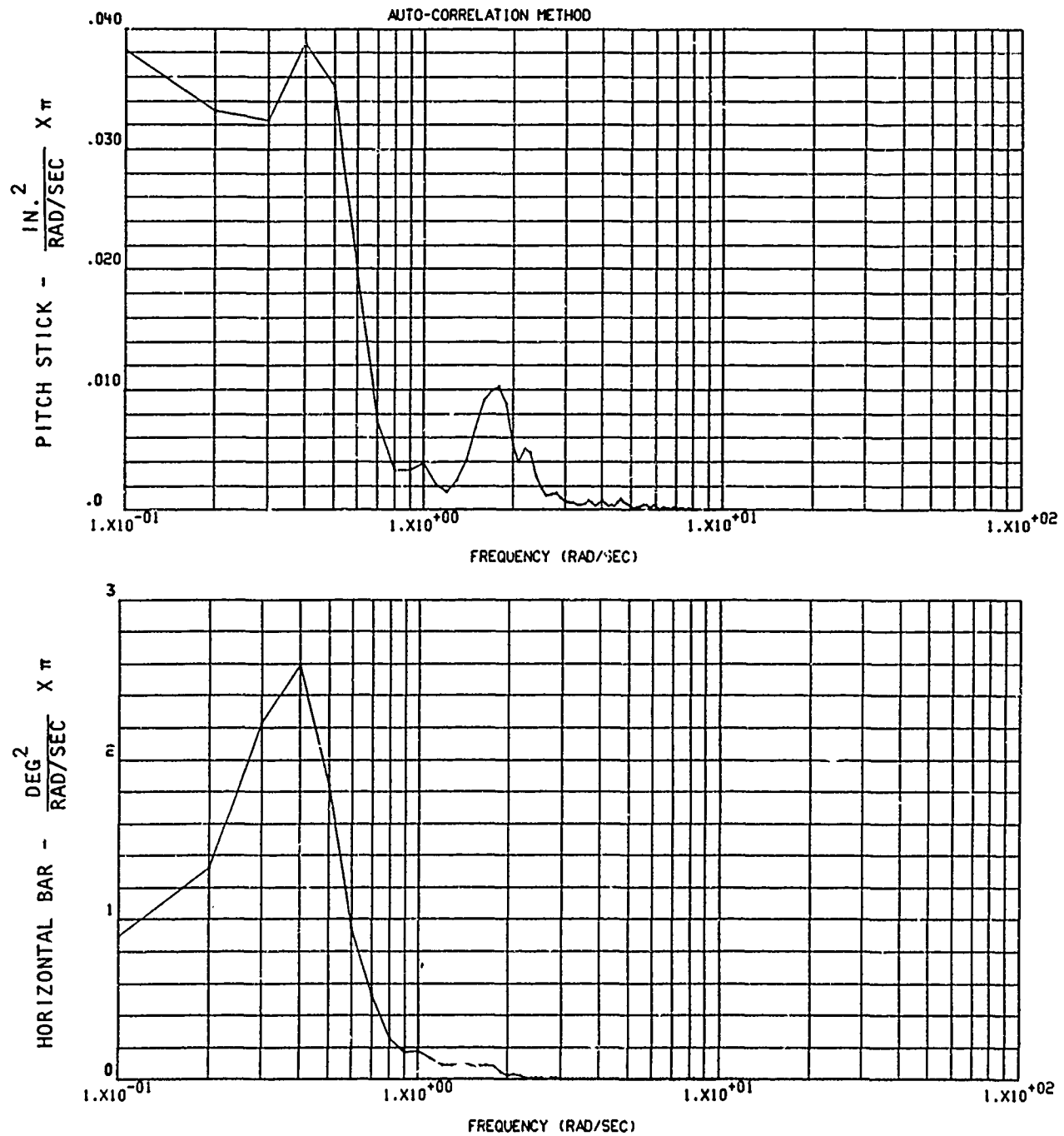
01A31 REFUEL ANALYSIS.

Figure 81. AR Simulation Run No. 01A31 Data (Concl)

297

Figure 82.   AR Simulation Run No. 01A32 Data

01A32 REFUEL ANALYSIS.

Figure 82. AR Simulation Run No. 01A32 Data (Cont)

299

Figure 82. AR Simulation Run No. 01A32 Data (Cont)

C1A32 REFUEL ANALYSIS.

SPECTRAL DENSITY FUNCTIONS

Figure 82. AR Simulation Run No. 01A32 Data (Cont)

301

01A32 REFUEL ANALYSIS.

Figure 82. AR Simulation Run No. 01A32 Data (Cont)

302

01A32 REFUEL ANALYSIS.
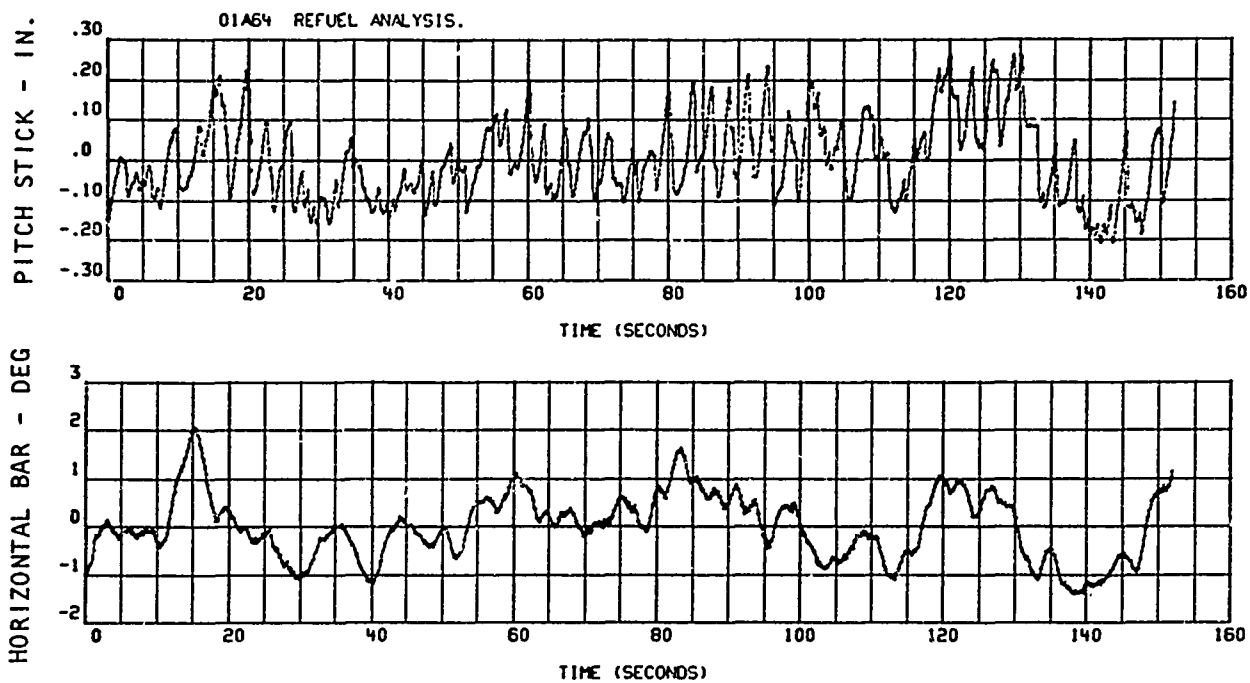

Figure 82. AR Simulation Run No. 01A32 D.ta (Concl)

303

Figure 83. AR Simulation Run No. 02A49 Data

AUTO CORRELATION FUNCTIONS

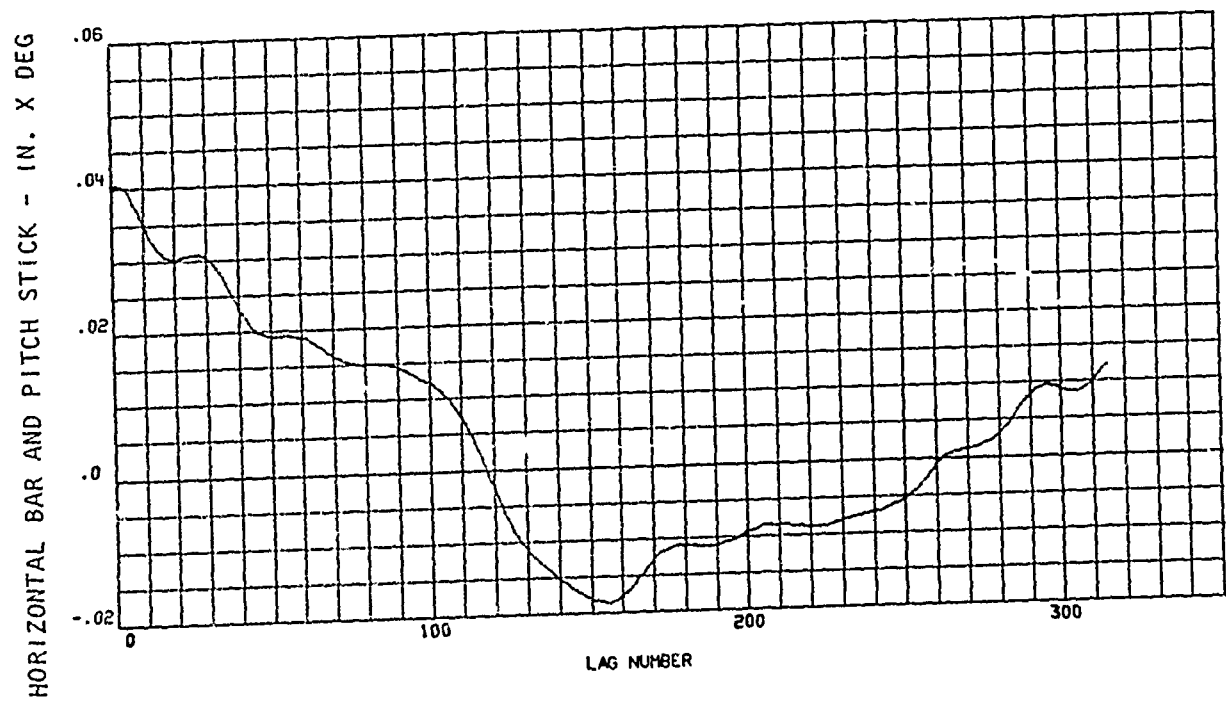
Figure 83. AR Simulation Run No. 02A49 Data (Cont)

305

Figure 83.   AR Simulation Run No. 02A49 Data (Cont)

306

02A49 REFUEL ANALYSIS.

SPECTRAL DENSITY FUNCTIONS

Figure 83. AR Simulation Run No. 02A49 Data (Cont)

307

Figure 83. AR Simulation Run No. 02A49 Data (Cont)

308
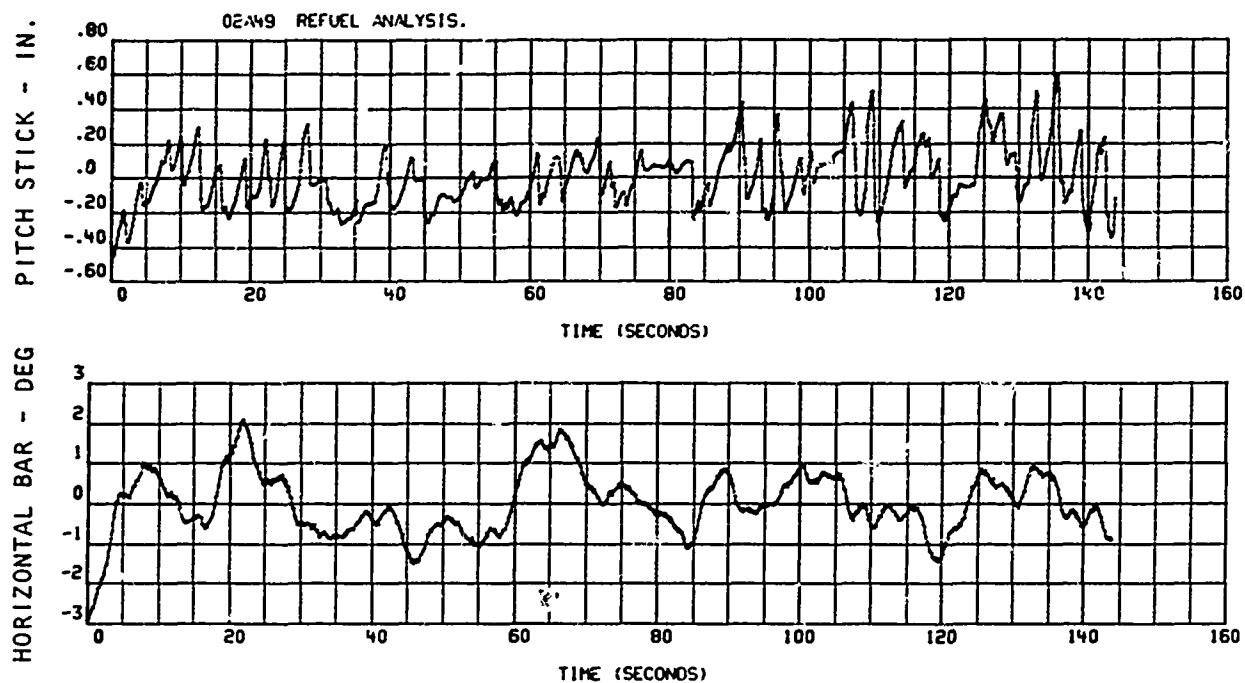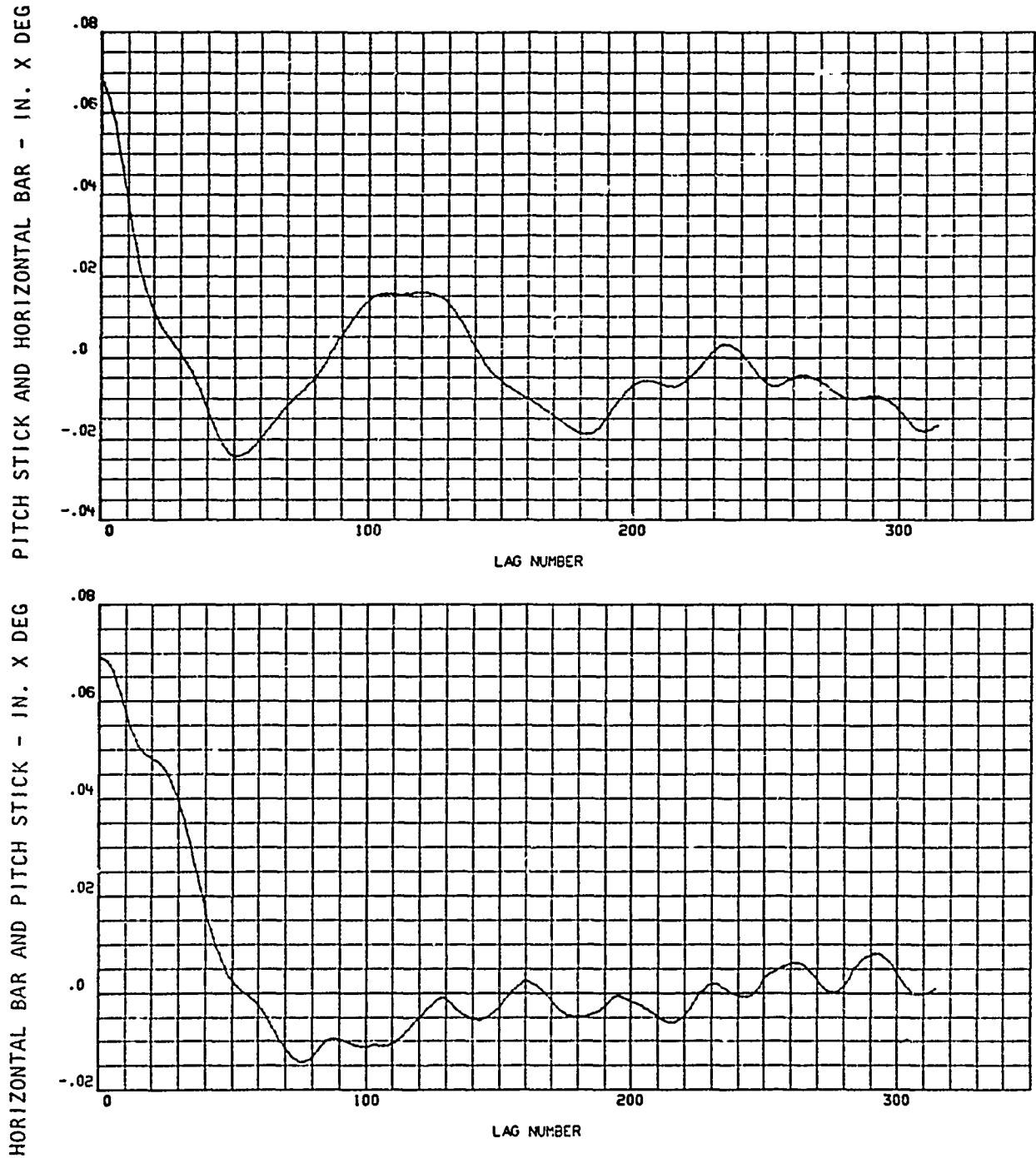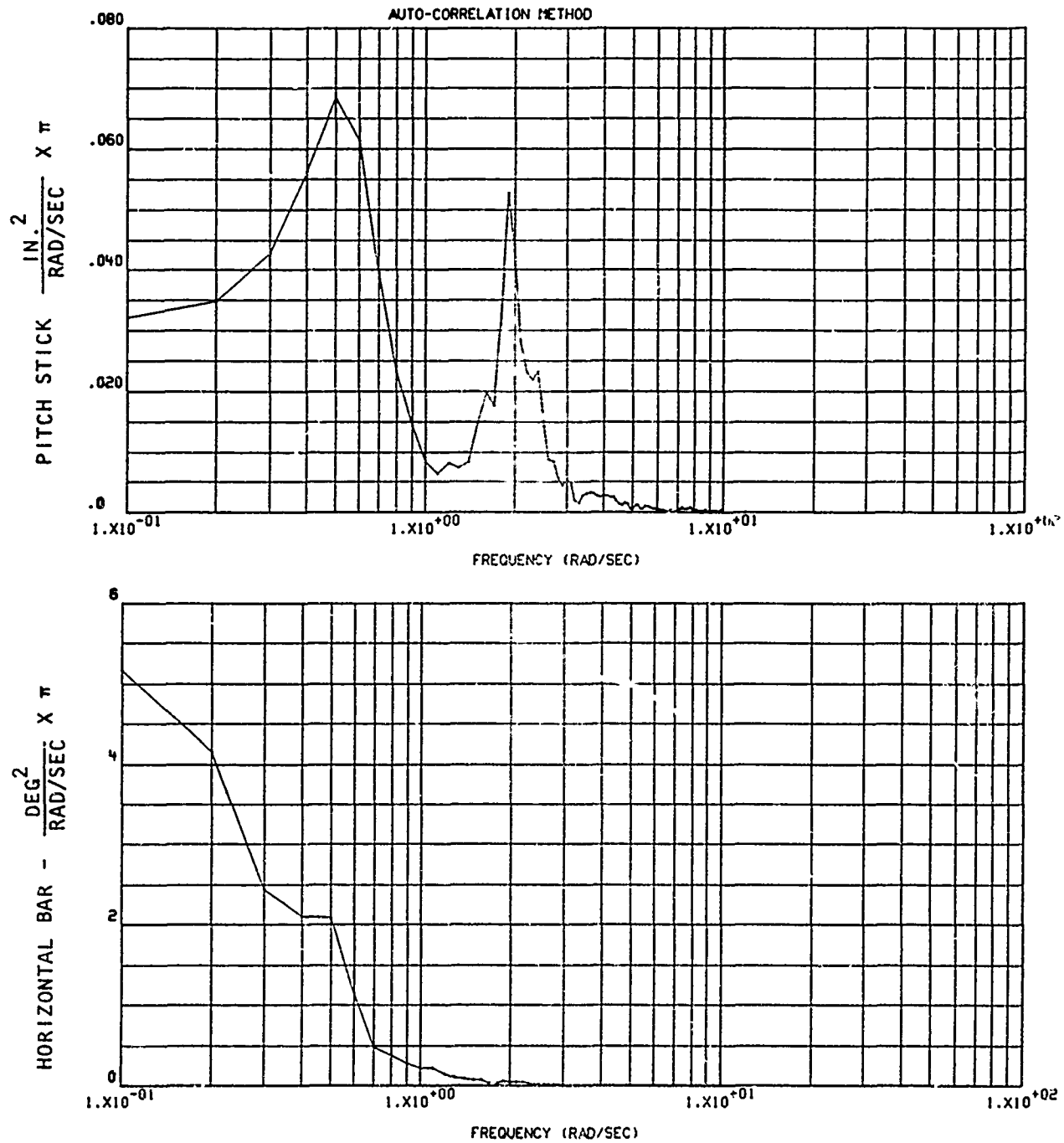
02A49 REFUEL ANALYSIS.

Figure 83. AR Simulation Run No. 02A49 Data (Concl)

309

Figure 84. AR Simulation Run No. 01A50 Data

310

GIA50 REFUEL ANALYSIS.

AUTO CORRELATION FUNCTIONS

Figure 84.   AR Simulation Run No. 01A50 Data (Cont)
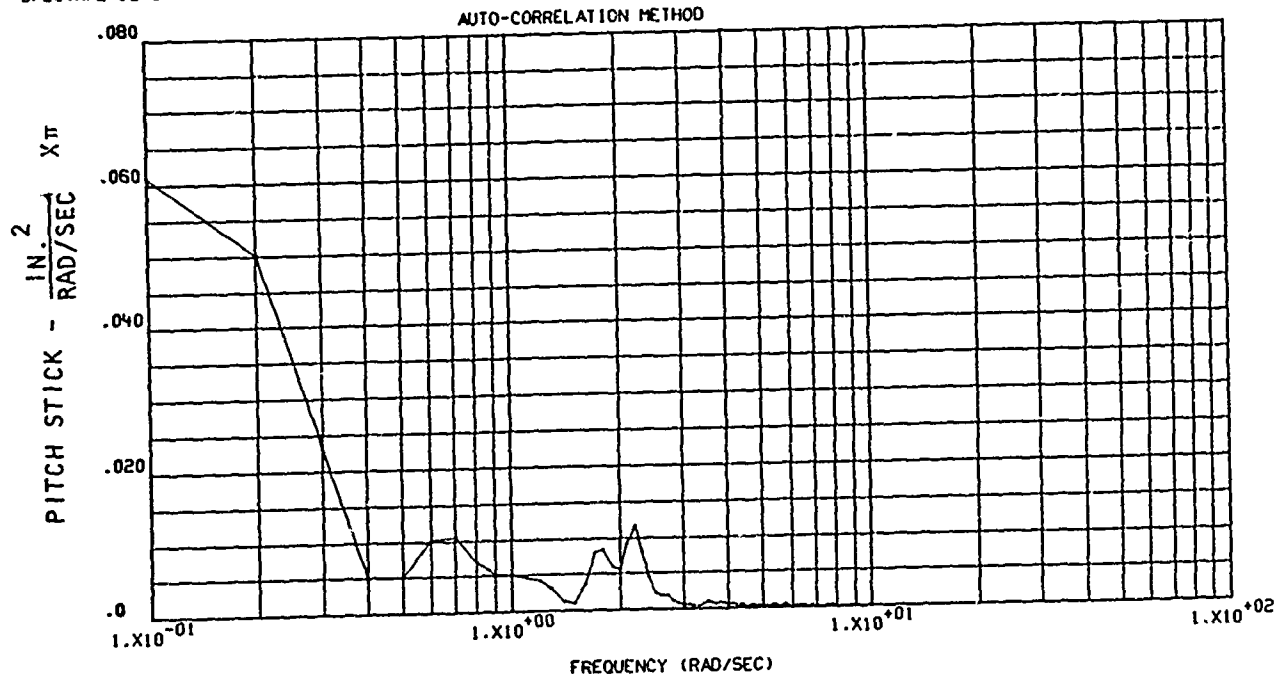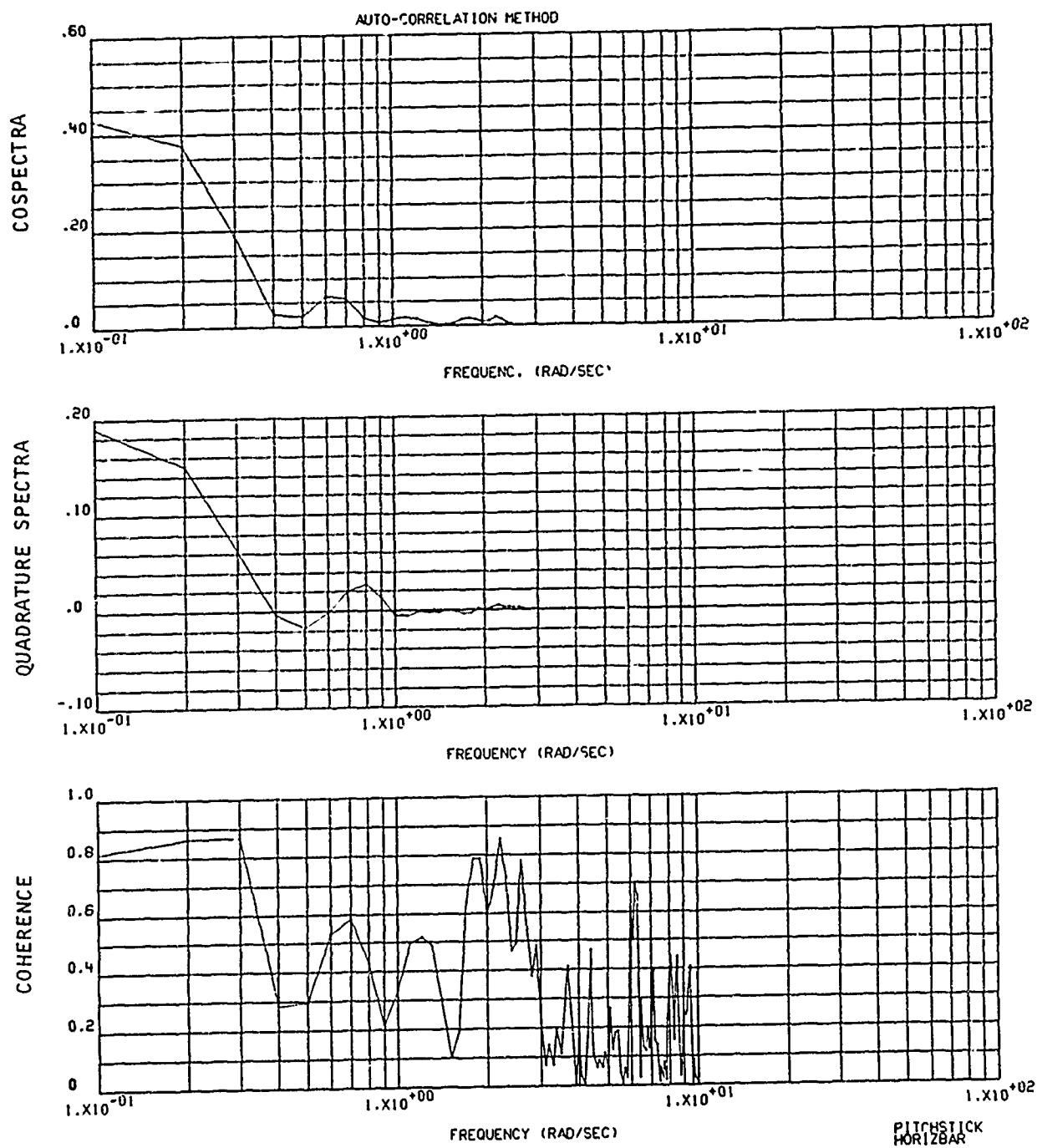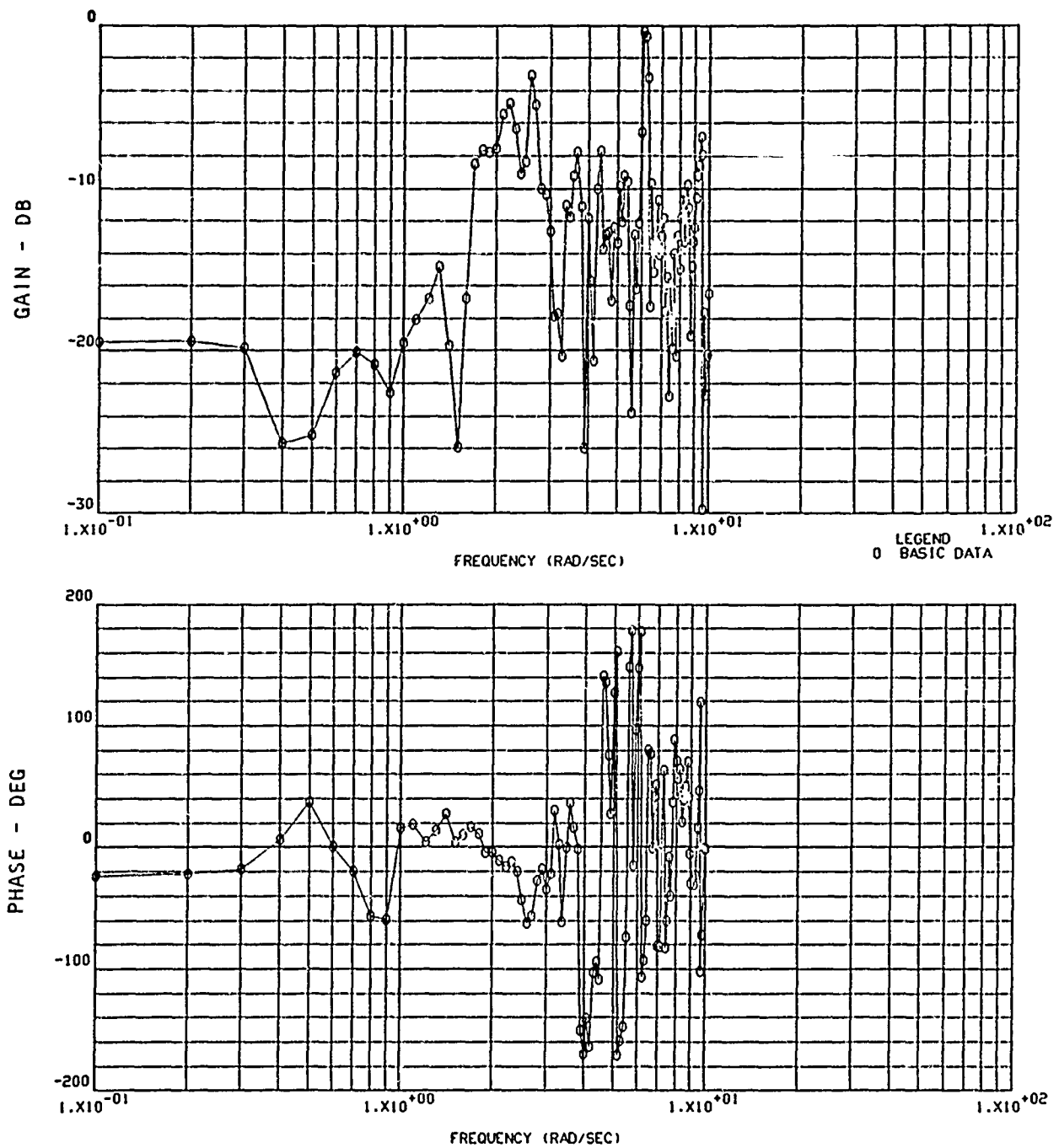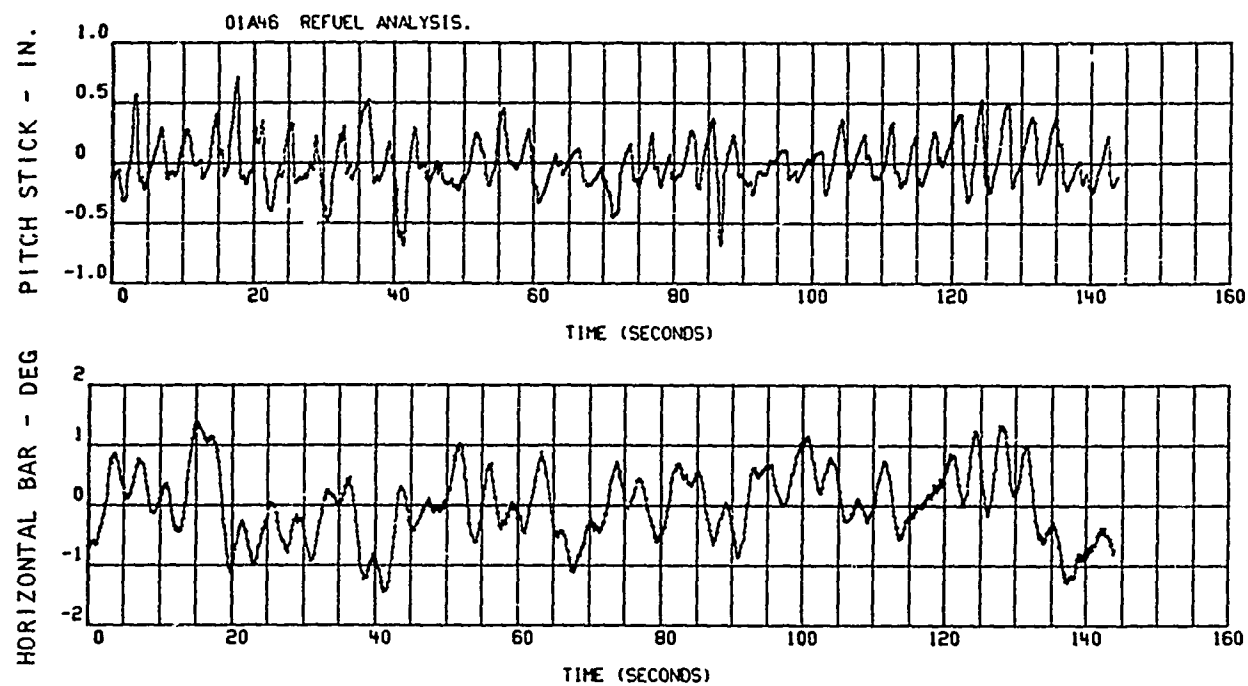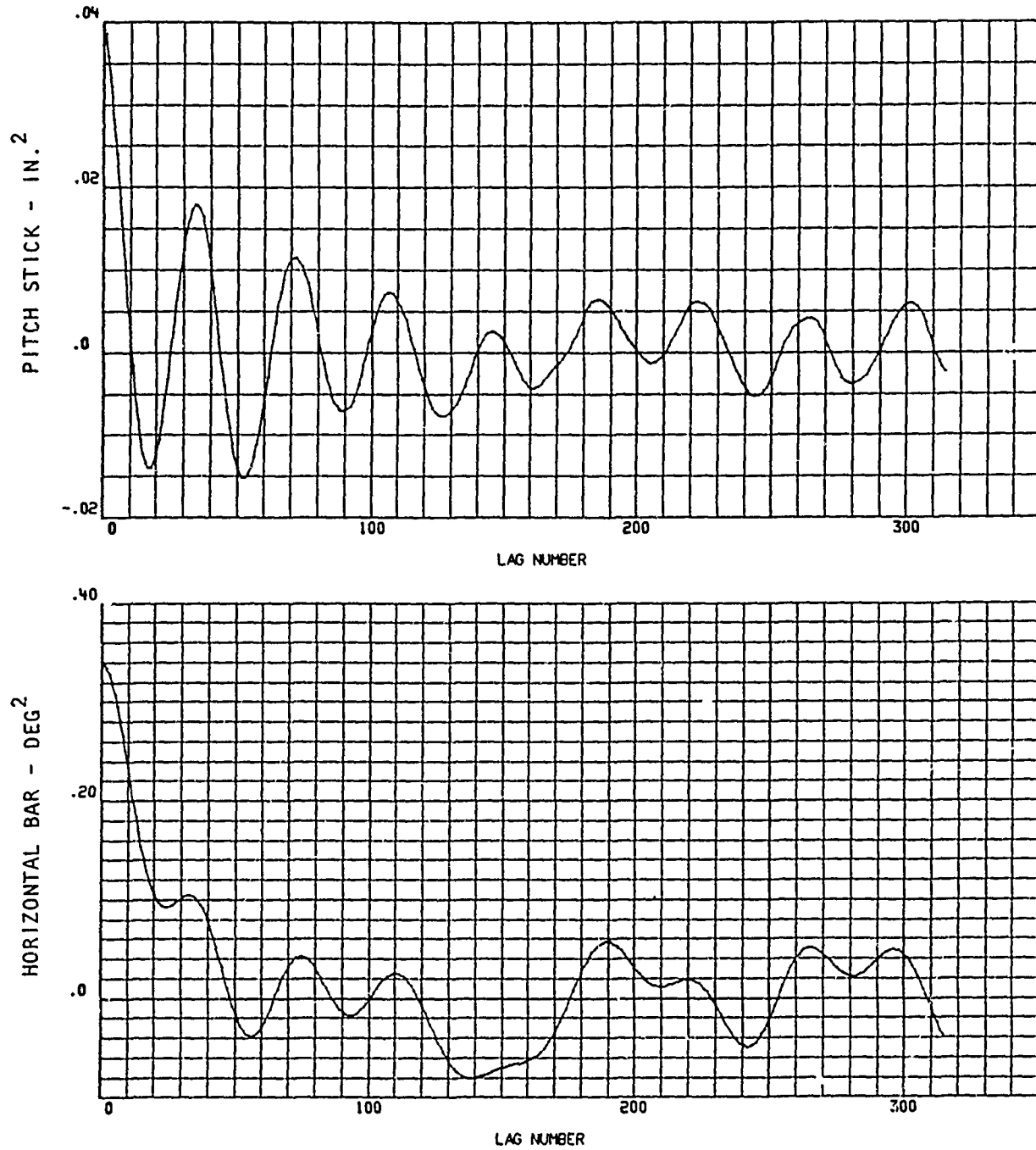
01A50 REFUEL ANALYSIS.

CROSS CORRELATION FUNCTIONS

Figure 84. AR Simulation Run No. 01A50 Data (Cont)

312

Figure 84. AR Simulation Run No. 01A50 Data (Cont)

313

01A50 REFUEL ANALYSIS.

Figure 84. AR Simulation Run No. 01A50 Data (Cont)

314
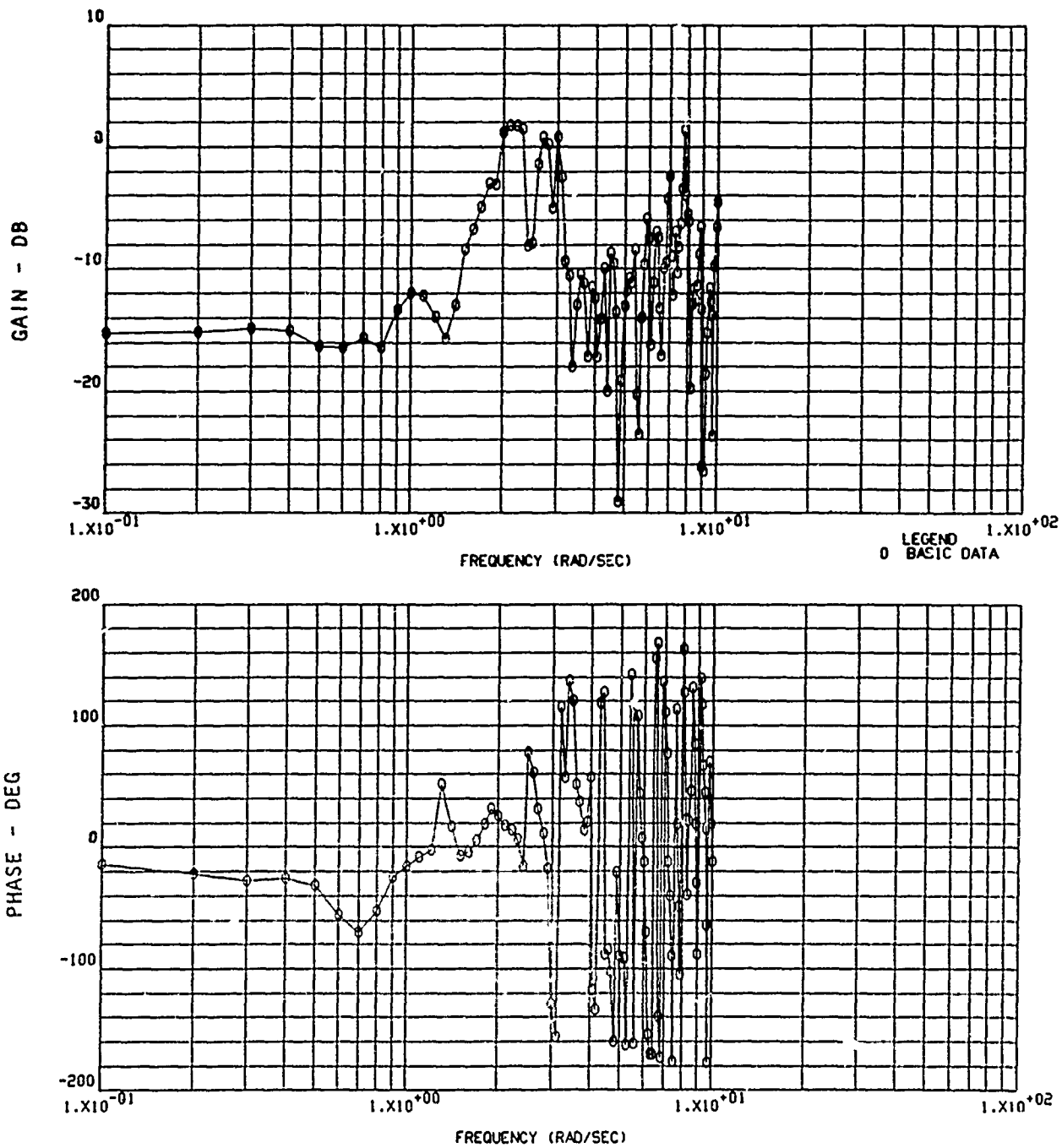
Figure 84. AR Simulation Run No. 01A50 Data (Concl)

315

Figure 85. AR Simulation Run No. 01A51 Data

316

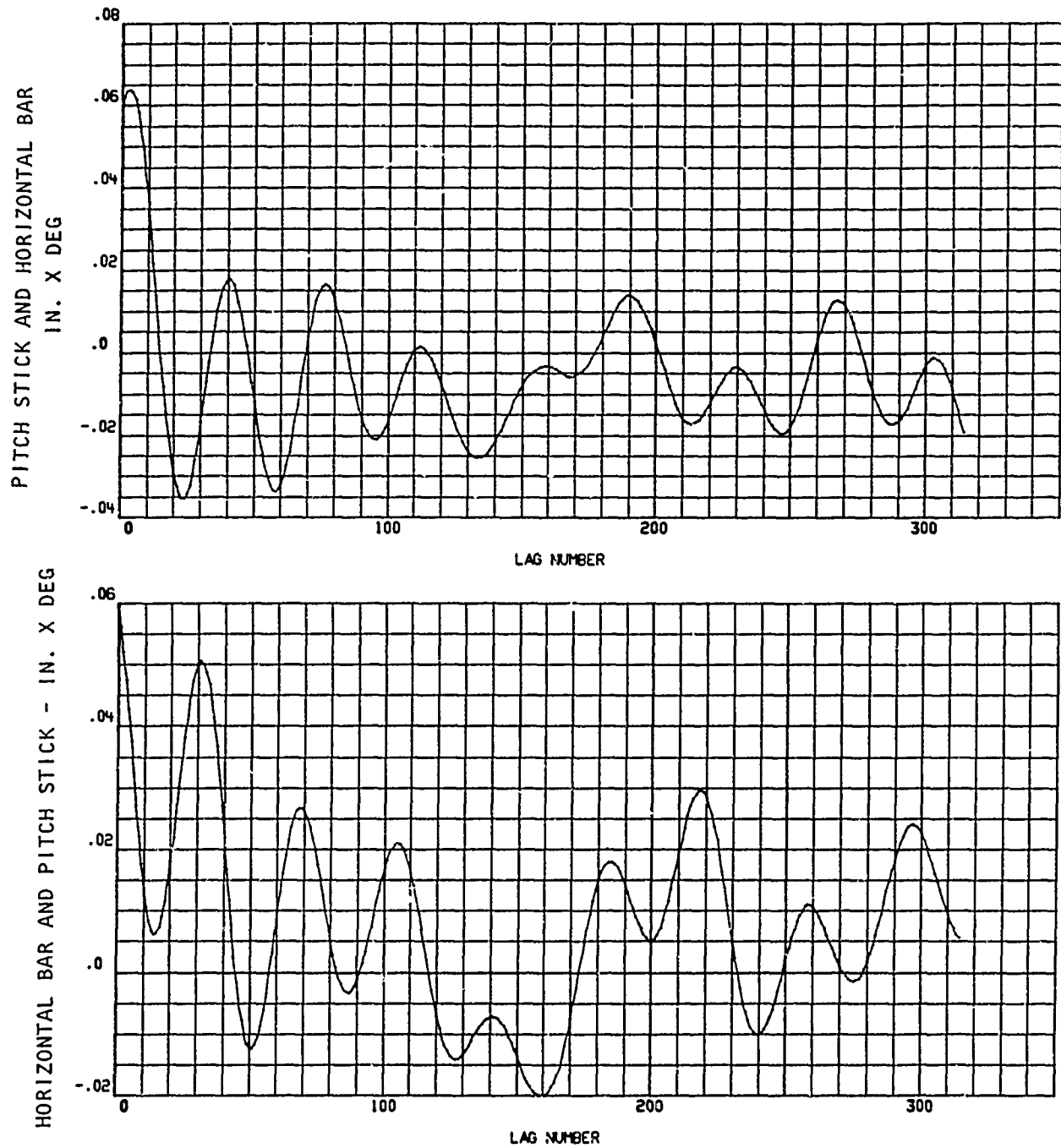Figure 85.   AR Simulation Run No. 01A51 Data (Cont)

317

Figure 85.   AR Simulation Run No. 01A51 Data (Cont)

318

01A51 REFUEL ANALYSIS.

SPECTRAL DENSITY FUNCTIONS

Figure 85. AR Simulation Run No. 01A51 Data (Cont)

319

01A51 REFUEL ANALYSIS

AUTO-CORRELATION METHOD

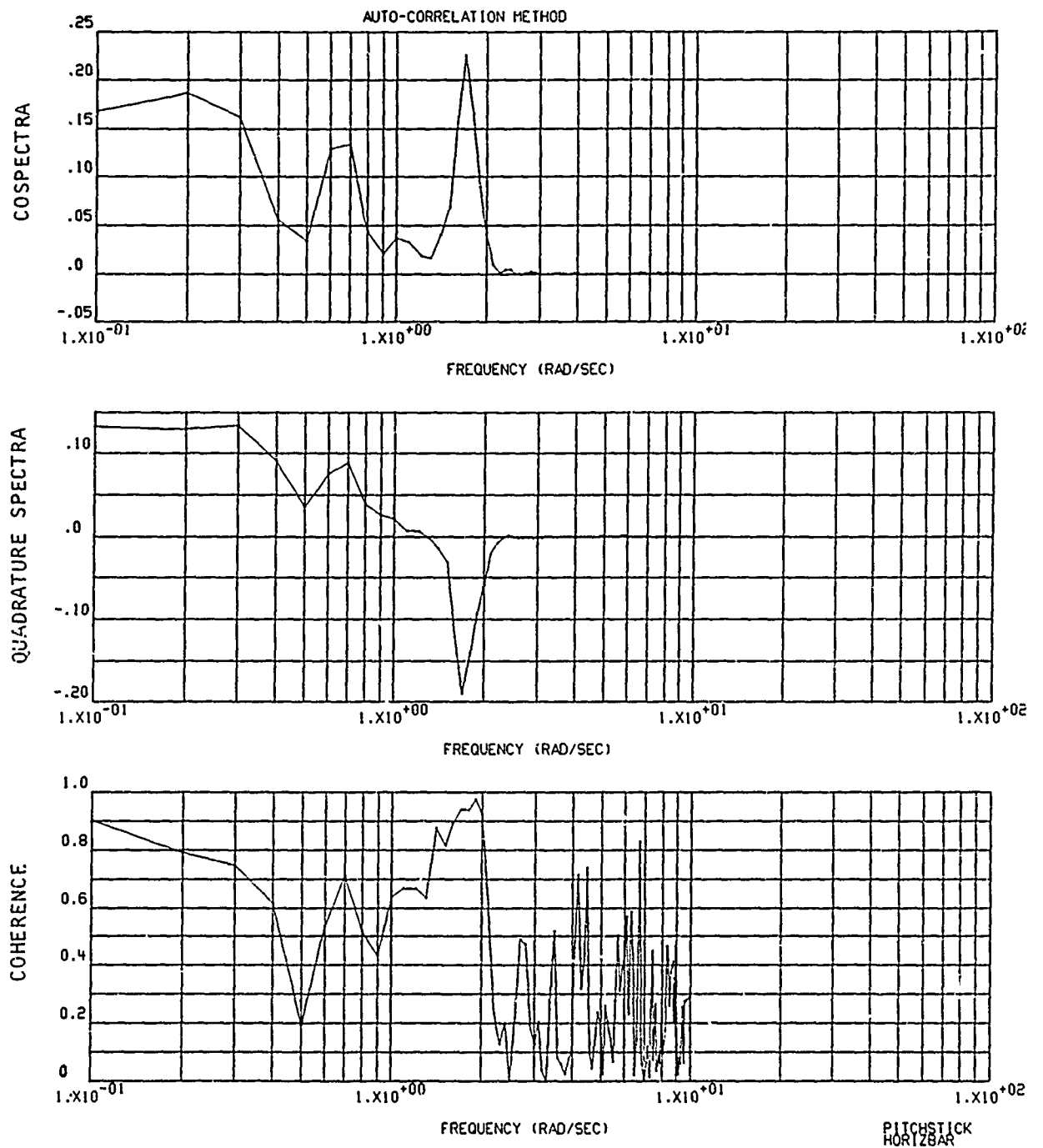Figure 85. AR Simulation Run No. 01A51 Data (Cont)

320
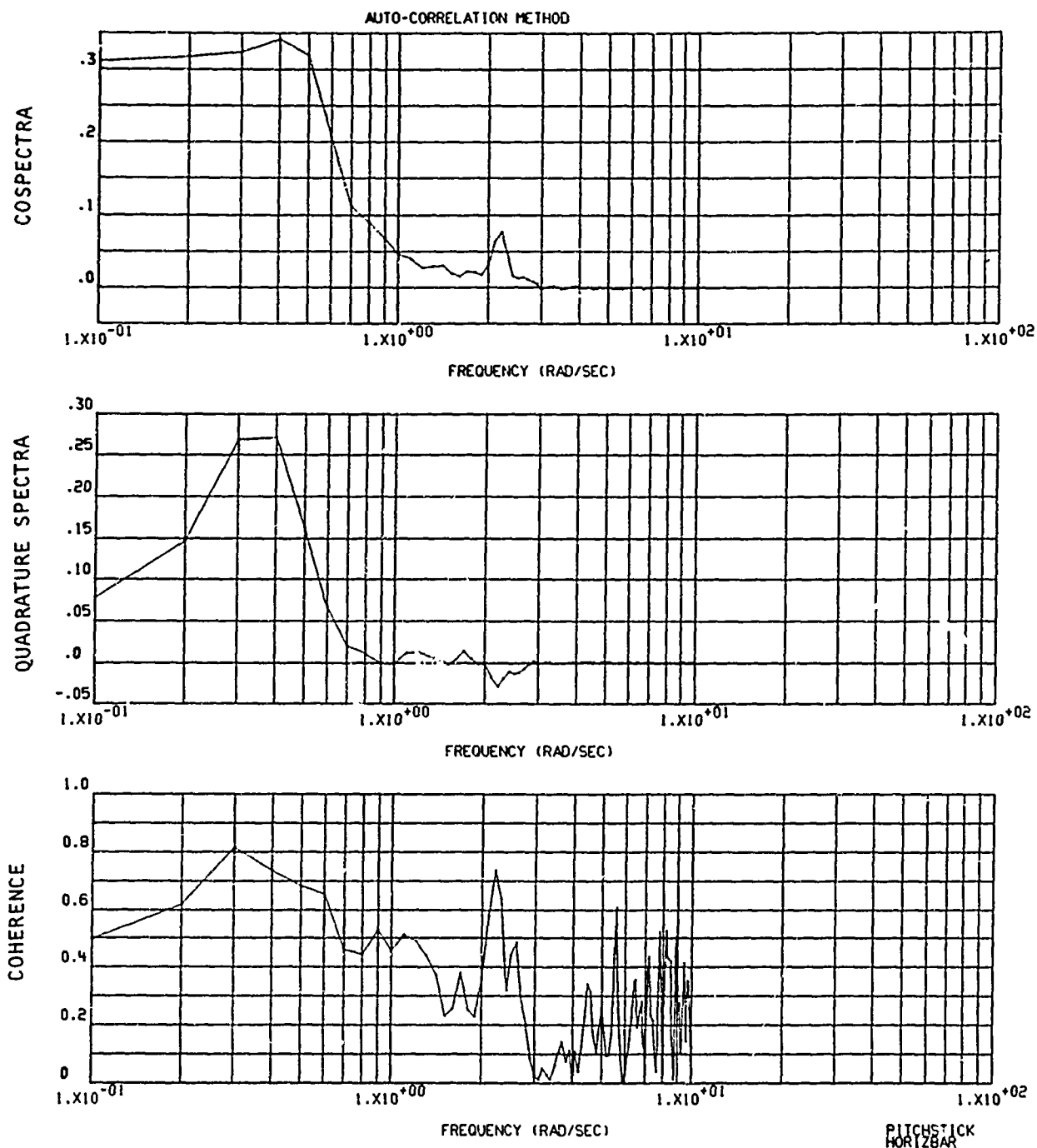
01A51 REFUEL ANALYSIS.
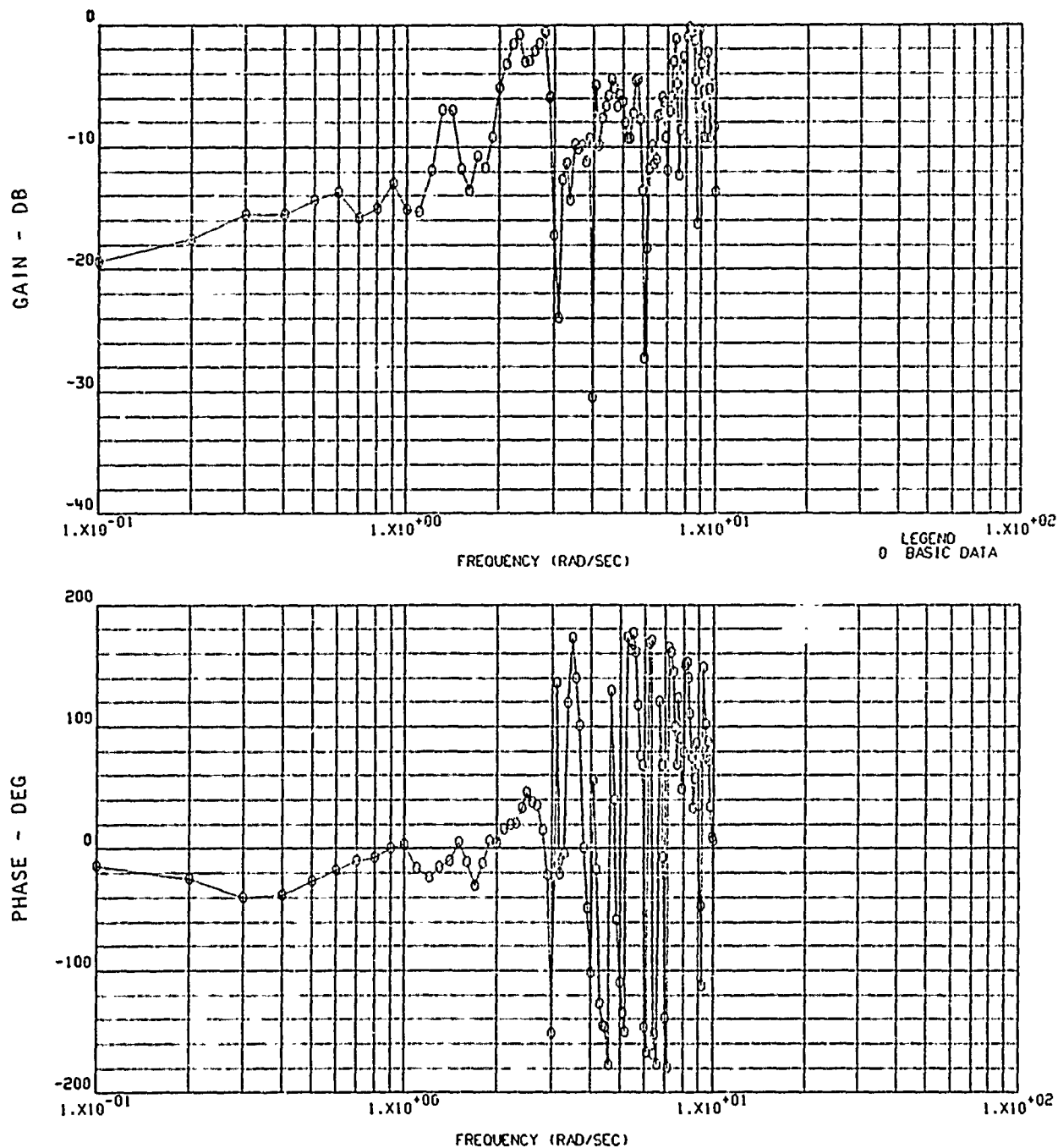
Figure 85. AR Simulation Run No. 01A51 Data (Concl)

321

Figure 86. AR Simulation Run No. 01A52 Data

Figure 86. AR Simulation Run No. 01A52 Data (Cont)

323

01A52 REFUEL ANALYSIS.

CROSS CORRELATION FUNCTIONS

Figure 86. AR Simulation Run No. 01A52 Data (Cont)

Figure 86. AR Simulation Run No. 01A52 Data (Cont)

325

01A52 REFUEL ANALYSIS.

AUTO-CORRELATION METHOD

FREQUENCY (RAD/SEC)

FREQUENCY (RAD/SEC)

FREQUENCY (RAD/SEC)

PLICHSTICK
HORIZBAR

Figure 86. AR Simulation Run No. 01A52 Data (Cont)

326

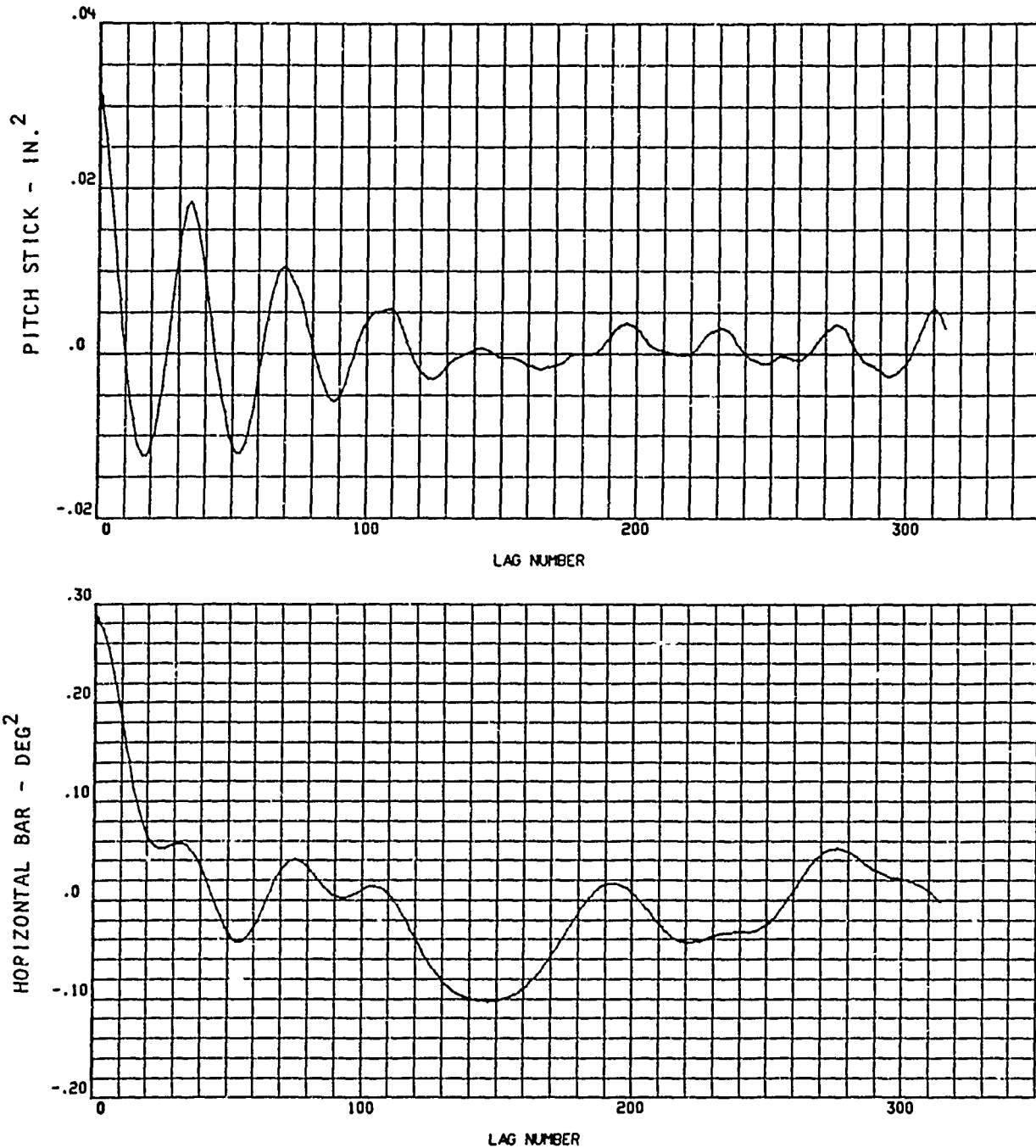01A52 REFUEL ANALYSIS.

Figure 86.   AR Simulation Run No. 01A52 Data (Concl)
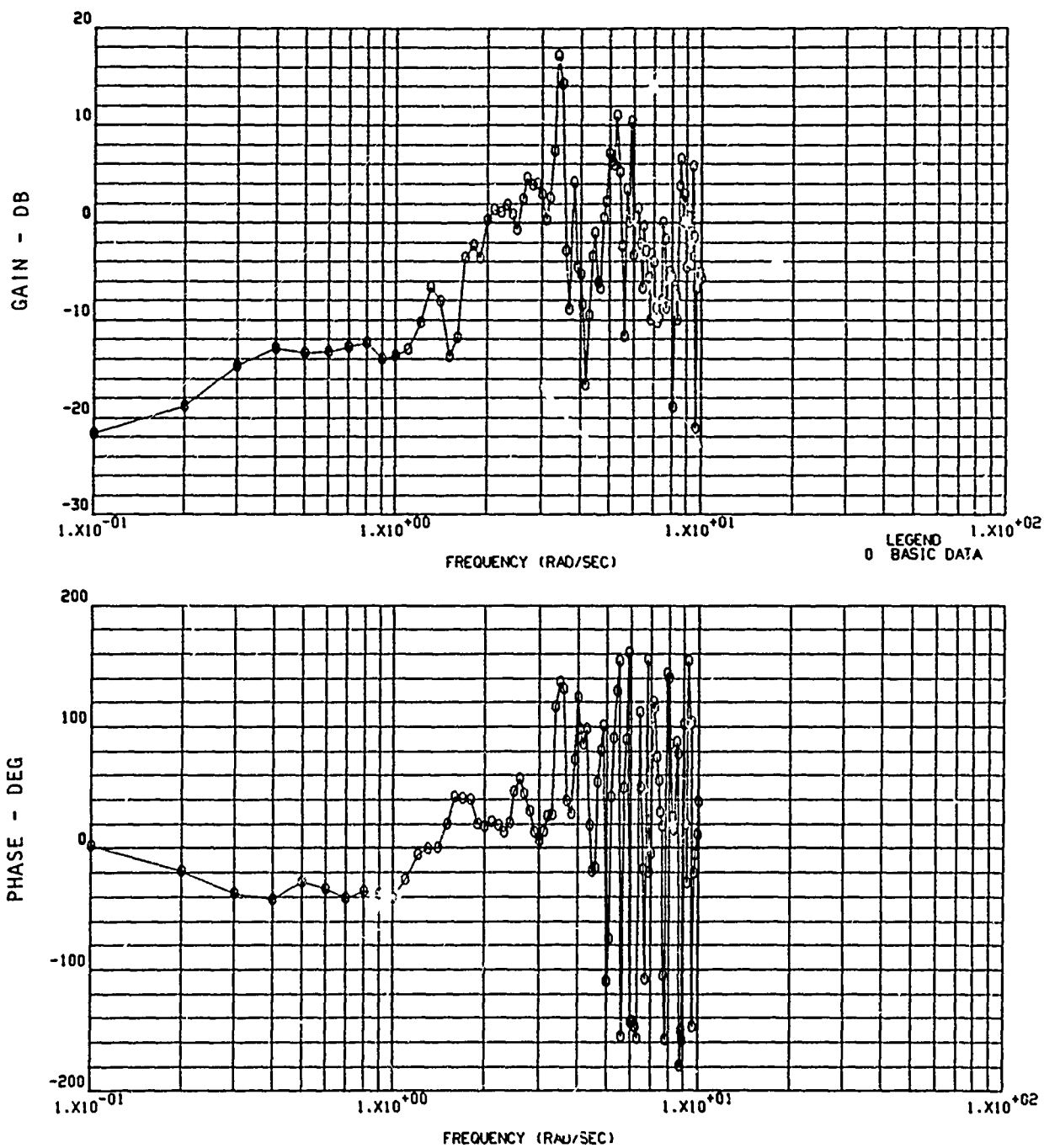
327

Figure 87. AR Simulation Run No. 01A56 Data

AUTO CORRELATION FUNCTIONS

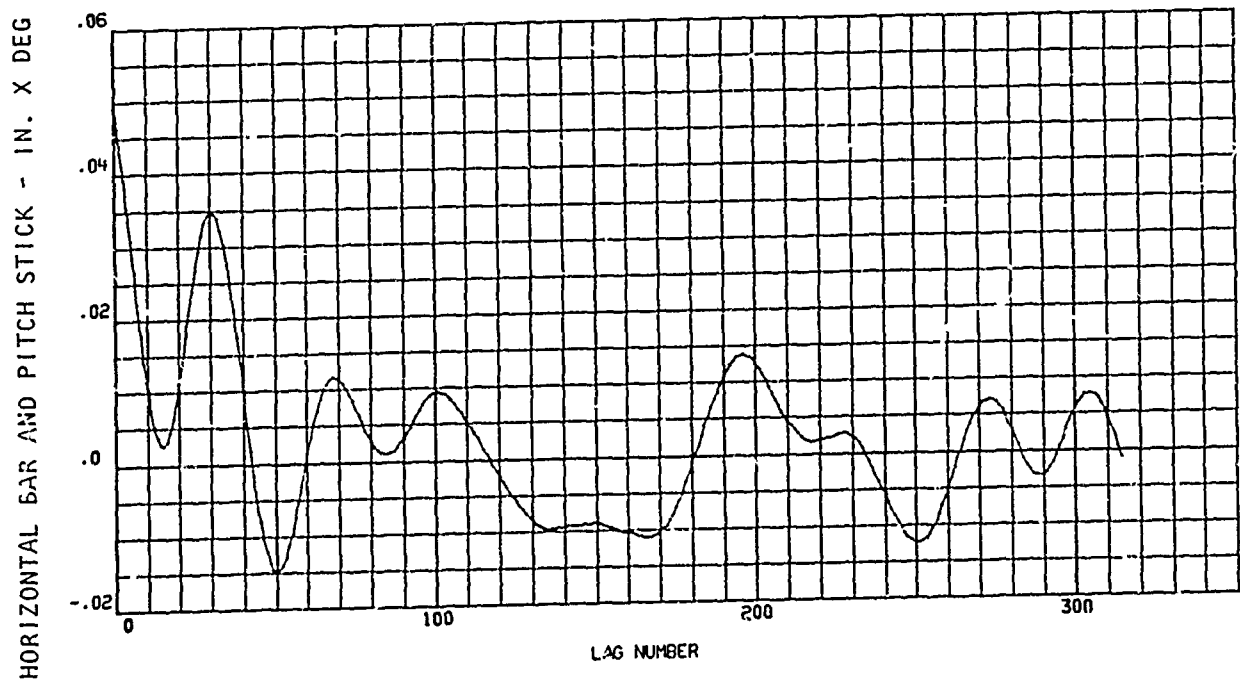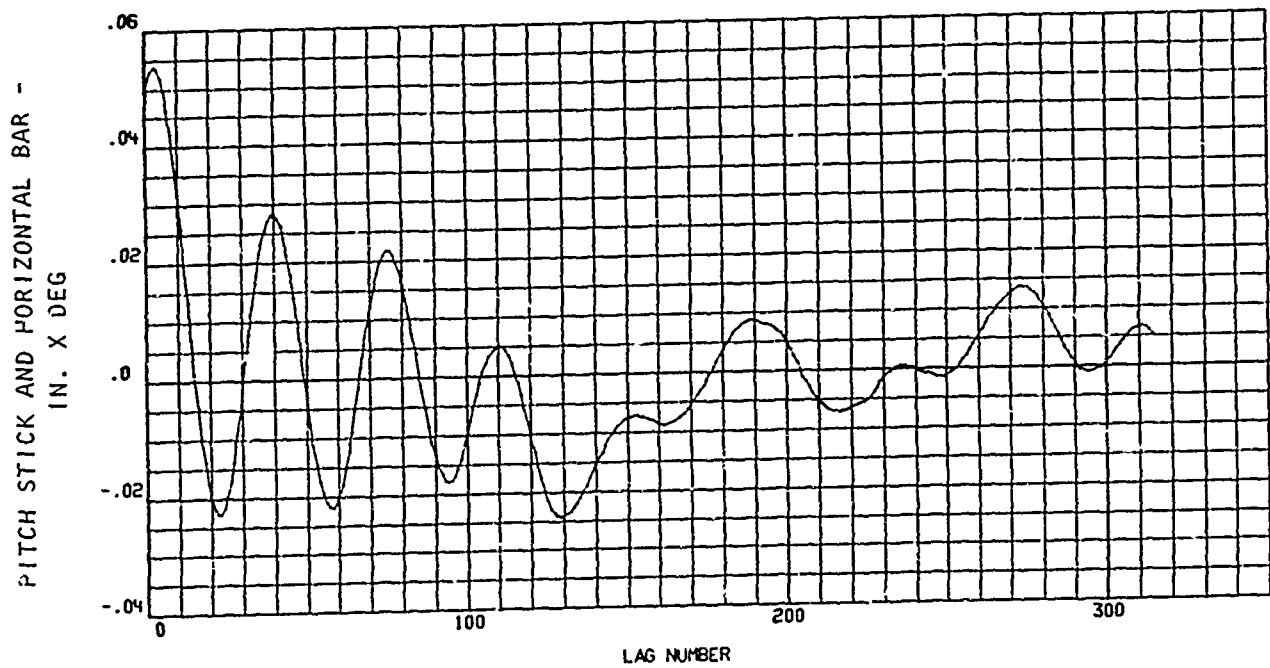Figure 87. AR Simulation Run No. 01A56 Data (Cont)

329

Figure 87. AR Simulation Run No. 01A56 Data (Cont)

330

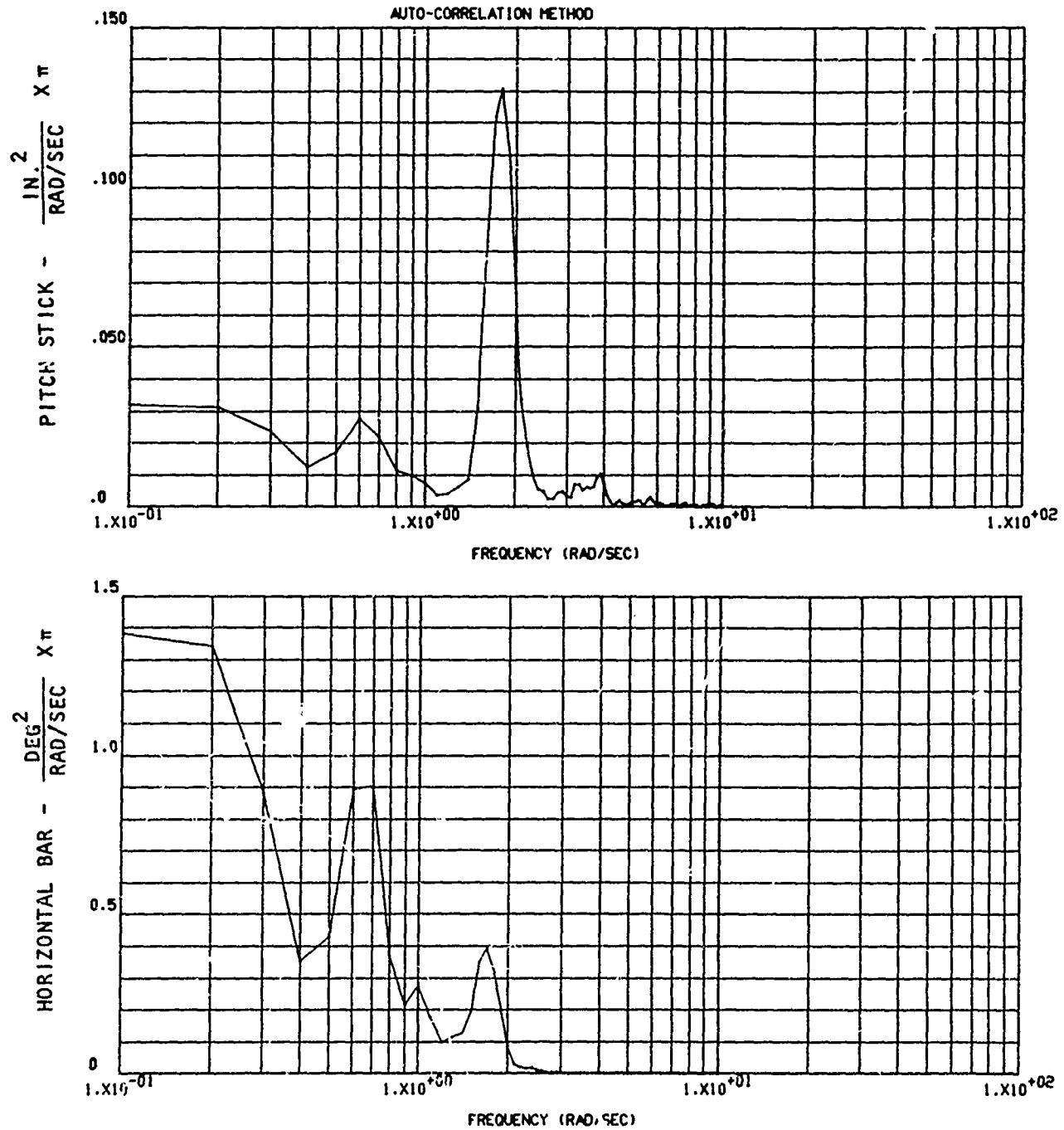01A56 REFUEL ANALYSIS.

SPECTRAL DENSITY FUNCTIONS

Figure 87.   AR Simulation Run No. 01A56 Data (Cont)

331

OIA55 REFUEL ANALYSIS.

Figure 87. AR Simulation Run No. 01A56 Data (Cont)

332

01A56 REFUEL ANALYSIS.

GAIN - DB vs FREQUENCY (RAD/SEC)

PHASE - DEG vs FREQUENCY (RAD/SEC)

LEGEND
0 BASIC DATA

Figure 87.   AR Simulation Run No. 01A56 Data (Concl)

333

Figure 88. AR Simulation Run No. 01A57 Data

Figure 88. AR Simulation Run No. 01A57 Data (Cont)

335

Figure 88.   AR Simulation Run No. 01A57 Data

336

Figure 88.   AR Simulation Run No. 01A57 Data (Cont)

337

01A57 REFUEL ANALYSIS.

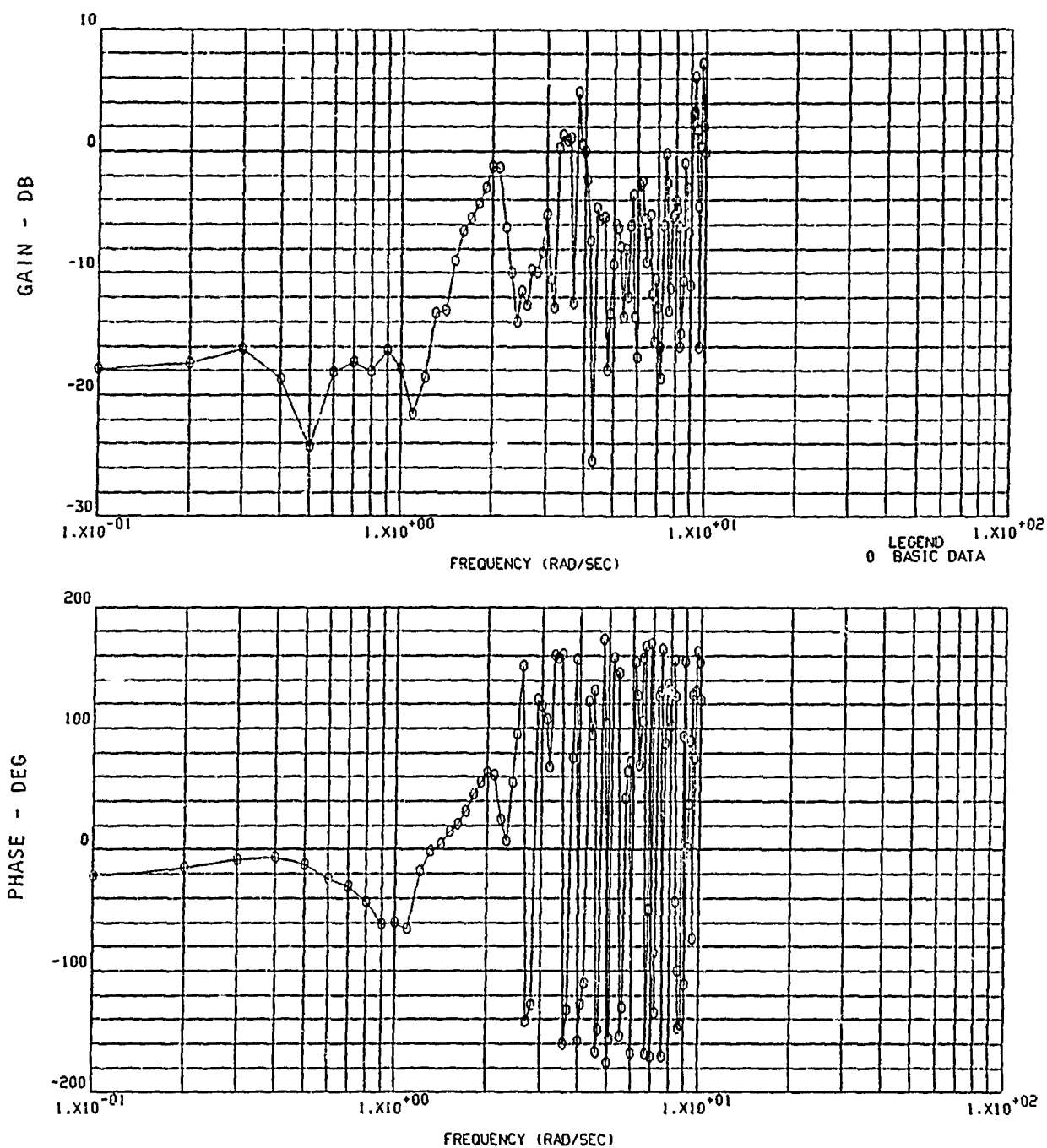Figure 88.   AR Simulation Run No. 01A57 Data (Cont)

338
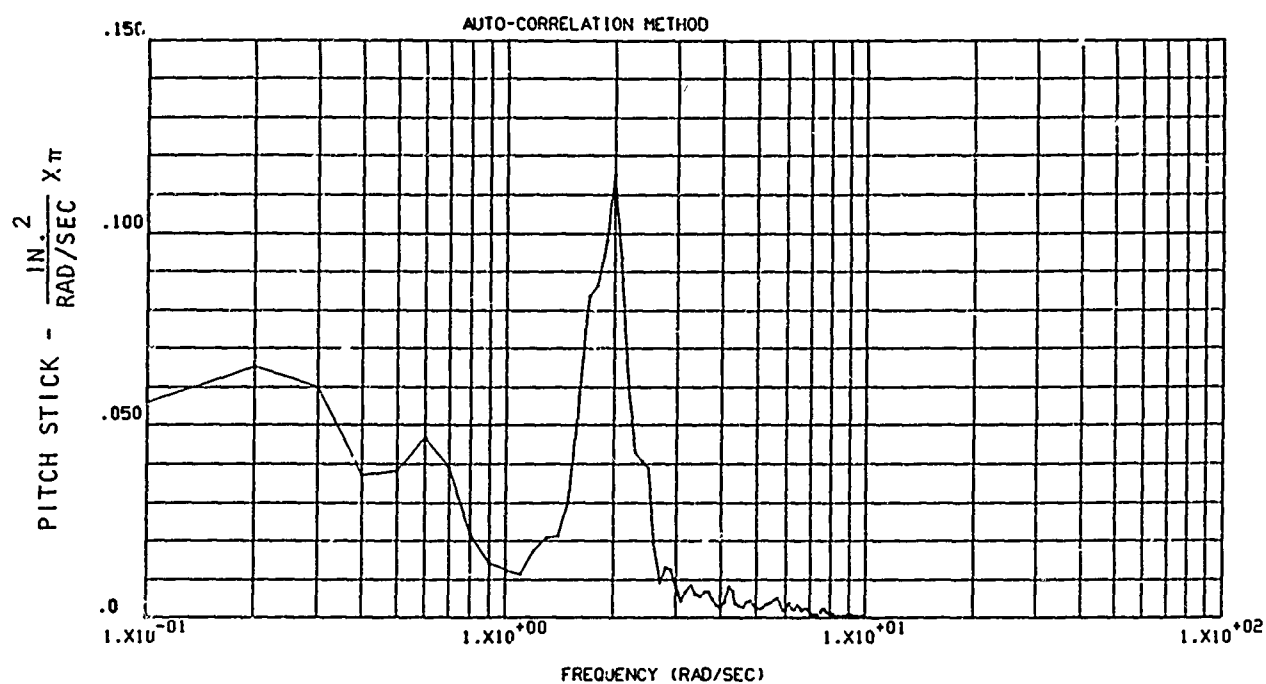
01A57 REFUEL ANALYSIS.

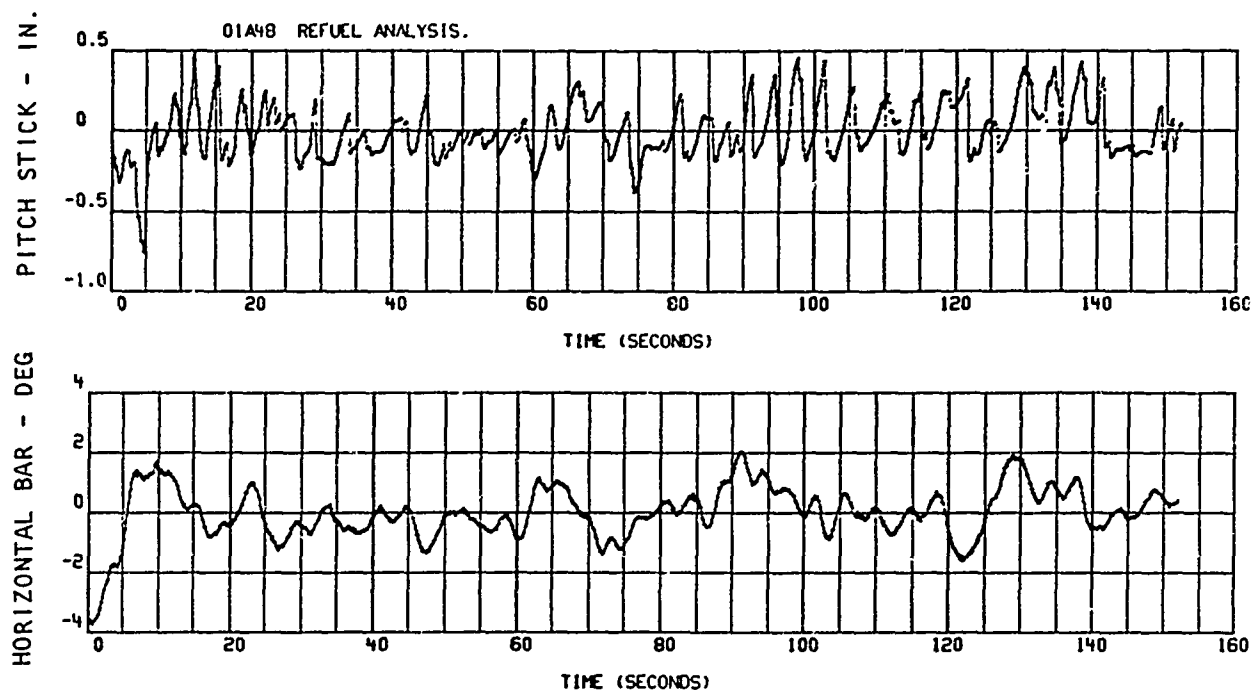Figure 88. AR Simulation Run No. 01A57 Data (Concl)

339

Figure 89.   AR Simulation Run No. 01A58 Data
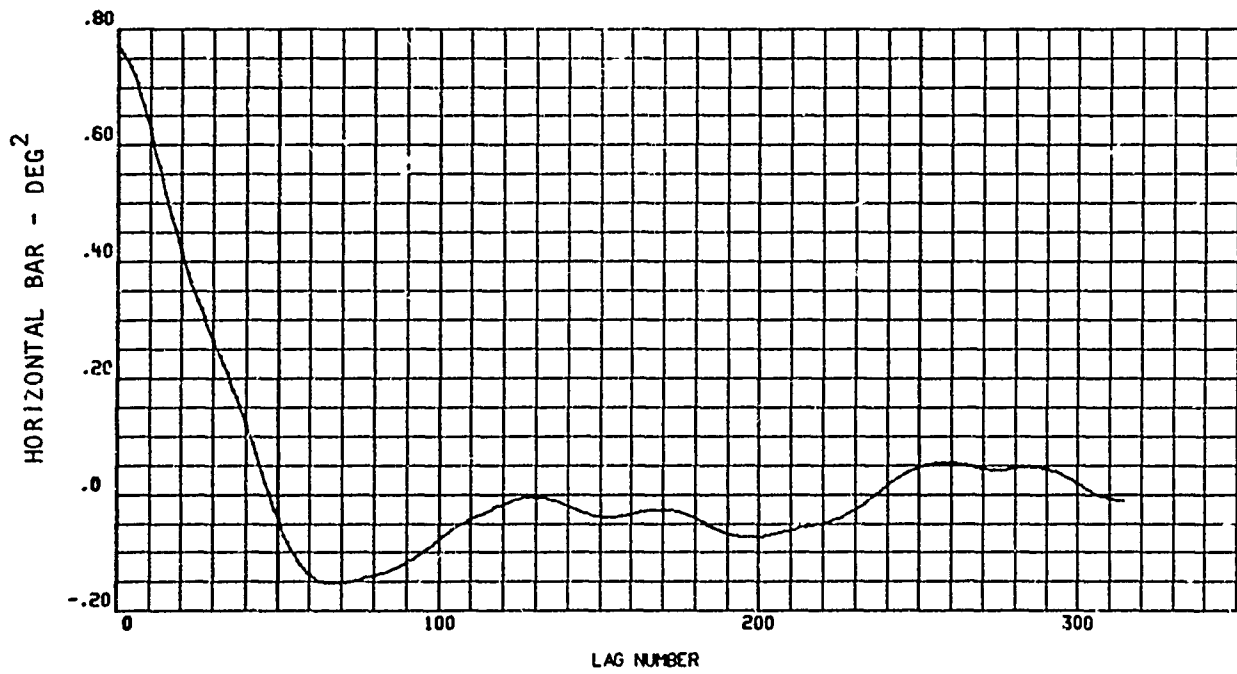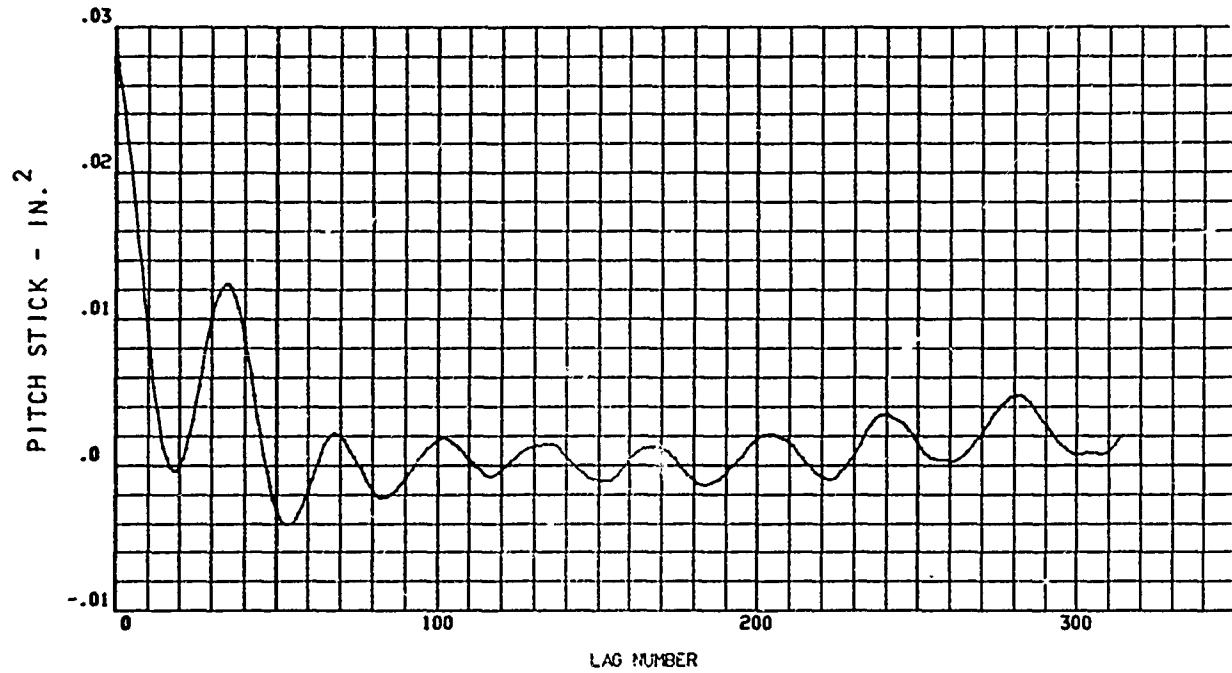
AUTO CORRELATION FUNCTIONS

Figure 89. AR Simulation Run No. 01A58 Data (Cont)
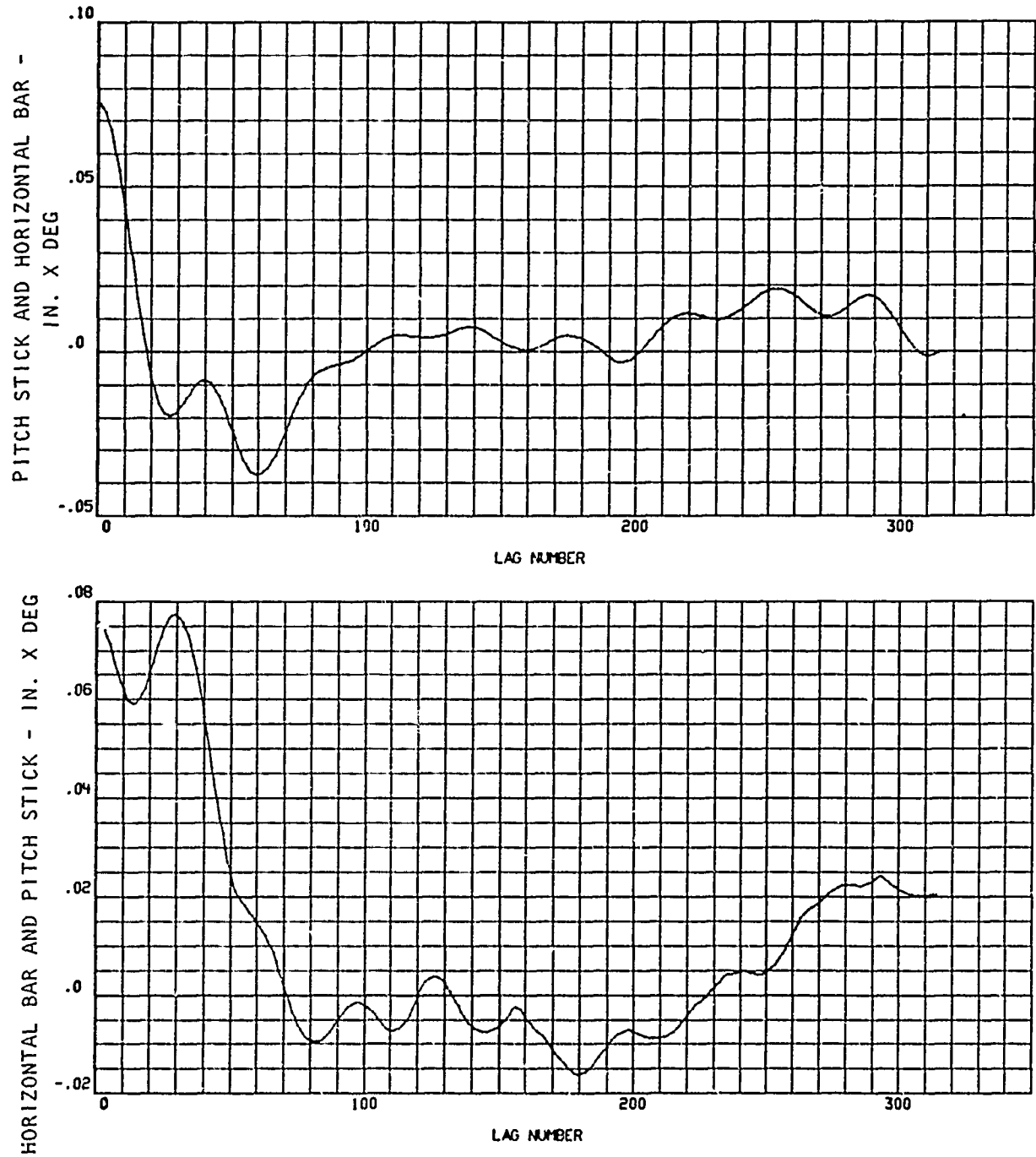
341

01A58 REFUEL ANALYSIS.

CROSS CORRELATION FUNCTIONS

Figure 89. AR Simulation Run No. 01A58 Data (Cont)

Figure 89. AR Simulation Run No. 01A58 Data (Cont)

343

Figure 89. AR Simulation Run No. 01A58 Data (Cont)

344

01A58   REFUEL ANALYSIS.

Figure 89.   AR Simulation Run No. 01A58 Data (Concl)

345

Figure 90. AR Simulation Run No. 01A63 Data

346

01A63 REFUEL ANALYSIS.

AUTO CORRELATION FUNCTIONS

Figure 90. AR Simulation Run No. 01A63 Data (Cont)

347

Figure 90. AR Simulation Run No. 01A63 Data (Cont)

348

01A63 REFUEL ANALYSIS.

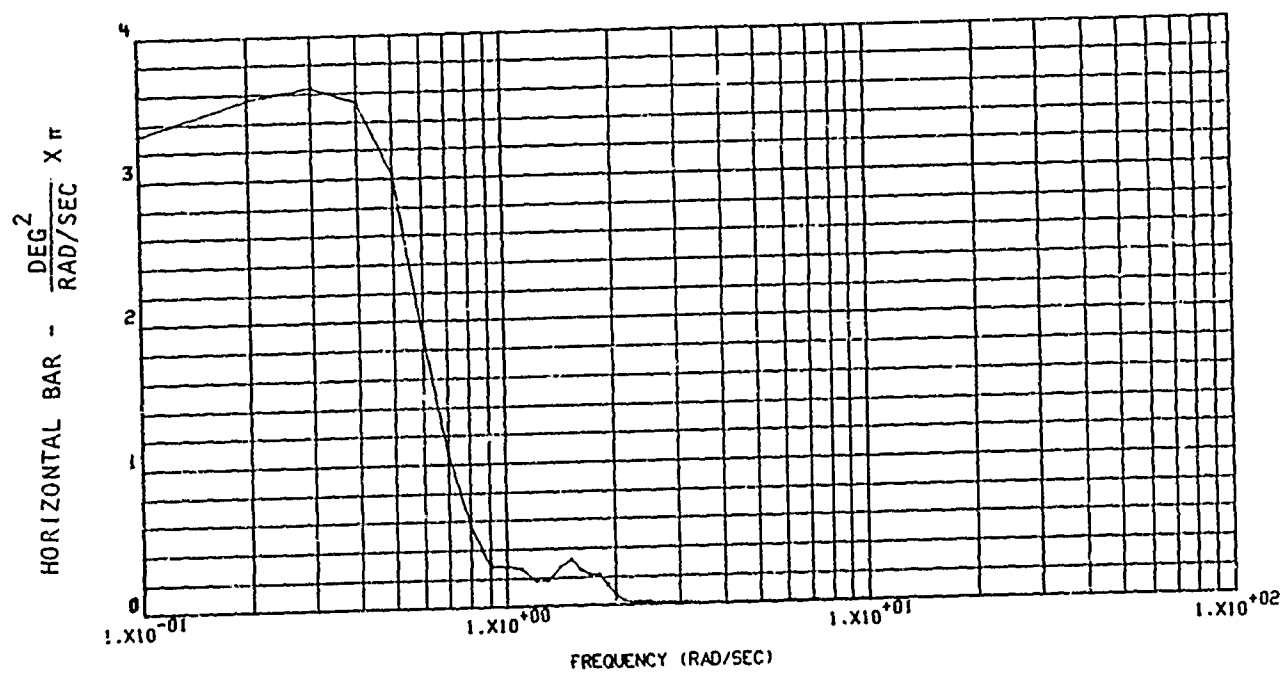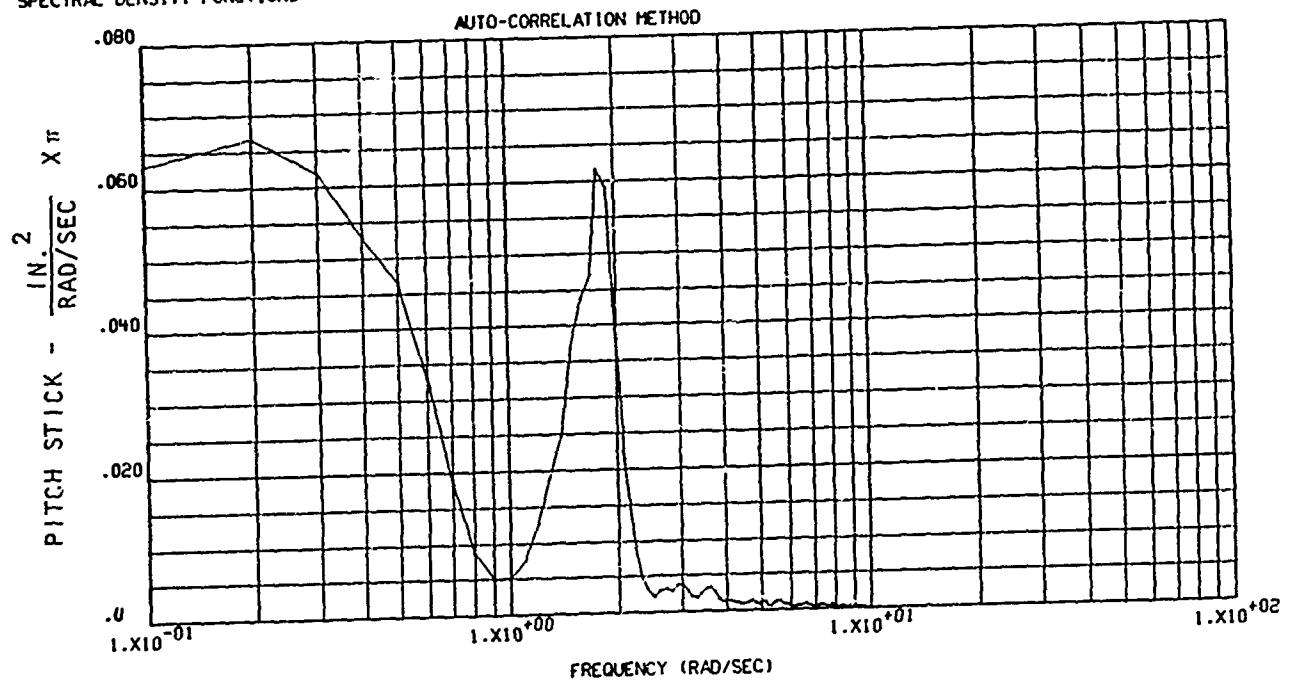SPECTRAL DENSITY FUNCTIONS

AUTO-CORRELATION METHOD

Figure 90. AR Simulation Run No. 01A63 Data (Cont)

349

01A63 REFUEL ANALYSIS.

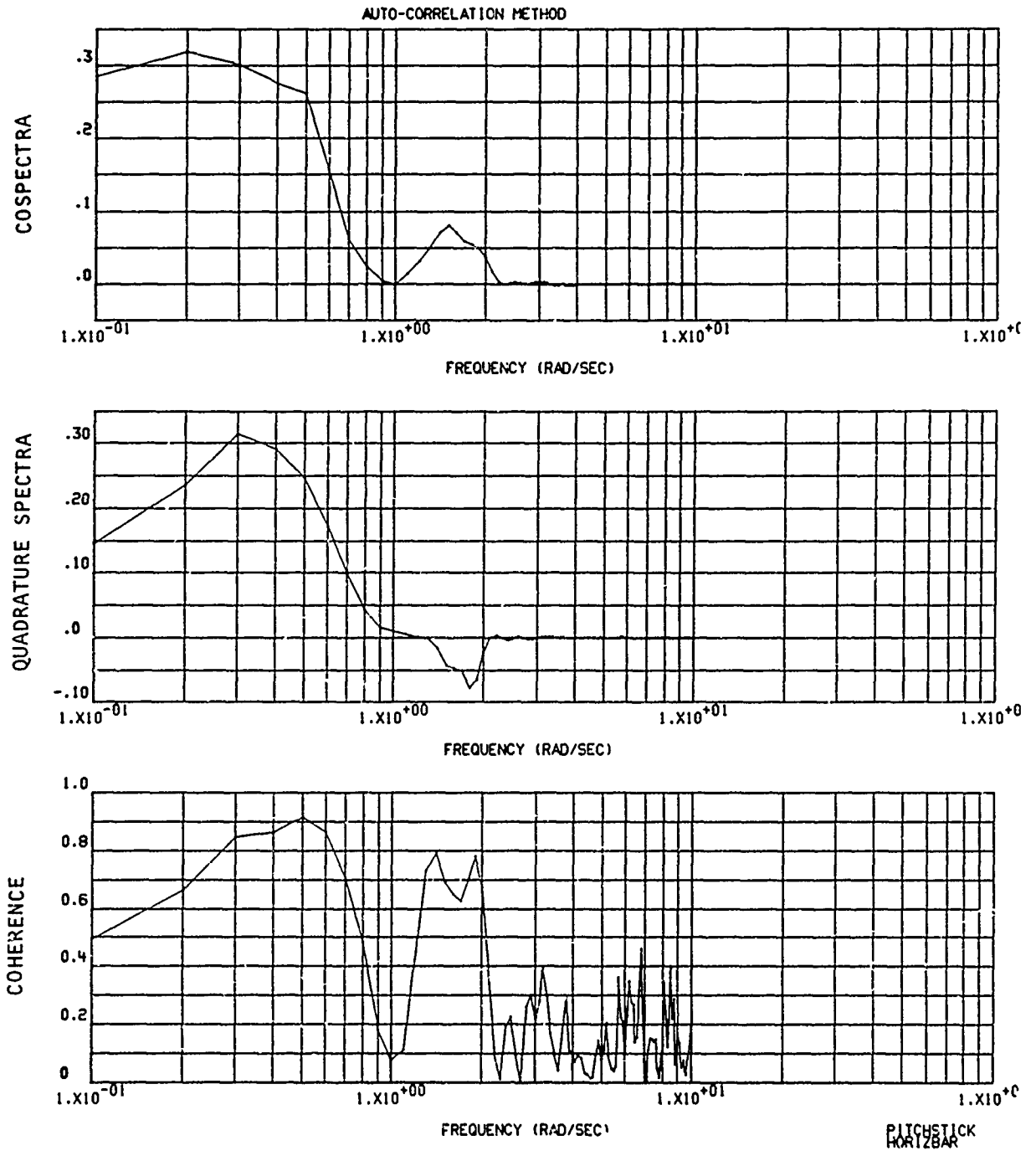Figure 90. AR Simulation Run No. 01A63 Data (Cont)
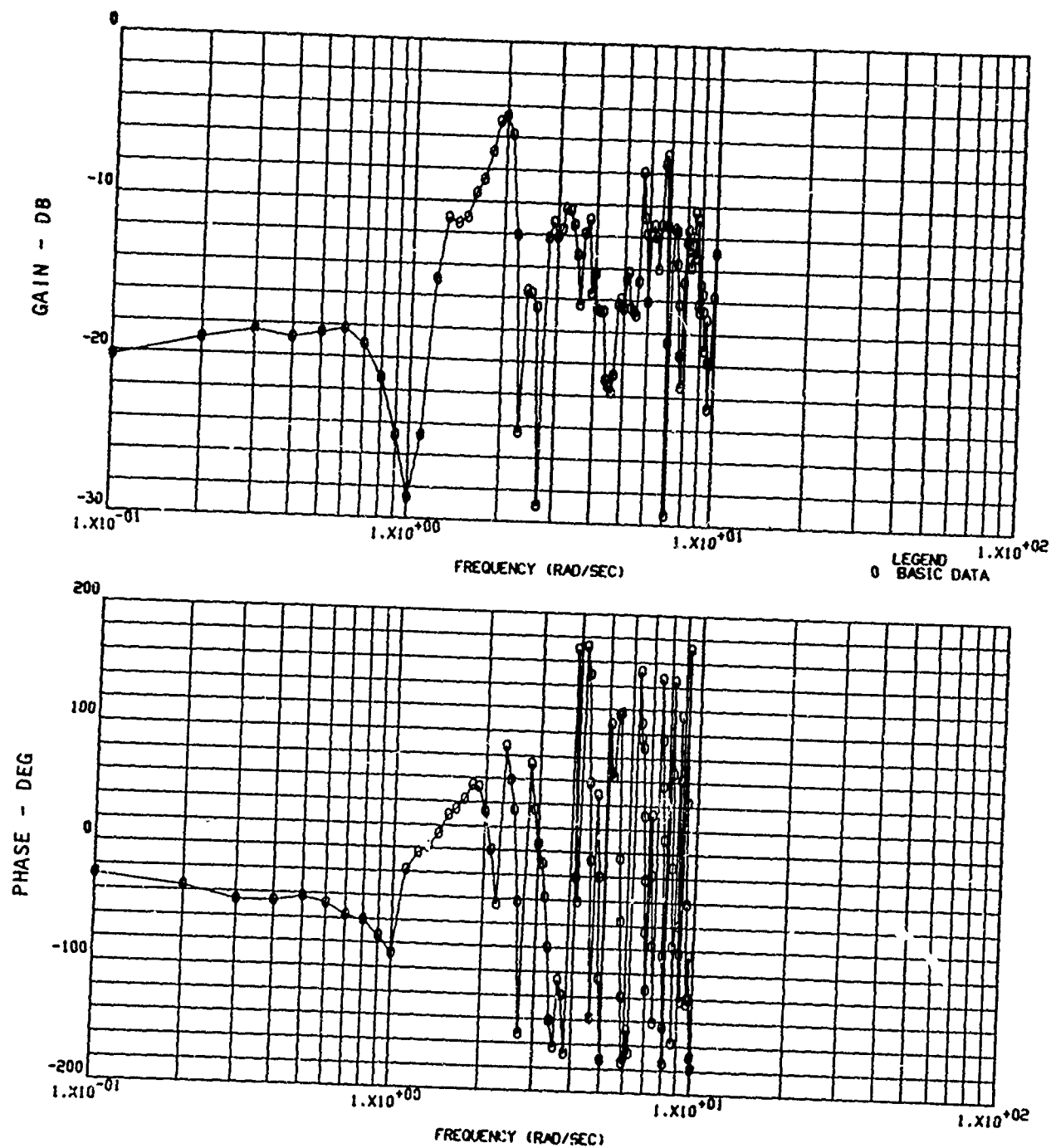
350

01A63 REFUEL ANALYSIS.

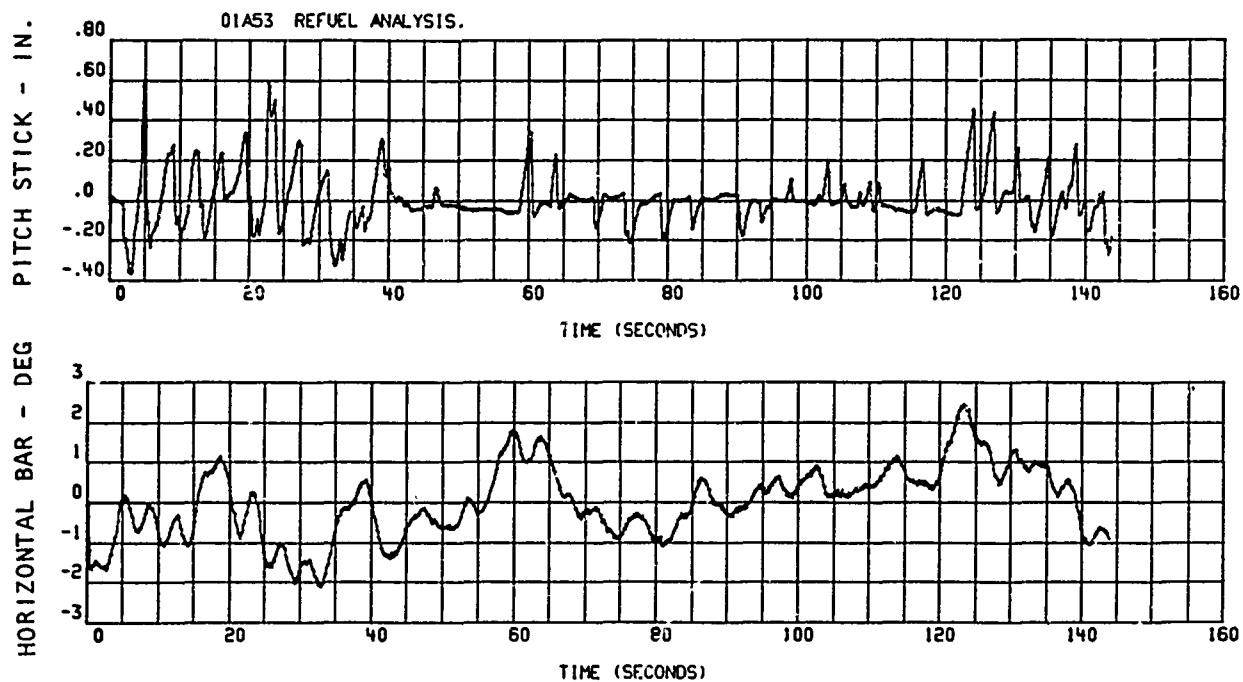Figure 90. AR Simulation Run No. 01A63 Data (Concl)

351

Figure 91. AR Simulation Run No. 01A64 Data

01A64. REFUEL ANALYSIS.
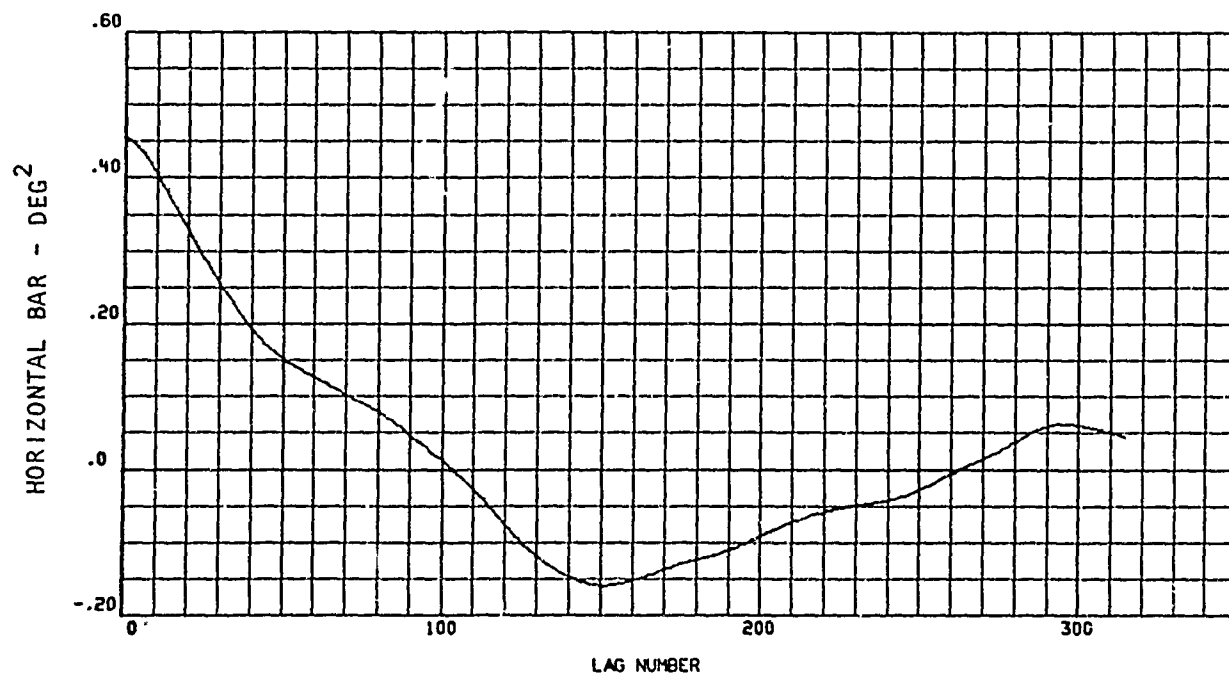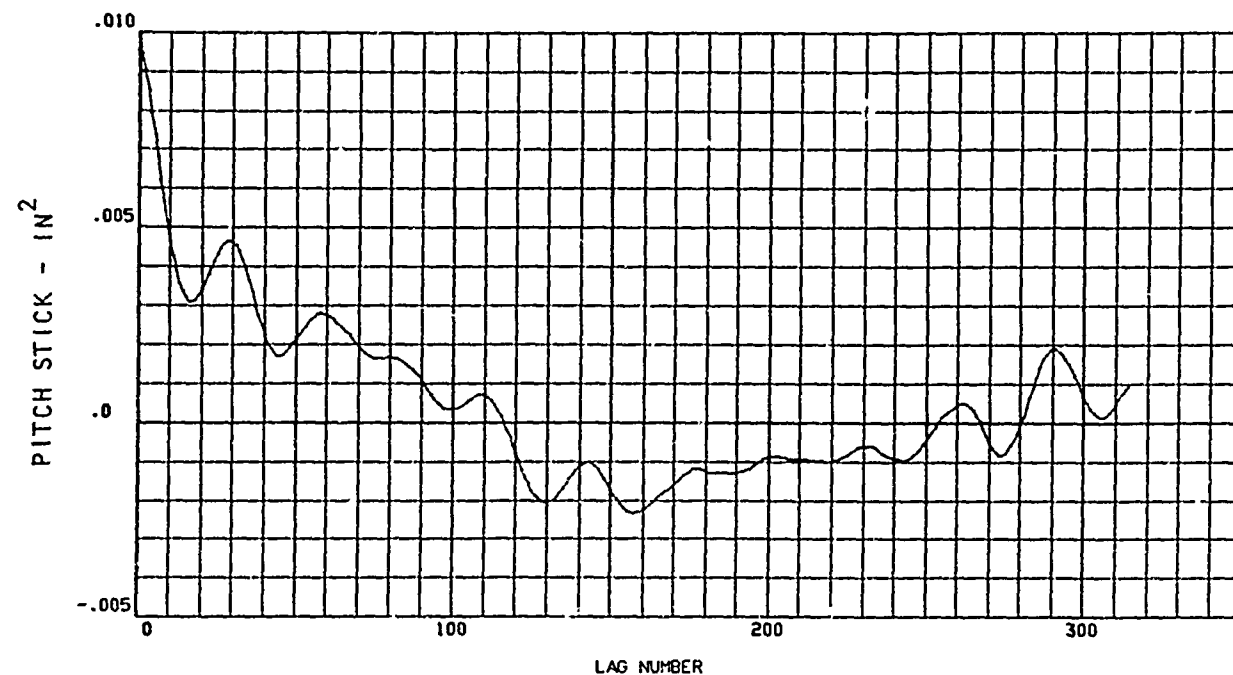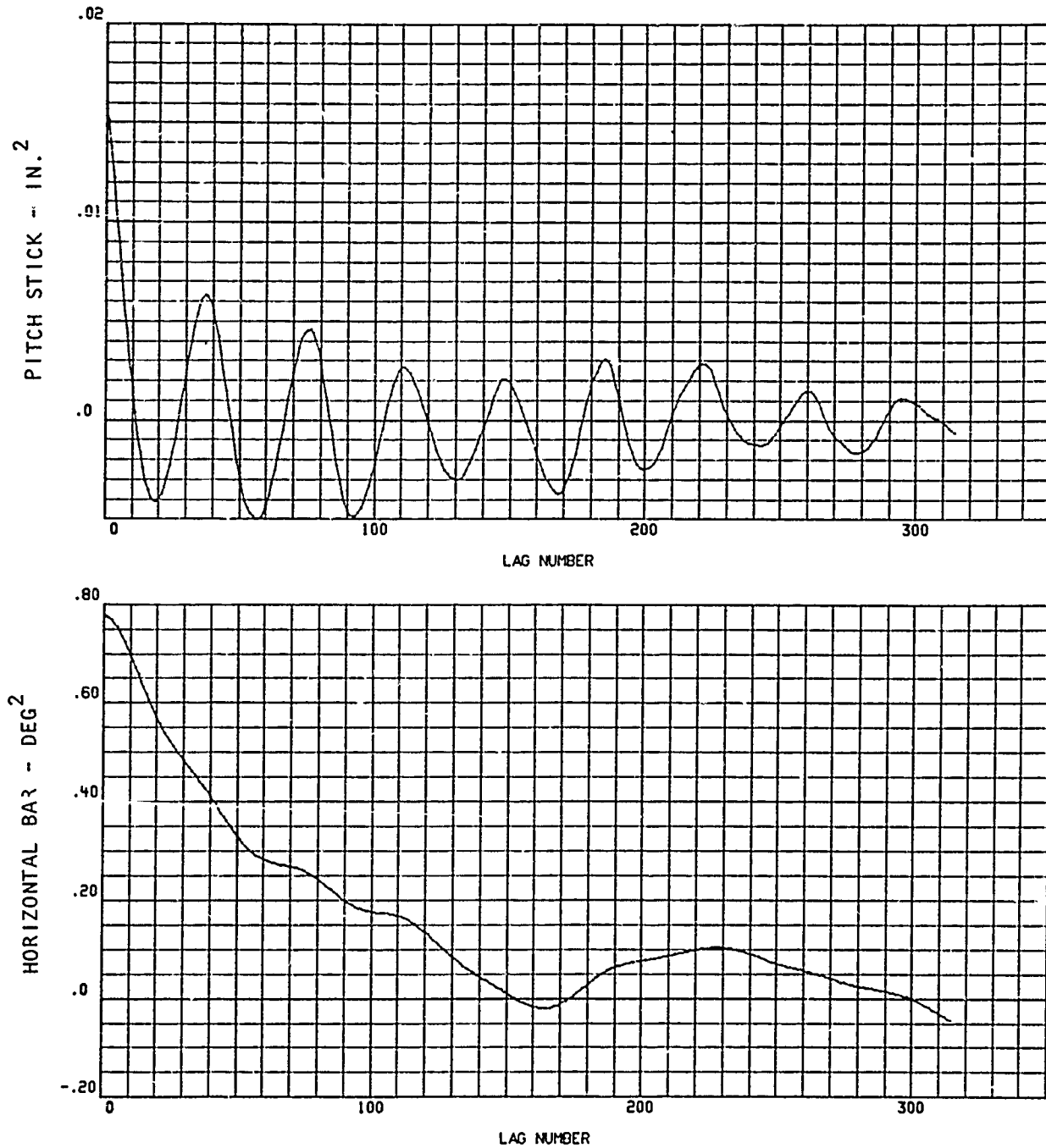
AUTO CORRELATION FUNCTIONS

Figure 91.   AR Simulation Run No. 01A64 Data (Cont)
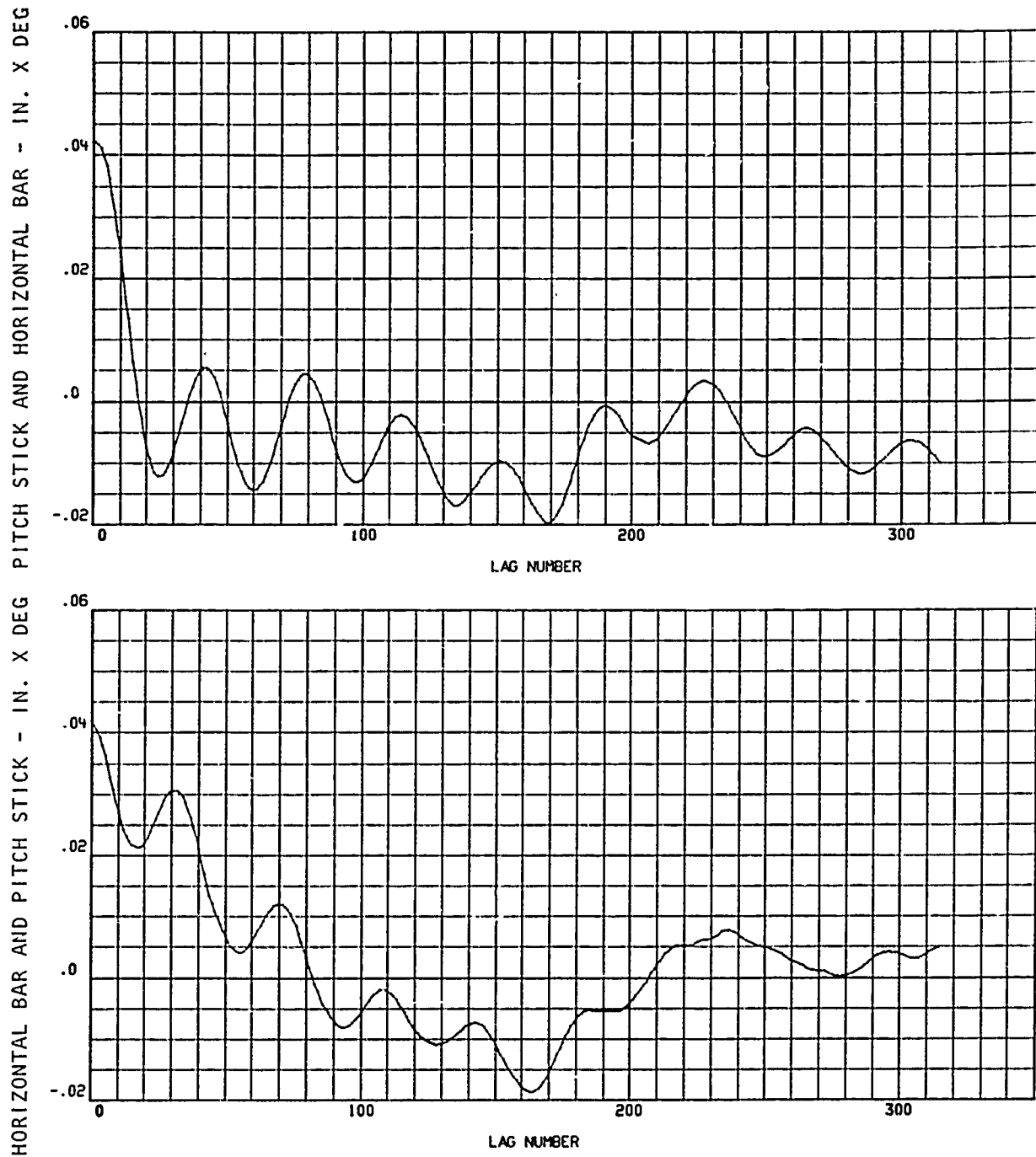
353

CROSS CORRELATION FUNCTIONS

Figure 91. AR Simulation Run No. 01A64 Data (Cont)

354

01A64 REFUEL ANALYSIS.

SPECTRAL DENSITY FUNCTIONS

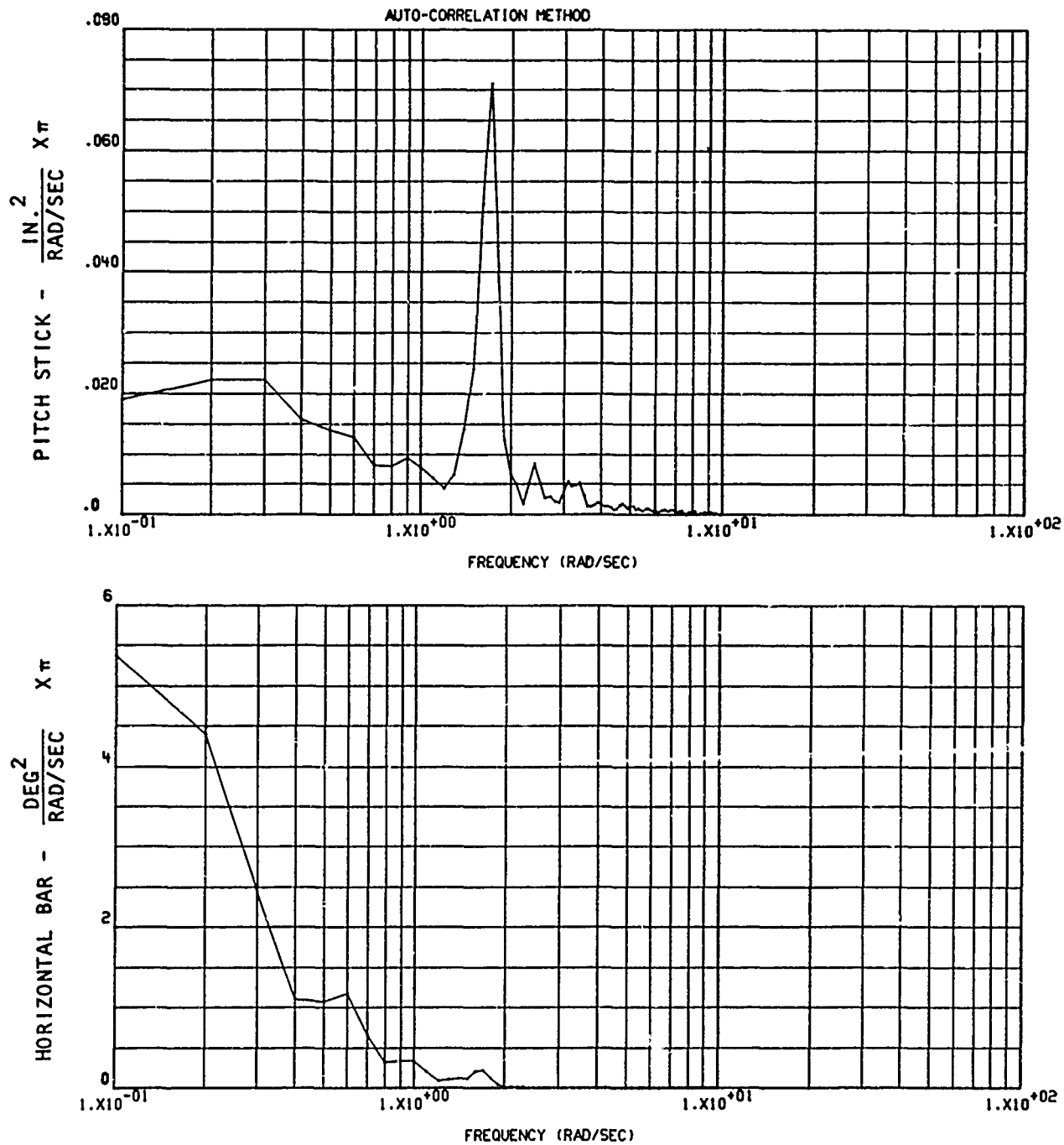Figure 91. AR Simulation Run No. 01A64 Data (Cont)

355
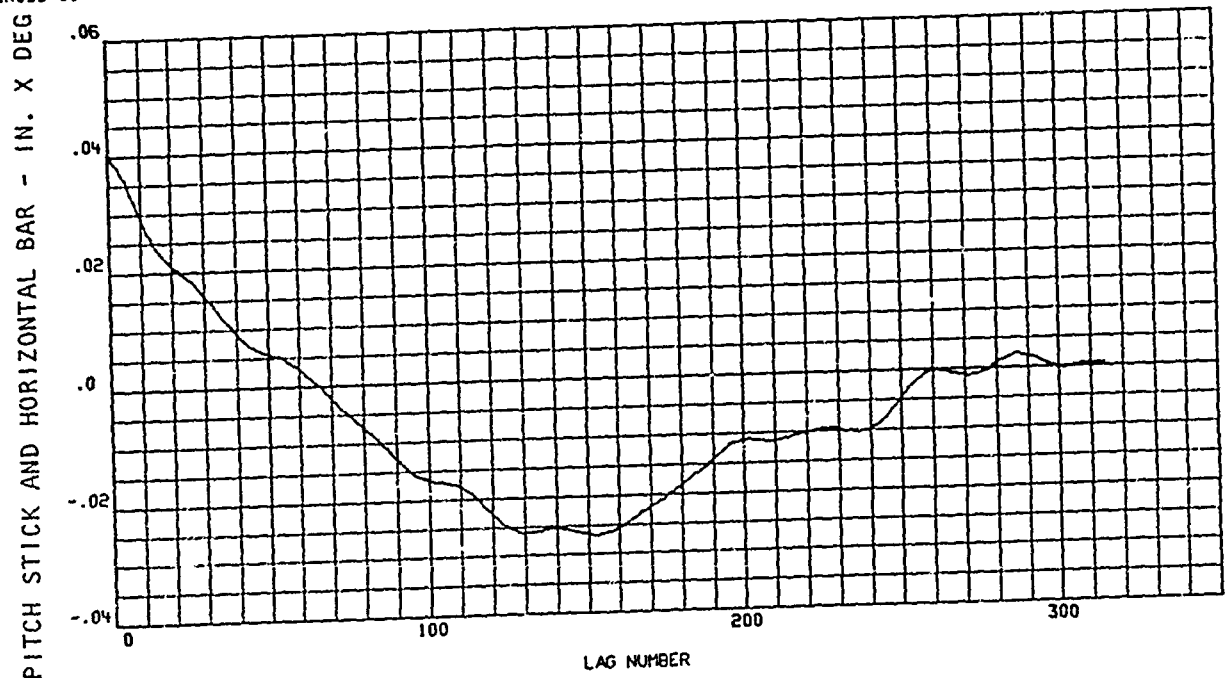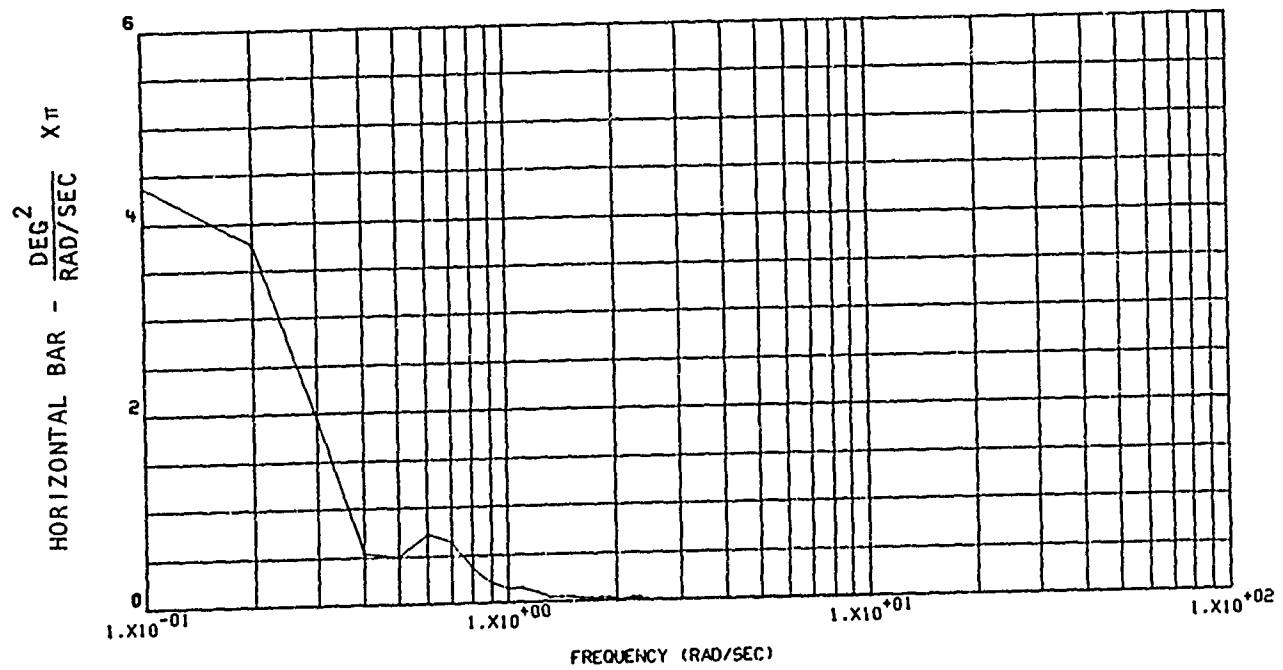
01A64 REFUEL ANALYSIS.

Figure 91. AR Simulation Run No. 01A64 Data (Cont)

356

Figure 91.   AR Simulation Run No. 01A64 Data (Concl)

Figure 92. AR Simulation Run No. 01A46 Data

AUTO CORRELATION FUNCTIONS

Figure 92. AR Simulation Run No. 01A46 Data (Cont)

01A46 REFUEL ANALYSIS.

CROSS CORRELATION FUNCTIONS

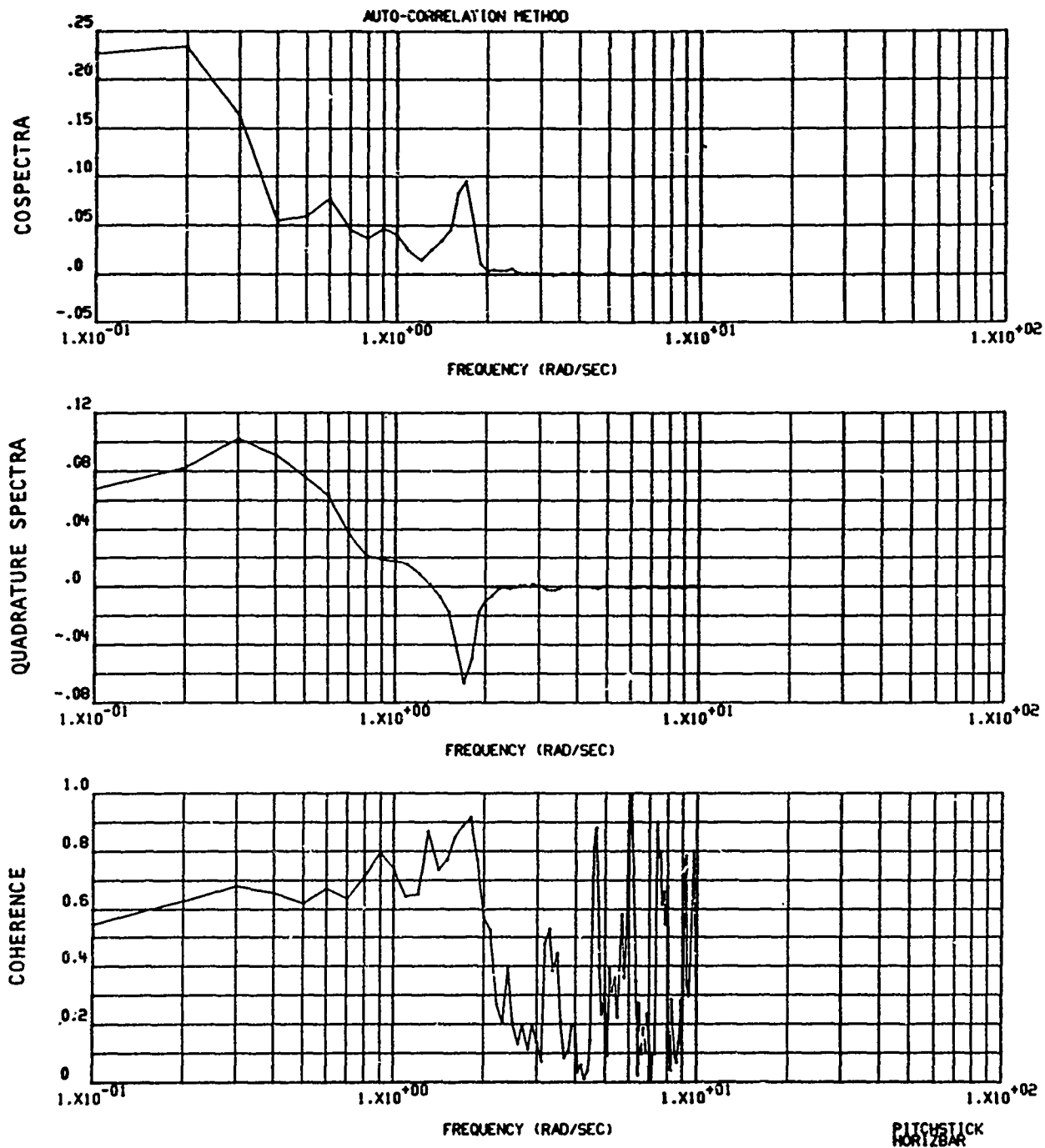Figure 92.   AR Simulation Run No. 01A46 Data (Cont)

Figure 92. AR Simulation Run No. 01A46 Data (Cont)

361

01A46 REFUEL ANALYSIS.

Figure 92.   AR Simulation Run No. 01A46 Data (Cont)
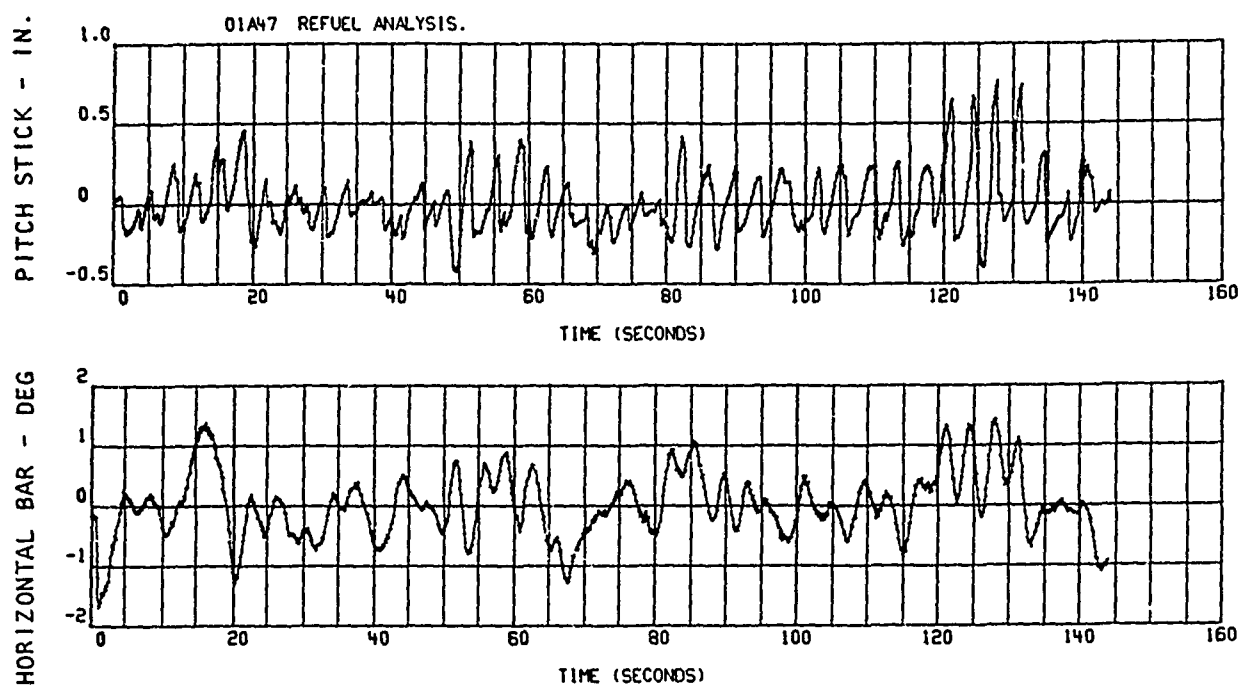
362

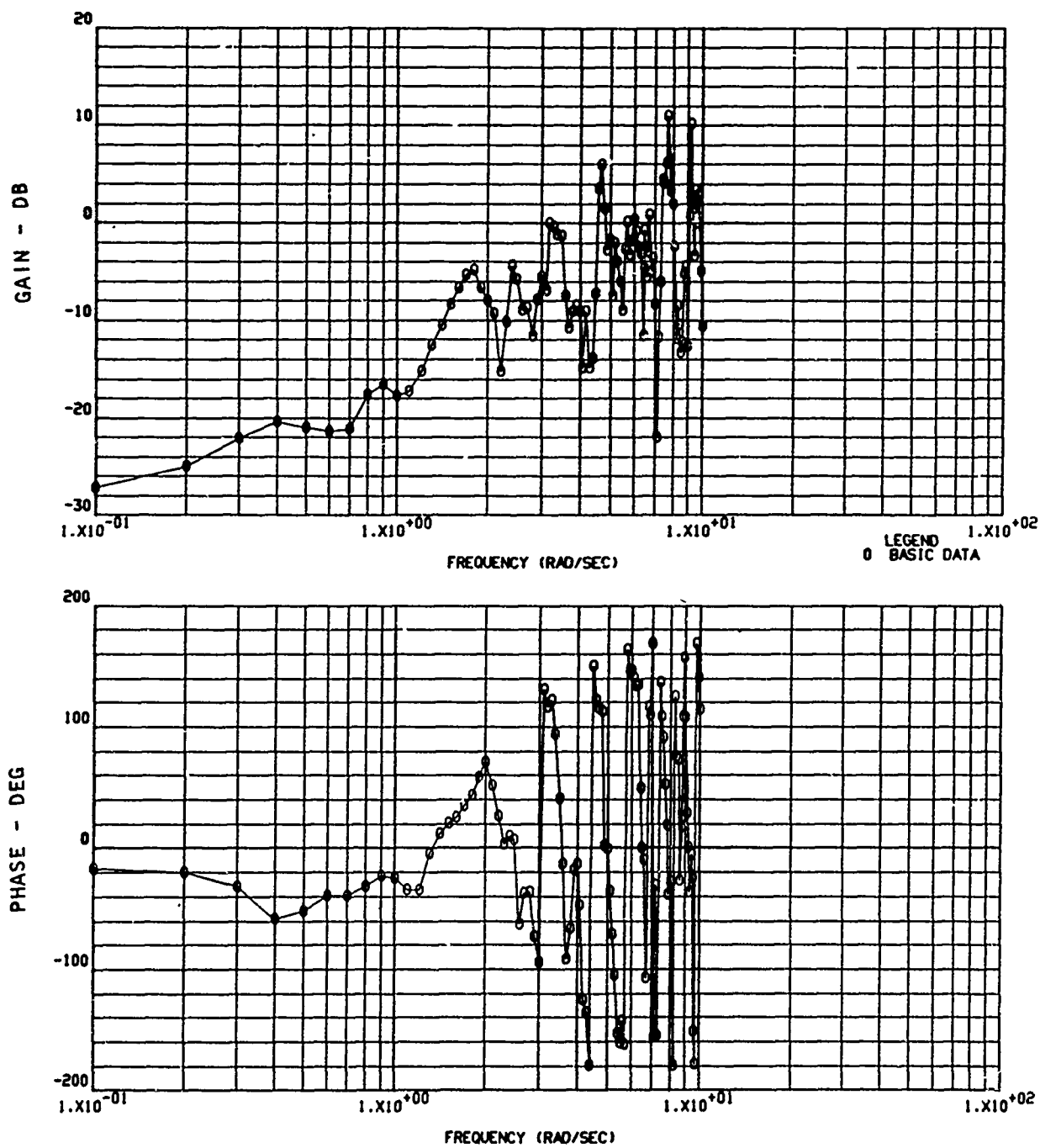Figure 92.   AR Simulation Run No. 01A46 Data

363

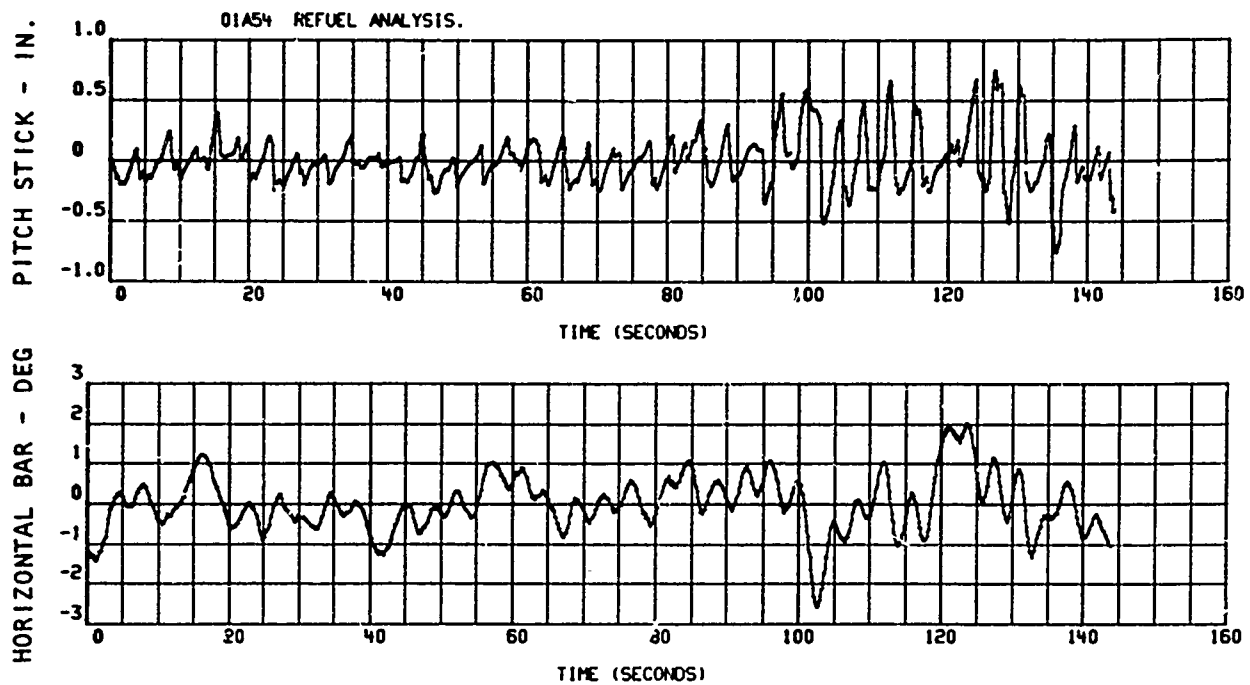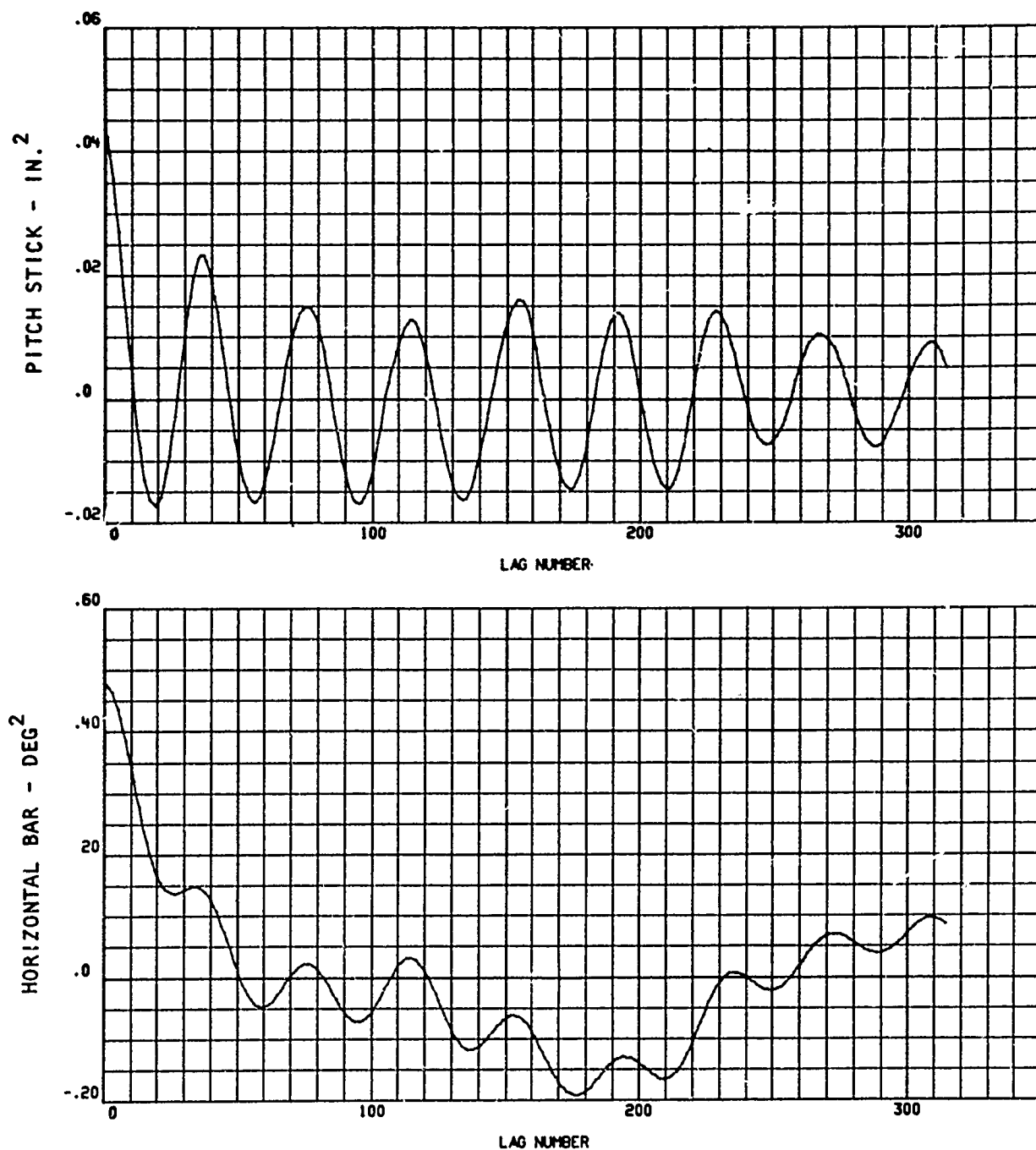Figure 93.   AR Simulation Run No. 01A47 Data

Figure 93. AR Simulation Run No. 01A47 Data (Cont)

365

01A47 REFUEL ANALYSIS.

CROSS CORRELATION FUNCTIONS

Figure 93. AR Simulation Run No. 01A47 Data (Cont)

366

Figure 93.   AR Simulation Run No. 01A47 Data (Cont)

367

Figure 93. AR Simulation Run No. 01A47 Data (Cont)

368
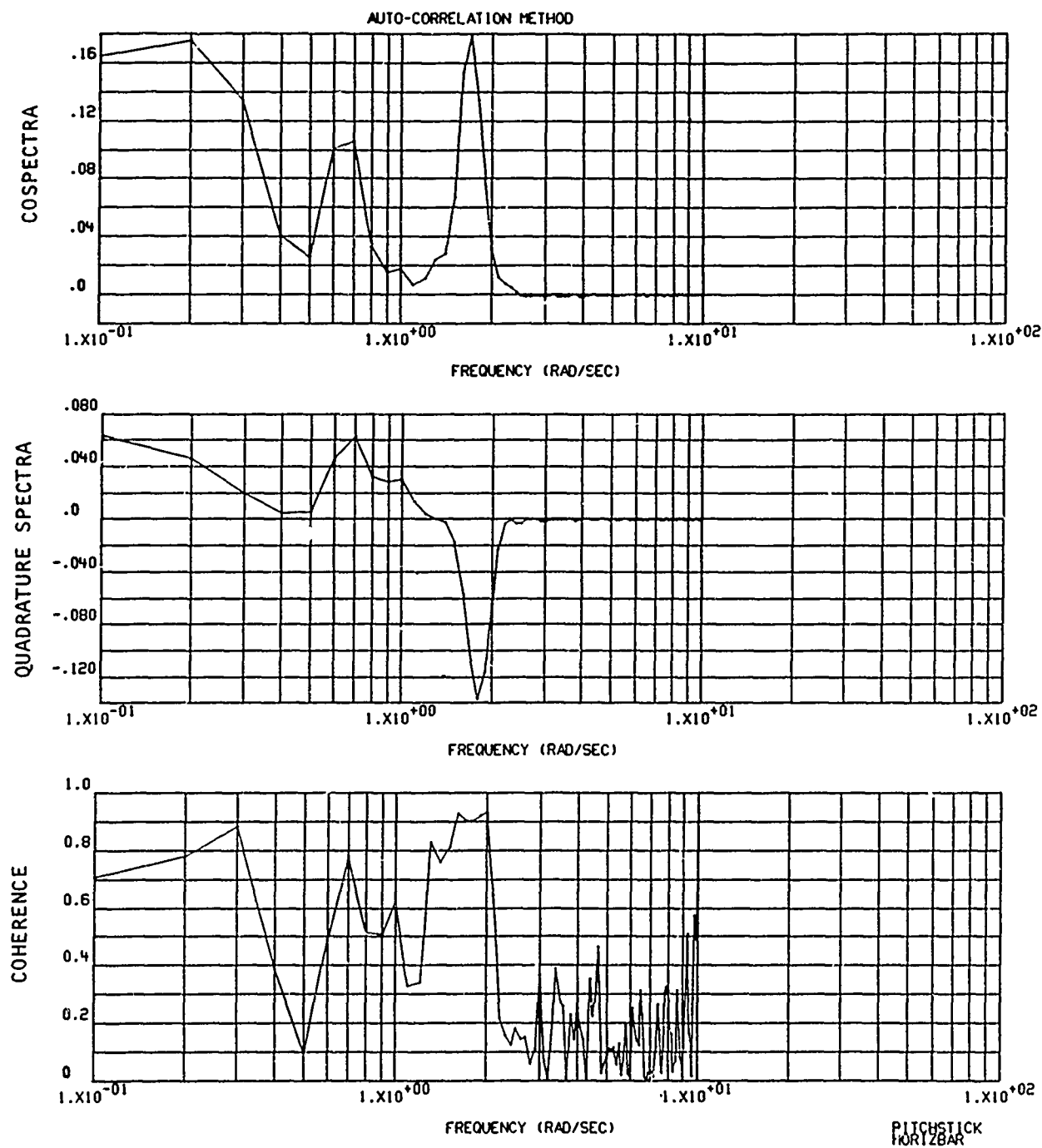
01A47 REFUEL ANALYSIS.

Figure 93. AR Simulation Run No. 01A47 Data (Concl)

369

Figure 94. AR Simulation Run No. 01A48 Data

AUTO CORRELATION FUNCTIONS

Figure 94. AR Simulation Run No. 01A48 Data (Cont)

371

Figure 94. AR Simulation Run No. 01A48 Data (Cont)

Figure 94. AR Simulation Run No. 01A48 Data (Cont)
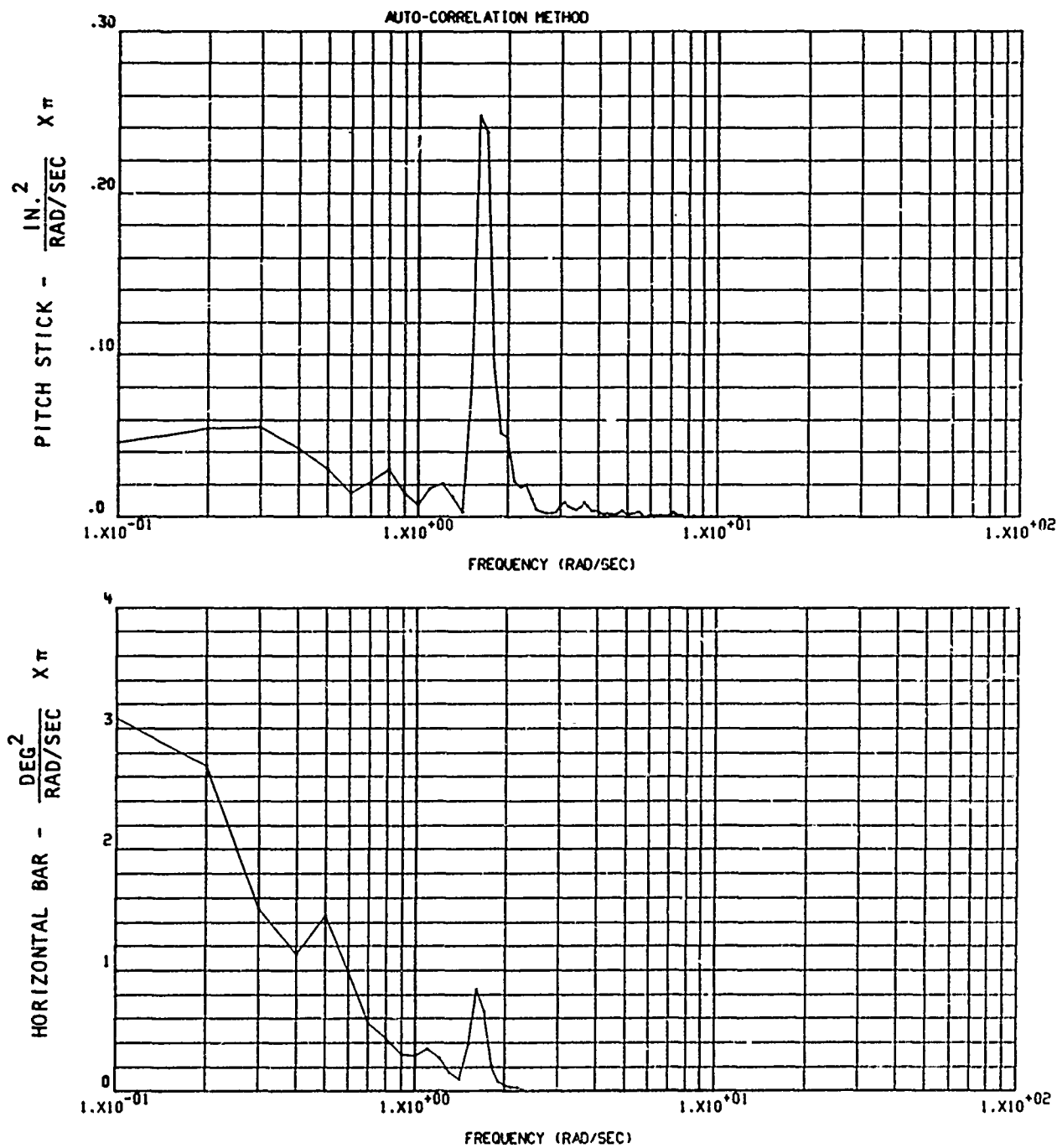
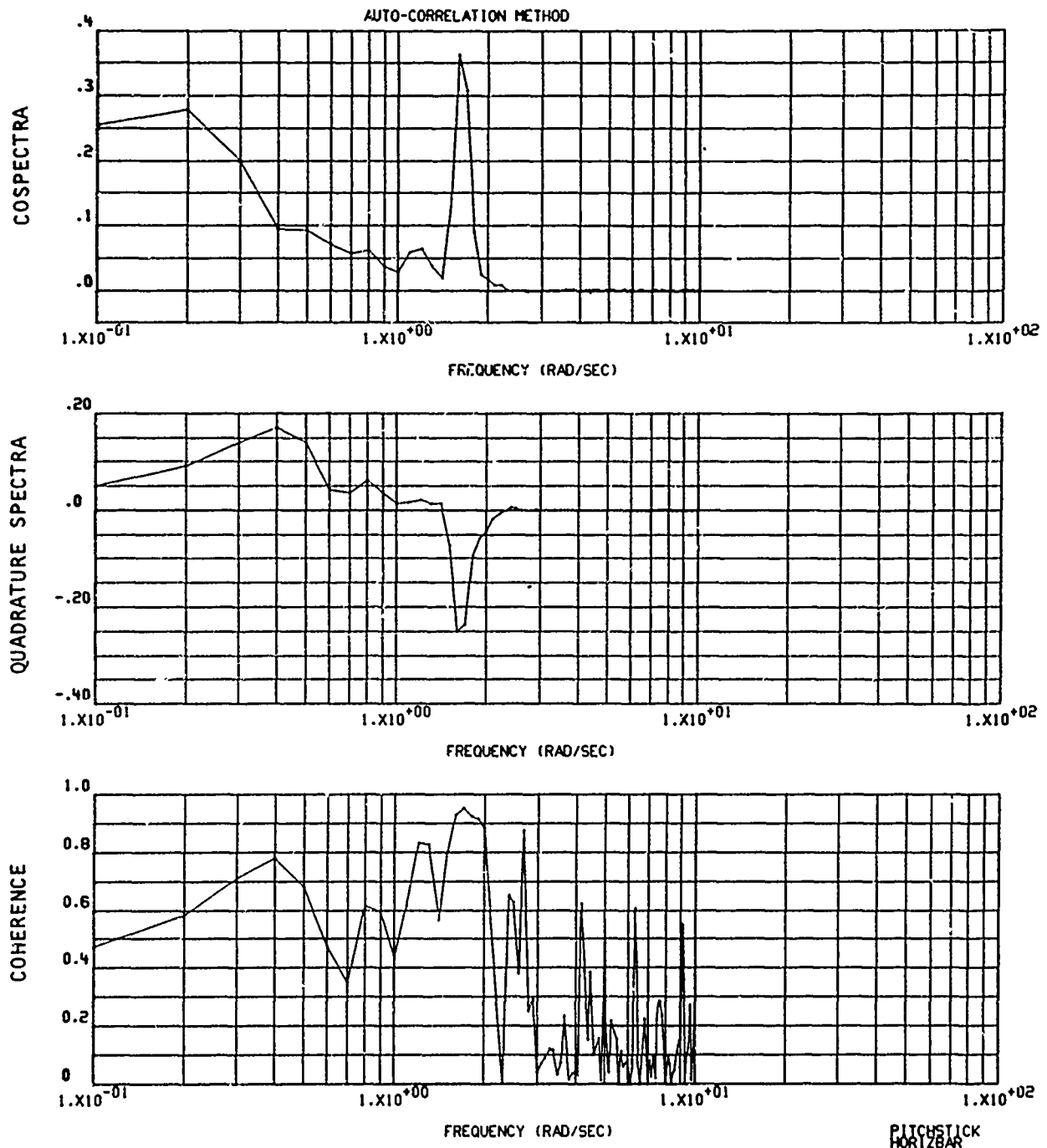01A48 REFUEL ANALYSIS.

AUTO-CORRELATION METHOD

Figure 94. AR Simulation Run No. 01A48 Data (Cont)
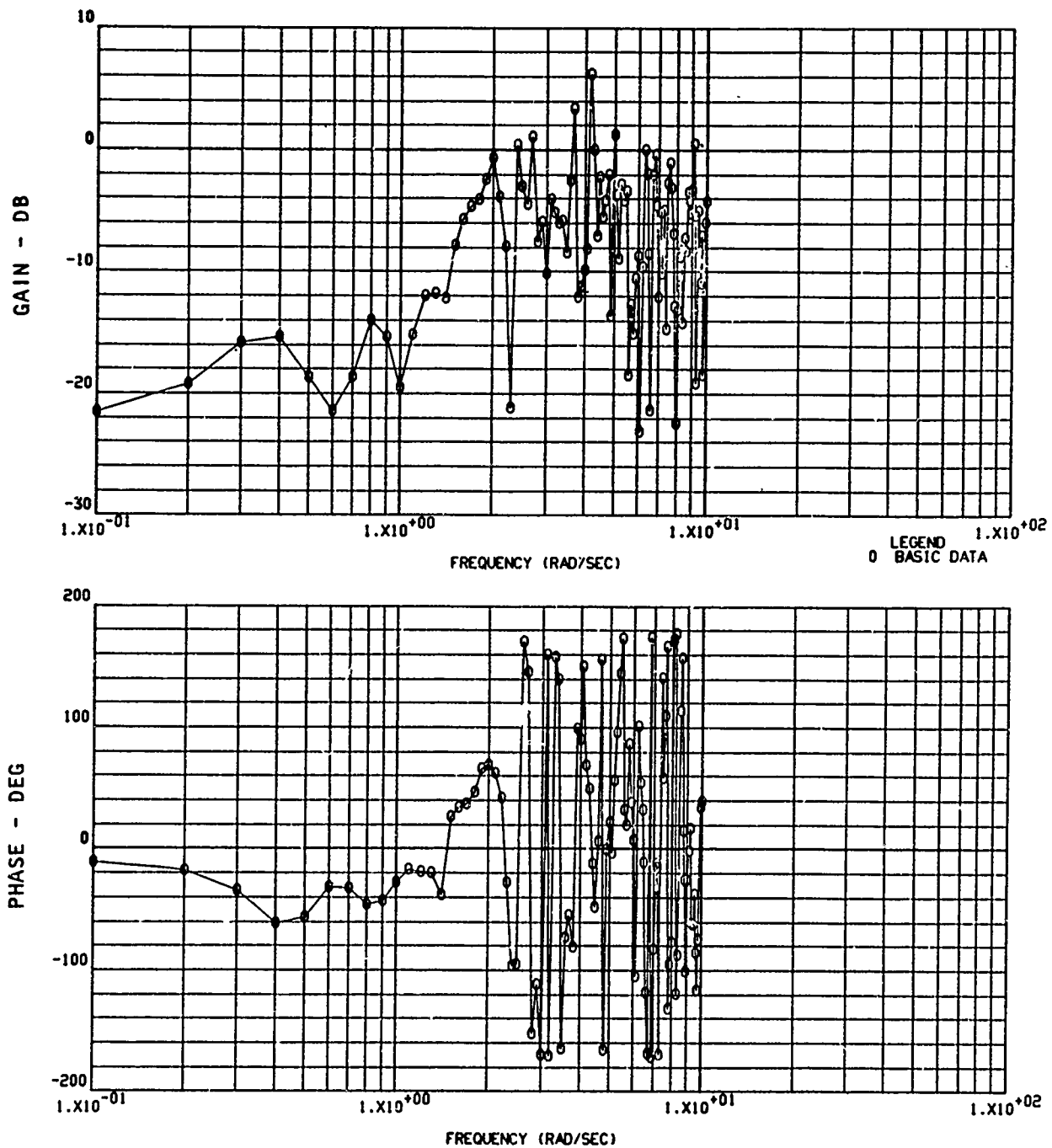
374

01A48 REFUEL ANALYSiS.

Figure 94. AR Simulation Run No. 01A48 Data (Concl)

375
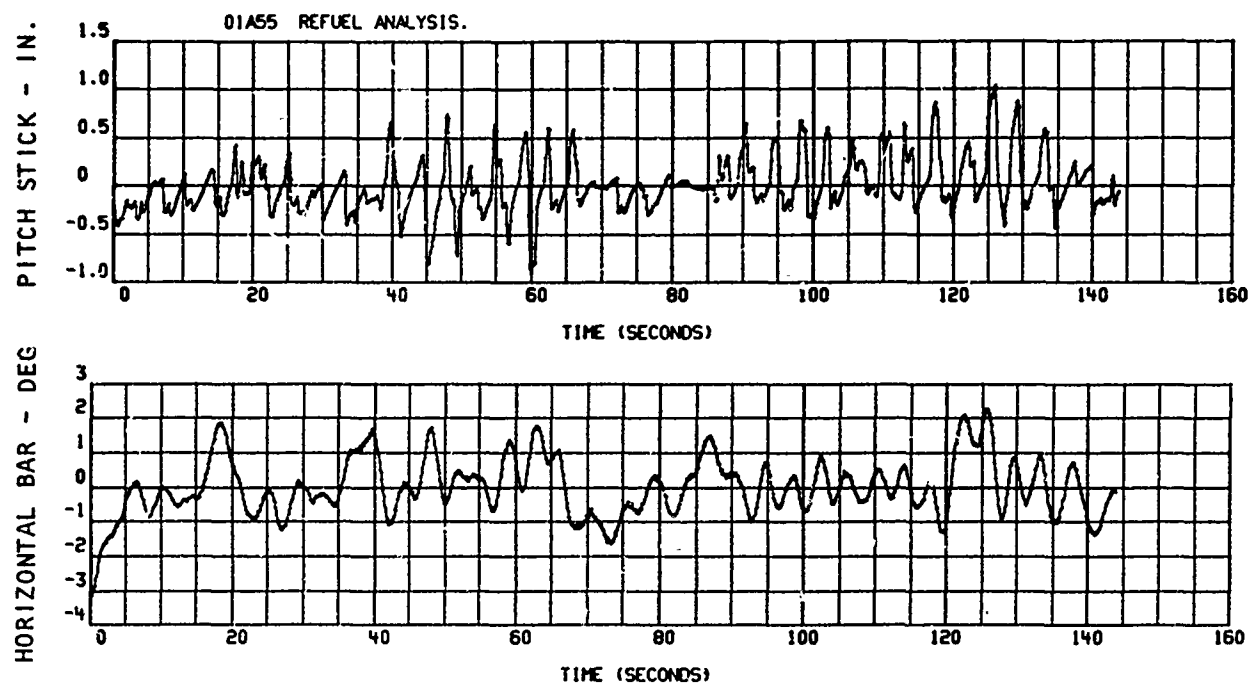
Figure 95. AR Simulation Run No. 01A53 Data

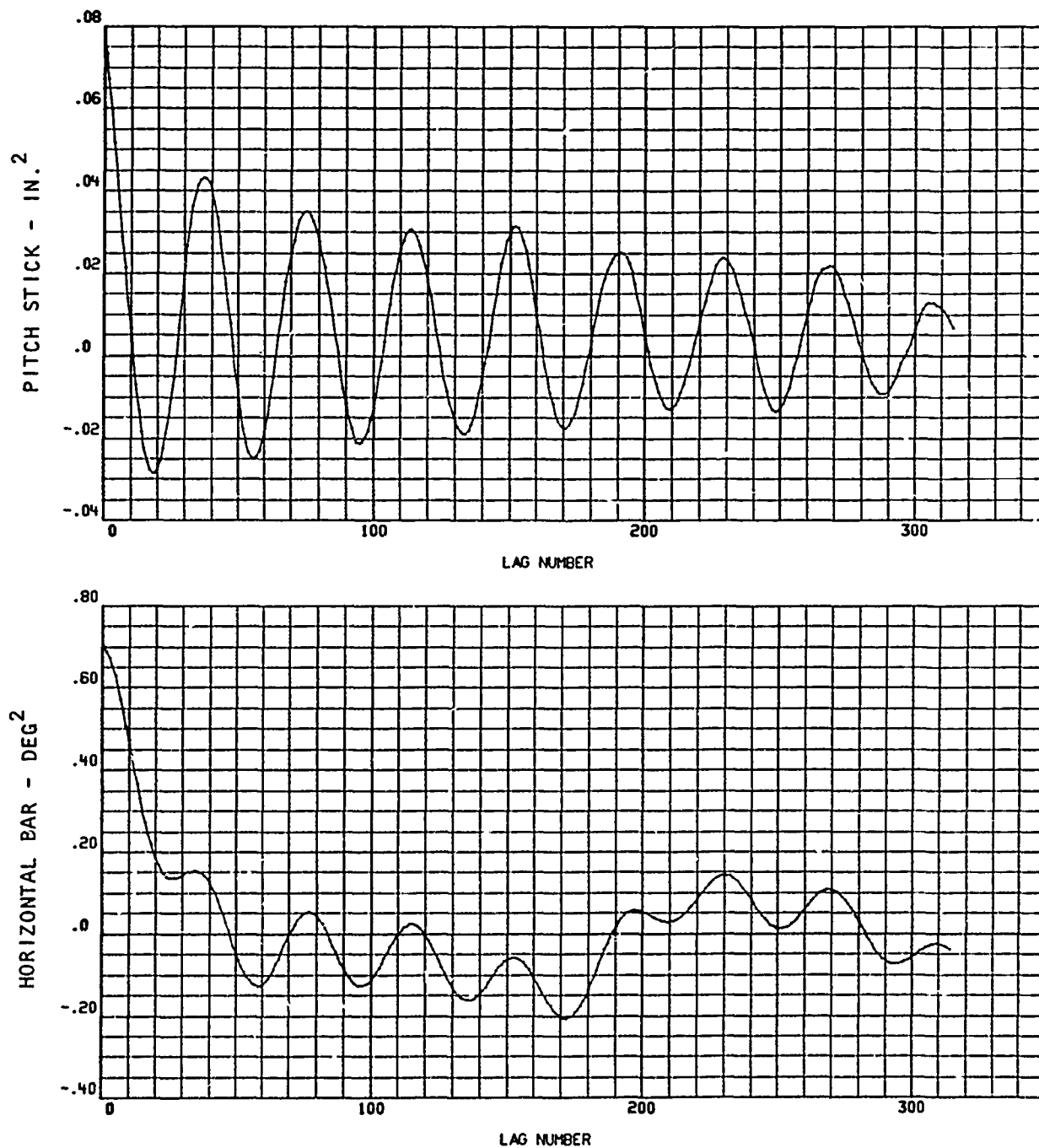01A53 REFUEL ANALYSIS.

AUTO CORRELATION FUNCTIONS

Figure 95. AR Simulation Run No. 01A53 Data (Cont)

377

01A53 REFUEL ANALYSIS.

CROSS CORRELATION FUNCTIONS

Figure 95. AR Simulation Run No. 01A53 Data (Cont)

378

01A53 REFUEL ANALYSIS.

SPECTRAL DENSITY FUNCTIONS

AUTO-CORRELATION METHOD

Figure 95. AR Simulation Run No. 01A53 Data (Cont)

379

01A53 REFUEL ANALYSIS.

Figure 95. AR Simulation Run No. 01A53 Data (Cont)

380

01A53 PEFUEL ANALYSIS.

Figure 95. AR Simulation Run No. 01A53 Data (Concl)

Figure 96. AR Simulation Run No. 01A54 Data

AUTO CORRELATION FUNCTIONS

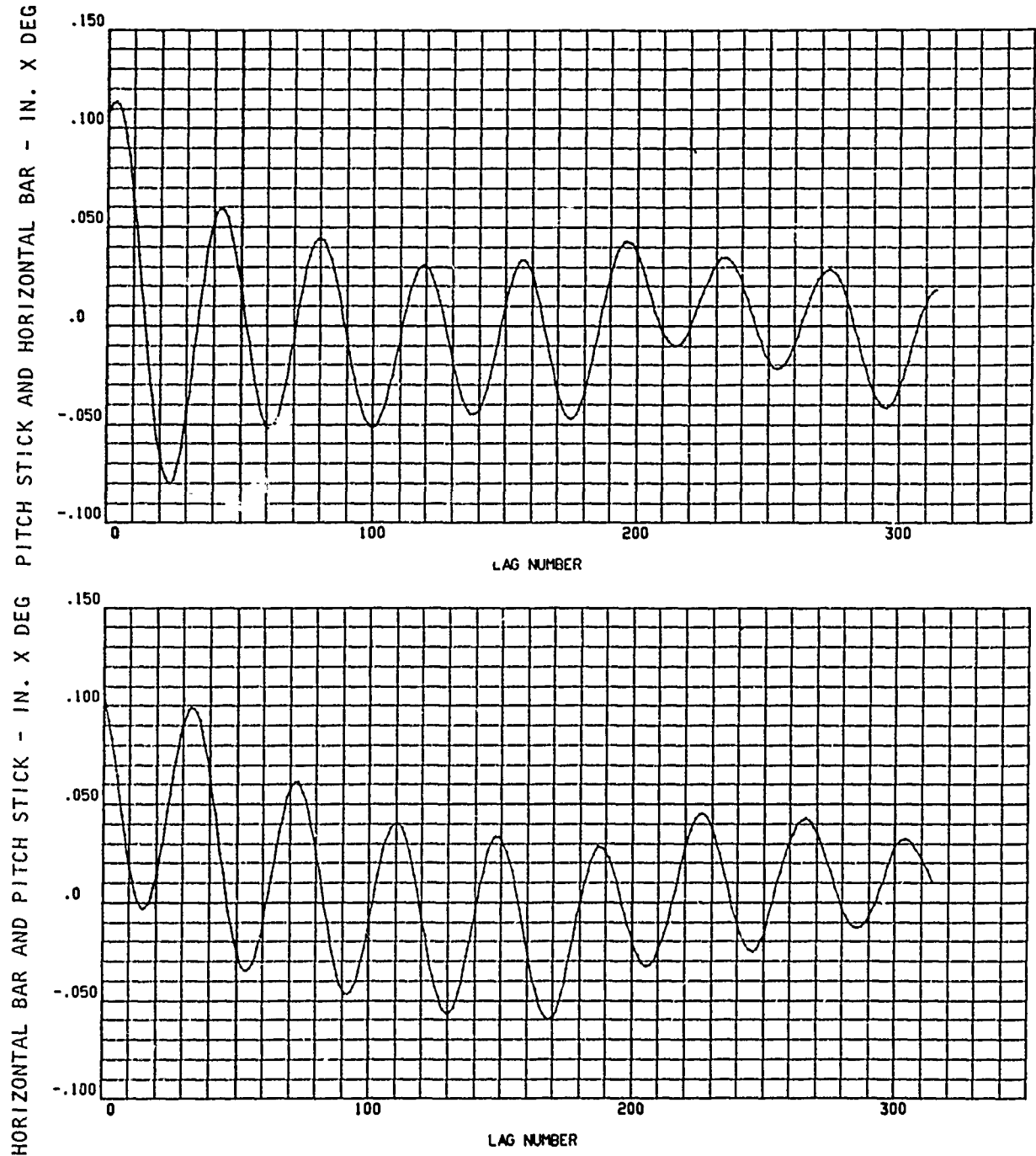Figure 96.   AR Simulation Run No. 01A54 Data (Cont)

383

Figure 96.   AR Simulation Run No. 01A54 Data (Cont)

01A54   REFUEL ANALYSIS.

SPECTRAL DENSITY FUNCTIONS
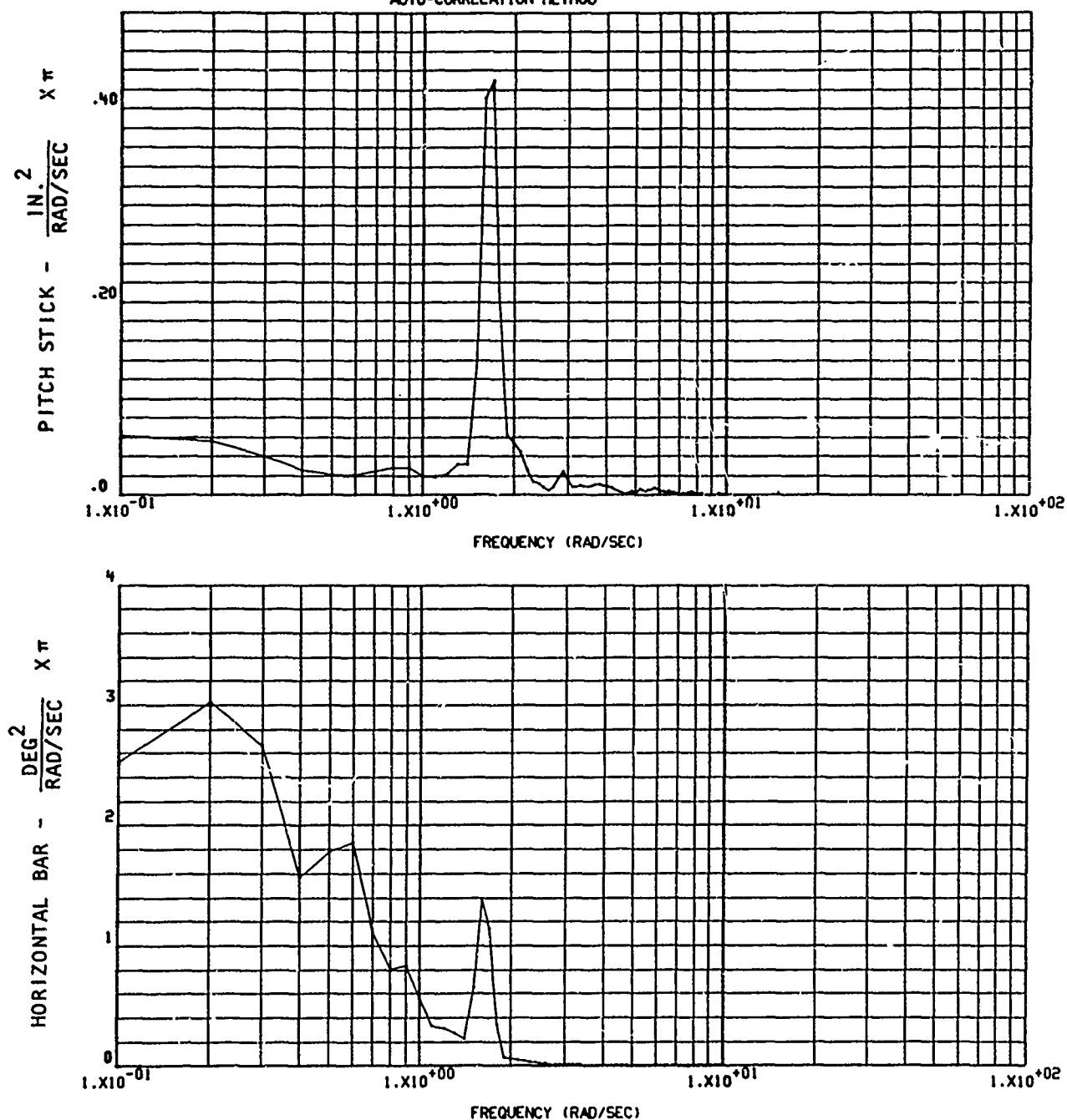
AUTO-CORRELATION METHOD

Figure 96.   AR Simulation Run No. 01A54 Data (Cont)
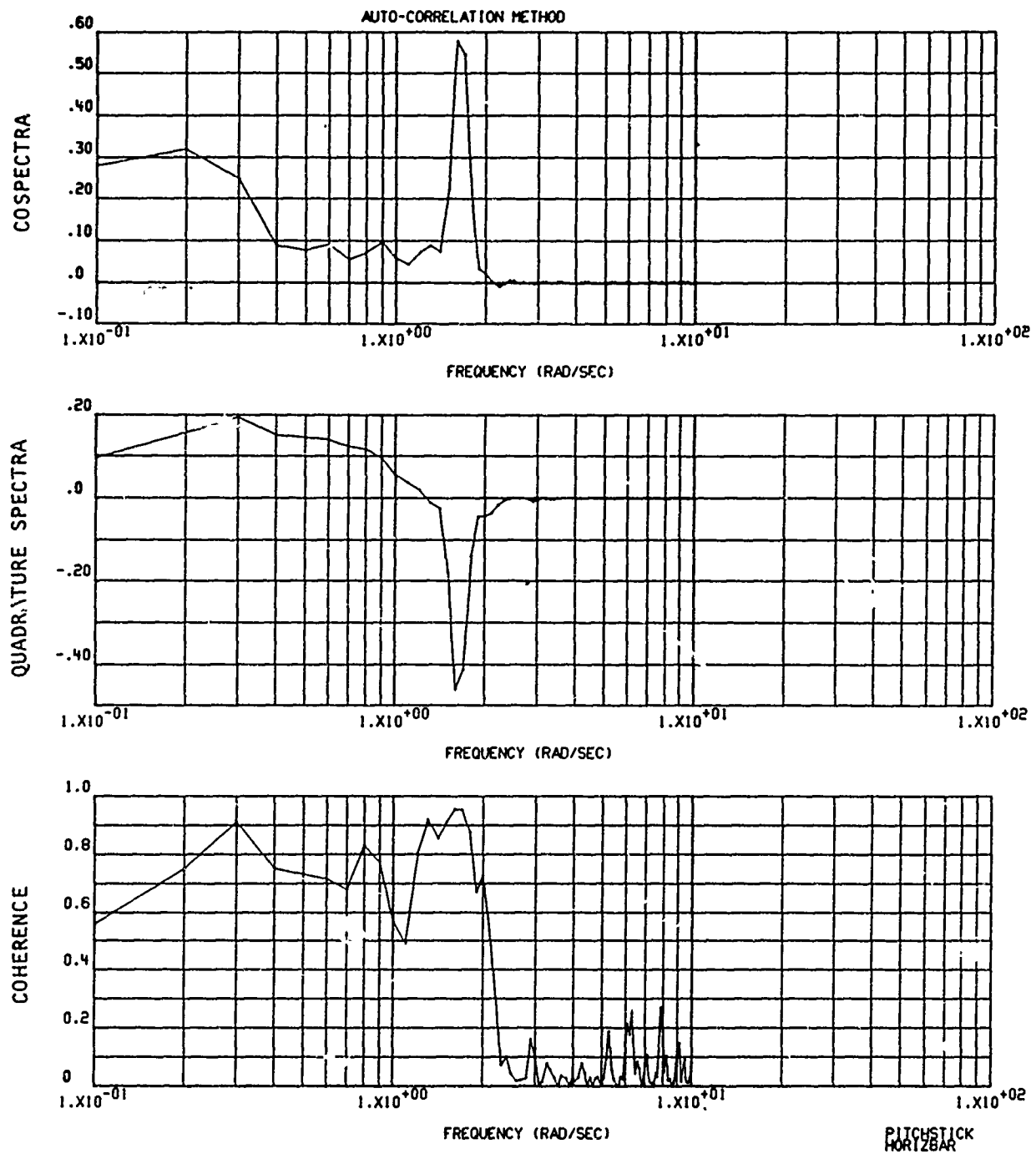
385

01A54 REFUEL ANALYSIS.

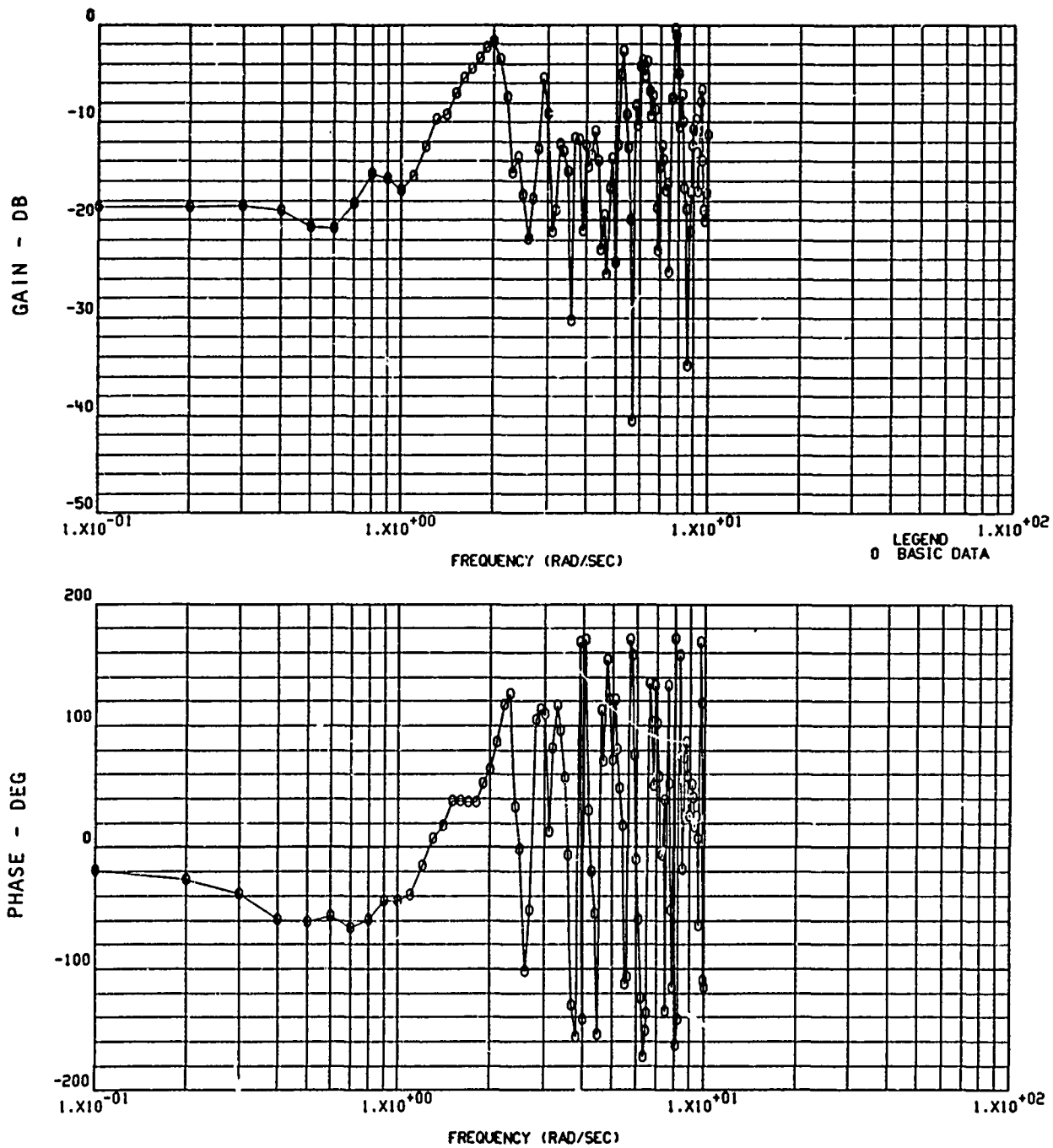Figure 96. AR Simulation Run No. 01A54 Data (Cont)

386

01A54 REFUEL ANALYSIS.

Figure 96.   AR Simulation Run No. 01A54 Data (Concl)

387

Figure 97. AR Simulation Run No. 01A55 Data

388

AUTO CORRELATION FUNCTIONS

Figure 97.   AR Simulation Run No. 01A55 Data (Cont)

389

Figure 97. AR Simulation Run No. 01A55 Data (Cont)

01A55 REFUEL ANALYSIS.

SPECTRAL DENSITY FUNCTIONS

AUTO-CORRELATION METHOD

Figure 97. AR Simulation Run No. 01A55 Data (Cont)

391

01A55 REFUEL ANALYSIS.

Figure 97.   AR Simulation Run No. 01A55 Data (Cont)
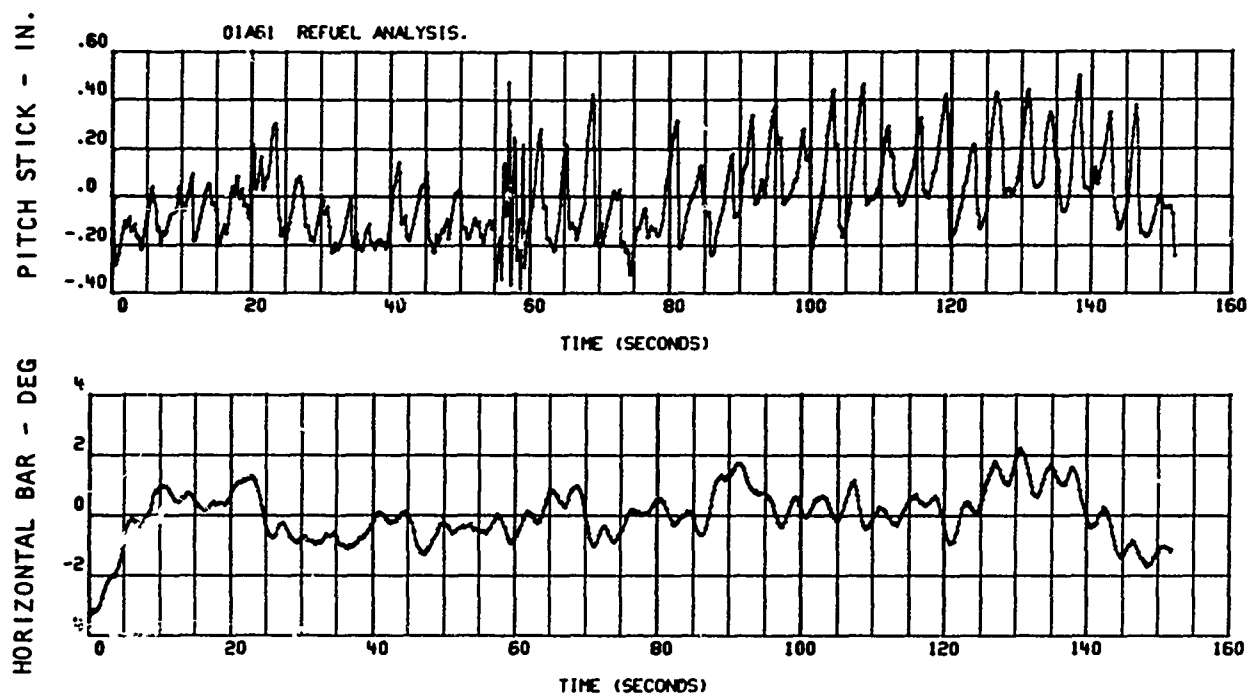
392

Figure 97. AR Simulation Run No. 01A55 Data (Concl)

Figure 98. AR Simulation Run No. 01A61 Data

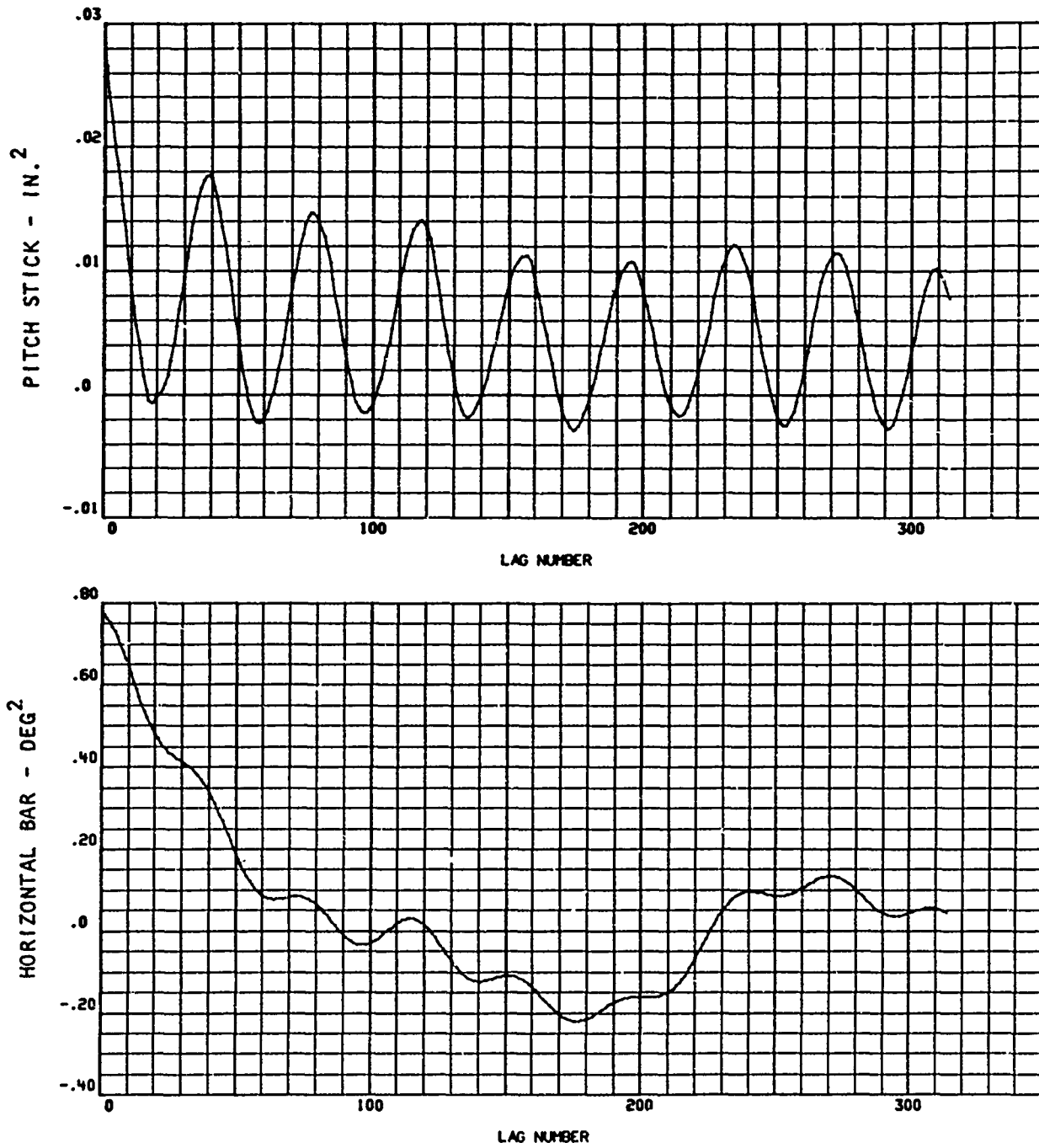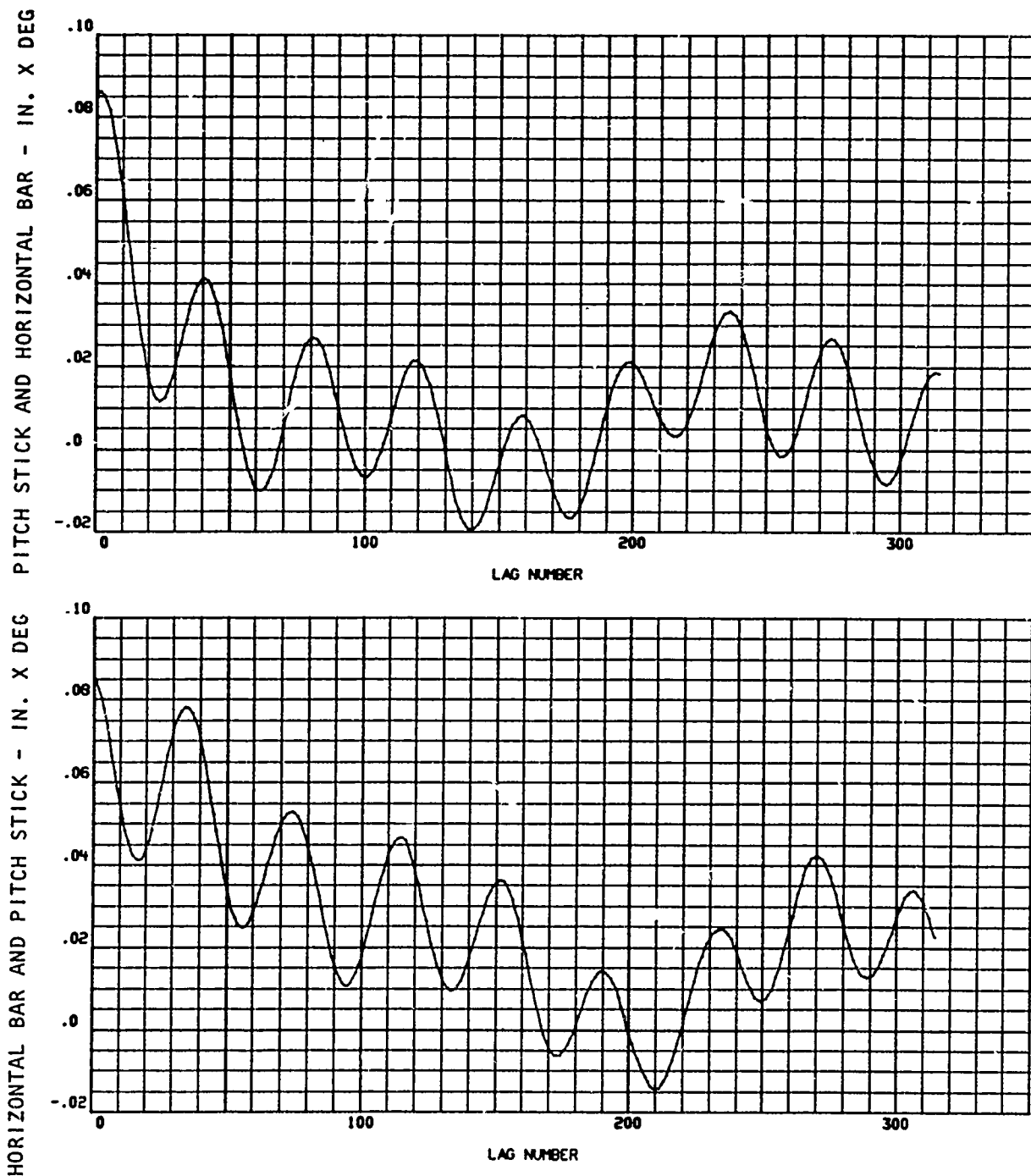Figure 98. AR Simulation Run No. 01A61 Data (Cont)

395

Figure 98. AR Simulation Run No. 01A61 Data (Cont)

01A61 REFUEL ANALYSIS.

SPECTRAL DENSITY FUNCTIONS
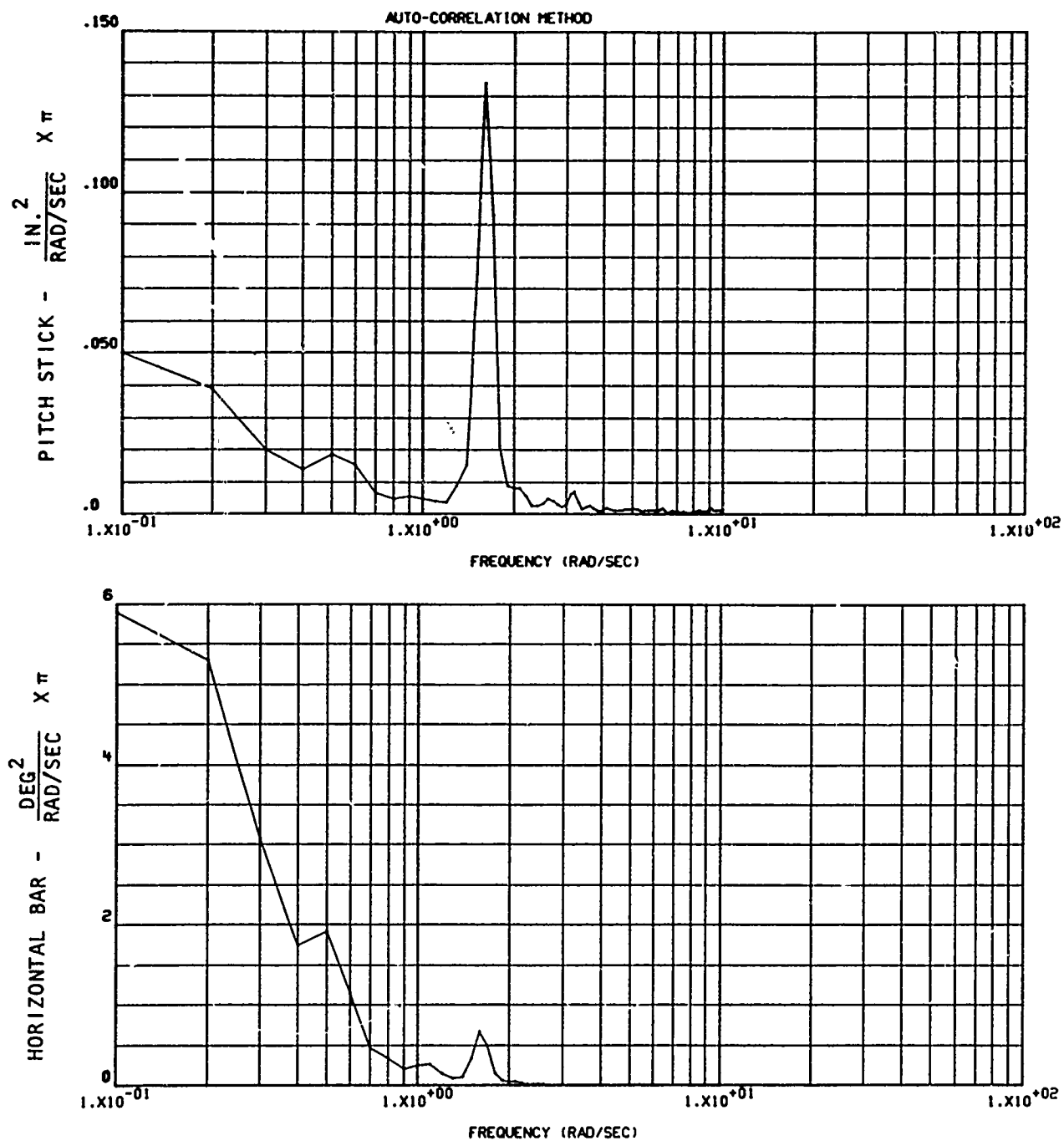
Figure 98. AR Simulation Run No. 01A61 Data (Cont)
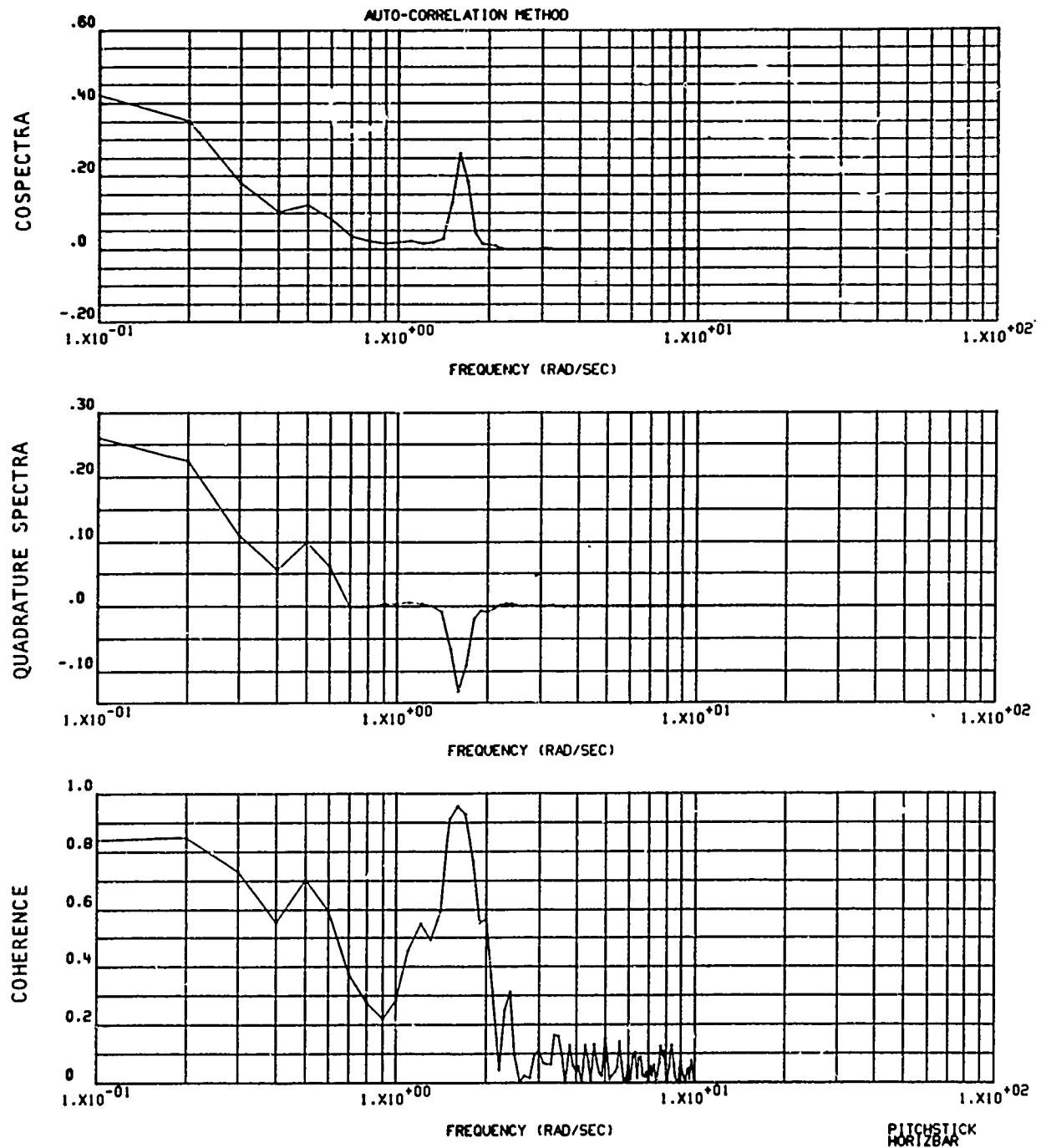
397

Figure 98. AR Simulation Run No. 01A61 Data (Cont)

01A61 REFUEL ANALYSIS.

Figure 98. AR Simulation Run No. 01A61 Data (Concl)

399

Figure 99.   AR Simulation Run No. 01A62 Data

Figure 99. AR Simulation Run No. 01A62 Data (Cont)

401

01A62 REFUEL ANALYSIS.

CROSS CORRELATION FUNCTIONS

Figure 99. AR Simulation Run No. 01A62 Data (Cont)

01A62 REFUEL ANALYSIS.

SPECTRAL DENSITY FUNCTIONS

Figure 99. AR Simulation Run No. 01A62 Data (Cont)

403

01A62 REFUEL ANALYSIS.

Figure 99. AR Simulation Run No. 01A62 Data (Cont)
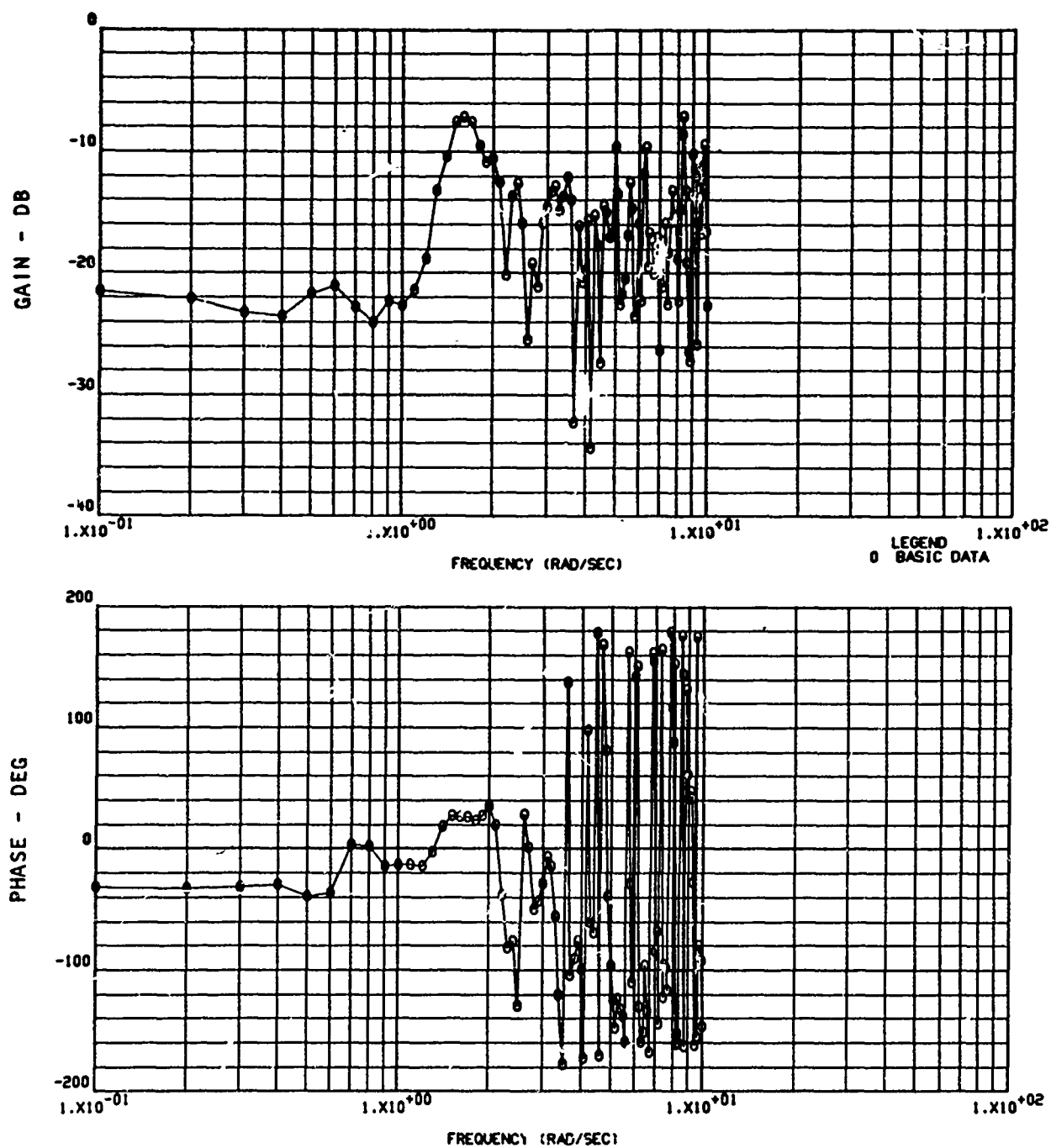
404

01A62 REFUEL ANALYSIS.
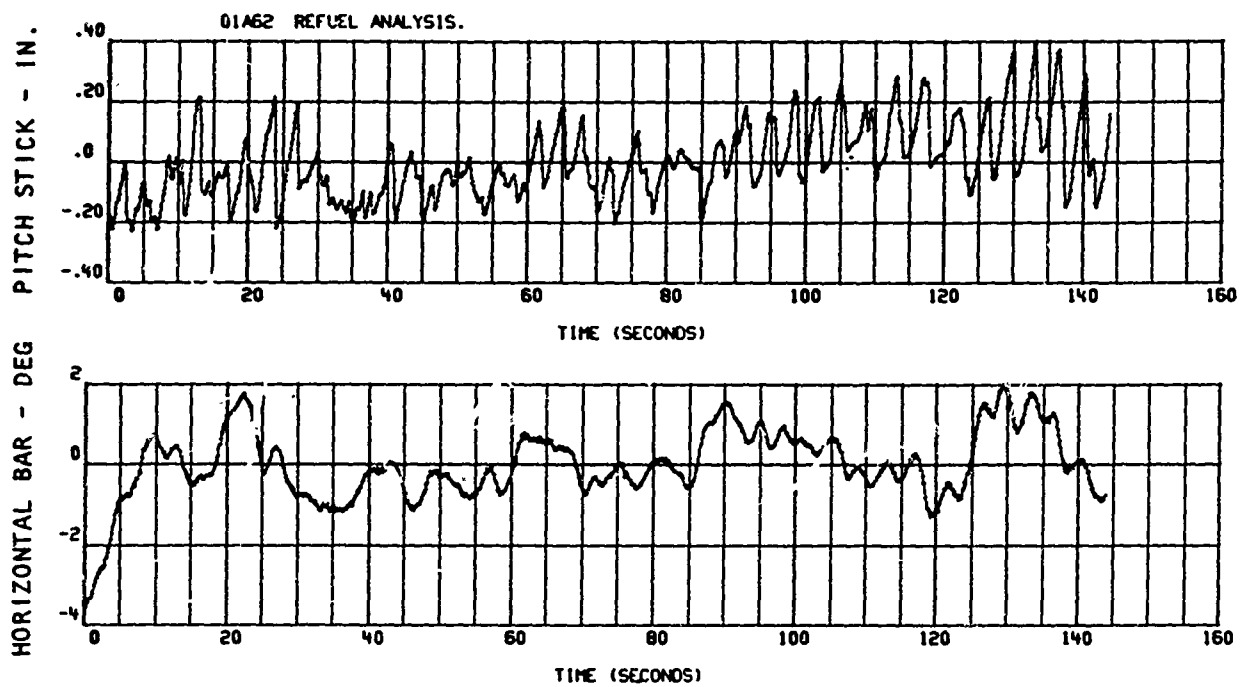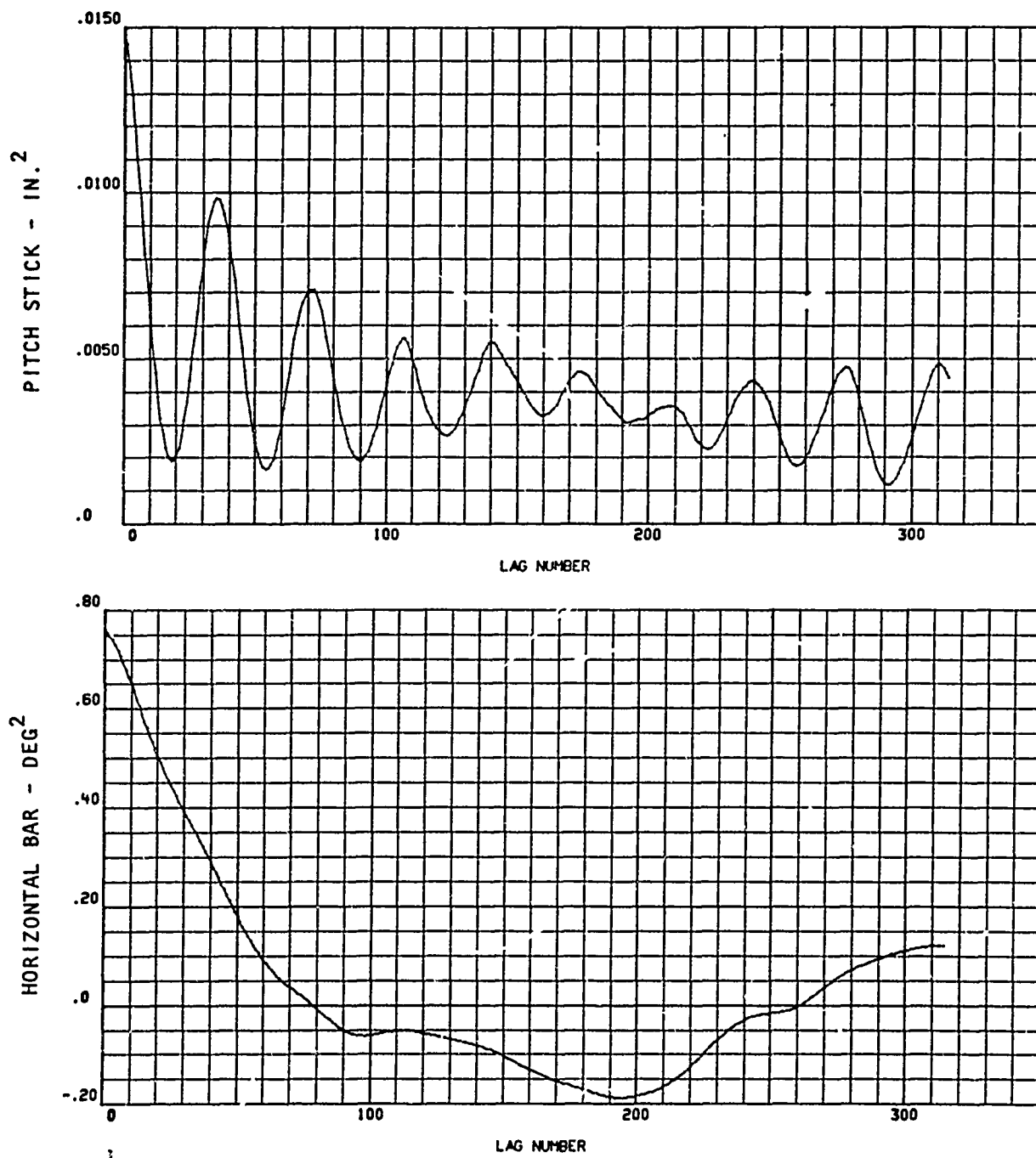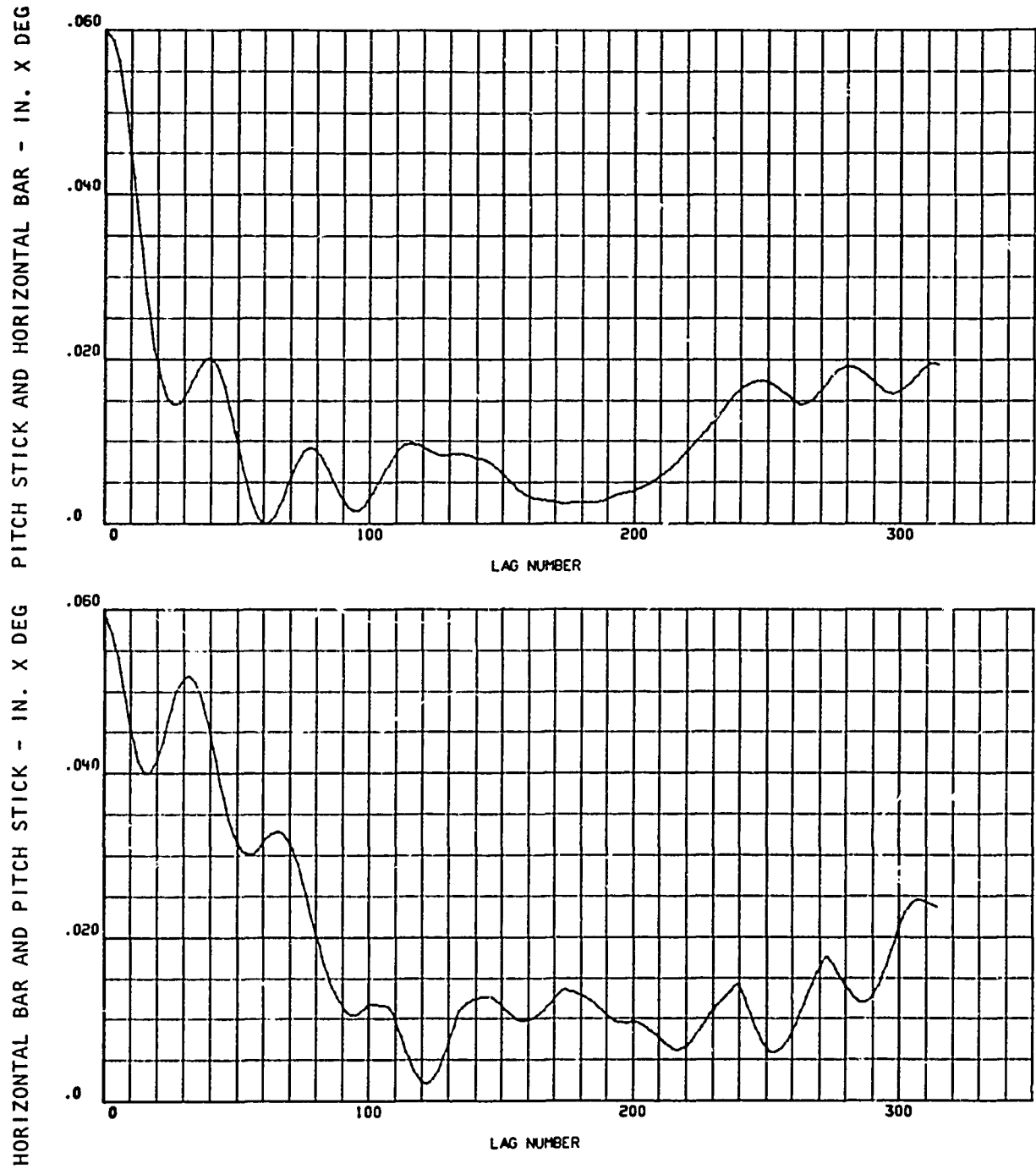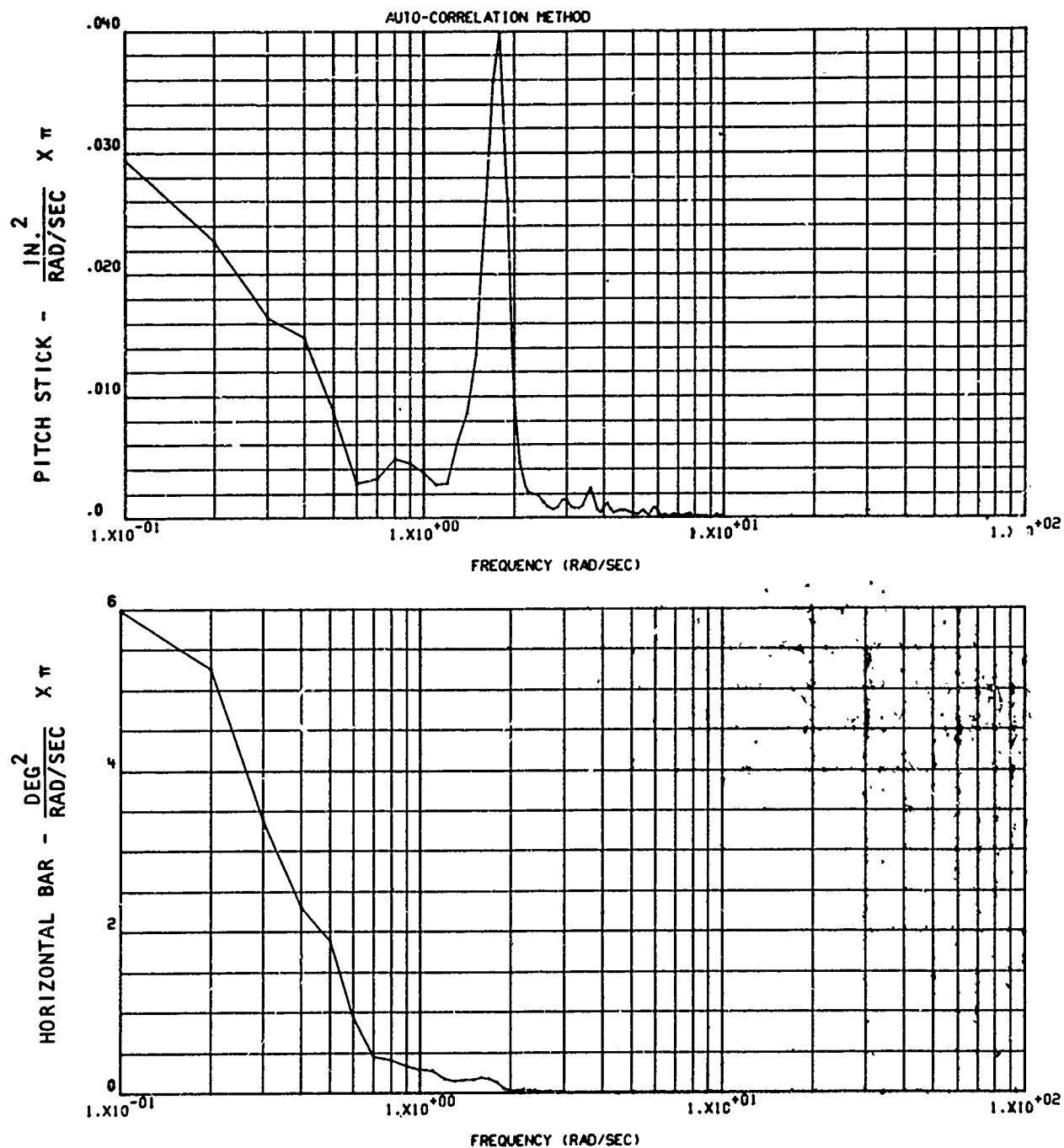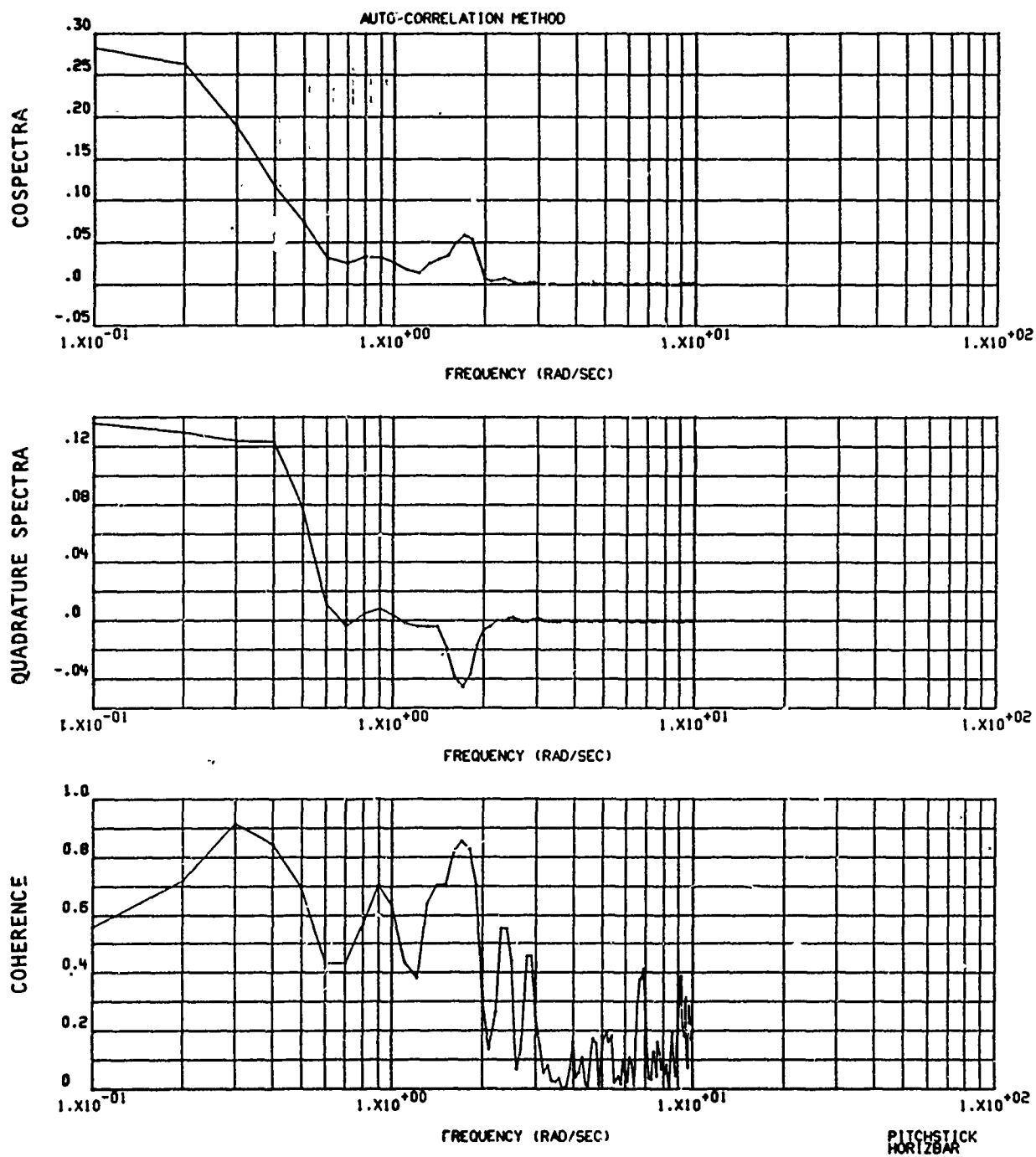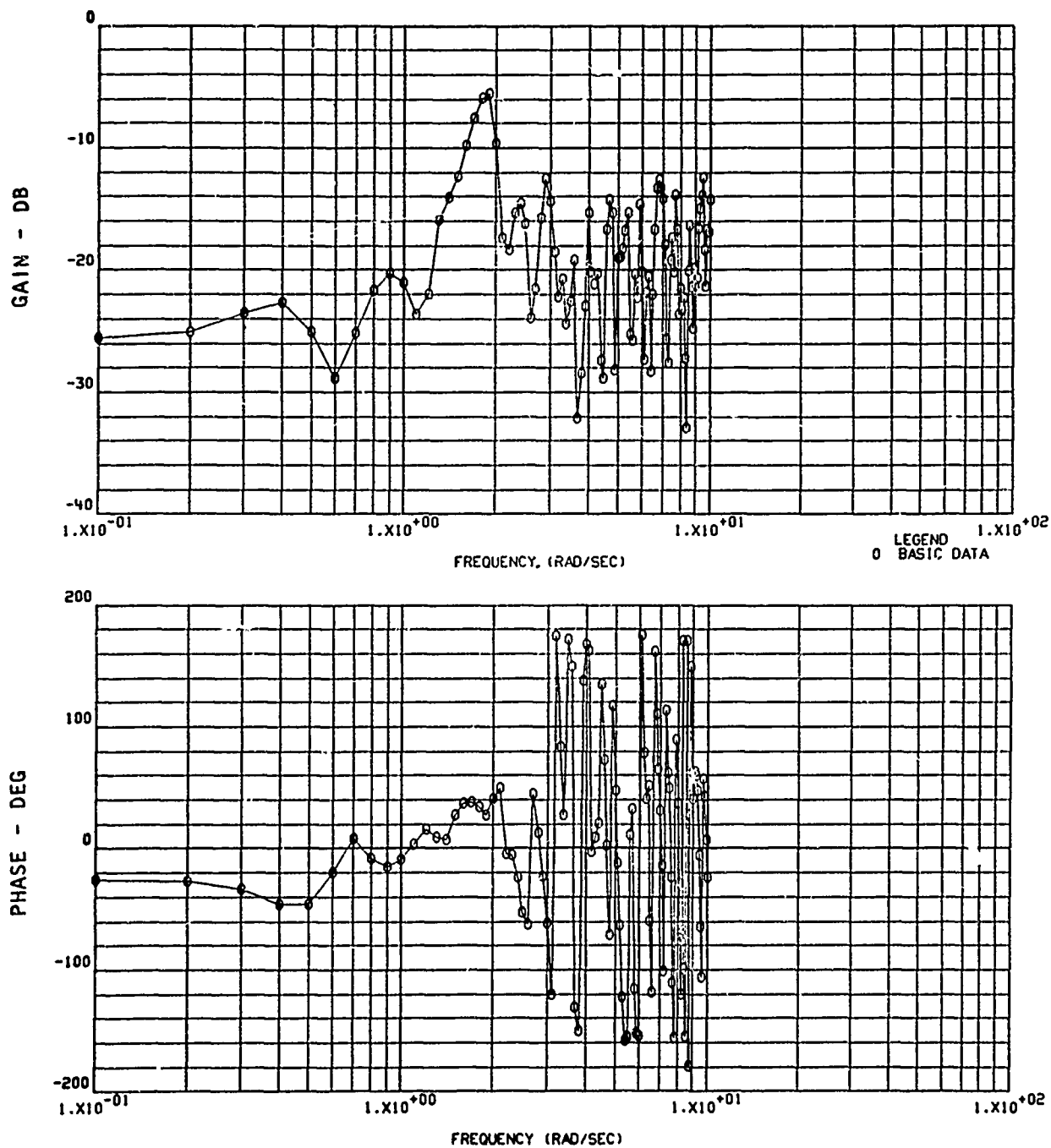
Figure 99. AR Simulation Run No. 01A62 Data (Concl)

405

REFERENCES

1. Anderson, R. O., "A New Approach to the Specification and Evaluation of Flying Qualities," AFFDL-TR-69-120, June 1970

2. Anderson, R.O., Connors, A. J., and Dillow, J. D., "Paper Pilot Ponders Pitch," AFFDL/FGC-TM-70-1, November 1970

3. Onstott, E. D., and Salmon, E. P., "Airplane Flying Characteristics in Turbulence," AFFDL-TR-70-143, November 1970

4. Dillow, J. D., "The 'Paper Pilot' - A Digital Computer Program to Predict Pilot Rating for the Hover Task," AFFDL-TR-70-40, March 1971

5. Teper, G. L., "An Assessment of the 'Paper Pilot' - An Analytical Approach to the Specification and Evaluation of Flying Qualities," STI TR No. 1006-1, November 1971

6. Wykes, J. H., "B-1 Flexible Vehicle Equations of Motion for Ride Quality, Terrain Following, and Handling Qualities Studies," B-1 Division, Rockwell International Corp, TFD-71-430-1, January 1973

7. McRuer, D. T., and Krendel, E. S., "Dynamic Response of Human Operators," WADC TR 56-524, October 1957

8. Bendat, J. S., "Measurement and Analysis of Power Spectra and Cross-Spectra for Random Processes," WADD Technical Report 60-681, October 1960

9. Hamming, R. W., Numerical Methods for Scientists and Engineers, McGraw-Hill, 1962

10. Dubman, M. R., and Byars, B. J., "Rocketdyne Cross-Spectral Analysis Computer Program," Research Report No. 64-10, 31 December 1964

11. Blackman, R. B., and Tukey, J. W., The Measurement of Power Spectra, Dover Publications, Inc, 1958